Design of Collective Motions from Synthetic Molecular Switches, Rotors, and Motors

Damien Dattler, Gad Fuks, Joakim Heiser, Emilie Moulin, Alexis Perrot, Xuyang Yao, Nicolas Giuseppone

Design of collective motions from synthetic molecular switches, rotors, and motors

*Damien Dattler, Gad Fuks, Joakim Heiser, Emilie Moulin, Alexis Perrot, Xuyang Yao and Nicolas Giuseppone**

SAMS research group – University of Strasbourg – Institut Charles Sadron, CNRS – 23 rue du Loess, BP 84047, 67034 Strasbourg Cedex 2, France.

Dedicated to Prof. Jean-Marie Lehn on the occasion of his 80th birthday

ABSTRACT. Precise control over molecular movement is of fundamental and practical importance in physics, biology, and chemistry. At nanoscale, the peculiar functioning principles and the synthesis of individual molecular actuators and machines has been the subject of intense investigations and debates over the past 60 years. In this review, we focus on the design of collective motions that are achieved by integrating – in space and time – several or many of these individual mechanical units together. In particular, we provide an in-depth look at the intermolecular couplings used to physically connect a number of artificial mechanically active molecular units such as: photochromic molecular switches, nanomachines based on mechanical bonds, molecular rotors, and light-powered rotary motors. We highlight the various functioning principles that can lead to their collective motion at various length scales.

We also emphasize how their synchronized – or desynchronized – mechanical behavior can lead to emerging functional properties and to their implementation into new active devices and materials.

TABLE OF CONTENT.

1. INTRODUCTION

1.1. General objective of the review

The increasing complexity of chemical systems is often related to their propensity in generating more elaborated molecular movements, as for instance observed in living matter. Indeed, biologists and physicists teach us that the intrinsic properties of life as we know it (*e.g.* reproduction, metabolism, mutation, and homeostasis)[1,2] are sustained by out-of-equilibrium situations which, at some point, require – but also generate – directional molecular motion through the involvement of biomolecular machines.[3]

Often inspired by nature in their quest to conceive always more complex molecular objects, chemists have also been for a long time interested in designing and synthesizing artificial molecular systems capable of precise mechanical actuation and of energy transduction. To do so, they had first to finely

understand the thermodynamic parameters that rule motion at nanoscale, and then to practically overcome a number of related physical constraints. For instance, individual molecular actuators are typically submitted to Brownian motion and their internal movements cannot be harnessed at larger scales without the conception of appropriate methods to orientate and interface them with other elements. Moreover, the extraction of a useful mechanical work at nanoscale from a simple molecular motion is not possible without the necessary introduction of very specific elements to rectify thermal fluctuations also known as Brownian ratchets – a notion popularized 60 years ago by Richard Feynman along with his visionary talks on nanotechnologies.[4–6]

The recent progresses made by researchers and engineers to harness nano-mechanical actuation have been remarkable, and they can be roughly divided between two main categories. On the one hand, a series of very fruitful endeavors has been directed by a large research community strongly influenced by polymer chemists and materials scientists. They made use of relatively simple bistable molecules (such as *E*/*Z* configurational isomers in photochromic switches) in order to exploit their collective mechanical actuation by properly integrating them in responsive materials and devices.[7] On the other hand, a series of breakthroughs has been achieved by another research community mostly influenced by synthetic organic chemists, and partly inspired by the functional principles of biological machines. They succeeded in designing more complex switchable chemical entities capable of large amplitude motion of submolecular components, in particular based on the development of the so-called "mechanical bond".[8] In addition, they developed complementary chemical tools conferring to these machines the advanced property to function autonomously out-of-equilibrium when fueled by a constant source of external energy. Notably, initial endeavors and achievements in the design and synthesis of such artificial molecular machines have been awarded by the 2016 Nobel Prize in Chemistry to Jean-Pierre Sauvage, Sir Fraser Stoddart, and Ben Feringa.[9–11] In general, the functional tasks that can be performed using these machines have been pursued on their own scale (*e.g.* transport of nanometric cargo, mechanochemical

catalysis, molecular pumping). However, the recent literature shows that artificial molecular machines can also be integrated and interfaced with other elements to harness their collective motion up to microscopic and even macroscopic scales.

The objective of this article is to discuss some of the progresses towards collective molecular actuations made by these two communities which have only limited interactions with one another, but which could further benefit to be mutually influenced. More specifically, we review the integration and synchronization of controlled molecular motions, whether they come from minimal photochromic switches or more advanced synthetic machines. We first show how individual nano-actuators can be engineered as elementary modules and coupled into larger mechanically active assemblies towards higher length scales. We then discuss the differences and the similarities between these systems depending on the nature of the molecular actuators involved. Finally, by highlighting the various functioning principles at work in these mechanical systems, we propose a general classification which relates their molecular structures with their hierarchical dynamics, their potential functions, and their applications at micro- and macroscopic scales.

1.2. Directional motion at low Reynolds number

The term of motion relates to the spatial and temporal displacement of an element within a frame of reference. The concepts and methodologies that have been developed to understand and control motion at different length scales revealed some of the most important scientific principles which stand at the foundation of modern physics.[6] At macroscopic scale, movements of objects are mainly ruled by the gravitational force, and they can be predicted accurately by deterministic physics. Conversely, at molecular scale, positional changes of single particles are dominated by random collisions which can be described in the form of Brownian motion by statistical physics.[12] The Reynolds number (R), which decreases with the radius of the particles, quantifies this transition from the macroscopic world (dominated by momentum and inertia) to the nanoworld (dominated by random thermal energy and viscosity). This

is why, at low Reynolds number, finely controlled molecular motion (*e.g.* translational or rotational) is achieved in a way that is largely counterintuitive based on what we experience with macroscopic machines in our everyday life.[13]

A number of "thought experiments"[14] (such as Maxwell's demon,[15] Smoluchowski's trapdoor,[16] and Feynman ratchet-and-pawl[17]) have early explored the implications of the Second Law of Thermodynamics – which stipulates that entropy increases to a maximum in an isolated system – in order to permit directional motion at nanoscale. The general answer to the apparent paradoxes raised by these approaches is that the local decrease in entropy caused by directional motion should be somehow payed by fueling the system with an external source of energy. In the particular case of the Feynman ratchet-and-pawl device, directional motion (which breaks spatial and time-reversal symmetries) cannot be obtained from a single thermal bath. However, the production of an effective mechanical work becomes in principle possible if the device is submitted to a very local thermal gradient (which breaks detailed balance and leads to a non-equilibrium situation).[18] A number of refinements on the understanding and design of Brownian ratchet mechanisms have been discussed in the literature.[19–22] Two main categories can be distinguished:[14,22] *i*) *energy ratchets* that have no reference to the position of the particle and in which biased potential-energy minima and maxima are repeatedly modified by an external signal (pulsating ratchets), or in which biased potential-energy surface remains constant but detailed balance is broken by using an unbiased driving force to cross energy barriers (tilting ratchets); and *ii*) *information ratchets* which rely on modifying the height of an energy barrier depending on the position of the particle on the potential-energy surface (and thus by a transfer of information from the particle to the energy profile powered by an external source of energy). Therefore, mechanically active molecular systems can make use of ratcheting strategies to move a particle up to an energy gradient and to exchange energy – and thus to potentially exchange information – with their environment.[23]

Ratcheting strategies are notably adopted by biomolecular machines in order to bias random thermal motion for the production of a mechanical work. These complex protein machineries ensure key functions by transduction of this mechanical energy from – and into – other types of energies (that is most often chemical energy).[24,25] For instance, the key energetic molecule of adenosine triphosphate (ATP) is produced within mitochondrial matrices by a protein rotary motor (ATP-synthase), which uses a gradient of proton as a primary source of energy.[26] Other complex protein machineries are responsible for the translation of nucleic acids (*e.g.* ribosome),[27] for intracellular transport (*e.g.* kinesin),[28] for the creation of concentration gradients (*e.g.* Na^+/K^+ pump),[29] for controlling the highly dynamic structure of the Golgi apparatus (*e.g.* dynein),[30] for bacterial flagellar motion (*e.g.* salmonella H^+-driven motor),[31] or for the production of integrated movements of large amplitudes (*e.g.* myosin in muscular tissues).[32] The structural complexity of biologic machines is certainly driven by an evolutionnary process which addresses a number of heavy constraints in the cell, including the need of spatial and temporal specificity for binding events in a highly dense medium of competitors, and including specific catalytic activations and correlations with networks of chemical reactions.

These constraints should be in principle less demanding in simpler environments, and it has been shown that more rudimental artificial molecular systems can indeed achieve precise motion, and can even produce a continuous work on their environment, although they are built with only a few number of atoms. Synthetic machines can also be supplied by various sources of energy (*e.g.* chemical, electrical, and optical), thus leading to various peculiarities. For artifical systems, the use of light is of utmost interest for several reasons: it is a low cost source of energy; its wavelength is finely tunable; its spatial and temporal delivery can be precisely controlled from very large to very small domains; it can directly activate a molecular motion through excited states without the production of chemical waste; and it can directly generate a force on a machine (known as “power stroke”) due to the absence of microscopic reversibility in light-driven excitation.[33] This later specificity has important consequences for the fine

functioning principles which differ drastically between chemically-gated and light-powered molecular motors.[34,35] On the other hand, light has also some drawbacks which can partly explain the choice made by Darwinian evolution to work with biomolecular machines using chemical fuels. Indeed, sunlight cannot be stored and delivered on demand, it produces highly energetic radiations which can damage other chemical parts of the system, and it cannot easily penetrate at lower wavelengths neither within tissues, nor within materials when discussing artificial systems.

1.3. Terminology used in this review

Although the artificial construction of nanomachines reaching the complexity of their biological counterparts is very far from any practical realization, the fundamentals of what should be their functioning principle is progressively diffusing into the chemical community. This knowledge has already helped chemists in formalizing a number of now well-accepted terms to characterize mechanically active molecules (*e.g.* "machine", "switch", "motor", "ratchet", "linkage", "escapement", *etc.*).[14] Because the functioning principles of directional motion at nanoscale can be counterintuitive based on our macroscopic perceptions, the use of an appropriate scientific vocabulary is of first importance to discuss this topic, and we will be rigorous on that aspect throughout this review. In particular, the term of "molecular machine" describes a molecular entity in which the subcomponents can be moved relative to one another, in a controlled manner, and with the potential to use that mechanical actuation as a functional – and therefore "useful" – tool. Such machines can be divided between two main categories: switches and motors. *Molecular switches* are bistable (or multistable) entities which can be actuated back and forth upon external stimulation (*e.g.* by optical, electrical, or chemical means), and which influence the system as a function of state. Importantly, because of microscopic reversibility principle, when an isolated switch returns to its original position, the backward motion between the submolecular components leads to the cancellation of any work done during the forward motion. In a striking difference, *molecular motors* move their subcomponents following a non-reversible pathway that influence the system as a function of their

spatial trajectory. A motor can repeat this motion again and again, for instance by processing with a full directional rotation of 360°, and can even possibly cycle motion autonomously when supplied with a constant source of external energy. Therefore a molecular motor – although more challenging to synthesize – is able to constantly and progressively increase the work it performs on its environment. In addition, we will discuss in this review a limiting number of examples involing *molecular rotors*. They are defined as molecules consisting of two parts that can easily rotate relative to each other. In principle, this one-dimensional rotation (that is changing in a single angle) involves very low energy barriers and cannot be ratcheted to produce any work. However, when properly designed, several of these rotors can be coupled together to lead to collective gearing motion, which constitute an interesting entry to construct mechanical modules which could be eventually connected to an active motor part for instance.

The language necessary to describe the coupling between molecular actuators and their hierarchical dynamics across all length scales will also be of first importance in the following discussion. Terms such as self-assembly, bottom-up, interfacing, orientation, transmission, correlation, gearing, anisotropy, synchronization / desynchronization, oscillations, and cooperativity will be introduced along the description of the systems selected for this review, and they will be used to precisely characterize and classify the various effects at work in a more general perspective.

1.4. Organization of the review

To keep this review comprehensive, we will mainly restrict our discussion to systems in which collective motions are the direct consequence of local mechanical interactions between their various elements. Hence, we will not consider collective motions only involving phase transition phenomena or being only induced by long range orientation in external fields. The selected systems will be classified in three chapters, depending on the chemical nature and functioning principles of their individual actuating units as defined in this introduction. This subdivision is justified by the fact that it represents the current trend by which these systems have been mainly developed, that is along relatively separated approaches

which have been pursued by relatively different communities. Therefore, we will start by discussing collective motion extracted from photochromic switches that make use of local configurational isomerization as a source of molecular actuation. We will then turn to actuators built on the mechanical bond, which involve controlled molecular motions of larger amplitudes, often by making use of molecular binding events, and whose complex topologies can also be integrated in dynamic collective systems. We will finally outline correlated rotary motion, either produced by simple rotors showing gearing effects, or by the integration of more advanced light-driven rotary motors capable of generating a continuous unidirectional rotation when fueled by an external source of photons.

For each family of actuator, a brief introduction – including both seminal works and key reviews – will describe their basic chemistry and their intramolecular motions, because they are essential information to subsequently understand their intermolecular coupling in space and time. Then, collective mechanical motions will be comprehensively described as well as their potential practical applications in devices or materials. The organization of the works within each chapter will be partly based on chronology – in order to highlight original research –, partly based on the mechanisms of collective actuation at work, and partly based on the increasing complexity and performances of the systems described. Some typical criteria that have been considered for this last item are: the complexity of the chemical structures involved, the number of elements coupled with one another, the dimensional order of that coupled elements (from 1D to 3D objects), the amplitude and speed of the generated motion, and the profound physical nature of the actuation, going from simple reversible switches to more advanced motors functioning out-of-equilibrium. Finally, in a last part on conclusions and perspectives, we will try to extract a global classification of all these systems by discussing their similitudes, differences, and complementarities in more general and common terms.

2. MOTION FROM PHOTOCHROMIC MOLECULAR SWITCHES

Molecular switches are defined as chemical species possessing at least two thermodynamically (meta)stable states and capable of reversible interconversion between them in response to external stimuli. Such switches are typically activated by chemical, electrochemical, or photochemical triggers, and their isomers should be stable enough to avoid spontaneous thermal relaxation when not desired.[36] Kinetic aspects are also important when considering a switchable molecule, because its time response must be compatible with its functional use (e.g. as a molecular probe, as part of a drug delivery system, or as a bit of information for data storage). Among the various types of switches, the present section will discuss only those involving isomerization of photochromic compounds, some of which have been widely studied for more than a century.[37,38] Photochromism is simply described as the reversible color change of a molecular species induced by light. More specifically, this phenomenon corresponds to a molecular isomerization activated by photo-irradiation with UV, visible, or IR wavelengths. Photo-isomerization is of particular interest and remains unequalled by any other approach because it is a non-invasive tool, which can be easily tuned, and spatially resolved, and it is compatible with a large selection of phases.[39] One should point out in the context of this particular review that, for the reasons mentioned above, and although other triggers could be in principle used instead,[40] light is the only stimulus that has been used so far to switch isomerizable molecules in order to generate controlled collective motion. In addition, among all the photochromic switches that have been elaborated in the literature, only a few of them have been implemented into such collective systems. To enter in this field of intense investigations, we will first detail the intrinsic mechanism of molecular photochromic actuation, and we will then present an exhaustive list of the papers describing the elaboration of a collective motion using such compounds, with a particular emphasis on the most impressive examples.

2.1. Introduction to photochromic molecular switches

Azobenzene, diarylethene, and spiropyran are amongst the most studied molecular switches and, as a consequence, they are predominant in the elaboration of collective motion systems. Fulgide, spirooxazine and stilbene derivatives can also be found in the literature of this particular field, although the number of examples still remains limited. Finally, photochromic hydrazones have emerged in the literature quite recently, and the very first collective systems have been now developed. In the following, we will provide an introductory overview of these molecular actuators based on their two main mechanisms of photo-activation, namely: *i*) the *cis–trans* isomerization (i.e. with azobenzene, stilbene, and hydrazone), and *ii*) the electrocyclization (i.e. with diarylethene, fulgide, spiropyran, and spirooxazine).

Azobenzene was first used as a dyeing agent in the industry, and it is only in 1937 that G. S. Hartley discovered its propensity to undergo *cis-trans* photoisomerization.[41] This compound, formed by two phenylamines whose nitrogen atoms are linked together by a double bond, is one of the most popular photoswitches nowadays because of its simple structure and its reliability (Figure 1a). Usually, the switch requires to be irradiated by UV light in order to perform the *trans→cis* isomerization. This process is generally thermally reversible, the *trans* isomer being often more stable than the *cis* isomer. Therefore, the *cis→trans* interconversion may occur through the absorption of visible light but also in the dark, thus lowering the global yield of the *trans→cis* conversion. The lack of emission at the excited states and the absence of obvious side-photoreaction lead to an almost quantitative quantum yield for both isomerizations.[42] Although this switch stands out by its great stability and fatigue resistance, degradations can still occur in some specific conditions,[43] leading to photocyclization[44] or photoreduction.[45] Even if the photoreaction seems simple at first sight, its mechanism has not yet been fully elucidated; inversion, concerted inversion, rotation, and inversion-assisted rotation are the four main processes that have been proposed so far to explain this isomerization.[46] The polarity and the viscosity of the solvent, the nature and the position of the substituents, the temperature and even the pressure may have a tremendous impact on the isomerization quantum yield, on the absorption wavelengths, and on the mechanism involved.[46–48]

For instance, it has been shown that the presence of strong electron-withdrawing moieties allows the *cis→trans* isomerization to occur under visible light.[49–51] These days, azobenzene has been explored thoroughly and numerous synthetic approaches have been developed; two essential reviews cover almost all the different synthetic pathways and detail their corresponding mechanism.[52,53] The main synthetic method is the azo-coupling reaction in which a primary phenylamine is diazotized at low temperature before being placed in the presence of an aromatic nucleophile. This approach is usually quick and efficient although it remains pH sensitive. In order to form exclusively symmetrical compounds, the reductive coupling of nitrophenyl derivatives may be preferred. One of the main interests of the azobenzene structure lies in the important change of its geometry and polarity. Indeed, the *trans* isomer has almost no dipole moment and is planar, whereas the corresponding *cis* isomer is twisted and possesses a dipole moment close to 3 Debye.[54] Moreover, with its two aryl rings, azobenzene can be easily substituted and functionalized by many different moieties. Finally, this switch may isomerize selectively, depending on its orientation, when irradiated with linear polarized light.[55,56] As a result, this photochromic moiety has been incorporated in a plethora of applications related to many different domains. For example, it is used in the field of memory devices[57,58] and it is also promising in order to form photo-responsive polymers,[42,56,59–61] metal-organic frameworks,[62] and self-assemblies.[59]

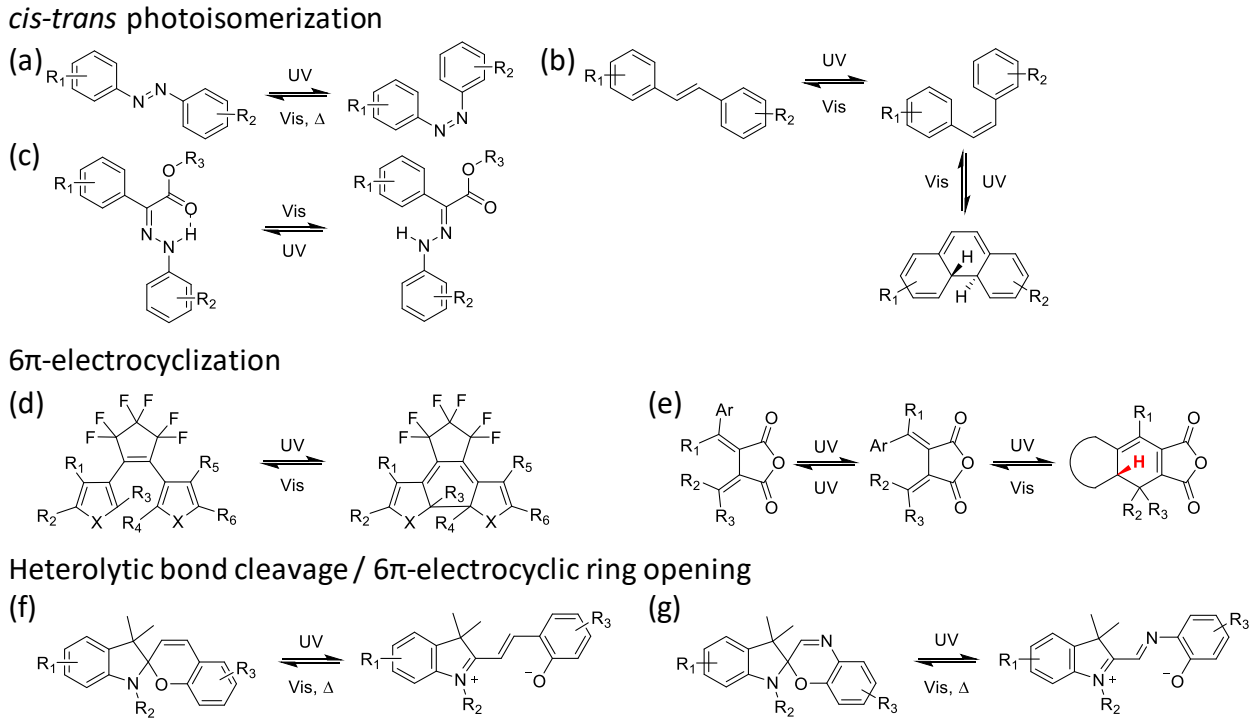

Figure 1: Chemical structures of photoisomerizable (a) azobenzene, (b) stilbene, (c) hydrazone, (d) diarylethene, (e) fulgide (labile hydrogen highlighted in red), (f) spiropyran and (g) spirooxazine.

The synthesis of *stilbene* was first reported in 1843 by Laurent,[63] but it is only in 1940 that its photochemical properties have been reviewed by G. Lewis.[64] Nowadays, the book published by G. Likhtenshtein is absolutely unequalled in order to get a better understanding of this system and of its main applications.[65] The stilbene structure is quite simple, composed of two phenyl rings linked together by a double bond. When photo-irradiated, this switch reacts similarly to azobenzene (Figure 1b). Indeed, the *trans→cis* isomerization takes place under UV, whereas the *cis→trans* reversed reaction occurs typically in the visible range. It is important to note that, unlike the previous system, the *cis* isomer cannot be thermally isomerized back to the *trans* isomer,[66] but that it can undergo a photocyclization leading to the formation of dihydrophenanthrene. This side reaction possesses a quantum yield of approximatively 0.1[67] and remains reversible as long as the product is not oxidized by dioxygen or by any other oxidizing agent. Therefore, stilbenes are usually present as a starting material in the synthesis of phenanthrene

derivatives.[68] [47] The chromophore properties of these switches are extremely dependent on the solvent viscosity, polarity, and temperature, but also on the presence of other species such as heavy atoms.[69] Stilbene derivatives can be synthesized in many different approaches.[65] The main pathway is the aldol-type condensation, which can lead to a disubstituted product, at the cost of a relative low yield. Alternatively, the Siegrist method or the Wittig reaction may be preferred in order to reach higher selectivity or yield. In a general way, this switch can be found in different systems such as molecular probes, photoresponsive materials, or drugs.[65]

In 2009, the research team of Aprahamian developed a pH-responsive rotary switch based on *hydrazones*.[70,71] This system was further improved in order to control the *E/Z* isomerization with transition metals, such as Zn,[72,73] or with photo-acids, such as spiropyran,[74,75] and a negative feedback loop system has even been elaborated.[76] However, it is only in 2017 that the first photochromic hydrazone derivatives were synthesized.[77] Their structures are usually based on the presence of an α-ester phenylhydrazone linked to an aryl moiety (Figure 1c). The *Z* isomer possesses an intramolecular H-bond between the carbonyl of the ester and the hydrogen of the hydrazone, and its irradiation with visible light allows the formation of the *E* isomer. The latter does not possess intramolecular H-bond and is also thermally stable, thus photoirradiation at a shorter wavelength is often necessary to reverse it to its initial form. It is interesting to note that the interconversion may also be triggered by a two-photon excitation process.[78] The nature of the solvent and of the substituents seems to have a great effect on the absorption and emission spectra,[78] though few studies have been conducted so far to establish a general conclusion. Compared to some other switches, hydrazone derivatives are relatively straightforward to synthesize. They are formed through the condensation of an aryl hydrazine with a ketone.[77] Having been recently developed, the number of applications present in the literature is still limited. However, with their high fatigue resistance, slow thermal isomerization and important quantum yield, one can assume that

hydrazones will be investigated in depth in order to create novel systems. So far, they have been integrated to liquid crystal to induce a photo-control of the material phase transition.[79]

Theoretically predicted and synthesized in 1988 by the team of Irie,[80,81] *dithienylethene* has become one of the most popular photoswitching units. Its structure, based on a diarylethene, is composed of two thiophene groups that are linked together by a (perfluoro)cyclopentene (Figure 1d). Upon photoirradiation, this compound performs a reversible reaction from an open-ring isomer to a closed-ring one, the latter possessing a cyclohexadiene structure.[82] This photocyclization follows the Woodward–Hoffmann rules, with the 6π-electrocyclization that requires UV light to occur, and with the reverse opening that requires visible light. The (perfluoro)cyclopentene moiety is an important part of this photochromic unit because it precludes *cis*→*trans* isomerisation of the double bond and hence increases the efficiency of the switch.[83] It has been demonstrated that this process is fatigue-resistant, thermally irreversible, and that the nature of the molecular substituents influences greatly the photoresponse of the system.[84] The presence of electron-donating groups induces an increase in the absorption maxima concomitantly with a diminution of the quantum yield of the cyclization and ring-opening reactions. Inversely, electron-withdrawing substituents have no effect on the absorption maxima nor on the ring-opening quantum yield, but they induce a bathochromic shift of the spectrum and an increase of the cyclization efficiency.[85,86] The synthesis of diarylethenes has been explored relentlessly since its discovery and, nowadays, the most popular approach to obtain dithienylperfluorocyclopentene compounds is the mono- or bis-elimination reaction of a (perfluoro)cyclopentene with aryllithium derivatives.[84] This method allows the formation of symmetrical or asymmetrical compounds in accordance with the ratio of the cyclopentene used. This molecular switch can therefore be functionalized in a variety of ways, facilitating its integration in any system, whether involving collective motion or not, and many different applications have progressively been developed.[87–90] Dithienylethenes appear particularly promising for the design of memory devices,[91,92] of multi-responsive agents[93] and smart

receptors,[94] and it has been coordinated to transition metals[95] and incorporated into various chemical structures[96] and self-assembled systems.[97]

The photoreaction of *fulgides* was observed for the first time by Stobbe in 1907,[98] but only accurately characterized in 1968 by the team of Becker.[99] Their structure is based on a succinic anhydride substituted at positions 3 and 4 by two alkenyl groups (Figure 1e). In addition, in order to obtain a photochromic molecule, it is essential that one of the methylene carbons bears an aryl moiety. Similarly to diarylethenes, this switch can perform a thermally irreversible 6π-electrocyclization from the *E*-hexatriene structure to the colored form.[100] Most of the time, this photocyclization occurs under UV light and the reverse ring opening reaction under visible light. It is important to note that the *E*-*Z* isomerization is a side-photoreaction that leads to a decrease of the electrocyclization quantum yield. Numerous papers reported on the influence of the steric hindrance over this isomerization, showing that bulkier substituents lower the quantum yield of *E*-*Z* isomerization.[101–103] The electronic nature of the substituents and their position on the ring are also of importance. In the case of electron-donating groups, a strong bathochromic shift of the closed-form absorption spectrum can be observed, along with an important reduction of the electrocyclization and ring-opening quantum yields.[104,105] In the case of electron-withdrawing groups, hypsochromic shifts in the absorption spectra of the *E* isomer and of the closed form are observed, together with an increase of the ring-opening quantum yields.[106] Nowadays, the most popular synthetic pathway in order to access fulgides remains the Stobbe condensation.[107] Unfortunately, because of the anhydride moiety, fulgides tend to react easily with nucleophilic species such as water, amines, and alcohols. Moreover, the presence of a labile hydrogen (Figure 1e) in the closed isomer may lead to the formation of a stable non-photochromic aryl ring.[38] Even if it is possible to avoid this side reaction by replacing that labile hydrogen with an alkyl moiety, this switch is not as fatigue-resistant as dithienylethenes, and its applications have been therefore comparatively limited.[100]

Originally noticed in 1927 by Dickinson and Heilbron for their thermochromic properties,[108] *spiropyrans* were only characterized as photoswitches in 1952 by Fischer and Hirshberg.[109] Since then, this family of compounds has been extensively studied and reviewed in a number of papers.[110–113] The spiropyran structure is commonly considered as formed by a benzopyran moiety linked to an indoline part by a spiro bond (Figure 1f). The UV photoirradiation of a spiropyran leads to the formation of its open-ring isomer, also called merocyanine. The latter may undergo the reverse reaction thermally or through the absorption of visible light. The specificity of this switch lies in the large variety of stimuli capable of triggering and/or modulating its isomerization. For instance, spiropyran responds to mechanical force,[114] to the nature of the solvent,[115,116] and to the presence of ions in solution.[117] Moreover, this switch stands out by the large difference of properties between its two isomers, may it be their charge, polarity, absorption spectra, or solubility. The interconversion process is ruled by two competing mechanisms.[118] The first one is a heterolytic bond cleavage with the presence of a polar transition state. The charge separation, between the indoline nitrogen and the benzopyran oxygen, is stabilized by polar solvent and electron-withdrawing substituents, especially in the *ortho* and *para* positions relative to the chromene phenolate. The second mechanism is similar to an electrocyclization and involves a less polar intermediate, with the formation of a ketone, stabilized by non-polar solvents and electron-donating substituents. Hitherto, the synthesis of spiropyrans has remained quite constant overtime.[119] Indeed, the main pathway consists in the condensation of a Fischer's base with an *o*-hydroxy aromatic aldehyde in ethanol. However, the downside of this approach is definitely the presence of undesired reactions, such as the condensation of the obtained spiropyran with another Fischer's base. Besides, this switch unfortunately also stands out by its poor fatigue resistance under UV light, with two main photodegradations pathways. The first one requires the presence of triplet oxygen which may irreversibly oxidize the switch.[120] The second one involves a bimolecular mechanism with spiropyran units in their triplet excited states, a detrimental situation that depends on the solvent polarity and on the concentration

as merocyanines tend to easily aggregate. Thus, it has been attested that working under inert atmosphere, along with immobilizing the switch on a surface, are favorable conditions to greatly limit those side reactions[121]. Despite those downsides, spiropyrans have been integrated in many different systems,[112] such as metal[111,122] and stress[114] sensors, polymer viscosity[123] or catalyst activity[124] photoregulators, and in memory devices.[110]

The synthesis of *spirooxazine* was first reported by Fox in a patent of 1961.[125] It is only in 1980 that Hovey and Chu noticed the amazing fatigue resistance of this photoswitch.[126] Since then, spirooxazine has been involved in many different patents mainly linked to its integration into chromophoric lenses and sunglasses. So far, the number of academic papers related to this compound remains quite limited in comparison to spiropyran, however some enlightening reviews have still been published on this subject.[38,110,113,127] The spirooxazine structure is quite similar to the spiropyran one, the main difference lying in the presence of a nitrogen atom replacing a carbon on the chromene moiety (Figure 1g). The UV photoirradiation of the closed-ring isomer leads as well to the formation of a merocyanine including a central Schiff base moiety, and the reverse reaction is also promoted by a thermal process or by visible light. As for spiropyran, the mechanism of interconversion along with the ratio between the different isomers are ruled by the solvent polarity as well as by the position and electronic nature of the substituents.[127] Historically, the synthesis of spirooxazine was based on the approach used for the formation of spiropyran.[127] It required the coupling of an *o*-hydroxynitrosoaryl with an alkydiene derivative. Unfortunately, the nitroso moiety is less reactive than the corresponding chromene and, moreover, the intermediate formed is often sensitive to degradations. These difficulties are at the root of the slow development of novel spirooxazine derivatives. Nowadays, optimized synthetic strategies have been elaborated, such as, for instance, the use of toluene as solvent or the addition of a drying agent.[128] The main quality of this photoswitch remains its remarkable resistance to photodegradation in comparison to its spiropyran counterpart. Therefore, different systems have been elaborated to exploit this asset, and

spirooxazines have been indeed implemented as photoresponsive ligands[111] and liquid crystals,[110] or as dyes in bioimaging.[129]

The above introduction on photoswitches will sustain the following discussions on their implementation to produce collective motion of molecules and polymers in devices and materials. However, due to the huge number of systems and applications developed so far, it is primordial to set some limits and to restrict the scope of what will be presented in this review. Therefore, we will focus on 2D and 3D systems in which the collective photoisomerizations of multiple molecular units lead to mechanical motion of much larger amplitude than the molecular switch itself. As a result, changes of conformation of single macromolecules, such as folding or helicity, will not be considered. Also, concerted changes of physical properties, such as viscosity or phase transitions and photoalignments, will not be part of this paper unless they involve the mechanical motion of connected ensembles of molecules. Furthermore, collective motion which have been proved to be solely induced by photothermal effect will not be addressed. Indeed, this approach relies on the phase transition at the surface of a liquid crystal by a local increase of temperature, the presence of a photoswitching unit is thus not required, even if it can result in remarkable systems, like the self-oscillating film developed by Meijer, Broer and coworkers.[130] However, for the readers interested by these different subjects, reviews already exist in the literature.[131–133] Finally, the actuating materials developed with mechanically-bonded molecules and incorporating photoswitches will be described in Chapter 3.

Considering these constraints, the comprehensive overview of the remaining systems is divided into four main sections. The first one discusses the motion of micro- or macroscopic objects driven by an interfacial force, which is often caused by a gradient in the surface energy that results in the mechanical motion of liquids, solids, and colloidal objects. The second part focuses on mechanical deformation of bidimensional materials, either planar or spherical, and on their photomechanical motion. Finally, the third part on tridimensional materials is divided in two sections: the first one discusses the manipulation

of their surface topology, mainly with surface relief gratings (SRG), and the second one presents their overall structure deformation. The various phenomena presented in the following paragraphs have already been widely discussed since their discoveries, and some of the corresponding reviews will be indicated for the readers who wish to go further into each topic.

2.2. Interface driven motion of liquids, solids and colloids

In the introduction to this chapter, we have seen that the *cis* isomer of azobenzene is more polar than its *trans* form because of its twisted configuration. Also, whereas the closed spiropyran isomer is neutral, its opened merocyanine form is charged, and thus more polar. Therefore, the isomerization of these photoswitches can in principle modify the polarity of materials in which they are integrated. In particular, with a careful design of such systems, one can build a surface energy gradient driving the macroscopic motion of an object in contact with its interface. The following paragraphs present materials in which such motions have been achieved. We will first consider the examples of liquid photoactuation, we will then turn to solid photoactuation, and we will finish with systems where the motion of colloidal particles and micromotors has been demonstrated.

2.2.1. Photodriven actuation of liquids

In microfluidic systems, surface energies have a great impact on the motion of liquids. Hence, a remote control of the interfacial properties is of prime interest for the successful application of microfluidic devices.[134] The basic principle of the motion of liquids on solid surfaces relies on the wettability switching of the substrate. This phenomenon has been widely investigated and reviewed with photoswitches.[135–140] The preparation of the solid substrates can for instance involve the grafting of photochromic molecules directly onto its surface *via* a siloxane spacer (Figure 2a),[141,142] or it can be coated with a photoactive polymer (Figure 2b).[136,143]

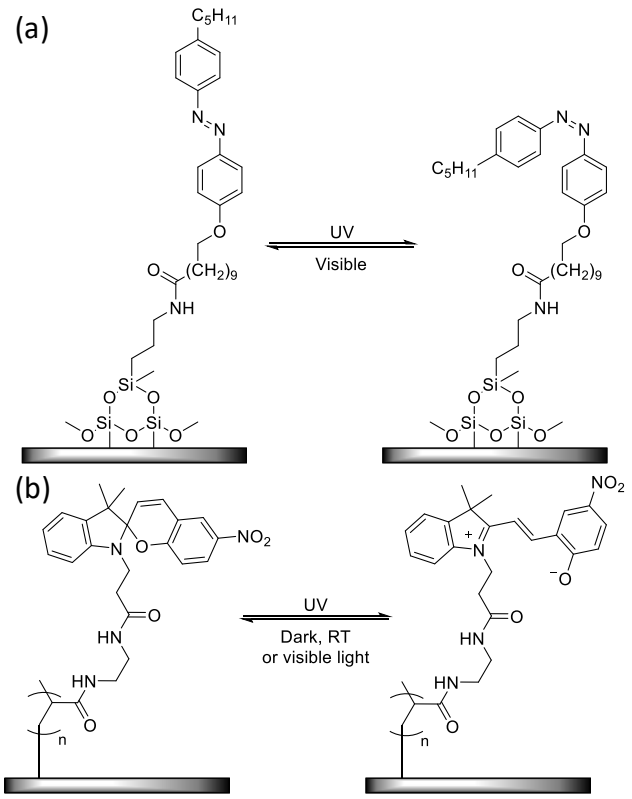

Figure 2: Examples of methods for the functionalization of solid substrates with photochromic molecules. (a) Chemical structure of an azobenzene derivative grafted on the surface *via* a siloxane spacer, and corresponding isomerization process upon light irradiation.[141] (b) Chemical structure of a spiropyran derivative attached to the surface *via* a polymer backbone, and corresponding isomerization process upon light irradiation.[136]

The most commonly used chromophores in such systems are based on azobenzenes, but some examples incorporate spiropyran[144,145] or diarylethene[146] derivatives. One should mention that the mechanism of wettability switching for the diarylethene-based systems is slightly particular: the light irradiation and subsequent isomerization induces the crystallization of the molecule, and it is that resulting morphological change of the surface which modifies its wettability.[146] One should also note that it is possible to enhance the functional efficiency of a switch by structuring the surface[147] and taking advantage of the Lotus effect,[148] or by incorporating hydrophobic moieties in its chemical structure (typically with

fluorination).[149] When the wettability change is modulated in space, so that a surface energy gradient is built, it may cause the motion of a droplet at the surface.[150] The most famous system for this purpose has been proposed in 2000 by Ichimura and coworkers.[151,152] The authors designed a calix[4]resorcinarene bearing four pendant azobenzene derivatives (Figure 3a). By immersing an aminosilylated glass substrate into a solution of this photoactive compound, they obtained the corresponding responsive surface. The photoinduced motion of several liquids was investigated. Figure 3b shows the result for an olive oil droplet placed on the substrate. First, the surface is enriched in *cis* isomers under UV illumination (λ = 365 nm) with hidden carboxylic acid moieties, leading to the spreading of the droplet due to the higher surface energy (Figure 3b, (i)). The surface energy gradient was achieved by irradiating the liquid with the edge of a blue light beam (λ = 436 nm), isomerizing the azobenzene back to its *trans* form, exposing carboxylic acids at the surface and causing the droplet to move towards the area with the highest surface energy (i.e. towards the *cis*-rich areas) (Figure 3b, (ii)). Because the beam can be displaced along with the movement, there is intrinsically no limitation to the distance that the droplet can travel. The motion can be stopped by homogeneous illumination of the surface with blue light, forming the *trans* isomers back on all the surface (Figure 3b, (iii)). The authors further showed that the process is fully reversible by simply repeating this procedure and by adjusting the position of the light beam (Figure 3b, (iv)).[151] The typical speed achieved was in the order of 35 μm.s^{-1}.

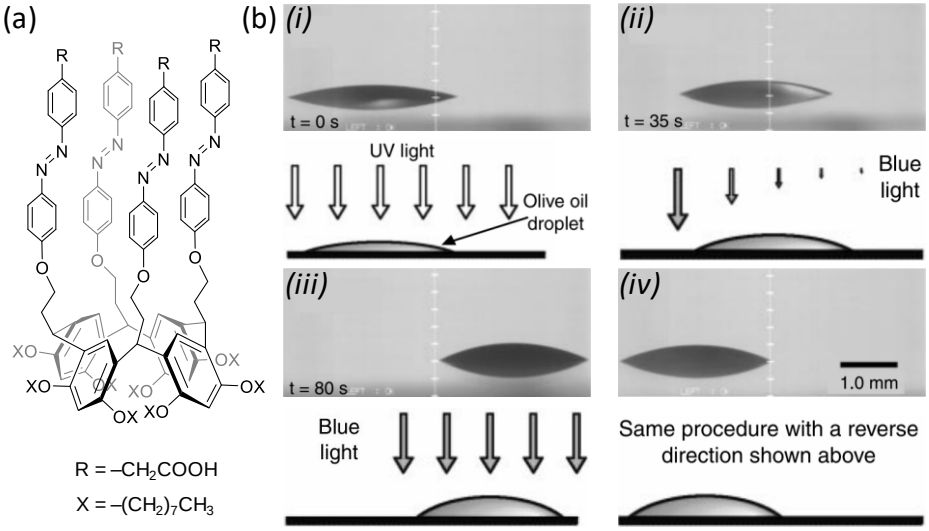

Figure 3: Photoinduced liquid actuation on a solid substrate. (a) Chemical structure of the tetra-azobenzene calix[4]arene derivative used for the functionalization of the surface. (b) Procedure for the photocontrolled motion of an olive oil droplet and the corresponding optical microscopy images, with first a homogeneous illumination with UV light (λ = 365 nm) to have the *cis* isomer all over the surface (i), followed by asymmetric irradiation with the edge of a blue light beam (λ = 436 nm) inducing the motion of the droplet towards the *cis*- rich area of higher surface energy (ii). The motion is stopped by homogeneous irradiation with blue light (iii) and the process is fully reversible by adjusting the direction of the UV illumination (iv). Part (b) is adapted with permission from reference [151], Copyright 2000, American Association for the Advancement of Science.

The same motion was achieved for other liquids, such as the liquid crystalline compounds NPC-02 (mixture of two alkoxyphenylcyclohexane derivatives) and 4-cyano-4'-pentylbiphenyl (5CB), 1-methylnaphtalene, and 1,1,2,2-tetrachloroethane. However, no motion was observed with water, formamide, ethylene glycol, and a low molecular weight poly(ethylene glycol). Since the motion of a liquid on a solid substrate is controlled by the contact angle hysteresis, that is, the difference between the advancing contact angle θ_{adv} and the receding contact angle θ_{rec} on a tilted surface, the authors investigated this phenomenon for the considered liquids on *trans*- and *cis*-rich surfaces (Table 1). They concluded that a motion can be achieved if the receding contact angle on the *trans*-surface is larger than the advancing contact angle on the *cis*-surface.[152] This requirement was further confirmed by the work of Picraux *et al.*[141] This behavior is theoretically possible for any system containing stimuli-responsive molecules switching their polarity, and has been, for instance, also achieved with rotaxanes (see Section 3.2.2) and overcrowded alkenes (see Section 4.3.2).

Table 1: Contact angles (°) measured for various liquids on a surface functionalized with azobenzene.[152]

	trans- rich		*cis*- rich	
	θ_{adv}	θ_{rec}	θ_{adv}	θ_{rec}
No motion				
Water	94	**40**	**86**	51
Formamide	68	**17**	**62**	19
Ethylene glycol	61	**36**	**56**	39
Poly(ethylene glycol) M_w = 400 g.mol^{-1}	42	**37**	**38**	31
Motion				
1-methylnaphtalene	26	**24**	**20**	18
1,1,2,2-dichloroethane	18	**16**	**12**	11
5CB	43	**37**	**22**	19
NPC-02	28	**24**	**11**	10
Olive oil	29	**25**	**17**	13

Garcia and coworkers developed the functionalization of a glass substrate with spiropyrans for the photoactuation of liquids (Figure 4a).[153] For the photoswitch to have enough free volume to isomerize under illumination, the authors decreased its surface density by first coating the glass with *t*-butyldiphenylmethylsilane. They subsequently introduced a spiropyran derivative bearing an aminosilylated linker (Figure 4a). This procedure was applied to a capillary tube and the authors observed that upon irradiation with UV light (λ = 366 nm), the water level in the tube rose of 2–3 mm after 300–1500 s. They described this phenomenon as a "photocapillary" effect and suggested that the extent of motion could be larger with a capillary tube of a smaller diameter.[153]

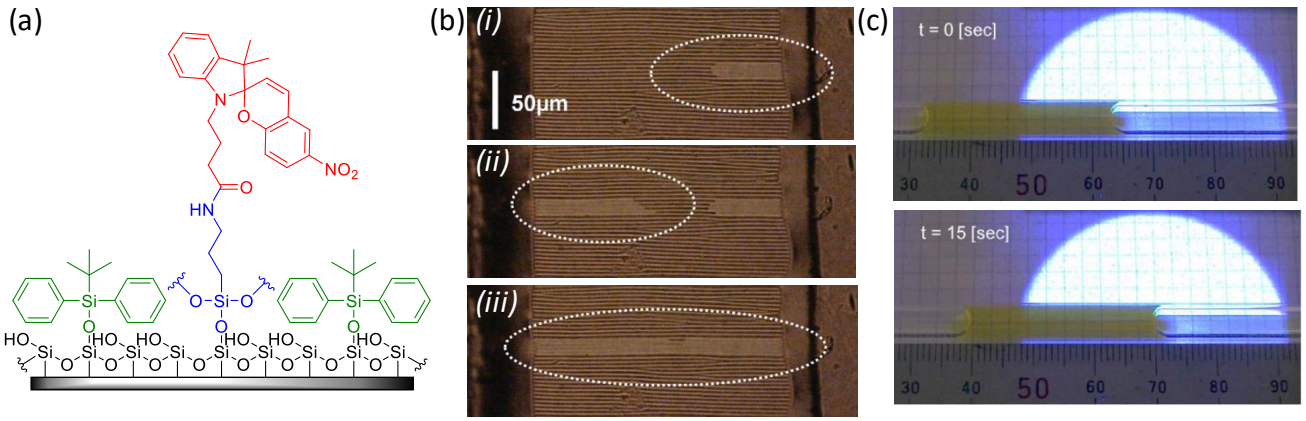

Figure 4: Spiropyran-based examples of liquid photoactuation. (a) Representative chemical structure of the substrate used in reference 153 with the spiropyran in red, the silylated spacer in blue, and the *t*-butyldiphenylsilyl used to « dilute » the surface in green. (b) Optical microphotographs of the motion of "liquid filaments" in the grooves of the photoactive material that have been irradiated with UV light (λ = 365 nm); (*i-iii*) localization of the irradiation. (c) Snapshots of the photoactuation in a capillary tube of a solution containing an azobenzene surfactant upon UV irradiation (λ = 365 nm). Parts (b) and (c) are adapted with permission from references [154], Copyright 2012 American Chemical Society, and [155], Copyright 2017 Springer Nature, respectively.

More recently, Monobe *et al.* described a system for the manipulation of “liquid filaments” (LF).[154] Microwrinkles were prepared on a polyimide film by applying a strain to the material during the curing step, and an azobenzene-containing polymer was subsequently coated on the substrate. Upon UV irradiation (λ = 365 nm), the LF wet the material only within the grooves (hence the term “liquid filament”) of the isomerized area (Figure 4b). Interestingly, photoactuation of liquids on a glass substrate was also observed with the photochromic molecule in solution instead of being at the surface. Hence, Motosuke *et al.* described the motion of an aqueous solution of an azobenzene surfactant in a capillary tube upon UV irradiation (Figure 4c).[155]

Let's now consider examples in which the controlled motion of a liquid is achieved on a liquid surface. Baigl and coworkers engineered a system to optically trap a droplet of oleic acid at the surface of a solution containing an azobenzene surfactant.[156] They first demonstrated that, upon irradiation with appropriate wavelengths, the droplet was moving from areas with a high surface energy (i.e. *cis*-rich areas) towards areas with a low surface energy (i.e. *trans*-rich areas). Hence, they developed an optical device where a localized spot is irradiated with blue light (λ = 435 nm) circled by a circular irradiation with UV light (λ = 365 nm), creating an optical trap for the oil droplet (Figure 5a). They named this phenomenon as the "chromocapillary effect" and they succeeded in "drawing" several patterns by moving the Petri dish containing the solution (Figure 5b and 5c) with a maximal speed of approximately 400 µm.s^{-1}. Independently, Okano, Yamashita *et al.* described the expansion and the contraction of a liquid crystalline droplet of an azobenzene derivative on a water surface upon irradiation.[157]

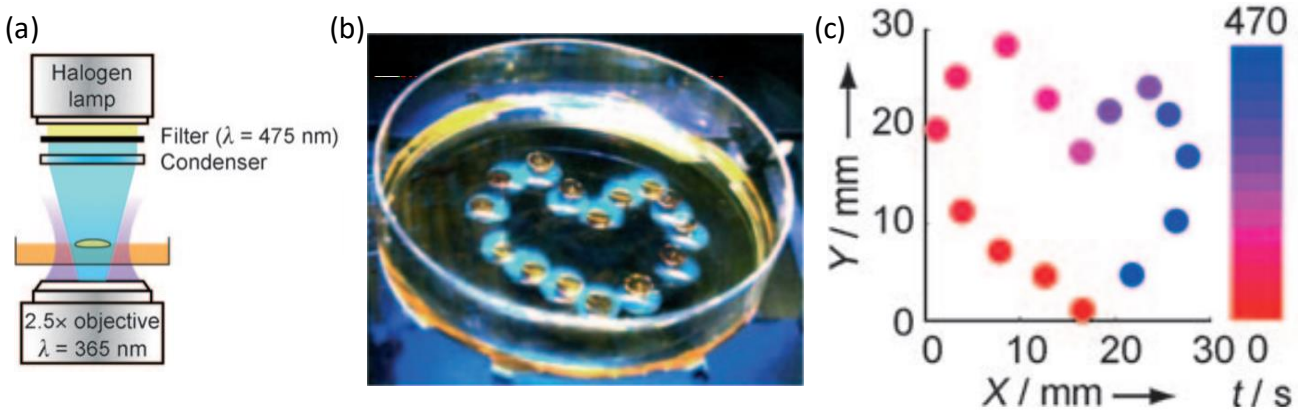

Figure 5: The "chromocapillary effect". (a) Experimental setup for the trapping of an oil droplet on the surface of an azosurfactant solution. (b) Example of the controlled motion of the droplet, with a drawing of a heart. The picture has been built by the overlap of snapshots from a video. (c) Corresponding positions of the droplet in the (x,y) plane as a function of time, represented here with the color going from red to blue. Adapted with permission from reference [156], Copyright 2009 John Wiley and Sons.

An interesting device where the liquid motion is no longer caused by a surface energy gradient, but instead driven by osmotic pressure, has been designed by Masiero *et al.*[158] They described a system based on an azobenzene derivative capable of supramolecular aggregation in its *trans* form by intermolecular H-bonds (Figure 6a). When dissolved in acetone, the *trans* isomers exist as oligomers of H-bonded molecules that can further grow to lead to insoluble aggregates; conversely, the *cis* isomer forms only intramolecular H-bonds and is soluble. The two compartments of an osmotic cell were filled with this solution (Figure 6b, (i)).

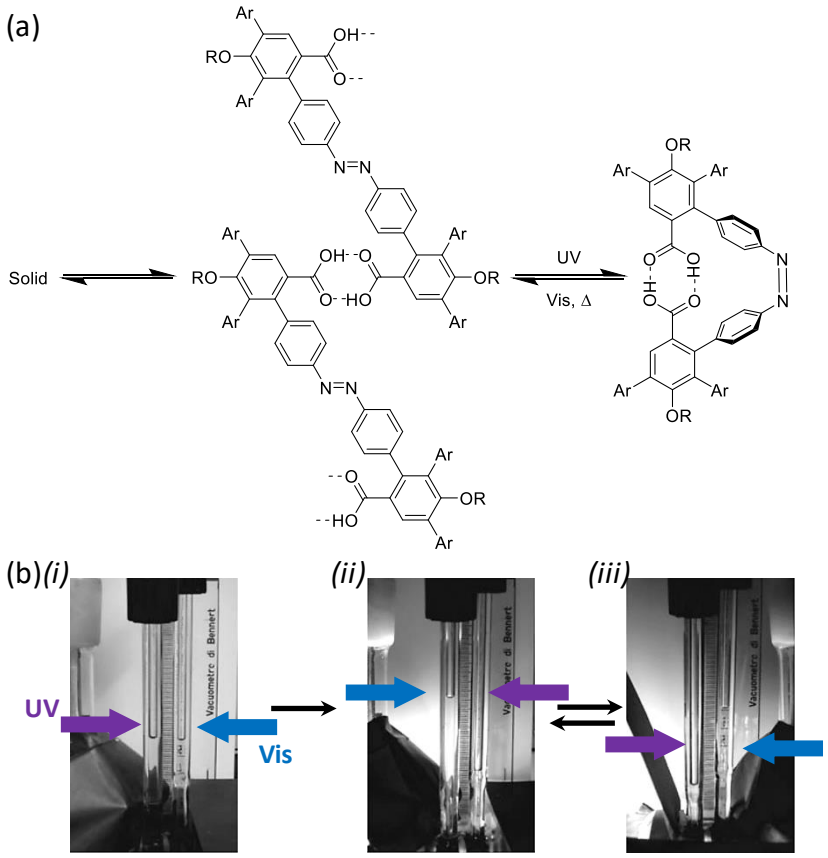

Figure 6: Liquid photoactuation driven by osmotic pressure. (a) Chemical structure of the azobenzene derivative and equilibrium between the *cis* isomer, with intramolecular H-bonding, and the *trans* isomer forming a supramolecular aggregate. (b) Snapshots of the osmotic cell containing the photoactive solution: *(i)* at the initial state, *(ii)* after irradiation of the left compartment with UV light (λ = 365 nm) (*trans* → *cis*) and the right compartment with visible light (λ = 436 nm) (*cis* → *trans*), causing the level

to rise in the left compartment, and *(iii)* the opposite process. Part (b) is adapted with permission from reference [158], Copyright 2008 John Wiley and Sons.

The irradiation with UV light (λ = 365 nm) of the left compartment causes the *trans*→*cis* isomerization, and thus the disaggregation and dissolution of the azobenzene molecules which increase their effective concentration. The irradiation with visible light (λ = 435 nm) of the right compartment enforces *cis*→*trans* isomerization and decreases the effective concentration in photoswitch. Overall, the opposite photoisomerization processes on each side lead to an osmotic pressure-driven liquid motion from the right compartment to the left compartment (Figure 6b, *(ii)*). By reversing the UV and visible irradiations on each side, the opposite flow can occur (Figure 6b, *(iii)*).[158]

Finally, motion of a liquid marble has also been achieved. Liquid marbles consist of aqueous droplets coated by a hydrophobic powder, and the interest for these objects is raising in fields such as microfluidics,[159] mainly because they can move with very low friction forces and they do not leave liquid residues on their path. Baigl and coworkers deposited such a liquid marble – consisting of a water droplet coated with silica nanoparticles – on an azobenzene/surfactant solution (Figure 7a).[160] Upon irradiation with UV light (λ = 365 nm), they observed the motion of the object, either away or towards the beam, depending on the thickness of the underlying solution. Below a critical thickness H^{crit} (2 mm in their case), the Marangoni flow[161] caused by the formation of the *cis* isomer at the point irradiated by UV light deforms the surface, and the liquid marble then moves away from the light beam (Figure 7b, (i)). Above H^{crit}, however, the surface deformation becomes negligible. The motion of the liquid marble is then governed by the Marangoni flow at the interface, and the object moves towards the light beam (Figure 7b, *(ii)*).[160]

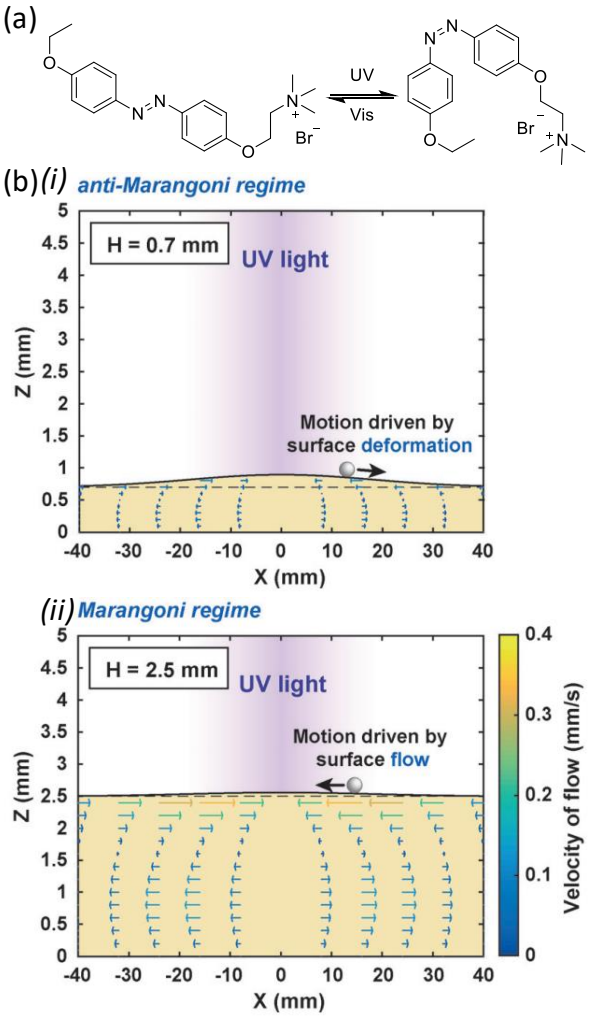

Figure 7: Photoactuation of a liquid marble on the surface of an azobenzene-based surfactant solution. (a) Chemical structure of the azobenzene derivative used as surfactant. (b) Proposed mechanism for the motion of the liquid marble at the surface. In both case, irradiation of the solution causes a Marangoni flow at the interface. Below a critical thickness H^{crit}, this flow deforms the surface and the liquid marble moves away from the light source *(i)*. Above H^{crit}, the surface deformation is negligible and the liquid marble moves in the same direction as the liquid flow, that is, towards the light beam *(ii)*. Part (b) is adapted with permission from reference [160], Copyright 2016 John Wiley and Sons.

2.2.2. Motion of solid objects on liquid surfaces

The motion of microscopic solids has been achieved on azobenzene doped polymer films[162] or azo-doped liquid crystalline (LC) films.[163–166] For instance, Kurihara and coworkers prepared a chiral azobenzene derivative by grafting a *L*- or *D*-menthol group to the photoswitch. They used it (along with another chiral mesogenic compound) to prepare a cholesteric LC phase (Figure 8a), whose pitch is determined by the helical twisting power (HTP) of the dopant.[166] They first demonstrated that the helical twisting power (HTP) of the chiral azobenzene changed upon UV or visible light irradiation (Table 2), with the *D*-isomer and *L*-isomer showing right- and left-handed helical structures, respectively.

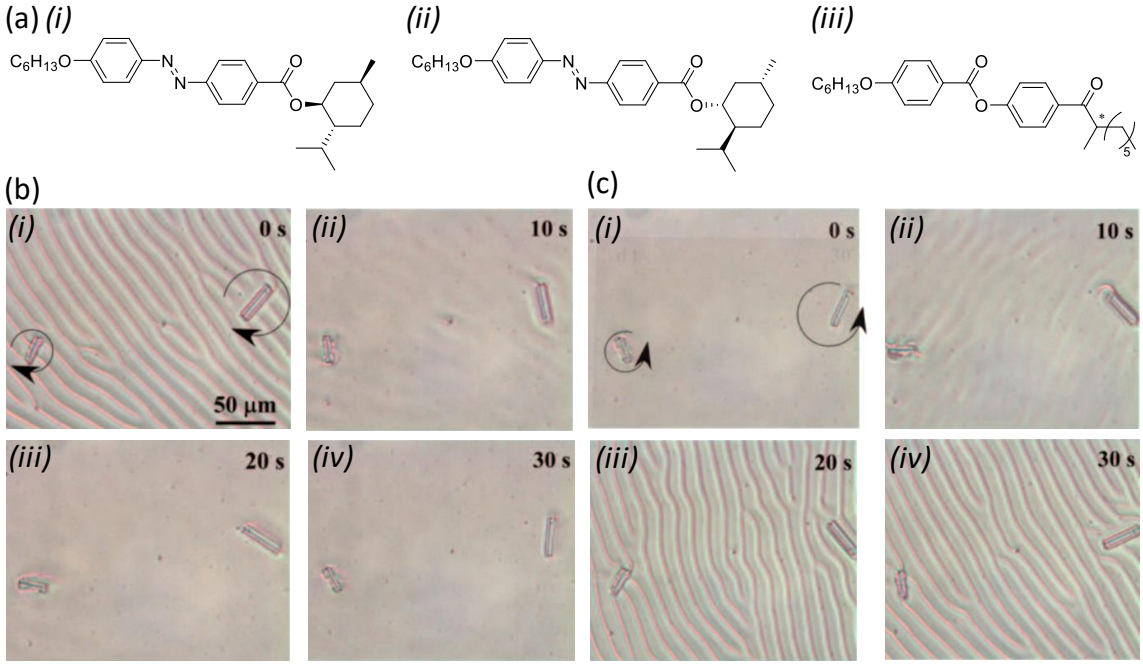

Figure 8: Pictures of the rotational motion of a glass microrod on a azodoped LC film observed by optical microscopy. (a) Chemical structure of mesogenic dopants: *(i)* is *D*-azomenth, *(ii)* is *L*-azomenth, and *(iii)* is a non-photochromic mesogenic chiral dopant, either *R*- or *S*-811. (b) Snapshots of the clockwise rotation of glass microrods on an *D*-azomenth-doped LC film upon irradiation with UV light (λ = 365 nm). (c) Reverse motion upon irradiation with visible light (λ = 436 nm). In both cases, note the

disappearance/appearance of the cholesteric texture as a function of irradiation time. Parts (b) and (c) are adapted with permission from reference [166], Copyright 2010 John Wiley and Sons.

Table 2: Helical Twisting Powers (HTP) of chiral azobenzene compounds in an E44 LC phase.[166]

	HTP ($\times 10^8$ $m^{-1}.mol^{-1}.g^{-1}$ E44)	
	Before UV (*trans*)	After UV (*cis*)
D-azomenthol	49.4	10.4
L-azomenthol	49	10.8

A rubbed polyimide substrate was then coated with the LC mixture and glass microrods were dispersed on the surface in an attempt to observe the same phenomenon that was reported earlier by Feringa and coworkers with molecular motors based on overcrowded alkenes (see section 4.3.3).[167] When illuminated with UV light (λ = 365 nm), the rods rotated clockwise or counterclockwise when doped with the *D*- or *L*-isomer, respectively; the opposite motion took place upon irradiation with visible light (λ = 436 nm) (Figure 8b and 8c). As expected, the cholesteric texture disappeared during UV irradiation, and reappeared when the isomerization to the *trans* form took place. The authors went one step further by preparing a compensated nematic LC phase, that is by mixing the *trans*-azomenthol derivative and the non-photochromic chiral compound (with an opposite twisting power) in such proportions that their HTP compensate, so that a nematic phase instead of a cholesteric phase is formed. In this case, upon irradiation with UV light, the HTP are not balanced anymore and the apparition of the cholesteric phase comes along with the rotation of the glass microrods. Finally, they succeeded to linearly move the microrods in by irradiating with blue light (λ = 488 nm) where both *trans* and *cis* isomers absorb, and with the glass pieces moving away from the irradiation area.[166]

It has also been demonstrated that the motion of microscopic solid objects can take place on the surface of an aqueous solution containing an azo-surfactant.[168,169] Varanakkottu, Hardt, and coworkers developed an optical system where the surface of the solution can be irradiated with several light beams, hence addressing several particles at the same time (Figure 9a).

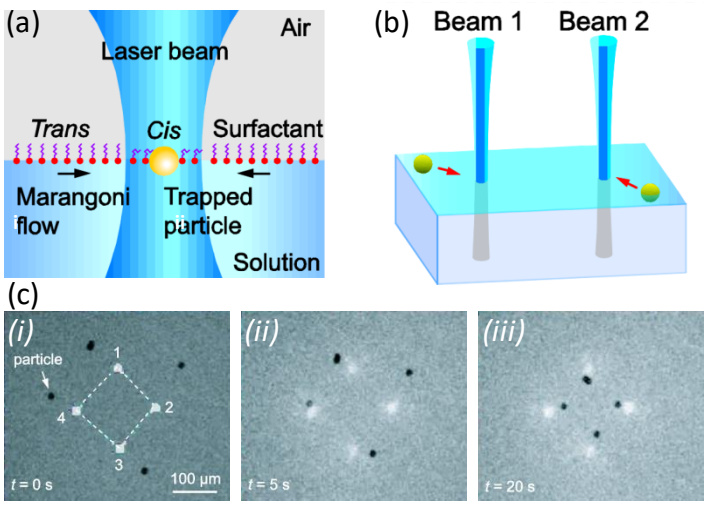

Figure 9: The "Light-Actuated Marangoni Flow" (LAMF). (a) Scheme of the Marangoni flow induced towards the irradiated spot of the surface, trapping a particle. (b) Scheme of the motion of microparticles towards the irradiated areas. (c) Snapshots of the motion of polystyrene microspheres (black dots) towards the irradiated spot with blue light (λ = 442 nm) (bright dots). Adapted with permission from reference [169], Copyright 2018 American Chemical Society.

The solution is prepared by dissolving an azo-surfactant at a concentration above its critical micellar concentration (CMC) so that the isomers fully occupy the air/water interface. Upon irradiation with blue light (λ = 442 nm) the *trans*→*cis* isomerization takes place on the spot, leading to an increase of the surface tension of approximately 10 $mN.m^{-1}$, and hence, a Marangoni flow[161] takes place from the low surface tension area towards the high surface tension area, that is towards the irradiated spot (Figure 9b). Polystyrene microspheres at the interface then move towards the laser beam (Figure 9c).

In another type of approach, Norikane *et al.*[170] prepared a photoswitchable crystal of *trans*-4-methoxyazobenzene (Figure 10a) that was placed at the water surface, and they observed a motion of the material away from the UV light beam (λ = 365 nm) (Figure 10b). Supported by the observation that the crystal and the solution change color upon irradiation, they proposed that during *trans*→*cis* isomerization the more polar *cis* isomer dissolves in water, thereby creating a self-propelling motion caused by the local change in surface energy. Based on the same principle, a filter paper was soaked in a *trans* isomer solution to prepare a photoactive "boat", and the same dissolution-induced motion was observed upon UV irradiation.[170]

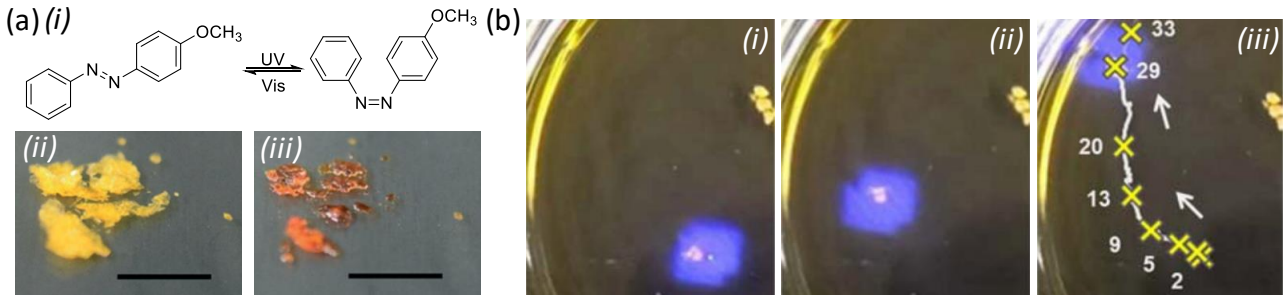

Figure 10: Motion of an azobenzene crystal on a water surface. (a) *(i)* Chemical structure of 4-methoxyazobenzene, and snapshots of the corresponding compounds before *(ii)* and after *(iii)* UV irradiation (λ = 365 nm). The scale bars are 5 mm. (b) Motion of the crystal upon UV irradiation (λ = 365 nm), caused by the dissolution of the *cis* isomer (*i, ii*) and the resulting trajectory of the solid *(iii)*, where the numbers correspond to the distance from the initial position (mm) and crossbars indicate the position at every second. Adapted with permission from reference [170], Copyright 2016 The Royal Society of Chemistry.

2.2.3. Motion of colloidal particles and micromotors

The controlled and autonomous motion of colloidal particles and micromotors has been widely studied and reviewed,[171–174] with the development of drug delivery systems for biomedical applications,[175] and

pollutants capture devices for environmental treatment.[176] In the case of photoactive systems, the photochromic molecules can be dissolved either in the solution,[177–179] in the colloidal droplet,[180] or used as a surfactant at the interface.[181] The motion of nanoparticles can also be controlled when functionalized with photoswitches,[182] and there are several examples where the motion is achieved in a liquid crystalline phase.[183–185]

Liu and coworkers designed a hyperbranched polymer containing spiropyran moieties that aggregate in water to form colloidal microparticles (Figure 11a).[186] When suspended in a H_2O/DMSO mixture, the microspheres move straight towards the center of the spot irradiated with UV light (λ = 365 nm) (Figure 11b), and the authors observed that, at the end of the horizontal motion, the particles moved vertically in the direction of the light source. They explained the motion by a surface tension gradient built by the illumination gradient (causing the opening of the spiropyran molecule to its merocyanine form), itself caused by the optical properties of the microparticles.[186]

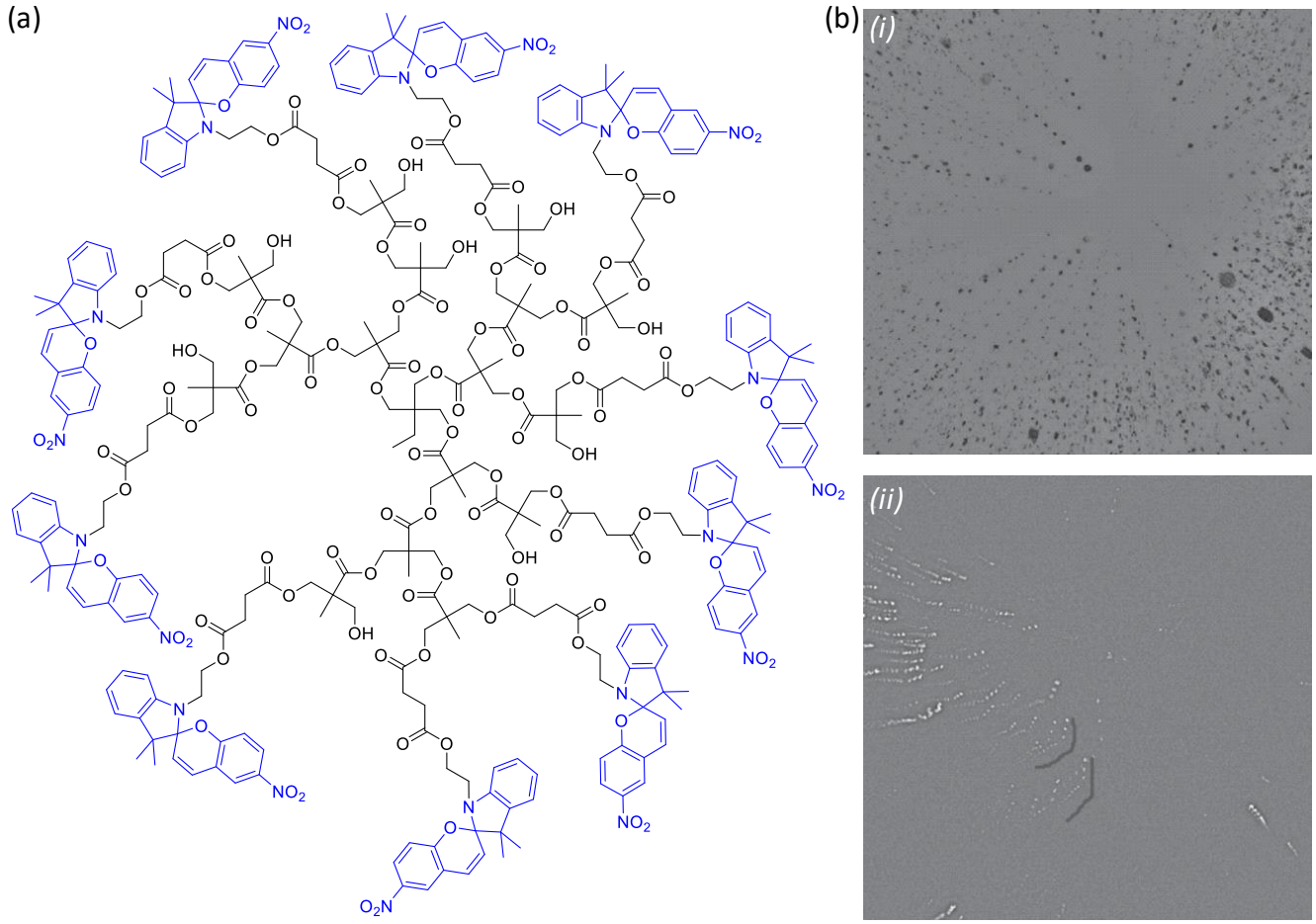

Figure 11: Motion of colloidal particles driven by UV light. (a) Structure of the hyperbranched polymer used in reference [186] to form the microparticles; the spiropyran moieties are colored in blue. (b) (i) Motion of the microparticles towards the center of the UV irradiation (λ = 365 nm), and (ii) disturbance of the motion by a vortex. The images were made by superimposing 20 consecutive snapshots of the video (interval of 1 s) captured by fluorescence microscopy. The particles have an average diameter of approximately 2 μm. Part (b) is adapted with permission from reference [186], Copyright 2016 John Wiley and Sons.

Another example of a spiropyran-based system has been published by Benito-Lopez, Diamond, and coworkers.[178] By mixing a chromoionophore (CI) with 2-hexyldecanoic acid (DA), an acid-base equilibrium takes place, and their charged forms (Figure 12a) can act as surfactants for the formation of

dichloromethane microdroplets in an aqueous solution. This solution contains a merocyanine-sulfonic acid derivative in an acid-base equilibrium, reaching a pH around 5 (Figure 12b). Upon irradiation with white light, the photochromic molecule isomerizes back to its spiropyran form, liberating protons and reaching a pH close to 3.4. At this pH, 2-hexyldecanoate gets protonated, and therefore breaks its assembly with the charged chromoionophore (CI-H$^+$), which is released in solution. This chemical process results in a local decrease of the surface tension with the droplet moving away from the white light (Figure 12c).

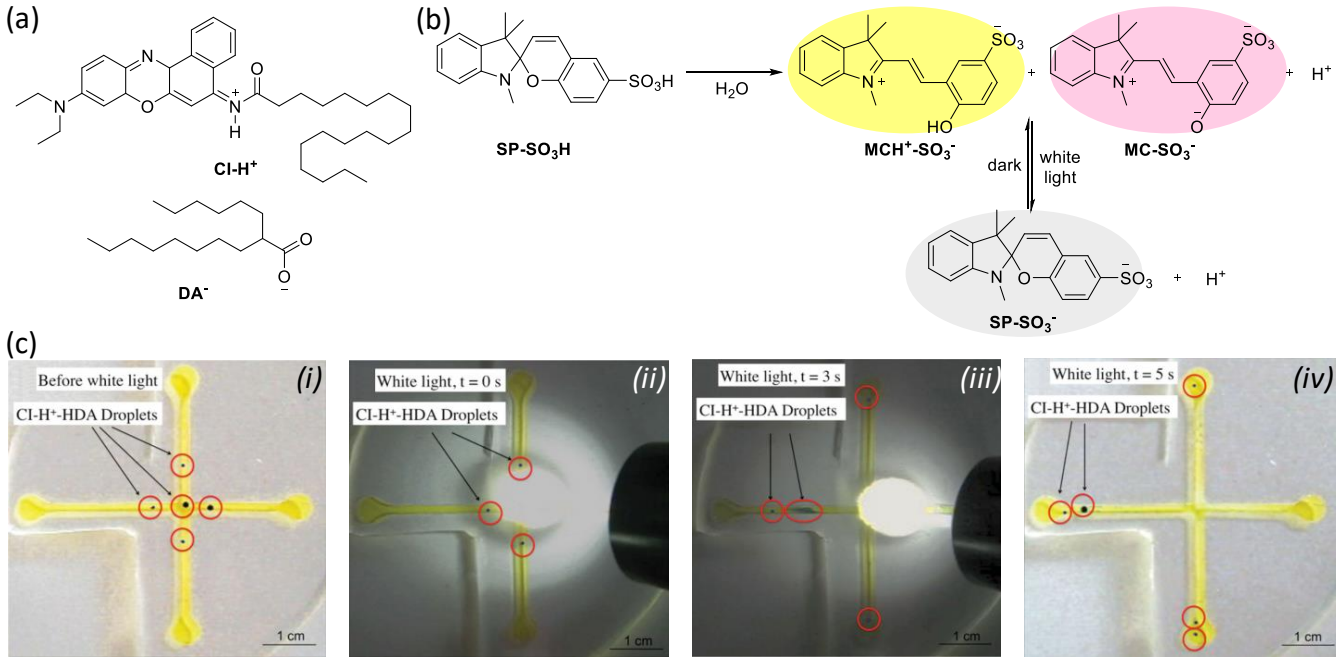

Figure 12: Motion of colloidal particles driven by the acido-basic equilibrium of a spiropyran-sulfonic acid. (a) Chemical structure of the protonated chromoionophore (CI-H$^+$) and 2-hexyldecanoate (DA$^-$) used as surfactants to form the dichloromethane microdroplets in water. (b) When dissolved in water, SP-SO$_3$H opens to its merocyanine form and an acid-base equilibrium takes place in the solution between MCH$^+$-SO$_3^-$ (yellow, λ_{max} = 408 nm) and MC-SO$_3^-$ (red, λ_{max} = 508 nm), reaching pH ≈ 5. Upon irradiation with white light, the merocyanine form closes back to a colorless spiropyran form SP-SO$_3^-$, generating even more protons (pH ≈ 3.4). (c) Motion of DCM droplets (circled in red) upon irradiation with white light. Part (c) is adapted with permission from reference [178], Copyright 2014 John Wiley and Sons.

Smalyukh *et al.* recently reported the out-of-equilibrium rotational motion of silica microplatelets coated with azobenzene monolayers when immersed in a nematic liquid-crystalline phase and irradiated with linearly polarized blue light.[187] As it will be explained in more details in Section 2.4.1, azobenzene molecules tend to orient parallel to the polarization direction of the incoming light beam. Also, due to surface anchoring conditions, the orientation of the photochromic moieties imparts directly the orientation of the liquid crystalline phase close to the surface of the microplatelet, which in turn rotates locally the light polarization direction and, hence, reorients the azobenzene monolayer again (Figure 13). This feedback mechanism coupled with the torque associated with the LC phase deformation drives the continuous rotational motion of the silica microplatelets in suspension.

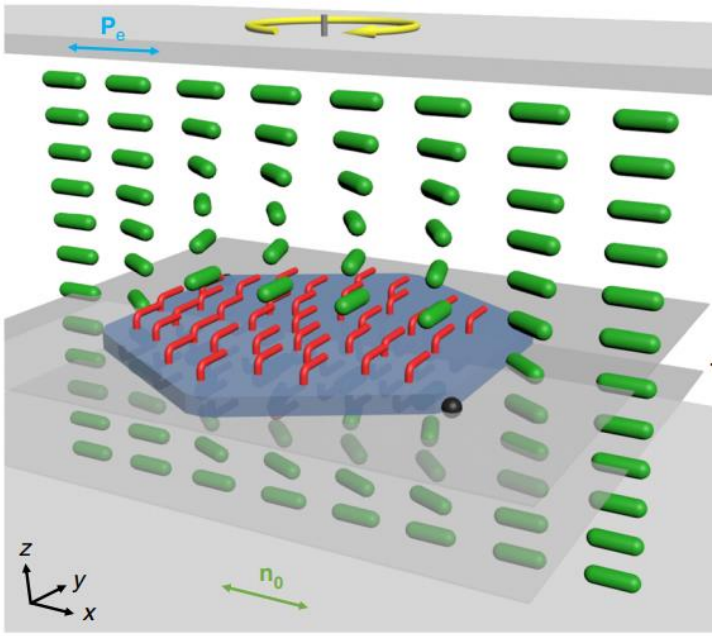

Figure 13: Schematic representation of the mechanism of rotation of silica microplatelets coated with azobenzene moieties. Pe represents the direction of polarization of the beam. n0 represents the main director of the LC phase. The mesogens are represented by green rods and the azobenzene moieties by red rods. The yellow arrow represents the rotational motion of the silica platelet in blue. Upon irradiation, the azobenzene molecules orient perpendicularly to the polarization direction of the light, inducing a

reorientation of the LC phase near the surface, which in turn locally deviates the polarization direction of the light beam. This feedback mechanism induces the continuous rotation of the platelet. Reproduced with permission from reference [187], Copyright 2018 Springer Nature.

Although all the above examples demonstrate remote control of the actuation of liquids and solid microobjects, their functioning principles do not allow to alter the shape of solid materials. In the upcoming section, we will discuss examples of photomechanical deformations, starting with bidimensional materials.

2.3. Photomechanical deformation of mono- and bilayers

Early examples of mechanical effects in bidimensional photoactive materials were observed by surface pressure-area isotherms of Langmuir-Blodgett films or by nanometric expansion of these films transferred onto a mica surface.[188] In this section, we will focus on such systems where mechanical deformation of micro- or macroscopic objects has been observed.

Concerning planar materials, the first direct observation of photomechanical deformation of a bidimensional film was done by Brewster Angle Microscopy (BAM).[189–191] Seki, Ichimura, and coworkers designed an experimental setup to allow simultaneous irradiation with UV light and observation through the BAM objective (Figure 14a). After 700 s of illumination, the monolayer of an azopolymer formed at the air-water interface spread to approximately three times its initial area.

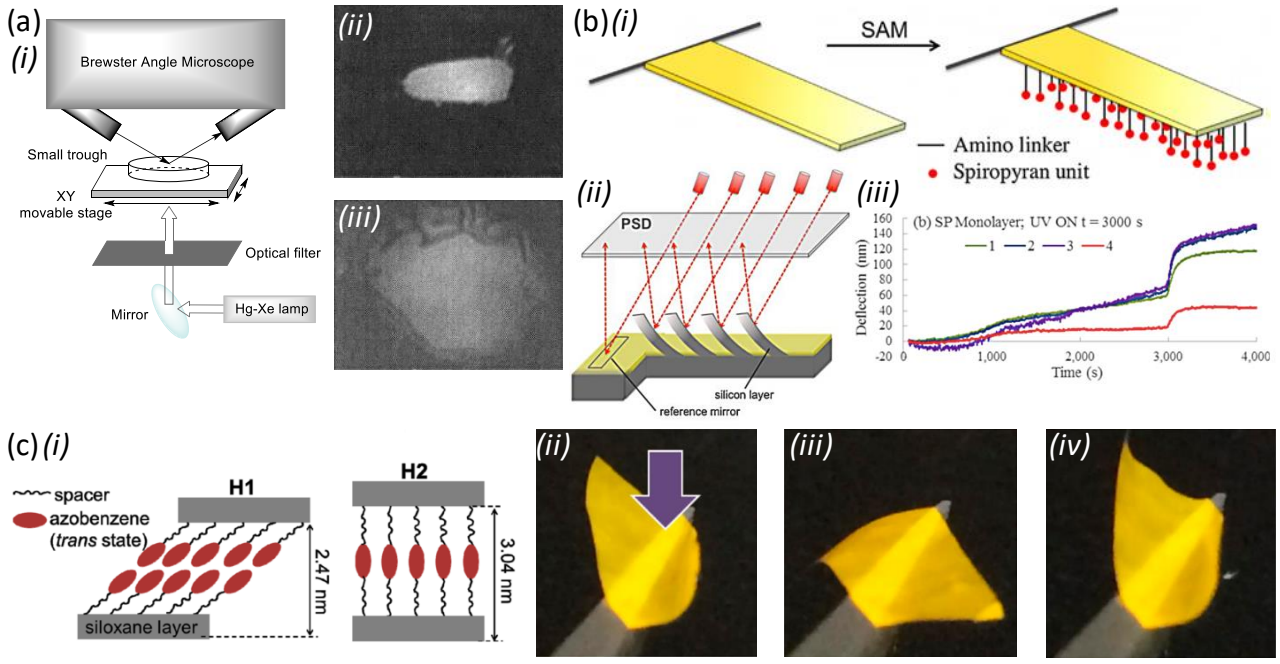

Figure 14: Photomechanical effects in planar bidimensional assemblies. (a) (*i*) Scheme of the experimental setup used in reference [191] to observe the mechanical deformation of a azobenzene-containing Langmuir film. Microscopy images of the Langmuir film (*ii*) before and (*iii*) after 500 s of UV irradiation (λ = 365 nm). The diameter of the microscope field was 0.6 mm. (b) (*i*) Spiropyran-functionalized cantilever prepared *via* a self-assembled monolayer to measure the stress generated by the isomerization. (*ii*) Experimental setup used for the detection of the deflection (PSD = single position sensitive optical detector), (*iii*) Evolution of the deflection (nm) of the four functionalized cantilevers under UV irradiation (λ = 365 nm). (c) (*i*) Schematic representation of the structure of a sandwiched bilayer (H1) or monolayer (H2) of azobenzene derivatives between two polysiloxanes networks, depending on if the photochrome bears two or one spacer, respectively. When a mixture of the two azobenzene derivatives is prepared, a free-standing film is obtained, which bends upon irradiation (λ = 365 nm). (*ii*) Initial state, (*iii*) after irradiation from the top side and (*iv*) recovery of the initial shape. The sample dimension is approximately 4 mm × 20 mm × 10 µm. Part (a), (b) and (c) are adapted with

permission from references [191] Copyright 1998 American Chemical Society, [192] Copyright 2016 Elsevier, and [193] Copyright 2015 American Chemical Society, respectively.

The photomechanical deformation of monolayers has also been shown by functionalizing microcantilevers and measuring their deflection upon irradiation.[192,194] For instance, Florea, Raiteri, and coworkers[192] functionalized an array of cantilevers with a self-assembled monolayer of silylated amines, followed by the reaction with a spiropyran derivative, so that one side of the cantilever is covered by photochromic molecules (Figure 14b, (*i*)). They measured the deflection of the cantilever upon UV irradiation (λ = 365 nm) *via* the reflection of a laser beam on the material (Figure 14b, *(ii)* and *(iii)*), and they calculated the corresponding force for such motion. They found that the stress generated by an 8 nm thick monolayer of spiropyran was equal to 446 $N.m^{-1}$.

In another example, Shimojima and coworkers reported a composite composed of an azobenzene mono- or bilayer sandwiched between two polysiloxane networks (Figure 14c, *(i)*).[193] When a mixture of these two azobenzene derivatives (bearing either one or two spacer groups) is prepared, a free-standing film is obtained and it can bend upon irradiation (λ = 365 nm) (Figure 14c, *(ii)-(iv)*). Other lamellar composites had already been reported with clay,[195,196] but no free-standing films were obtained and the amplitude of motion was several scales lower.

Micrometric vesicles may also be formed with bilayers. One of the main applications of photosensitive vesicles is their controlled assembly/disassembly for drug delivery applications.[197] Since it resembles a phase transition, however, we will focus here only on their mechanical deformation, and that is when the object is not destroyed. Along the same line, and in order to stay in the scope of this chapter, we will not discuss the deformation of nanometric objects such as found in many interesting papers of the literature.[198,199] There are, however, few examples where the distortion of vesicles has been observed due to the isomerization of photochromic molecules.[200–202] A common example of photoinduced deformation

is the shrinking/swelling behavior of these objects upon irradiation.[203–208] For instance, Zhang and coworkers synthesized a block copolymer comprising poly(N-isopropylacrylamide) (pNIPAAm) and poly(6-[4-(4-pyridyazo)phenoxy] hexylmethacrylate) (pAzPy) that self-assembled into vesicles in a THF/water mixture (Figure 15a).[206]

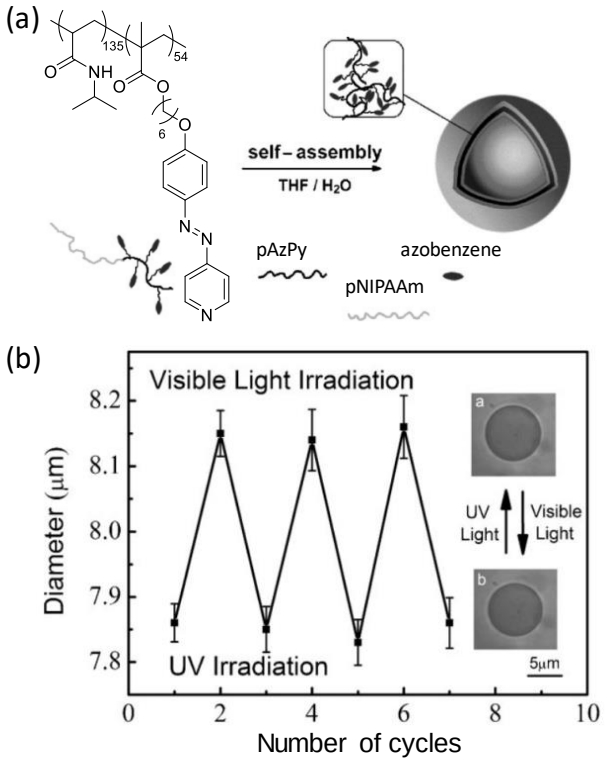

Figure 15: Swelling/shrinking behaviour in vesicles. (a) Self-assembly of poly-(N-isopropylacrylamide)-*block*-(6-[4-(4-pyridyazo)phenoxy] hexylmethacrylate) (pNIPAAm-*b*-PAzPy) in a THF/water mixture. (b) Evolution of the diameter of the vesicle upon alternative UV (λ = 365 nm) and visible (λ = 436 nm) light irradiation. The insets are images obtained by optical microscopy. Parts (b) and (c) are adapted with permission from reference [206], Copyright 2008 John Wiley and Sons.

Upon alternative irradiation with UV (λ = 365 nm) and visible light (λ = 436 nm), the diameter changed from approximately 7.85 μm to approximately 8.15 μm, respectively, corresponding to a volume change of 17 % (Figure 15b). Interestingly, this change in size of the 3D object results from the 2D motion of the

bilayer. However, the examples of photomechanical deformation of bidimensional materials are still relatively scarce. Indeed, the focus of the research on the deformation of photoactive objects has been, up to now, mainly towards the tridimensional materials. These systems are addressed in the following sections, starting with the examples where light has been used to manipulate the surface topology of the materials.

2.4. Photomechanical deformation of the surface topology in tridimensional materials

2.4.1. Surface relief grafting

The first examples of surface relief grating (SRG) were independently reported in 1995 by Rochon, Batalla, and Natansohn on the one hand,[209] and by Tripathy and coworkers on the other hand,[210,211] during their investigation for the holographic inscription in azomaterials. Since then, numerous papers have been published in order to enhance the SRG inscription, to understand their mechanism of formation, and to find innovative applications of these patterned materials. We do not aim here to detail every aspect of the SRG principles and other reviews deal more precisely with this field of research.[212–214] We wish, however, to provide a comprehensive overview of what has been done, and we will focus on original applications explored with these objects. One fundamental principle to understand the formation of SRG is the photoalignment process of azobenzene derivatives. Upon irradiation with polarized light of an appropriate wavelength, only molecules having a component of their dipole moment parallel to the polarization direction of the light undergo isomerization. This process slightly reorients the molecule and, for those aligning in the perpendicular direction of the incoming beam, the photoswitch will not isomerize (and reorient) anymore. Consequently, over time, the material will enrich in azobenzene derivatives aligned perpendicularly to the polarization of the incoming light beam (Figure 16a). The resulting material therefore present a higher birefringence, a property of interest to implement azopolymers in the field of optical data storage.[215]

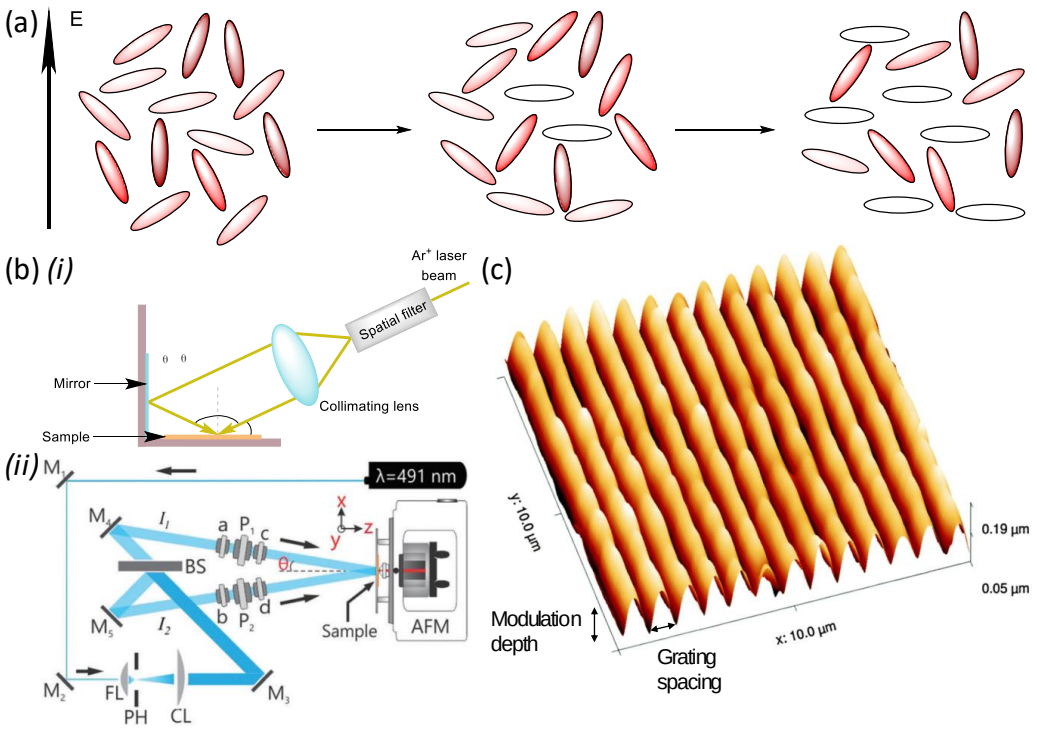

Figure 16: (a) Mechanism for the alignment process of azobenzene molecules in a polarized light field. The arrow on the left represents the direction of polarization. Only the azobenzene molecules having a component of their dipole moment parallel to the field can isomerize. The likelihood of isomerization is represented by the color: the darkest color (brown) represents molecules that have a high probability to isomerize, while the lightest color (white) represents the molecules that cannot isomerize, and, hence, will not change their orientation anymore. This process, over time, enriches the material in azobenzene molecules oriented perpendicularly to the light polarization (from left to right). (b) Examples of experimental setups for the inscription of SRG with interfering light beams, with an incident angle θ. *(i)* Lloyd's mirror. *(ii)* Experimental setup for simultaneous irradiation and AFM measurement. FL: focusing lens; PH: pinhole; CL: collimating lens; a and b: half wave plates; c and d: either half wave or quarter wave plates and/or their combinations. P1 and P2: polarizers; AFM: atomic force microscope; S: computer controlled beam shutter; M1 to M5: mirrors; BS: 50/50 beam splitter; I1 and I2: intensity of the beams. (c) Example of SRG measured by AFM. Parts (b) *(i)* and *(ii)* are adapted with permission from reference

[211] Copyright 1998 American Chemical Society, and reference [216] Copyright 2016 The Royal Society of Chemistry, respectively. Part (c) is adapted with permission from reference [217], Copyright 2015 Centre National de la Recherche Scientifique (CNRS) and The Royal Society of Chemistry.

Different experimental setups have been designed for the effective inscription of the gratings (Figure 16b). Upon irradiation with an interfering light beam, crests and troughs are formed at the material surface, forming a tridimensional periodic structure. Typically, SRG have a period in the range of micrometers, and a modulation depth of a few hundreds of nanometers, meaning that the motion takes place at a scale several orders of magnitude higher than that of the photochromic molecule alone (Figure 16c). The grating spacing Λ_g can be modulated by tuning the incident angle θ of the interfering beams at a wavelength λ, following the equation:[211]

$$\Lambda_g = \frac{\lambda}{2}\sin\theta \quad (1)$$

Even if SRG are widely explored in the literature, the mechanism of their formation is still under debate.[216,218–276] Briefly, two main ideas are usually opposed: *i*) the photofluidization concept, and *ii*) the alignment effect. For the former, it is suggested that the continuous *trans→cis* and *cis→trans* isomerization processes soften the polymer matrix around the photochromic molecules, like a thermal fluidization. Because the material is not homogeneously irradiated due to the interference pattern, the interaction between "fluidized" areas and non-illuminated areas results in the formation of gratings. Differently, the alignment effect suggests that, during the orientation of the photochromic molecules under polarized illumination, a stress occurs between the non-irradiated areas and the irradiated areas, with a resulting force important enough to cause the deformation of the material. A recent paper by Hurduc (for the photofluidization effect) and Santer (for the optomechanical stress effect)[216] details experiments favoring one effect over the other, and presenting common conclusions. Both agreed that the necessary condition to observe SRG is to have an optomechanical stress in the material, but the resulting motion can

then be seen either as a flow or as a mechanical deformation. Interestingly, Santer and coworkers reported the formation of cracks on a metallic layer coated on an azopolymer during the inscription of SRG, indeed supporting a mechanism with a built-up stress in the material.[277] More recent studies proposed a mechanism based on the Marangoni flow,[278] or on an optical tweezing effect.[218] To complement the studies about the mechanism, several papers have focused on the formation and relaxation kinetics of SRG.[279,280]

Regardless of its mechanism of action, the inscription of SRG needs an interference pattern, either in intensity (IIP) or in polarity (PIP), and some comparative studies between both methods have been conducted.[281–283] Numerous studies have been conducted to tune irradiation patterns and the most usual ones are summarized in Table 3.

Table 3: Usual interference patterns used for the inscription of SRG. RCP and LCP stand for right-handed and left-handed circularly polarized light, respectively.

	Polarization of the interfering beams	Spatial distribution of the interference				
		+ λ/2	+ λ/4	0	- λ/4	- λ/2
Intensity Interference Pattern (IIP)	s- ; s-					
	p- ; p-					
	-45° ; -45°					
	RCP ; RCP					

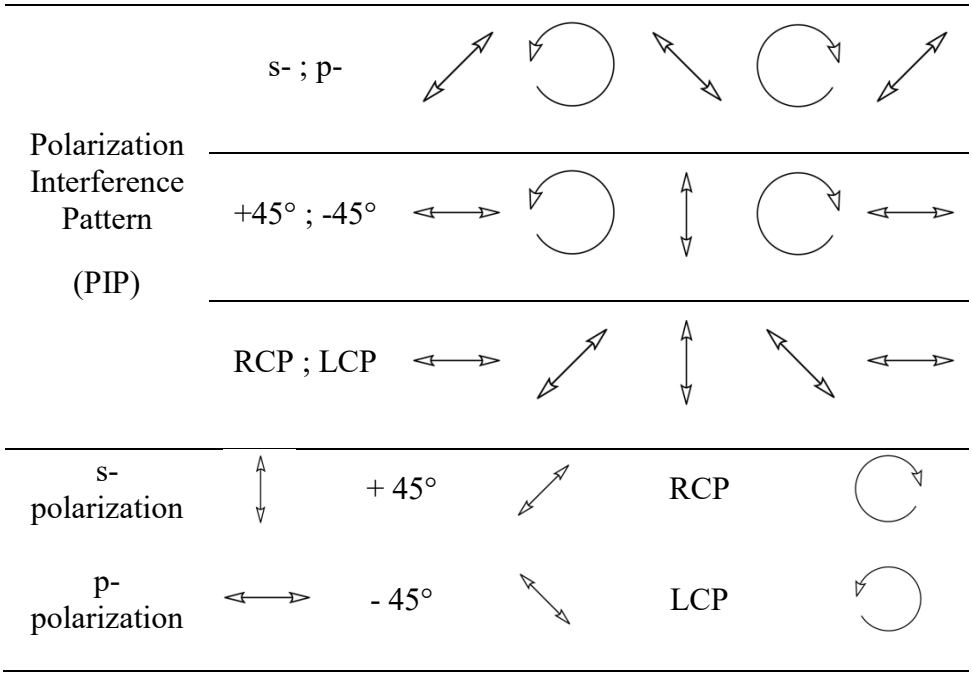

It is possible to inscribe SRG by using interfering beams at different wavelengths,[284–288] by adding "assisting beams" to increase the isomerization rate,[289,290] by using more than two interfering beams,[291] and even when incoherent light is used.[292,293] Some examples used pulsed irradiation.[294–301] The interference can also be achieved when light is irradiated through a photomask.[302–306] Half-grating spacing has also been achieved by Miniewicz and coworkers[307] when they used an s-/p- interference pattern that they attributed to the interference between the zeroth- and first-order scattered beams. Interestingly, elliptic interference patterns can be used to fabricate asymmetric SRG.[308–312] For instance, Kawatsuki *et al.*[310] experimented a variety of polarization interference patterns, and they observed the formation of blazed SRG when two orthogonal elliptically polarized light beams where used (Figure 17a).

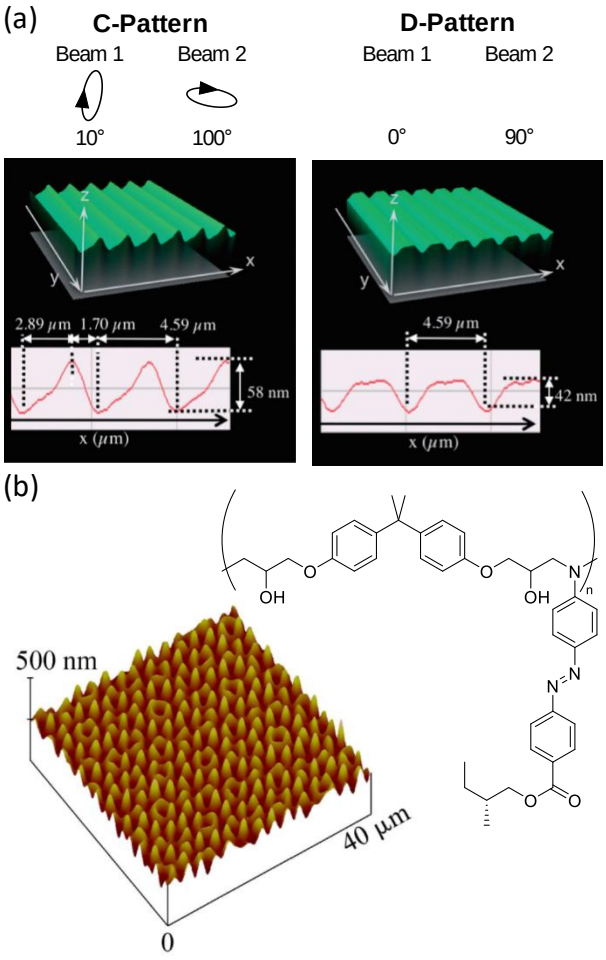

Figure 17: (a) Formation of asymmetric SRG by irradiation with elliptic light beams (λ = 325 nm). The top part shows the polarization of the interfering beams, with below the corresponding height profiles of the SRG. (b) Chemical structure of the epoxy azopolymer used to form 10-fold quasi-crystal SRG by successive inscription/rotation of the sample, as observed by AFM. Parts (a) and (b) are adapted with permission from reference [310] and reference [313], Copyright 2015 Optical Society of America, respectively.

Nunzi and coworkers generated SRG with a single beam *via* a water droplet, suggesting that the interference pattern is created with the different refraction and reflection angles generated at the air/water interface.[314] Peretti and coworkers alternatively switched the polarization interference pattern (between s- and p-polarization) during an AFM measurement of SRG growth, and observed that the migration is

directional for their system, that is, either away or towards the irradiated area for p-interference and s-interference, respectively.[315] Gritsai, Stumpe, and coworkers designed a system where several layers inscribed with SRG can be superimposed, with a passive layer in between, in order to obtain a tridimensional material that could be of use in the domain of photonics.[316] Lee, Park and coworkers investigated the "field gradient effect",[317] i.e. the fact that the deformation cannot take place after a certain depth of material due to its inherent absorption.

Multidimensional gratings can be obtained by rotating the sample holder after successive unidimensional SRG inscription. For instance, Wang and coworkers investigated this phenomenon to create quasi-crystal structures on a surface.[313,318] These structures have a rotational symmetry and aperiodic long-range order, and they are useful for photonic applications for instance.[313] Their latest example considers the SRG on an epoxy polymer with an azobenzene derivative (Figure 17b). 2n-fold quasi-crystal SRG are fabricated with an LCP/RCP interference pattern, followed by a rotation of π/n, these two steps being repeated n times; the authors succeeded in preparing a quasi-crystal structure from 6- to 72-fold symmetry with this procedure (Figure 17b).

The erasure of SRG most commonly takes place when the sample is either heated above its glass transition temperature (T_g) or under the illumination of a homogeneous circularly polarized light beam. Several studies have been devoted to the improvement of the erasing procedure efficiency.[319–321] Recently, Lee, Cho, and coworkers reported that after the erasure of a damaged SRG with circularly polarized light, and reinscription of the initial gratings with an interfering light beam, the triboelectric nanogenerator prepared could recover its initial efficiency.[322] In addition, hierarchical secondary gratings can be obtained by using an adequate polarization interference pattern,[311,323] using masks[324,325] or by the creeping of previously formed domes induced during the SRG formation.[326] Lee, Cho, and coworkers reported the fabrication of a bioinspired hierarchical surface by inscribing SRG on a prepatterned wavy surface.[327]

Importantly, we stated earlier the relation between the grating spacing and the wavelength of the light used for the inscription (Eq. 1), so as the spatial periodicity is inherently limited by the diffraction limit. Nevertheless some studies demonstrated that it is possible to prepare smaller gratings by using plasmonic waves[328–332] or evanescent waves.[333,334]

Having highlighted that SRG can come in almost all shapes and sizes, we continue hereafter by making a list of the wide variety of polymeric backbones that have been used over the years to create them. The most used polymers are based on polyacrylates,[279,335–367] especially the commercially available poly(Disperse Red 1 methacrylate) (pDR1m) (Figure 18a). pDR1m has the advantage of bearing a push-pull azobenzene derivative, with absorption spectra partially overlapped for the *trans* and *cis* isomers. Hence, when irradiated with an appropriate wavelength, continuous *trans→cis* and *cis→trans* isomerization events take place, improving the inscription of SRG. Polyimides have often been used for the inscription of SRG as well.[294,295,297,368–385] These polymers are already common in optical applications, for instance for the alignment of liquid crystalline materials. Sava *et al*. synthesized a variety of azopolyimide derivatives to study their applicability as photoactive materials (Figure 18b).[373] Some reported examples, notably by Santer and coworkers, use poly(1-[4–(3-carboxy-4-hydroxyphenylazo)benzenesulfonamido]-1,2-ethanediyl, sodium salt) (PAZO) (Figure 18c)[386–389] to determine its ability to form SRG as compared with a molecular glass containing azobenzene derivatives.[389] Epoxy polymers have also been reported for the inscription of SRG,[390–400] and we have already discussed the example showing the formation of quasi-crystal structures (Figure 17b).[313] It is also possible to find examples with conjugated azopolymers, such as polydiacetylenes,[401] polyfluorene,[402] or polycarbazole (Figure 18d-f).[403] Zettsu *et al.* doped an azopolyacrylate film with poly(3-dodecylthiophene).[404] Azopolyurethanes were used for the inscription of SRG as well;[346,351,405–413] for instance, Rochon and coworkers synthesized a polyurethane where the azobenzene derivative was in the hard segment (Figure 18g).[409] A few examples are available with poly(aryl ether):[414–420] Kim and

coworkers prepared one with a perfluorocyclobutane moiety, because these materials are stable towards temperature and mechanical forces, transparent, and easily synthesized and processed (Figure 18h).[420]

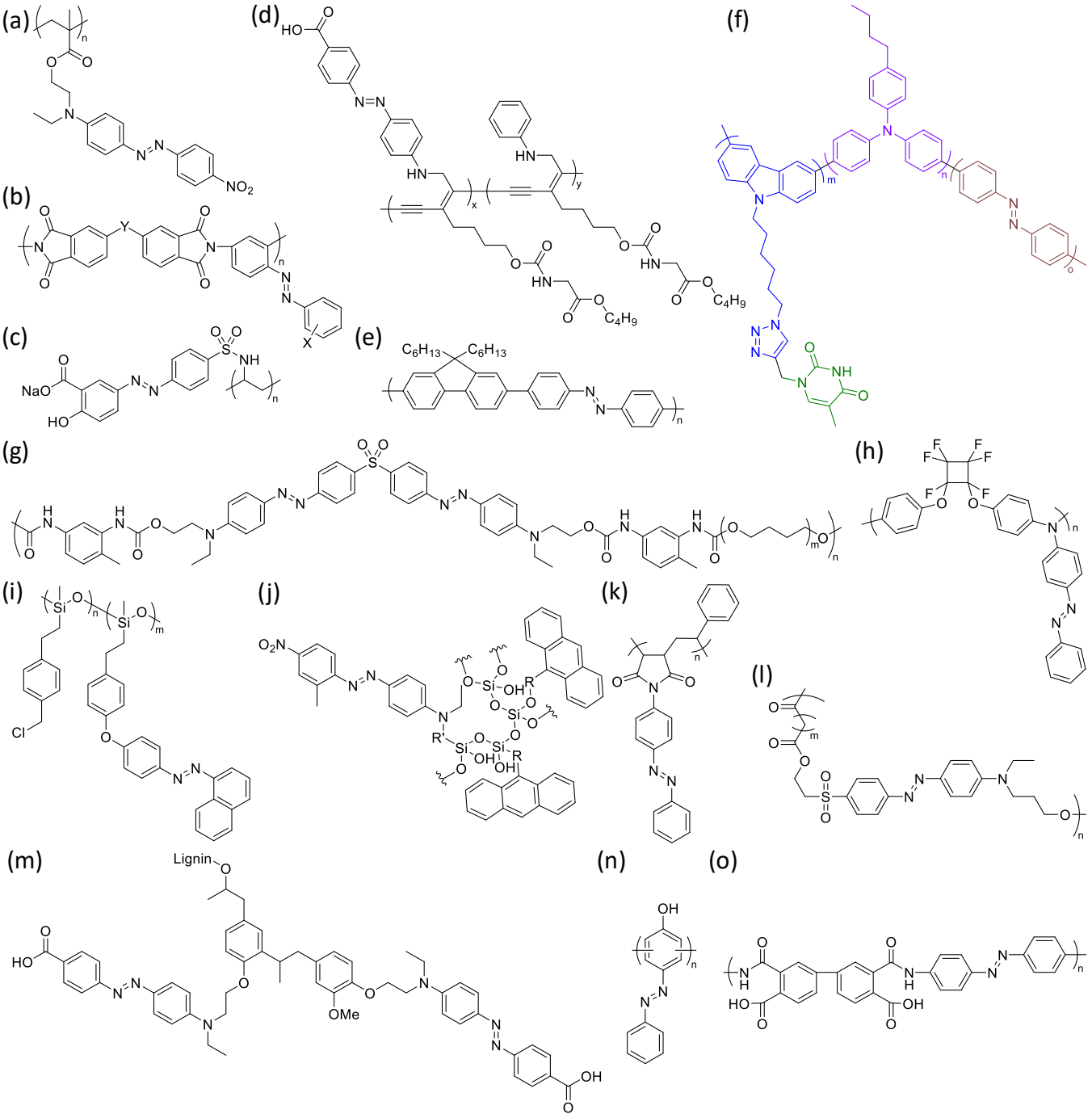

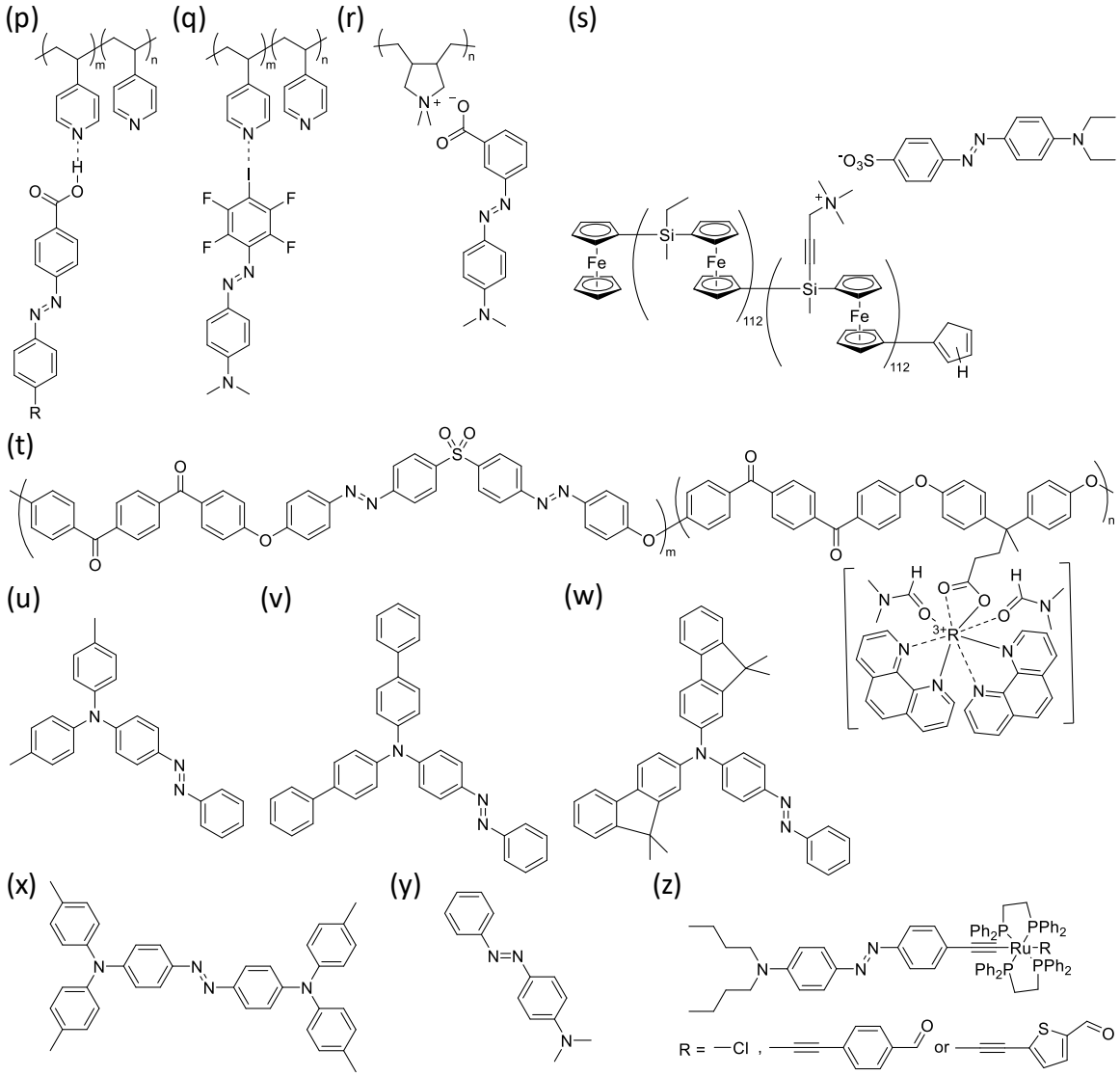

Figure 18: Chemical structures of systems used for the formation of SRG. (a) poly(Disperse 1 methacrylate) (pDR1m). (b) Azopolyimides with X = *o*-Me, *p*-Cl or *p*-Me, and Y = CO or C(CF_3).[373] (c) poly(1-[4–(3-carboxy-4-hydroxyphenylazo)benzenesulfonamido]-1,2-ethanediyl sodiumsalt) (PAZO).[389] (d) Polyacetylene.[401] (e) Poly(fluorene-azobenzene).[402] (f) Copolymer of carbazole (blue), triarylamine (purple) and azobenzene (brown) with a thymine moiety (green).[403] (g) Polyurethane.[409] (h) Azopoly(aryl ether) with a perfluorocyclobutane moiety.[420] (i) Azopolysiloxanes.[296] (j) Representative example of the structure of the sol-gel hybrid material with anthracene and an azobenzene derivative, R = -$(CH_2)_3$-NHCOO-CH_2-, and R' = -$(CH_2)_3$-NHCOO-$(CH_2)_2$-.[421] (k) Azopolymaleimide-*co*-styrene.[422] (l) Structure

of the azopolyester.[423] (m) Example of functionalization with azobenzene for the lignin.[424] (n) Azopoly(4-phenol) synthesized with horseradish peroxidase.[425] (o) Poly(amic acid).[426]. (p) Poly(4-vinylpyridine) and H-bonded azobenzene derivative, R = -NH-CH_3, -$N(CH_3)_2$ or –O-CH_3.[427] (q) Poly(4-vinylpyridine) and X-bonded azobenzene derivative.[428] (r) Chemical structure of the polyelectrolytic complex between poly(diallyldimethylammonium) and 2-(4- dimethylaminophenylazo)benzoate.[429] (s) Poly(ferrocenylethylmethylsilane)-*block*-(ferrocenylaminomethylsilane) and Ethyl Orange complex.[430] (t) Azopoly(aryl ether) bearing a rare earth metal complex, with R being either Eu or Tr.[431] (u-x) Azotriarylamine derivatives.[432] (y) 4-(dimethylazobenzene) where the formation of SRG has been observed.[433] (z) Ruthenium acetylide complexes with azobenzene derivative.[434]

The flexible polysiloxanes also got their share in the SRG field.[296,370,372,435–437] Rocha, Hurduc, and coworkers prepared such polymers and studied the inscription of SRG under pulsed irradiation (Figure 18i).[296] Another kind of siloxane derivatives can be obtained with sol-gel silica coatings;[421,438,439] an example of such material has been prepared by Peretti, Gacoin, and coworkers by mixing a silylated anthracene, a silylated azobenzene, and tetraethyl ortho silicate (Figure 18j).[421] Zhu and coworkers reported the synthesis of an azocopolymer of maleimide and styrene for the formation of SRG (Figure 18k),[422] while Fukada *et al.* used the same kind of polymer (along with an azopolyacrylate) to study the influence of the functionalization degree on the SRG inscription.[440] A few azopolyesters have been reported,[441,442] for instance by Xu *et al.* where the photochromic molecule is part of the main chain (Figure 18l).[423] An interesting instance has been published by He and coworkers, where they successfully functionalized a biobased lignin with azobenzene derivatives (Figure 18m).[424] Tripathy and coworkers reported the enzymatic synthesis of azopoly(4-phenol) and the corresponding inscription behavior for SRG (Figure 18n),[425] whereas Zhang and coworkers reported the use of a poly(amic acid) backbone (Figure 18o).[426]

Polymers backbones interacting with azobenzene derivatives by supramolecular bonds have also been proven to be suitable materials for SRG.[368,383,386,403,437,443–448] Poly(4-vinylpyridine) (P4VP) is the most common macromolecule that has been described for relief gratings. Many examples use azobenzene derivatives that are H-bonded to their polymer backbone.[319,323,427,449–456] Zhang and coworkers described a hydrogen-bonded P4VP-azobenzene system (Figure 18p), for which they observed the formation of gratings with a modulation depth of up to 312 nm, depending on the azo-content of the material.[443] A few years later, Priimagi, Metrangolo, Resnati, and coworkers presented the first example of a halogen-bonded azobenzene derivative with P4VP for the inscription of SRG (Figure 18q);[428] halogen-bonded systems have been subject to further investigation since then.[428,451] Several studies aimed to compare supramolecular systems to their covalent counterparts[457] or to compare hydrogen-bonded and halogen-bonded systems.[444,445,458] Forni, Resnati, Metrangolo, Priimagi and coworkers demonstrated that the higher directionality of the X-bond compared to the H-bond made them better candidates for the photoalignment of azosupramolecular materials.[445] The inscription of SRG has also been done on various polyelectrolytic systems;[429,459,460] Stumpe and coworkers prepared such a system by mixing poly(diallyldimethylammonium chloride) and sodium 2-(4- dimethylaminophenylazo)benzoate (Figure 18r).[429] Polyelectrolytic complexes have also been used for the fabrication of layer-by-layer (LbL) assemblies, where a cationic and an anionic layer are alternatively coated on the substrate.[461,462] Faul, Manners, and coworkers prepared a polyelectrolytic complex based on a poly(ferrocenyl) cationic backbone and an anionic azobenzene derivative (Figure 18s).[430] Some rare earth metallic complexes with azopoly(aryl ether) have also been reported:[431,463] Zhang and coworkers prepared such polymers with europium and terbium complexes (Figure 18s).[431]

In addition, different polymer topologies of azobenzene derivatives have been explored for the inscription of SRG. Several examples used polymer brushes,[464–468] dendrimers[469–472] and star-shaped compounds,[473–478] and some of them have been directly compared to their linear counterpart.[479]

The inscription of SRG has also been explored on amorphous low molecular weight molecular materials.[217,389,432,480–500] Nakano *et al.* compared the gratings formation between several amorphous films composed of azotriarylamine derivatives (Figure 18u-x),[432] and Ishow *et al.* performed a comparative study of several molecular glasses.[501] There are in addition several examples where the authors proved that their material was in a crystalline phase.[433,502–506] Nakano *et al.*, for instance, observed the formation of SRG at the surface of a single crystal of 4-(dimethylamino)azobenzene (Figure 18y). Several papers were aimed at comparing molecular materials to their polymeric counterparts.[507,508] Many examples have been described where the systems are in a liquid-crystalline phase.[335,336,360,362,478,489,509–520] Ruthenium acetylides derivatives can also be used for the inscription of SRG.[434,521,522] These compounds are used in the field of non-linear optics because they are stable, easily prepared, and redox-responsive. Sahraoui *et al.* synthesized such complexes with azobenzene derivatives (Figure 18z) and studied the ability to form relief gratings on these materials.[434] Interestingly, Gopalan and coworkers reported the synthesis of Single-Wall Carbon NanoTubes (SWCNT) functionalized with DR1m and the subsequent inscription of relief gratings on the corresponding film.[523]

In order to enhance the stability of SRG over time, several studies aimed at developing a post-inscription crosslinking step.[336,347,359,524–529] Moreover, since azobenzene derivatives are colored, there have been reports where the photochromic molecule was removed after the formation of the relief gratings, while still conserving the surface topology,[447,530] in order to obtain transparent materials.

SRG have mainly been inscribed on planar surface, but a few examples show also that mass transport can take place at the surface of colloidal particles[531,532] or along the length of an azopolymer nanotube.[533]

The main part of the available literature about SRG deal with azobenzene derivatives, as already discussed,[335,384,519,534,535] but bisazobenzene derivatives have also been reported.[352,374,395,414,454,456,536,537] For instance, Vapaavuori, Goulet-Hanssens, *et al*. observed that the use of a *meta*-bisazobenzene (Figure 19a) resulted in better relief inscription than its monoazo counterpart.[536]

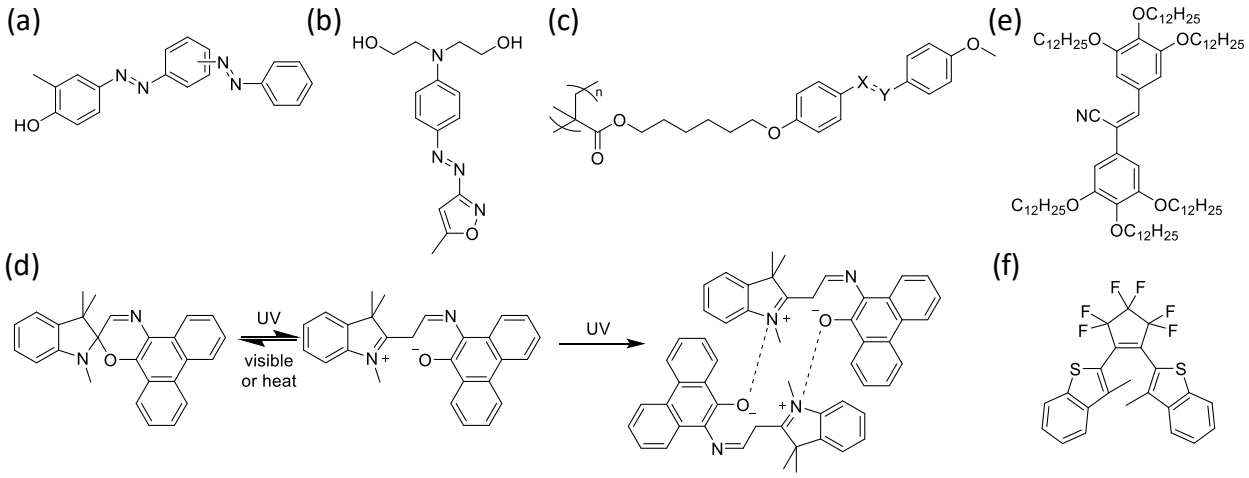

Figure 19: (a) Bisazobenzene structure with the second azo unit either at the *para* or *meta* position.[536] (b) Azoisoxazole derivative.[407] (c) Polymethacrylate with benzylidene aniline derivative with X = Y = C=N or N=C.[538] (d) Phototriggered merocyanine aggregation.[539] (e) Cyanostilbene derivative.[540] (f) Diarylethene derivatives.[541]

Kucharski, Ortyl, and coworkers investigated the formation of SRG in materials containing azoisoxazole units (Figure 19b).[407,542] There are also a few reports where benzylidene aniline has been used (Figure 19c).[538,543–545] Kawatsuki *et al.* studied the inscription kinetics of SRG in such a system, and observed that it differed from the azobenzene-based system because of the concomitant degradation of the C=N of the photochromic unit.[538] A few examples consider spiropyran and spirooxazine derivatives,[539,546–548] but the mechanism differs from the azobenzene-based systems and is not perfectly understood. Ubukata *et al.* suggested a mechanism where the diffusion coefficients difference of the spiropyran and its merocyanine isomer between the irradiated and shaded areas drives the formation of SRG,[546] while Fu, Zhang, Liu, and coworkers explained the formation of SRG in their system with a phototriggered merocyanine aggregation (Figure 19d).[539] Park and coworkers used a cyanostilbene derivative to form SRG in a crystalline film;[540] in this case, the authors proposed that the efficient

inscription is driven by a photodriven crystallization of the photochrome (Figure 19e). Ubukata *et al*. also reported the formation of SRG in diarylethene-containing PMMA films (Figure 19f).[541]

Having now established an exhaustive catalog of all the possible general chemical structures reported so far for the inscription of SRG with photoswitches, we will now focus on some examples of original applications of such materials, that is apart from the classical optical data storage.

In optics, SRG have been used, for instance, to increase the light extraction of Organic Light-Emitting Diodes (OLED).[549,550] The internal quantum efficiency of these devices are close to 100 %, but due to the multilayered structure and the internal reflection, the overall light extraction of the material is usually closer to 20 % (Figure 20a).[549]

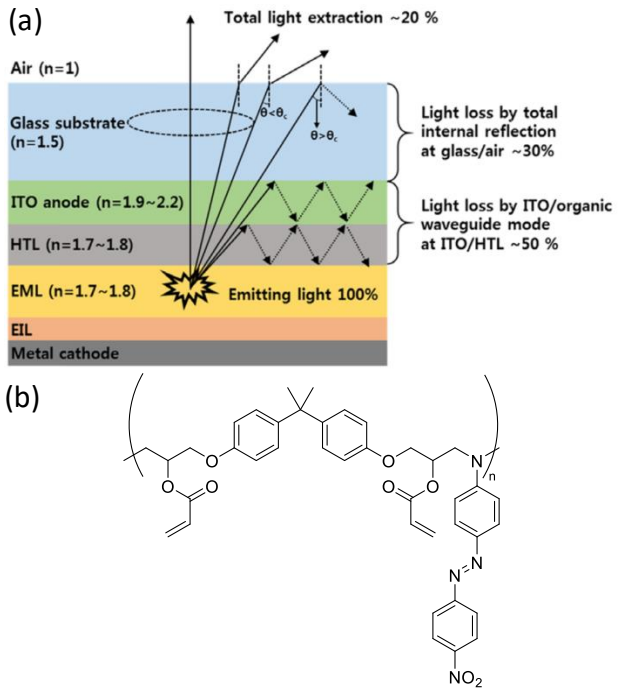

Figure 20: (a) Scheme of the light loss in an OLED device. EIL = Electron-Injecting Layer, EML = EMission Layer, HTL = Hole-Transport Layer, ITO = Indium Tin Oxide. (b) Chemical structure of the modified poly(Disperse Orange 3) used for the inscription of SRG.[550] Part (a) is adapted with permission from reference [549], Copyright 2017 Springer Nature.

The incorporation of microstructures at the interfaces lowers the internal reflection loss; for instance, Kim and coworkers inscribed SRG in a modified poly(Disperse Orange 3) (Figure 20b) for this purpose [550] and observed an increase in the luminescence of the device of approximately 10 % to 20 %, compared to its non-microstructured analogue. An early example by Rochon and coworkers reports the use of azopolymers with inscribed SRG as slab waveguides.[551] SRG have also been used to fabricate Distributed FeedBack (DFB) lasing devices.[552–556] Briefly, DFB lasers make the use of a periodic variation of properties along a material, like its refractive index, for the emission of a coherent and monochromatic light beam. On this basis, Ubakata *et al.* studied the DFB lasing ability of a device (Figure 21b) based on the laser dyes sulforhodamine and malachite green (Figure 21a), with a pDR1m layer for the inscription of SRG.[555]

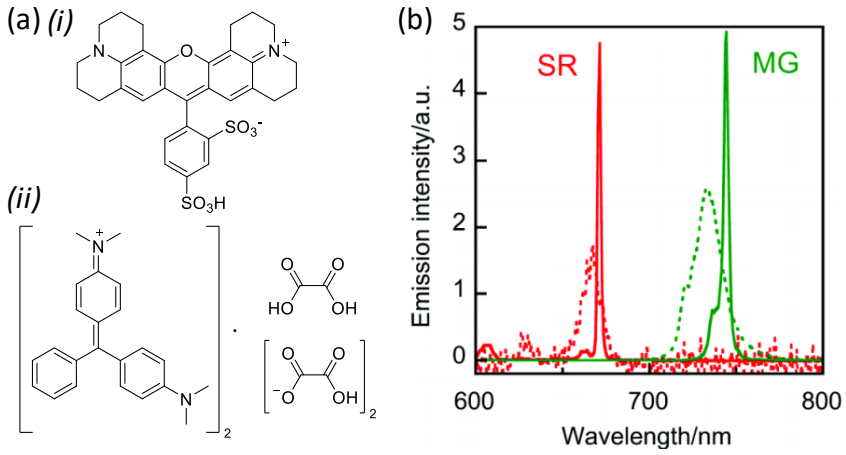

Figure 21: (a) Chemical structure of the laser dyes (i) sulforhodamine (SR) and (ii) malachite green oxalate (MG).[555] (b) Emission of the SRG-inscribed DFB device, where the dotted line represents the assisted spontaneous emission and the solid line the DFB lasing. Part (b) is adapted with permission from reference [555], Copyright 2006 Taylor & Francis.

SRG can also be used to pattern fluorescent substrate:[557–559] Ishow *et al.* used an azotriarylamine derivative (Figure 22a) to form a 2D array of fluorescing spots (Figure 22b).[559] Oh and coworkers reported

the formation of SRG at the tip of an optical fiber for applications such as beam splitter or diffractive lens.[560]

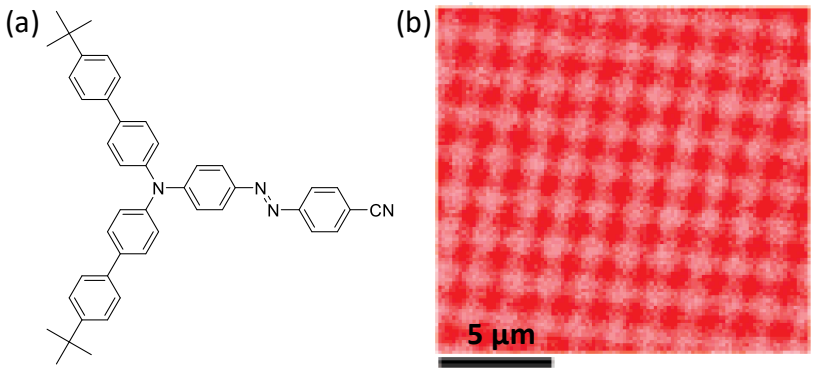

Figure 22: (a) Chemical structure of the azotriarylamine used for the formation of SRG,[559] and (b) the resulting Two-Photon Fluorescence imaging of the patterned fluorescence. Part (b) is adapted with permission from reference [559], Copyright 2007 American Chemical Society.

There are also examples of the use of SRG in the fields of organic solar cells.[561–567] For instance, Kim and coworkers transferred the SRG pattern to a layer of poly(3-hexylthiophene) *via* a PDMS stamp, in order to increase its sunlight absorption without increasing its thickness.[564]

Other examples made use of the transfer of SRG to substrates with a PDMS stamp[568–570] but, in some cases, the pattern can be directly inscribed onto the substrate or a coating material.[387,455,571–573] Samuelson, Kumar, and coworkers reported a system where, after the formation of the pattern, they coated the material with a LbL assembly of poly(4-styrene sulfonate) and TiO_2 particles. After a calcination step at 500 °C which sinters the TiO_2 in the grooves of the SRG and degrades the organic material, they obtained titania nanowires and nanodots over a large area (Figure 23).[572] The same procedure was later used by the same group for the formation of gold nanostructures.[574]

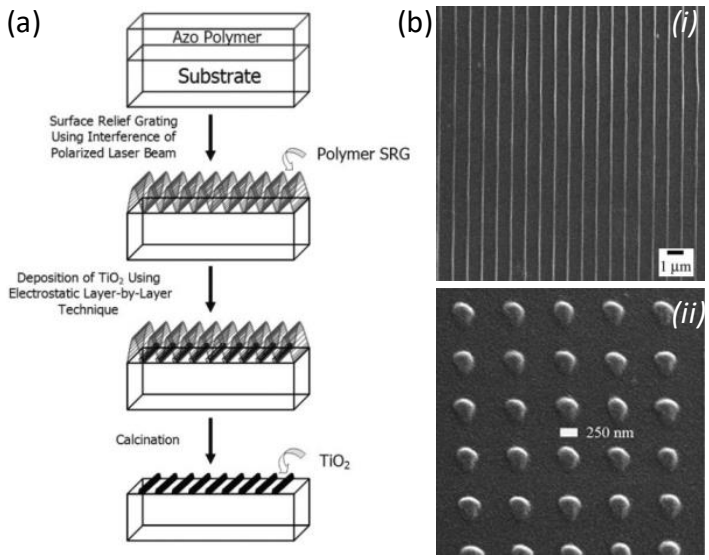

Figure 23: (a) Schematic representation of the procedure used to fabricate titania nanostructures. (b) *(i)* Resulting titania nanowires and *(ii)* nanodots observed by SEM. Adapted with permission from reference [572], Copyright 2006 John Wiley and Sons.

Other procedures can be used to form nanostructures with SRG, with numerous examples being based on an etching step.[575–580] For instance, Shevchenko and coworkers formed nanostructures in silicon through the reactive ion etching of a patterned azopolymer with the eventual use of an intermediate Al_2O_3 photomask (Figure 24).[578]

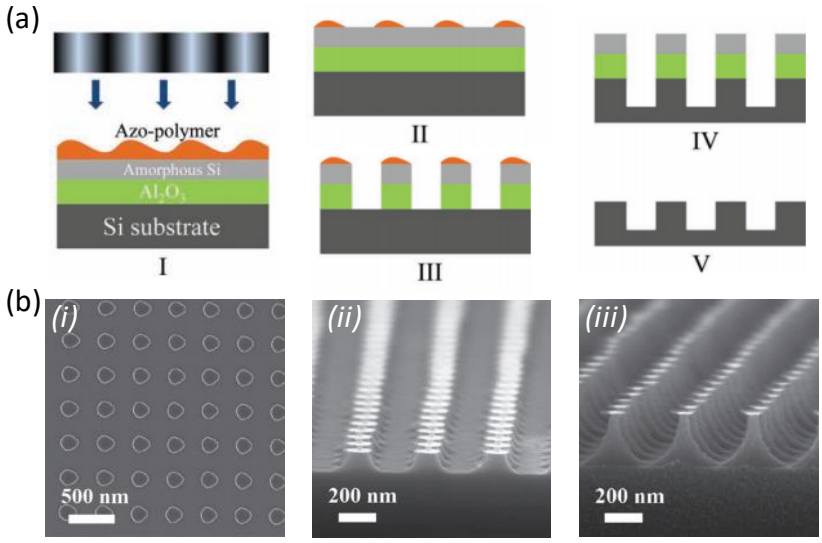

Figure 24: (a) Schematic representation of the procedure used to fabricate silicon nanostructures (I) Formation of SRG. (II) Partial etching of the organic matrix in O_2. (III) Dry etching of the silicon. (IV) and (V) Stripping of the mask. (b) The corresponding structures observed by SEM, with *(i)* the Al_2O_3 photomask, *(ii)* the etched silicon substrate, *(iii)* another etched silicon substrate with a different etching procedure. Adapted with permission from reference [578], Copyright 2011 John Wiley and Sons.

Santer and coworkers widely investigated a system where anionic poly(methacrylate) are grafted onto a silica substrate and loaded with cationic azobenzene derivatives (Figure 25a).[363,465–468,581]

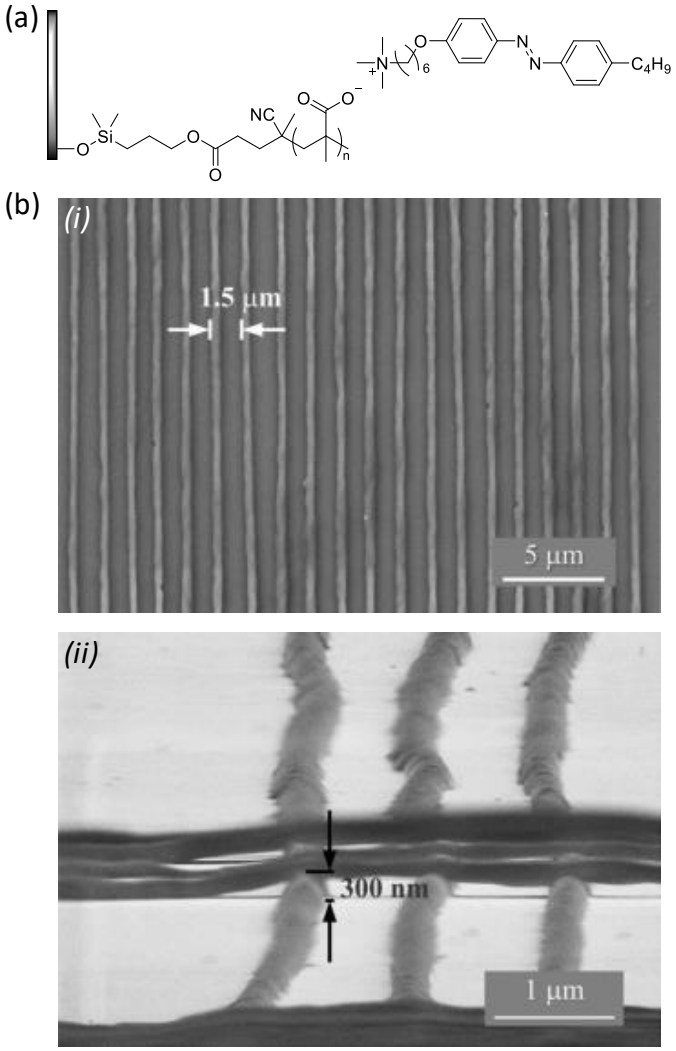

Figure 25: (a) Chemical structure of the anionic PMMA layer loaded with cationic azobenzene derivative, along with gold nanoparticles. (b) Nanowires obtained after the inscription of SRG and subsequent washing with DMF, as observed by SEM. Part (b) is adapted with permission from reference [581], Copyright 2017 Nature Springer.

The inscription of SRG to this material leads to the chain scissions in the grooves of the pattern, and the residues can be washed by a good solvent, like DMF.[466] They used this system to form nanowires with gold nanoparticles that were loaded, along with the azobenzene derivative, within the polymer layer (Figure 25b).[581]

The inscription of SRG has been also reported in the biomedical field. Sabat, Escubedo, and coworkers explored the application of bidimensional SRG as nanoplasmonic biosensors for the detection of biotin-streptavidin binding events[582] and for the detection of uropathogenic bacteria.[583] Briefly, they prepared orthogonal bidimensional gratings on a DR1m glass, and they further coated the surface with gold (Figure 26a).

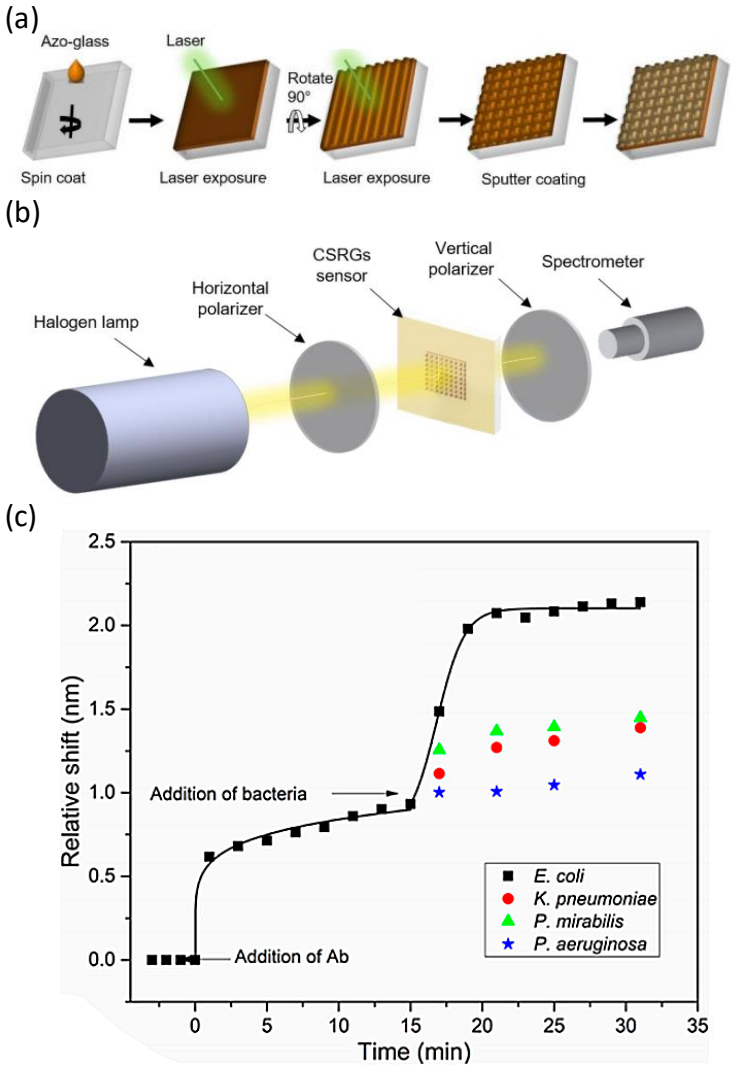

Figure 26: (a) Procedure for the preparation of the crossed surface relief gratings (CSRG) for nanoplasmonic biosensing. (b) Schematic representation of the setup used for the detection of binding events in the device. (c) Evolution of the relative shift (nm) as a function of time (min); the bacteria *E. coli* shows the strongest response. Parts (a-b) and (c) are adapted with permission from reference [582] Copyright 2017 American Chemical Society, and reference [583], respectively.

When irradiated with horizontally polarized light, surface plasmons can be excited at the metal-glass interface, and energy can be reemitted in the orthogonal component, that is, vertically polarized. Hence, by placing a vertical polarizer after the device (so that any residual incident signal is removed), a

spectrophotometer can detect the signal caused by the surface plasmon resonance (SPR) (Figure 26b). The shift of the signal peak is quantitatively related to the objects adsorbed at the surface, and the authors showed that they could detect *E. coli* bacteria (Figure 26c).[583] Moreover, since cells are sensitive to the topology of their environment, several studies have been conducted for the patterning of cell culture media through SRG.[436,464,584–587] Recently, Cavalli, Netti, and coworkers observed that human umbilical vein endothelial cells (HUVEC) oriented preferentially along the pattern direction (Figure 27).[464]

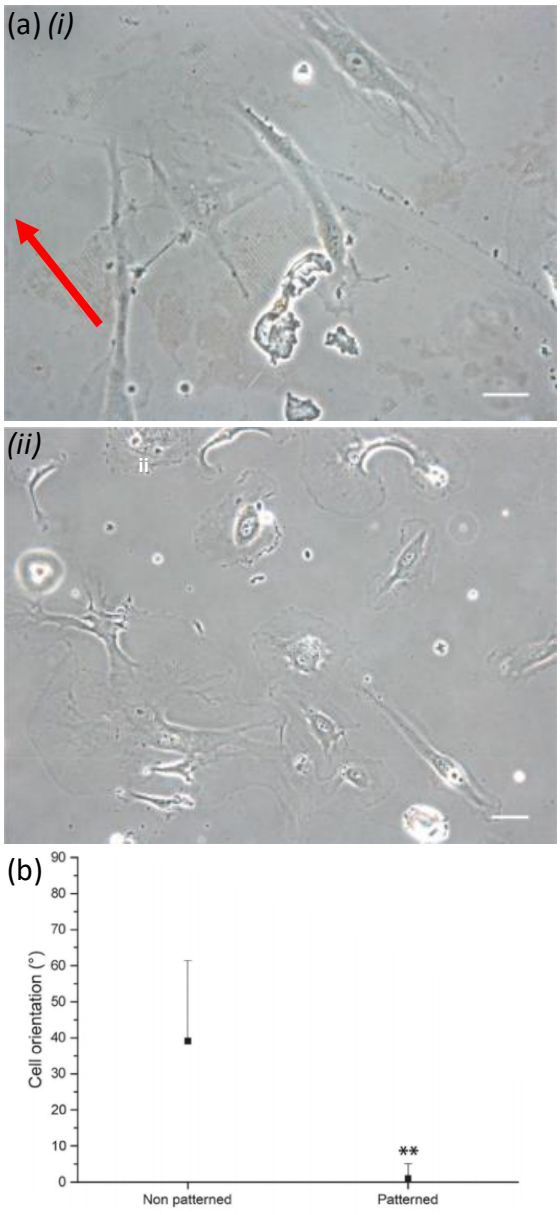

Figure 27: (a) Phase contrast images of incubated human umbilical vein endothelial cells (HUVEC) on *(i)* patterned surface with SRG (red arrow shows the pattern direction) and *(ii)* non-patterned surface. The scale bars represent 30 μm. (b) Corresponding cell orientation of the surfaces. The wide distribution with an average of approximately 45° indicates a random orientation on the non-patterned surface, while the narrow distribution with an average of 0° indicates a highly preferential orientation on surfaces patterned with SRG (the asterisks represent a significant statistical difference between the two cases). Adapted with permission from reference [464], Copyright 2010 The Royal Society of Chemistry.

Since SRG occurs because of a directional mass migration in the material, several examples report the orientational motion of nanoobjects[588–591] or dyes[592] embedded in the matrix. For instance, Ishow and coworkers reported the selective alignment of polystyrene nanoparticles either in the crests of SRG (for nanoparticles deposited before inscription of the pattern), or on the troughs (for nanoparticles deposited after inscription) (Figure 28).[589]

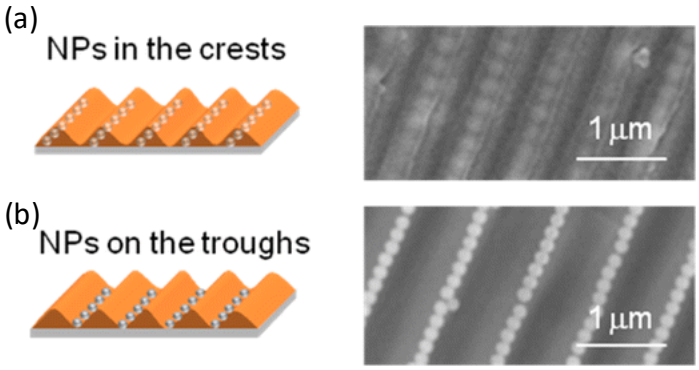

Figure 28: (a) Schematic representation of the linear alignment of polystyrene nanoparticles in the crests of the SRG and the corresponding SEM image, when the particles are deposited before the inscription of the pattern. (b) Scheme of the linear alignment of polystyrene nanoparticles in the troughs of the SRG and the corresponding SEM image, when the particles are deposited after the inscription of the pattern. Adapted with permission from reference [589], Copyright 2014 American Chemical Society.

Finally, SRG can also be used for the orientation of liquid crystalline materials coated on it,[593–596] or for the organization of block copolymer phases.[597] They have also been used to change the wettability of materials, since this property is closely related to the surface topology.[598]

So far, we mainly discussed SRG fabricated with an inhomogeneous light field, either through IIP, PIP, or a photomask. However, there are some reports describing the interesting formation of "spontaneous" SRG under illumination with a single polarized light beam.[326,338,364,394,452,474,488,587,599–605] The resulting pattern, named recently the "willow structure" by Noga *et al.*, is less periodic than the classical SRG (Figure 29a).[606]

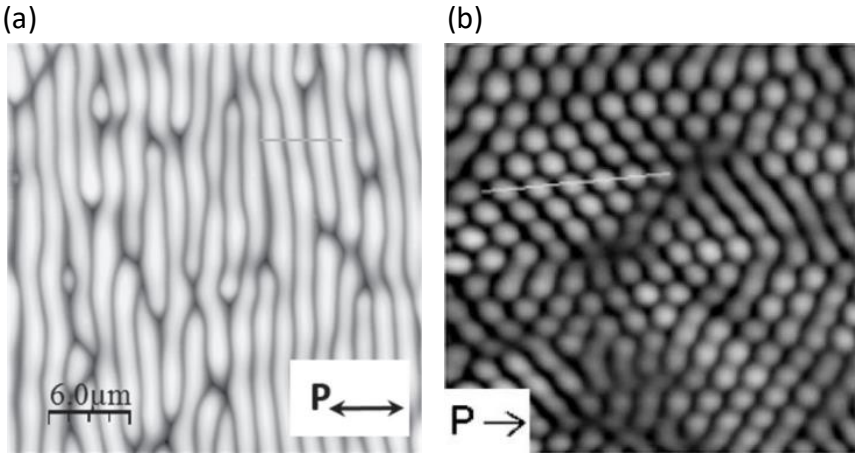

Figure 29: (a) « Willow structure » obtained on a supramolecular azopolymer upon irradiation with a single linearly polarized beam, observed by AFM. (b) AFM image of the hexagonal array of domes obtained after irradiation with a single linearly polarized beam. Parts (a) and (b) are adapted with permissions from reference [606], Copyright 2016 John Wiley and Sons, and [607], Copyright 2002 John Wiley and Sons, respectively.

It seems that these structures result from the interference patterns generated at the surface by defects, but model and experiments are still ongoing to fully understand how such patterns can appear.[608,609] An

early example of “spontaneous” inscription of structure has been reported by Hubert *et al.*, where they observed the formation of hexagonal arrays of domes after the illumination with a single linearly polarized light beam (Figure 29b).[607,610] These arrays could further be organized to hierarchical SRG after illumination with an interference pattern.[611]

2.4.2. Local photopatterning

SRG are formed on large areas, but the mass motion upon polarized irradiation can also be achieved on localized spots, either with focused beams[612–620] or by the near-field generated by metallic structures (that is, surface plasmons).[621,622] The latter case has actually been used to map such near-fields generated by metallic nanostructures.[328,623–629] Hubert *et al.* described a system where they coated pDR1m on an array of silver and gold nanostructures. After irradiation with polarized light, they observed by AFM the formation of surface reliefs, close to the theoretical calculations of the photogenerated near-fields (Figure 30).[628]

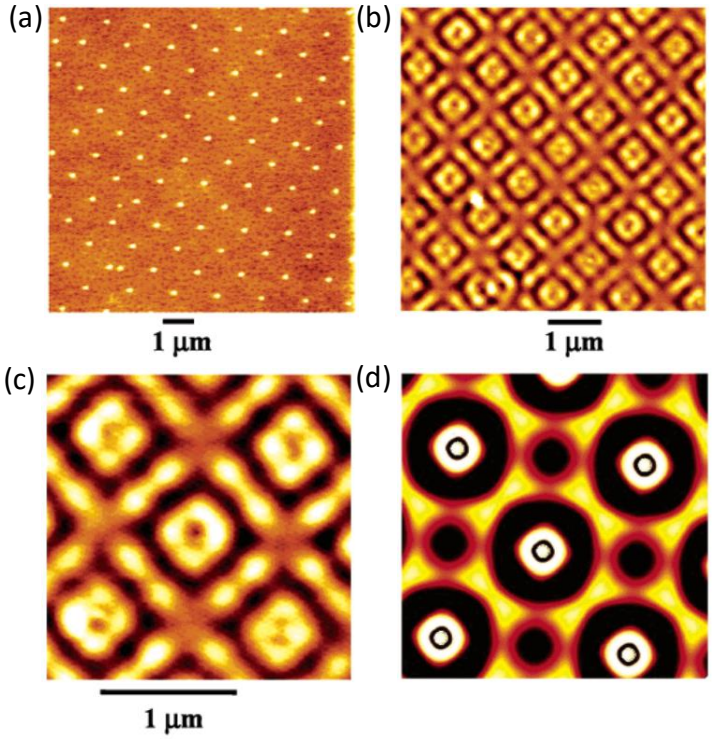

Figure 30: AFM images of the mapping of near-fields generated by silver nanostructures coated with pDR1m, (a) Before irradiation. (b) After irradiation with RCP light. (c) Close-up of the structure seen in (b), and (d) corresponding theoretical negative field image. Adapted with permission from reference [628], Copyright 2005 American Chemical Society.

Santer and coworkers used the same phenomenon to map the interaction between silver and gold nanoantennas.[629] Concerning the patterning with a single focused light beam, various shapes of surface reliefs has been achieved, for example, some helical structures (Figure 31a),[630–632] or some doughnut-shaped structures (Figure 31b).[633]

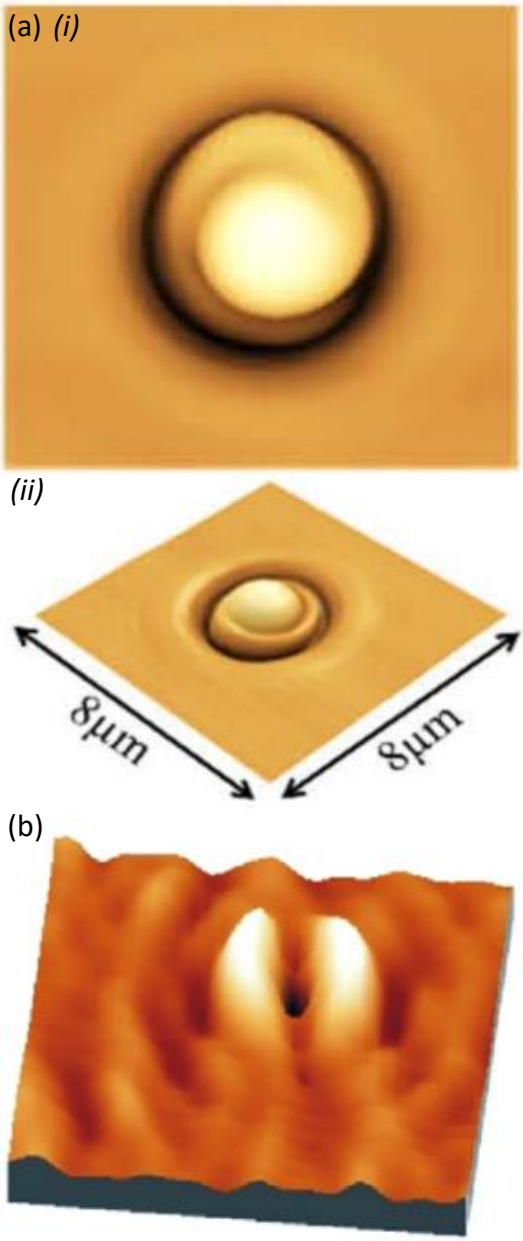

Figure 31: AFM images of localized photopatterning achieved with a single focused light beam. (a) *(i)* Top view and *(ii)* perspective view of a helical structure. (b) Doughnut shape (the image represents 3 μm × 3 μm). Parts (a) and (b) are adapted with permissions from reference [630], Copyright 2017 Optical Society of America, and reference [633], Copyright 2017 Elsevier, respectively.

More recently, Netti, Cavalli, Attanasio, Ventre, and coworkers used confocal microscopy to pattern cell media with various shapes (Figure 32) and study the behavior of cells on the modified substrate.[634–636]

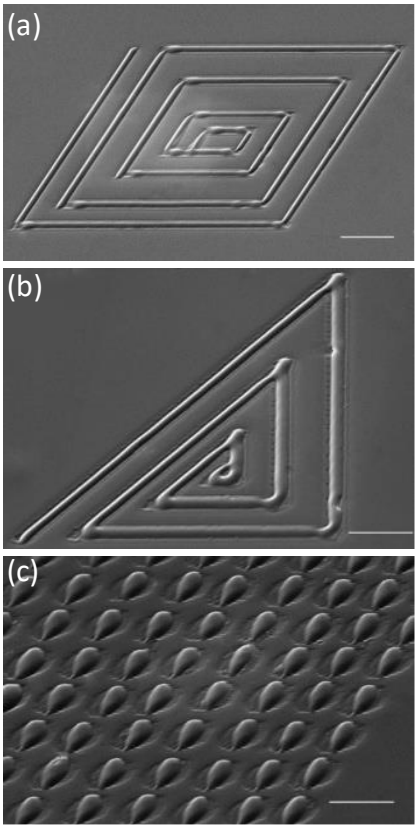

Figure 32: SEM images of patterned surfaces formed with a confocal microscope. (a) Concentric squares. (b) Concentric triangles. (c) Sphere-like geometries. Scale bars: 10 μm. Adapted with permission from reference [635], Copyright 2016 John Wiley and Sons.

2.4.3. Other examples

A switchable surface topology can also be achieved by using poly(N-isopropylacrylamide) (pNIPAAm) hydrogels functionalized with spiropyran moieties.[637–639] (*n.b.* the photoswitchable shrinking/swelling mechanism of these systems will be discussed later (section 2.5.2)). For instance, Broer, Schenning, and coworkers prepared such a hydrogel layer on a glass substrate, and varied the degree of crosslinking in

the material, thus pre-patterning the surface topology. Switchable topologies are produced by irradiation with blue light (λ = 455 nm) because the volume difference between the swollen and shrunk states is higher in the areas where the material is less crosslinked (Figure 33).[637]

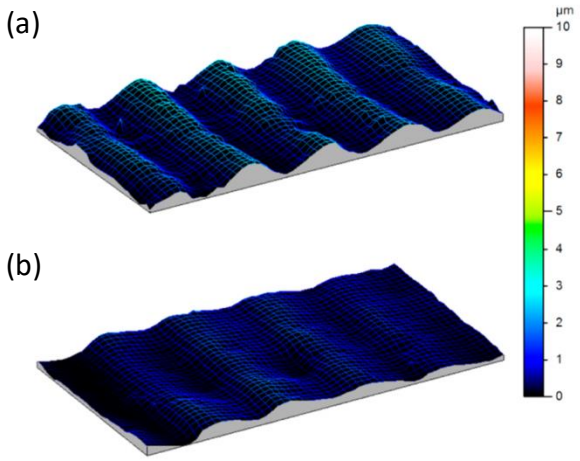

Figure 33: Modification of the topography of a spiropyran-pNIPAAm hydrogel surface observed by interferometry, (a) before and (b) after light irradiation (λ = 455 nm). The represented area is 505 × 946 µm^2. Adapted with permission from reference [637], Copyright 2014 American Chemical Society.

Liquid-crystalline (LC) materials doped with molecular photoswitches have been used to tune the surface topology as well (*n.b.* the mechanism will be also discussed later in section (2.5.3.)). Shortly, the local disorder caused by the *trans*→*cis* isomerization of azobenzene under light irradiation is amplified by the liquid-crystalline phase, resulting in an overall contraction or expansion of the material. This localized change of volume has paved the way for surfaces topology photocontrol.[213,640–645] Nowadays, many systems possessing light-responsive surfaces have already been elaborated.[646–649] However, they may require the pre-organisation of the material such as an alternation of chiral nematic and isotropic phases.[646] A recent paper describes a promising material through the study of an *ortho*-fluorobenzene Liquid-Crystalline Elastomer (LCE) film.[335] A mask is used to filter the green light triggering the isomerization of the photoswitch and to impose a precise topography on the surface (Figure 34).

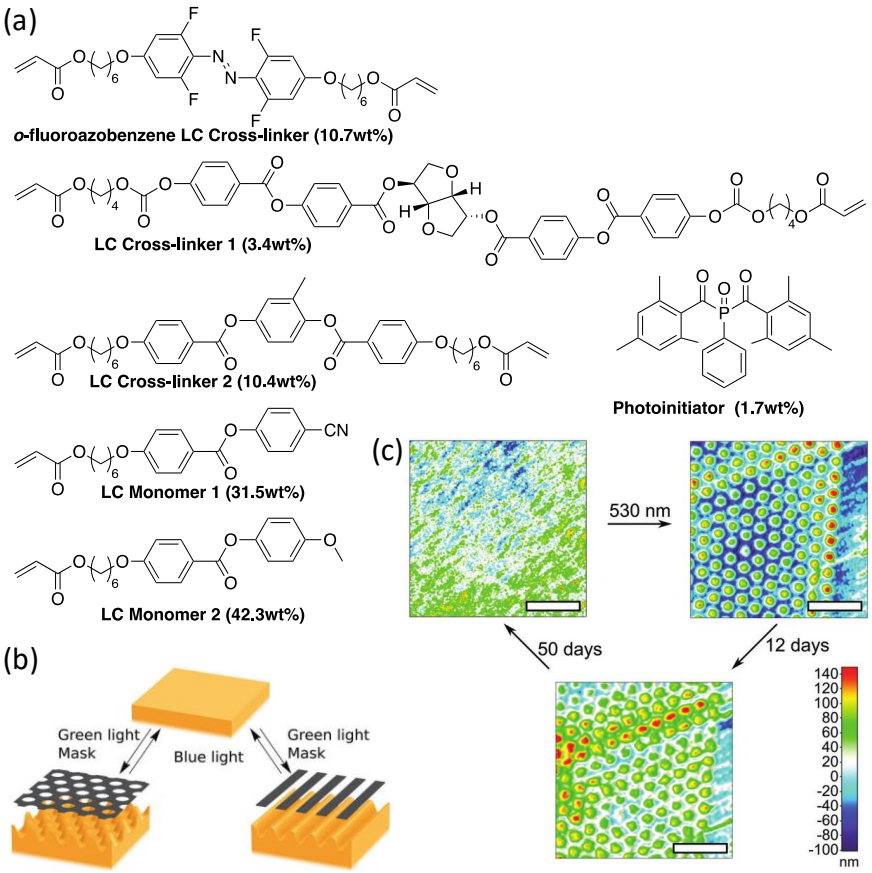

Figure 34: (a) Chemical structures of the liquid crystal components. (b) Illustration of the configuration of the surface topography with the use of a mask. Writing with green light and erasing with blue light. (c) Microscope pictures of the surface evolution over time (scale bar: 100 µm). Parts (b) and (c) are adapted with permission from reference [335], Copyright 2018 John Wiley and Sons.

The process is reversible as the sample only needs to be placed under blue light to recover its initial shape. Therefore, multiple topographies can be successively obtained by changing the form of the mask. The presence of the fluorides allows the surface to be preserved for at least 12 days in the dark, since it confers an important thermal stability to the switch.

2.5. Photoinduced shape deformation of tridimensional materials

Photocontrollable macroscopic mechanical deformation has been widely reviewed over the years, mainly for LC systems. The present section starts with the deformation based on the directional photomanipulation (DPM) method, closely related to SRG. We will then move on with systems manipulated by other methods, usually when the shape change is caused by the modification of the geometrical dimensions of the photochromic molecule. We will consider first amorphous polymers, followed by liquid crystalline materials, and finish this section by discussing examples with molecular crystals.

2.5.1. Directional photomanipulation

Directional photomanipulation (DPM) has also been commonly called directional photofluidization, but since it seems that its mechanism is closely related to the mechanism of inscription of SRG, and, hence, not evidently a fluidization process, we will prefer the more general term in this review. There have been some reports focused on the mechanism of DPM,[650,651] and there are actually examples where the initial DPM of particles leads to the formation of SRG.[652] Again, we do not aim to conclude on a mechanism here, and we invite the reader to refer to the previous section for a general discussion. Besides, we will not discuss the examples with the DPM of nanoparticles,[653–660] considering the scale limitations that we established at the beginning of this chapter.

DPM refers to the mechanical deformation of a photosensitive object along the polarization direction of the incident light. While the most recent reports do not use interfering beams, one of the first example of DPM was observed during the irradiation of microspheres with an interference pattern. Wang and coworkers showed the elongation of epoxy-based amphiphilic azopolymers colloidal particles along the direction of polarization of blue light (λ = 488 nm), which deformed from spheres to rods with an aspect ratio of almost 2.4 (Figure 35).[661]

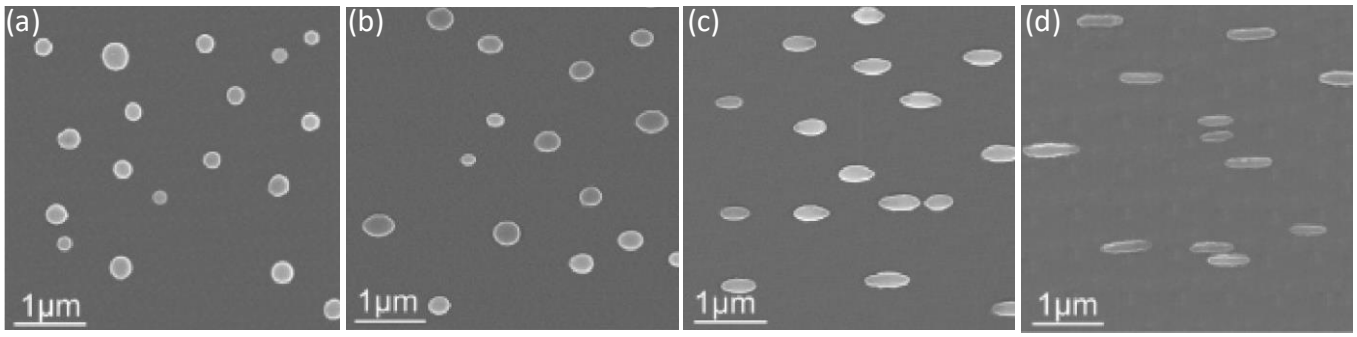

Figure 35: Directional photomodulation of amphiphilic azopolymer colloidal particles. The light beam is linearly oriented from left to right. The SEM images are obtained (a) before, (b) after 5 min, (c) after 12 min and (d) after 15 min of irradiation (λ = 488 nm). Adapted with permission from reference [661], Copyright 2005 American Chemical Society.

Other authors also observed this effect under an interference pattern.[532,662–664] Interestingly, in an attempt to explain the formation of SRG, such deformation was observed earlier by Helgert and coworkers, with the directional deformation of an azopolyester film deposited on a water surface along the direction of polarization of the visible light (λ = 532 nm) (without any interference pattern) and restoration of the initial shape with circularly polarized light (Figure 36a-c);[665] we believe that it is the first example of DPM of an azobenzene-containing material.

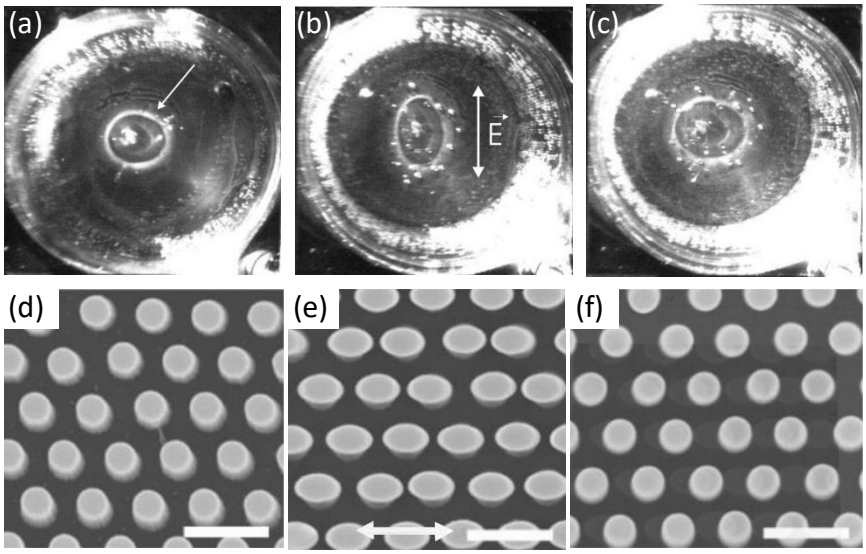

Figure 36: (a-c) Optical microscopy images of the deformation of an azopolyester film deposited on water. The film contour appears white. (a) Before irradiation, with the arrow highlighting the film contour. (b) After irradiation with LPL (λ = 532 nm), as indicated by the double arrow. (c) Restoration of the initial shape after irradiation with CPL. The film is approximately 1 cm in diameter; (d-f) SEM images of the reversible directional photomanipulation on a crosslinked azopolyacrylate material. (d) Before irradiation. (e) After irradiation with LPL (λ = 532 nm), as indicated by the double arrow. (f) Restoration of the initial shape after a heating treatment. Scale bars are 1 μm. Parts (a-c) and (d-f) are adapted with permission from reference [665], Copyright 2000 Nature Springer, and reference [666], Copyright 2018 John Wiley and Sons, respectively.

The initial shape can indeed be recovered with illumination with homogeneous CPL,[667] but also by crosslinking the material: Li and coworkers recently reported such a system with a crosslinked azopolyacrylate.[666] They observed the DPM of an array of micropillars upon irradiation with LPL (λ = 532 nm) and restored the initial shape by heating the material (Figure 36d-f). Interestingly, they also observed a patterned DPM under irradiation with interfering light beams.The materials used for DPM can be based on polyacrylates,[361,668,669] polyurethanes,[670,671] epoxy-based polymers[391,672,673] (with an example with a hollow microsphere[674]), various block copolymers[675–678] or supramolecular systems with poly(4-vinylpyridine).[679] Wang and coworkers reported a systematic study of the DPM depending on the size of epoxy-based microparticles.[680]

DPM has also been achieved on molecular materials.[681–684] For instance, Xu, Wang, and coworkers prepared microspheres of azobenzene derivatives (Figure 37a) *via* a microfluidic processing method and observed the deformation of the top layers of the particles, highlighting the field gradient effect stated earlier (Figure 37b). Moreover, it can be noted that the final shape of the spheres does look like a directed fluidization of the polymer matrix.

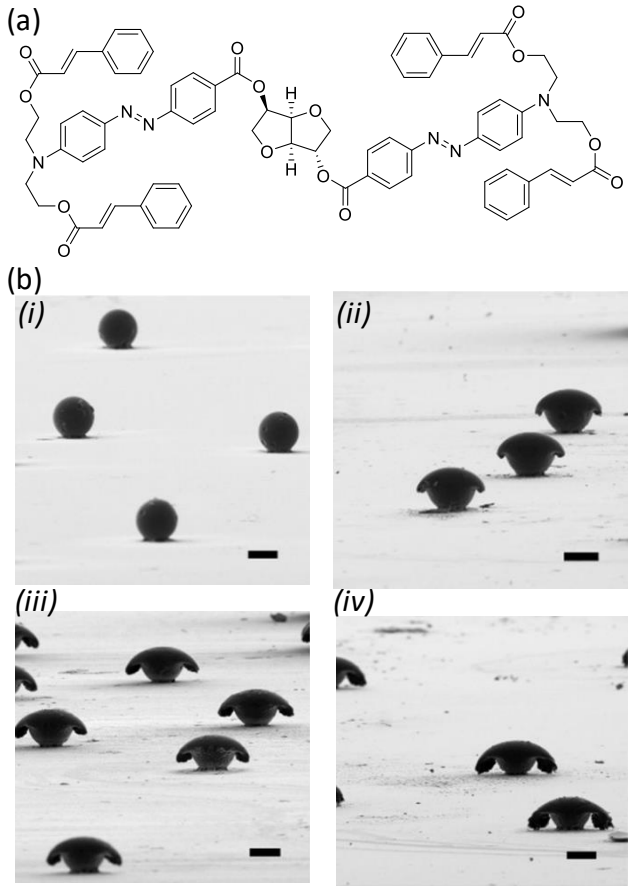

Figure 37: (a) Chemical structure of an azobenzene isosorbide derivative. (b) Directional photomanipulation of the resulting microspheres observed by SEM: *(i)* before irradiation, *(ii)* after 1 h, *(iii)* after 2 h and *(iv)* after 3 h of irradiation with LPL (λ = 488 nm). Scale bars are 10 μm. Part (b) is adapted with permission from reference [681], Copyright 2018 The Royal Society of Chemistry.

As discussed earlier, the core of the literature about DPM is based on colloidal systems with the deformation of microspheres, but we have also presented an example of system with micropillars, and similar geometries have been reported by other groups.[667,685–689] The DPM can also be achieved on spherical arrays (Figure 38a),[663,664,690] stripes (Figure 38b)[691] or even holes (Figure 38c).[692–698]

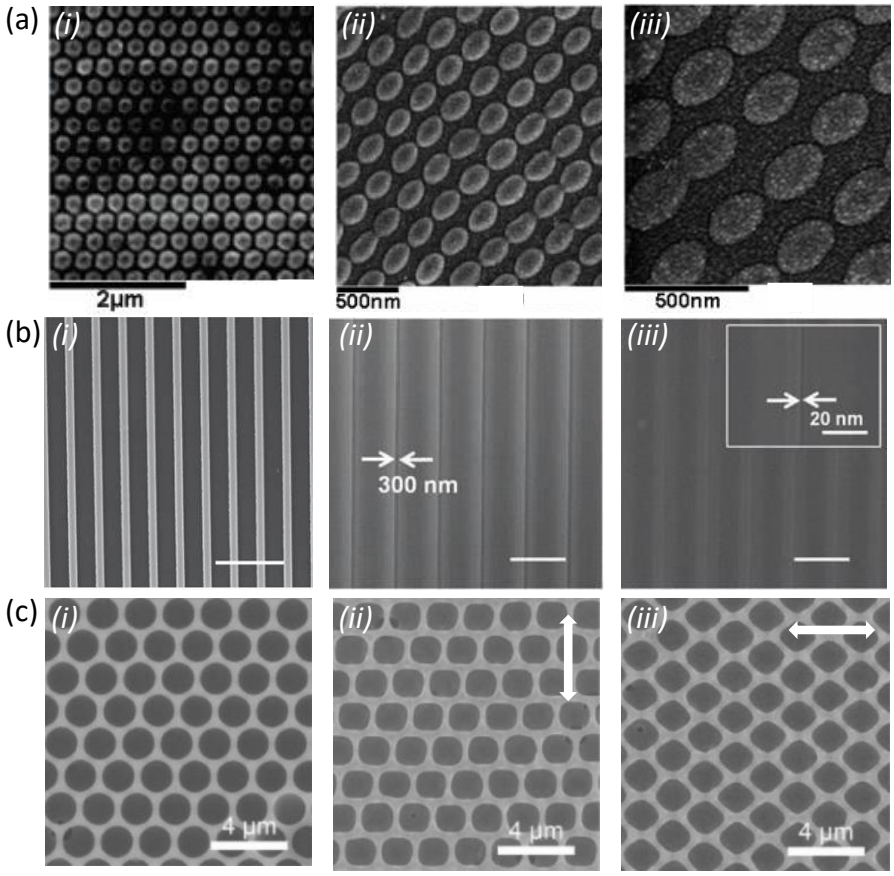

Figure 38: (a) SEM images of the directional photomanipulation of spherical cap arrays. *(i)* Before irradiation. *(ii)* After 2 h of irradiation with LPL (λ = 488 nm). *(iii)* After 3 h of irradiation. (b) SEM images of the directional photomanipulation of stripes. *(i)* Pristine azopolymer stripes (scale bar: 10 µm). *(ii-iii)* Topography of the same material *(ii)* after 8 minutes, and *(iii)* after 12 minutes of directional photomanipulation with LPL (λ = 488 nm) oriented from left to right (scale bar: 5 µm). (c) SEM images of the directional photomanipulation of holes. *(i)* Pristine azopolymer stripes. *(ii)* Topography of the same material after irradiation with LPL (λ = 450 nm, white double arrow shows the direction of the polarization). *(iii)* Subsequent irradiation with an orthogonal LPL (white double arrow shows the direction of the polarization). Parts (a), (b) and (c) are adapted with permission from reference [664], Copyright 2007 American Chemical Society, reference [691], Copyright 2011 John Wiley and Sons, and reference [694], Copyright 2017 American Chemical Society, respectively.

He, Lin, and coworkers reported the DPM of azobenzene-based micelles upon irradiation with LPL (λ = 450 nm) (Figure 39).[699]

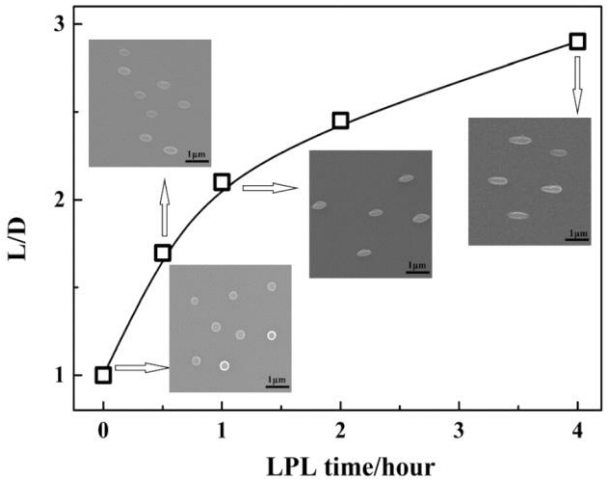

Figure 39: Evolution of the aspect ratio (L/D) of azobenzene-based micelles as a function of irradiation time with LPL (λ = 450 nm). The insets show the corresponding SEM images. Adapted with permission from reference [699], Copyright 2017 The Royal Society of Chemistry.

Nakano and coworkers described the DPM of a separated microphase containing an azobenzene derivative.[700] Several examples also consider the DPM of Janus particles.[701–704] For instance, Wang and coworkers showed that the DPM of these particles takes place exclusively on the phase containing the azobenzene derivative (Figure 40a).[704] Nakano and coworkers observed the DPM of molecular glass fragments fixed in agar gel (Figure 40b).[705–707]

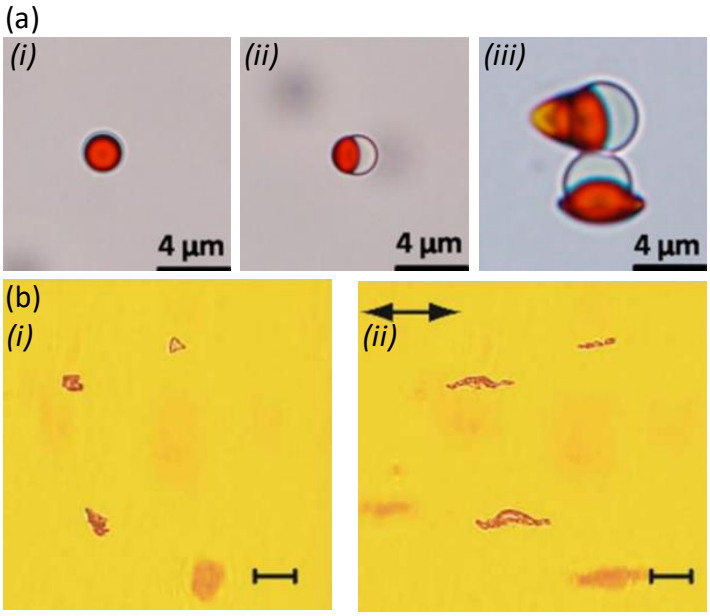

Figure 40: (a) *(i-ii)* Optical microscopy images of Janus particles where the azobenzene-containing part appears red, and *(iii)* after deformation by directional photomanipulation with LPL (λ = 488 nm). (b) *(i)* Optical microscopy images of molecular glass fragments of azobenzene derivatives fixed in an agar gel. *(ii)* Same fragments after directional photomanipulation with LPL (λ = 488 nm, direction of polarization indicated by the black double arrow). Scale bars: 20 µm. Parts (a) and (b) are adapted with permission from reference [704], Copyright 2016 American Chemical Society, and reference [705], Copyright 2018 American Chemical Society, respectively.

Recently, Kang, Kim, and coworkers presented an interesting procedure for the patterning of azopolymer films through DPM, *via* a process they named "vertical DPM". Basically, a PDMS mold is applied on the photoactive film, and an oblique irradiation with LPL (λ = 532 nm) moves the polymer matrix up in the cavities of the mold. The structure obtained in this way is asymmetric, so a leveling irradiation with LPL at normal incidence is necessary in order to obtain a symmetric relief (Figure 41).[708]

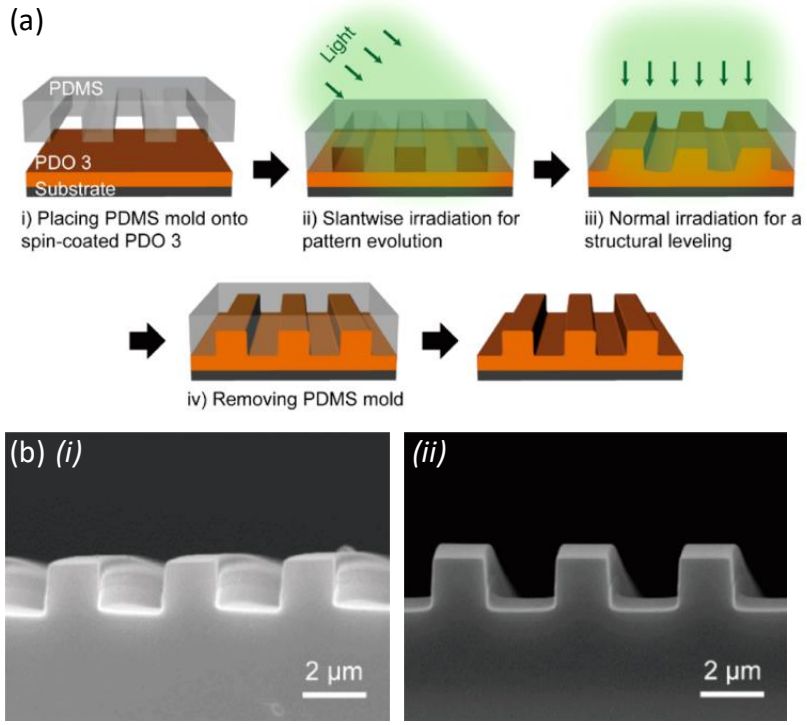

Figure 41: (a) Scheme of the procedure for vertical directional photomanipulation. (b) Resulting SEM images after *(i)* the oblique illumination and *(ii)* the normal irradiation for levelling (λ = 532 nm). Adapted with permission from reference [708], Copyright 2017 American Chemical Society.

Concerning the examples leading to original application, DPM has been used to control the wettability of substrates.[686,687] Li, Lin and coworkers recently showed the design of an anisotropic superhydrophobic substrate, biomimicking the "rice leaf". It was obtained by the DPM of a microsphere array, and they showed that the sliding angle was different between the direction parallel and perpendicular to the substrate orientation (Figure 42).[709]

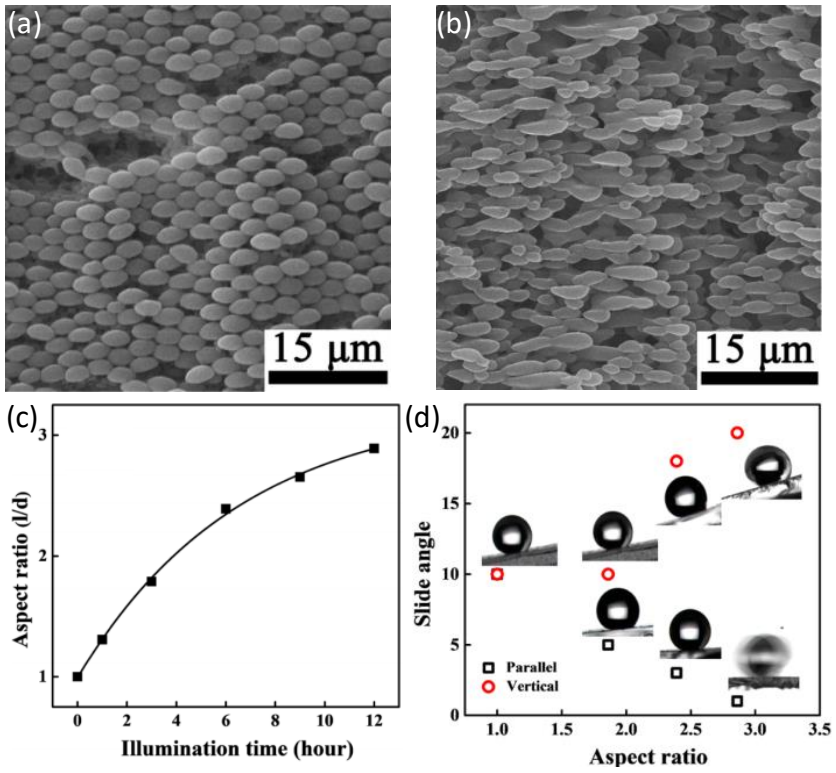

Figure 42: SEM images of the microspheres array obtained from a homopolymer decorated with azobenzene side chains after directional photomanipulation for (a) 3 h and (b) 12 h. (c) Evolution of the aspect ratio of the microparticles as a function of irradiation time. (d) Evolution of the sliding angle of water droplets deposited on the patterned substrate as a function of the aspect ratio, in the parallel direction (black squares) and in the orthogonal direction (red circles) to the orientation direction. Insets represent the corresponding pictures of the droplet on the tilted surface. Adapted with permission from reference [709], Copyright 2018 American Chemical Society.

DPM has also been used to align nanoobjects embedded in a polymer matrix.[710,711] For instance, Lee, Yoo, and coworkers reported the linear orientation of ZnO nanowires by this method (Figure 43).[710]

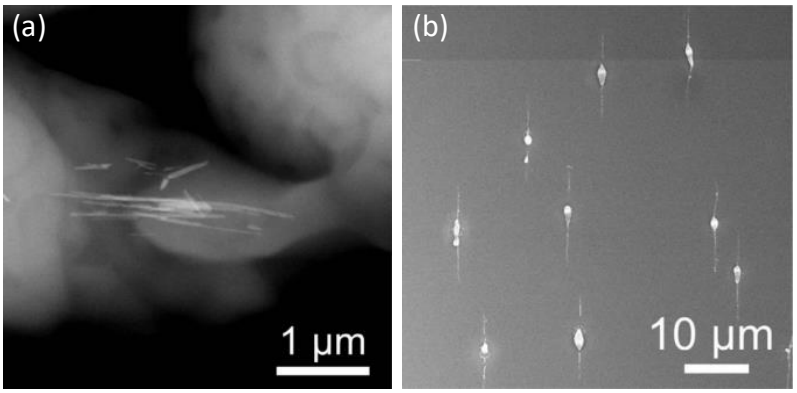

Figure 43: (a) High-angle annular dark-field scanning transmission electron microscopy images of the elongated azomicrospheres containing the ZnO nanowires. (b) Resulting nanostructure after etching the organic matrix. Adapted with permission from reference [710], Copyright 2018 Elsevier.

Kim, Park, Lee, and coworkers reported the healing of a crack in an azopolymer film (Figure 44), and they applied it for the restoration of a wearable electronic device.[712] Park and coworkers also reported the use of DPM to create patterns for gold nanostructures.[713,714]

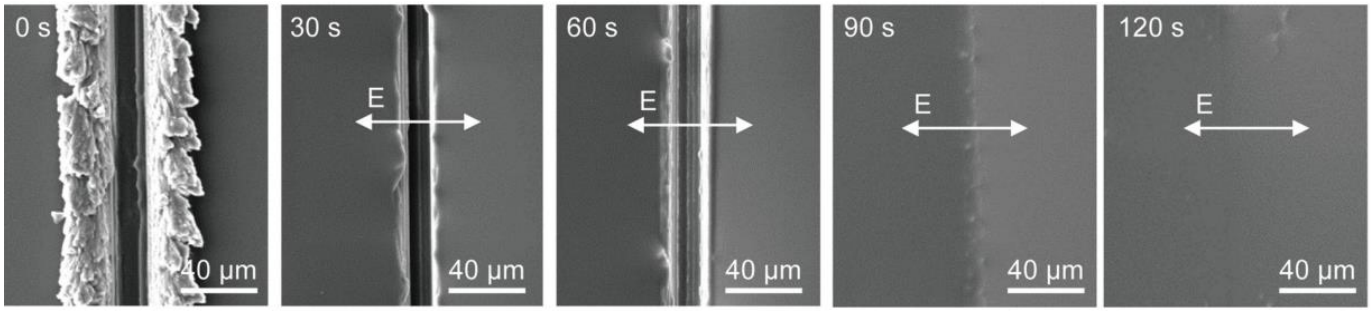

Figure 44: SEM images of different stages of healing of an azopolymeric material upon directional photomanipulation with LPL (λ = 532 nm, direction of polarization indicated with the white double arrow). Adapted with permission from reference [712], Copyright 2014 John Wiley and Sons.

White, Tan, and coworkers widely studied the macroscopic bending of polyamide and polyimide films under LPL, motion that they attribute to the reorientation of the azobenzene moieties. Concerning non-

crosslinked materials, they showed the bending of an azopolyamide film upon irradiation with polarized blue light (λ = 445 nm), and they attributed the important mechanical response to a cooperative anisotropic disruption of the H-bonded network of the material (Figure 45).[715]

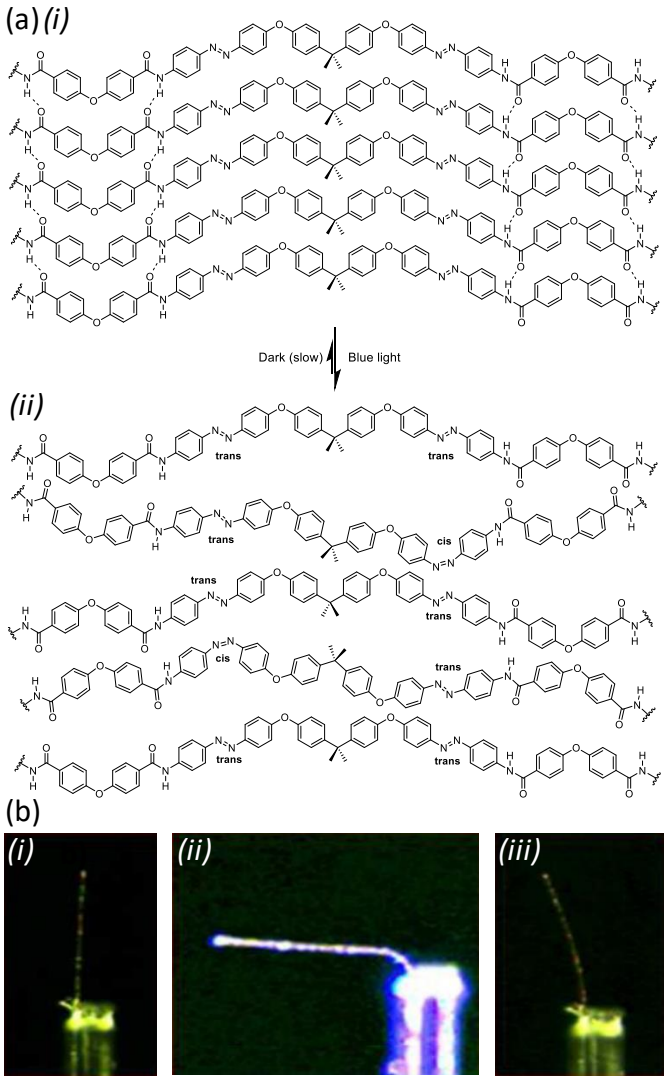

Figure 45: (a) *(i)* Idealized chemical structure of the hydrogen-bonded structure of the polyamide containing azobenzene derivatives and *(ii)* chemical structure of the disrupted material upon LPL (λ = 445 nm). (b) Bending of a film made of the azopolyamide, *(i)* initial film, *(ii)* after 60 min of irradiation, *(iii)* after subsequent relaxation in the dark for 60 min. The film has a length of approximately 6 mm. Part (b) is adapted with permission from reference [715], Copyright 2013 The Royal Society of Chemistry.

The same group also investigated systems based on azopolyimides films,[716–718] and they recently reported that a bulkier substituent on the polymer backbone (Figure 46a,b) induces a higher photomechanical response of the material (Figure 46c).[716]

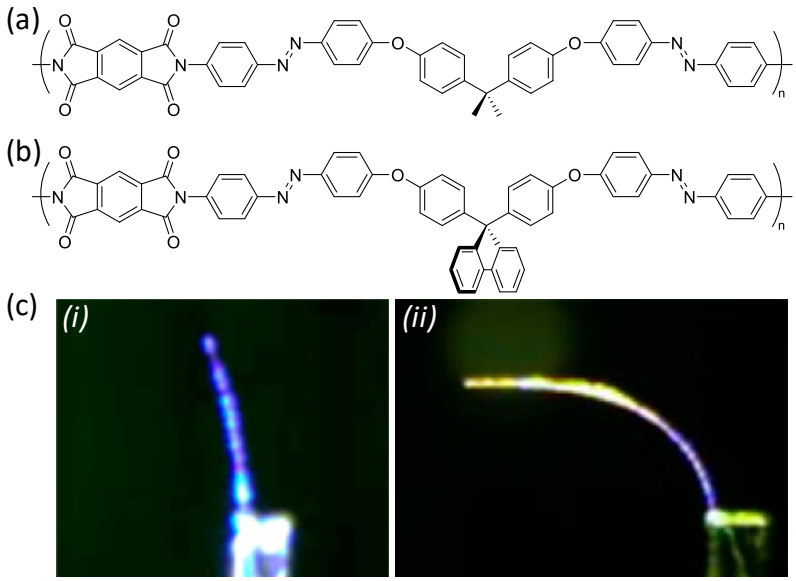

Figure 46: (a-b) Chemical structures of polyimides with different substituents and (c) their corresponding photomechanical actuation, using *(i)* polymer (a) and *(ii)* polymer (b). Part (c) is adapted with permission from reference [716], Copyright 2017 American Chemical Society.

For crosslinked materials, they mainly focused on polyimide films;[719–721] they studied the effect of the crosslinking degree[722,723] and even optimized their system by physical ageing.[724] They also designed a composite of polyimide with poly(vinylidene fluoride) for its piezoelectric properties, and, hence, the conversion of light to electrical energy.[725] Finally, Nakano reported the bending of a triarylamine derivative bearing azobenzenic groups, and proposed that the irreversible mode of deformation of the material was caused by DPM.[726] The same authors presented the directional motion of pieces of molecular glasses containing azobenzene derivatives upon angled irradiation with a LPL beam (λ = 488 nm); the motion was attributed to an anisotropic softening of the matrix.[727,728]

With SRG, local photopatterning, and DPM, we mainly considered until now the mass migration of objects caused by the photoalignment of azobenzene derivatives. In the upcoming sections, we will consider the shape deformation of objects that are not the consequence of such alignment, but rather caused by either the geometry or polarity change of the photochromic molecule. We will first start with amorphous polymers, then consider liquid crystalline systems, and we will end this chapter with the macroscopic motion of molecular crystals.

2.5.2. Photoactuation in amorphous polymers

As it will be seen in Section 2.5.3, liquid crystalline systems are usually the materials of choice for photoactuation, mainly because only a small quantity of photochromic moieties are sufficient to induce a huge shape change of the object. However, the first examples of macroscopic motion were based on amorphous systems.

We will start the discussion with non-crosslinked materials. To the best of our knowledge, the first example of the photoinduced contraction of an azomaterial was reported by Merian in 1966, [729,730] where he observed that a 140 cm long dyed acetate fabric containing an azobenzene derivative contracted upon irradiation of about 1.2 mm (that is, approximately 0.09 %), and that a 30 cm long dyed piece of Nylon fabric contracted of about 0.33 mm (approximately 0.1 %). In 1980, Blair and Lau reported the contraction of Nylon-6,6 film, dyed with either β-carotene or cyanostilbene, by 0.6 % and 0.8 % of their original size, respectively.[731] The study of non-crosslinked amorphous azomaterial was then abandoned, until the beginning of the 2000s. Zhang, Hu, and coworkers also reported a few years back the bending of a silk fibroin fiber that was coated with an azopolysiloxane layer only on one side.[732]

Azobenzene derivatives are again the main photochromic moieties used in these systems, but one recent example by Zhang and coworkers use a bridged azobenzene derivative in a polyurea backbone (Figure 47a).[733] Due to its structure, the bridged azobenzene derivative is more stable in its *cis* form. Hence, upon

irradiation with blue light (λ = 405 nm), the *cis*→*trans* isomerization takes place, leading to an anisotropic expansion of the material. The process is reversible with the irradiation using green light (λ = 532 nm) (Figure 47b). The authors prepared a film of the material, and indeed observed the reversible bending of the film upon alternative irradiation (Figure 47c and d).

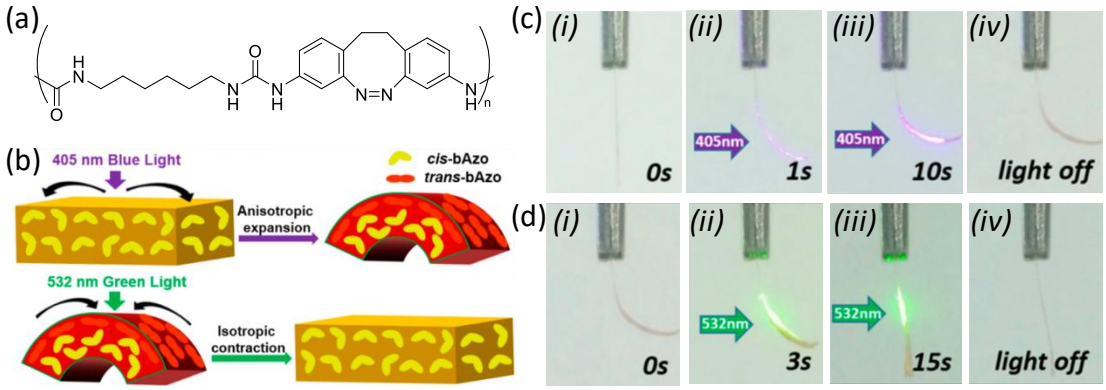

Figure 47: (a) Chemical structure of a light-responsive polyurea with a bridged azobenzene derivative. (b) Scheme of the mechanism of reversible deformation of the azomaterial upon irradiation. (c) Bending of the azopolymer film upon blue irradiation, and (d) reverse motion upon green light irradiation. The length of the film is approximately 2 cm. Parts (b-d) are adapted with permission from reference [733], Copyright 2018 American Chemical Society.

Athanassiou *et al.* reported the bending of a polyacrylate film doped with spiropyran derivatives[734–736] that they attributed to the aggregation of the merocyanine isomers (Figure 48).

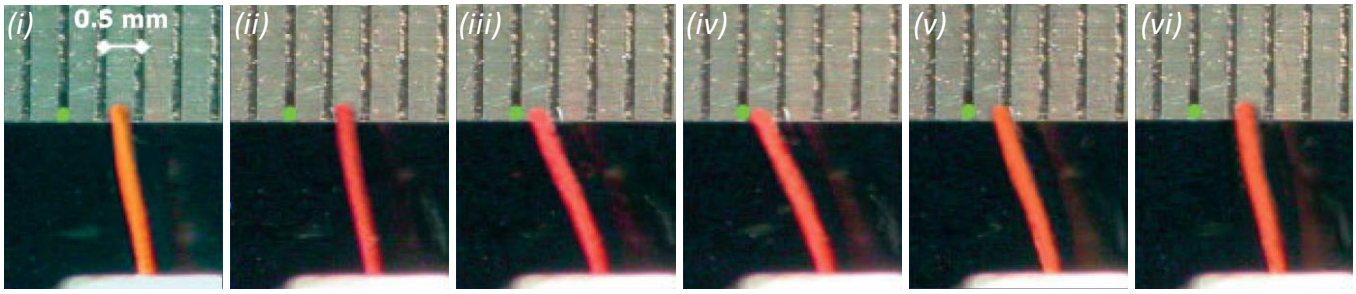

Figure 48: Bending of a film made of a polyacrylate doped with spiropyran derivatives. The irradiation is done on the left side of the material. *(i)* Initial shape. *(ii)* After 10 UV pulses (λ = 308 nm). *(iii)* After 20 green pulses (λ = 532 nm). *(iv)* After 40 green pulses. *(v)* After 100 green pulses. *(vi)* After 160 green pulses. Reproduced with permission from reference [734], Copyright 2005 John Wiley and Sons.

Barrett and coworkers reported the deflection of an AFM cantilever coated with an azopolyacrylate upon irradiation.[737] Endo and coworkers reported the use of poly(vinyl ether) blends containing azobenzene derivatives as side chains, either with a polycarbonate[738] or poly(caprolactone).[739] In the former case, they observed the reversible expansion of the stretched film upon irradiation, which they explained by the disaggregation of the *trans* isomers;[738] in the latter case, they observed an anisotropic photomechanical response of the stretched film, that is a contraction in the direction parallel to the stretching force and an expansion in the orthogonal direction.[739] They explained this behavior in a way similar to that of the liquid crystalline networks, which will be discussed more thoroughly later. Briefly, isomerization of the azobenzene derivatives that are in the "oriented" amorphous phases (because of the stretching force) lead to an isotropization of the domains, and therefore to a contraction in the parallel direction and an expansion in the perpendicular direction of the stretching force. For the same reasons, Shepherd and coworkers also used a stretching step before irradiating their azopolyurethane film for actuation; moreover, the addition of hydrogen-bonding units in the system resulted in a self-healing material.[740] Recently, Naumov, Wu, and coworkers reported the sunlight-driven bending of a film based on an azobenzene derivative in agarose,[741] following previous studies on dual humidity- and light-sensitive polymeric films.[742,743] Theato and coworkers presented a composite system where the azopolymer is coated onto polypropylene fabric.[744] Fang, Yu, and coworkers described a system with a shape-memory effect (SME) based on a polyurethane doped with an azobenzene derivative and graphene oxide, where a second temporary shape can be achieved via UV irradiation.[745] Zhang and coworkers

observed the bending of an azopoly(amic acid) as well.[426] Kuzyk and coworkers studied the bending of a PMMA fiber doped with azobenzene derivatives.[746,747]

Polymer networks containing photochromic units have also been investigated for their photomechanical behavior. Examples of the photoactuation of dry covalent networks (as opposed to gels and supramolecular systems) are quite scarce, probably because the crosslinking reduces the mobility of the chains. Zhang and coworkers reported the bending of a recyclable azopolyacrylate crosslinked with disulfide bonds.[748] Endo and coworkers, studied the photomechanical response of interpenetrated polymer networks of azopoly(vinyl ether) and polycarbonate,[749,750] obtaining the same mode of deformation as discussed earlier for their blend systems.[738]

Gels have been way more studied as photoactive networks and we will detail hereafter some examples. While pNIPAAm networks incorporating spiropyran moieties are the most common examples (*vide infra*), some examples deal with azobenzene derivatives.[751–757] For instance, back in 1984, Ishihara *et al.* reported the reversible swelling/shrinking behavior of an azopoly(hydroxyethylmethacrylate) having free hydroxyl groups.[754] They attributed this phenomenon to the fact that, upon UV irradiation and formation of the *cis* isomer, the hydroxyl groups of the polymer will preferentially interact with the polar azobenzene isomer than with water. Water being then driven out of the gel, shrinkage of the material is the direct macroscopic consequence. More recent examples use azosurfactants,[758–760] also based on the polarity switching of the photochromic molecule. A recent example by Hosono, Watanabe, Horie, and coworkers uses a rigid poly(amic acid) backbone bearing an azobenzene derivative (Figure 49a).[761]

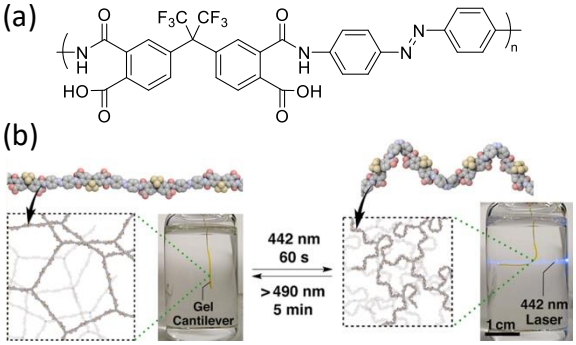

Figure 49: (a) Chemical structure of the poly(amic acid) bearing azobenzene units in the main chain. (b) Bending of the corresponding gel upon irradiation with blue light, because of the contraction of the rigid polymer backbone. The insets show the structure of the gel and the macromolecule. Part (b) is reproduced with permission from reference [761], Copyright 2013 American Chemical Society.

Upon irradiation with blue light (λ = 442 nm), the macromolecule contracts, leading to the gel shrinkage, and they observed the bending of the material (Figure 49b). Additionally, Neckers and coworkers reported a system with a spirooxazine derivative, with a similar behavior to the spiropyran-based ones.[762] Also, the same group presented the use of a superabsorbent polymer with an azobenzene moiety to cause water expulsion from the gel upon irradiation.[763]

The photomechanical motion of pNIPAAm-spiropyran gels is based on simple reversible shrinking/swelling behavior. Then, the design of the material can be tuned to obtain other modes of motion.[764–768] For instance, Sumaru and coworkers prepared rod-like gels of this material that bent upon irradiation (Figure 50a).[765] The proposed mechanism is the following: when dissolved in acidic water, spiropyran derivatives isomerize spontaneously to their protonated merocyanine form, which is easily solvated by water because of its polarity. Upon irradiation with blue light (λ = 436 nm) to induce the ring closure, the spiropyran isomer (more hydrophobic) is obtained; this leads to the dehydration of the chain, and, hence, the gel shrinkage (Figure 50b).

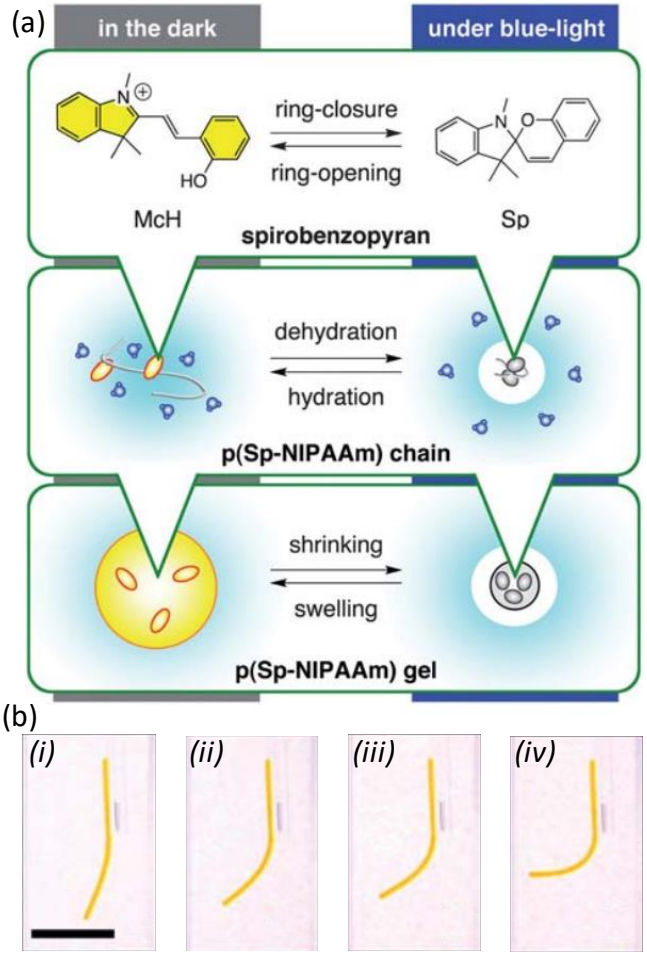

Figure 50: (a) Mechanism for the reversible swelling/shrinking behavior of pNIPAAm-spiropyran gels. (b) pNIPAAm-spiropyran rod-like gels at different stages of shrinking. The irradiation with blue-light (λ = 436 nm) was conducted from the left-side of the material. Scale bar: 5 mm. Adapted with permission from reference [765], Copyright 2005 The Royal Society of Chemistry.

Some reports attempted to enhance the efficiency of this effect.[769,770] For instance, Diamond and coworkers introduced PEG porophores in the material and removed it after the polymerization. The increased porosity facilitated the motion of water in and out of the material, overall increasing the kinetics of the shrinking/swelling behavior.[769] Another interesting example of material design has been reported

by Florea and coworkers, who presented the unidirectional motion of a bent pNIPAAm-spiropyran gel (the "walker") on a (macroscopic) ratcheted surface (Figure 51).[771]

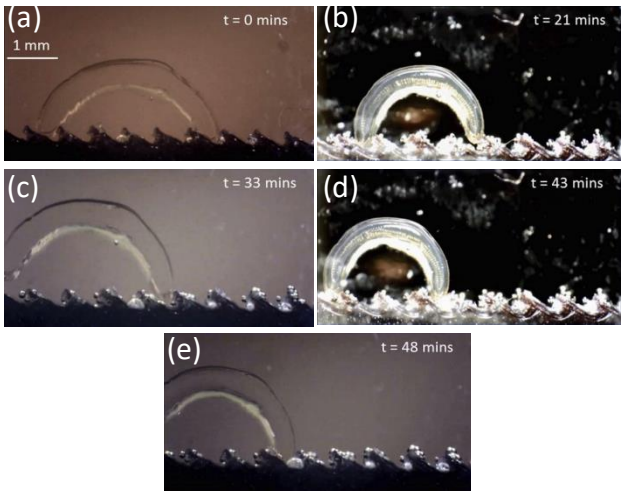

Figure 51: Unidirectional motion of the "walker" based on pNIPAAm-spiropyran. (a) Initial state. (b) and (d) Contraction of the gel under white light. (c) and (e) Swelling of the gel in the dark. The unidirectional motion is due to the ratcheted geometry of the surface. Adapted from with permission from reference [771], Copyright 2017 Elsevier.

As stated earlier, it is necessary to work in acidic conditions to ensure that the spiropyran moiety is mainly in its protonated merocyanine form. The necessity of an acidic aqueous solution can be overcome by copolymerizing acrylic acid in the polymer,[772,773] providing an internal source of protons to the gel. Moreover, it is possible to swell the material in an ionic liquid (IL), to form a so-called ionogel.[774–777] The advantage of ILs resides in their stability, low vapor pressure, and that their properties are easily tunable by changing the cation and/or the anion,[778] and incorporating these properties into "solid" gel structures could be advantageous.[777]

The main investigated application of pNIPAAm-spiropyran gels were made in the field of microfluidics.[774,779–784] An interesting example has been reported by Sumaru and coworkers.[783] The authors created on-demand microchannels on a microfluidic device by irradiating it with a micropatterned

light beam (λ = 436 nm), causing the localized gel shrinkage (Figure 52). It is not, however, the only example of applications that have been published. Schenning, Esteves and coworkers reported the functionalization of a cotton fabric with the gels[785] and the irradiation decreases the diameter of the fibers. The theoretical study of the mechanism of the photomechanical response has been investigated on these gels,[786–788] and, interestingly, some papers were published where the authors computationally designed devices based on this material.[789–791]

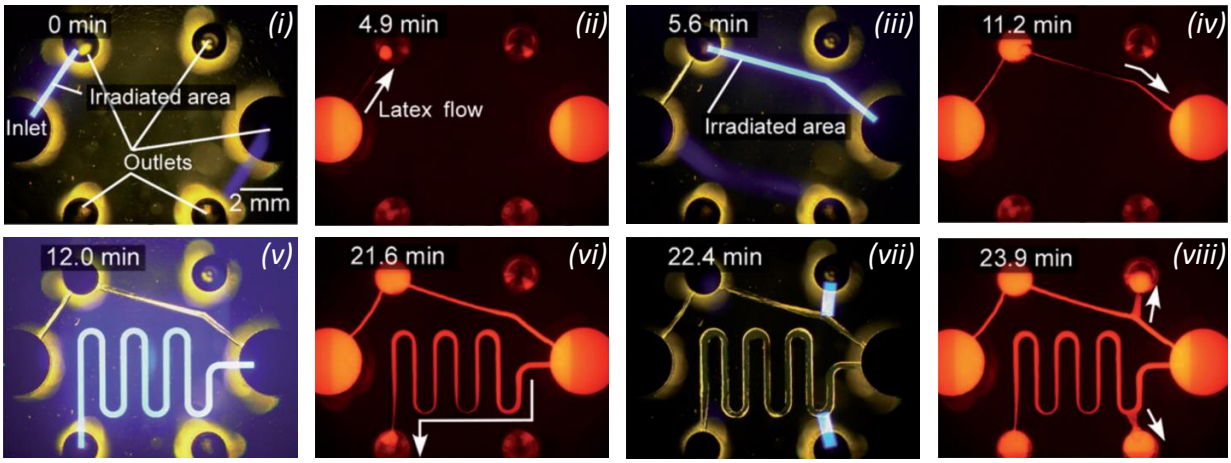

Figure 52: On-demand formation of microchannels in a microfluidic device based on pNIPAAm-spiropyran hydrogel observed by fluorescence microscopy. In *(i)*, *(iii)*, *(v)* and *(vii)*, the light blue area represents the irradiated area (λ = 436 nm) where the gel is locally shrunk. In *(ii)*, *(iv)*, *(vi)* and *(viii)*, the red areas are caused by fluorescing latex beads, and the direction of the flow is indicated by the white arrows. Adapted with permission from reference [783], Copyright 2001 The Royal Society of Chemistry.

Finally, we will here discuss examples of amorphous supramolecular systems. Feng, Feng, and coworkers reported a supramolecular azobenzene/polyimide assembly.[792] The cast film was initially oriented with LPL so that the cut films spontaneously form helices. However, the photoinduced deformation was done under unpolarized UV light (λ = 365 nm), inducing a stretching of the helices (Figure 53).

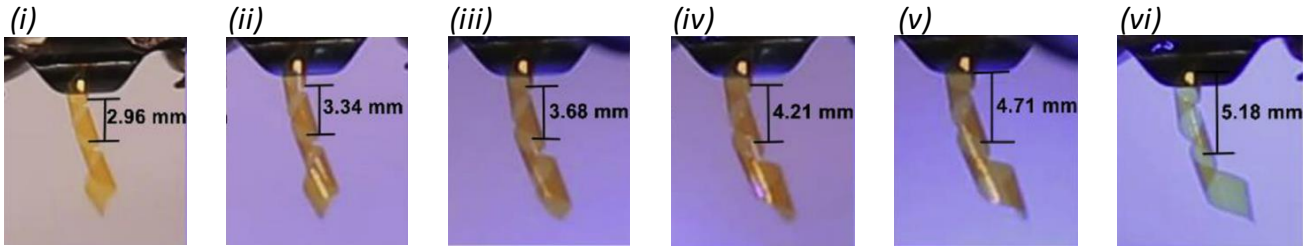

Figure 53: Augmentation of the helical pitch of the supramolecular azobenzene/polyimide assembly under UV irradiation (λ = 365 nm). 5 min separate image *(i)* from image *(vi)*. Adapted with permission from reference [792], Copyright 2019 Elsevier.

Feng and coworkers also reported the use of a supramolecular assembly of a polyammonium with an anionic azobenzene derivative to form films bending upon irradiation.[793,794] A supramolecular device designed as a "hand" by Feng, Feng, and coworkers has also been described.[795] Zhang, Li, and coworkers presented the use of the α-cyclodextrin (CD)/*trans*-azobenzene complex to form a supramolecular material with a shape-memory effect.[796] The mechanism is as follows: the material has an initial shape, and the *trans*-azobenzene forms crosslinking points with α-cyclodextrin, along with other physical crosslinking points between carbonyl groups and calcium ions (Figure 54a).

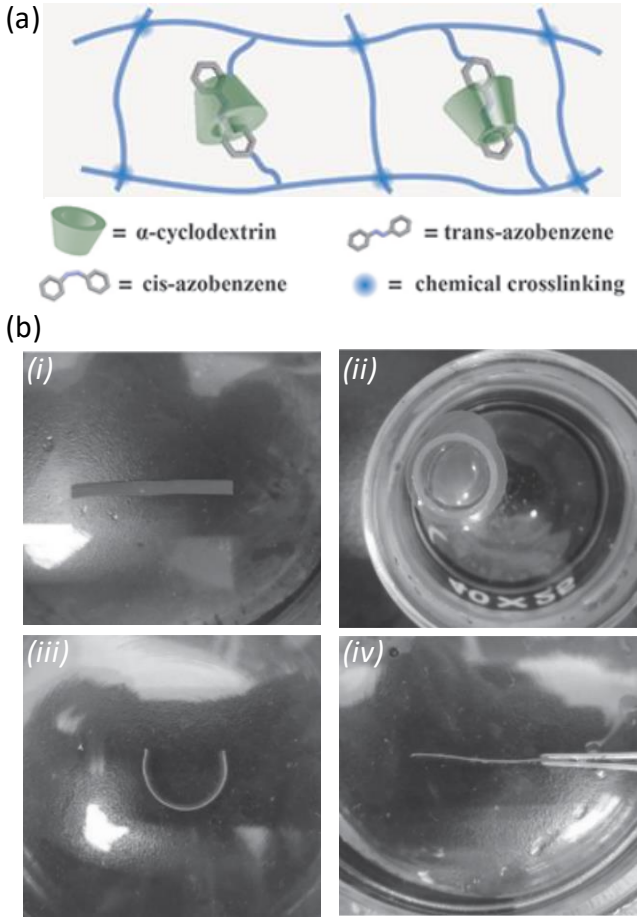

Figure 54: (a) Schematic representation of the polymer network containing both chemical and supramolecular crosslinks. (b) Shape-memory effect in a supramolecular material based on α-cyclodextrin and azobenzene. *(i)* Initial shape. *(ii)* Deformed shape fixed by UV irradiation (λ = 365 nm) followed by visible light irradiation. *(iii)* Temporary shape. *(iv)* Recovery of the initial shape upon irradiation with UV light (λ = 365 nm). The film has a length of approximately 2.5 cm. Part (b) is reproduced with permission from reference [796], Copyright 2016 John Wiley and Sons.

Upon UV irradiation (λ = 365 nm), the *cis* isomer is formed, so as the complex with the CD is broken with a subsequent deformation applied to the material. While the object is still deformed, visible light or heat is applied, forming the *trans* isomer back, and new complexes with CD are made, fixing the deformed shape. When the mechanical stress is removed, the material recovers a part of its initial shape, but is still

deformed overall (temporary shape). Then, upon irradiation with UV light, these azobenzene/CD complexes will break again, and the material fully recovers its initial shape that has been "memorized" by the carbonyl/calcium crosslinking points (Figure 54b).[796] Sun and coworkers also reported the photoinduced bending of a LbL film containing azobenzene moieties.[797]

As discussed in this section, amorphous polymers are already interesting to achieve a variety of mechanical deformation. We will now discuss LC systems in which only a small fraction of actuating molecules can induce a large-amplitude, macroscopic deformation.

2.5.3. Photoactuation in liquid crystalline elastomers

Liquid-crystalline elastomers (LCE) are slightly cross-linked networks incorporating mesogenic moieties, which can form materials characterized by their flexibility and their anisotropy. Finkelmann and coworkers published in 2001 the first example of a LCE coupled to a molecular switch, and they demonstrated its reversible contraction upon UV irradiation.[798] The amplification of the mechanical motion in such materials is induced by the disorder brought along the *trans→cis* isomerization of azobenzene derivatives involved as cross-linking units. This seminal paper is at the origin of a whole class of photoresponsive materials which have been intensively investigated over the years. In the following part of this review, we will focus on such LCEs containing photoswitches and capable of large actuation upon light irradiation. We will first explain the functioning principle of those systems and detail the various parameters that may influence their mechanical behaviour. Then, we will present different examples of complex motions together with the corresponding applications that have been achieved using those compounds. We will highlight here some of the most important examples, but the reader can also refer to a number of reviews already covering this particular topic. [643,645,799–810]

Motion in LCE can be easily achieved by perturbing the natural alignment of the mesogens using various stimuli. In the case of photoresponsive LCE, a molecular switch is introduced in the network, as

a main constitutive unit or as a doping agent and, most of the time, all the components are linked together by a polyacrylate polymer. Their synthesis often involves the use of a photoinitiator such as bis-acylphosphine oxide. H. Zhang and co-workers investigated the elaboration of unorthodox linkers,[811] to induce a reversibility in the network,[748] or to form a cross-link based on supramolecular interactions[812]. As already mentioned, the first switch integrated into an LCE matrix was an azobenzene derivative which remains nowadays predominantly used in this area. The main mechanism for the actuation of the material is closely related to the disorder brought by this photoswitch. Indeed, the *trans* isomer of the azobenzene, with its elongated shape, can easily pack with the liquid-crystal moieties and thus stabilize the nematic phase. Conversely, the corresponding *cis* isomer possesses an angled structure and therefore destabilizes this organisation. Consequently, the phase transition temperature will be lowered upon the *trans*-*cis* isomerization of the photoswitches and, as a result, the nematic phase becomes isotropic in an isothermal manner (Figure 55). Nanoscopic shifts of alignment at the surface are subsequently translated macroscopically by an expansion or a contraction of the material, depending of the director orientation, a subject closely investigated by Ikeda and co-workers.[813,814]

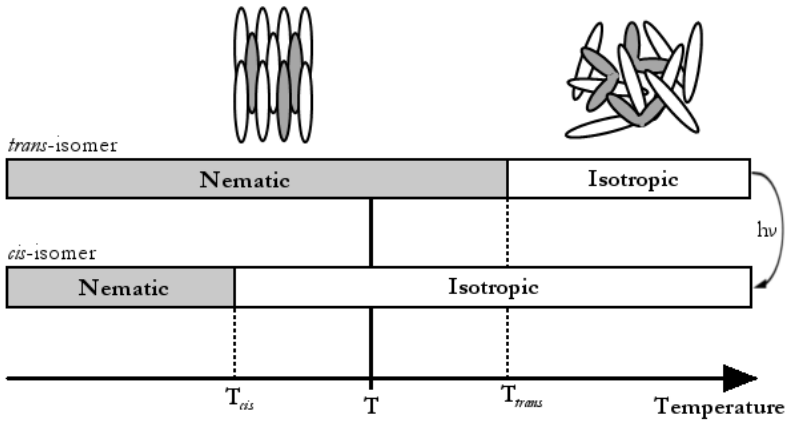

Figure 55: Phase transition temperature of a LCE involving *trans*- (T_{trans}) and *cis*-azobenzene (T_{cis}), T: Isothermal phase transition by photoisomerization.

In all cases, the liquid-crystalline network contracts in the direction parallel to the director and expands in the direction orthogonal to it. As a consequence, when the mesogens are oriented parallel to the irradiated surface, the material contracts upon light exposure. With an homeotropic alignment, however, the material expands, as it has been reported in details by Ikeda[813,814] and by White & Broer (Figure 56).[815] More complex deformation can be achieved with a proper patterning of the orientation of the LC phase, moreover, splayed alignment of the material (homeotropic on one face, planar on the other) may be used to obtain a fast, large amplitude actuation.[816–819]

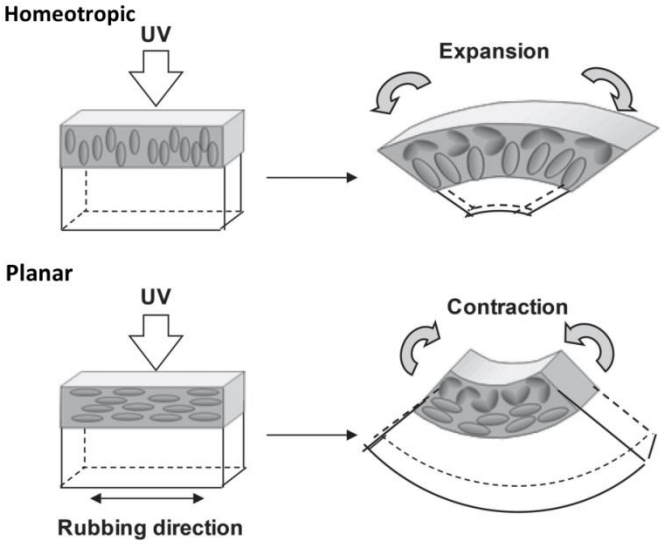

Figure 56: Proposed mechanisms for the expansion or contraction motions obtained for azobenzene-containing LC materials with homeotropic and planar alignment, respectively. Reproduced with permission from reference [814], Copyright 2014 John Wiley and Sons.

The whole process is completely reversible as the azobenzene can easily isomerize from *cis* to *trans* thermally (or under visible light) and therefore, LCE can reorganize back. Obviously, a rise of the surface temperature would have had a similar effect. As it has been stated in the introduction of this chapter (2.1), collective motion solely induced by photothermal effect[817] will not be addressed in this review. However, this phenomenon should not be overlooked so quickly. Indeed, even if the isomerization of a photoswitch

should, in theory, lead to an isothermal phase transition by destabilizing the mesogens organization, one cannot avoid a local rise of temperature at the surface induced by the absorption of light. Therefore, any collective motion in LCE systems involving a photoswitch might involve a synergy between photomechanical and photothermal effect. Interestingly, it is also possible to strongly limit the thermal process by substituting the *ortho* positions of azobenzenes by fluorides; the obtained LCE are thereby shape-persistent and can maintain their form for days.[335,820] In order to generate a unidirectional bending of the material, two main approaches have been developed so far. The first one, popularized by Ikeda and coworkers, consists in using linearly polarised light to induce a selective isomerisation of the azobenzene units based on their respective orientation.[821] The second one is based on the control of the mesogens global alignment. In this case, one can distinguish the use of a pre-organized surface from the application of an external force. The former consists of a "command surface" on which the LCE is simply deposited. The mesogens will then align themselves spontaneously without any other external stimulus, before being cross-linked, thus fixing their configuration.[817,822–825] Conversely, the latter requires the application of a force on the network. To that end, one way consists in stretching unidirectionally the LCE film while heating it (Figure 57).[826] The main drawback of this method lies in the lack of reversibility. Once irradiated by UV light, the formed isotropic phase loses the memory of the initial main director of the LCE. Thus, even after visible irradiation and recovery of the nematic phase, the obtained bending will not be exactly similar. To tackle this issue, it is possible to reticulate the material after stretching, thus trapping the LCE in a chosen organization. Shear forces during the viscous flow of the material, for instance in a microfluidic device, may also be sufficient to induce uniform alignment before reticulation.[827]

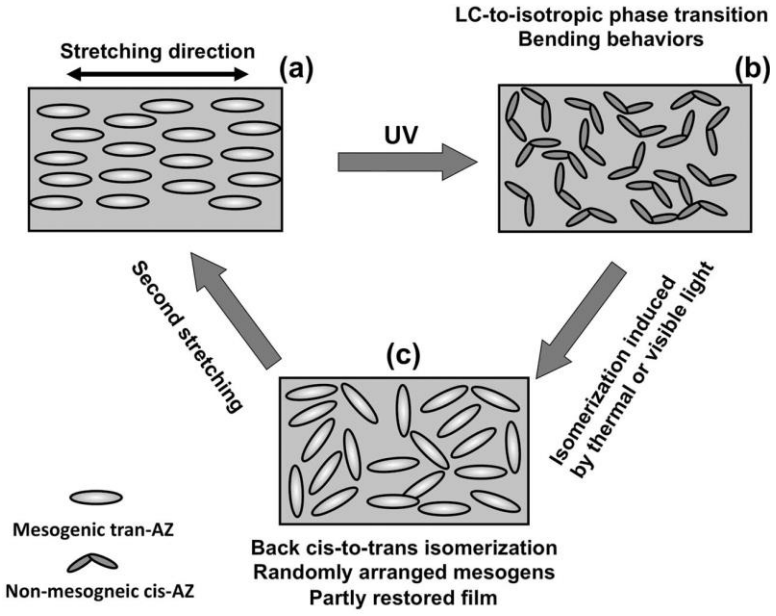

Figure 57: (a) Alignment along stretching direction (b) Photoisomerization upon UV exposure, formation of isotropic phase (c) Thermally- or light-triggered isomerization leading to restoring of the nematic phase. However, the global alignment is lost. Reproduced with permission from reference [826], Copyright 2011 John Wiley and Sons.

Ikeda and coworkers have shown that it is also possible to control the bending direction of a LCE film with linearly polarized UV light (Figure 58).[821,828] Indeed, as it has been described previously (section 2.4.1), polarized light can selectively isomerize microdomains of LCE with dipole moments parallel to the polarization direction, thus leading to an oriented contraction of the material.[829–833] Upon visible light exposure, it is then possible to revert the isomerization and to completely recover the material in its initial state. In that case it is interesting to mention that a unidirectional cyclic motion can be obtained by playing with the sequence of light polarizations and wavelengths, and thus leading to the increasing production of work and although extracted from purely reversible molecular switches which do not increase the work produced on their own scale.

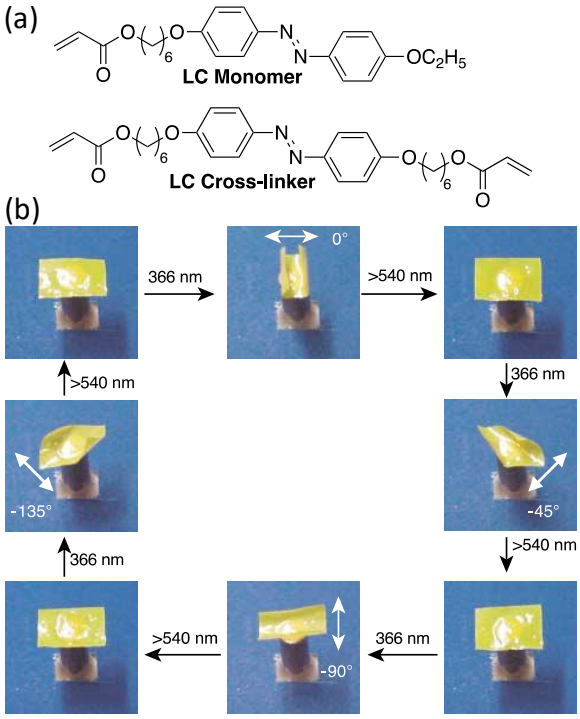

Figure 58: (a) Structures of the liquid crystalline monomer and cross-linking unit. (b) Pictures of a LC film actuated using a 366 nm linearly polarized light at, respectively, 0°, -45°, -90° and -135°. After bending, the film returns to its initial state by visible photoirradiation. The process is completely reversible. Part (b) is reproduced with permission from reference [821], Copyright 2003 Springer Nature.

More recently, another approach has been developed by the group of Katsonis.[834] It relies on a weakly chiral nematic phase in which the helical structures can be disrupted by the photoisomerization of an azobenzene cross-linker (Figure 59). In that case, the macroscopic actuation is highly dependent on the angular offset which can be defined as the angle between the mid-plane molecules orientation and the cutting direction of the material.[820,835] This time, the process is completely reversible upon visible light irradiation as there is no need to induce a global alignment of the mesogens as the glass substrate used is functionalized with a polymer to promote the directional alignment of the liquid crystal.

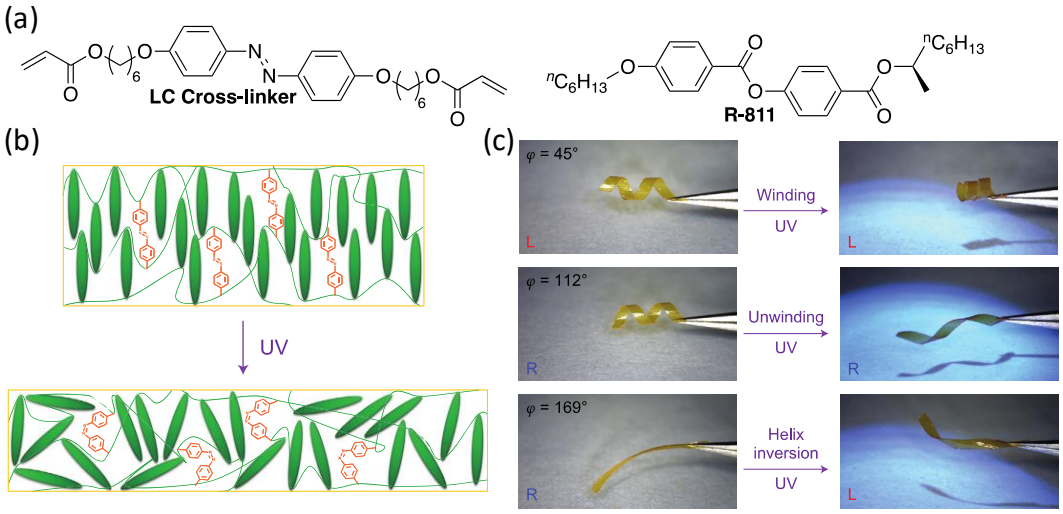

Figure 59: (a) Chemical structures of an azobenzene crosslinker and of the R-811 chiral agent used respectively to form right-handed helices in the LC network. (b) Illustration of the behaviour of the LC moieties upon irradiation with UV light. A decrease in the order parameter is observed leading to a contraction of the material along the director and an expansion in the perpendicular direction. (c) Pictures of different samples cut along various angular offsets (defined as the angle between the mid-plane molecules orientation and the cutting direction) before and after UV irradiation. Parts (b) and (c) are adapted with permission from reference [834], Copyright 2014 Springer Nature.

Various parameters have been investigated over the years in order to acquire a better comprehension of these mechanical behaviors. The research focused mainly on the influence of variables such as molecular switch concentration, relative position, topology in the network, size of the spacer, etc. As a result, it has been demonstrated that it is not necessary to introduce large amount of azobenzene to observe a modification of the mesogens alignment. Indeed, as low as 1 mol% already induce a macroscopic motion due to the cooperative collapse of the LCE nematic organisation.[719,836,837]

While the majority of the systems reported are based on chemically crosslinked polymer networks, a few materials also showed photoinduced actuation when crosslinked via supramolecular interactions[838–

[840] or not crosslinked at all.[841,842] Moreover, it has been proven that the connectivity of the photoswitch in the LCE greatly impacts the mechanical response of the material.[843,844] If employed as a cross-linking unit, the azobenzene triggers a stronger response than the same photoswitch used as a simple monomer.[836] Furthermore, it appears that the azobenzene moiety does not necessarily need to be covalently linked to the LCE network to generate a motion.[839] Finally, the length of the spacer between the azobenzene moiety and the acrylate linker also has to be taken into consideration.[845] Simultaneously, numerous studies have been done in order to investigate an approach to model and to predict the bending behaviour of such LCE.[846–851] Using DFT calculation, they have studied the influence of various parameters such as light intensity, density of mesogens, as well as orientation,[852–855] but also the different mechanisms involved in the generation of such motion.[238,856–859] Despite their demonstrated potential, photoisomerization of classical azobenzene moieties in LCE can nevertheless face limitations related to the use of UV light, such as photodegradation and/or formation of $^1O_2$, and novel chemical derivatives have been investigated.[804] Clark, Yang and coworkers report the use of an azobenzotriazole derivative (Figure 60a) in a polyurethane network.[860] Another example consists in using an azobenzene substituted with fluorides in the *ortho* positions of its aryl rings (Figure 60b).[335,818] The *trans→cis* isomerization occurs under blue-light energy, and the reverse interconversion under green light. A third approach involves an azobenzene derivative commonly named azotolane,[861] where an alkylbenzene is linked to the *para* position of one of the azobenzene aryl rings. In that case, visible light is used to trigger both *trans→cis* and *cis→trans* isomerization.[862,863] This photoswitch has been used in some actuators,[864] but it really stands out by its incorporation to infrared (IR) responsive LCEs. Indeed, Y. Yu and collaborators managed to create a LC material constituted by azotolanes doped with upconversion nanophosphors (Figure 60c).[865]

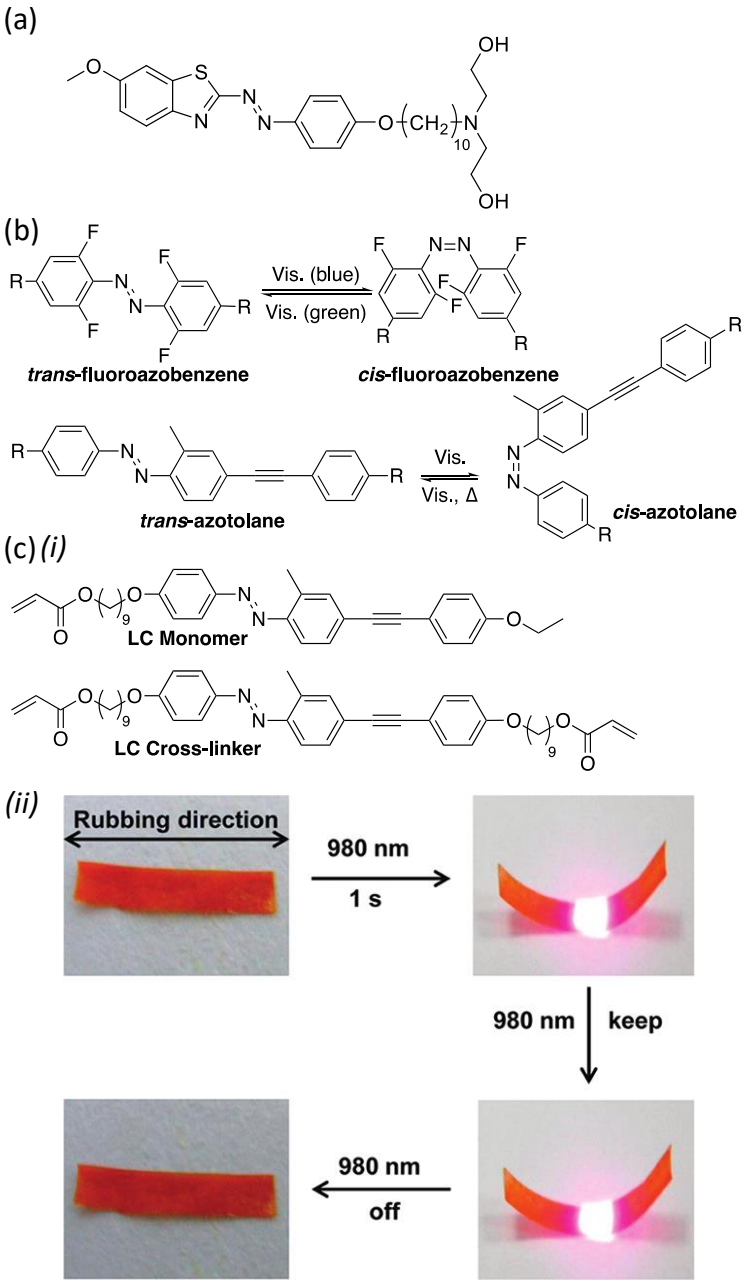

Figure 60: (a) Chemical structure of the azobenzotriazole used within a polyurethane network. (b) Photoisomerization of the *trans*-fluoroazobenzene and *trans*-azotolane derivatives. (c) *(i)* Chemical structures of the azotolane monomer and cross-linker used to form LC films, *(ii)* Pictures of a LC film containing *trans*-azotolane and macroscopic response observed upon irradiation at 960 nm, bending occurs toward the light source. Part (c) is adapted with permission from reference [865], Copyright 2011 American Chemical Society.

The latter is composed of sodium yttrium fluoride as well as thulium cations (Tm^{3+}), which are able to absorb light at 980 nm and to re-emit it at a lower wavelength. The peak of emission around 475 nm corresponds to the limit of the photoswitch absorption spectrum. However, overheating by photothermal effect being a major issue, another alternative has been devised. It is based on triplet-triplet annihilation procured by a coupling between bis(diphenylphosphoryl)anthracene and platinum-tetraphenyltetrabenzoporphyrin.[866] In this system, the required energy input is lowered, thus reducing the heating of the sample. On the other hand, the wavelength of activation is also decreased to 635 nm in this very example. Finally, it is also possible to find some systems responding to UV, visible, and IR light. While it is possible to incorporate compounds displaying two-photon absorption and energy transfer,[867] they usually combine both photothermal and photoisomerization motion, where an IR absorbing compound, such as graphene oxide[745,868] or gold nanorods[869] is integrated into the LCE film.

To our knowledge, only two examples of LCE possessing another photoresponsive unit than azobenzenes have been described so far in the literature. The first one is based on hydrazone photoswitches and has been developed recently by the groups of Katsonis and Aprahamian (Figure 61).[870] Conversely to azo-LCE, the motion in this very system is not triggered by the modification of the order parameter but by the increase of tension in the polymer chain due to the change of shape of the hydrazone moiety upon isomerization. Therefore, this photoswitch has to be used as a cross-link agent, and not as a simple side-chain, in order to produce a bending of the material. Moreover, this hydrazine-based LCE is thermally stable over long period of time and is thus shape persistent.

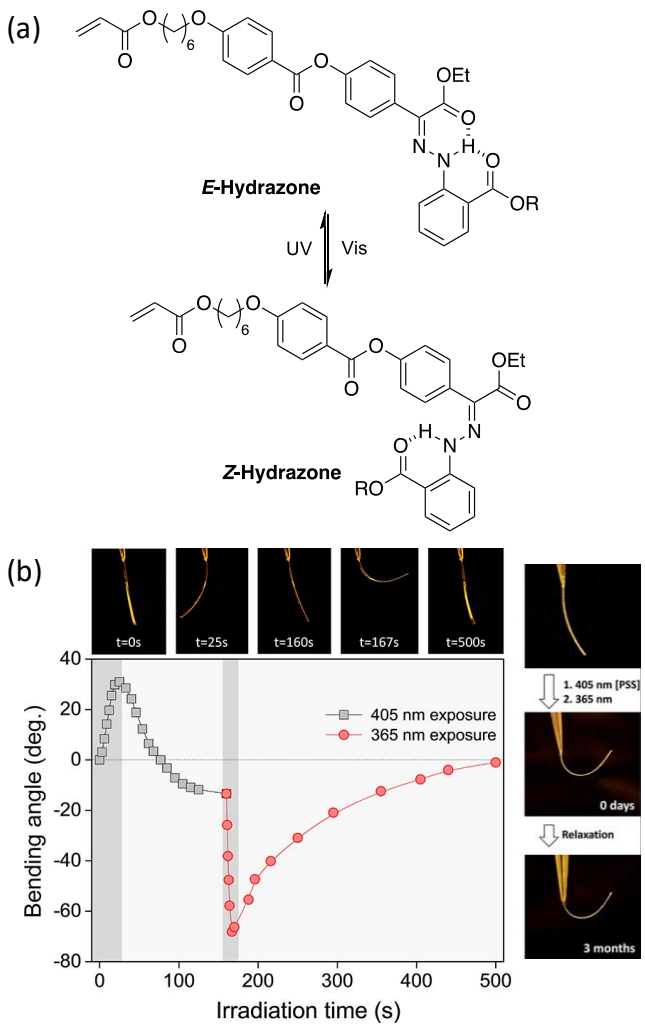

Figure 61: (a) Reversible photoisomerization of hydrazone. (b) Evolution of the bending angle of the hydrazone-based LCE over time upon exposure to light and shape persistency of the material after 3 months. Part (b) is adapted with permission from reference [870], Copyright 2019 American Chemical Society.

The second photoswitch integrated into such materials is an α-cyanostilbene derivative developed by H. Zhang and coworkers (Figure 62).[840] This novel system stands out as it is not covalently linked to the LCE and is also thermally stable. Even more interestingly, this material shows a configurable shape memory: a specific form can be created by localized UV irradiation and then, after mechanical stretching, this form can be obtained again through a simple heating process.

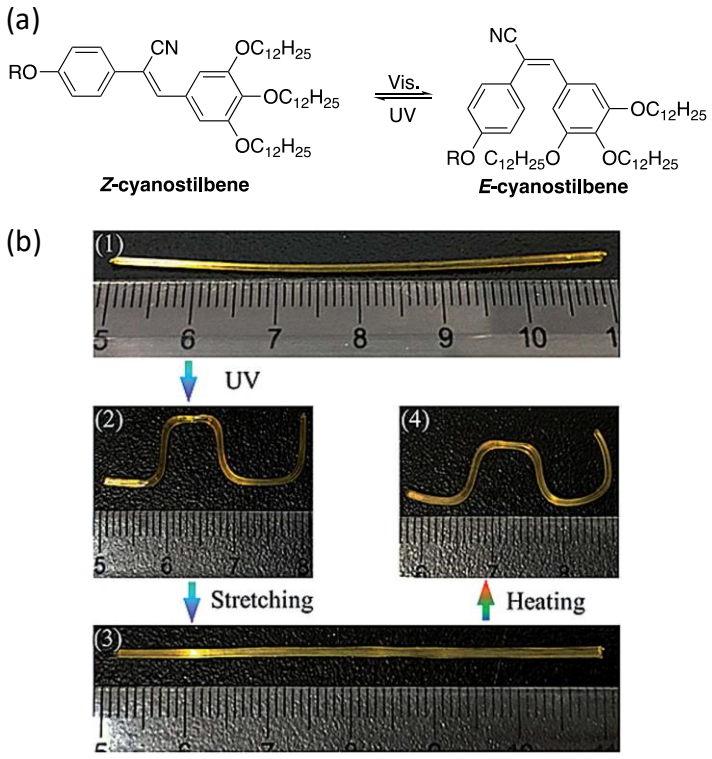

Figure 62: (a) Reversible photoisomerization of cyanostilbene. (b) Shape memory of the cyanostilbene-based material. Part (b) is adapted with permission from reference [840], Copyright 2013 The Royal Society of Chemistry.

Applications of light-induced collective motion in LCE can take different aspects and be used for various purposes; the research in this area has been fruitful for the past 20 years. Many examples are reported in the literature and we will now try to offer an overview of what has been done so far. The majority of the papers related to mesogens integrating azobenzene derivatives and generating motion upon light exposure are restricted to the simple bending[718,748,811,812,841,871–880] or change in volume of a LCE film.[881,882] However, structures involving more complex movements have also been developed, and many reviews are already covering this topic.[799,800,804–806,810,883–889]

Katsonis et al. achieved a biomimetic complex actuation with LCE incorporating azobenzene derivatives.[890] Its design relies on alternating stripes of different order parameters. The liquid-crystalline mixture is sandwiched in a glass cell coated with a rubbed polyimide layer, which induces a parallel orientation of the mesogens at the surfaces. In a first photopolymerization step under UV light through a photomask, bars of low order are crosslinked because of the concomitant *trans*→*cis* isomerization of azobenzene, reducing the order parameter of the liquid-crystalline mixture. In the second photopolymerization step, the photomask is removed, and the material is crosslinked under visible light where the photoisomerization of the photoactive unit does not occur, hence preserving the high order of the liquid-crystalline phase. The LCE is therefore composed of alternating stripes of high and low order parameters, which do respond equally under UV light; the highly ordered phase contracts along the director, while the low-ordered phase (almost) does not actuate. With a proper design of the film geometry, they obtained a fast actuation of the LCE because of the sudden release of potential energy stored during the irradiation, similar to the motion observe in chiral seedpods (Figure 63).

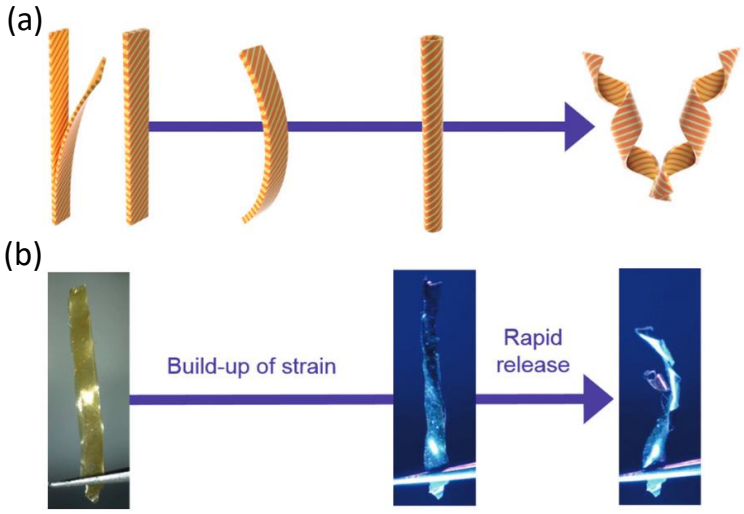

Figure 63: Fast actuation of a patterned liquid-crystalline elastomer due to the strain build-up, similar to seedpods. (a) Schematic representation of the deformation. The material consists of two stripes put together. Upon UV irradiation, a slight bending is observed and after further irradiation, the material forms a tube which will "pop" to release the strain stored in the material. The dark and light bars indicated low-

order and high-order regions, respectively. (b) Corresponding snapshots of the material. Dimensions: width ca. 770 mm, length ca. 1.2 cm. Reproduced with permission from reference [890], Copyright 2017 John Wiley and Sons.

In order to obtain a steady motion from the conversion of a continuous light exposure, two main strategies have been developed so far. The first approach rests on the irradiation of the LCE at two specific wavelengths, each one triggering a different interconversion of the photoswitch. Therefore, the azobenzene derivatives will constantly move from the *trans* to the *cis* isomer in a random manner. Macroscopically, it will be translated as a perpetual oscillating and chaotic motion of the material upon light exposure.[818,891–895] The most interesting example in this category is represented in Figure 64. Here, the presence of fluoride substituents allows the material to function under visible light instead of UV, reducing greatly its degradation over time.

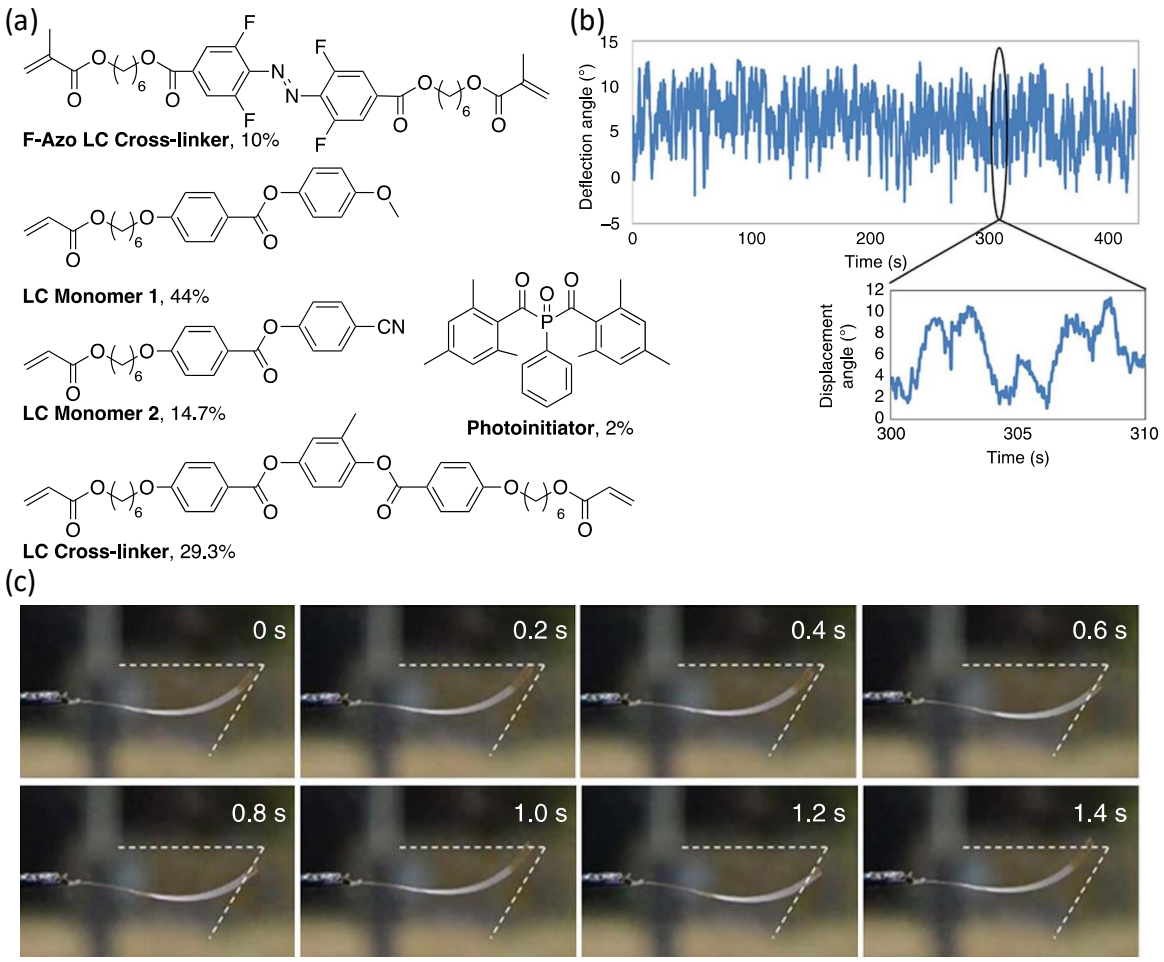

Figure 64: (a) Structures of the chemical components of the LC film and their respective ratio (in wt%). (b) Graph plotting the deflection angle versus time under sunlight exposure. (c) Pictures of the LC film under visible irradiation. Parts (b) and (c) are adapted with permission from reference [818], Copyright 2016 Springer Nature.

The second approach is also based on the irradiation of the LCE at two different wavelengths simultaneously, but not at the same position.[896] The system published by Ikeda and co-workers in 2008 can be considered as the first light-fuelled macroscopic motor based on LCE (Figure 65).[897] A film of LC mixture is deposited and cross-linked on an oriented substrate and then fixed around two pulleys of different sizes. On one side, the system is locally exposed to UV irradiation causing the contraction of the

material. On the other side, the irradiation of visible light leads to an expansion of the material. At the end, the synchronized motion generates a global rotational movement of the film around the pulleys, exposing unreacted parts of the film, hence the motor continues its course until one of the lights is switched off. One should insist on that such a system does not involve any molecular motor, as it is the case for other categories of materials such as some described in section 4.3, and that the continuous work produced here only comes from the differential macroscopic manipulations of simple molecular switches.

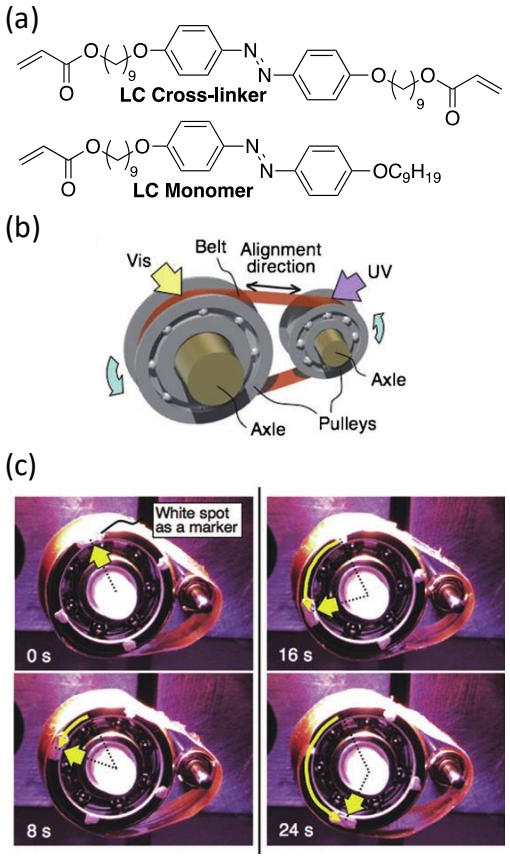

Figure 65: (a) Structures of the monomer and of the cross-linking agent. (b) Scheme of the experimental setup of the light-fuelled motor. A LC film is placed around two pulleys and irradiated by UV on one side and visible light on the other. Contraction of the film followed by its expansion allows the ribbon to move. (c) Pictures of the rotation of the motor overtime, the white spot can be used as a marker to follow the rotational motion. Parts (b) and (c) are adapted with permission from reference [897], Copyright 2008 John Wiley and Sons.

Even though continuous motions seem promising, only few examples involving LCE can be found in the literature. However, regarding stepwise motions, many more systems have been elaborated. In particular, the movement of structures through light irradiation has received a lot of interest in order to mimic systems found in nature or to develop soft actuators. One of the first published example concerns a UV-fuelled LCE able to swim at the surface of a solution,[898] and it is only in 2009 that the first example of a "walker" was elaborated (Figure 66).[899] Here, a film of photoresponsive mesogens is fixed on a substrate and then successively irradiated by UV and visible light. Upon UV exposure, the film expands towards the flat edge of the substrate, since the sharp side acts as a stationary point. Then the sample is irradiated by visible light causing the contraction of the material and its displacement in the same global direction. In the end, this UV-Visible cycle can be repeated numerous times in order to move the system over greater distances. More complex moving units have been synthesized since then, however their functioning remains usually based on a similar scheme. The interested readers can also refer to a number of published articles discussing other "walkers"[900–904] as well as rolling systems.[905–907]

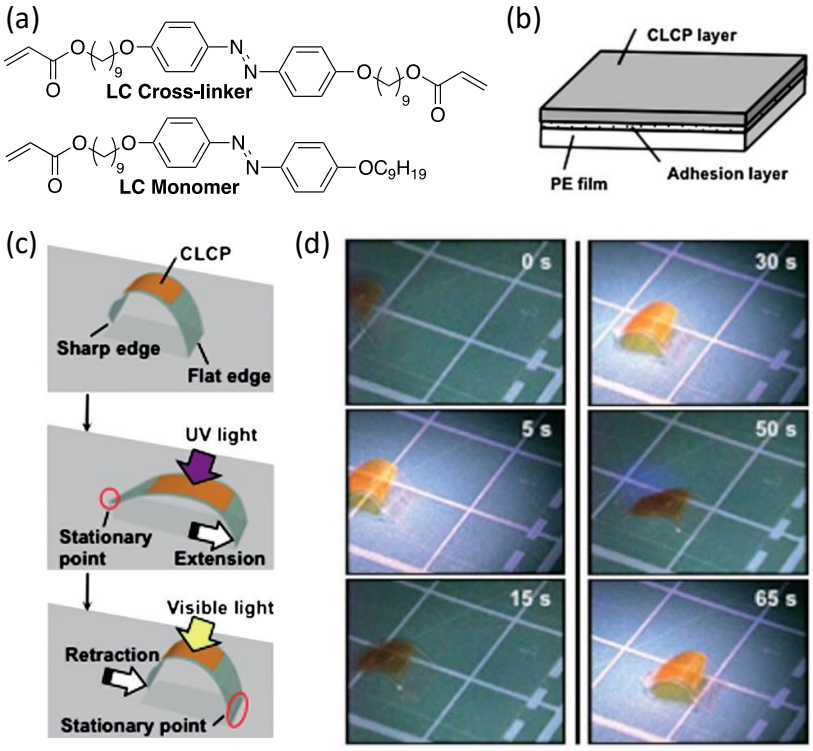

Figure 66: (a) Structures of the monomer and of the cross-linking agent used to form a LCE. (b) Schematic representation of the structure organization of the photomobile material. The Crosslinked Liquid-Crystal Polymer (CLCP) is attached to a PE film. (c) Illustration of the mechanism involved in the motion of the material. Upon UV irradiation, the LC film expands forward as the sharp edge acts as a stationary point. Then, when irradiated by visible light, the LC film contracts, and the material retracts toward a new stationary point. (d) Pictures of the LC film motion overtime, induced by the successive irradiation of the material by UV and visible light. Parts (b-d) are adapted with permission from reference [899], Copyright 2009 The Royal Society of Chemistry.

Photoresponsive LCE are particularly adapted to be used as soft actuators in the domain of soft robotics.[643,908,909] Indeed, being molecularly excited by light, these systems can be remotely controlled and do not need to possess wires or motors. An interesting system composed of successive LCE films, fixed on a polyethylene substrate and linked together by joints has been developed in 2010 by the group of Yu (Figure 67).[864] The photoswitch used is an azotolane, allowing the robot to be triggered by visible light. The local irradiation of the mesogens allows the system to pick, to hold, and to move an object weighting up to 10 mg, which is around 10 times its own weight. This structure does not show any sign of deterioration even after several uses.

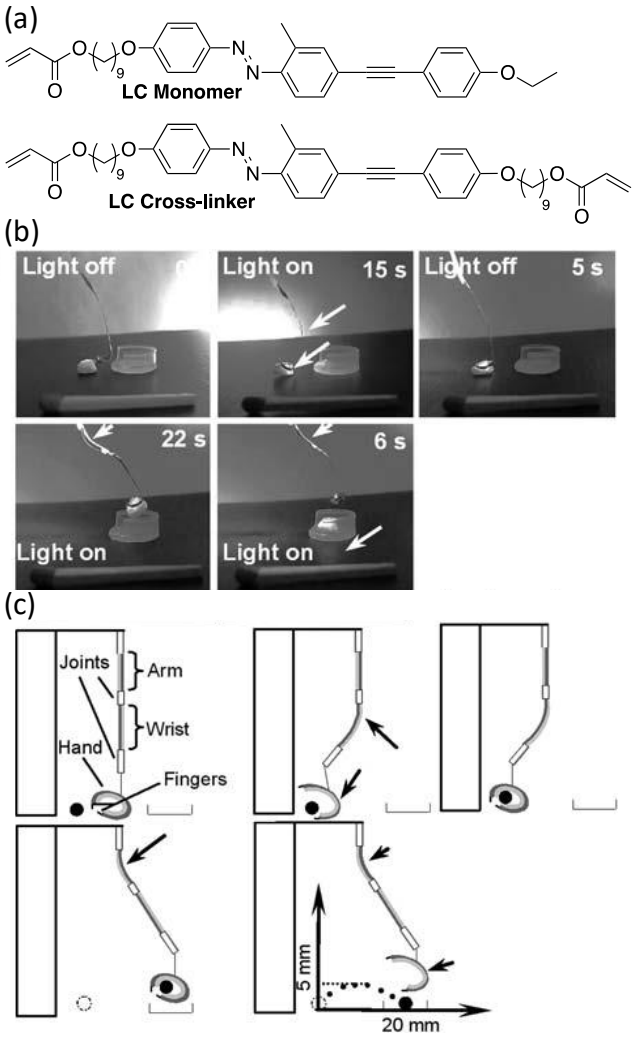

Figure 67: (a) Structures of the monomer and of the cross-linking agent used to form a mechanical arm, whose pictures in action are depicted in (b). (c) Schematic representation of the organization of the robots at different stages. The black arrows indicate the irradiated areas. Parts (b) and (c) are adapted with permission from reference [864], Copyright 2010 The Royal Society of Chemistry.

Since then, other examples of LCE clamp have been developed.[869,900,910] However, none of these systems are completely independent as a real robot should be, they still require controlled and localized irradiations to move in a coordinated manner. To this end, more complex systems have to be elaborated,[911] often inspired by what can be observed in nature.[912] For instance, a fully automated artificial flytrap has

been recently devised by Priimagi and co-workers.[913] Its chemical design is relatively simple as it is constituted by a photoresponsive polyvinyl alcohol substrate doped with azobenzene derivatives, leading to a material capable of contracting upon UV irradiation (Figure 68).

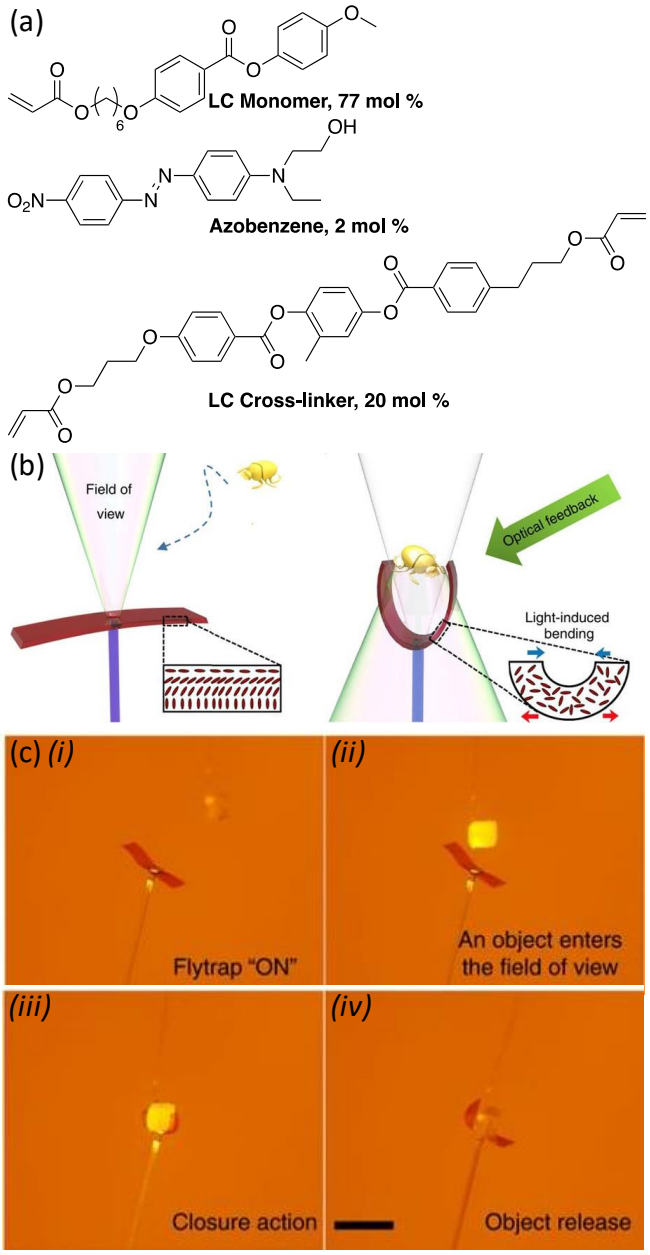

Figure 68: (a) Structures of the monomer and of the cross-linking agent, as well as the azobenzene dopant used to form a fully automated artificial flytrap. (b) Illustration of the system. At first, the object is out of the field of view, thus, it does not reflect the UV light; the trap remains inactive. Once the object is close

enough, the reflection allows the bending of the LC film, hence the trap is activated. (c) Pictures of the flytrap in action (Scale bar: 5 mm). The object is trapped and remains captured until the light is switched off. Parts (b) and (c) are adapted with permission from reference [913], Copyright 2017 Springer Nature.

An interesting trick was subsequently used in order to implement this material as a smart device: an optical fiber was inserted in a hole going across the material. In this configuration, when an object enters its field of view, the UV light coming from the centre of the film is reflected back, hence triggering the contraction of the material. The object can then be easily released by switching off the source of light. It is also possible to implement photoswichable LCEs towards the design micro-mechanical devices. The first example in this direction has been published by Oosten and co-workers, it corresponds to the elaboration of artificial cilia triggered by light (Figure 69).[914] This paper describes the formation, through a four-step process, of micro-structured cilia integrating a gradient of nitrobenzene concentration along the axis of each cilium. This variation of concentration allows the generation of a differential mechanical response depending of the irradiation wavelength. Upon UV exposure, only the portion containing the azobenzene cross-linker is bent. On the other hand, visible light leads to the isomerization of nitroazobenzene monomers, therefore creating a motion in the part of the material presenting an important concentration of this photoswitch. It is of course possible to combine both wavelengths in order to obtain a cumulative effect, as both interconversion will be triggered simultaneously. Light-triggered volume-change of cilia arranged in arrays have also been achieved,[915] as well as the thermocontrol of their photoinduced motion.[916]

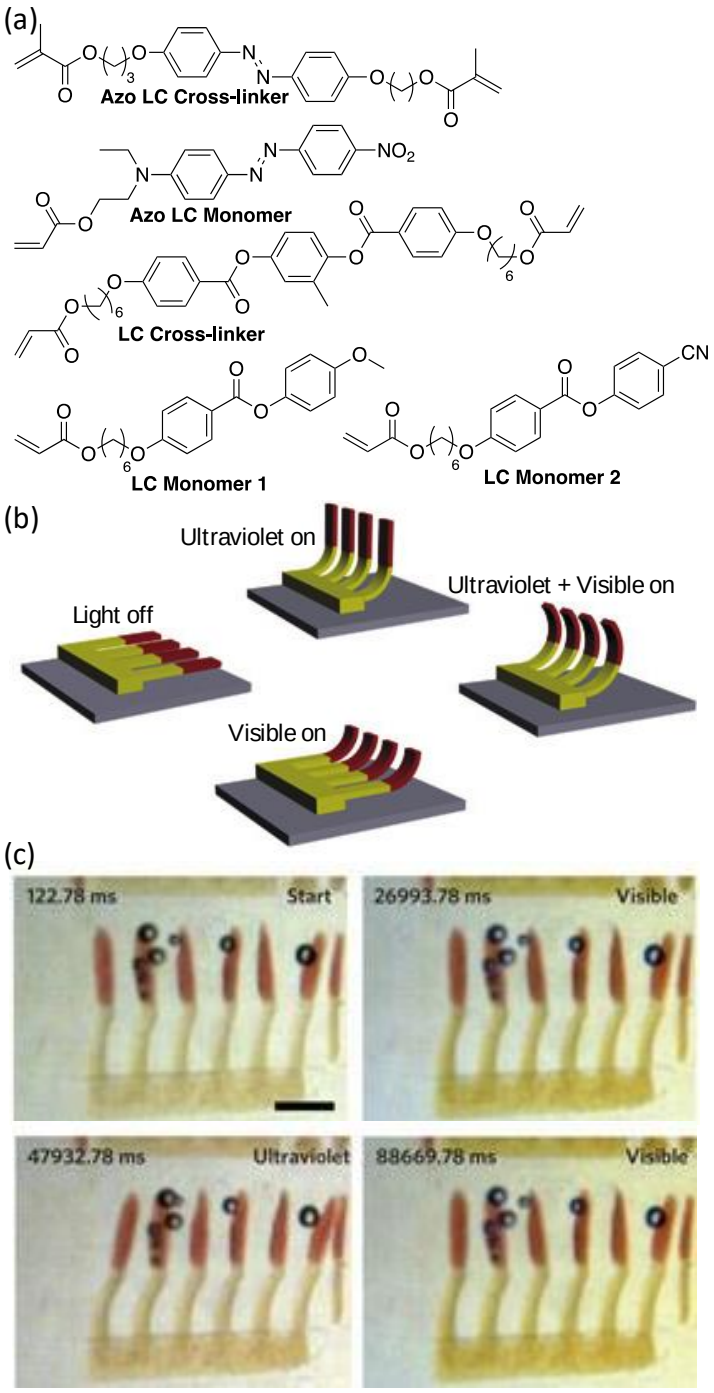

Figure 69: (a) Structures of two azobenzene derivatives used as cross-linking unit and monomer to form cilia. The two other molecules are used as a host LC matrix. (b) Illustration of the response of the material to different light irradiation. The red part contains mostly the nitroazobenzene-based LC monomer, triggered by visible light and the yellow portion is composed mainly of the azobenzene cross-linker, which

can be isomerized upon UV irradiation. (c) Pictures of the bending of the cilia as a function of light irradiation (scale bar: 0.5 mm). Parts (b) and (c) are adapted with permission from reference [914], Copyright 2009 Springer Nature.

Yu and coworkers processed photoactive liquid-crystalline films into microtubules resembling arteries. Irradiation with the side of a light beam, hence creating a gradient of illumination, causes an anisotropic extension of the cross-section of the tube; the resulting asymmetric capillary forces drive the motion of fluids in the tube towards the non-illuminated areas. The major advantage of this approach is that, since it relies on geometrical considerations, the photocontrolled motion could be achieved with a variety of different liquids and may therefore be of major interest in microfluidic systems.[917]

2.5.4. Molecular Crystals

We have presented until now the deformation of soft matrices incorporating photochromic molecules. Instinctively, it seems that achieving such motion in harder materials such as crystals might be complicated. It has however been reported, notably with systems based on diarylethene molecules.

The first example of the bending of a diarylethene crystal was achieved by Irie and coworkers in 2007, using a 1,2-bis-(thiazolyl)perfluorocyclopentene motif (Figure 70a).[918] The corresponding crystalline fiber bend towards the UV light source (λ = 365 nm) (Figure 70b), and with a force sufficient enough to move a gold microparticle (Figure 70c).

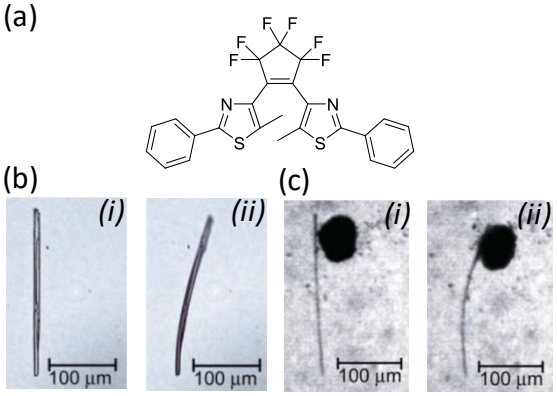

Figure 70: (a) Chemical structure of a diarylethene derivative used to form crystals. (b) Bending of this diarylethene crystal upon light irradiation (λ = 365 nm): (i) before and (ii) after UV irradiation. (c) The crystal deformation could move a gold microsphere (black spot): (i) before and (ii) after irradiation. Parts (b) and (c) are adapted with permission from reference [918], Copyright 2007 Springer Nature.

The same group later conducted crystallographic studies to correlate the molecular structure to the macroscopic motion.[919] They also studied a slightly different diarylethene derivative (Figure 71a) and determined the molecular packing of the corresponding crystal (Figure 71b). According to their experiments, the photochromic molecule is thinner once it is isomerized to its closed form, causing the macroscopic deformation in the c direction of the crystal (Figure 71c).

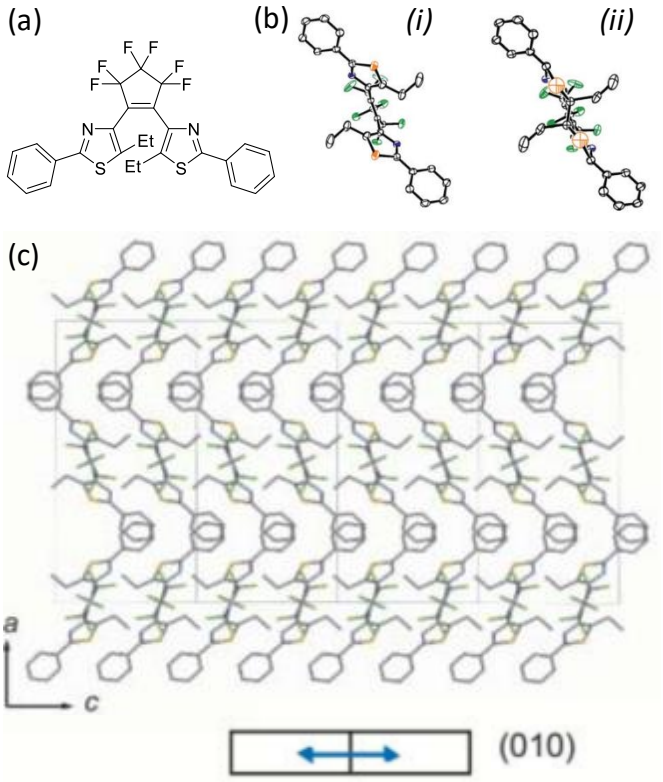

Figure 71: (a) Chemical structure of a diarylethene derivative used to form crystals. (b) ORTEP drawings of the diarylethene derivative *(i)* before and *(ii)* after UV irradiation, showing a change in dimension

between the open and closed form of the photochromic molecular. This molecular deformation causes the macroscopic deformation of the crystal. (c) Molecular packing of the diarylethene derivative before irradiation. Parts (b) and (c) are adapted with permission from reference [919], Copyright 2010 The Royal Society of Chemistry.

Several other studies have been conducted on thiazolyl derivatives of diarylethene,[920–924] but many examples are also available based on 1,2-bis-(thienyl)-perfluorocyclopentene derivatives.[920,925–931] Lu *et al.* observed the bending of crystals based on naphthylvinyl benzoxazole and naphthylvinyl benzothiazole.[932] Kobatake and coworkers reported recently an unusual bending behavior of such a crystal, that returns back to its initial shape after long UV exposure (λ = 365 nm).[926] The authors explain this motion by the existence of several crystalline structures depending on the relative amount of closed forms of diarylethene derivatives. Bending occurs as the two sides of the crystal possess different molecular packings, but it comes back to a linear shape once a homogeneous structure is obtained after long exposure (Figure 72).

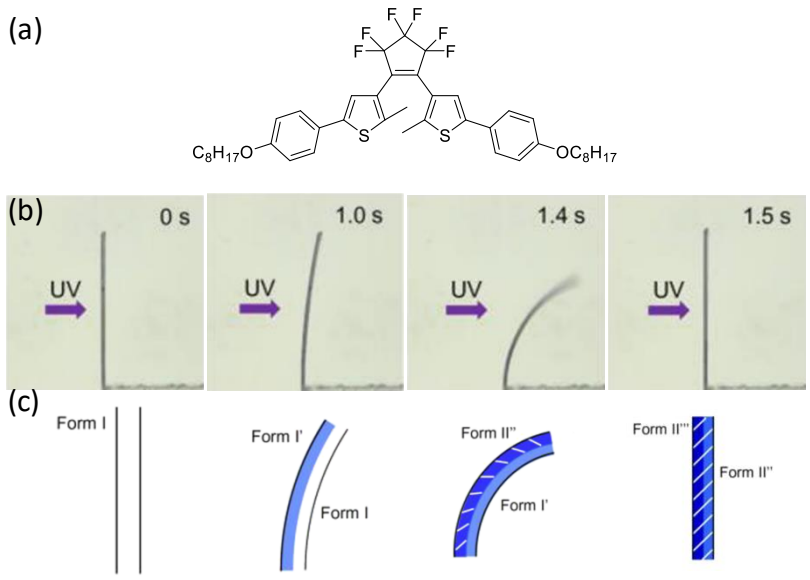

Figure 72: (a) Chemical structure of a diarylethene derivative used to form light-responsive crystals. (b) Bending of this diarylethene crystal upon light irradiation (λ = 365 nm) with (c) the corresponding schemes explaining the mechanism with the different crystalline structures on each side of the material. Parts (b) and (c) are adapted with permission from reference [926], Copyright 2017 American Chemical Society.

Irie and coworkers also reported a cocrystal of a diarylethene derivative with perfluoronaphtalene,[933] and Morimoto, Uchida, and coworkers published an example with a 1,2-bis-(thiazolyl)-perfluorocyclohexene.[934] Kobatake and coworkers also reported a twisting motion of a crystal of 1,2-bis-(thienyl)-perfluorocyclopentene derivative.[929]

Several parameters have been systematically studied in order to elucidate more precisely the mechanism of deformation of the diarylethene crystals, such as the light direction,[935] intensity,[936] wavelength,[921] as well as the crystal thickness.[922,928] Several papers were also focused on the theoretical computation of the photomechanical motion of these materials.[937,938]

Devices have been developed with diarylethene crystals. Kitagawa, Kobatake, Bardeen, and coworkers developed an optical setup for the detection of the deflection of a laser beam by a mirror displaced by diarylethene nanocrystals (Figure 73a).[939] Kobatake and coworkers also reported the use of a gold-coated diarylethene crystal that acts as an electrical photoswitch (Figure 73b).[940]

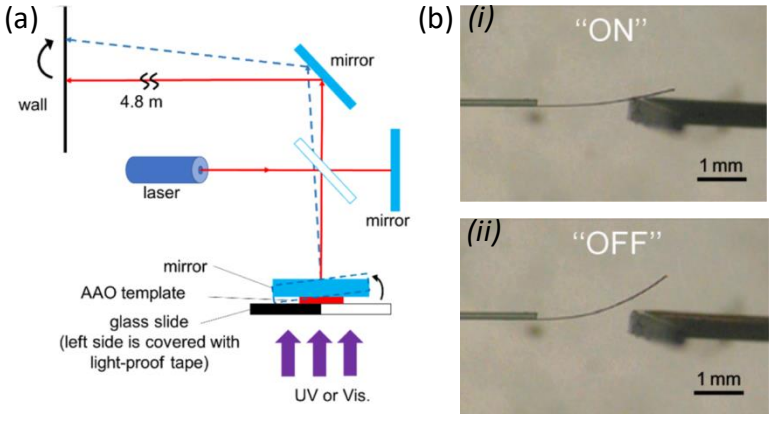

Figure 73: (a) Experimental setup for the detection of the deflection of a mirror caused by irradiated diarylethene nanocrystals. (b) « On » and « off » switching of an electrical circuit with a gold-coated diarylethene crystal upon irradiation (λ = 405 nm). Parts (a) and (b) are adapted with permission from reference [939], Copyright 2019 American Chemical Society, and reference [940], Copyright 2015 The Royal Society of Chemistry, respectively.

Photoactuation of crystals obtained with other photochromic molecules have also been described. Al-Kaysi, Bardeen, and coworkers reported materials with divinylanthracene derivative.[941,942] Upon irradiation with blue light (λ = 405 nm), the molecule undergoes a *cis-trans* isomerization, disrupting the molecular packing and, hence, causing the crystal bending (Figure 74a).

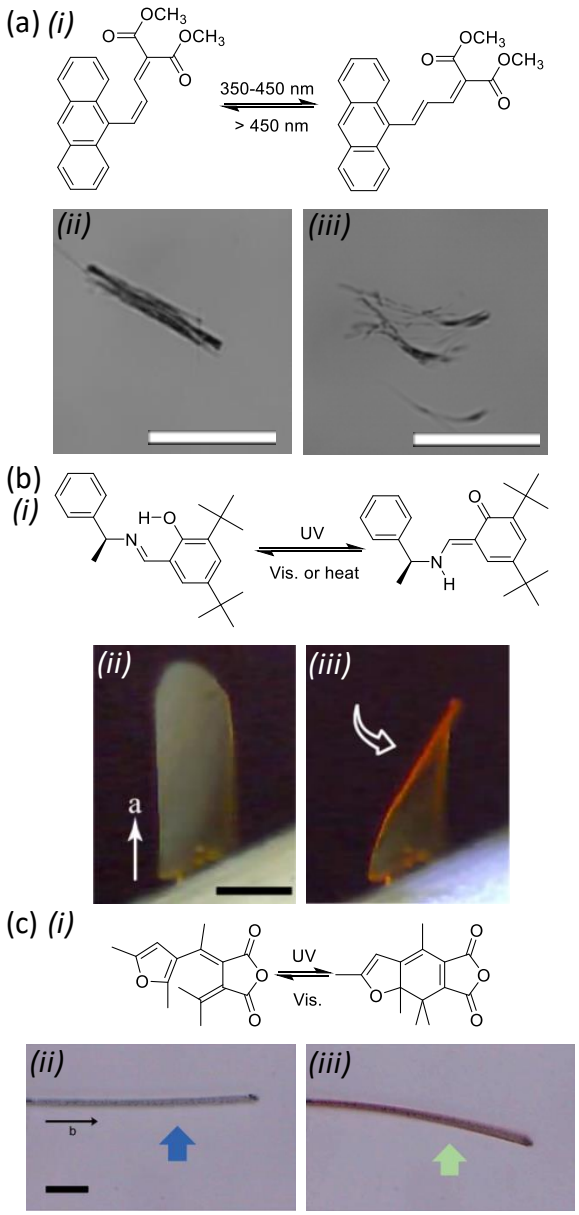

Figure 74: (a) *(i)* Chemical structure and isomerization of a divinylanthracene derivative, which forms crystals *(ii)* before and *(iii)* after UV irradiation (λ = 405 nm) (scale bars: 50 μm). (b) *(i)* Chemical structure and intramolecular proton transfer upon irradiation of the salicylidenephenylethylamines which form crystals *(ii)* before irradiation and *(iii)* after UV irradiation (λ = 365 nm) (scale bars: 100 μm). (c) Chemical structure and photocyclization of a furylfulgide derivative and its corresponding crystal *(ii)* before and *(iii)* after irradiation (λ = 365 nm) (scale bar: 20 μm). Parts (a), (b) and (c) are adapted with permission from reference [941], Copyright 2018 American Chemical Society, reference [943], Copyright 2016

American Chemical Society, and reference [944], Copyright 2012 The Chemical Society of Japan, respectively.

Several examples also deal with salicylidene amine derivatives.[943,945–947] This molecular unit is quite different compared to all the photoswitches encountered in this chapter, because it undergoes an intramolecular proton transfer upon irradiation with light (Figure 74b, *(i)*). Koshima, Asahi and coworkers reported the bending motion of a microcrystal of this photochrome under UV light (λ = 365 nm) (Figure 72b, *(ii)* and *(iii)*).[943] Koshima and coworkers also reported the use of furylfulgide derivatives, which undergo a photocyclization reaction similar to the one of diarylethenes (Figure 74c, *(i)*), and indeed observed the same photomechanical motion as their analogues (Figure 74c, *(ii)* and *(iii)*).[944]

Finally, we will discuss examples of the literature based on crystals of azobenzene derivatives.[948–953] For instance, Koshima *et al.* observed the bending of a single crystal of a simple 4-(dimethylamino)azobenzene,[951] as well as the twisting of a crystal based on chiral azobenzene derivatives upon light irradiation.[954] Interestingly, Yu and coworkers reported different modes of deformation of low-density polyethylene films coated with azobenzene derivatives caused by the photoinduced crystal to liquid phase transition (and corresponding volume change) of the photochrome (Figure 75).[955,956]

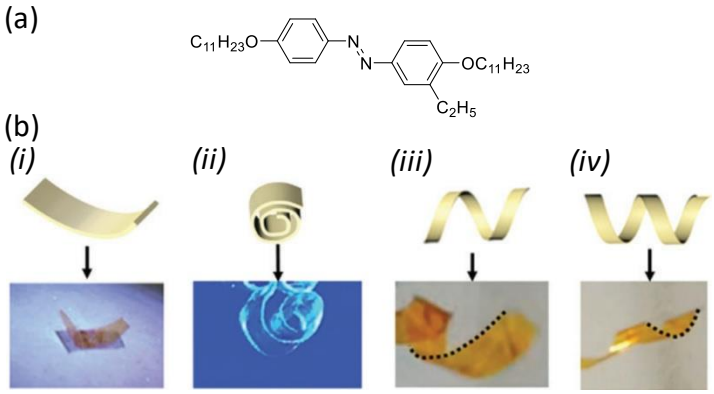

Figure 75: (a) Chemical structure of a azobenzene derivative used to form a composite material with commercially available low-density polyethylene films. (b) Different modes of deformation achieved by

the composite material upon UV irradiation at different powers. *(i)* bending, *(ii)* coiling, *(iii)* right-handed helix and *(iv)* left-handed helix. The dotted black lines highlight the contour of the helical materials. The films have a length between 15 mm and 20 mm. Part (b) is adapted with permission from reference [955], Copyright 2018 The Royal Society of Chemistry.

Kim, Je, and coworkers described the fabrication of nanoactuators and their bending behavior upon irradiation with UV light (λ = 365 nm).[957] Another interesting example has been published by Norikane and coworkers, where they achieved the motion of a crystal of an azobenzene derivative.[958] The crawling behavior of the material was done by oblique irradiation of UV light (λ = 365 nm) on one side, and visible light (λ = 465 nm) on the other side, so that the motion was attributed to an asymmetric photoinduced liquefaction and crystallization of the crystal on opposite ends, respectively (Figure 76).[958]

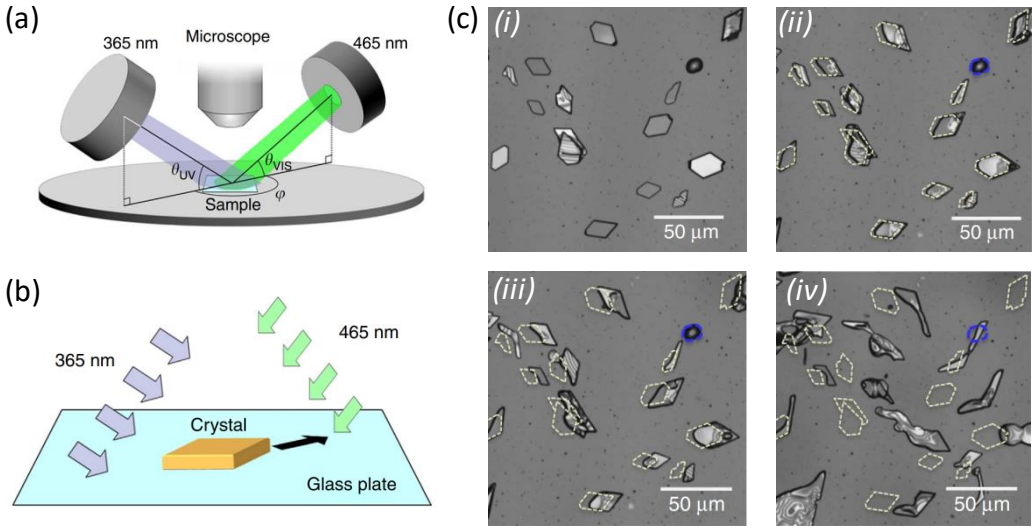

Figure 76: (a) Experimental setup for the asymmetric irradiation of an azobenzene crystal. (b) Scheme of the motion of the crystals induced by the oblique asymmetric irradiation with UV light and visible light. (c) Motion of the crystalline pieces of azobenzene derivatives observed by laser microscopy, with *(i)* the initial state, *(ii)* after 3 min, *(iii)* after 6 min and *(iv)* after 20 min of irradiation. Adapted with permission from reference [958], Copyright 2015 Springer Nature.

2.6. Conclusion

We have painted in this chapter an overview of all the current possibilities offered at the micro- and macroscopic scales by generating collective motion from simple molecular photoswitches. Many of these photoswitches have a polarity that depends on their isomeric form, leading to the manipulation of object driven by surface energy gradients, or to the reversible motion of 3D materials relying on the solvation of their polymer backbone. Also, azobenzene derivatives have the interesting property of orienting when exposed to a polarized light beam. When a gradient of intensity is applied over a large area of the material, it usually gives rise to SRG, while the homogeneous irradiation with of polarized light over a large area leads to the DPM of the object, depending on its size. The alignment phenomenon can also be focused on single spots for local photopatterning of the material. In addition, since the isomerization process usually changes the shape of photochromes, a careful design of the material may lead to a direct amplification of molecular motion to macroscopic motion, as it has been observed for mono- and bilayers, for crystals, and for various polymeric materials, either amorphous or liquid crystalline. In combination to these amplifications, the engineering of supplementary ratchets at the scale of the material, or of anistropic sequences of light irradiations, can produce oscillations and unidirectional cyclic motions leading to the continuous production of a work at macroscopic scale. This interesting aspect shows that despite their simplicity and their perfectly reversible nature as individual units, switchable photochromic molecules can take advantage of many engineering tools to generate more complex actuations in collective systems, up to their implementation in macroscopic motors.

In the next chapter, we explore the collective amplification of more complex nanoscale motions produced by switchable mechanical bonds.

3. MOTION FROM MECHANICALLY INTERLOCKED MOLECULES

3.1. Introduction to mechanically bonded molecules

The term of "mechanical bond" has been introduced relatively recently and is defined as a topological link that maintains together – two or several – interlocked molecular subcomponents which could not be separated without the breakage of at least one of their covalent bonds.[959] Classical examples are catenanes, where topologically interlocked macrocycles can freely move around one another. In addition of such mechanical bonds, the introduction of carefully designed molecular stations (*i.e.* binding sites where the subcomponents can typically interact by reversible supramolecular bonds) enables to control the relative positions of interlocked components by changing reversibly their energy profile. Therefore, the combination of mechanical bonds with molecular stations gives access to mechanical switches capable of producing internal motions of large amplitude (*i.e.* larger than those produced by the more classical *cis*/*trans* isomerization processes for instance).[14,960] In this chapter, we will focus on these switchable mechanically interlocked molecules (MIMs) including catenanes, rotaxanes, and daisy chains. After a general introduction on their molecular design, we will concentrate on their integration in larger systems which can mechanically operate at higher length scales. Because the number of examples involving mechanical bonds are much more limited compared to what has been described with photochromic switches, we have classified the following examples by types of objects, rather than by types of collective motion.

3.1.1. Catenanes

The first synthesis of a catenane (and more generally of a MIM) was reported by Wassermann in 1960.[961] During the preparation of an acyloin macrocycle in the presence of a cyclic hydrocarbon, he observed the formation of a "small but demonstrable yield of a catenane". This small yield was the direct

consequence of the low probability for the acyloin to thread the cyclic hydrocarbon before its own cyclization. For more than 20 years, the synthesis of interlocked structures has been limited by this statistical approach, until Sauvage and collaborators reported on a synthetic procedure which turned to be a game changer.[962] In 1983, they indeed managed to synthesize a catenane with a spectacular yield of 42 % by using a template approach to direct the pre-association of a ring and a thread based on coordination chemistry. Since then, catenanes lost their status of topological curiosities to become readily accessible molecules. More broadly, this pioneering work on synthetic template strategies opened an entire field of research to efficiently access all kinds of MIMs.

Further, the group of Sauvage reported the full control over the switching motion of a catenane in 1994.[963] In a first example, they synthesized a catenane bearing two phenantroline and one terpyridine which can bind copper ions. The switching motion was triggered electrochemically and then, they extended this system by adding a second terpyridine leading to a switching motion involving three states.[964] In this famous example (Figure 77a), the Cu(I) atom adopts a preferred tetrahedral geometry and thus binds with the two bidentate phenantroline ligands (in blue) contained in the two macrocycles. Upon oxidation of the central copper ion, Cu(II) is obtained and tends to adopt an octahedral geometry which is reached by a two-step rearrangement of the molecule. First, one of the rings undergoes a pirouetting motion in order to expose a terpyridine ligand (in red) to the metal center which becomes transiently penta-coordinated. Second, the other ring also moves in order to finally surround the central copper with two terpyridines and to satisfy its preferred octahedral geometry. The process is fully reversible, and the subsequent reduction to Cu(I) leads back to the initial state *via* the same penta-coordinated intermediate. Since this first example describing a synthetic molecular switch based on the controlled sliding motion of a bistable catenane, other types of stimuli have been successfully demonstrated in the literature.[965]

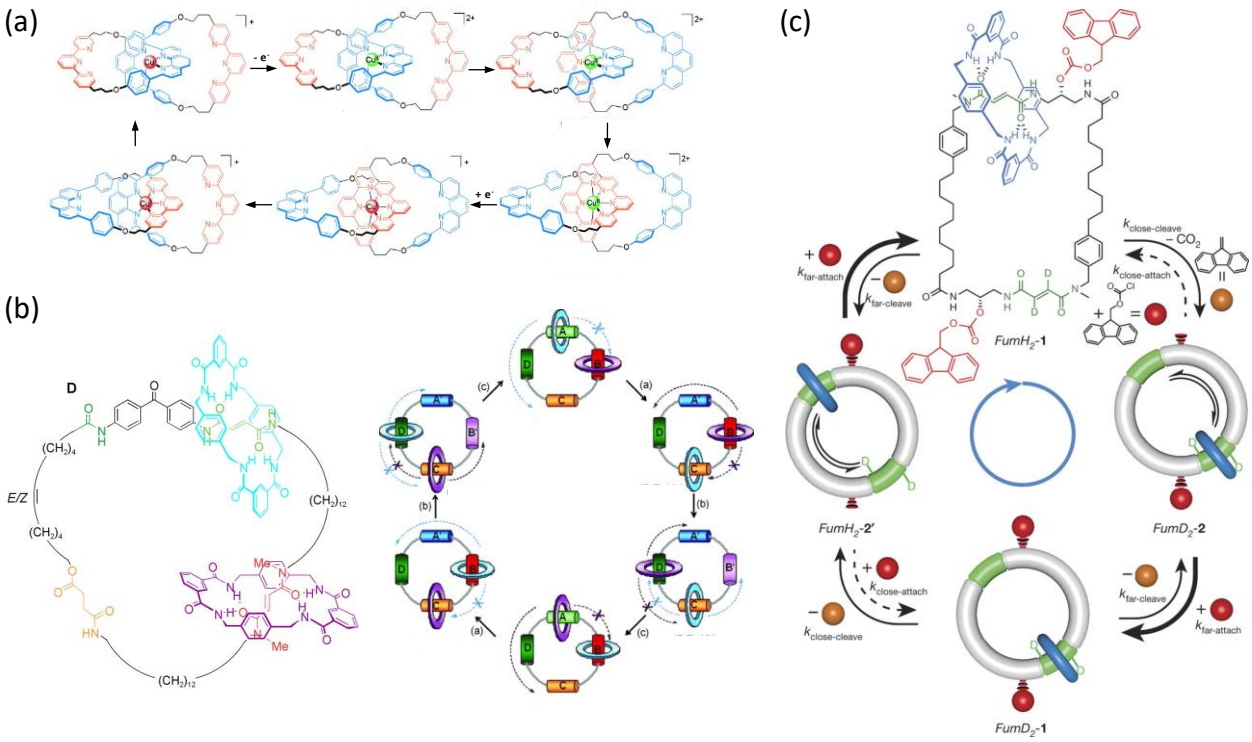

Figure 77: (a) Chemical structures of the intermediates involved in the red-ox actuation mechanism of one of the first switchable catenanes. (b) Unidirectional rotation in a [3]catenane. (c) Autonomous chemically fueled catenane-based molecular motor. Parts (a), (b) and (c) are adapted with permission from reference [966], Copyright 2015 John Wiley and Sons, reference [967], Copyright 2003 Springer Nature, and reference [968], Copyright 2016 Springer Nature, respectively.

In addition, an important question related to the internal motion in catenanes concerns the possible directional control over the mechanical rotations. The answer to this question by bringing experimental evidences remained a challenge for years, until the group of Leigh reported in 2003 the unidirectional rotation of two rings around a larger one in a [3]catenane (Figure 77b).[967] This system is chemically designed on a large macrocycle bearing four different stations on which two smaller macrocycles can slide. Two stations (light green A and red B) are based on fumaramide groups (with B being methylated to reduce its affinity with the sliding rings for steric reasons). It is also important to mention here that the light green fumaramide station A is positioned close to a benzophenone moiety which can act as

photosensitizer to trigger the *E*→*Z* isomerization of station A at a wavelength that does not isomerize station B. Then, the third station (orange C) is made of a succinic amide ester, and the fourth one (dark green D) is a simple amide group. The two sliding rings are based on benzylic amide motifs that are able to selectively interact with the different stations through hydrogen bonding. In the initial state, one of the rings (in blue) is interacting with station A which is the most favored site of interaction and the second ring (in purple) rests on the second best station which is the methylated fumaramide B. After irradiation at 350 nm, an energy transfer from the benzophenone to the fumaramide A triggers the isomerization to the *Z* isomer. As a consequence, the blue ring moves to the best available station which is the succinic amide C, this motion can only occur counterclockwise as the clockwise path is blocked by the purple ring. In a second step, irradiation at 254 nm results in the isomerization of the methylated fumaramide B. The purple ring does not interact anymore with station B and thus moves to the only available binding site which is station D. In a third step, heating or irradiation in the visible range allows the fumaramide stations to recover their initial *E* configurations and, as a consequence, the purple ring will position above station A, and the blue one over station B. Applying this 3 steps sequence a second time allows to reset the system in the initial situation, with the two rings having performed unidirectional rotations of 360° each. One year later, the same group described a system consisting in a [2]catenane where the controlled motion is unidirectional and reversible.[969] In addition, in 2016, they reported the first synthesis of a chemically-fueled motor capable of functioning autonomously using an information ratchet mechanism (Figure 77c).[968] The design of this molecular motor is based on a catenane consisting of a large macrocycle that bears two fumaramide stations (in green) and two fluorenylmethoxycarbonyl (Fmoc) bulky groups (in red) that can be cleaved in order to allow gliding of the smaller macrocycle made of benzylic amides (in blue). The autonomous rotation in this system is made possible because the Fmoc blocking group has a faster rate of attachment on the site far from the blue macrocycle (as compared to the nearest site), whereas the kinetics of cleavage is the same for both positions. Interestingly, this kinetic bias was shown to induce

a directional motion within the catenane. At initial time, the fully blocked system is put in presence of Fmoc-Cl (as chemical fuel), of trimethylamine (to allow the Fmoc cleavage), and of $KHCO_3$ (to deprotonate the triethylammonium after cleavage). The clockwise rotation begins by the cleavage of the Fmoc close to the blue ring, which allows that ring to shuttle between the initial station (at the top) and the deuterated one (at the bottom). When, the blue ring is at the bottom station, it subsequently favors the attachment of a blocking group far from the ring (*i.e.* at the top station). Then, cleavage of the blocking group from the bottom allows the shuttling between the two stations. But here again, when the blue ring is positioned on the top station, it favors the attachment of a blocking group at the bottom of the track. The initial situation is thus recovered when the blue ring has performed a full clockwise rotation. Taking into account the relative energies of states, the anticlockwise motion is thermodynamically favored; nevertheless, as it involves the attachment of the Fmoc group close to the blue ring, which is kinetically disfavored by allosteric interactions, the clockwise motion takes place eventually. This interesting mechanical system, based on the relative kinetic rates of chemical reactions, was shown to rotate over 360° every 12 hours, and to keep rotating as long as a chemical fuel is present.

3.1.2. Rotaxanes

The first synthesis of a rotaxane – in which a mechanical bond maintains the topological association between a macrocycle and a thread – was reported by Stoddart and coworkers in 1991.[970] By using a non-covalent templating strategy, they managed to synthesize a bistable molecular shuttle with both binding sites being identical, and thus leading on average to an equal distribution of the macrocycle over the two stations. The same group pushed the approach further in 1994 by breaking the rotaxane symmetry to access a chemically and electrochemically switchable molecular shuttle (Figure 78a).[971] In this new

design, the two stations of the thread are different and consist of benzidine and biphenol electron donating groups, whereas the macrocycle is an electron accepting tetracyclophane. Initially, the electron-poor macrocycle prefers to stay close to the best electron donating benzidine, which results in an 84/16 distribution in favor of the benzidine. Protonation – or oxidation – of the benzidine leads to the appearance of repulsive positive charges on the benzidine station, with the macrocycle shuttling towards the bisphenol station with a ratio of 98/2. In this paper, and interestingly enough for the present review, the authors concluded by pointing out that one of the next challenges faced by scientists would be to "wire" these molecules to the macroscopic world.

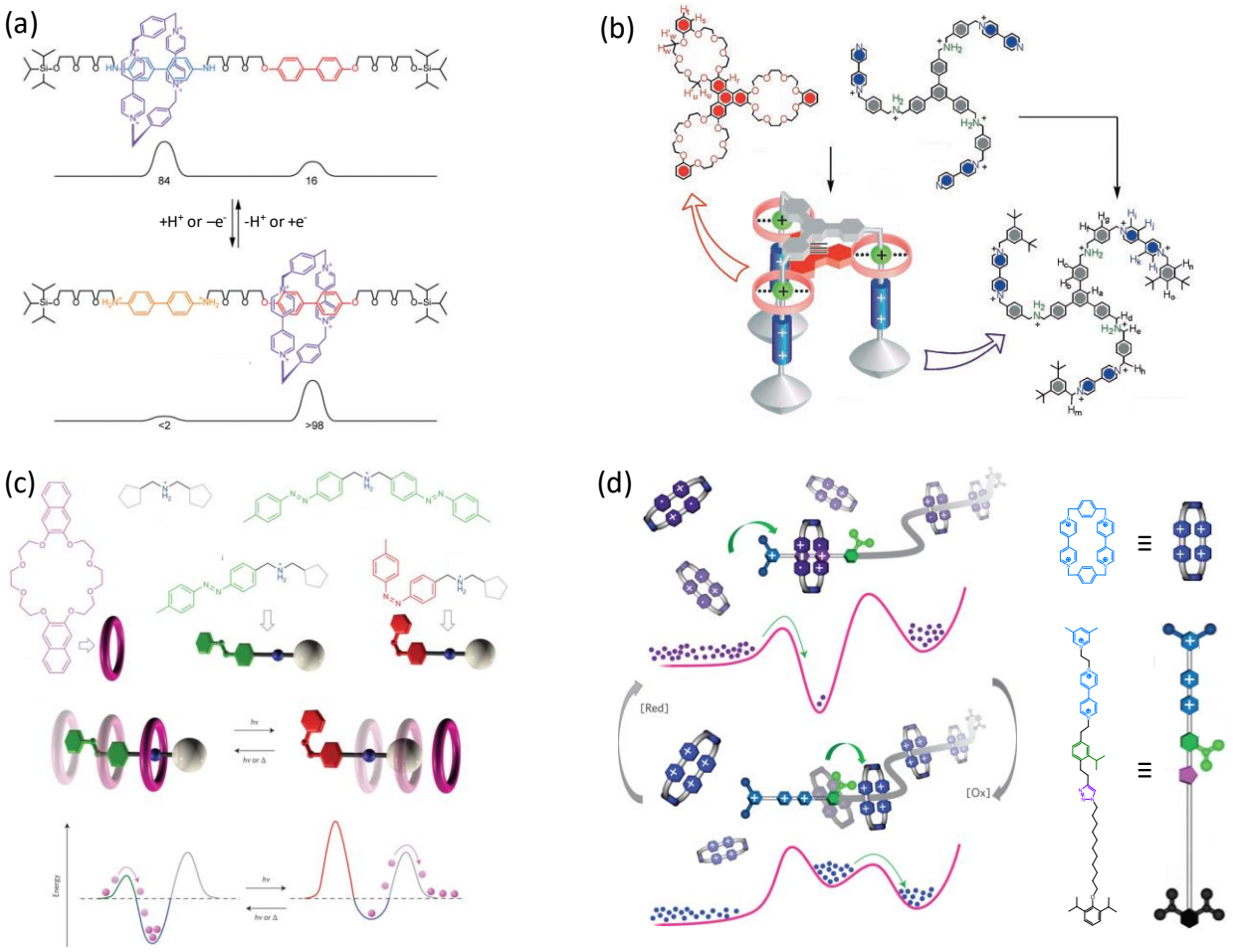

Figure 78: (a) First example of a switchable rotaxane described in the literature, controlled by either pH or redox processes. (b) Molecular structure and schematic representation of a tripodal "molecular

elevator" actuated by pH. (c) Molecular structure and schematic representation of an autonomous linear motion using the light-driven unidirectional threading of a rotaxane. (d) Operating principle of an artificial molecular pump based on a rotaxane topology, and capable of concentrating macrocycles on a thread against entropy. Parts (a), (b), (c) and (d) are adapted with permission from reference [14], Copyright 2006 John Wiley and Sons, reference [972], Copyright 2004 American Association for the Advancement of Science, reference [973], Copyright 2014 Springer Nature, and reference [974], Copyright 2015 Springer Nature, respectively.

Shortly after, the same group designed another system where the switching process is controlled only by pH.[975] In this design, the authors used an axle where the first station is an aliphatic amine and the second one a bypiridinium. Upon protonation of the amine, the macrocycle (a dibenzo[24]crown-8 (DB24C8)) interacts with the bipyridinium station, whereas the amine in its neutral form has the best affinity for the macrocycle. This design has been nicely extended for the preparation of a molecular elevator (Figure 78b).[972] Here, the system consists in a tritopic host containing three DB24C8 units linked through a triphenylene core. This host is triply threaded by a guest which contains three axles displaying two stations (one amine and one bipyridinium) linked by a benzene core. ^{1}H NMR, UV-Visible spectroscopy as well as cyclic voltammetry have been used to demonstrate the pH-controlled motion of the molecular elevator that can move over a distance of 0.7 nm. During the past 20 years, other outstanding achievements have been reported using rotaxanes. For instance, light has been used to fuel their shuttling process,[976] they have been implemented to design an information ratchet[977] as well as a peptide synthesizer,[978] and unidirectional motion has been reached.[979] In a recent example, the group of Credi reported an elegant system with a minimalistic molecular design that can function out of thermodynamic equilibrium (Figure 78c).[973] This pseudo-rotaxane (that is without bulky stoppers) is built on an azobenzene switch linked to a secondary ammonium and a cyclopentadiene moiety. When the azobenzene

is in its *E* configuration, the macrocycle can be threaded and interacts with the ammonium. Upon photoswitching of the azobenzene, the interaction between the macrocycle and the ammonium is destabilized due to steric reasons and it results in the dethreading of the macrocycle. Interestingly, and also for steric reasons, the direction of the threading preferentially occurs by the *E* azobenzene tip, while the dethreading occurs by the cyclopentadiene one. In addition, the same wavelength can be used for the *E*→*Z* as well as the *Z*→*E* isomerizations at 365 nm. This implies that, upon constant irradiation, the macrocycle is continuously (and directionally) threaded when the azobenzene is in its *E* configuration, and is continuously (and directionally) dethreaded when the azobenzene switches to its *Z* configuration. Overall, this biased operational principle could be envisaged as an element of a molecular pump that would concentrate macrocycles on an axle. Such a molecular pump capable of concentrating rings on a thread was achieved in 2015 by the group of Stoddart (Figure 78d).[974] Here, on the one hand, the dumbbell part is composed of a dimethoxypyridinium acting as an electrostatic stopper, a viologen dicationic station, an isopropylphenyl, a triazole, an alkyl chain, and a tilted diisopropylphenyl stopper. On the other hand, the macrocycle that can be pumped on the rotaxane consists of a cyclobis(paraquat-*p*-phenylene) tetracationic ring. Upon reduction, the resulting dicationic diradical ring can interact with the cationic radical viologen unit of the dumbbell to form a stable tricationic triradical complex between the axle and the threaded macrocycle. Subsequent oxidation destabilizes the inclusion complex by electrostatic repulsion, and the macrocycle is pushed away from the viologen with sufficient potential energy to pass over the tilted diisopropylphenyl unit and to sit on the alkyl chain. This occurs without dethreading because of the higher energy to cross the bulky diisopropylphenyl stopper from the other direction. This red-ox cycle can be repeated to pump another macrocycle against entropy with the same operation principle.

3.1.3. Daisy-chains

In 2000, Sauvage and coworkers described the first example of a bistable [*c2*]daisy chain which was nicknamed by the authors as a "molecular muscle" (Figure 79a).[980] Indeed, upon actuation, an immediate analogy exists between the sliding motion observed in such a synthetic system and the gliding motion of a sarcomere unit within muscular tissues. Chemically, this bistable [*c2*]-daisy chain is composed of two interpenetrating rotaxanes, each one made of a macrocycle covalently attached to an axle. Each axle contains two binding sites (one terpyridine and one phenantroline), and each macrocyle contains a phenantroline unit. The operating principle is based on the difference of affinity of these binding sites between two metal cations, namely Cu(I) and Zn(II). In the initial state, two Cu(I) ions bind two phenantroline ligands with a tetrahedral geometry. Subsequent removal of Cu(I) ions by KCN and addition of Zn(II) ions triggers the sliding motion as the Zn(II) ions prefer adopting a pentacoordinated geometry involving one phenantroline and one terpyridine ligand around the metal center. This sliding motion results in a net contraction of the daisy chain of about 1 nm, which is 22 % from its original size (a relative variation similar to the one observed in sarcomeres).

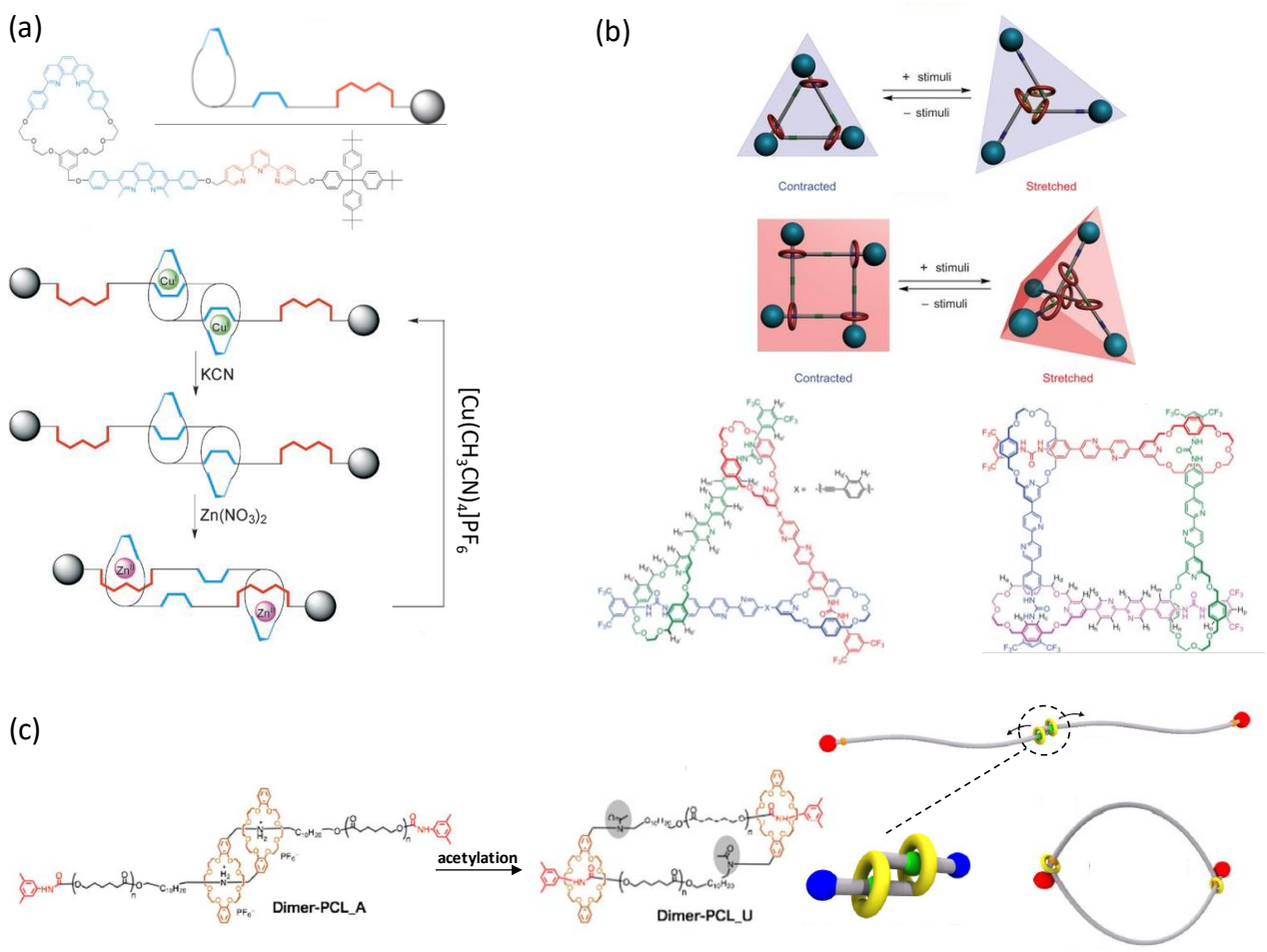

Figure 79: (a) Molecular structure and schematic representation of the first example reported in the literature describing the double-threated topology of a [*c2*]daisy chain rotaxane. (b) Chemical structures and actuation principle in [*c3*] and [*c4*]daisy chain rotaxanes that can switch between 2D and 3D structures. (c) Chemical structures and schematic actuation of a [*c2*]daisy chain embedded in the main chain of a polycaprolactone; the mechanical switch is accompanied by a global change of the polymer chain from a linear to a macrocyclic topology. Parts (a), (b) and (c) are adapted with permission from reference [14], Copyright 2006 John Wiley and Sons, reference [981], Copyright 2016 Springer Nature, and reference [982], Copyright 2017 American Chemical Society, respectively.

In 2008, the groups of Stoddart and Coutrot described independently pH-switchable [*c2*]daisy chains. In Stoddart's design, the macrocycles are based on DB24C8 crown ethers whereas the two stations consist in a secondary ammonium and a bipyridinium.[983] Initially, the macrocycles sit on top of the ammonium stations but upon deprotonation, the electron-rich macrocycles slide towards the bipyridinium stations resulting in a 29 % reduction of size. Using the same macrocycle and the same first ammonium station, the group of Coutrot designed another pH-switchable [*c2*]daisy chain.[984] In this example, the authors used mannosyl stoppers which were introduced through copper-catalyzed azide-alkyne cycloaddition (CuAAC). The triazole ring formed during the "click" reaction was then methylated to form a methyltriazolium, and thus providing a second competing station for the macrocycle. The use of the CuAAC reaction has proved here to be particularly useful as it allows to attach a stopper and at the same time to provide a second station for an electron-rich macrocycle. This strategy to obtain pH-switchable daisy chains has since been reported in the preparation of other [*c2*]daisy chains,[985] including unsymmetric ones.[986] In addition, various research groups developed new [*c2*]daisy chains for which the linear contraction / extension can be triggered by different *stimuli* such as light,[987] solvent polarity,[988] or even electric field.[989] Very recently, the group of Chiu showed the possibility to access daisy chains of higher order (namely [*c*3] and [*c*4]) that are able to contract and extend in the 2D and 3D spaces (Figure 79b).[981] The chemical design is based on a thread featuring urea and bipyridine binding sites, and macrocycles that contain pyridine ligands. Depending on the size of the linker and on the stoichiometry, it is possible to access trimers and tetramers in presence of Zn(II) ions which chelates to both the bipyridine and the pyridine. After removal of Zn(II) ions by addition of a competing ligand, the macrocycles slide towards the terminal urea stations. Upon actuation, the trimer switches between a contracted and a stretched triangular geometry, whereas the tetrameric assembly switches between a contracted 2D square planar geometry and a stretched 3D tetrahedron. Interestingly, in another approach to change the topology of such a MIMs upon actuation, the group of Takata has introduced a [*c*2]daisy chain at the center of a

polycaprolactone polymer chain (Figure 79c).[982] The hydroxyl-terminated polymer was reacted with 3,5-dimethylphenylisocyanate in order to introduce a stopper and also to generate a second station (a carbamate) for the macrocycle. In the initial state, the macrocycles sit around the central ammonium stations, and the actuation is performed upon acetylation with acetic anhydride which hinders the central ammonium stations. As a consequence, the macrocycles slide towards the terminal carbamate stations. This process is accompanied by a spectacular switch in topology, as the polymer chain goes from a linear geometry to a macrocyclic one.

We have seen in the introduction of this chapter a selection of switching systems based on mechanical bonds, displaying various kinds of molecular architectures and topologies, and which can be actuated by various *stimuli*. In the next sections, we will show how chemists have succeeded in integrating such MIMs in larger systems in order to transfer their collective motion over larger length scales and up to our macroscopic world.

3.2. Collective motion from mechanically interlocked molecules

As described in the above introduction, initial efforts related to mechanically interlocked molecules have focused on their synthesis and their study as individual actuating units.[990,991] In this section, we will highlight how the molecular motions of molecular catenanes, [n]rotaxanes and [*c*2]daisy chains can be used to produce new functions at higher length scales by collective actuations.

3.2.1. Collective motion from catenanes

The general topology of catenanes has been significantly diversified by synthetic chemists in order to build architectures of increasing complexity such as [n]catenanes, Salomon links, Borromean rings, etc.[966] Although, these structures have also been inserted into main-chain and side chain polymers, into MOFs, and even anchored on surfaces, the study of their concerted dynamics at higher scales has remained limited

to date. The first example featuring a response corresponding to the collective motion of catenanes in a device was reported 20 years ago by the group of Stoddart (Figure 80).[992]

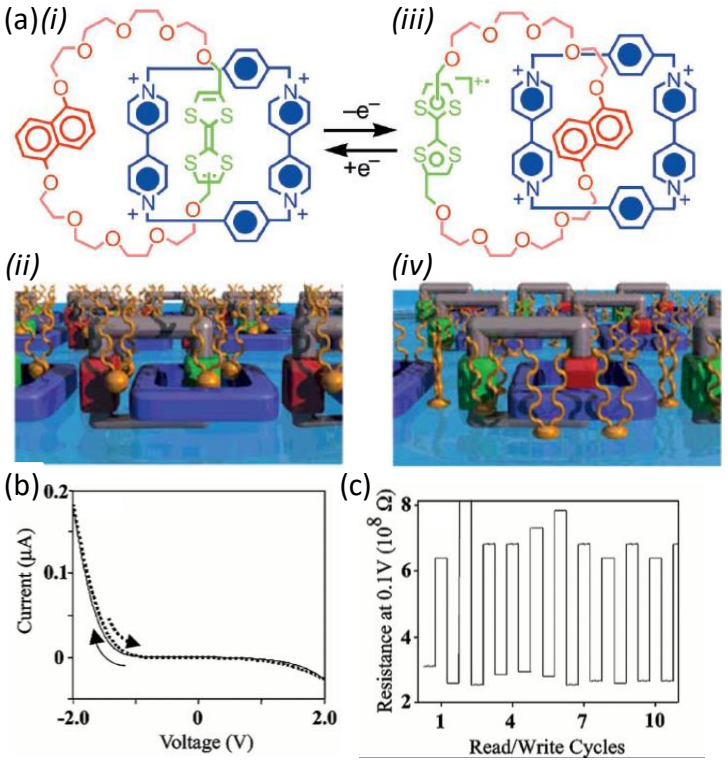

Figure 80: (a) Chemical structure of the [2]catenane used by the group of Stoddart to build the first molecular switch tunnel junction from MIMs *(i)* Reduced form of the [2]catenane and *(ii)* schematic representation of its behavior in a Langmuir monolayer with $DMPA^-$ at the air/water interface, *(iii)* Oxidized form of the [2]catenane and *(iv)* schematic representation of its behavior in a Langmuir monolayer with $DMPA^-$ at the air/water interface; DMPA: dimyristoylphosphatidyl; (b) Current-Voltage hysteresis loop of a device build from a Langmuir monolayer made of these catenanes and recorded at 291 K; (c) Performance of this device in terms of measured resistance at 0.1 V upon several on/off cycles. Panels (a) (*i, iii*), (b) and (c) are adapted with permission from reference [992], Copyright 2000 American Association for the Advancement of Science. Panels (a) (*ii, iv*) are adapted with permission from reference [993], Copyright 2005 Springer Nature.

The MIM used in the device consisted in an electrochemically switchable bistable [2]catenane built from a cyclophane ring with two bipyridinium stations on one hand, and a crown ether macrocycle with two opposite stations, namely a tetrathiafulvalene (TTF) and a 1,5-dioxynaphtalene, on the other hand.[994] A Langmuir monolayer composed of these interlocked molecules on supporting phospholipids was sandwiched between a 7 μm-wide n-type poly-silicon bottom electrode and a 10 μm-wide titanium-aluminum top electrode. The electrical response of this device was characterized by a large hysteretic current voltage behavior (Figure 80b) associated with the bistable nature of the [2]catenane, that is only slightly pronounced when analyzed in solution. The device could be switched *on* and *off* by applying +2 V and -2 V respectively and, cycled several times (up to few hundred times over a period of 2 months under ambient conditions, Figure 80c) without loosing efficiency. This work demonstrate the possibility to access molecular switch tunnel junction (MSTJ) devices with a global electrical response originating from the molecular level and with possible applications as memory devices. A similar MSTJ device was also obtained using a similar [2]catenane with diazapyrenium stations instead of bipyridinium ones and single-walled carbon nanotubes as bottom electrodes.[995]

Some years later, the groups of Stoddart and Grzybowski reported the functionalization of metal nanoparticles (gold, palladium and platinum) with similar redox-active catenanes.[996] Interestingly, oxidation of the [2]catenane-functionalized gold nanoparticles using iron perchlorate (III) resulted in an increase by a factor of ~1.5 of the zeta potential of the nanoparticles in agreement with the oxidation of the MIM from 4+ to 6+ (Figure 81a). This process could be cycled several times in a reversible manner in the presence of ascorbic acid as reducing agent (Figure 81b). Cyclic voltammetry experiments of these functionalized nanoparticles showed similar oxidation and reduction peaks compared to the free catenane in solution but with much higher values (~ +300 mV for each peak, Figure 81c) as a result of a high density of positive charges on the surface leading to a destabilization of the oxidized tetrathiafulvalene units in comparison to the solution. Overall, these examples demonstrate the ability of redox-sensitive

[2]catenanes to work in concert at surfaces even in dense molecular arrays, and to produce functional macroscopic response.

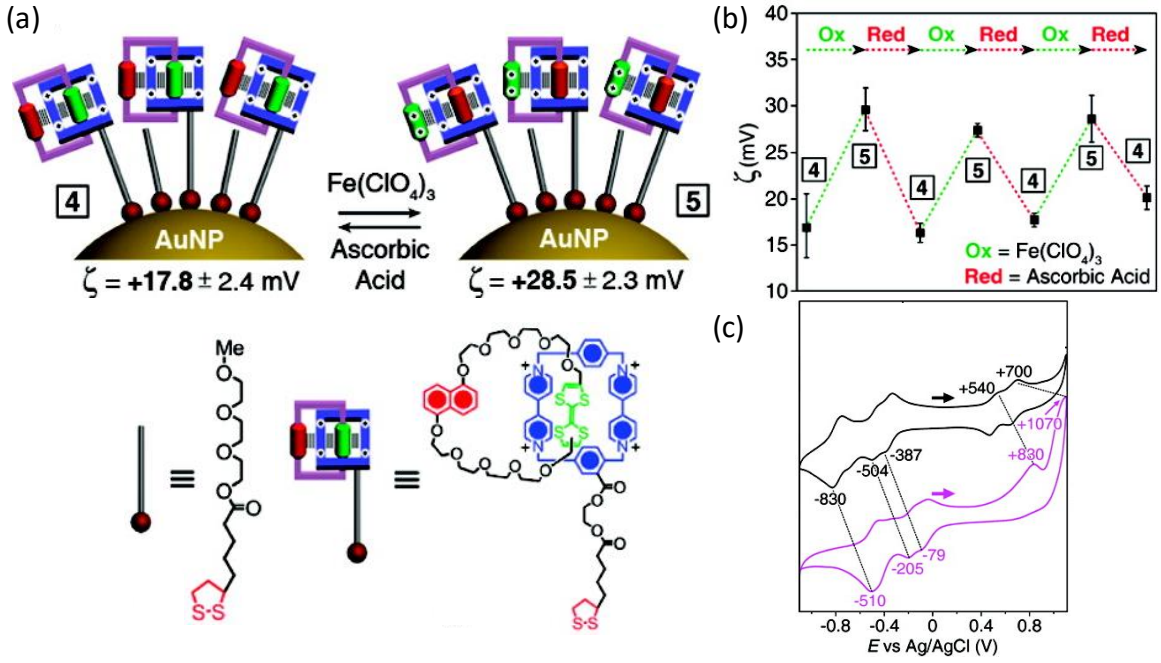

Figure 81: (a) Schematic representation of gold nanoparticles decorated with redox-active [2]catenane, their respective zeta potential and the chemical structure of the ligands; (b) Evolution of the zeta potential of the functional nanoparticles upon chemical oxidation and reduction; (c) cyclic voltammogram of the free catenane in solution (black) and of the [2]catenane-functionalized gold nanoparticles with a fractional coverage of 0.50 (purple). Adapted from reference [996], Copyright 2009 American Chemical Society.

Alternatively, the group of Rowan studied the reversible stimuli-responsive behavior of poly[*n*]catenanes in solution and in the bulk (Figure 82).[997] A new synthetic methodology was designed – involving first the formation of a metallo-supramolecular polymer, followed by a ring closing metathesis step, and finally a demetallation – to access these mechanically interlocked polymers as a mixture of branched, linear, and cyclic architectures. Further separation by preparative gel permeation chromatography afforded four fractions, the main one (60 %) being constituted of mainly linear poly[7-

27]catenanes (85 %) and cyclic poly[4-7]catenanes, as determined using a combination of ^{1}H NMR, MALDI-TOF and multi-angle light scattering experiments. Interestingly, upon addition of Zinc ions which can bind the BIP ligands of the catenane, an increase of the hydrodynamic radius in solution was observed for both the predominantly linear and branched polymers (~70 % and ~50 % respectively), while almost no effect was observed for the cyclic one (Figure 82a). DSC analysis of the bulk materials indicates that metallation induces an increased glass transition temperature (T_g) for the linear and branched polycatenanes, in agreement with a reduced flexibility of the structures (Figure 82b). This work demonstrates the first example of collective motion of catenanes in a polymeric structure by making use of changes in the conformational flexibility of the macromolecule.

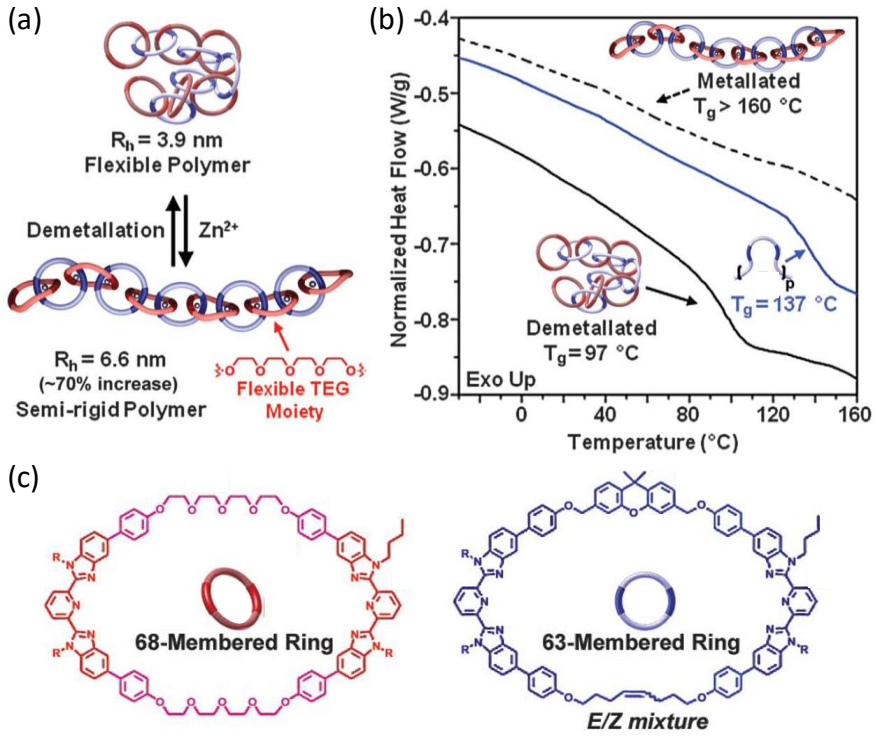

Figure 82: (a) Reversible evolution of the hydrodynamic radius (R_h) of a linear poly[*n*]catenane upon metallation/demetallation; (b) Evolution of the glass transition temperature (T_g) of a linear poly[*n*]catenane upon metallation/demetallation as indicated by DSC analysis; (c) Chemical structure of

the two rings that compose the poly[*n*]catenanes. Adapted from reference [997], Copyright 2017 American Association for the Advancement of Science.

More recently, pH- and temperature-sensitive [2]catenanes were inserted as reticulating units in poly(ethylene glycol) chains using thiol-ene chemistry (Figure 83).[998] While hydrogen bonding interactions between the rings are favored for pH values above 7, a decrease in pH leads to an increased mobility of the rings as illustrated by ^{1}H NMR.

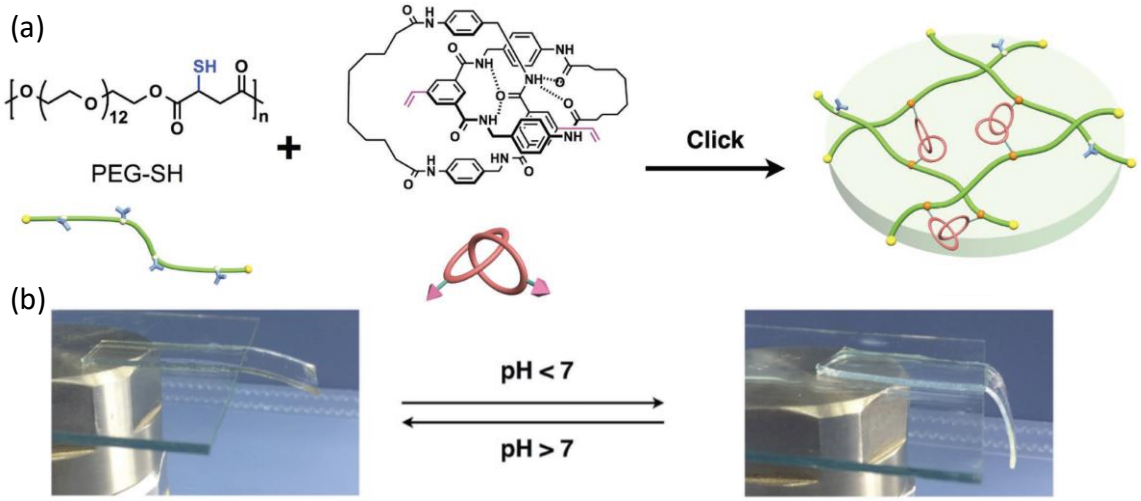

Figure 83: (a) Chemical structures of the polyethylene glycol chain and of the [2]catenane used to build a chemical gel with MIMs as reticulating units; (b) Evolution of the material upon pH stimulation. Adapted with permission from reference [998], Copyright 2017 John Wiley and Sons.

In the chemical gel, the rigidity of the material was reduced at low pH as determined by measurements of the storage and loss moduli. Similar observations were made when measuring the rheological properties of the material at high temperatures. Tensile stress-strain measurements on the chemical gels at low (1.7) and neutral pHs further demonstrated the reversible soft and tough characters of the materials respectively, in agreement with a more constrained material at neutral pH. Comparison with control gels, i.e. with either

blocked hydrogen bonding interactions or without catenane but a cross-linked chemical network, indicate that the "motion" of the rings is responsible for the mechanical behavior of the gel.

3.2.2. Collective motion from rotaxanes

Inspired by their success on using bistable [2]catenane as active unit in MSTJ devices,[992] Stoddart, Heath and co-workers further studied the behavior of a series of [*n*](pseudo-)rotaxanes at surfaces using an electrical stimulus. The molecular structures consisted in an axle bearing one TTF and one 1,5-dioxynaphtalene (DNP) units as stations surrounded by a cyclobis(paraquat-*p*-phenylene) ($CBPQT^{4+}$) macrocycle.[999] The Langmuir monolayer made of the [2]pseudorotaxane was transferred to a n-type polycrystalline (poly-Si) bottom electrode and further covered with a titanium-aluminum top electrode (Figure 84a*(i)*).[1000] The corresponding MSTJ device was characterized by a hysteretic current-voltage response between two conductivity states (high and low). Compared to the same device made of the bistable [2]catenane, larger conductance changes (10^2 compared to 2-3) were recorded between the switch-open and switch-closed states, but the devices exhibited lower cycling reproducibility. This was explained by the presence of domain structure in the Langmuir monolayer as observed by Brewster angle microscopy. Importantly, the bistable nature of the rotaxane proved to be of particular importance to reach devices with good general performances. By introducing a bulky hydrophilic stopper on the bistable [2]pseudorotaxane thus leading to a bistable [2]rotaxane, the same groups demonstrated the absence of structure domains, due to a higher molecular area (Figure 84a*(ii)*).[1001] This amphiphilic interlocked structure was then studied in micrometer- and nanometer-scale MSTJ devices (Figure 84b). Electrical signatures similar to the ones recorded for the [2]catenane, namely large hysteretic current-voltage behavior, opening and closing voltage at +2 V and -2 V respectively, were measured for both devices. In the case of the nanometer-scale one, up to 35 opening/closing cycles were recorded without losing efficiency.

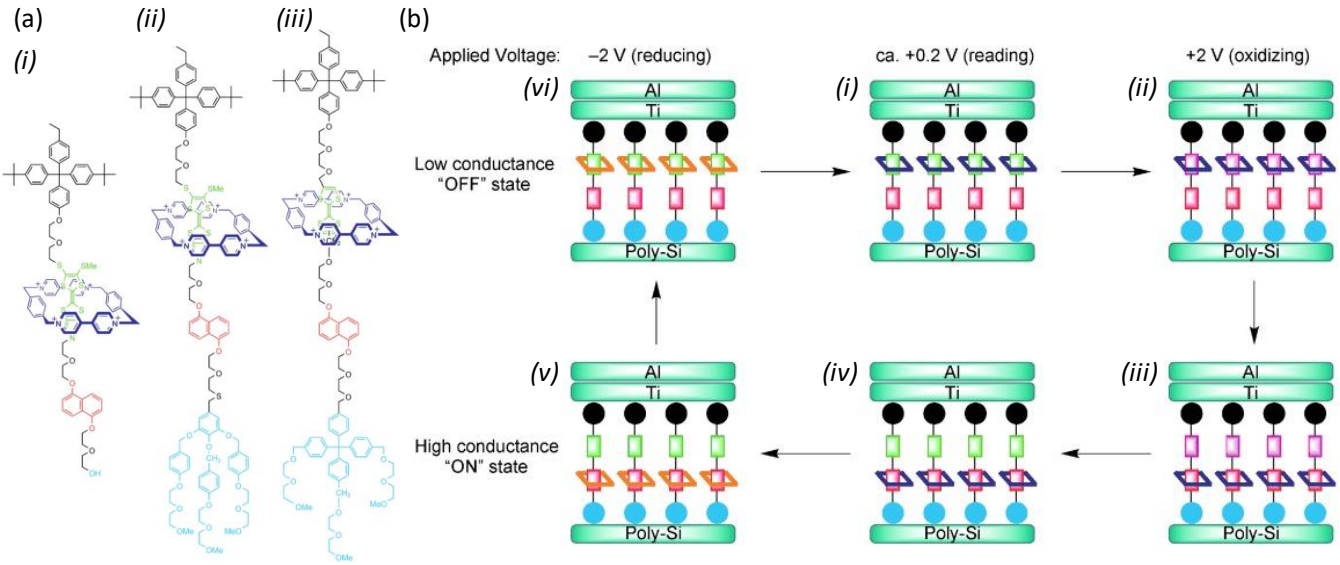

Figure 84: (a) Chemical structures of (*i*) [2]pseudorotaxane and (*ii-iii*) [2]rotaxanes studied in MSTJ devices; (b) Working principle of a molecular switch tunnel junction (MSTJ) based on [2]rotaxane: *(i)* Ground state device with the $CBPQT^{4+}$ macrocycle (dark blue) surrounding the TTF station (green) – this state presents a low conductance, *(ii)* Oxidation of the TTF units (2e-, pink) using a positive bias and *(iii)* subsequent shuttling of the $CBPQT^{4+}$ macrocycle to the DNP unit (red), *(iv)* Reduction of the oxidized TTF unit when the electrical bias is lowered to ~0V – this state presents a high conductance, *(v)* Reduction of the cyclophane macrocycle to its radical dication (orange) using a negative bias and *(vi)* subsequent shuttling of the macrocycle to the TTF unit (green), further increase of the electrical bias to ~0V regenerates the ground-state device *(i)*. Reproduced with permission from reference [14], Copyright 2006 John Wiley and Sons.

By slightly modifying the chemical nature of the TTF unit (Figure 84a*(iii)*), the micrometric MSTJ devices were subsequently used to fabricate 2D crossbar circuits, in order to produce 64-bit random access memory devices which could be cycled several times. Importantly, in subsequent work, the group of Bjornholm demonstrated by surface-sensitive synchrotron X-ray reflectometry that the motion of the cyclobis(paraquat-*p*-phenylene) ring of such [2]rotaxane can be efficiently controlled by a redox process

within a densely ordered Langmuir monolayer.[1002] Some years later, the groups of Stoddart and Heath succeeded in producing a 160-kilobit molecular electronic memory fabricated at a density of 10^{11} bits.cm^{-2}.[1003] The crossbar memory device was built by sandwiching a monolayer of an analogous bistable [2]rotaxane between 400 Si bottom-nanowire electrodes crossed by 400 Ti top-nanowire electrodes. Each cross-section of the electrodes was considered as an individual MSTJ device containing ~100 interlocked molecules. Although a large number of defects of several types were detected by electrical testing, and although failures of the device occurred after cycling for more than ten times, the crossbar memory device could be operationally used to store and retrieve information. However, this lack of robustness along with some engineering issues have currently limited the use of this technology as the next-generation of memory device.[1004,1005]

The groups of Stoddart and Ho also studied the switching ability of bistable [2]rotaxanes preorganized in densely-packed Langmuir films using a chemical oxidant and a reducing agent as stimuli.[1006] First, [2]rotaxane molecules were dispersed over an aqueous subphase, and a chemical oxidant ($Fe(ClO_4)_3$) was further injected into this aqueous phase while compressing the monolayer (Figure 85a-b). By monitoring the evolution of the surface pressure as a function of mean molecular area, the authors could demonstrate that the threaded molecules present a switching behavior similar to the one observed in the non-pressurized state (Figure 85c).

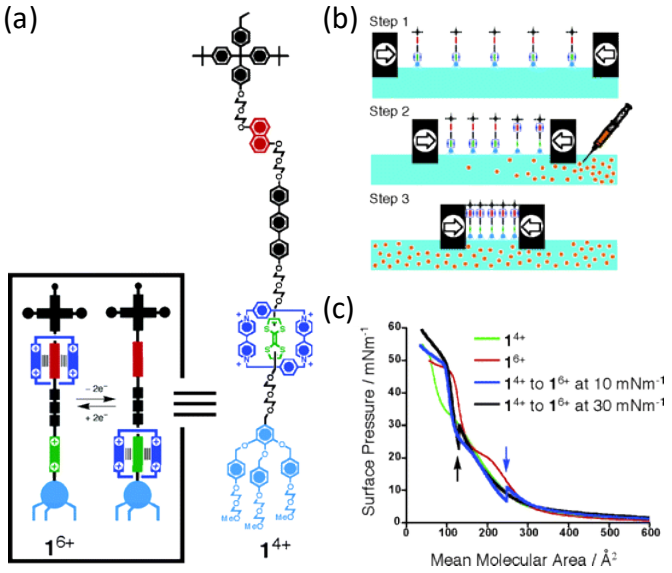

Figure 85: (a) Chemical structure of an amphiphilic [2]rotaxane and schematic representation of its redox behavior; (b) Schematic representation of the procedure used to induce oxidation of [2]rotaxane while building a highly packed Langmuir film, Step 1: dispersion of the reduced [2]rotaxane over an aqueous subphase, Step 2: Injection of a chemical oxidant ($Fe(ClO_4)_3$) into the subphase and simultaneous compression of the subphase, Step 3: formation of a Langmuir monolayer with oxidized [2]rotaxanes; (c) Evolution of the surface pressure as a function of mean molecular area for Langmuir films built from the starting rotaxane upon oxidation during the formation of the Langmuir monolayer according to (b) and at two different pressures (blue and black), comparison with the isotherm curves obtained directly from the 4+ (green) and 6+ (red) rotaxanes. Adapted with permission from reference [1006], Copyright 2004 American Chemical Society.

Subsequently, the Langmuir monolayers were transferred to silicon dioxide substrates and the shuttling motion was monitored by X-ray photoelectron spectroscopy (XPS). This technique revealed in a quantitative manner that a complete movement of the ring occurs from one station to the other when these solid substrates are immersed in an oxidant solution. An identical behavior was observed on Langmuir-Blodgett double layers but only for the molecules involved in the outermost layer of the film. The results

were very encouraging for the use of rotaxanes as mechanical units in nanometric chemomechanical systems. To reach such objectives, the same groups designed a bistable [3]rotaxane bearing two TTF and two naphthalene stations on the dumbbell surrounded by two cyclobis(paraquat-*p*-phenylene) rings which served as attachment points to a gold surface (Figure 86a).[1007,1008] A self-assembled monolayer of these molecules deposited on a gold-coated silicon cantilever array was sequentially immersed in an aqueous solution of oxidant and of reductant under constant flow. The deflection of a laser beam was then used to monitor the mechanical bending of the cantilever as a result of the cooperative motion of the [3]rotaxanes. Reversible bending of the cantilever array was observed up to 25 times with a noticeable decrease of the deflection at each cycle due to chemical and/or physical passivation such as degradation of molecules and movement of gold atoms (Figure 86b).

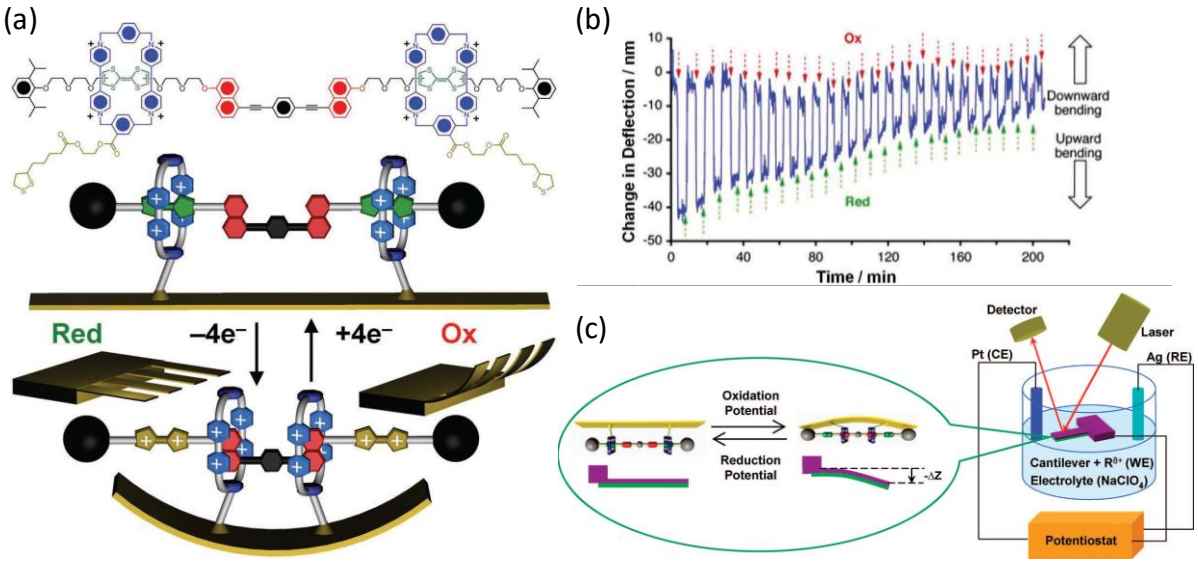

Figure 86: (a) Chemical structure of a [3]rotaxane used to functionalize a cantilever array and schematic representation of the bending occurring upon oxidation; (b) Evolution of the deflection of a laser beam upon successive oxidation / reduction cycles (up to 25); (c) Experimental set-up used to electrochemically actuate the cantilever array. Panels (a-b) are adapted with permission from reference [999], Copyright 2012 John Wiley and Sons. Panel (c) is reproduced with permission from reference [1009], Copyright 2009 American Chemical Society.

Control experiments further confirmed that the redox-controlled molecular motion of the macrocyclic rings is the only collective phenomenon at the origin of the deflection of the beam. The experimental deflection of the cantilever beam was found to be in good agreement with theoretical predictions, which consider that 6 billion of individual "molecular muscles" are required to fully cover the surface. Further work demonstrated that the same nanomechanical device can be controlled electrochemically using oxidizing (> +0.4 V) and reducing (< +0.2 V) potentials (Figure 86c).[1009] Compared with the use of a chemical oxidant as stimulus, this device operates more easily (no need to alternate the redox solution), much faster (~40 seconds for a cycle vs. ~10 minutes), and with larger responses (up to 550 nm vs. max 40 nm). Nevertheless, these improved performances were also accompanied by a so-called "creep" phenomenon which was attributed to the reorganization of molecules at the surface. These examples clearly highlight the possibility for [3]rotaxane to work in concert in order to produce a higher scale motion.

Based on their experience in using bistable [n]rotaxanes in a cooperative manner in nanomechanical and molecular electronics devices, the groups of Stoddart and Huang further demonstrated that the plasmonic properties of a gold nanodisc array can be switched by controlling the redox-state of bistable [2]rotaxane molecules (Figure 87).[1010] In solution, such molecules display different extinction spectra and a wavelength-dependent refractive index for their ground and oxidized states, which could be used to control the local surface plasmon resonance (LSPR) properties of metal nanoparticles. Thus, gold nanodisk arrays were coated with a monolayer of [2]rotaxanes using gold thiol chemistry. Using optical extinction spectroscopy, a red shift by ~10 nm of the LSPR peak at 690 nm of the gold nanodisk was monitored upon chemical oxidation with $Fe(ClO_4)_3$ (Figure 87b). Reversibility of this peak was observed when immersing the nanodisk in an aqueous solution of ascorbic acid, and over several redox cycles. A modification of the refractive index of the nanodisk from 1.31 to 1.37 accompanied this change in the LSPR peak position upon oxidation. Control experiments with bare naodisks and nanodisks decorated

only with the dumbbell confirmed that the observed optical phenomena are uniquely related to the synchronized switching mechanism of the rotaxane.

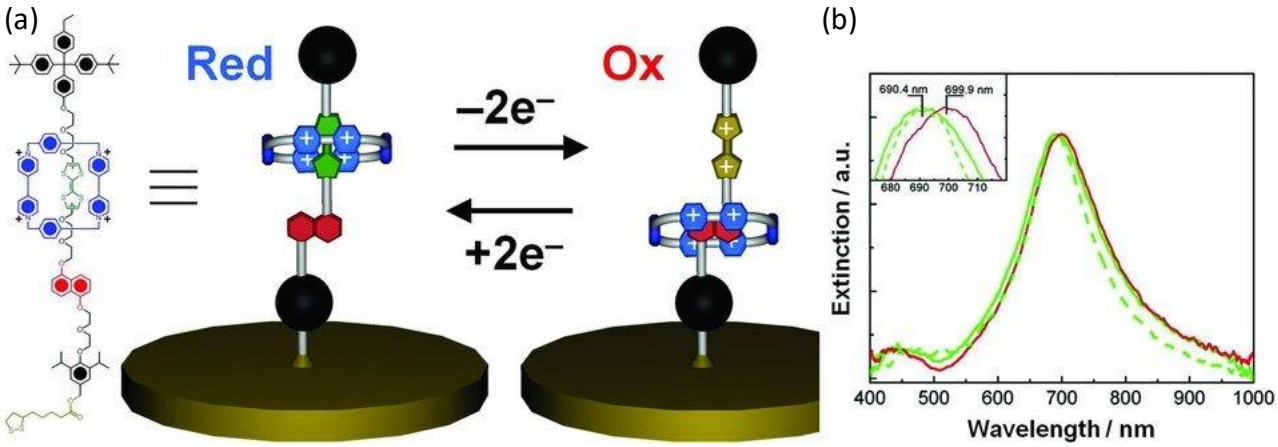

Figure 87: (a) Schematic representation of a gold nanodisk functionalized with a redox-active [2]rotaxane and its chemical structure; (b) Extinction spectra of the [2]rotaxane-functionalized gold nanodisk array just after functionalization (green), after oxidation (red) and after subsequent reduction (dashed green). Reproduced from reference [999], Copyright 2012 John Wiley and Sons.

More recently, the group of Stoddart in collaboration with the one of Guo reported the successful construction of a hybrid redox-bistable [2]rotaxane-graphene photoswitch with interesting electronic properties.[1011] The device consisted in a conductive single-layer graphene sheet, non-covalently decorated by a monolayer of light-responsive bistable [2]rotaxanes (Figure 88a). Characterization by UV-Vis absorption, XPS, Fourier transform infrared and Raman spectroscopies confirmed the successful grafting of the MIMs at the graphene surface. Upon reduction using triethanolamine and light under air-free conditions, shuttling of the $CBPQT^{4+}$ ring from the DNP station to the bipyridinium unit induced a large decrease (~12 %) in the source-drain current of the graphene, which could be reversibly restored in the dark and in the presence of oxygen (Figure 88b). Importantly, the low conductance state observed in the reduced form could be maintained if the device was stored under oxygen-free conditions, either with or

without light. Following a series of control experiments, the authors demonstrated that the photoswitching properties are directly related to the light-directed actuation of the [2]rotaxane molecules, which leads to the formation of a very stable bipyridinium/CBPQT$^{2(\bullet+)}$ complex that confers a non-volatile stability to the device (Figure 88c).

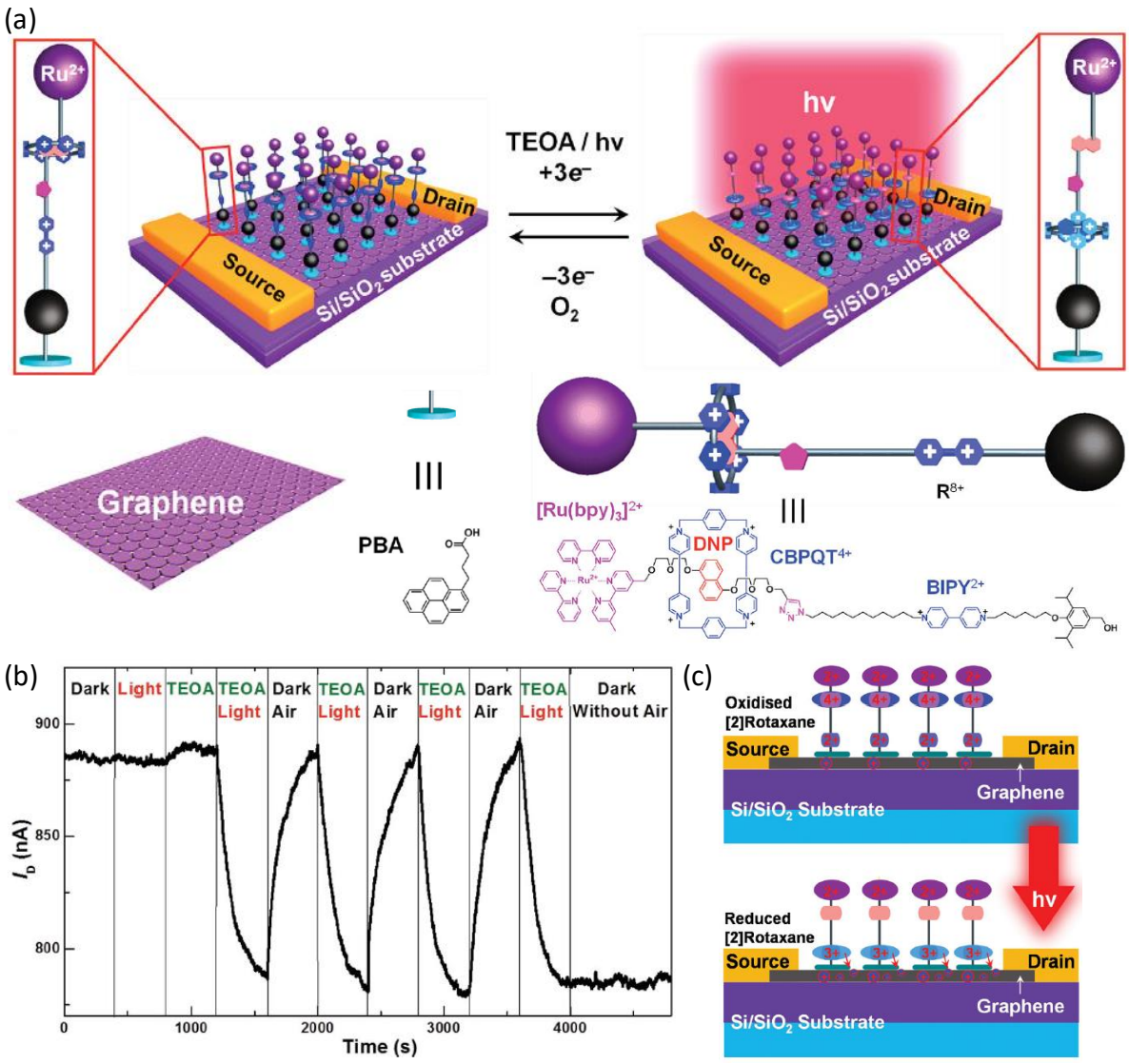

Figure 88: (a) Schematic representation of the redox-responsive graphene transistors built using a single monolayer of [2]rotaxanes and its chemical structure; (b) Evolution of the source-drain current (I_D) of the devices with time under different conditions, TEOA: triethanolamine; (c) Schematic representation of the

concerted reduction occurring at the rotaxane level during photoswitching. Adapted with permission from reference [1011], Copyright 2013 John Wiley and Sons.

The actuation of [2]rotaxanes has also been used to control the wettability of surfaces. For instance, the group of Willner reported the formation of a self-assembled monolayer of monostable redox-active [2]rotaxanes directly on a gold electrode (Figure 89).[1012] Upon reduction, the $CBPQT^{4+}$ ring is dissociated from the π-donor diaminobenzene unit and shifted toward the electrode, while oxidation restores the original position, as characterized by chronoamperometry and impedance experiments. By combining in situ electrochemical measurements with contact angle experiments, modification of the surface properties from hydrophilic to hydrophobic occurred upon reduction and in a reversible manner over several cycles.

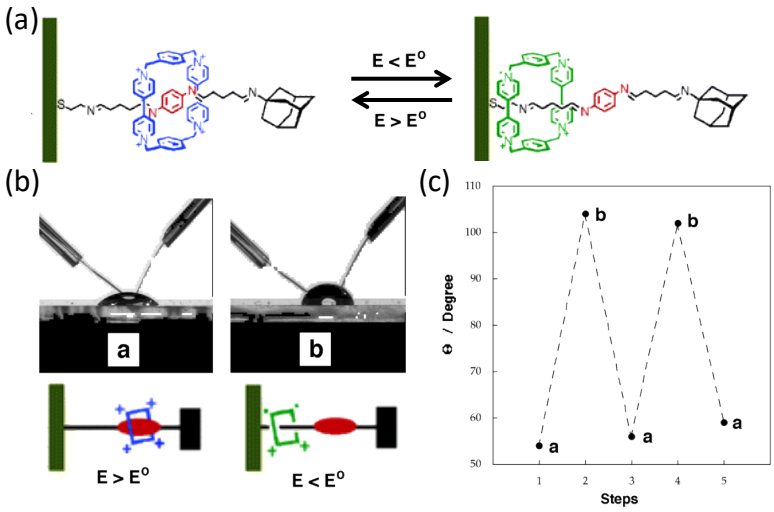

Figure 89: (a) Electrochemical switching on an imine-based [2]rotaxane immobilized on a gold surface; (b) Contact-angle measurements performed on the functionalized surface in the oxidized state a and reduced state b; (c) Variation of the contact angle values measured over 3 cycles of in-situ electrochemical switching of the rotaxane. Adapted with permission from reference [1012], Copyright 2004 American Chemical Society.

Shortly after, the groups of Leigh and Zerbetto reported the formation of a photoresponsive surface built from photo-switchable bistable [2]rotaxanes physisorbed on a gold surface modified with a thiol linker (Figure 90).[1013] This device is based on the *E*→*Z* photoisomerization of a fumaramide station, which induces a shuttling of the catenated macrocycle to a tetrafluorosuccinamide station (Figure 90a).

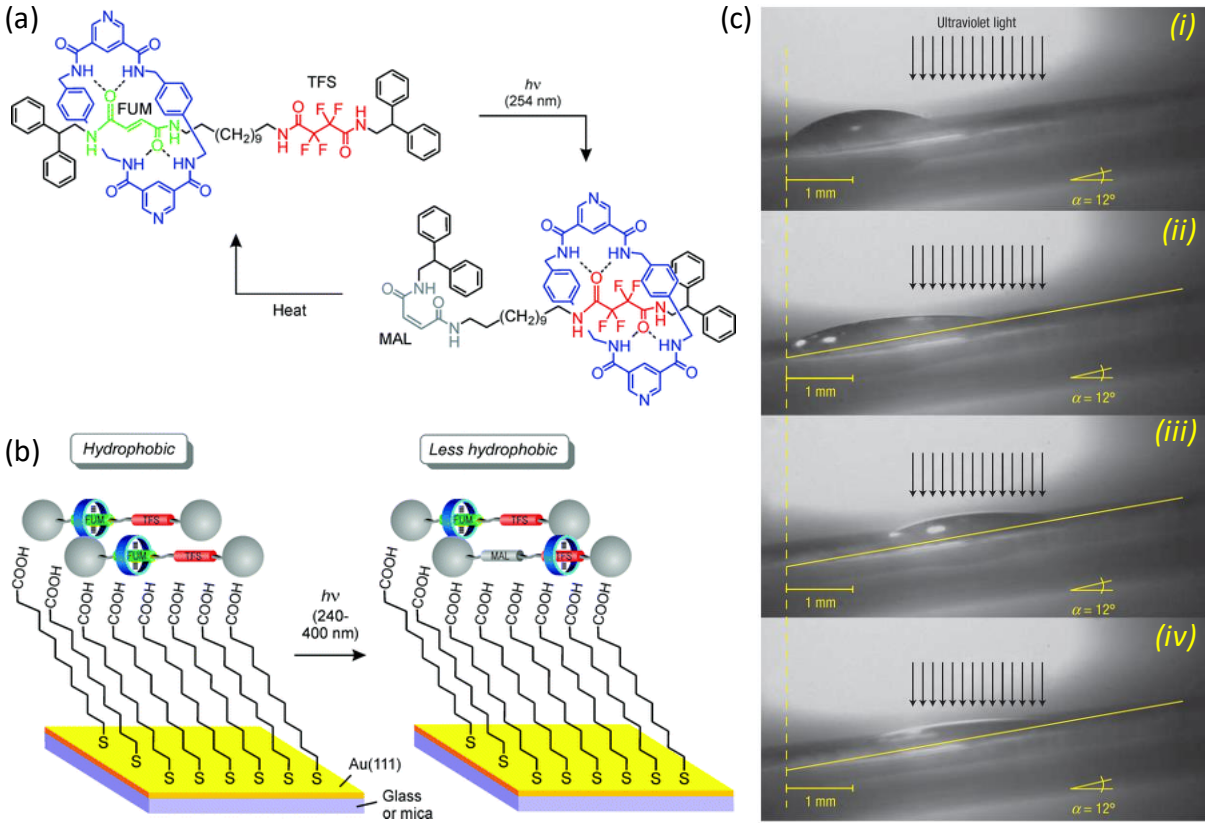

Figure 90: (a) Chemical structure of the bistable [2]rotaxane studied by Leigh and its reversible photocontrolled switch; (b) Schematic representation of the gold-surface modified by the physisorbed rotaxanes and the associated change in surface properties; (c) Evolution of the transport of a drop of iodomethane on a 12° incline surface over time, *(i)*: 0 s, *(ii)* 160 s, *(iii)* 245 s and *(iv)* 640 s of UV irradiation. Panels (a-b) are reproduced with permission from reference [990], Copyright 2009 The Royal Society of Chemistry. Panel (c) is reproduced with permission from reference [1013], Copyright 2005 Springer Nature.

Contact angle measurements were used to monitor the evolution of the surface properties after irradiation with UV light. For several low-volatility liquids including water and diiodomethane, a decrease in the contact angles occurred after irradiation because of the motion of the macrocycle towards the fluoroalkane residues present on the dumbbell. Interestingly, when a drop of diiodomethane was irradiated on one of its side with a perpendicular beam of light, one can observe the unidirectional motion of the drop at the micrometer scale in the direction of the light irradiated surface due to modification of the surface energy, following the same principle as for surfaces functionalized with azobenzene (see Section 2.2.1). Such drop could even be transported over ~1.4 mm against gravity on a 12° incline surface (Figure 90c). Considering that ~2 * 10^{12} molecules are located under the drop before transport and that only 40 % of them are properly isomerized during the transport, the authors estimated to ~9 kJ.mol^{-1} the contribution of each molecular machine to the collective motion against the gravity, which represents ~50 % of the absorbed photon energy. More recently, the groups of Schalley and Unger designed a new series of bistable [2]rotaxanes reversibly switchable using chloride anions.[1014] These rotaxanes were either covalently attached to a gold surface via an azide-alkyne click reaction leading to the formation of an ordered monolayer, or polymerized by supramolecular terpyridine/iron interactions to produce multilayer surfaces (Figure 91). Characterization of the mono- and multilayer (up to 20 layers of rotaxanes) surfaces was achieved thanks to a combination of spectroscopic and imaging techniques. Upon addition of chloride anions, these surfaces showed a decrease of their contact angles by ~20°, which could be attributed to the switching of the macrocycle from one station to another. Additional near-edge X-ray absorption fine structure (NEXAFS) spectroscopy provided further evidence for the collective motion of the threaded structures at the surface in ordered well-packed mono- and multilayers. Based on these experiments, the authors proposed that the switching process occurs through a nucleation/growth mechanism, which consists in a) the switching of one rotaxane as a rate-limiting step, b) the formation of a small nucleus of switched rotaxanes necessary to induce c) the quicker switching of the neighboring rotaxanes. The same

group subsequently developed a photoactivable [2]rotaxane which motion could be controlled over several cycles in a monolayer deposited on glass and silicon surfaces.[1015]

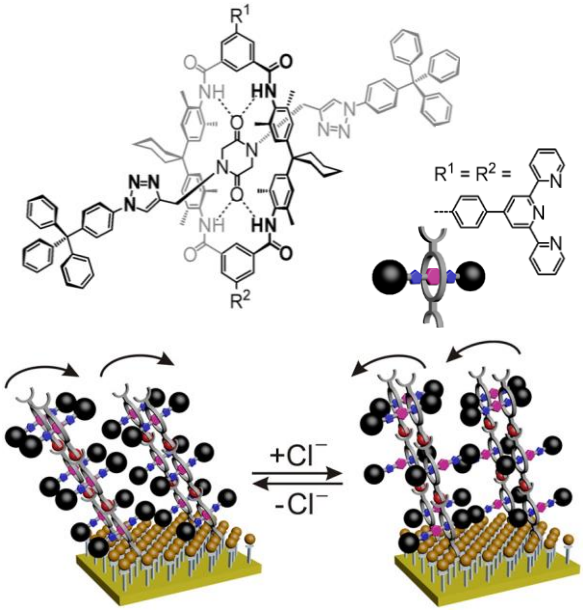

Figure 91: Chemical structure of the [2]rotaxane developed by the groups of Schalley and Unger which can be polymerized on surfaces by metal-ligand interactions to form chloride-responsive multilayers. Adapted with permission from reference [1014], Copyright 2015 American Chemical Society.

Finally, by covalently anchoring bistable redox-switchable [2]rotaxane on silica nanoparticles, the groups of Stoddart and Zinck demonstrated their possible utility for the controlled release of guest molecules (Figure 92).[1016,1017] The [2]rotaxane used to form the molecular valve is very similar to the ones previously mentioned that operate at surfaces. Porous silica nanoparticles (MCM-41) with an average diameter of 620 nm and with pore size of 1.5-2.0 nm were functionalized with these threaded structures using urethane chemistry. The nanovalves were originally synthesized as open forms, loaded with guest molecules such as luminescent iridium complexes Tris(2,2'-phenylpyridyl)iridium(III) or rhodamine B, and finally closed by adding a chemical oxidant ($Fe(ClO_4)_3$). Upon addition of ascorbic acid with switches the $CBPQT^{4+}$ macrocycle from the dioxynaphthalene to the TTF stations, fluorescence spectroscopy

showed an immediate and fast increase of the emission intensity, in agreement with the release of the guest molecules. Precise location of the rotaxanes on the nanoparticles, and modification of the size of the linker depending of the size of the molecules to release, are among important parameters to achieve a controlled release of the guests.[1017]

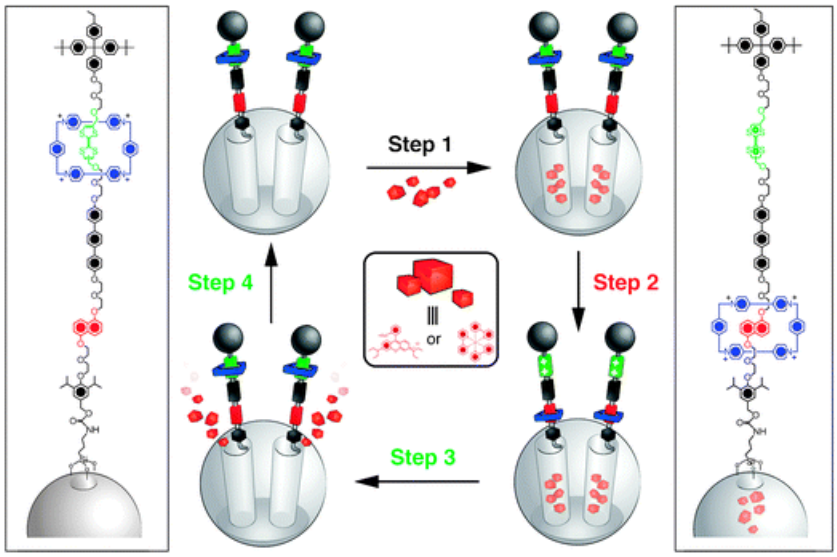

Figure 92: Schematic representation of silica nanoparticles decorated by [2]rotaxanes, their loading with guest molecules such as Rhodamine B or iridium complexes (Step 1); closing of their pores after oxidation of the TTF stations (green) (and shuttling of the CBPQT macrocycle (blue) over the DNP station (red)) (Step 2); opening of the pores upon addition of ascorbic acid to reduce the TTF unit (Step 3); releasing of the guest molecules (Step 4). Reproduced with permission from reference [1005], Copyright 2012 The Royal Society of Chemistry.

Some years later, in a more fundamental study, the group of Stoddart in collaboration with the one of Grzybowski reported the functionalization of metal nanoparticles with bistable redox-switchable [2]rotaxane.[1018] Similarly to their observations on gold nanoparticles decorated with [2]catenanes,[996] they showed that the rotaxane-based gold nanoparticles can change their zeta potential upon oxidation (from +20.1 mV to +30.4 mV in the reduced and oxidized forms respectively) in a reversible manner over

several cycles. Using cyclic voltammetry experiments, the authors showed that the modified nanoparticles exist as two metastable- and ground-state co-conformations. The relaxation kinetics between these two states can be controlled by different parameters including the density of rotaxanes on the surface and occurs at a faster rate when the rotaxanes are located on metal nanoparticles compared to their behavior at surfaces or in polymer matrix. The group of Qu further functionalized silica nanoparticles with pH-sensitive rotaxane units and demonstrated the reversible pH-modulation of the fluorescence properties in solution and in the bulk, thanks to the concerted motion of the mechanically active units on a single nanoparticle.[1019]

Many developments have been made also in the field of rotaxane-crosslinked polymers, leading to materials with very interesting gliding topologies and unconventional mechanical behaviors.[1020] However, because the molecular components are not bistable, no collectively switchable motions have been reported so far, and these systems fall out of the scope of this review. However, a few examples report the use of polyrotaxane with a micro-/macroscopic behavior related to the controlled collective motion at the molecular level. In the early 2010s, the groups of Stoddart and Heath reported the synthesis of poly[*n*]rotaxanes incorporating 1,5-dioxynaphtalene and TTF stations for $CBPQT^{4+}$ macrocycles.[1021] The synthetic strategy designed to reach these polymers consisted in the synthesis of a main chain polymer with the electroactive stations, which then serve as guest units for clipping the cyclophane rings. Polymers with molecular weights ranging from 8 to 94 kDa were synthesized, containing from 90 to 72 % of $CBPQT^{4+}$ units of the TTF moieties (as determined by ^{1}H NMR studies). Cyclic voltammetry studies on the polymer in solution confirmed their reversible redox-active properties, in agreement with previous works involving similar individual molecules. Finally, studies on the electroactive behavior of the polymer in solid-state switches showed electrical signatures (hysteresis and bistability) similar to the ones observed in the aforementioned examples on small-molecule analogues. This example clearly establishes that the physical properties observed at the micrometric level are related to the collective motion of the

rings at the polymer scale. Recently, the group of Ke reported the synthesis of polyseudorotaxane hydrogels from micellar solutions of triblock copolymers, which serve as host for α-cyclodextrin guests.[1022] After 3D-printing, photo-irradiation to cross-link the micellar aggregates and rinsing to remove any excess of cyclodextrin, polyrotaxane monoliths with a millimeter size were obtained (Figure 93). The presence of several cyclodextrin rings interconnected by hydrogen bonding on a single polymer chain in the different materials (hydrogel and monolith) proved to be important for their mechanical robustness as they form crystalline domains that act as rigid supramolecular struts and non-covalent crosslinkers. This was exemplified by the behavior of the monolith in DMSO, which completely spread out and lost their mechanical robustness as determined by rheology experiments.

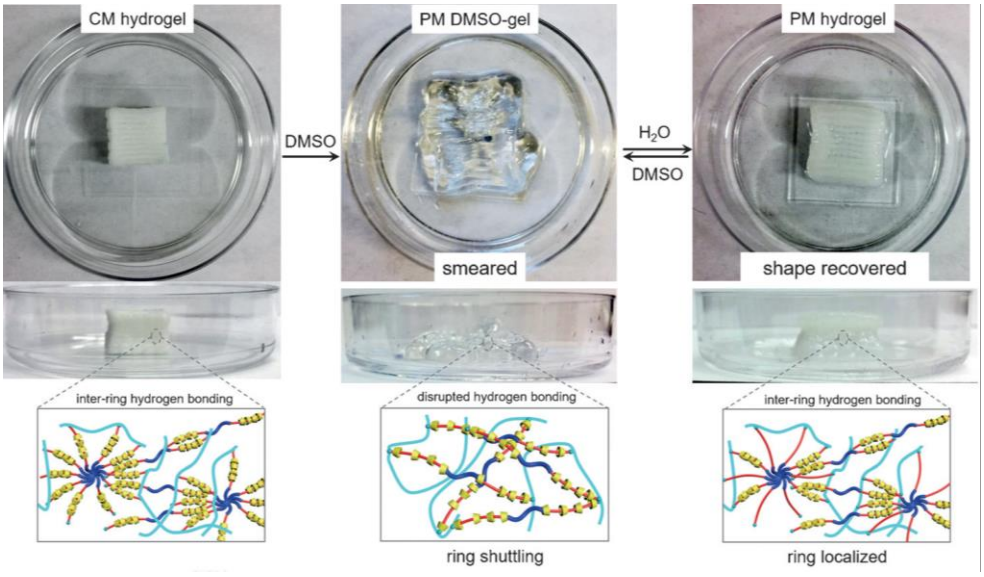

Figure 93: Top-view and side-view images of the cross-linked monolith hydrogel (CM hydrogel) obtained after polymerization, its evolution as smeared gel after soaking in DMSO for several hours (PM DMSO-gel) and its shape recovery after rinsing with water (PM hydrogel). Insets show a cartoon representation of the cross-linked network and the behavior of the cyclodextrin rings (yellow) when changing the solvent. Adapted with permission from reference [1022], Copyright 2017 John Wiley and Sons.

Recovery of the shape occurred after immersing the material in water for a few hours. These monoliths also behave as shape-memory materials able to transfer chemical energy (solvent exchange) into mechanical work by simple reorganization of their structures at the molecular level. Overall, the macroscopic change recoveries observed in this work are related to the different behavior of the cyclodextrin rings at the molecular level on the poly[*n*]rotaxane chains, i.e. free shuttling motion in DMSO and localization in water. In relation with their work on [*c*2]daisy chain rotaxanes (see next part), the group of Harada succeeded in developing a polymeric actuator involving [2]rotaxane as mechanically-active light-responsive units (Figure 94a).[1023] A [2]rotaxane motif built from an α-cyclodextrin surrounding an azobenzene unit was polymerized via a polycondensation reaction with a poly(ethylene glycol) chain. Upon light irradiation with UV or visible light, the material in its hydrogel or xerogel state could be reversibly deformed because of the *trans* to *cis* isomerization of the azobenzene units which further displace the cyclodextrin units. For the xerogel, actuation toward the light source occurred within 3 seconds and shining light on the other side induced reversibility to the initial shape (Figure 94b-c). This material was also shown to convert light energy to mechanical energy within 10 seconds. These interesting mechanical properties are mainly related to the orientation of the rotaxane within the polymer network and their concerted motion upon light stimulation. All these recent examples should stimulate the use of polymers based on [n]rotaxanes to develop new materials with interesting physical properties.

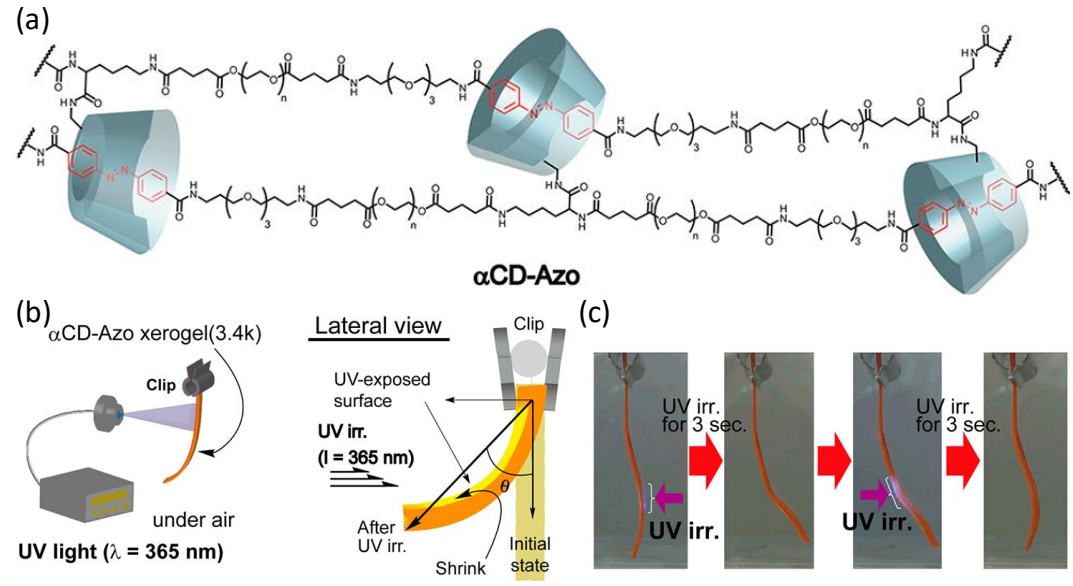

Figure 94: (a) Chemical structure of the light-responsive polymeric actuator based on [2]rotaxanes developed by the group of Harada; (b) Schematic representation of the experimental set-up used to actuate this polymeric actuator and lateral view of the bending phenomenon occurring in the xerogel state; (c) Images showing the evolution of the xerogel upon UV irradiation for 3 seconds from the right side and the left side successively. Adapted with permission from reference [1023], Copyright 2018 American Chemical Society.

Mechanically interlocked molecules such as catenanes and rotaxanes have also been considered as potentially interesting structures to form liquid-crystalline (LC) phases.[1024] The work related to catenanes is not described in this review as it just describes the formation of LC phases without considering the possible motion of the interlocked rings. On the other hand, the groups of Stoddart and Kato described the synthesis of a bistable [2]rotaxane decorated with dendritic mesogenic stoppers, which present smectic A LC phase behavior up to 146 °C (Figure 95a).[1025,1026] The electrochemical switching of the $CBPQT^{4+}$ macrocycle occurs in the mesophase as demonstrated by cyclic voltammetry and spectroelectrochemistry measurements. In their initial work, the LC phase did not change upon shuttling probably because of the

staggered molecular arrangement of the mesogens in the LC phase.[1025] However, when electrochemical cells were fabricated with the LC films in the presence of an electrolyte, a marked change in the UV-Vis-NIR spectrum of the cell upon oxidation corresponding to the oxidation of all TTF units and shuttling of the CBPQT ring towards the naphthalene station was observed.[1026] This spectral change was associated with a visible color change of the film upon oxidation, which can be reversibly changed to its original greenish brown color by applying a negative potential (Figure 95b). This example further expands the possible applications of [n]rotaxanes in devices which properties are controlled at the molecular scale by the concerted motion of mechanically interlocked molecules.

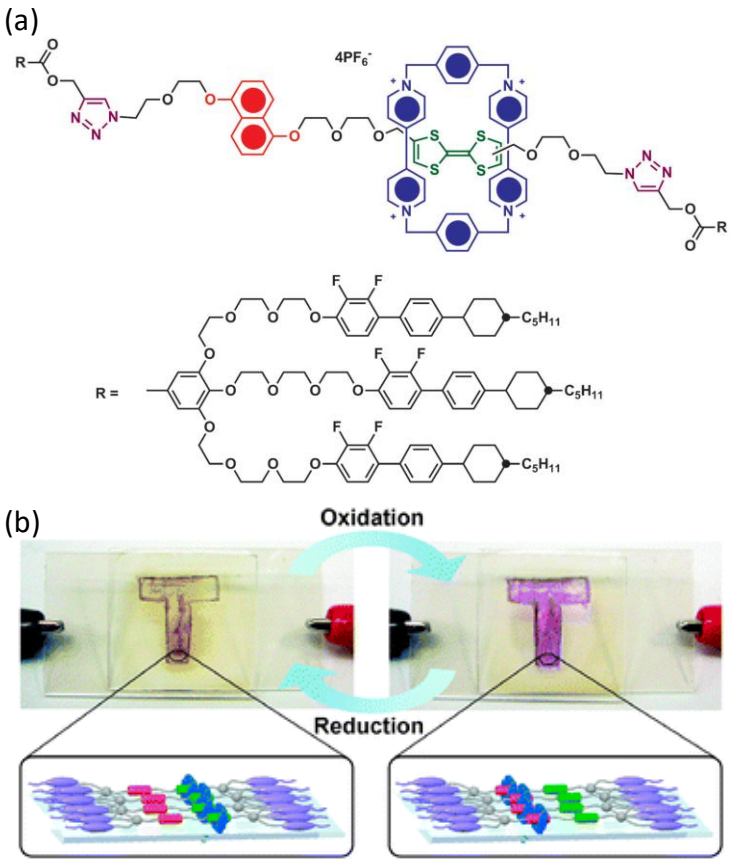

Figure 95: (a) Chemical structure of a bistable redox-sensitive liquid crystalline [2]rotaxane; (b) Photographs showing the change in color occurring in an electrochemical cell upon oxidation and reduction, cartoons represent the [2]rotaxanes in their reduced (left) and oxidized (right) form. Parts (a)

and (b) are reproduced with permission from reference [1024], Copyright 2012 John Wiley and Sons, and reference [1026], Copyright 2010 The Royal Society of Chemistry, respectively.

Over the last ten years, the group of Loeb has pioneered the incorporation of [2]rotaxanes within metal-organic framework (MOF) structures.[1027–1029] Using various solid state NMR experiments, internal motion of the macrocycle within the MOF,[1027] phase change of the MOF induced by the motion of the macrocyclic ring[1028] but also movement of the macrocyclic ring between struts of the MOF[1029] was observed. However, the motion observed in these systems does not involve a controlled motion of the mechanical bond. Similarly, the group of Horie reported several studies on the motion of crystals incorporating pseudo-rotaxanes upon light irradiation.[1030–1033] In all these examples, lighting of a metallocene ligand present on the pseudo-rotaxane leads to changes of the size and shape of the crystal resulting from a different packing of the molecular structures. Although these crystals showed interesting properties in terms of cycling or for transport, it is clear that there is no motion of the mechanical bond at the origin of these properties. Thus, all these examples incorporating mechanically interlocked molecules within MOFs and crystals will not be discussed further in this review but are mentioned as a potential source of inspiration for further developments.

Finally, some polymer backbones decorated with pendant rotaxane units have been reported.[1034–1036] Upon pH stimulation, a change of fluorescence related to the motion of the macrocyclic unit within the polymer chain was observed in solution and in the solid state.[1034,1035] When a single rotaxane side-chain was present on the polymer backbone, this polymer could be used to pattern surfaces which showed sensing properties for DMSO and protons in the form of an "INHIBIT" Boolean logic gate.[1036] In another example, a polymer backbone decorated with pendant macrocyclic bis-pyridinium units was used to aggregate different nanoparticles.[1037] When this polymer was mixed in a solution containing gold nanoparticles with naphtalene units and silver nanoparticles with TTF units, chemical oxidation/reduction

of the TTF units leads to reversible optical changes related to the presence of a single population of nanoparticle in solution. Finally, the mechanical oscillation of a "polyrotaxane-interlocked" gel was reported.[1038] The change in topological structure of the gel (contraction and extension) is driven by the oscillating Belousov-Zhabotinsky reaction which occur thanks to the presence of ruthenium-terpyridine ligands on the polymer chains.

3.2.3. Collective motion from [*c*2]daisy chain rotaxanes

Biology has always been an incredible source of inspiration for chemists. In the context of collective motion, muscles are known to actuate thanks to the synchronized motion of sarcomere units that are polymerized into myofibrils filaments.[1039] The development by the group of Sauvage[1040] of individual [*c*2]daisy chains capable of reversible contraction and extension events thanks to metal ligand interactions has been instrumental for the molecular machine community to simplistically mimic such macroscopic events. With the goal to amplify this molecular sliding movement at higher length scales, initial efforts have focused on the possibility to access polymers made of [*c*2]daisy chains rotaxanes.[1041] In 2006, using an N-alkylation polymerization reaction, the group of Kaneda reported the formation of dimers, trimers, tetramers and pentamers of [*c*2]daisy chains built on α-cyclodextrin as macrocyclic units complexing azobenzene moieties as stations on the axle in 33 %, 14 %, 4 % and 2 % yield after recycling preparative gel permeation chromatography (GPC), respectively.[1042] Upon light stimulation at 366 nm, the cyclodextrin which originally sits around the azobenzene unit in the *trans* form is displaced as the azobenzene motif switches to its *cis* form. This contraction event could be monitored on both the individual [*c*2]daisy chain and its trimer by ^{1}H NMR and UV-Vis absorption experiments. On the single molecule after irradiation, NMR experiments demonstrated the presence of three photoisomers *E,E*, *E,Z* and *Z,Z* in a 75:20:5 ratio, which could be reversibly switched to one single *E,E* isomer upon heating at 90 °C. On the trimer, broad signal corresponding to isomeric mixtures were observed after light

irradiation, confirming that each azobenzene unit can be switch independently but with a theoretical content of Z_6-isomer as low as 0.013 %. Some years later, in 2009, the groups of Stoddart and Grubbs independently reported the covalent polymerization of [*c*2]daisy chain rotaxanes using the copper-catalyzed [3+2] Huisgen cycloaddition reaction.[1043,1044] The monomer designed by Stoddart and co-worker involves a 24-crown-8 macrocycle as host for either a secondary ammonium or a bipyridinium station, thus leading to a bistable pH-responsive interlocked structure. Step-growth polymerization between the bis-alkyne-terminated [*c*2]daisy chain and 1,4-bis(2-azidoethoxy)benzene led to main-chain polymers composed of ~11 repeating units and a dispersity of 1.85 as estimated by GPC (Figure 96a). Acid-base switching of the oligomers was monitored by ^{1}H NMR, UV-Vis absorption spectroscopy and cyclic voltammetry, demonstrating the reversible bistable character of the macromolecule (Figure 96b).

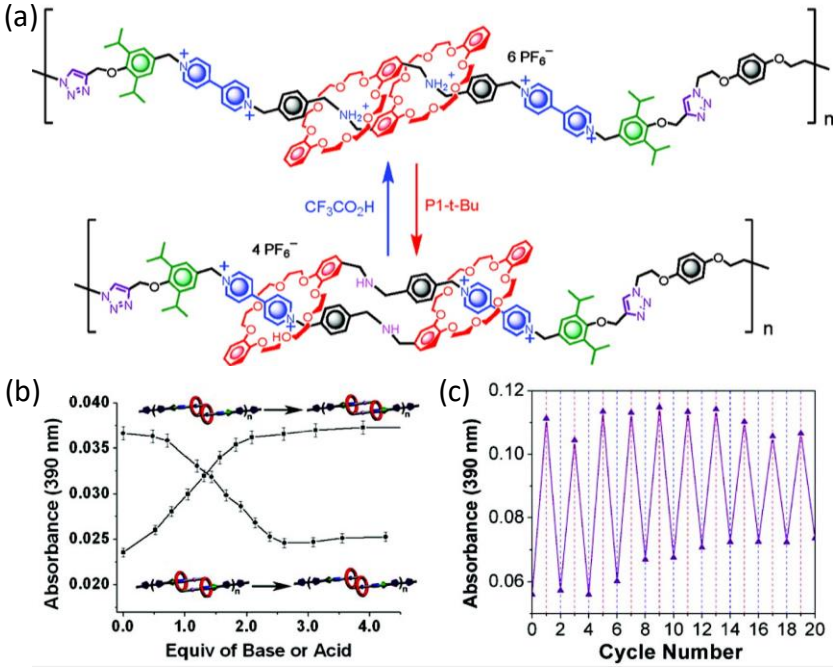

Figure 96: (a) Structure of the [*c*2]daisy chain polymer synthesized by the group of Stoddart and its actuation upon changing the pH; (b) Evolution of the absorbance of the polymer at 390 nm corresponding to the charge-transfer band between the bipyridinium station and the crown ether macrocycle upon

addition of base or acid; (c) Evolution of this absorbance for up to 20 acid / base cycles. Adapted with permission from reference [1043], Copyright 2009 American Chemical Society.

Further analyses using stopped-flow spectrophotometry techniques established that the presence of more destabilized kinetic intermediates leads to a faster acid-triggered extension compared to the base-induced contraction and a slower actuation for the monomer compared to the polymer.[1045] However, the small size of the polymers, mainly because of solubility issues occurring during the polymerization, precluded any conclusion on the possible amplification of molecular motion to higher length scales. In parallel, Grubbs and coworkers designed a monostable bis-azide-terminated [*c*2]daisy chain which could be polymerized with 1,4-diethynylbenzene, leading to a step-growth main chain polymer composed of 22 repeating units and with a radius of gyration R_g of ~14.8 nm as estimated by GPC using a multiangle laser light scattering (MALLS) detection (Figure 97). While deprotonation of the secondary ammonium stations did not lead to extension of the polymer chain probably because of favored π-π slipped-stacking interactions between bis-aryl units, their acylation and thus increased bulkiness led to a forced slippage which resulted in an extension up to 21.4 nm (R_g), representing a 48 % increase in size in agreement with the expected dimer extension (Figure 97b(*ii*-*iii*)).

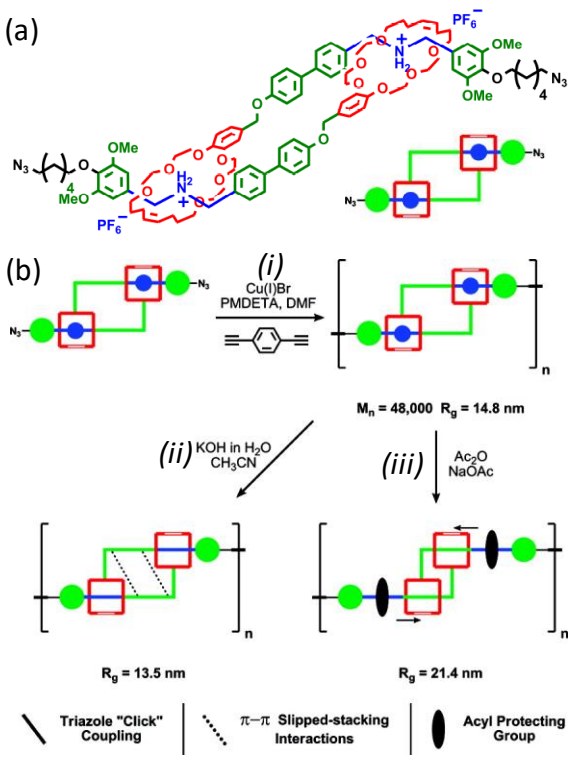

Figure 97: (a) Chemical structure of the [*c*2]daisy chain monomer synthesized by the group of Grubbs, (b) *(i)* Polymerisation of this monomer by step-growth polycondensation with 1,4-diethynylbenzene and actuation of the polymer using either *(ii)* base or *(iii)* acetic anhydride leading to macromolecules with various radius of gyration (R_g). Adapted with permission from reference [1046], Copyright 2009 American Chemical Society.

The first example demonstrating the collective motion of [*c2*]daisy chain units embedded in a single chain polymer (from nanometric to micrometric scale length) was reported by our group in 2012.[1047] Bistable pH-switchable [*c*2]daisy rotaxanes were decorated with terpyridine units as end groups and polymerized using zinc(II) or iron(II) metal ions via supramolecular metal-ligand interactions (Figure 98a-b).

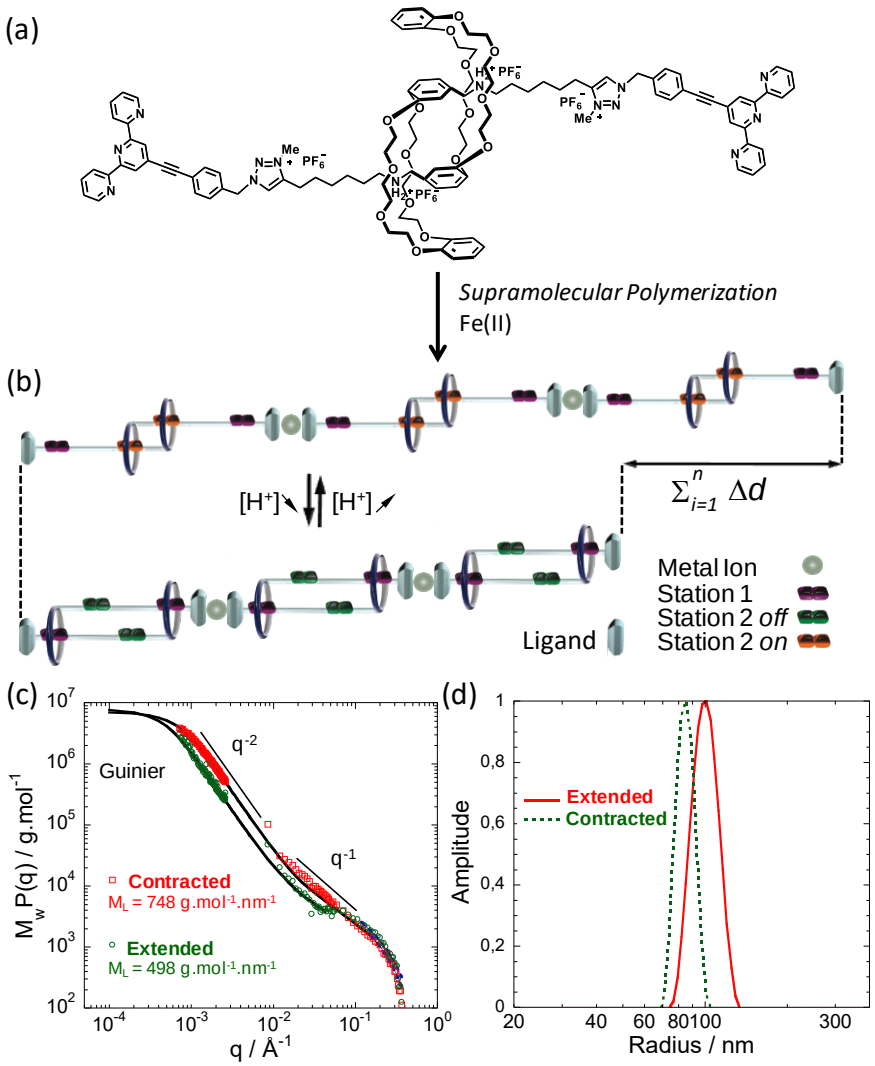

Figure 98: (a) Chemical structure of the [*c2*]daisy chain monomer functionalized with terpyridine stoppers developed by the group of Giuseppone; (b) Schematic representation of the supramolecular polymer obtained using Fe(II) ions and its bistability upon pH stimulation; (c) Evolution of the light and neutron scattering curves for the contracted and extended Fe(II) polymers highlighting the difference in linear mass density M_L; (d) Difference in hydrodynamic radius measured by light scattering experiments between the contracted and extended Fe(II) polymers confirming the actuation at the microscopic scale. Adapted with permission from reference [1047], Copyright 2012 John Wiley and Sons.

Characterization of the shape and size of the polymers was performed using a combination of light and neutron scattering experiments (Figure 98c-d). For both polymers, the scattering profile consisted in q^{-2} and q^{-1} domains at low and intermediate scattering vectors q and a Guinier regime at high q range. Such scattering variations are characteristic of a perfectly soluble single wormlike chain polymer. For the ones made of iron, data fitting suggests the same degree of polymerization (DP) as high as ~2900 units, a decrease in the linear mass density M_L (- 250 $g.mol^{-1}.nm^{-1}$) and an increase in contour length L_C (+ 6463 nm) for the extended polymer compared to the contracted one. Actuation of the polymer chains proved to be reversible by acid/base stimulation. These data are in agreement with the dimensions expected from the DP and the size of the monomers and were further supported by theoretical explanations provided by the group of van Hove.[1048,1049] Overall, this work demonstrates the possibility to amplify the molecular motion of [*c*2]daisy chain rotaxanes via their concerted actuation by four order of magnitudes from the nanometer to the 10 micrometer scale. Using the same polymerization technique with iron ions and terpyridine ligands, the group of Huang subsequently reported the solvent-sensitive actuation of polymers made of [*c*2]daisy chains based on pillar[5]arenes.[1050] While TEM and SEM microscopy experiments showed the presence of fibrillar aggregates for different solvent compositions, dynamic light scattering experiments highlighted an increase of the hydrodynamic radius of the aggregates from 104 nm in pure chloroform to 254 nm in pure DMSO, in agreement with the extension of the interlocked unit upon increasing solvent polarity. In 2016, our group reported the possibility to bundle single wormlike polymer chains by changing the nature of the supramolecular polymerization while keeping the actuation properties.[1051] [*c*2]daisy chain rotaxanes with 2-aminopyridine end groups were successfully polymerized via hydrogen-bond interactions with a complementary rigid hydrophobic bis-uracil-terminated linker, as determined by ^{1}H NMR experiments (Figure 99a). Interestingly, TEM and AFM microscopy experiments revealed marked morphological differences between the contracted and extended states, as qualitatively determined by a combination of light and neutron scattering experiments. While micrometer-long

entangled fibers were observed for the extended polymer, more discrete coffee-grain-like structures with an average length comprised between 200 and 400 nm were imaged for the contracted one (Figure 99b).

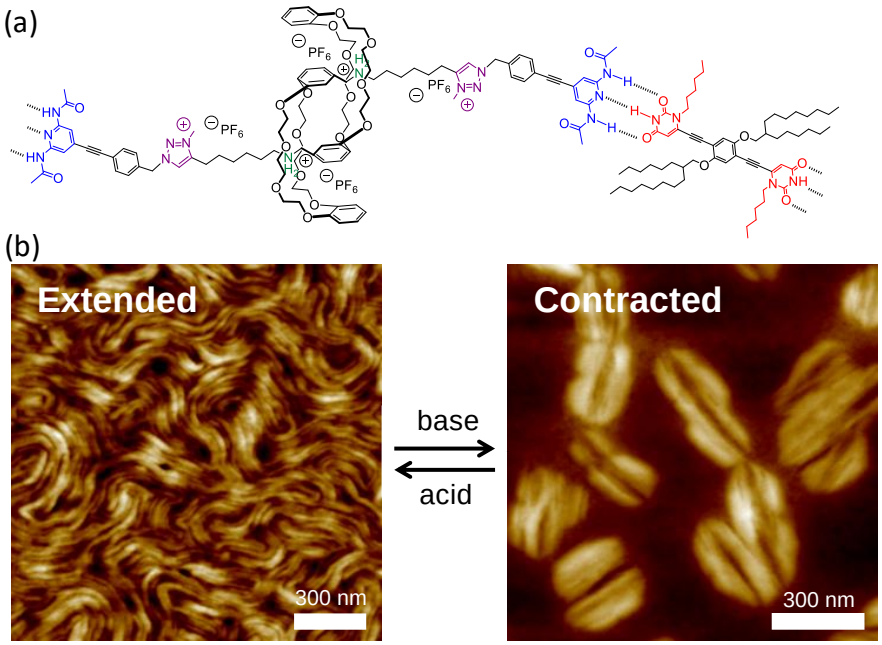

Figure 99: (a) Chemical structures of the [*c*2]daisy chain monomer functionalized with 2,6-diamidopyridine stoppers and polymerized with a bis-uracil linker; (b) AFM images of the entangled fibers and the coffee-grain-like structures observed in the extended and contracted states, respectively. Adapted with permission from reference [1051], Copyright 2015 John Wiley and Sons.

Importantly, AFM imaging at high magnification demonstrated that both kinds of objects are composed of single polymer chains with an internal diameter of ~4 nm bundled into larger aggregates thanks to a combination of lateral π-π and van der Waals interactions from the linker. The difference in morphologies can be explained by the difficulty of the polymer to sustain the contraction event due to the relatively low stability of the considered hydrogen bond motif,[1052] as already observed for supramolecular systems[1053] and thus leading to partial depolymerization in addition to a mechanical actuation. Nevertheless, this work

highlights the possibility to modulate the microscopic properties of polymers by actuating molecular machines.

In order to achieve collective motion at the macroscopic scale, two strategies have been proposed, based either on the physical reticulation of single polymer chains or on the formation of covalent polymer networks. For the first approach, our group designed a bistable [*c*2]daisy chain rotaxane capped with ureidopyrimidinone (UPy) end groups.[1054] These hydrogen-bond motifs are known to form dimers with high association constants in organic solvents, which further aggregate by stacking interactions.[1055] In toluene, photodeprotection of the 2-nitrobenzyl-protected UPy-modified rotaxanes leads to the formation of a gel for the extended monomer and to a solution for the contracted one, which could be reversibly switched to the gel state upon protonation (Figure 100). In both cases, small angle neutron scattering experiments confirmed the formation of a hydrogen-bonding supramolecular polymers with a DP estimated to 22 for the contracted one, in agreement with the low dimerization constant of the UPy measured by isothermal titration calorimetry for the contracted solution as a result of the proximity of the crown ether macrocycle. Importantly, in-depth neutron and X-ray scattering studies on the extended gel phase provided valuable information on its internal structure, which consists in a crystal-like phase with stacks of UPy dimers acting as physical reticulation nodes.[1056] These experiments suggest that, in the contracted state, the presence of the crown ether macrocycle in the vicinity of the UPy motif prevents dimers stacking, which in turn preclude the formation of a gel by physical reticulations. A similar gel-sol transition was later on observed for a [*c2*]daisy chain with hydrogen-bonding tri-alkylated stoppers.[1057] These examples demonstrate the possibility to achieve collective motion at the macroscopic scale using supramolecular polymers based on [*c2*]daisy chain rotaxanes and to change interesting properties of the materials therefrom, but also raise the problem of maintaining material integrity with supramolecular polymers upon actuation.

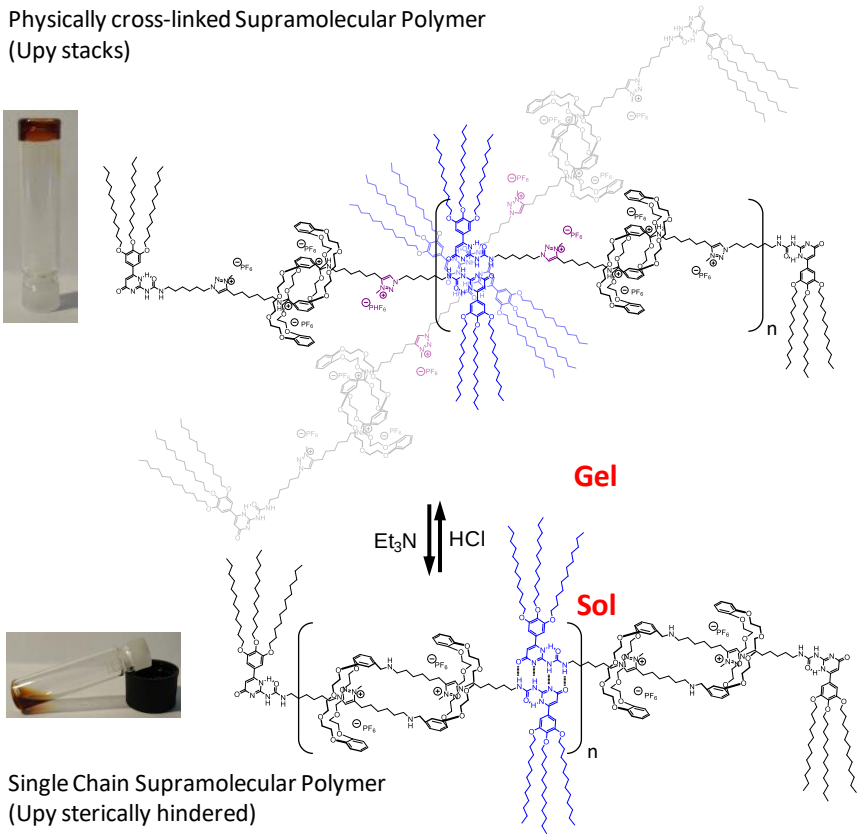

Figure 100: Supramolecular polymers made of [*c*2]daisy chain rotaxanes polymerized using self-complementary ureidopyrimidinone (UPy) stoppers giving rise to a physical gel in the extended form (due to stacking interactions between the UPy dimers) and to a solution made of a single chain supramolecular polymer (n = 22 at c = 4 mM) in the contracted form due to steric hindrance of the crown ether macrocycle preventing any stacking of the UPy. Adapted with permission from reference [1054], Copyright 2017 American Chemical Society.

To date, the only way envisioned to circumvent this limitation has focused on integrating [*c*2]daisy chain units into covalent polymer networks. In 2016, the group of Harada prepared photoresponsive polymeric hydro- and xero-gels from cyclodextrin-based [*c*2]daisy chain units with a single azobenzene station and reticulated by a four-arm poly(ethylene glycol).[1058] Upon UV irradiation, the hydrogel was

shown to contract due to the *trans*→*cis* isomerization of the azobenzene units, while the use of visible light could reversibly restore the initial size of the gel (Figure 101a).

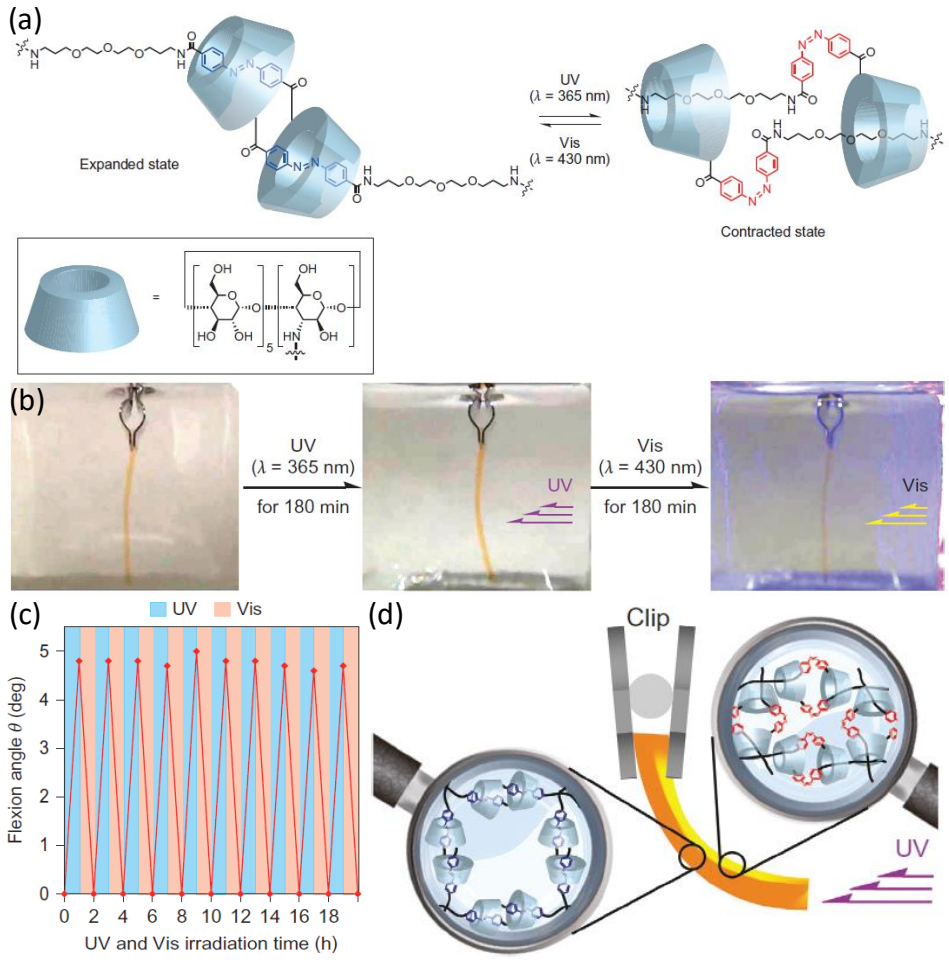

Figure 101: (a) Chemical structure of the bistable photoresponsive [*c*2]daisy chain rotaxane unit used to formed chemically cross-linked polymer gels; (b) Photoresponsive behavior of a small plate of [*c*2]daisy chain hydrogel upon UV and visible light irradiation; (c) Reversible cycling of this hydrogel over 10 irradiation cycles; (d) Cartoon showing how the azobenzene unit located on the side of the irradiation are isomerized to the *cis* form while the ones on the other side remain in their trans form, thus explaining why the materials bend. Adapted with permission from reference [1058], Copyright 2016 Springer Nature.

Interestingly, the same material in the absence of [*c*2]daisy chain but with remaining azobenzene units presented a reversed swelling behavior upon UV irradiation, as a result of increased mesh sizes of the network in the *cis* form. In water, a thin plate of [*c*2]daisy chain gel could be reversibly actuate more than ten times with the material bending towards the source of UV light as a result of partial light penetration and without significant alteration of the material (Figure 101b-d). This actuation proved to be much slower (hours versus seconds) than for the xerogel but, in this latter case, no reversible motion was observed using visible light. As only UV light could be used to photoactuate the xerogel, recovery of the bending could only be observed by sequentially shining UV light on the right and left side of the material. This pseudo-reversiblity was proposed to arise from the weak hydrophobic interactions occurring between the azobenzene units and the cyclodextrin ones in the dry state. Nevertheless, this material was found to be stiff enough to lift a match (~100 mg). A similar system involving stilbene instead of azobenzene units was further developed by the same group (Figure 102).[1059] While contraction of the hydrogel occurred upon UV-A irradiation at 350 nm, extension of the material was performed with UV-C at 280 nm. Compared to the previous system, actuation was found to occur 60 times faster (30 seconds versus 3 hours) due to higher reaction rate, conversion and quantum yield of the stilbene in the photoisomerization process. The authors also studied the influence of the size of the four-arm poly(ethylene glycol) units on the deformation and mechanical properties of the hydrogel (Figure 102b). The higher the molecular weight of the four-arm polymer was, the higher volume change as well as the Young modulus and fracture energy were upon contraction. In the dry state, a quasi-reversible actuation of the material was observed and could be repeated up to 15 times in a row over ~1 minute without apparent loss of efficiency (Figure 102c). Compared to the first system involving azobenzene units, the mechanical work produced by the xerogel is 150 times higher, as illustrated by the possibility to lift a weight which is 15 times heavier than the actuating material.

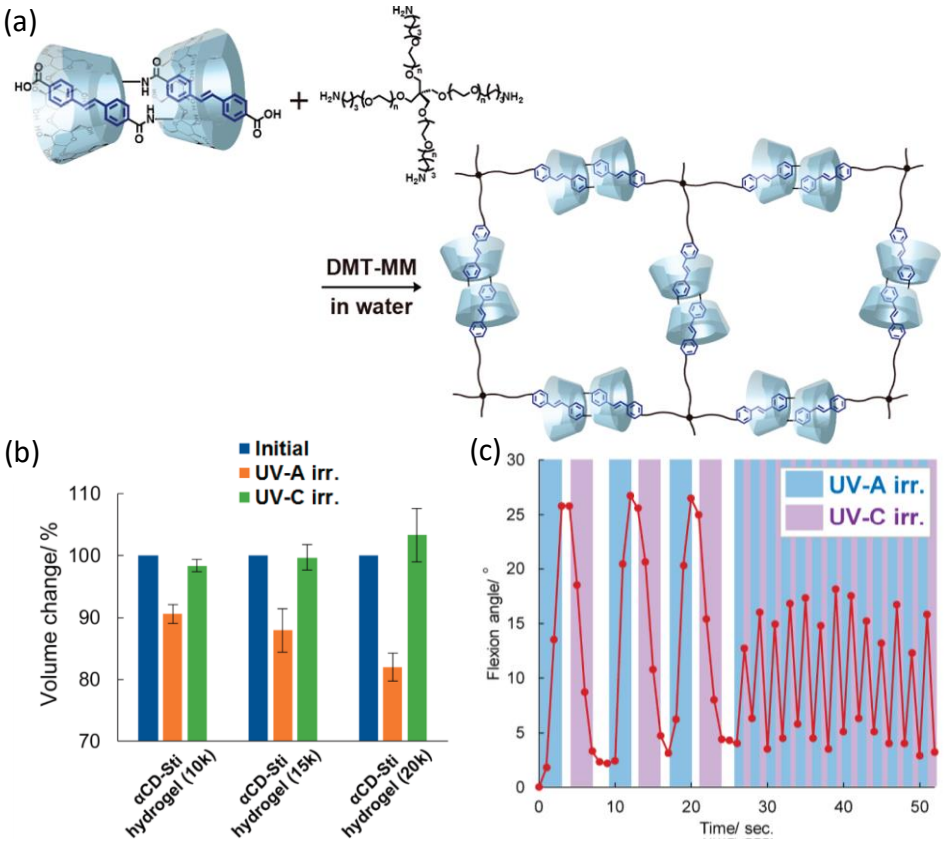

Figure 102: (a) Chemical structure of the [*c*2]daisy chain polymer network synthesized from a tetra-PEG unit and a [*c*2]daisy chain monomer based on stilbene; (b) Reversible evolution of the volume change measured during the contraction and extension of a hydrogel made of tetra-PEG units with different sizes under UV-A and UV-C irradiation, respectively; (c) Evolution of the flexion angle measured during the bending of a xerogel cycled several times over less than one minute upon different UV irradiations. Adapted with permission from reference [1059], Copyright 2018 American Chemical Society.

Alternatively, our group reported the possible pH-actuation of chemical gels built from our previously used [*c*2]daisy chain pseudorotaxane covalently reticulated by azide-alkyne click chemistry with ditopic and tritopic oligo(ethylene glycol) linkers (Figure 103a).[1060] These chemical gels could be reversibly actuated by immersion in basic solutions for contraction and acidic ones for extension, leading to materials reaching contraction down to ~60 % of their initial volume. Actuation occurred several times without

apparent degradation. Importantly, high-resolution magic angle spinning (HRMAS) NMR along with neutron scattering experiments confirmed that the macroscopic actuation of the material results from the local controlled motion of the polymer chains (Figure 103b). This was made also particularly clear from the scattering experiments showing an increase by ~50 % in linear mass density of the polymer chains upon contraction, in agreement with our results obtained on single wormlike polymer chains.[1047] All these works clearly establish the possibility to achieve collective motion of molecular machines in a synchronized manner at the macroscopic scale by connecting them within soft polymer materials.

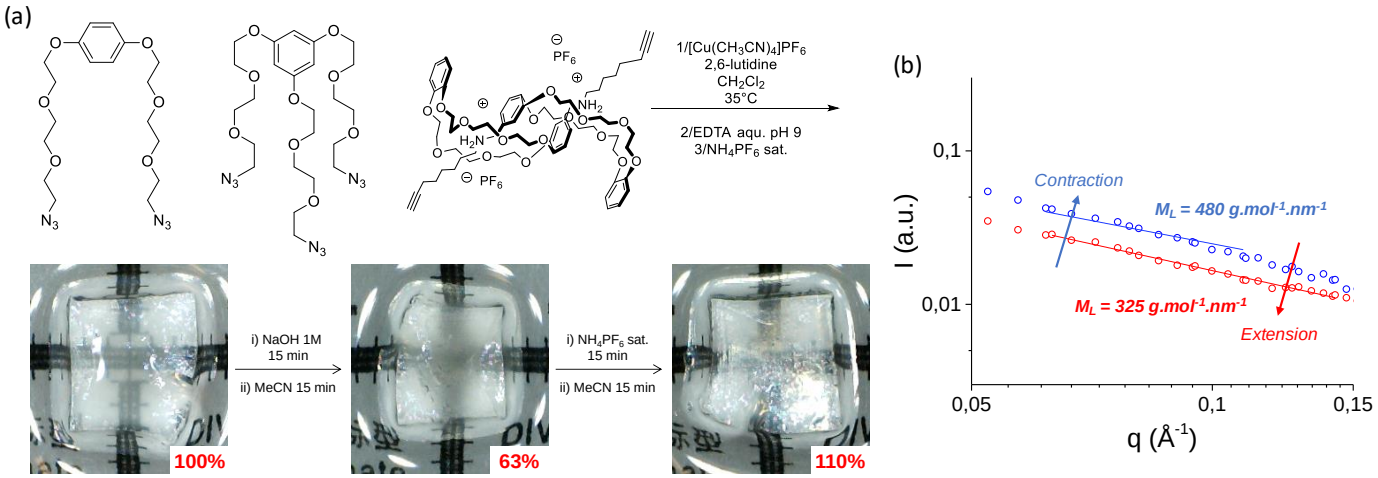

Figure 103: (a) Synthesis of a chemically cross-linked [*c*2]daisy chain rotaxane gel and its actuation upon pH stimulation, values in red indicate the changes in volume observed at each event; (b) Neutron scattering curve demonstrating the local actuation of the polymer chains resulting in a higher linear mass density for the contracted polymer (blue) compared to the extended one (red). Adapted with permission from reference [1060], Copyright 2017 American Chemical Society.

With a different approach to the one consisting in amplifying motion at macroscopic scale, the manipulation of nano-objects was also envisioned. Compared to systems developed to do so by achieving collective motion with [*n*]rotaxanes, only one example reported the concerted actuation of [*c*2]daisy chain rotaxanes at surfaces.[1061] Very recently, the group of Tian reported the functionalization of 60 nm gold

nanoparticles with bistable [*c*2]daisy chain rotaxanes bearing tris-thiol stoppers at their extremities (Figure 104a-b). Upon actuation of the daisy chains using an acid-base stimulus, a blue shift of the plasmonic oscillation upon contraction and a red shift upon extension were observed by dark-field microscopy suggesting that nanoparticles come closer to each other upon contraction and in a reversible manner (Figure 104c). This shift of ~6.2 nm can be correlated to a change in distance between the nanoparticles comprised between 3.34 and 1.17 nm, in agreement with the actuation of the daisy chains. This work opens the doors for applications of [*c*2]daisy chain rotaxanes at surfaces as already demonstrated for [*n*]rotaxanes.

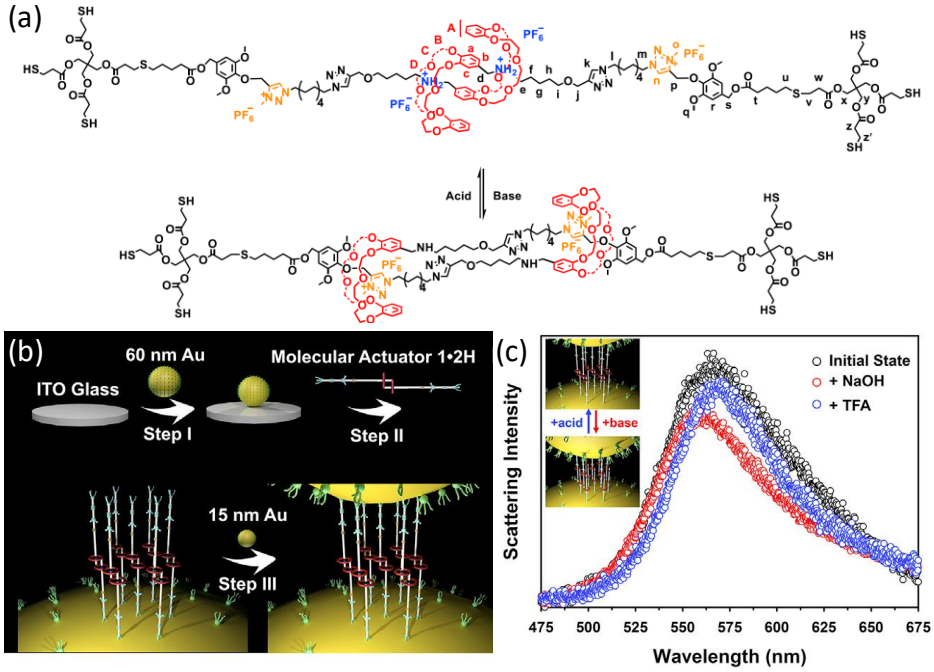

Figure 104: (a) Chemical structure of the [*c*2]daisy chain monomer used to covalently connect gold nanoparticles; (b) Schematic representation of the three-step construction of the gold nanoparticles dimer crosslinked by [*c*2]daisy chains; (c) Evolution of the scattering intensity of the gold nanoparticles dimer crosslinked by [*c*2]daisy chains showing a blue shift of ~6.2 nm upon addition of base. Adapted with permission from reference [1061], Copyright 2018 Elsevier.

3.3. Conclusion

We have seen in this chapter that individual switches based on mechanical bonds are able to produce molecular motions of relatively larger amplitudes compared to photochromic molecules. Interestingly, they can also be driven by chemical or red-ox stimuli to modify their energy profile and trigger very selective binding events. This makes them for instance very attractive for the design of sensors and of various responsive materials. When ordered in 2D domains at surfaces and interfaces (Langmuir monolayers, self-assembled monolayers, nanoparticles, mesoporous materials), or in 3D self-assembled systems, liquid crystals, or polymers, their collective actuation can give rise to amplified responses of interest for data storage, surface engineering, drug delivery, or mechanical actuations. In some cases, the transmission phenomena at work cannot be reached by simpler photochromic switches, because of the peculiarities of the mechanical bond which, for instance, include the gating of mesopores to deliver cargos or the mechanical sliding of polymer chains. However, we believe that one of the most promising futures for these systems remains to be accomplished. We have seen in the introduction that by properly ratcheting mechanical motions in catenanes and rotaxanes, it becomes possible to make them functioning along a non-reversible energy profile, thus progressively increasing the work they do on their environment, and there is certainly a lot to be created in this direction. In parallel, one can also imagine taking advantage of the macroscopic engineering tools that were cleverly developed with photoswitches and to implement them with machines based on mechanical bonds in order to combine the best of both worlds.

In the next section, we turn to a number of systems that include rotary motions, going from simple rotors to more complex light-driven motors.

4. MOTION FROM MOLECULAR ROTORS AND MOTORS

4.1. Introduction to molecular rotors

In the nanoscience community, the term of *molecular rotor* describes molecules composed of two parts rotating against one another, or of only one part rotating against a macroscopic entity such as a surface. The part with a larger moment of inertia is commonly designed as the *stator*, and the other one as the *rotor*. This field of research has been thoroughly reviewed by Michl[1062] and, following his definitions, even a small molecule as ethane is considered as a molecular rotor (with a very low rotation energy barrier of ≈ 3 kcal.mol^{-1}).[1063] Obviously, molecules of higher complexity are generally needed to create interesting functional objects. In particular, by focusing on the collective mechanical aspects that we want to discuss in the present review, it might be useful to classify molecular rotors depending on their organization order. One can distinguish *i*) individual molecular rotors suspended in an isotropic media (Figure 105a), *ii*) rotors at surfaces or in condensed phase matter with a possible anisotropic molecular order (Figure 105b), and *iii*) rotors which display mechanically correlated units and which consequently enter the scope of our review (Figure 105c).[1064]

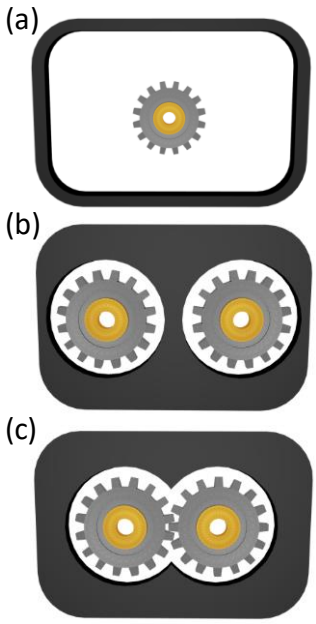

Figure 105: Schematic representation of the increasing spatial and mechanical interaction between molecular rotors. a) Individual molecular rotor in an isotropic medium, b) rotors with spatial molecular order and c) mechanically correlated molecular rotors.[1064]

In the first category, individual molecular rotors are subject to random collisions leading to a wide distribution of trajectories that preclude controlled mechanical interactions between them. In the two other categories, when ordering molecular rotors with one another, collective, synchronized, or even cooperative motions can emerge. The main feature of a collective behavior is that "an individual unit's action is dominated by the influence of the others; and that the unit behaves entirely differently from the way it would behave on its own."[1065] Considering the relation between molecular structure, phase order, and molecular dynamics in condensed media, Garcia-Garibay proposed a phase-order−molecular-dynamics diagram (Figure 106).[1066,1067]

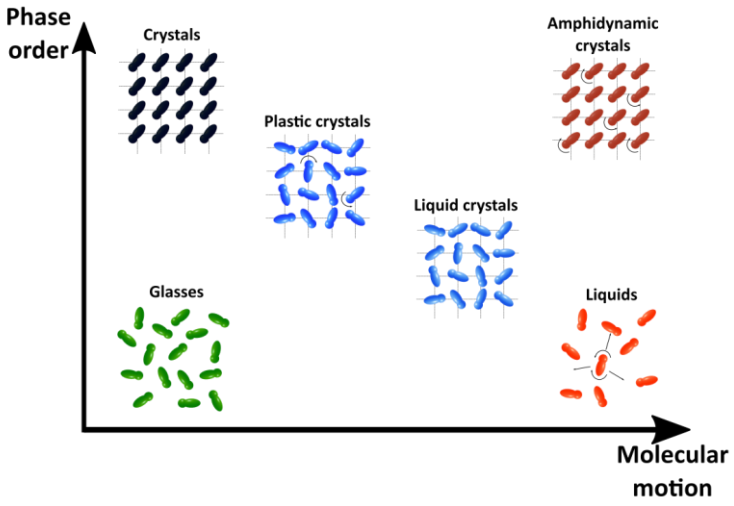

Figure 106: Phase order versus molecular motion for condensed-phase matter as proposed by Garcia-Garibay.[1067]

Here, the glassy state has low anisotropy and low molecular mobility, both incompatible with ordered collective motion. Then, crystals have the highest degree of order but concomitantly the lowest molecular mobility. Conversely, liquid phases have a high degree of freedom but this high mobility is detrimental to ordering. In addition, intermediate phases possessing molecular dynamics and phase order are commonly found such as liquid crystals and plastic crystals. Liquid crystals possess the typical properties of a liquid, such as fluidity and the inability to support shear, but also crystalline properties such as anisotropy of optical, electrical, and magnetic properties. Their structural dynamics is supported by molecules having several degrees of internal freedom such as molecular rotation, translational motion, and collective reorganization.[1068] Plastic crystals can be considered as a transitional stage between crystals and isotropic liquids. The phase is composed of molecules with a low translational mobility but where orientation disorder is caused by the rotations of entire molecules in the crystal with a homogeneous periodic arrangement.[1069] Finally, and very interestingly, Garcia-Garibay and coworkers proposed the description of a new hybrid phase in which the nanoporous structural properties give a static frame for the inclusion of rotor arrays with high internal mobility. This last class of objects was named amphidynamic crystals.

Amphidynamic crystals can be synthesized based on nanoporous crystal engineering to produce materials with highly ordered cavities that are controlled in size, stability, and chemical environment.[1028] Such materials provide a platform to precisely place molecular rotors in their voids. Typical synthetic pathways to form functional amphidynamic crystal have been reported either via structural collapse induced by weak supramolecular bonds (hydrogen, halogen, van der Waals), or via the formation of more robust networks using coordination and covalent bonds.[1070–1073] By a proper design of fully organic and rigid molecular structures, the self-assembly process forms rigid frameworks which generate large free volumes that can hold ordered molecular rotors with a high internal mobility. Many methods are instrumental to study dynamic processes and to determine the physical properties of amphidynamic

crystals. Solid state NMR measuring spin-lattice relaxation times ($T_1(^{13}C)$), as well as spin-echo deuterium NMR, are the most powerful methods for describing the reorientation frequencies and the trajectories of their mobile elements.[1074–1076] Diffraction experiments, including X-ray and neutron, also provide access to structural and dynamic information in such materials. In addition, dielectric spectroscopy is useful to investigate the dynamic of dipole-functionalized rotators and more generally the dielectric permittivity of the material.

Very important contributions in this field of research, including the design of rotational dynamics and physical properties of such systems, have been already reported in numerous reviews.[1062,1066,1067] The combination of anisotropic rotor alignment and of fast molecular dynamic in a same system paves the way to molecular collective motion inherent to dipole-dipole or spin state interactions and that can be implemented to achieve switchable properties of materials including ferroelectricity, birefringence, electric conductivity, sensing, capture and release of chemicals, etc. However, the collectivity of these motions being not directly related to the mechanical interactions between the rotational units, we will not discuss them further in this review. Instead, we will focus hereafter on interpenetrated molecular rotors leading to gearing effects. Although such rotors are not molecular machines by themselves, as they do not produce an effective work on their environment, they are very interesting to transfer mechanical motion from other elements, and as such they can be envisioned as modules in more complex molecular machines.

4.2. Mechanically correlated rotors

One of the most straightforward idea to mechanically correlate molecular rotors in space, and thus to transfer forces, movements, and energy, is to precisely arrange them in a gearing system. In an analogy with macroscopic machines, molecular gears can be imaged as wheels with serrated teeth presenting complementary steric interactions when the rotors are arranged in a regular way. Rotary transmission in molecular gears requires matching structural symmetry and connectivity in order to have a proper

positional relationship between the connected rotors. Chemists have developed multiple strategies to achieve gearing-type transmissions. Following pioneering works on restricted rotations within molecules,[1077–1082] intramolecular gears were naturally the first examples to emerge. Subsequently, larger assemblies of intermolecular gears were developed to transmit motion over longer distances. Following that classification, and by highlighting the different topologies encountered within each of these two categories, we describe hereafter a series of important achievements of the literature.

4.2.1. Intramolecular gears

Initial investigations with hindered molecules of intramolecular correlated motions of alkyls, phenyl, and other functional groups provide the basis to understand gearing effects. A full discussion on these fundamentals (typically involving only two gearing units) would not fit with the scope of this review, and we prefer to direct the reader to already existing articles giving an in-depth coverage of the field.[1062,1083–1085] We will however describe hereafter collective systems of interest that contain complex and multiple gearing units. Different intramolecular transmission modes have been developed such as the so-called bevel, spur, and coaxial molecular gears.

The bevel gearing arrangement allows a rotational movement to be transmitted between two or several concurrent and non-parallel rotors. Iwamura and Mislow reported simultaneously the first synthetic molecular bevel gears capable of undergoing correlated disrotatory motions from one rotor to another one.[1086–1104] The structural design was based on versatile triptycene derivatives presenting a D3h symmetry.[1105–1113] In macroscopic systems, a cyclic arrangement of gears requires an even number of units, so that the disrotatory movement is effectively transferred from one gear to the other. Obviously, the same principle applies for molecular systems, as shown in examples with three rotators components synthesized in linear[1114] and cyclic[1095] arrangements (Figure 107).

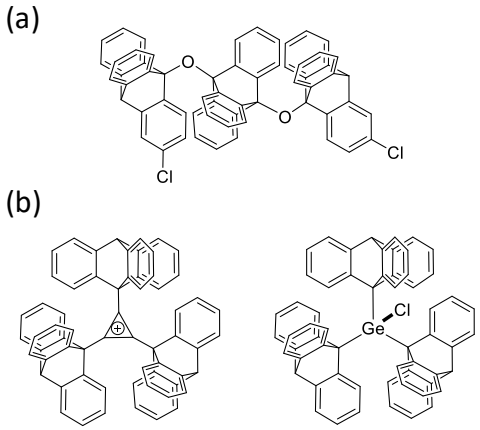

Figure 107: (a) Chemical structure of linear three rotors. (b) Chemical structure of cyclic three rotors.

As expected, the cyclic arrangement with three rotors locked the disrotary movements, while the linear structure presented smooth rotation (E_a < 2 kcal/mol) with phase isomerism (Figure 107a-b). Based on this principle, Iwanaga *et al.* described the synthesis and the highly dynamic behavior of covalent macrocyclic gear mashing of four triptycene.[1115] Shionoya and collaborators reported a gear meshing of four triptycene connected to a dirhodium complex revealing that exchangeable axial ligands greatly affect the gearing dynamic via steric interactions.[1116] The same research group reported the formation of a multigear platform composed of six triptycene covalently attached to a central benzene ring via an ethynyl linker (Figure 108a).[1117]

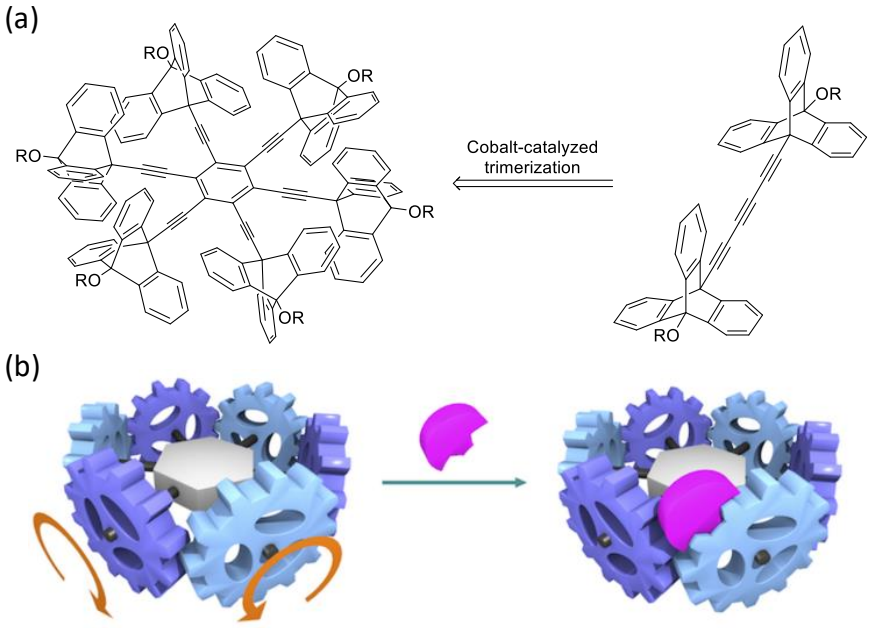

Figure 108: Design principle and realization of an intramolecular bevel gear. (a) Molecular structure and synthetic strategy to access the sextuple gear with six triptycene gears attached to the central benzene ring through ethynyl linkers. (b) Schematic representation of the gearing process and of its control by locking the triptycene rotation when complexed to bulky RuCp*. Adapted with permission from reference [1117], Copyright 2017 American Chemical Society.

This crowded device presents a high rotational dynamic estimated to be 2.7×10^4 s^{-1} at 300 K with the possibility to modulate gearing motions by using bulky ruthenium ions to complex and lock the active triptycene (Figure 108b). McGlinchey *et al.* also used this strategy to modulate the rotation speed of intramolecular gears by complexing the aromatic unit of triptycenes with a metal.[1118] Kira *et al.* introduced another tool to control the rotor transmission by using a clutch−declutch switching mechanism. They switched off the engagement of the two rotators by the reversible attachment of a fluoride ion on silicon-centered bis-triptycene system and leading to silane–silicates structural interconversion (Figure 109).[1119]

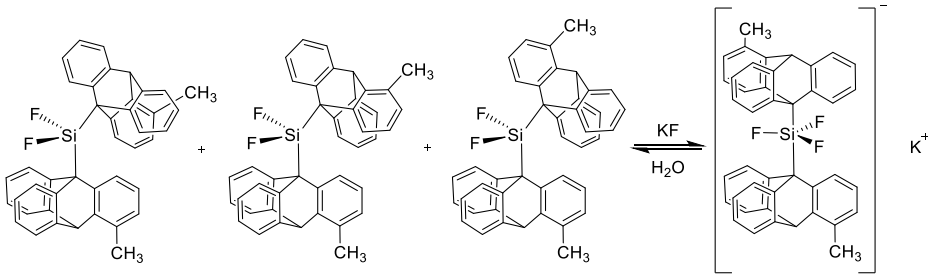

Figure 109: Chemical explanation of the clutching mechanism. The "clutched" structures of the bis-triptycene system (left side) can be unclutched upon addition of a fluorine atom to the silicon center, leading to the displacement of the triptycene groups to the apical positions of the complex (right side).

Shionoya and coworkers also reported Pt(II)-centered switchable gearing system based on photo- and thermally-driven *cis–trans* isomerization at the Pt(II) centre (Figure 110a). The stimuli-responsive configurational changes of the metal ion led to the reversible rotors engagement/disengagement (Figure 110b).[1120]

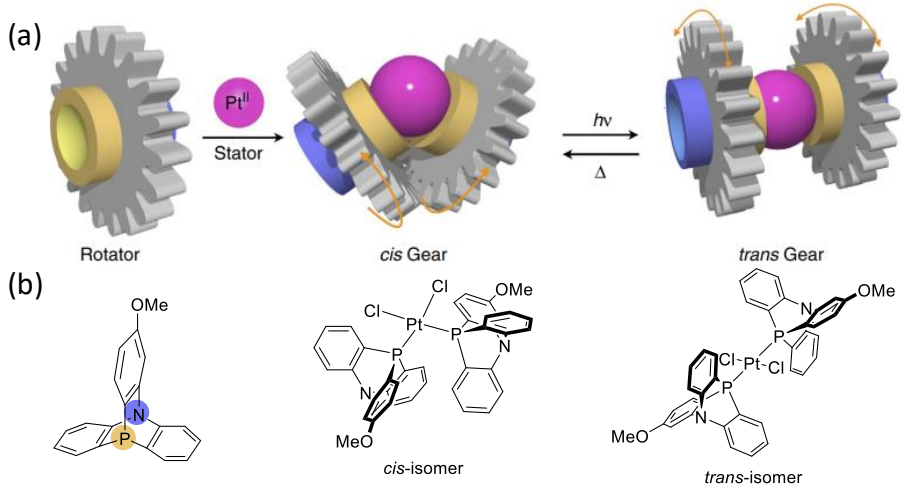

Figure 110: (a) Schematic representation of the mechanism of a molecular bevel gear and (b) the corresponding chemical structures. The "clutched" *cis*-gear is isomerized to its unclutched *trans* isomer upon UV irradiation (360 nm), and can be recovered by heating. Adapted with permission from reference [1120], Copyright 2017 Springer Nature.

Metal-bis(porphyrinate)s double decker complexes represent a class of synthetic molecular rotors in which two porphyrin rings rotate around a metal complex in a sandwiched configuration.[1121,1122] Based on previous investigations of Ru(II) and Os(II) porphyrin oligomers structured with mono-, di-, tri-, and tetrapyridylporphyrins,[1123–1128] Takeuchi *et al.* proposed to use double decker components as platforms for the building of molecular gears.[1129] They demonstrated the formation of a bevel gear by interlocking three molecular rotors composed of a La(III) bis-porphyrin double-decker and a Rh(III) porphyrin rotors (Figure 111). The dynamics of the rotary motions were evaluated by VT ^{1}H NMR spectroscopy, revealing activation energies of 30.1 and 30.7 kJ.mol^{-1} for the top and side rotors, respectively, and thus showing the rotational transmission through mechanical interactions. Further, by addition of a base to induce a conformational change of the rotors, going from a meshing state to an independent state, a rotational rate decrease for the top rotor only was measured. Upon neutralization, the gearing and correlated rotations were reinstalled.

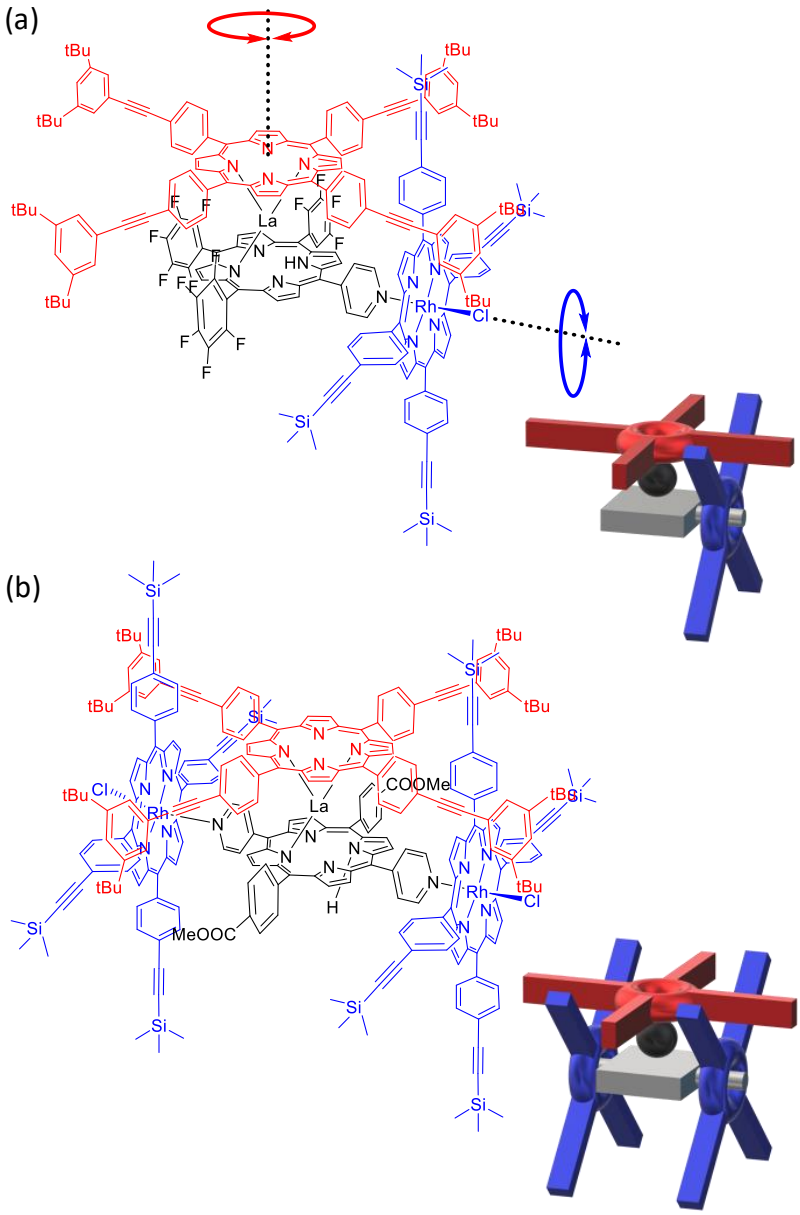

Figure 111: Chemical structures and schematic representation of bevel intramolecular gears built on a La(III) bis(porphyrinate) double decker (top unit, red) and either (a) one or (b) two Rh(III) porphyrins (side units, blue).[1129]

Based on the same principle, the structural and positional change of orthogonally arranged rotors was published later.[1130,1131] Other strategies to form molecular bevel gears have also been employed, including circumambulatory rearrangements[1132] or synchronism of fluxionality and rotation of ligands.[1133]

In spur gears, the axes of rotation lie in parallel and the gears have straight teeth relative to the axes (Figure 112a).

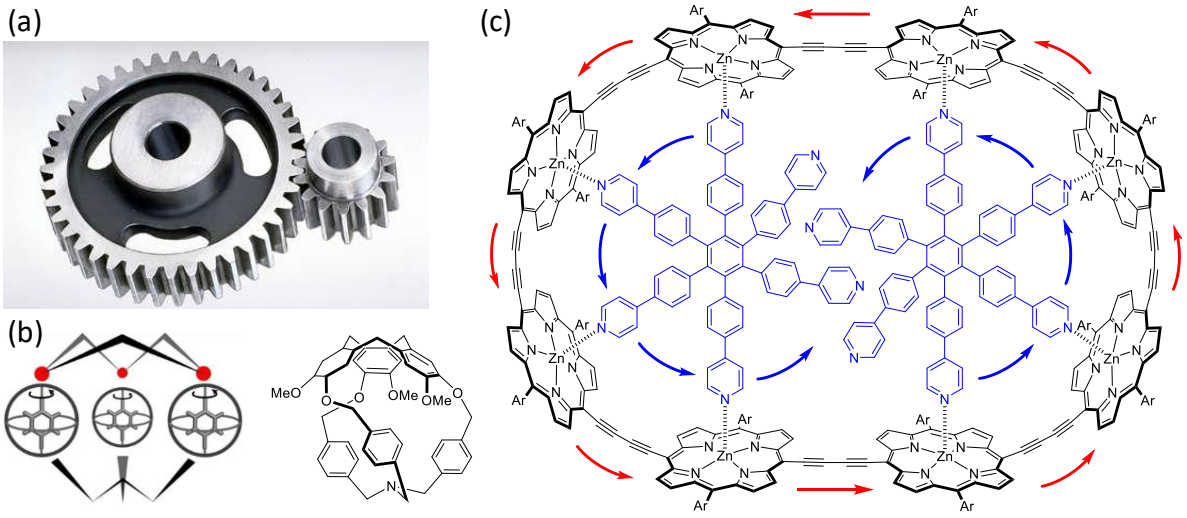

Figure 112: Representative examples of spur gear systems. (a) Macroscopic spur gears. Photograph courtesy from Emerson Power Transmission Corp (http://www.emerson-ept.com). (b) Schematic representation and chemical structure of the tribenzylamine hemicryptophane. The arrows represent the rotation of the units, but do not imply unidirectional motion. (c) Chemical structure of a molecular caterpillar track. The arrows represent the collective rotations within the system, with the red ones indicating the motion of the external macrocycle and the blue ones indicating the motion of the internal gears. Part (b) is adapted with permission from reference [1134], Copyright 2011 American Chemical Society.

To form molecular spur gears, Wakamatsu *et al.* investigated the design of molecules with two triptycene gear axes mounted on a rigid 1,8-anthrylene platform in the same direction.[1135] Similarly, Siegel

and coworkers synthesized a molecular spur gear with a rigid bisbenzimidazole platform holding two triptycene rotors with parallel axes at the proper distance to permit a gearing correlation.[1136] Computational studies suggested that the molecular dynamic preferentially undergoes geared rotation over gear slippage, though experimental VT-NMR studies did not confirm that mechanism. Inspired by the clutch mechanism developed on molecular bevel gears, Jiang *et al.* reported the control of spur gears by external stimuli. Upon complexation and decomplexation of $AgPF_6$ on the stator part, the molecule exhibit a structural change of large amplitude with a subsequent clutch−declutch mechanism of the gear.[1137] A surprising but elegant architecture based on the gyroscopic structure with three phenylene in parallel also showed a low spur gear mechanism between three rotors (Figure 112b).[1134] Finally, one original and complex synthetic structure, that presents some similarities with spur gears, and mimicking a macroscopic caterpillar track, has been reported by Anderson and collaborators (Figure 112c). This system is composed of a macrocyclic hexa-zinc-porphyrin belt coordinated to two star-shaped oligo-pyridines. NMR exchange spectroscopy (EXSY) revealed conrotatory rotation of the two template wheels correlated with the macrocyclic rotation.[1138]

Coaxial gearing mimics the rotation transmission of ball bearings correlated on a same axis (Figure 113a). Interestingly, if the use of macroscopic coaxial gears is uncommon, supramolecular chemistry has provided access to such tools at nanoscale. In particular, Shionoya *et al.* have developed a correlated motion in a molecular device based on disk-shaped ligands coaxially stacked by metal coordination.[1139–1142] Different hexasubstituted benzene molecules (Figure 113b) were arranged into rotor–transmitter–rotors metal complexes $[Ag_6M_3\mathbf{L^1}_2{\cdot}\mathbf{L^3}_2]^{(3n+6)+}$ (M=Ag^I (n=1) or Hg^{II} (n=2)) (Figure 113c). The motion of the two terminal rotors studied by VT ^{1}H NMR spectroscopy was shown to be strongly correlated – over a total distance of 1.5 nm – via intramolecular ligand exchange and flipping motions, constraining the central supramolecular transmitter $[M_3\mathbf{L^3}_2]^{3n+}$, located between the two rotors, to undergo helix inversion (Figure 113d).[1143]

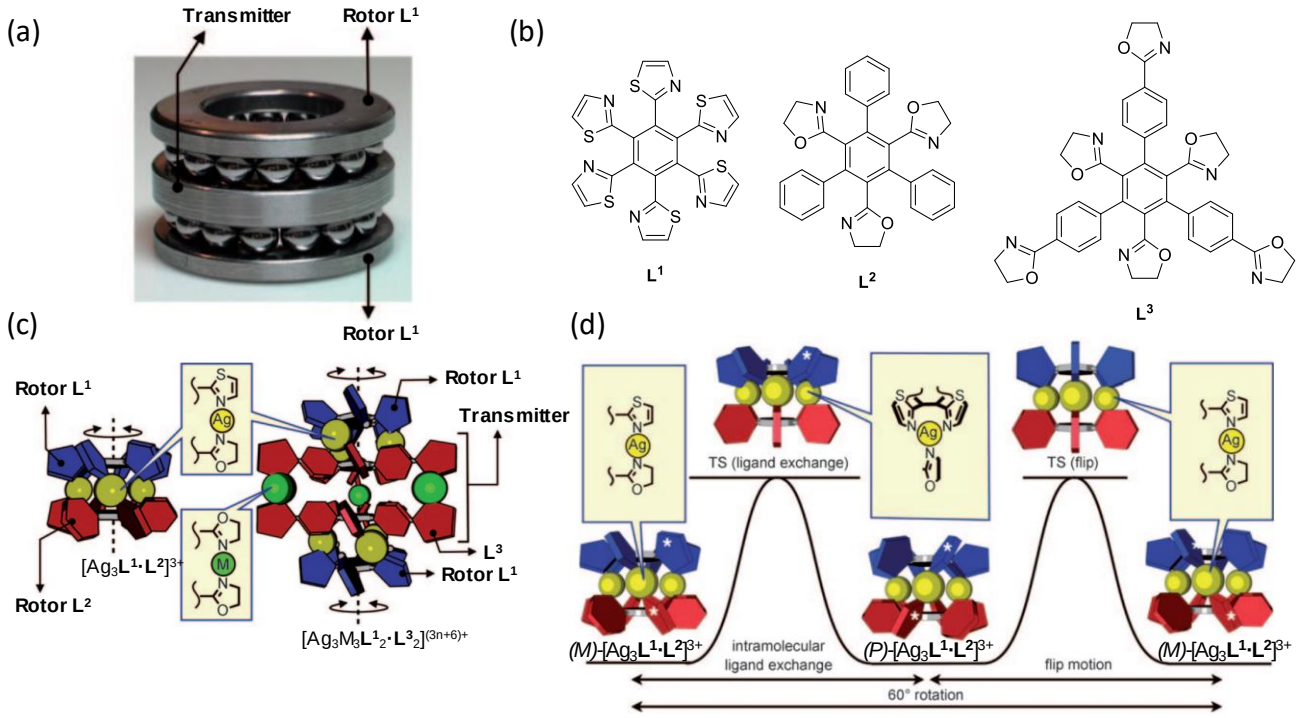

Figure 113: Examples of coaxial gearing: (a) Macroscopic double ball bearing. (b) Chemical structure of the subcomponents of the system. (c) Schematic representation of the corresponding trinuclear molecular ball bearing (left side) and nonanuclear molecular double ball bearing (right side). (d) Rotation mechanism of the rotors in the molecular ball bearing. Rotation takes place through alternate intramolecular ligand exchange and flip motion, both of which are accompanied by helix inversion between *M* and *P* forms (TS = transition state). Adapted with permission from reference [1142], Copyright 2010 John Wiley and Sons.

4.2.2. Intermolecular gears

Intermolecular correlated rotors involving gearing processes represent a potentially powerful approach to produce large collective motions within molecular assemblies and to generate emergent properties in materials therefrom. This approach requires to precisely control the spatial distribution between the

rotating units, and we will discuss hereafter the currently existing systems depending on their dimensionality.

Tabe and Yokoyama have reported a coherent collective procession of chiral molecular rotor in a Langmuir monolayer and driven by the transmembrane transfer of water molecules.[1144] Rod-like molecules spread at the air–glycerol interface display a tilted conformation and reflected-light polarizing microscopy established oscillation patterns similar to those observed in Belousov–Zhabotinsky reactions, which is explained by boundary conditions between each domain. The authors estimated the torque applied to an individual molecule to be several orders of magnitude lower than thermal energy. Hence, they conclude that the explanation for the observation of such macroscopic patterns is only possible with a cooperative mechanical motion of adjacent rotors. Without this cooperativity, thermal noise would "hide" the motion of single isolated molecules (Figure 114).

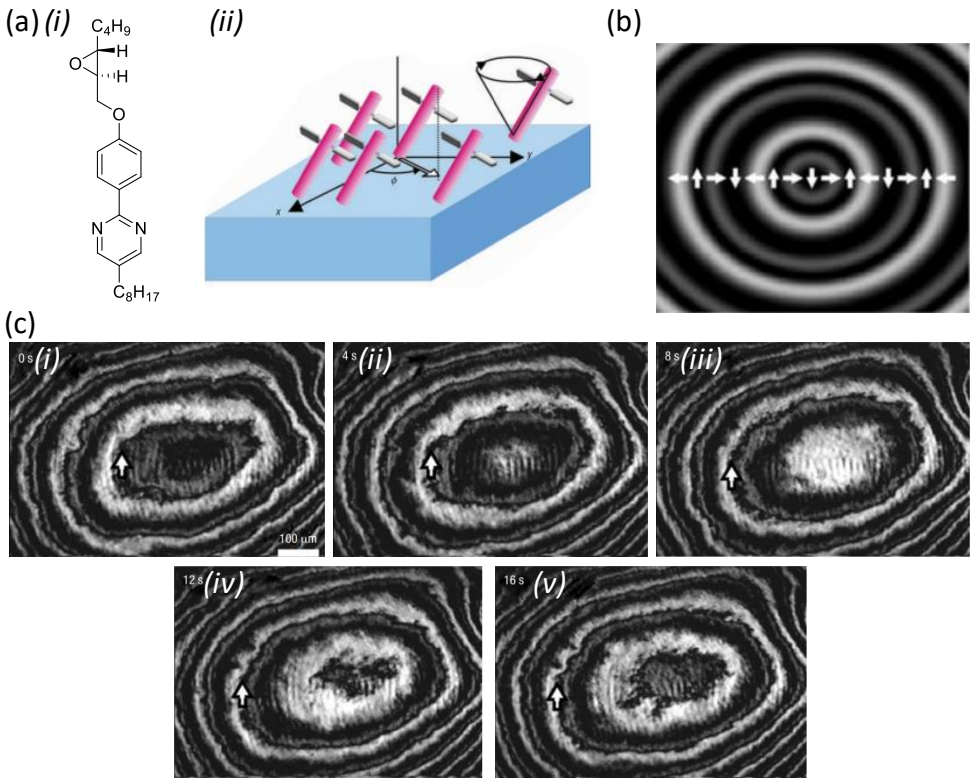

Figure 114: (a) *(i)* Chemical structure of the rod-like rotor and *(ii)* idealized representation of the corresponding Langmuir film at the air/glycerol interface. The angle Φ represents the molecular azimuth.

(b) Simulation of the response of the monolayer under reflection-type polarized microscopy, where the white arrows represent the direction of the molecular azimuth Φ. (c) Experimental images obtained by reflection-type polarized microscopy at different times (*(i)* 0 s, *(ii)* 4 s, *(iii)* 8 s, *(iv)* 12 s, *(v)* 16 s) displaying oscillations pattern comparable to Belousov-Zhabotinsky reactions. Adapted with permission from reference [1144], Copyright 2003 Springer Nature.

In recent years, solid surfaces have also emerged as promising platforms to control precisely the molecular orientation and position of rotors in ordered monolayer arrays. Computational simulations on the transmission mechanism of rotational motion on surfaces,[1145] with gear performance depending on linkers flexibility,[1146] have been used to predict an ideal chemical design.[1147] Experimentally, collective rotations of highly packed molecular rotors absorbed on surfaces have been imaged and manipulated with the tip of a scanning tunneling microscope (STM).[1148,1149] Sykes and coworkers reported the on-surface synthesis of interlocked molecular structures in two-dimensional crystals exhibiting correlated switching.[1150] Multidecker porphyrin complexes have also recently attracted particular attention for the engineering of molecular machines on surfaces. Their sandwiched structures provide for the top porphyrin a free rotational behavior, while the bottom one is anchored at the surface.[1151] Triggered by electrical pulses, and resulting from intermolecular correlated motions, highly ordered interlocked dipolar multi-decker molecules can display change in chirality (Figure 115a)[1152] and phase transition.[1153] Hla *et al.* reported synchronized rotations of dipolar double-decker porphyrins deposited on Cu(111) surfaces,[1154] with coordinated movements resulting from the minimization of dipole interaction energies and induced by the application of an electric field by the STM tip (Figure 115b).

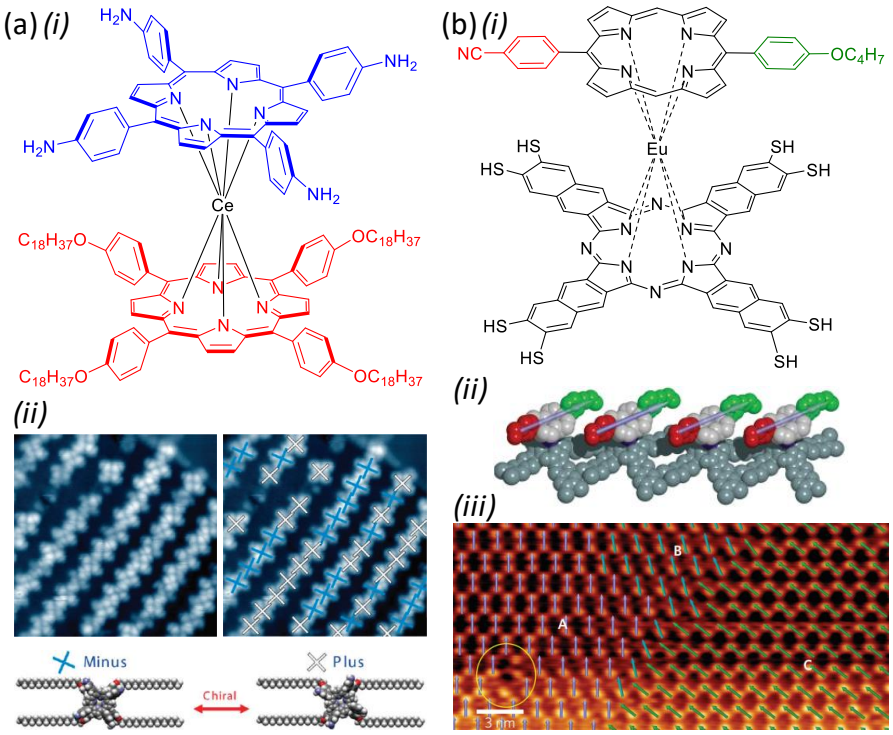

Figure 115: (a) *(i)* Chemical structure of a double-decker porphyrin complex and *(ii)* STM image of the corresponding self-assembled layer on an Au(111) surface (X = 20 nm). The insets below show the space-filling models of the complex depending on their chirality. (b) *(i)* Chemical structure of a double-decker porphyrin rotor and *(ii)* corresponding molecular model of its arrangement on the Cu(111) surface. *(iii)* STM image showing a sudden switching of rotators revealing the formation of different rotator domains (labelled 'B' and 'C') ($V_t = 1$ V, $I_t = 3.2 \times 10^{-10}$ A). Parts (a) and (b) are adapted with permission from reference [1152], Copyright 2011 American Chemical Society, and reference [1154], Copyright 2016 Springer Nature, respectively.

The search for amphidynamic crystals led the group of Garcia-Garibay to the discovery of gearing rotors in such configurations. The spatial distribution of rotor was driven by the self-assembly of a steroid frame and leading to an ideal short distance between the rotors in ^{1}D domain (Figure 116). On the basis of single-

crystal X-ray structures and VT ^{2}H NMR spectra, the authors postulated fast collective rotations ($\geq 10^{8}$ Hz).[1155]

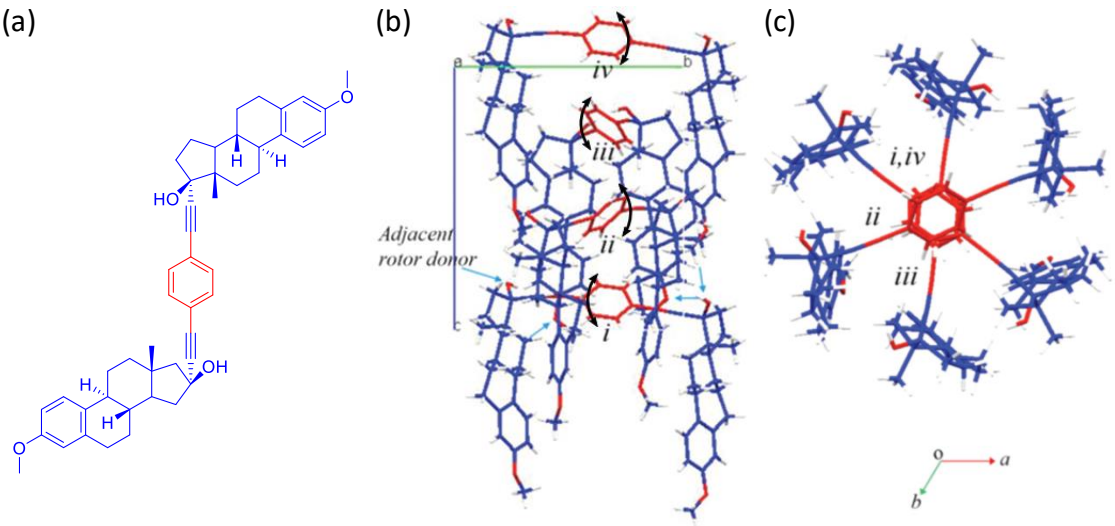

Figure 116: (a) Chemical structure of a mestranol rotor. (b) Columnar 1D arrangement of the nested molecular rotors in crystals. The black arrows represent the correlated motion between the phenylene rotors (*i*, *ii*, *iii*, *iv*). (c) View down the crystal 1D packing. Adapted with permission from reference [1155], Copyright 2011 American Chemical Society.

In 2013, Michl and coworkers reported a self-assembled structure of linear polyrotors connected by alkyne linkers.[1156–1158] Intermolecular hydrogen bonds between end pyridine unit have served to direct the self-assembly with an ideal close packing of the rotors.[1156,1159,1160] By combining X-ray diffraction, variable temperature ^{1}H spin–lattice relaxation, and computational simulation, the authors demonstrated that rotational motions are correlated between adjacent rotors in such a close packing (with rotor–rotor contacts shorter than 2.4 Å) (Figure 117).[1161] Similarly, the same group developed periodic self-assembled structures through iodine-iodine interactions harboring correlated movements of adjacent rotors.[1162]

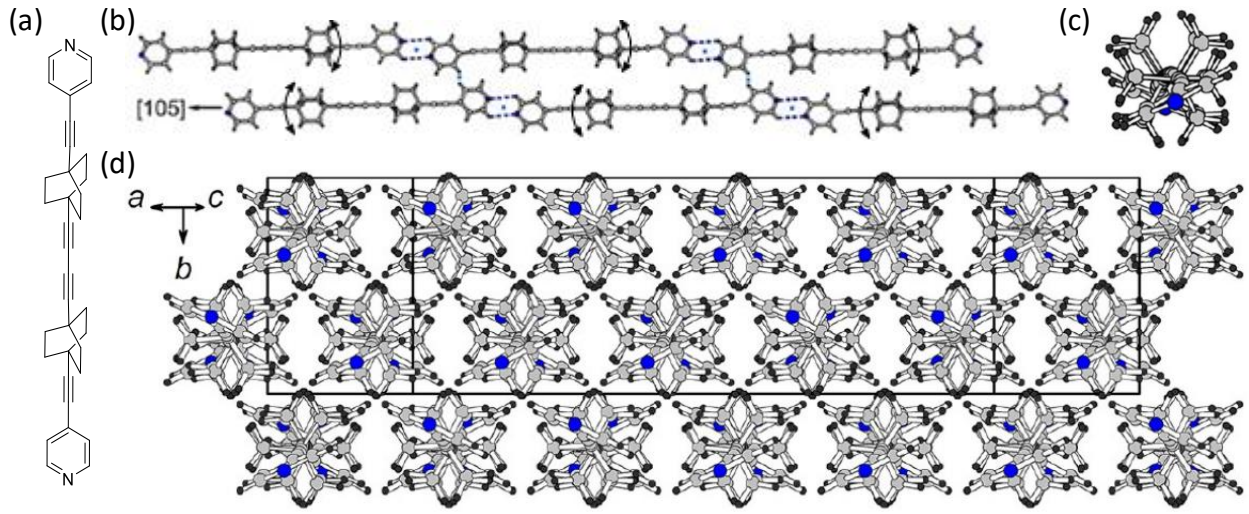

Figure 117: (a) Chemical structure of linear polyrotors developed by Michl *et al.* (b) 2D arrangement of linear polyrotors through hydrogen bonding interactions (c) Projected view along the backbone showing the helical structure of the linear polyrotors and (d) representation of the crystalline packing projected along the same view. Adapted with permission from reference [1161], Copyright 2013 American Chemical Society.

4.3. Rotary molecular motors

4.3.1. Introduction to rotary molecular motors

As already described in the general introduction of this review, molecular motors are molecular machines capable of continuously cycling a motion under an energy input – such as a directional rotation – and to increase progressively the work they perform on their environment.[1163] The most striking examples of such nanomotors are found in nature as part of biological machines. For instance, ATP synthase harnesses the potential energy of a gradient of protons created along the respiratory chain within the mitochondria in order to produce a mechanical energy of rotation, which is in turn used to catalyze the condensation of ATP from ADP and phosphate.[1164] In the past decades, chemists have proven the

possibility to create synthetic molecular motors and to progressively achieve energy conversion and functional tasks.[1163] That capability of performing a continuous (*i.e.* repetitively cycling) and possibly autonomous (*i.e.* under a constant input of energy) mechanical work, is the most significant distinction between a molecular motor and the above-mentioned molecular switches (which cancel the work produced in one direction when coming back to their initial state) and rotors (which do not produce any work). In the introduction to this chapter, we will focus more particularly on the functioning principles of synthetic light-powered molecular rotary motor.

One of the most important breakthrough in the field of artificial molecular motors was brought by Ben Feringa and coworkers in 1999, when reporting the first synthetic molecular motor capable of undergoing a unidirectional 360° rotation around an overcrowded alkene.[1165] The so-called first-generation of motor possesses two identical halves on each sides of a double bond that serves as a rotary axle (Figure 118a-b). The stereogenic methyl groups in the fjord region dominate the helical chirality of both halves and the direction of the rotation. One full cycle of rotation can be divided into four progressive steps: two photochemical and energetically uphill steps and two thermally-activated and energetically downhill steps. Irradiation with UV light (>280 nm) induces a *trans*→*cis* isomerization around the double bond of (*P,P*)-*trans*, yielding its isomer (*M,M*)-*cis* with opposite helical chirality. This photoisomerization is reversible and a photostationary state (PSS) is reached under continuous irradiation, with a *cis* to *trans* ratio of 95:5 for the structure shown in Figure 118a-b.

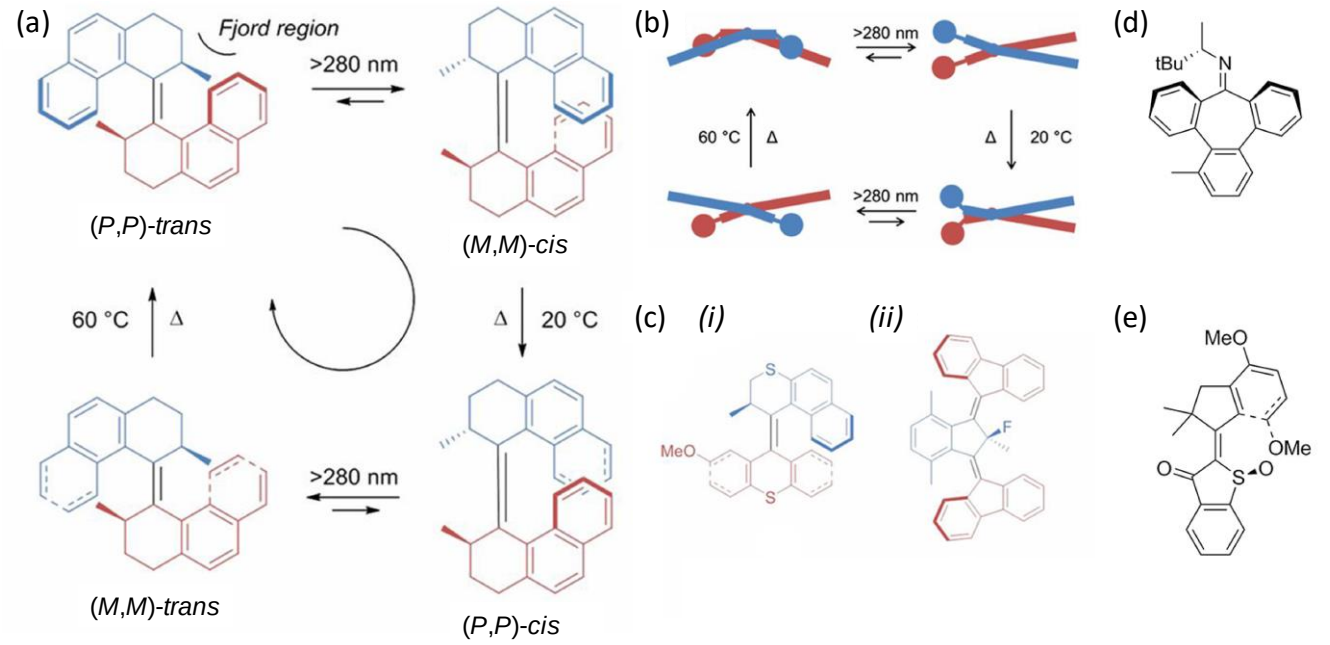

Figure 118: Schematic representation of various molecular motors capable of unidirectional rotations around sterically overcrowded double-bond axles. (a) Rotary cycle of a first-generation Feringa's motor. (b) Top view of the rotary cycle. (c) Structures of (*i*) second-, and (*ii*) third-generation molecular motors, (d) imine-based molecular motors and (e) hemithioindigo-based molecular motors. Adapted with permission from reference [1166].

Because in (*M,M*)-*cis* the methyl substituents hold an energetically-less-favorable pseudo-equatorial position, they tend to readopt the energetically-favored pseudo-axial orientation. The release of this strain is made possible by a thermally-activated helix inversion, in which both halves of the motor slide along each other and change their chiral conformation from a left-handed (*M,M*) to right-handed (*P,P*) helicity. With the methyl groups recovering their pseudo-axial conformation, the global thermal helix inversion is energetically favorable and effectively converts the higher-energy isomer such as (*M,M*)-*cis* to the thermally-stable (*P,P*)-*cis* form and hence completes the unidirectional 180° rotary motion. The second part of the cycle proceeds in a similar fashion, that is with a second photoisomerization step which affords (*M,M*)-*trans* (PSS *trans*→*cis* ratio of 90:10) with the methyl substituents again in the pseudo-equatorial

position. A second thermal helix inversion then regenerates (*P,P*)-*trans* with a full 360° rotation cycle being completed. Later on, the group of Feringa designed the so-called second-generation of rotary molecular motors (Figure 118c (*i*)). Here, the stereogenic information is reduced from two methyl groups to a single one, which therefore involves a desymmetrization of the upper and lower halves of the motor. As for the first generation, a full 360° rotary motion can be achieved by a sequential combination of two photochemical and two thermal steps. However, due to decreased steric hindrance in the fjord region, the energy barrier of the thermal helix inversion is significantly lowered, resulting in a dramatic increase of rotation speed that can reach the MHz regime. In order to go even further and test whether unidirectional rotation can be achieved in the absence of any stereocenters, symmetrical motors were synthesized bearing one stator and two rotor units (Figure 118c (*ii*)). This third generation of motors only presents a pseudo-asymmetric center, in the form of a fluorinated quaternary carbon, but still proved to rotate unidirectionally around both axles.

In addition to Feringa's motors based on overcrowded alkene, light-powered motors derived from imines and hemithioindigo molecules were also reported in recent years. In 2006, an imine-based motor was first proposed in a conjecture by Lehn (Figure 118d).[1167] The chemical design is based here on the two types of *E*/*Z*-isomerization processes that imines can undergo, and which are photochemical isomerization and thermal nitrogen inversion. Further, a preferred direction was assumed for the photochemical isomerization if adding a stereogenic center next to the imine. Based on this principle, Greb and Lehn reported experimentally the first example of an imine-based rotary motor.[1168] Through photochemical isomerization at 254 nm, and subsequent nitrogen inversion by heating at 60 °C for 15 h, an overall full rotation was demonstrated. In 2015, Dube and coworkers introduced a light-driven molecular motor based on a thioindigo unit fused with a stilbene fragment (Figure 118e).[1169] The structural analogy with the previously described overcrowded alkene allows a similar four steps rotation process, in

which two sets of photochemical and thermal isomerization take place alternately. Interestingly, a sulfoxide group in the lower part acts as the stereogenic center in thioindigo-based motor.

In the past two decades, great efforts have been made in the design and improvement of light-powered rotary molecular motors. For additional information about their chemical design, their mechanistic studies, and their implementations into dynamic systems at molecular level (such as chiral catalysts,[1170] chirality transfer agents,[1171] active elements to regulate DNA duplex stability[1172] or to drill holes in membranes[1173]), interested readers are referred to recent reviews.[1163,1174] Hereafter, we will highlight further examples based on the collective motion of rotary molecular motors, and which can produce integrated mechanical responses up to the macroscopic level. We will divide the discussion depending on the medium in which the molecular motors are integrated, namely surfaces, liquid crystals, self-assembled nanostructures, and polymer-based materials. We will also highlight in these examples whether the functioning principle of the collective motion observed makes only use of a biased distribution between the different isomers of the motors (*i.e.* influencing the system as a function of their state), or if they make use of their full potential to continuously rotate out-of-equilibrium (*i.e.* influencing the system a function of their trajectory) – and thus to progressively increase the mechanical work they perform.

4.3.2. Collective behaviors of molecular motors on surfaces

As for switches, immobilizing motors at surfaces and interfaces is one of the main strategies to coordinate in space and time their mechanical actuation.[39,1175] Examples of surfaces functionalized by azobenzene or spiropyran derivatives and capable of changing their wettability upon molecular switching have been already discussed in the above section 2. Though many approaches of immobilization have been developed with these photoswitches, including polymer-based surfaces and mixed layers that increase surface roughness, the variation of the water contact angle on flat and smooth surfaces has been limited in the typical order of 2-14°. Using some of their motor derivatives as simple *cis-trans* molecular

switches, Feringa and coworkers attached them by a bipodal anchoring group at a quartz surface.[1176] However, the thermal helix inversion of the motor was found to be strongly inhibited by the crowding of the self-assembled monolayer. To address this problem, a large tripodal stator with thiol groups was used to decrease the molecular density around the motor itself, as located in the upper part of the monolayer (Figure 119).[1177] In addition, the motor was designed to adapt an altitudinal-oriented position, so that the hydrophobic fluorinated chain of the rotor can be switched up or down, with a maximum effect on the wettability of the surface. The irradiation with UV light (λ_{max} = 365 nm) of the self-assembled monolayer (SAM) starting with the *cis* isomer results in a change of the water contact angle (WCA) from 60 ± 1° to 76 ± 1°. Conversely, the irradiation of SAM starting with the *trans* isomer results in a change of the WCA from 82 ± 1° to 68 ± 1°. However, recovery of initial WCA value is not possible for this system. Indeed, after several cycles of irradiation the wettability reaches an intermediate situation because both isomers have similar stabilities, leading to a mixture of *cis*- and *trans*- states. Nevertheless, this molecular design could be used for the translational motion of droplets on surfaces, as it was observed for photochromic switches (see Section 2.2.1) and rotaxanes (see Section 3.2.2).

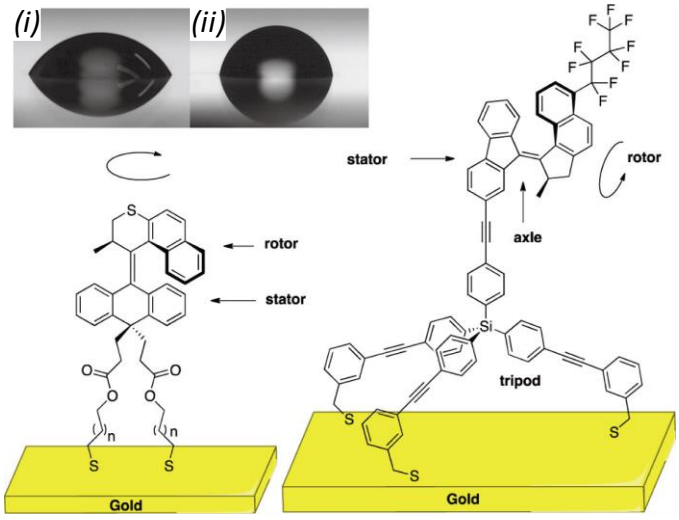

Figure 119: Azimuthal-oriented (*bottom left*) and altitudinal-oriented (*bottom right*) configurations of molecular motors at a surface. Insert (*top left*): water droplets on a self-assembled monolayer (SAM) made

of (*i*) an altitudinal-oriented *cis* motor and of (*ii*) an altitudinal-oriented *trans* motor. Adapted with permission from reference [1177], Copyright 2014 American Chemical Society.

The fabrication of discrete nano-objects that combine several molecular motors in order to access defined collective mechanical motions is another important direction of research for nanotechnologies. In the recent years, a great excitement appeared for the design of the so-called "nanocars",[1178] having their wheels made of rotary molecular motors powered by light, chemical, or electrical energy in order to propel them at a surface. In 2011, Feringa and coworkers managed to achieve the electrically driven directional translation of a four-wheeled nanocar over a copper surface.[1179] This mechanically active single molecule was designed by combining four chiral rotary motors as the four wheels surrounding a rigid chassis (Figure 120a). After landing onto the Cu(111) surface by sublimation, individual molecules were imaged by a scanning tunneling microscopy (STM) at 7 K, revealing the presence of three or four brighter spots corresponding to the linked rotary motors (Figure 120b).

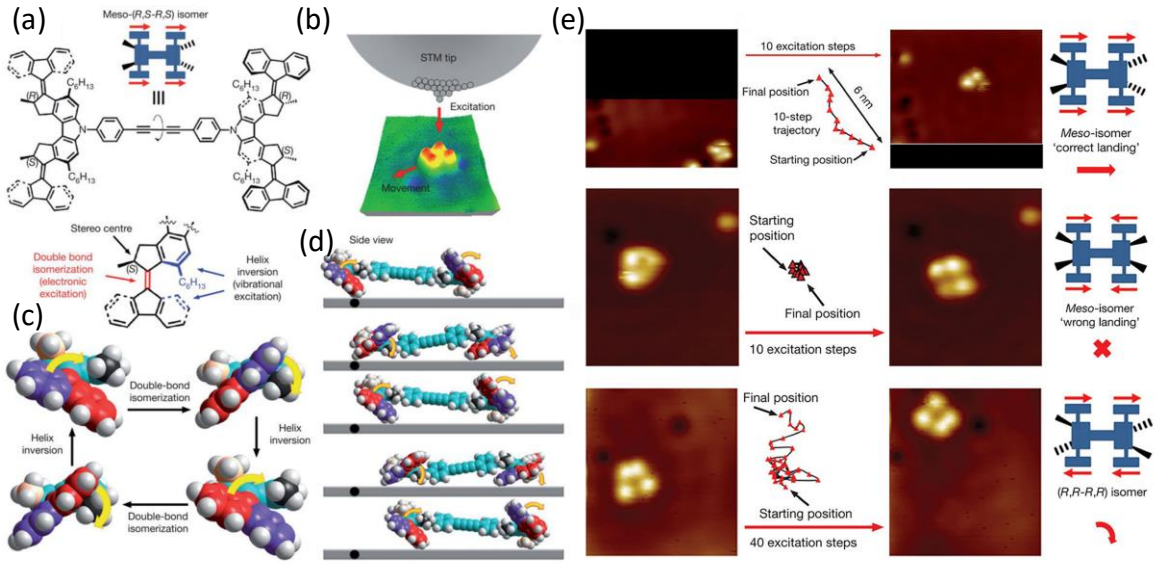

Figure 120: (a) Chemical structure of the Feringa's nanocar and cartoon representation of the meso-(*R*,*S*-*R*,*S*) diastereomer. The red arrows correspond to the direction in which the properly combined clockwise

and anticlockwise rotations of the individual motors propel the entire molecule. (b) Schematic representation of the experiment with the STM tip: electrons tunneling through the molecule excite vibrational and electronic states and induce a translational movement over the surface. (c) Side view representation of the 360° rotation of a single rotary motor, and (d) of a four-wheel nanocar. (e) STM images of trajectories of 'correctly landed' (linear) (surface area: 10.2 nm × 9.3 nm) and 'wrongly landed' (circular/random) nanocar molecules (surface area: 7.0 nm × 7.8 nm). Adapted with permission from reference [1179], Copyright 2011 Springer Nature.

Under STM excitation (voltage pulse larger than 500 mV), geometric changes of the wheels were imaged, revealing their sequential configurational and conformational isomerizations (provided by electronic and vibrational excitation, respectively). Interestingly, three scenarios of directionality were observed depending on the individual chirality of the motors and on the subsequent global geometry of the four-wheel nanocar. When the heterochiral meso-(*R*,*S*-*R*,*S*) isomer is properly adsorbed onto the surface in a "flat" "orientation, the four motor units display a conrotatory motion, that is for instance with the two left-hand-side motors of the chassis turning clockwise, and the two right-hand-side motors of the chassis turning anticlockwise (see red arrows on Figure 120a). The net result of this cooperative system is the propulsion of the nanocar in a straight trajectory after several rotations, even if this trajectory is not perfect because not all the four motor units are able to receive simultaneous excitation during each step. A translational distance of 6 nm over the surface was achieved after ten excitation steps. In contrast, for the homochiral enantiomers (*R*,*R*-*R*,*R*) and (*S*,*S*-*S*,*S*), the motor units display a disrotatory motion, resulting in a net spinning or random trajectory of the nanocar at the surface. Although only four molecular motors are integrated in the nanocar, this example is relevant in the context of this review because it demonstrates the importance of chirality and global geometry of mechanically active modules in order to efficiently synchronize their motions.

4.3.3. Collective behaviors in liquid crystals

As mentioned in above sections, owing to their high sensitivity to the presence and the nature of dopants, liquid crystalline (LC) matrices are commonly used to couple with photo-switches in order to generate light-induced alignment reorganization.[1180] Following general rules, it is well-known that the pitch of a cholesteric LC film in the presence of a chiral dopant is inversely proportional to its concentration (*c*), its enantiomeric excess (*ee*), and its helical twisting power (β). As stated earlier in Section 2.2.2, the helical twisting power is a property of a dopant-LC couple. In other words, the same dopant will have different HTPs in different (nematic) liquid crystal hosts. When the dimension of the pitch is in the range of the visible light wavelength, a well-defined, bright reflection with a distinct color can be observed. For switchable dopant molecules, high stability, good reversibility, high helical twisting power (β), as well as a large change in β values upon switching are required to achieve an efficient color tuning in liquid crystalline films. Feringa's rotary motors are intrinsically photo-dynamic chiral molecules and their first incorporation into a LC matrix was accomplished in 2002 (Figure 121a).[1181] In this work, the helical twisting power values of first-generation motors in a E7 LC matrix were determined by the Grandjean Cano technique for (*P,P*)-*trans*-**1a** (β = +75 μm^{-1}), (*P,P*)-*cis*-**2a** (β = +8 μm^{-1}) and (*M,M*)-*trans*-**1b** (β = -18 μm^{-1}). Under UV irradiation (λ>280 nm), the efficiency of the isomerization was found to be lower in E7 LC films than that in solution, which was attributed to the absorption of the matrix up to 340 nm. But the high helical twisting power of (*P,P*)-*trans*-**1a** in combination with the large β-value change between different states was sufficient to achieve tunable reflection wavelength throughout the visible spectrum simply by changing the irradiation time (Figure 121d). Because of the high energy barrier in the second thermal helix inversion step, heating to 60 °C is required to recover the original state. To work at room temperature, the same group designed a chiral dopant (2'*S*)-(*P*)-**1** based on a second-generation molecular motor (Figure 121b).[1182] The fluorene moiety was chosen for the lower part of the motor because its structure resemblance to the biphenyl LC host compound E7, thus potentially enhancing the interaction between the dopant and the matrix. Photochemical isomerization resulted in an inversion of helicity from (2'*S*)-(*P*)-**1a** to (2'*S*)-(*M*)-**1b** and the subsequent thermal helix inversion from *M* to *P* occurs readily at

room temperature in toluene ($t_{1/2}$ = 9.9 min). The β value of the motor can be switched here reversibly between +90 μm^{-1} (initial (2'*S*)-(*P*)-**1a** state) and -59 μm^{-1} (at PSS). Thus, a color change of the LC film across the visible spectrum can be addressed (Figure 121e). Benefiting from the faster thermal helix inversion process with that second-generation motor, recovery of the original state was achieved in 33 min, and the whole process showed good fatigue resistance (Figure 121f).

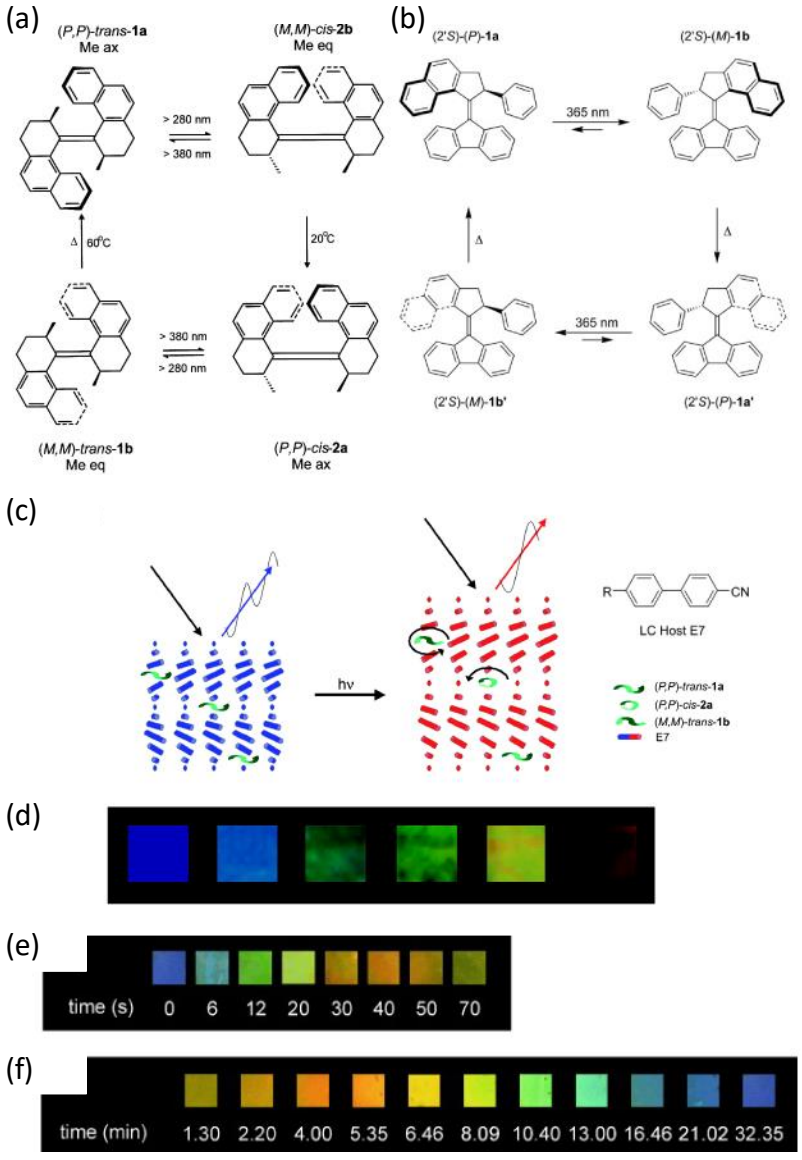

Figure 121: (a) Four-step unidirectional rotation cycle of a first-generation molecular motor used as a chiroptical switch in a LC phase. (b) Unidirectional rotation cycle of second-generation molecular motor used in a LC phase. (c) Schematic representation of the chiral switch of a molecular motor in a LC phase E7, and subsequent induced elongation of the LC pitch together with the associated change in light reflection wavelength. (d) Colors of a LC phase doped with a first generation molecular motor (6.16

weight% in E7), as a function of irradiation time (280 nm), and starting from pure (*P,P*)-*trans*-1a at RT. The colors shown from left to right correspond to 0, 10, 20, 30, 40, and 80 s of irradiation time, respectively. (e) Colors of a LC phase doped with a second generation molecular motor (6.8 weight% in E7), as a function of irradiation time (365 nm), and starting from (2'S)-(P)-1a, and (f) during subsequent thermal helix inversion at RT. Panels (a, c, and d) are reproduced with permission from reference [1181]. Panels (b, e, and f) are reproduced with permission from reference [1182], Copyright 2006 John Wiley and Sons.

Further, Feringa and coworkers used the same rotary molecular motor as a dopant (1 wt%) in a unidirectionally-aligned cholesteric liquid-crystalline film showing a polygonal fingerprint texture (Figure 122a).[1183]

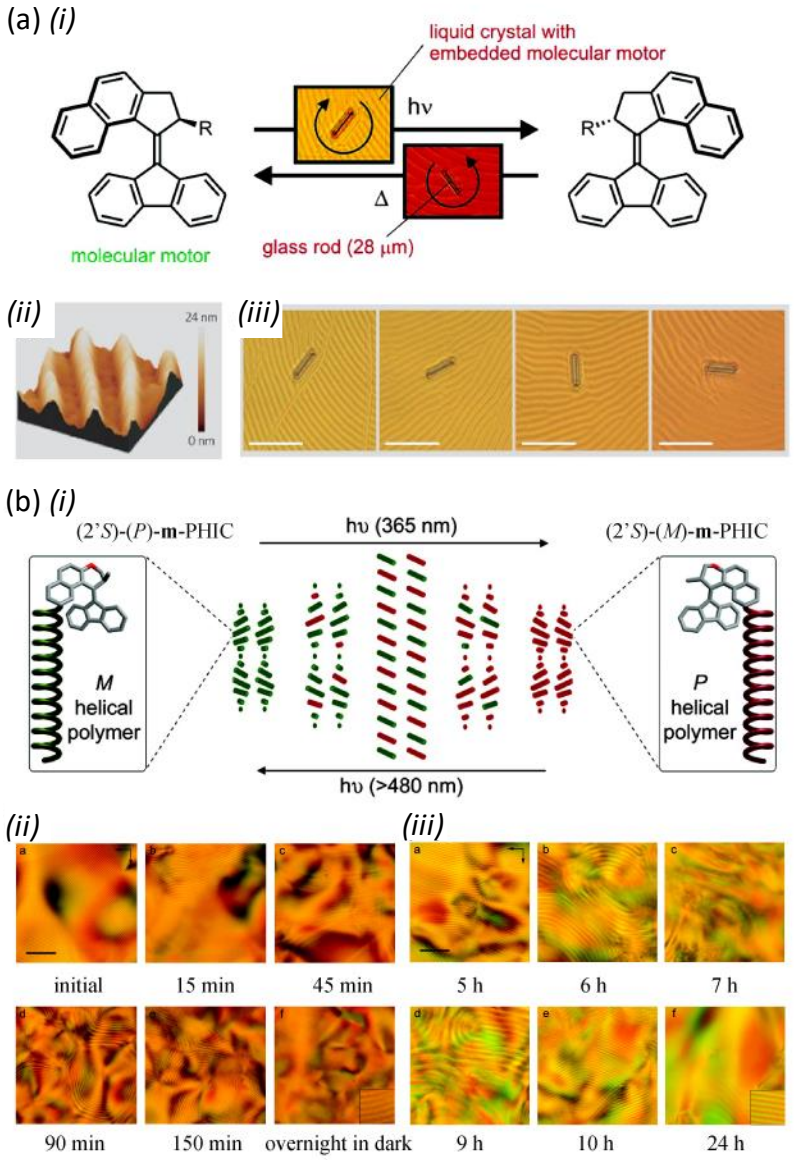

Figure 122: (a) *(i)* General observation of the rotation of a micrometric glass rod at the surface of a LC phase doped with a rotary molecular motor upon light irradiation or heating. *(ii)* Surface structure of the liquid-crystal film (atomic force microscopy image; 15 μm^2). *(iii)* Glass rod rotating on the liquid crystal during irradiation with ultraviolet light. Frames 1–4 (from left) were taken at 15-s intervals and show clockwise rotations of 28° (frame 2), 141° (frame 3) and 226° (frame 4) of the rod relative to the position in frame 1 (atomic force microscopy image; 15 μm^2). (c) *(i)* schematic representation of the reversible inversion of the preferred helical twist of a polymer backbone induced by a chiroptical molecular switch at its terminus. (2'*S*)-(*P*)-m-PHIC induces a preferred *M* helical twist of the polymer backbone. UV irradiation (λ= 365 nm) of the photochromic switch yields to (2'*S*)-(*M*)-m-PHIC and to an induced preferred *P* helicity of the polymer. Subsequent irradiation with visible light (λ > 480 nm) reverts the

system to (2'*S*)-(*P*)-m-PHIC with a preferred *M* helicity of the polymer. *(ii)* Optical micrographs of a thin film (thickness, 200 μm) of (2'*S*)-(*P*)-m-PHIC in toluene (30 wt %) at various times (0 to 150 min) of UV irradiation (λ = 365 nm). After 150 mn, a PSS mixture is obtained that consists of a large excess of (2'*S*)-(*M*)-m-PHIC. Scale bar, 50 μm. *(iii)* Optical micrographs of a thin film (thickness, 200 μm) of (2'*S*)-(*M*)-m-PHIC in toluene (30 wt %) at various times (0 to 24 h) of UV irradiation (λ > 480 nm). After 24 h, a PSS mixture is obtained that consists of a large excess of (2'*S*)-(*P*)-m-PHIC. Scale bar, 50 μm. Panel (a *(ii, iii)*) are adapted with permission from reference [1183], Copyright 2006 Springer Nature. (Panel (a (i)) is reproduced with permission from reference [1184], Copyright 2006 American Chemical Society. Panel (b) is adapted with permission from reference [1185], Copyright 2008 American Chemical Society.

Strikingly, it was observed by optical microscopy under UV irradiation at 365 nm that the polygonal texture reorganizes in a rotational (clockwise) fashion. The rate of rotation gradually decreases until the process halts after about 10 min. Removal of the light source causes the rotation of the texture to resume, this time in the opposite (anticlockwise) direction. The direction of rotation of the liquid-crystalline texture was proven to be determined by the change in helicity of the motor. The authors then demonstrated that the rotation of the texture can be harnessed to rotate a micrometric glass rod on the top of the film. A 20-nm height surface relief was observed by non-contact atomic force microscopy on the doped liquid-crystalline film, and the reorganization of the relief was believed to generate a torque to rotate the microscopic object. Note that such a rotation was later on observed by Kurihara with simple photoswitches as described in section 2.2.2.[166] In a later paper using motors,[1184] more comprehensive studies on the above system based on other liquid-crystalline matrices and alternative photo-switchable dopant were carried out, and a possible mechanism of rotational reorganization was given. The pitch change in response to the chirality change of the motor dopant requires a rotational reorganization of the mesogens perpendicular to the helix axis and that is cumulative along this axis. This unfavorable enormous reorganization promotes the change of the helix axis direction so that a longer pitch can be

achieved while minimizing the orientational reorganization of the mesogens. This changing then results in the change of local director angle and a local reorganization takes place to align the regions with similar directors. This reorganization can be considered as a defect passing through the film, which drastically changes the orientation and results in the amplification of the rotation at the microscopic scale. The specific mechanism of rotation was elucidated, based on the hybrid anchoring of the confined liquid crystal film.[1186] This hybrid (PH) anchoring mode of the cholesteric film at the liquid-air interface plays a key role in the formation of the texture and their rotation is indeed the result of pitch adjustment to the isomers of the motor having HTPs of opposite signs. The β_0, the angle between the normal to the stripes of the textures and the direction of the rubbed surface, was found to have an approximate linear relationship with 1/p for film with certain thickness. So the pitch changes ($p \approx c\ HTP_P$) induced by photoisomerization (or thermal relaxation) of the motor molecules consequently result in the variation of the β_0 angle. This process is recognized as the texture's rotation in a microscopic observation. Reorganization of the system is thus essentially dependent on the transmission of mechanical effects mediated by a change in elastic free energy.

The same group also demonstrated that the molecular chirality of the motor can be transmitted transiently to a macromolecular level by covalent attachment to a helical polymer,[1187] and then to the supramolecular level of a cholesteric LC phase (Figure 122b).[1185] This was accomplished by covalently functionalizing one end of a polyisocyanate with a modified motor, which here acts as a photochemical chiroptical switch between two thermally-stable states. This characteristic allows transmission and reversion of chirality between two stable *P* and *M* conformations of the polyisocyanate. Importantly, switching between the two chiroptical states is fully photo-addressable by tuning the irradiation wavelength either at 365 nm (Figure 122b(*ii*)) or over 480 nm (Figure 122b(*iii*)). In both photo-isomerization processes, the pitch of the LC matrix was found to increase at first and then elongate to such an extent that the cholesteric lines are no longer detectable by eye. At this point, the system contained equal amounts of *M* and *P* helical polymer in the LC film, effectively canceling the global helical torque of the LC. However, as expected, further irradiation resulted in the recovery of fingerprint texture,

indicating a shortening of the pitch that reflects the enantiomeric enrichment of the helical mixture. Although the thermal reorganization of the LC phase was found to be quite slower than the photoisomerization process, this work successfully achieved a fully photo-addressable hierarchical transmission of chiral information, from molecular to macromolecular and to supramolecular levels in the LC phase.

Katsonis, Brasselet, and coworkers used subnanowatt light activation of second-generation molecular motors to harness the reversible topological structuring of chiral frustrated LCs (Figure 123a).[1188]

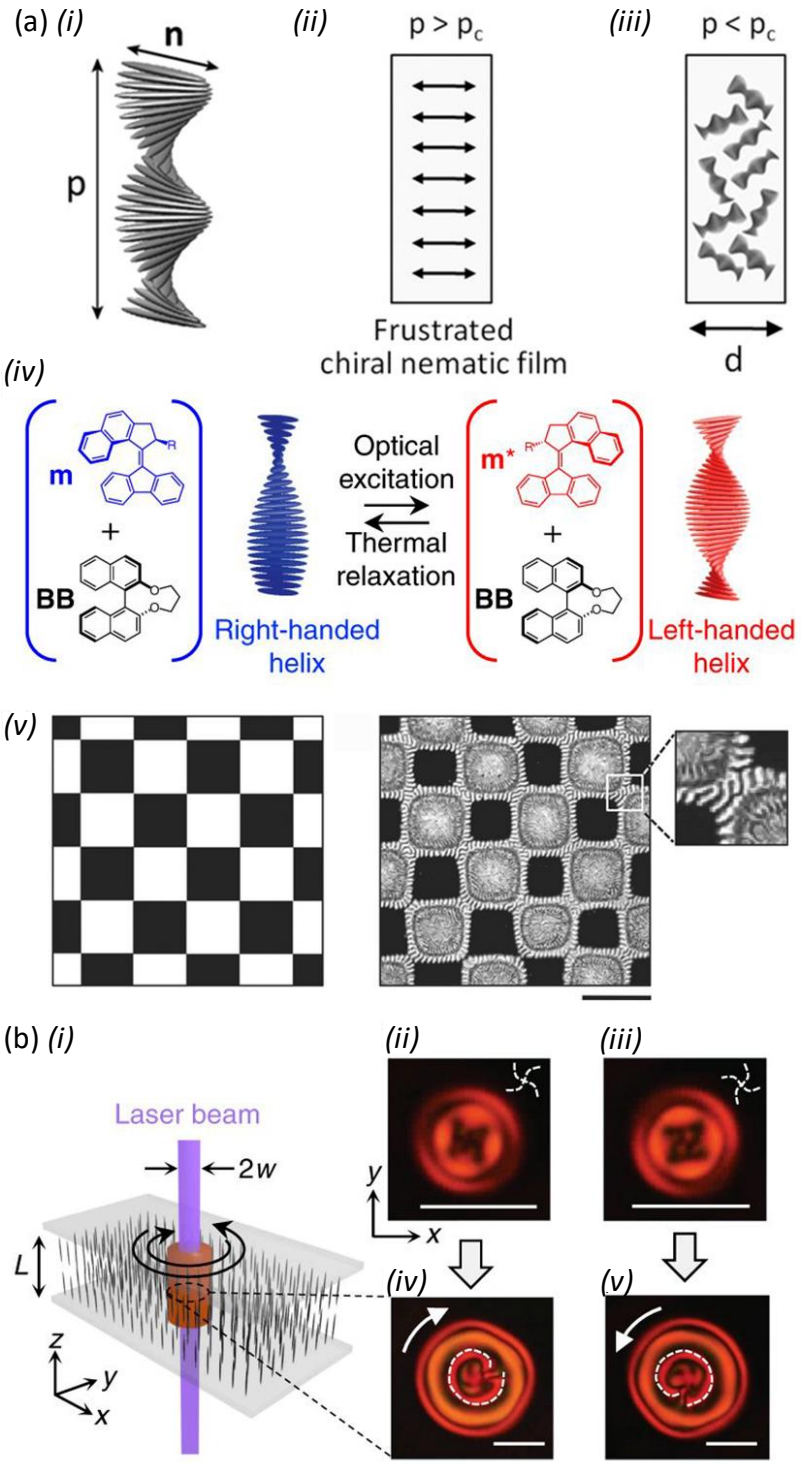

Figure 123: (a) *(i)* Helical twisting of a cholesteric LC of director *n* and pitch *p*. *(ii)* Frustrated LC film in a cell of thickness *d* ($p>p_c$). *(iii)* Twisted defect texture for large enough *d/p*. *(iv)* Molecular motor used as photo-active dopant, with a substituent R on the stereogenic center. Two derivatives were used: Ph-m (R = phenyl group), and Me-m (R = methyl group). A bridged binol BB was used as a passive co-dopant. *(v) Left*: Original image of the amplitude mask. Right: Image recorded of the imprinted checkerboard

pattern at PSS (light intensity:1 $mW.cm^{-2}$; Scale bar: 250 µm). (b) *(i)* 10 µm thick motor-doped LC film confined between two glass slides promoting perpendicular orientation of the molecules and illuminated locally using a Gaussian laser beam. *(ii-iii)* Axisymmetric chiral patterns with opposite handedness observed by polarized optical microscopy between crossed linear polarizers. *(iv-v)* A secondary structural symmetry breaking takes place spontaneously as the power increases up to $P \sim 2\ P_{min}$, and leads to a non-axisymmetric self-organized pattern that rotates continuously clockwise or anticlockwise, depending on the axisymmetric pattern from which it results (*ii* or *iii*). Scale bars of 20 µm. Panels (a *(i-iii, v)*) are adapted with permission from reference [1188], Copyright 2014 John Wiley and Sons. Panels (a (iv)) and (b) are adapted with permission from reference [1189], Copyright 2018 Springer Nature.

The so-called "geometric frustration" of a LC film can occur when the pitch p is larger than a critical pitch value p_c for a film of thickness d which is submitted to homeotropic boundary conditions, while a decrease of p to $p<p_c$ enables the chirality expression at supramolecular level. The commercially available E7 mixture was used as the nematic host and doped with a molecular switch **m**. In order to set an initial situation with $p>p_c$**,** a certain proportion of shape-persistent enantiopure co-dopant was used to favor a left-handed helicity of the LC, and to compensate the right-handed twist promoted by **m**. Upon UV irradiation, the left-handed cholesteric helix wound from an initial pitch p = 18 µm to a final pitch p = 1.7 µm at the photo-stationary state. Thus, in a homeotropic cell of thickness d = 10 µm, the cholesteric helix is unwound at thermodynamic equilibrium in the dark, whereas frustration can be relieved under irradiation with UV light. Based on this technology, large area checker-board pattern can also be achieved using a stencil as a binary amplitude phase mask, with photo-stationary patterns being typically obtained after 1 min of irradiation (Figure 123a(*iv*)).

In 2017, the same research groups reported on a very interesting phenomenon emerging from the same chemical system (Figure 123b).[1189] Above a critical light irradiation power of $\sim 2P_{min}$ (with P_{min} referring here to the minimum power necessary to generate twisted structures), a spontaneous axial symmetry

breaking takes place in the chiral pattern, resulting in the emergence of an oscillating rotation pattern. Based on the experimental data showing the dependence of the chiral pattern diameter on the incident power, a simple reaction-diffusion model was used to calculate the corresponding diffusion coefficient of the molecular motors. A good agreement of calculated value with those from literatures confirmed that diffusion plays an important role in the emergence of these structures. However, experimental data also showed an exponential dependence of the period of rotation with the diameter of the patterns, suggesting that diffusion is not the only parameter involved. In particular, the helix inversion plays a key role in preserving the rotation pattern and, overall, the out-of-equilibrium process rests on a non-local feedback loop that involves the local concentrations of the motor isomers, their spatial gradients, as well as twist gradients that occur across the liquid crystal structure. The diffusion of the chiral motors and the chirality of the liquid crystal in which they diffuse always influence mutually. Specifically, whereas the pitch distribution follows the spatial distribution of the molecular motors, further in return, the elastic relaxation and the differential diffusion rates of the motor isomers is also creating a new chiral landscape in the matrix. Thus, the access to oscillating patterns requires the collective interplay between the light-powered diffusion/rotation of chiral motors and the long-range orientation gradients of LCs. Of course, one may also consider whether a simple chiroptical molecular switch would be already sufficient to sustain such a rotation pattern, although the high efficiency of overcrowded alkenes to induce large pitch and handedness changes upon illumination, thanks to their axial chirality, remains unmatched by other photo-responsice chiral dopants.[1190]

Recently, Yang, and coworkers also reported on another light-powered dynamic reconfiguration of LC helical structures (Figure 124).[1191] Here again, second-generation molecular motors (with a methyl benzoate substitution) were used as chiral dopants in a rod-like LC host. In contrast to Katsonis and Brasselet's work, the initial state of the liquid crystal molecules was set in a homogeneous alignment under the boundary condition imposed, and in which the molecules align parallel to the substrate with the helical axes perpendicular to the substrate. UV irradiation of this device with a 365 nm light results in the photochemical isomerization of the motor accompanied with a chirality change. The pitch of the LC can

thus be varied from an initial state with p_0 = 2.0 μm, to the photostationary state with p_{PSS} = 0.5 μm. The compression of helical pitch involves reorganization with defects, resulting in the metastable opaque regions originating from the mismatch of refractive indices among the disordered helical domains.

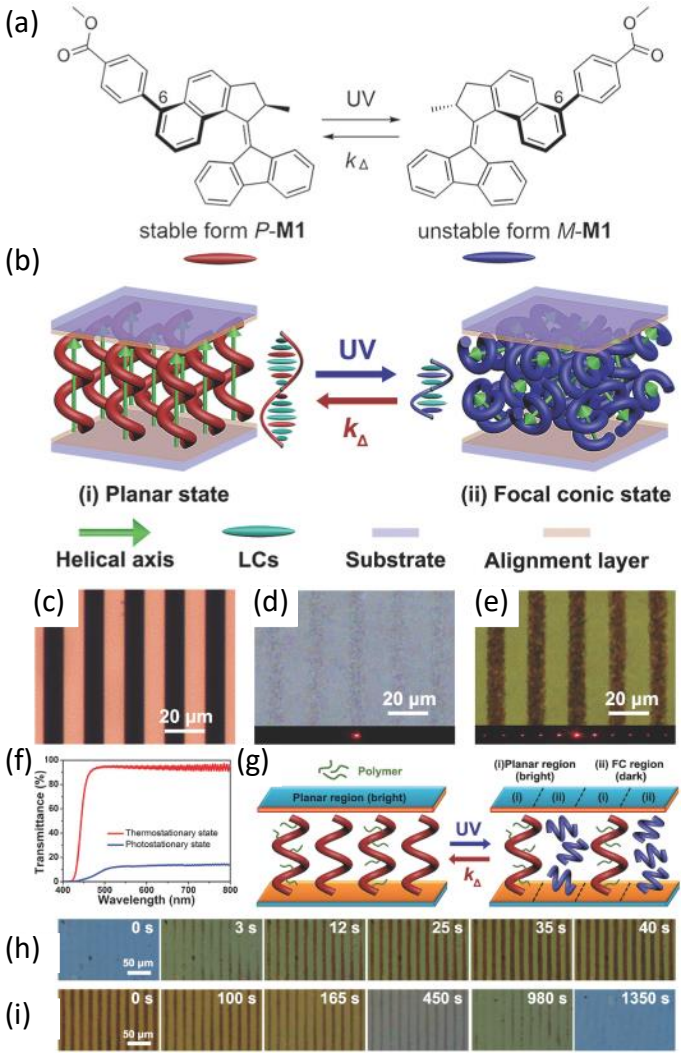

Figure 124: (a) Photoisomerization and thermal helix inversion of chiral motors with a methyl benzoate substituent at the 6-position. (b) Reversible structural reconfiguration of motor-doped helical LCs between homogeneous helical axis (thermal relaxation) and random helical axis (upon UV irradiation). (c) Optical micrograph of the striped photomask for fabricating the motor-doped LC grating. POM images of the motor-doped LC with (d) homogeneous planar configuration after thermal relaxation and (e) binary pattern at the PSS of alternating planar and focal conic states. (f) Transmittance spectra of the motor-doped LC at the TSS and the PSS, respectively. (g) Schematic illustrations of the patterns observed in (d)

and (e). (h) POM images of LC grating as a function of time during irradiation during photoirradiation (80 mW.cm^{-2}) and (i) during thermal relaxation. Adapted with permission from reference [1191].

On this basis, the authors also demonstrated a light-directed dynamic diffraction grating (Figure 124c-i). **M1**-doped polymer-stabilized cholesteric LCs grating was covered by a stripe photo-mask and the UV exposure created binary-stripe pattern with alternate transparent planar and opaque focal conic configurations, which resulted in the appearance of diffraction pattern from a probe beam with a grating period of ≈20 μm.

4.3.4. Collective behaviors within self-assembled structures

Self-assembled nanostructures, which can be perturbed by small energies in the order of a few k_BT, just as liquid crystalline phases, are highly sensitive to their environment and, hence, represent another very attracting domain for the implementation of rotary molecular motors, with the promise to access responsive soft nano-objects. In this direction, a few examples of the literature have been recently described. For instance, an over-crowded alkene was inserted within the so-called tryptophan zipper ("trpzip") monomeric β-hairpin sequence, which folds into a secondary structure without requiring metal ion binding (Figure 125).[1192] The over-crowded alkene molecular switches functionalized with dicarboxylic acid were protected at one half and then used as a starting building block in solid-phase peptide synthesis to attach the β-hairpin sequence. Both the light- and heat-induced isomerizations were shown to retain their efficiency even in the presence of the peptide. The self-assembling behavior and resultant secondary structure were studied by CD, NMR and TEM. In methanol, the *trans* isomer forms a single population of vesicles, while the *cis* isomer forms a mixed population of vesicles and fibers. Interestingly, the transition state going from vesicles to fibers can be observed in TEM images, and the fibers showed strong similarity with those formed by amyloidogenic peptides. In water, the *trans* isomer shows sheet-like structures which can be disrupted by irradiation and subsequent heating, while the *cis* isomer forms small apolar aggregates, invisible by TEM but probed by Nile red. The aggregates formed

by the *trans* isomer are very different from the ones formed by azobenzene-based β-hairpin, a variation explained by the much more hydrophobic core of the overcrowded alkene.

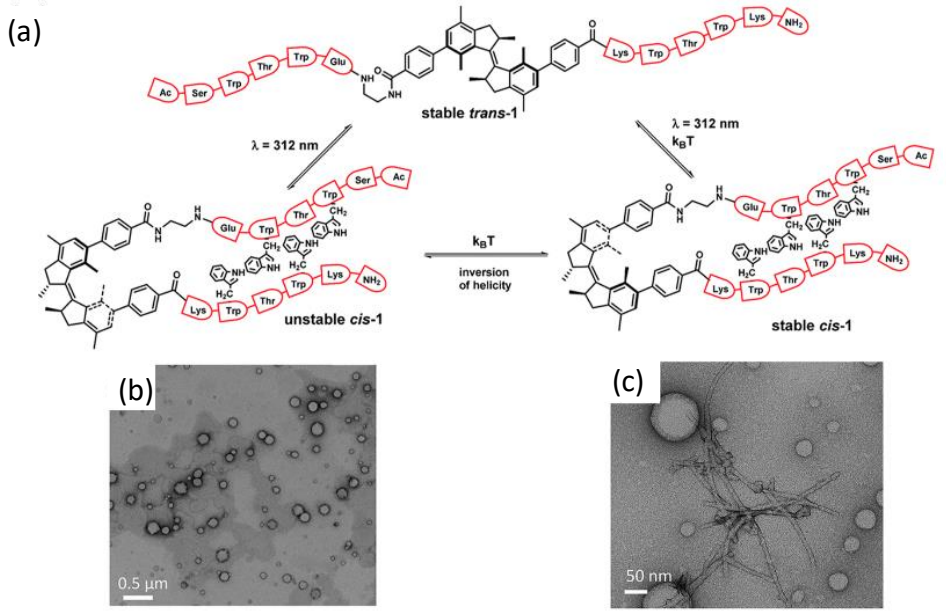

Figure 125: (a) Rotary cycle for an overcrowded alkene functionalized with a Trpzip sequence. (b) TEM image of the *trans* isomer in methanol. (c) TEM image of the stable *cis* isomer in methanol. Adapted with permission from reference [1192], Copyright 2015 The Royal Society of Chemistry.

The group of Feringa also demonstrated the first example of a molecular motor incorporating amphiphilic moieties, and leading to well-defined self-assembled structures in water (Figure 126). In addition, they proved a reversible change of their morphology by using external light and heat stimulations.[1193] In this work, and in reference to their speed of rotation, "fast" (A) and "slow" (B) amphiphilic molecular motors were designed and studied using cryo-transmission electron microscopy (cryo-TEM) and UV-vis absorption spectroscopy. On the one hand, amphiphile (A) forms toroided nanotubes when co-assembled with DOPC in water. However, its half-life time was determined to be of 40 ns by transient absorption spectroscopy, which was too short to observe any changes in the aggregates upon irradiation of the motor. On the other hand, amphiphile (B) self-assembles into straight nanotubes in water and, upon light irradiation, isomerization of the molecular component from its stable to its unstable form causes the tubular structures to reorganize into vesicles. However, in order to regenerate

the nanotube structure, subsequent freeze-thawing process had to be applied after heating the sample, thus meaning that spontaneous reorganization at higher length scales does not take place. Nevertheless, the authors demonstrated that it is possible for a motor to retain its function in aqueous solutions and utilized its light-induced isomerization to reorganize the structure of soft self-assembled nanostructures.

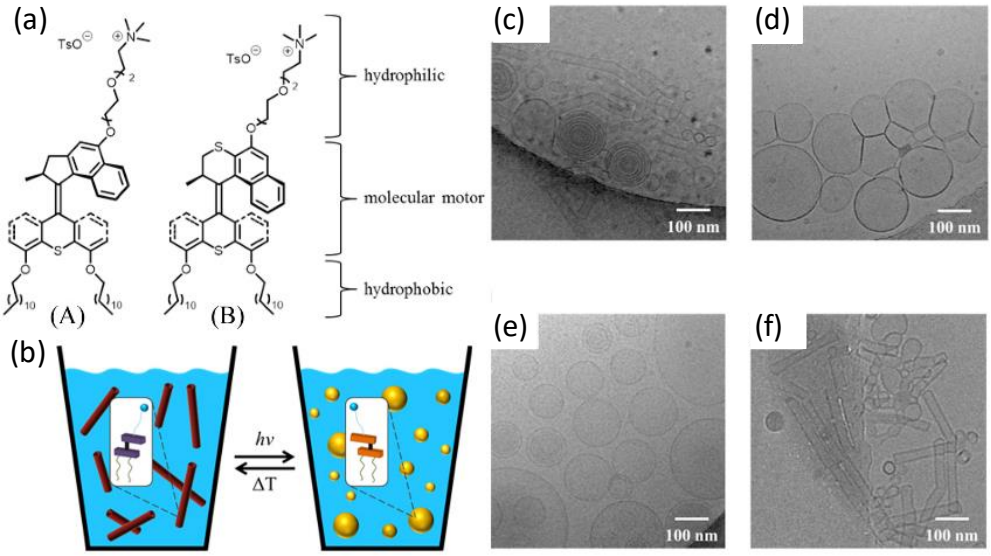

Figure 126: (a) Chemical structures of amphiphilic molecular motors A (fast) and B (slow). (b) Schematic representation of the morphological changes taking place in the supramolecular nanostructure upon isomerization of the motor. (c) Cryo-TEM micrographs of co-assemblies of amphiphile B and DOPC (1:1) in water at a total concentration of 1 mg.mL^{-1} before irradiation (stable B); (d) after irradiation for 15 min at 365 nm (unstable B); (e) after heating at 50 °C for 16 h (stable B); and (f) after freeze-thawing 3 times. Adapted with permission from reference [1193], Copyright 2016 American Chemical Society.

To reach responsive supramolecular structures with higher complexity and lager dimensions, Feringa and coworkers subsequently implemented amphiphilic motors in a hierarchical supramolecular assembly, which turned out expressing a muscle-like behavior (Figure 127).[1194] The molecular motor was functionalized with a dodecyl chain at its upper part, and two carboxyl groups at its lower part to allow its water solubility. This amphiphile is indeed able to undergo self-assembly in water to form nanofibers with high water content of 95 %. Further, aligned bundles of nanofibers can be obtained by drawing the

aqueous solution of motor into an aqueous solution of Ca(II), a technique which also provides electrostatic screening to avoid complicated processes like crystallization.

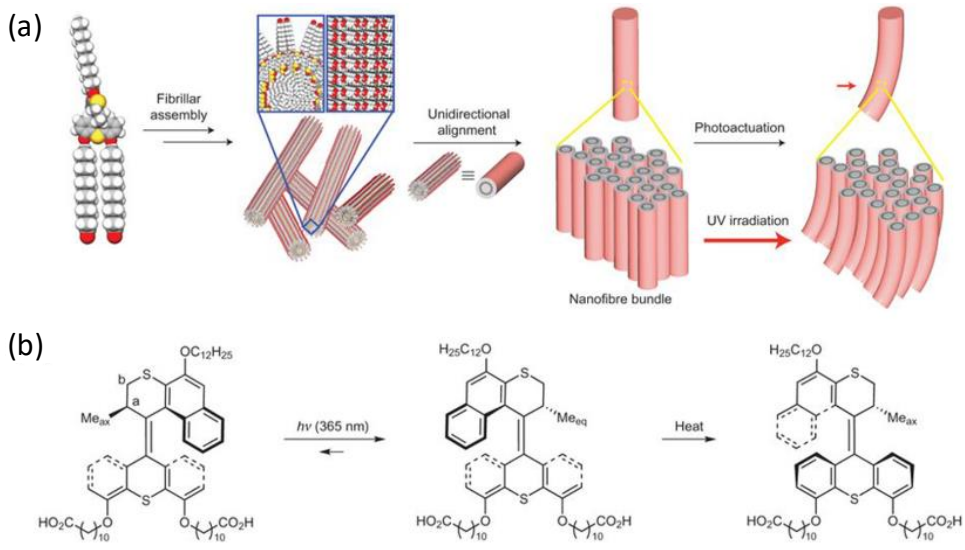

Figure 127: Schematic representation of the hierarchical organization and photoactuation of a self-assembled macroscopic string. (a) CPK structure of the photoresponsive rotary motor used and its self-assembly into nanofibers. The nanofiber-containing solution is manually drawn from a pipette into a $CaCl_2$ solution to achieve unidirectional alignment in bundles, generating a string that is able to bend upon exposure to UV irradiation (represented by red arrows). (b) Photochemical and thermal helix inversion steps of the motor used in this study. A single enantiomer is shown; the two stable isomers shown are identical but viewed from different angles. Adapted with permission from reference [1194], Copyright 2017 Springer Nature.

The photochemical and thermal isomerization processes within the self-assembled nanofibers in water were proven to be fully preserved by NMR and UV-vis spectroscopy study. Very interestingly, the UV irradiation causes the self-assembled string to bend towards the light source from an initial angle of 0° to a flexion angle of 90° in 60 seconds. A subsequent heating process at 50 °C in the dark restores its original conformation within 3 hours. However, a retardation of the system is observed for the second photoirradiation in which the same string only bends with a flexion angle of ~45°, a phenomenon attributed to the relatively low thermal stability of the supramolecular string. In addition, a lifting

experiment was performed with a 0.4 mg piece of paper adhered to the end of the string. Under photoirradiation, the collective actuation of the switches is able to bend the string by 45° towards the light source, and thus to produce a sufficient power to lift the weight. Based on in-situ small angle X-ray scattering (SAXS) measurements of the string, the bending actuation was proven to be the direct consequence of structural disordering and of the subsequent local contraction of the packing at the photo irradiated side only.

The group of Qu also made use of an amphiphilic overcrowded alkene switch (OAS) to construct photo-responsive nano-containers (Figure 128).[1195]

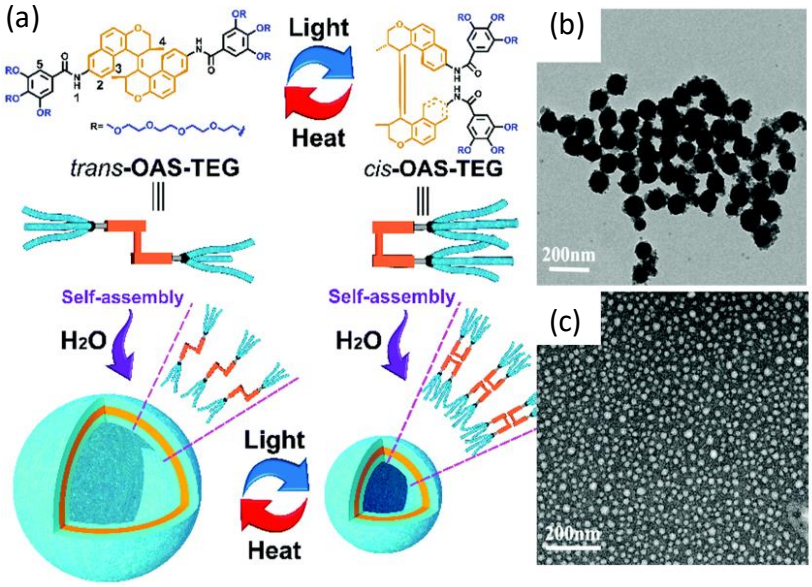

Figure 128: (a) Chemical structures of *trans* and *cis* OAS-TEG derivatives (which are isomerized by light and heat), and schematic representation of their responsive – stretchable – vesicular self-assembly in aqueous solution. (b) TEM images of *trans*-OAS-TEG vesicles. (c) TEM images of *cis*-OAS-TEG vesicles obtained after 15 min of UV irradiation at 365 nm from (b). Adapted with permission from reference [1195], Copyright 2016 The Royal Society of Chemistry.

Tetra(ethylene glycol) (TEG)-functionalized OAS, with a hydrophobic core and two hydrophilic arms, were shown to self-assemble into well-defined vesicles (with a diameter of ≈100 nm for the *trans*-OAS-TEG isomer). Upon 15 min of UV irradiation (365 nm), structural changes of the isomerized OAS-TEG

amphiphile resulted in the contraction of the pre-formed large vesicles into smaller ones. The larger vesicles were recovered by heating the *cis*-OAS-TEG in aqueous solution under darkness at 40° for 10 min. Interestingly, the vesicles with switchable diameters have remarkably different volumes to contain cargoes in their cavities. Calcein dye was loaded into larger vesicles, and its full releasing was monitored by fluorescence after 150 min of UV irradiation.

4.3.5. Collective behaviors in polymers and gels

Coupling molecular motors in polymer main chains, as well as in polymer networks, for instance in the form of chemical of physical gels, is of primary interest to couple their motions into mechanically active materials. Here again the transmission of the chiral information over length scales can be envisaged as a dynamic hierarchical process. For instance, in this direction, the group of Feringa demonstrated that the chirality from a molecular motor can be transferred to a helical polymer *via* supramolecular ionic interactions (Figure 129a).[1196] In this study, a molecular motor was functionalized with two carboxylic acid groups in order to provide ionic interactions with the ammonium side groups of a polyphenylacetylene (in addition to basic hydrophobic interactions). Interestingly, the CD spectrum of the helical polymer doped with the (*P,P*)-*trans*-motor is the mirror image (i.e. opposite helicity) of the CD spectrum of the helical polymer doped with the (*P,P*)-*cis*-motor, even though the *trans* and *cis* isomers have the same absolute configuration at their stereogenic centers and same helical chirality in their core. Based on the distance between the two carboxylic acids (11 Å for (*P,P*)-*trans*-motor and 6 Å for (*P,P*)-*cis*-motor), distinct binding modes were proposed to explain the preferred polymer handedness. Irradiation of a sample doped with (*P,P*)-*cis*-motor resulted in a mixture of (*M,M*)-*cis*-motor and (*P,P*)-*trans*-motor at PSS, which gave an inversion of CD signal indicating the inversion of the polymer handedness. However, when a sample doped with (*P,P)-trans*-motor was irradiated, no inversion of the CD signal was observed although the resultant (*M,M*)-*cis*-motor has a shorter distance between carboxylic acid groups. This sharp contrast was explained in the way that the (*M,M*)-*cis*-motor, as it is a pseudo-enantiomer of (*P,P*)-*cis*-motor, also induces the opposite helicity (compared to (*P,P*)-*trans*-motor).

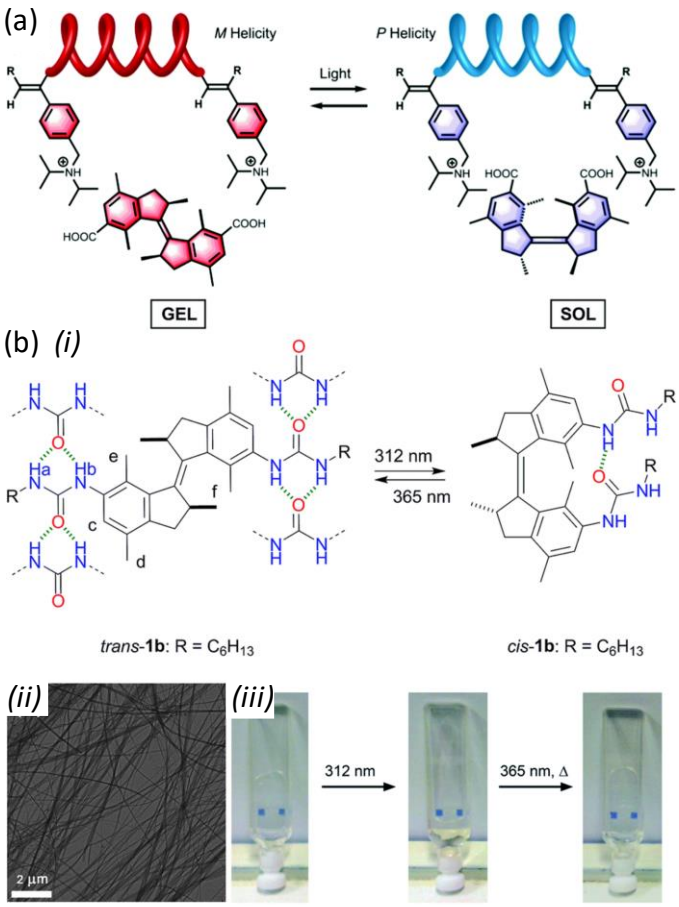

Figure 129: (a) Proposed control over the helicity of a polymer backbone using a photoresponsive molecular motor as dopant. (b) *(i)* Photoisomerization behavior and predicted urea hydrogen bonding pattern of trans and cis bis-urea LMWGs 1a-c. *(ii)* Transmission electron microscopy (TEM) of a gel in toluene (0.5 mg mL-1) of trans-**1b**. *(iii)* Images of a gel of trans-**1b** in toluene (0.5 mg mL-1) before and after an irradiation of 15 min at 312 nm and showing the gel to sol transition. The resulting solution was irradiated for 15 min at 365 nm and gently heated to regenerate the gel upon slow cooling. Panel (a) and (b) are adapted with permission from reference [1196], Copyright 2017 The Royal Society of Chemistry, and reference [1197], Copyright 2016 The Royal Society of Chemistry, respectively.

In 2016, the same group reported the first overcrowded-alkene-based bis-urea low-molecular-weight gelator (LMWG), which was able to undergo a *trans-cis* isomerization under UV irradiation and to show a different gelation behavior in each of these two states (Figure 129b).[1197] The LMWG was synthesized

by attaching urea end-groups with alkyl chains of different lengths to the overcrowded-alkene core. Remarkably, the hexyl derivative (*trans*-**1b**) forms gels in toluene and xylene at a concentration as low as 0.4 $mg.mL^{-1}$ (which ranks it among the family of "supergelators"). TEM images showed self-assembled thread-like fibers, fused and intertwined to form an entangled network (Figure 129b(*ii*)). In addition, a complete gel-to-sol transition was observed by starting from *trans*-**1b**, and by irradiating the system at 312 nm to enforce a *trans*-to-*cis* photo-isomerization. A transparent gel was then recovered by irradiating at 365 nm and subsequent gentle heating (Figure 129b(*iii*)). As illustrated in Figure 129b(*i*), all structural analyses supported the fact that in the *trans* configuration, intermolecular hydrogen bonds dominate the gelation process. In particular, single-crystal X-ray crystallography of the *trans* isomer clearly showed the existence of intermolecular hydrogen bonds between urea functions. In contrast, density functional theory (DFT) geometry optimization of the *cis* isomer indicates the possible formation of an intramolecular hydrogen bond, thus leading to a sol transition when switching the motor.

Covalent polymer networks were also recently reported to serve as a very attractive transmission relay between rotary molecular motors and our macroscopic world. In order to produce a useful work in a self-standing material, our research group integrated light-driven unidirectional molecular rotors as active reticulation units in a chemical polymer gel (Figure 130a).[1198] The enantiopure motor core was synthesized by a diastereoselective synthetic pathway compatible with scale-up up to the gram scale.[1199] After attaching four poly(ethylene glycol) (PEG) chains to the motor, the irreversible chemical cross-linking of the gel was performed by a copper-catalyzed Huisgen ("click") reaction. When swollen at a concentration of 10 % wt/wt in toluene, a macroscopic contraction is observed at room temperature upon simple irradiation at 365 nm. A maximum contraction of ~80 % in volume is reached after 120 min (Figure 130b).

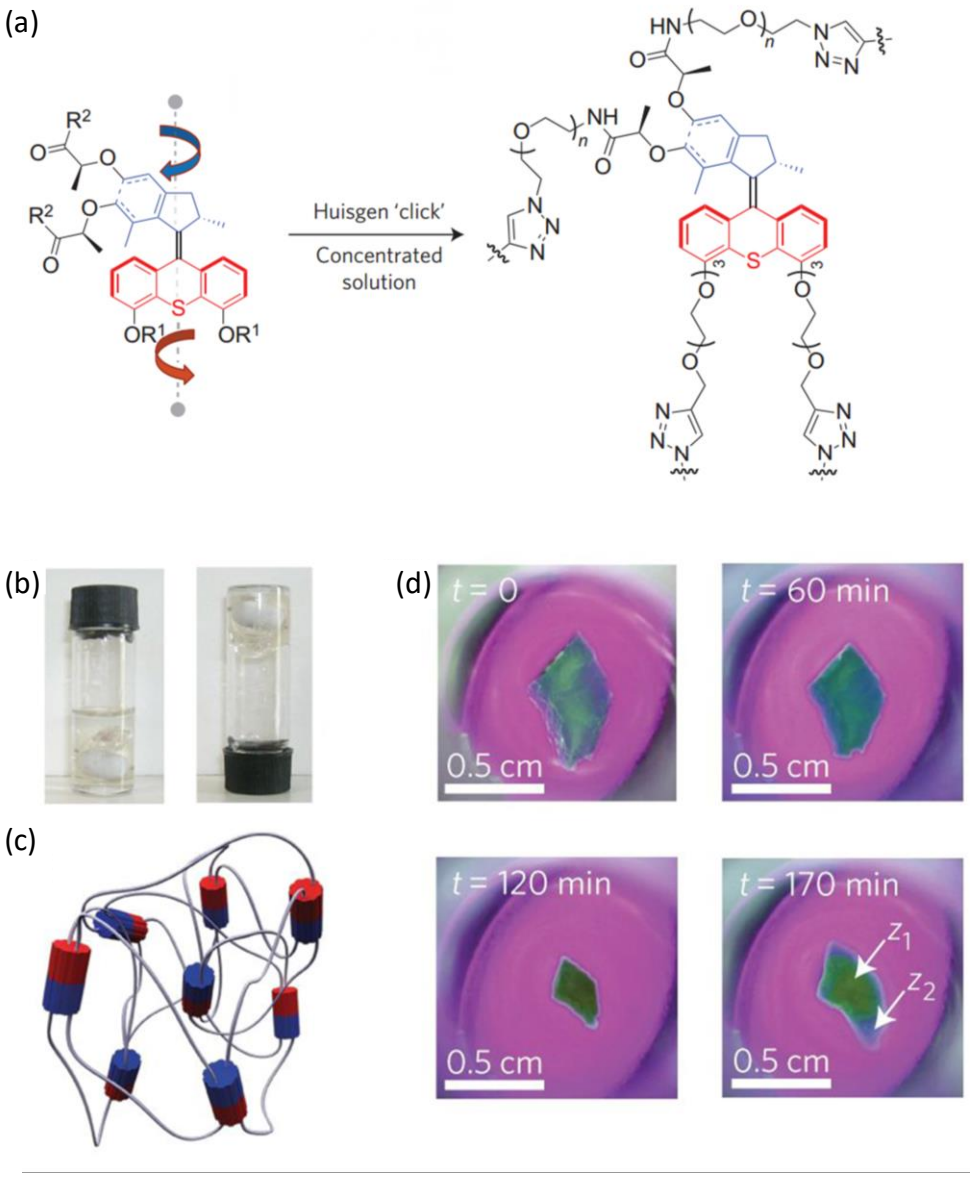

Figure 130: (a) Chemical design of enantiopure polymer–motor conjugates crosslinked by click reaction to access chemical gels (R_1 = $CH_2CH_2(OCH_2CH_2)_2$-OCH_2-C≡CH, R_2= NH-$CH_2CH_2(OCH_2CH_2)_n$-$OCH_2CH_2N_3$, n = 107 or 237). (b) Typical active gel (10 % wt/wt in toluene). (c) Schematic representation of a crosslinked polymer–motor conjugate network, which, due to its mechanically active topology, twists the polymer chains and reduces the entire size of the network upon light-driven rotations. (d) Snapshots showing time-dependent macroscopic contraction of a piece of gel upon UV irradiation. Adapted with permission from reference [1198], Copyright 2015 Springer Nature.

As a universal behavior, it has been shown by rheology that the ratio of the shear modulus before and after the gel contraction is equal to its volume ratio, and that a maximum mechanical efficiency is reached when the gel is crosslinked at the critical overlap concentration of the starting macro-monomers (c^*).[1200] By looking in details at the experimental kinetic and thermodynamic parameters of the system, one can reveal that the macroscopic contraction at the level of the whole material is achieved by amplification of the continuous rotation of the individual motors in a collective way. This system uses the incoming light to operate out-of-equilibrium at the individual motor level, which means that the motor is constantly twisting the polymers chains under continuous light irradiation. The work produced by the motor at PSS is transferred in elastic energy within the newly created conformational twists between pairs of polymer chains. However, as the twisting of the polymer chains cannot be reversed without inversion of chirality at the motor level, the resulting twisted conformation is persistent and the process is limited to a unique contraction event at the level of the entire material. To overcome this limitation, a so-called "modulator" unit was integrated in a second generation of materials (Figure 131).[1201] This modulator, based on a tetrasubstituted dithienylethene photoswitch, can act as an on-demand elastic releaser that operates at a different wavelength to the one actuating the motor. Interestingly, the untwisting of the polymer chains (at the modulator) operates through a different energy pathway that lead to their twisting (at the motor), and thus creates a mechanistic hysteresis favorable to design a global out-of-equilibrium situation. The overall process now functions as follows: with UV light, the motor is continuously rotating and the modulator is in its cyclized form, thus sustaining the torsion of the polymer chains generated by the motor. These combined effects lead to the global contraction of the material. Conversely, when irradiated with visible light, the motor ceases its rotation and the modulator is switched to its open form, in which the free rotations around C–C single bonds can then release the elastic energy accumulated in the braided polymer chains. This basic concept to connect a nanomotor with a releasing elementary unit in a fully integrated system is of great importance. It provides a general solution to overcome the unidirectionality limitation associated with the necessary use of Brownian ratchets when working out of-equilibrium at the nanoscale. Moreover, by playing with the frequencies of rotation of the motor and of the modulator (in

particular by changing the intensities of UV and visible light), it becomes possible to control the actuation of the entire material out of thermodynamic equilibrium with a global PSS that transfers into an apparent frequency which combines clockwise and anticlockwise rotations with a given mechanical output. If the contraction process is fully motorized, the expansion process also partly relies on osmotic pressure and elastic modulus of the polymer chains which is, from a thermodynamic point of view, reminiscent of what is observed in nature with muscular fibers. Such an artificial self-standing material is currently quite unique because it really involves the full potential of molecular motors, which is to produce a progressive work by cycling a constant unidirectional actuation within a system that is characterized by new descriptors such as the spatial trajectories and frequencies of its modules.

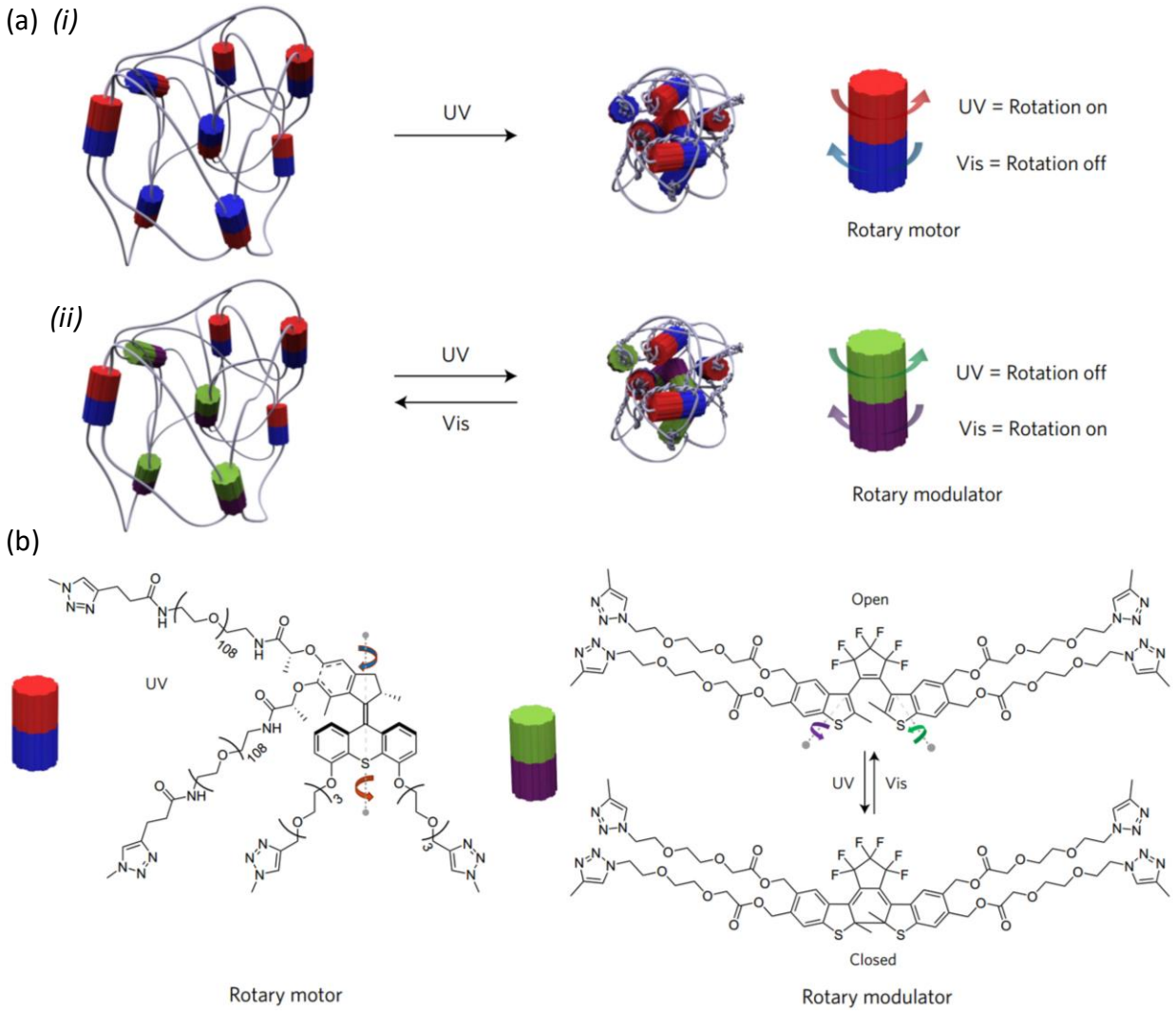

Figure 131: (a) Functioning principle and chemical design of an integrated motor/modulator system. (*i*) Schematic representation of a reticulated polymer–motor gel that, under UV light irradiation, produces a

continuous unidirectional out-of-equilibrium rotation of the motor part (red and blue cylinders) with subsequent twisting of the polymer chains, which leads to a macroscopic contraction of the entire network. A twist is defined as a new entanglement within a pair of polymer chains. (*ii*) Schematic representation of a polymer–motor–modulator gel that proceeds as in (*i*) when exposed to ultraviolet light, but that untwists the polymer chains when exposed to visible light by activating the modulator part (green and purple cylinders). Visible-light activation of the modulator allows its rotation in the opposite direction of the elastic torque initially produced by the motor, and thus leads to a full re-expansion of the network at thermodynamic equilibrium. (b) Chemical structures that compose the polymer–motor–modulator system shown in (a, (*ii*)). Adapted with permission from reference [1201], Copyright 2017 Springer Nature**.**

4.4. Conclusion

In this section, we have highlighted some examples of collective behaviors based on synthetic rotary molecular motors, either influencing their systems as a function of their state as simple switches, but also sometimes used for their capacity to constantly rotate out of thermodynamic equilibrium – and with the potential to achieve a progressive work on their environment. By means of surface immobilization, of doping in liquid crystal matrix, of self-assembling in nanostructures, or of hybridization with polymers, their motion at molecular level can be transferred across length scales up to supramolecular, microscopic, and even macroscopic levels. Various interesting functions have been achieved by these integrative systems, including the controllable wettability of surface, the patterning of LC media, the powering of nanomachines and of microscopic object, the switchable packing in self-assemblies, and the access to active self-standing materials at macroscopic scale. Beyond these recent achievements, new endeavors are still needed to gain a better understanding about the potential of such motors in the design of useful materials that can be implemented in relevant technologies with high efficiency and reliability. We believe that to cross this new scientific frontier, combined efforts between chemists, physicists, and engineers

will be instrumental and that it represents a particularly exciting and promising field for interdisciplinary research.

5. CONCLUSION AND PERSPECTIVES

This overview of the literature on the design of collective motions from synthetic molecular switches, rotors, and motors, reveals the richness of the systems developed so far, and their potential to access new kinds of functional materials.

First of all, this survey shows the high diversity of molecular actuators that can be involved, and which can be all considered as potential elementary building blocks for the construction of molecular machines (Figure 132, top panel). Various kinds of internal motional processes of different amplitudes can be implemented at molecular scales, and include: *cis-trans* isomerizations, electrocyclizations, mechanical bond actuations, axial rotations, and atropoisomerizations. From a more general point of view, one can probably better define these individual building blocks depending on the thermodynamic nature of their actuation, which determines their propensity to furnish different types of mechanical output. Hence, whereas molecular rotors do not produce work, molecular switches produce a reversible work as a function of their state, and motors produce a progressively increasing work as a function of their spatial trajectories. However, as it will be discussed below, such a basic thermodynamic situation at nanoscale can be changed by several means at higher length scales when these individual elements are integrated in systems.

This review also shows the high diversity of physical mechanisms that exist to couple those individual elements in space and time (Figure 132, middle panel). These phenomena are adapted to the chemical nature of the systems considered, as well as to their degree of organizational order. For instance, molecular actuation can generate variations of osmotic pressure or of interfacial energy, and can be therefore transmitted indirectly up to the macroscale. In many other examples, the transfer of the actuation takes advantage of ordered mesophases or even of crystalline organization to couple mechanical actuations with

phase transitions or molecular packing modifications. The last type of transmission is based on the direct mechanical amplification of molecular actuation such as encountered in molecular gearing or polymer twisting. In a parallel with supramolecular chemistry, which rests on the (non-covalent) self-assembly of structures from (covalent) molecular objects, such a hierarchical mechanics defines a continuum of controlled and integrated mechanical transmissions beyond the molecule.

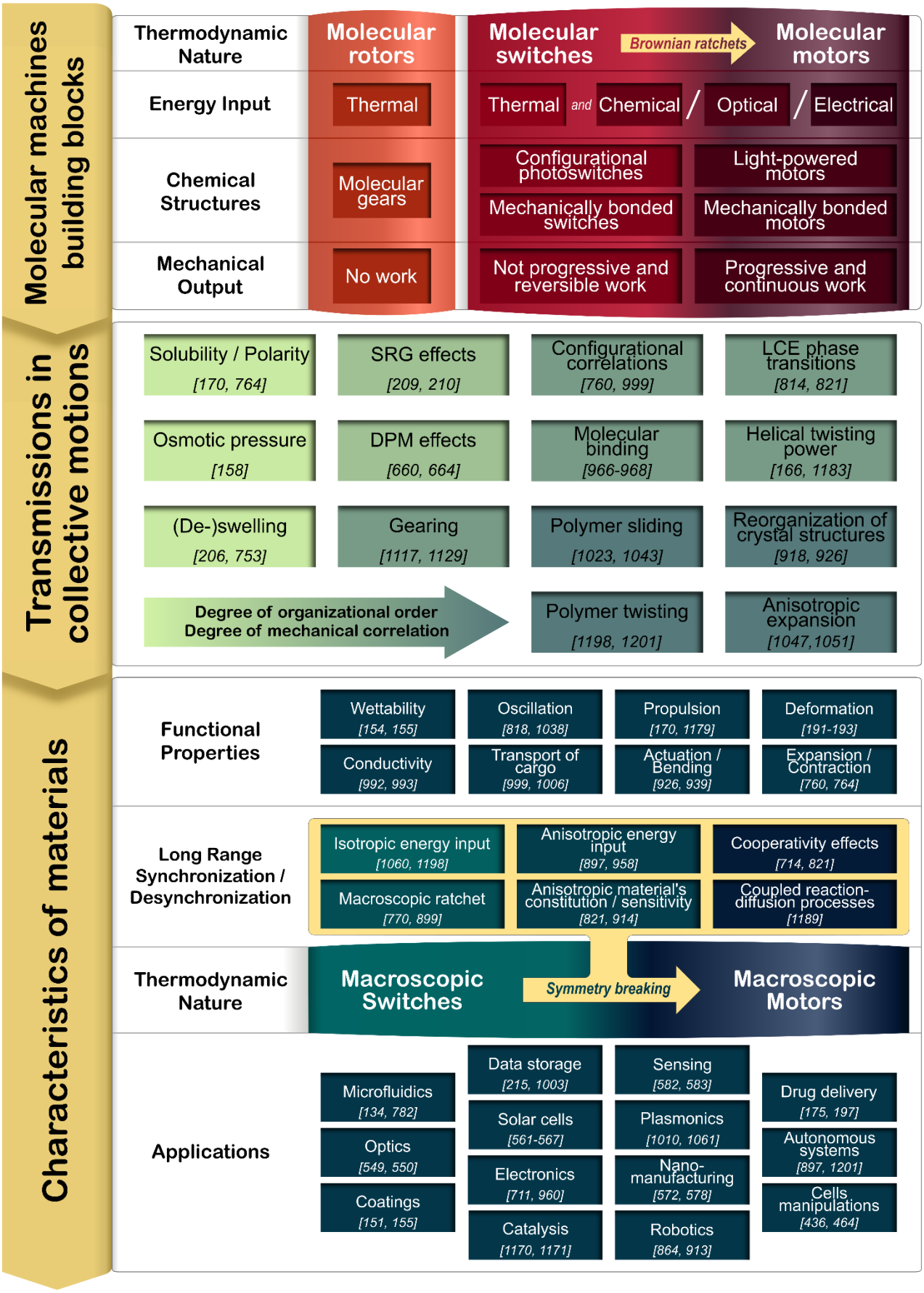
Molecular machines building blocks
Thermodynamic Nature
Molecular rotors
Molecular switches
Brownian ratchets
Molecular motors
Energy Input
Thermal
Thermal and Chemical / Optical / Electrical
Chemical Structures
Molecular gears
Configurational photoswitches
Light-powered motors
Mechanically bonded switches
Mechanically bonded motors
Mechanical Output
No work
Not progressive and reversible work
Progressive and continuous work
Transmissions in collective motions
Solubility / Polarity [170, 764]
SRG effects [209, 210]
Configurational correlations [760, 999]
LCE phase transitions [814, 821]
Osmotic pressure [158]
DPM effects [660, 664]
Molecular binding [966-968]
Helical twisting power [166, 1183]
(De-)swelling [206, 753]
Gearing [1117, 1129]
Polymer sliding [1023, 1043]
Reorganization of crystal structures [918, 926]
Degree of organizational order
Degree of mechanical correlation
Polymer twisting [1198, 1201]
Anisotropic expansion [1047,1051]
Characteristics of materials
Functional Properties
Wettability [154, 155]
Oscillation [818, 1038]
Propulsion [170, 1179]
Deformation [191-193]
Conductivity [992, 993]
Transport of cargo [999, 1006]
Actuation / Bending [926, 939]
Expansion / Contraction [760, 764]
Long Range Synchronization / Desynchronization
Isotropic energy input [1060, 1198]
Anisotropic energy input [897, 958]
Cooperativity effects [714, 821]
Macroscopic ratchet [770, 899]
Anisotropic material's constitution / sensitivity [821, 914]
Coupled reaction-diffusion processes [1189]
Thermodynamic Nature
Macroscopic Switches
Symmetry breaking
Macroscopic Motors
Applications
Microfluidics [134, 782]
Optics [549, 550]
Coatings [151, 155]
Data storage [215, 1003]
Solar cells [561-567]
Electronics [711, 960]
Catalysis [1170, 1171]
Sensing [582, 583]
Plasmonics [1010, 1061]
Nano-manufacturing [572, 578]
Robotics [864, 913]
Drug delivery [175, 197]
Autonomous systems [897, 1201]
Cells manipulations [436, 464]

Figure 132: Summary of the systems reviewed in this article highlighting the various objects and processes taking place from the molecular level to the macroscopic one. Numbers between brackets corresponds to references illustrating the notions highlighted.

Finally, this review shows the diversity of materials that can incorporate such dynamic elements, including: liquids, liquid crystals, amphidynamic crystals, crystals, mono- and bilayers, self-assembled soft materials, and various polymer systems. By integrating mechanically active building blocks, those materials can become stimuli-responsive, and can display new adaptable functions going from wettability to actuation (Figure 132, bottom panel). Interestingly, by playing appropriately with the long range synchronization/desynchronization of molecular actuators in materials, and by breaking spatial and time-reversal symmetries (*e.g.* by using anisotropic energy inputs or by designing macroscopic ratchets), it becomes possible to generate emergent behaviors such as oscillations, and even to modify the thermodynamic nature of the entire system compared to its elemental components, as for instance to transform a system made of molecular switches into a macroscopic motor, which can produce cycles of unidirectional actuations and deliver a repetitive and increasing work output (Figure 133). On the same topic, one can also notice that working with molecular motors is not a guarantee to reach a macroscopic motor when integrated in a collective system. Indeed, the necessity to reset the transmission processes (by binding/unbinding, twisting/untwisting, *etc.*) should take place in coherence with the molecular motors themselves in order to keep the entire system out-of-equilibrium.

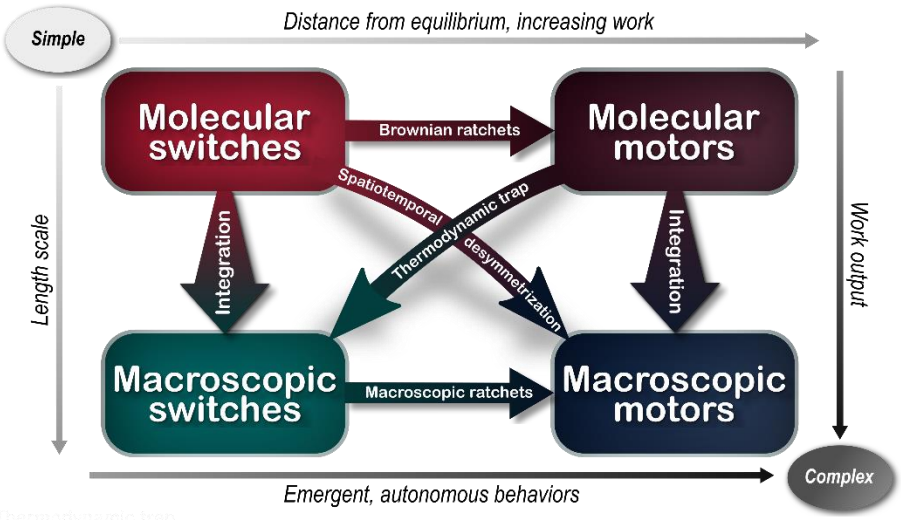

Figure 133: General relationship linking molecular machines building blocks with their collective behaviour at larger length scale.

It is finally interesting to notice within this review the high number of applications that such integrated systems have already touched, going from data storage and photonics, to drug delivery and robotics (Figure 132, bottom panel).

Overall, based on this precise classification (Figure 132), one can propose a more general, simple, and common vision of the various mechanical objects that are available and of the various mechanical pathways to connect them at all scales, going from simple to more complex systems (Figure 133). Here lies probably an interesting aspect of this review, which links numerous approaches – that have been pursued so far by relatively different communities – into a single domain of research, and which highlights the opportunities offered by harnessing molecular motion in order to produce new specific functions and applications. In addition, this general vision – even if simplistic – presents the advantage to show still missing parts of research that have remained fully untouched so far. For instance, one can obviously imagine combining other types of molecular actuators in collective motions, such as conformationally stretchable helical strands, reconfigurational DNA building blocks, or tautomeric species. One can also suggest the synthesis of complex systems integrating various types of modules (gears, switches and motors) functioning on their own mechanics but talking to one another. One can also see that most of the

integrated systems which include molecular motors so far are based on light-driven processes. As discussed in the introduction light has many advantages, but it could be of great interest now to extend similar integration principles with molecular motors fueled with a chemical source of energy. Although their individual functioning principle would be probably based on information ratchets, it does not preclude in principle that they can produce collective behaviors. This would be for instance particularly interesting to design biomaterials and smart implants or propellers to behave autonomously in the body by making use of ATP as a source of energy. One can also notice that often, the use of molecular motors has been underexploited, by implementing them in systems which *in fine* only act as switches. If recent examples have already introduced the basic elements to integrate molecular motors in global (macroscopic) motorized actuators, further temporal synchronization and/or spatial desymmetrization would be necessary to amplify the potential of these systems in order to produce large autonomous oscillations for instance.

In this direction, we believe that the implementation of top-down technologies involving engineering tools will be also of crucial importance in the future developments of such systems in order to confer them supplementary levels of hierarchical organizations (*e.g.* bundling, layering, and 3D printing). If these engineering approaches have been already well developed with simple photochromic switches, it is not yet sufficiently the case with more complex molecular machines and motors. In addition, the investigations pursued to date have been mainly oriented toward the amplification of molecular motion into other motions of larger amplitudes. But laws of physics permit that such actuations can be in turn transduced into other functions such as pumping molecules or catalyzing chemical reactions, as existing in living systems, and such functions would benefit to be integrated in large collective systems. Additionnally, programing aspects to control sequential tasks made of collective motion should be now explored. Combining all these aspects together, one can think of a multifunctional autonomous entity – that is a multitask macroscopic machine made of molecular machines, and possibly capable of making copies of itself (why not?) – as a considerable synthetic challenge. Finally, by considering more immediate and practical aspects, the performances of these systems should be much improved – in terms of speed,

workload, and robustness, but also in terms of production costs – because they will not become technically relevant without being performant enough and compliant with industrial requirements. Although it is a reality, and a true opportunity, that domains such as soft robotics are currently looking forward to these new technologies, the gap is still wide from practical applications.

To conclude, we believe that the entire field of research defined in this review represents a particularly interesting domain to express the creativity of researchers and engineers for many years to come. It is also a domain that should be included in our teachings in order to train the next generation of scientists in an interdisciplinary approach based on a number of fundamental concepts that will certainly give birth to practical realizations of major technological relevance.

AUTHOR INFORMATION

Corresponding Author

*giuseppone@unistra.fr

Author Contributions

The manuscript was written through contributions of all authors. All authors have given approval to the final version of the manuscript.

Funding Sources

Notes

ACKNOWLEDGMENTS

The authors thank the European Commission's Horizon 2020 Programme as part of the MSCA-ITN project ArtMoMa under grant no. 860434, the FET-Open project MAGNIFY under grant no. 801378, the

LabEx CSC, the CNRS, and the University of Strasbourg. J.H. thanks the FNR Luxembourg for an AFR individual PhD grant, and X.Y. thanks the USIAS-FRIAS for a post-doctoral fellowship.

REFERENCES

(1) Schrödinger, E. *What Is Life? The Physical Aspect of the Living Cell*; Cambridge University Press, 1944.

(2) Luisi, P. L. *The Emergence of Life*; Cambridge University Press: Cambridge, 2006.

(3) Kinbara, K.; Aida, T. Toward Intelligent Molecular Machines: Directed Motions of Biological and Artificial Molecules and Assemblies. *Chem. Rev.* **2005**, *105*, 1377–1400.

(4) Feynman, R. P. There's Plenty of Room at the Bottom. *Caltech Eng. Sci.* **1960**, *23*, 22–36.

(5) Feynman, R. P. *Richard Feynman Lecture on Nanotechnology: Tiny Machines*; https://cosmolearning.org/courses/richard-feynman-lecture-on-nanotechnology-tiny-machines-473/, 1984.

(6) Feynman, R. P.; Leighton, R. B.; Sands, M. *The Feynman Lectures on Physics, Vol. I The New Millennium Edition: Mainly Mechanics, Radiation, and Heat*; Basic Books, Ed.; New York, 2011.

(7) Russew, M.-M.; Hecht, S. Photoswitches: From Molecules to Materials. *Adv. Mater.* **2010**, *22*, 3348–3360.

(8) Bruns, C. J.; Stoddart, J. F. *The Nature of the Mechanical Bond*; John Wiley & Sons, Inc.: Hoboken, NJ, USA, 2016.

(9) Sauvage, J.-P. From Chemical Topology to Molecular Machines (Nobel Lecture). *Angew. Chem. Int. Ed.* **2017**, *56*, 11080–11093.

(10) Stoddart, J. F. Mechanically Interlocked Molecules (MIMs)-Molecular Shuttles, Switches, and Machines (Nobel Lecture). *Angew. Chem. Int. Ed.* **2017**, *56*, 11094–11125.

(11) Feringa, B. L. The Art of Building Small: From Molecular Switches to Motors (Nobel Lecture). *Angew. Chem. Int. Ed.* **2017**, *56*, 11060–11078.

(12) Einstein, A. Über Die von Der Molekularkinetischen Theorie Der Wärme Geforderte Bewegung von in Ruhenden Flüssigkeiten Suspendierten Teilchen. *Ann. Phys.* **1905**, *322*, 549–560.

(13) Purcell, E. M. Life at Low Reynolds Number. *Am. J. Phys.* **1977**, *45*, 3–11.

(14) Kay, E. R.; Leigh, D. A.; Zerbetto, F. Synthetic Molecular Motors and Mechanical Machines. *Angew. Chem. Int. Ed.* **2007**, *46*, 72–191.

(15) Maxwell, J. C. MOLECULAR THEORY OF THE CONSTITUTION OF BODIES. In *Theory of Heat*; Cambridge University Press: Cambridge, 2011; pp 281–312.

(16) Smoluchowski, M. S. XIII. On Opalescence of Gases in the Critical State. *London, Edinburgh, Dublin Philos. Mag. J. Sci.* **1912**, *23*, 165–173.

(17) Feynman, R. .; Vernon, F. . The Theory of a General Quantum System Interacting with a Linear Dissipative System. *Ann. Phys. (N. Y).* **1963**, *24*, 118–173.

(18) Jarzynski, C.; Mazonka, O. Feynman's Ratchet and Pawl: An Exactly Solvable Model. *Phys. Rev. E* **1999**, *59*, 6448–6459.

(19) Astumian, R. D. Thermodynamics and Kinetics of a Brownian Motor. *Science* **1997**, *276*, 917–922.

(20) Linke, H.; Downton, M. T.; Zuckermann, M. J. Performance Characteristics of Brownian Motors. *Chaos An Interdiscip. J. Nonlinear Sci.* **2005**, *15*, 026111.

(21) Reimann, P. Brownian Motors: Noisy Transport Far from Equilibrium. *Phys. Rep.* **2002**, *361*, 57–265.

(22) Astumian, R. D.; Derényi, I. Fluctuation Driven Transport and Models of Molecular Motors and

Pumps. *Eur. Biophys. J.* **1998**, *27*, 474–489.

(23) Maruyama, K.; Nori, F.; Vedral, V. Colloquium : The Physics of Maxwell's Demon and Information. *Rev. Mod. Phys.* **2009**, *81*, 1–23.

(24) Jülicher, F.; Ajdari, A.; Prost, J. Modeling Molecular Motors. *Rev. Mod. Phys.* **1997**, *69*, 1269–1282.

(25) Schliwa, M.; Woehlke, G. Molecular Motors. *Nature* **2003**, *422*, 759–765.

(26) Nakamoto, R. K.; Baylis Scanlon, J. A.; Al-Shawi, M. K. The Rotary Mechanism of the ATP Synthase. *Arch. Biochem. Biophys.* **2008**, *476*, 43–50.

(27) Steitz, T. A. A Structural Understanding of the Dynamic Ribosome Machine. *Nat. Rev. Mol. Cell Biol.* **2008**, *9*, 242–253.

(28) Hirokawa, N.; Noda, Y.; Tanaka, Y.; Niwa, S. Kinesin Superfamily Motor Proteins and Intracellular Transport. *Nat. Rev. Mol. Cell Biol.* **2009**, *10*, 682–696.

(29) Morth, J. P.; Pedersen, B. P.; Buch-Pedersen, M. J.; Andersen, J. P.; Vilsen, B.; Palmgren, M. G.; Nissen, P. A Structural Overview of the Plasma Membrane Na+,K+-ATPase and H+-ATPase Ion Pumps. *Nat. Rev. Mol. Cell Biol.* **2011**, *12*, 60–70.

(30) Brownhill, K.; Wood, L.; Allan, V. Molecular Motors and the Golgi Complex: Staying Put and Moving Through. *Semin. Cell Dev. Biol.* **2009**, *20*, 784–792.

(31) Minamino, T.; Imada, K. The Bacterial Flagellar Motor and Its Structural Diversity. *Trends Microbiol.* **2015**, *23*, 267–274.

(32) Cooke, R. The Sliding Filament Model. *J. Gen. Physiol.* **2004**, *123*, 643–656.

(33) Principle of Microscopic Reversibility. In *IUPAC Compendium of Chemical Terminology*; Compiled by A. D. McNaught and A. Wilkinson: Oxford (1997).

(34) Astumian, R. D. Optical vs. Chemical Driving for Molecular Machines. *Faraday Discuss.* **2016**, *195*, 583–597.

(35) Astumian, R. D. How Molecular Motors Work – Insights from the Molecular Machinist's Toolbox: The Nobel Prize in Chemistry 2016. *Chem. Sci.* **2017**, *8*, 840–845.

(36) Feringa, B. L. The Art of Building Small: From Molecular Switches to Molecular Motors. *J. Org. Chem.* **2007**, *72*, 6635–6652.

(37) Crano, J. C.; Guglielmetti, R. J. . *Organic Photochromic and Thermochromic Compounds*; Crano, J. C., Guglielmetti, R. J., Eds.; Springer US: Boston, MA, 2002.

(38) Dürr, H.; Bouas-Laurent, H. *Photochromism: Molecules and Systems*; Elsevier, 2003.

(39) Katsonis, N.; Lubomska, M.; Pollard, M. M.; Feringa, B. L.; Rudolf, P. Synthetic Light-Activated Molecular Switches and Motors on Surfaces. *Prog. Surf. Sci.* **2007**, *82*, 407–434.

(40) Harris, J. D.; Moran, M. J.; Aprahamian, I. New Molecular Switch Architectures. *Proc. Natl. Acad. Sci.* **2018**, *115*, 9414–9422.

(41) Hartley, G. S. The Cis-Form of Azobenzene. *Nature* **1937**, *140*, 281.

(42) Kumar, G. S.; Neckers, D. C. Photochemistry of Azobenzene-Containing Polymers. *Chem. Rev.* **1989**, *89*, 1915–1925.

(43) Griffiths, J. II. Photochemistry of Azobenzene and Its Derivatives. *Chem. Soc. Rev.* **1972**, *1*, 481–493.

(44) Lewis, G. E. Photocatalysed Cyclisation of Azobenzene. *Tetrahedron Lett.* **1960**, *1*, 12–13.

(45) Irick, G.; Pacifici, J. G. Photochemistry of Azo Compounds. I. Photoreduction of 4-Diethylamino-4′-Nitroazobenzene. *Tetrahedron Lett.* **1969**, *10*, 1303–1306.

(46) Bandara, H. M. D.; Burdette, S. C. Photoisomerization in Different Classes of Azobenzene. *Chem.*

Soc. Rev. **2012**, *41*, 1809–1825.

(47) Serra, F.; Terentjev, E. M. Effects of Solvent Viscosity and Polarity on the Isomerization of Azobenzene. *Macromolecules* **2008**, *41*, 981–986.

(48) Dokić, J.; Gothe, M.; Wirth, J.; Peters, M. V.; Schwarz, J.; Hecht, S.; Saalfrank, P. Quantum Chemical Investigation of Thermal Cis-to-Trans Isomerization of Azobenzene Derivatives: Substituent Effects, Solvent Effects, and Comparison to Experimental Data. *J. Phys. Chem. A* **2009**, *113*, 6763–6773.

(49) Bléger, D.; Schwarz, J.; Brouwer, A. M.; Hecht, S. O-Fluoroazobenzenes as Readily Synthesized Photoswitches Offering Nearly Quantitative Two-Way Isomerization with Visible Light. *J. Am. Chem. Soc.* **2012**, *134*, 20597–20600.

(50) Knie, C.; Utecht, M.; Zhao, F.; Kulla, H.; Kovalenko, S.; Brouwer, A. M.; Saalfrank, P.; Hecht, S.; Bléger, D. Ortho-Fluoroazobenzenes: Visible Light Switches with Very Long-Lived Z Isomers. *Chem. Eur. J.* **2014**, *20*, 16492–16501.

(51) Ahmed, Z.; Siiskonen, A.; Virkki, M.; Priimagi, A. Controlling Azobenzene Photoswitching through Combined Ortho-Fluorination and -Amination. *Chem. Commun.* **2017**, *53*, 12520–12523.

(52) Merino, E. Synthesis of Azobenzenes: The Coloured Pieces of Molecular Materials. *Chem. Soc. Rev.* **2011**, *40*, 3835–3853.

(53) Hamon, F.; Djedaini-Pilard, F.; Barbot, F.; Len, C. Azobenzenes-Synthesis and Carbohydrate Applications. *Tetrahedron* **2009**, *65*, 10105–10123.

(54) Fliegl, H.; Köhn, A.; Hättig, C.; Ahlrichs, R. Ab Initio Calculation of the Vibrational and Electronic Spectra of Trans- and Cis-Azobenzene. *J. Am. Chem. Soc.* **2003**, *125*, 9821–9827.

(55) Ichimura, K. Photoalignment of Liquid-Crystal Systems. *Chem. Rev.* **2000**, *100*, 1847–1874.

(56) Natansohn, A.; Rochon, P. Photoinduced Motions in Azobenzene-Based Polymers. In *Photoreactive Organic Thin Films*; Elsevier, 2002; Vol. 102, pp 399–427.

(57) Matharu, A. S.; Jeeva, S.; Ramanujam, P. S. Liquid Crystals for Holographic Optical Data Storage. *Chem. Soc. Rev.* **2007**, *36*, 1868–1880.

(58) Ikeda, T.; Tsutsumi, O. Optical Switching and Image Storage by Means of Azobenzene Liquid-Crystal Films. *Science* **1995**, *268*, 1873–1875.

(59) Wang, D.; Wang, X. Amphiphilic Azo Polymers: Molecular Engineering, Self-Assembly and Photoresponsive Properties. *Prog. Polym. Sci.* **2013**, *38*, 271–301.

(60) Wei, Y. bo; Tang, Q.; Gong, C. Bin; Lam, M. H. W. Review of the Recent Progress in Photoresponsive Molecularly Imprinted Polymers Containing Azobenzene Chromophores. *Anal. Chim. Acta* **2015**, *900*, 10–20.

(61) Zhao, Y.; Ikeda, T. *SMART LIGHT-RESPONSIVE MATERIALS: Azobenzene-Containing Polymers and Liquid Crystals*; Wiley, 2009.

(62) Kanj, A. B.; Müller, K.; Heinke, L. Stimuli-Responsive Metal-Organic Frameworks with Photoswitchable Azobenzene Side Groups. *Macromol. Rapid Commun.* **2018**, *39*, 1–14.

(63) Gmelin, L. *Hand-Book of Chemistry: Organic Chemistry, Vol. 6. Organic Compounds Containing Fourteen Atoms of Carbon*; 1858; Vol. 12.

(64) Lewis, G. N. The Absorption and Re-Emission of Light by Cis- and Trans-Stilbenes and the Efficiency of Their Photochemical Isomerization. *J. Am. Chem. Soc.* **1940**, *62*, 2973–2980.

(65) Likhtenshtein, G. *Stilbenes*; Wiley-VCH Verlag GmbH & Co. KGaA: Weinheim, Germany, 2009.

(66) Bejarano, F.; Alcon, I.; Crivillers, N.; Mas-Torrent, M.; Bromley, S. T.; Veciana, J.; Rovira, C. Study of the E-Z Stilbene Isomerisation in Perchlorotriphenyl-Methane (PTM) Derivatives. *RSC*

Adv. **2017**, *7*, 15278–15283.

(67) Muszkat, K. A.; Fischer, E. Structure, Spectra, Photochemistry, and Thermal Reactions of the 4a,4b-Dihydrophenanthrenes. *J. Chem. Soc. B Phys. Org.* **1967**, No. 662, 662.

(68) Laarhoven, W. H. Photochemical Cyclizations and Intramolecular Cycloadditions of Conjugated Arylolefins: Part 2: Photocyclizations without Dehydrogenation and Photocycloadditions. *Recl. des Trav. Chim. des Pays-Bas* **2010**, *102*, 241–254.

(69) Waldeck. D.H. Photoisomerization Dynamics of Stilbenes. *Chem. Rev.* **1991**, *91*, 415–436.

(70) Landge, S. M.; Aprahamian, I. A PH Activated Configurational Rotary Switch: Controlling the E/Z Isomerization in Hydrazones. *J. Am. Chem. Soc.* **2009**, *131*, 18269–18271.

(71) Su, X.; Aprahamian, I. Switching around Two Axles: Controlling the Configuration and Conformation of a Hydrazone-Based Switch. *Org. Lett.* **2011**, *13*, 30–33.

(72) Su, X.; Robbins, T. F.; Aprahamian, I. Switching through Coordination-Coupled Proton Transfer. *Angew. Chem. Int. Ed.* **2011**, *50*, 1841–1844.

(73) Ray, D.; Foy, J. T.; Hughes, R. P.; Aprahamian, I. A Switching Cascade of Hydrazone-Based Rotary Switches through Coordination-Coupled Proton Relays. *Nat. Chem.* **2012**, *4*, 757–762.

(74) Tatum, L. A.; Foy, J. T.; Aprahamian, I. Waste Management of Chemically Activated Switches: Using a Photoacid To Eliminate Accumulation of Side Products. *J. Am. Chem. Soc.* **2014**, *136*, 17438–17441.

(75) Aprahamian, I. Hydrazone Switches and Things in Between. *Chem. Commun.* **2017**, *53*, 6674–6684.

(76) Pramanik, S.; Aprahamian, I. Hydrazone Switch-Based Negative Feedback Loop. *J. Am. Chem. Soc.* **2016**, *138*, 15142–15145.

(77) Qian, H.; Pramanik, S.; Aprahamian, I. Photochromic Hydrazone Switches with Extremely Long Thermal Half-Lives. *J. Am. Chem. Soc.* **2017**, *139*, 9140–9143.

(78) Shao, B.; Baroncini, M.; Qian, H.; Bussotti, L.; Di Donato, M.; Credi, A.; Aprahamian, I. Solution and Solid-State Emission Toggling of a Photochromic Hydrazone. *J. Am. Chem. Soc.* **2018**, *140*, 12323–12327.

(79) Moran, M. J.; Magrini, M.; Walba, D. M.; Aprahamian, I. Driving a Liquid Crystal Phase Transition Using a Photochromic Hydrazone. *J. Am. Chem. Soc.* **2018**, *140*, 13623–13627.

(80) Nakamura, S.; Irie, M. Thermally Irreversible Photochromic Systems. A Theoretical Study. *J. Org. Chem.* **1988**, *53*, 6136–6138.

(81) Irie, M.; Mohri, M. Thermally Irreversible Photochromic Systems. Reverisble Photocyclization of Diarylethene Derivatives. *J. Org. Chem.* **1988**, *53*, 803–808.

(82) Matsuda, K.; Irie, M. Diarylethene as a Photoswitching Unit. *J. Photochem. Photobiol. C Photochem. Rev.* **2004**, *5*, 169–182.

(83) Nakayama, Y.; Hayashi, K.; Irie, M. Thermally Irreversible Photochromic Systems. Reversible Photocyclization of 1,2-Diselenenylethene and 1,2-Diindolylethene Derivatives. *J. Org. Chem.* **1990**, *55*, 2592–2596.

(84) Irie, M.; Uchida, K. Synthesis and Properties of Photochromic Diarylethenes with Heterocyclic Aryl Groups. *Bulletin of the Chemical Society of Japan*. 1998, pp 985–996.

(85) Irie, M.; Sakemura, K.; Okinaka, M.; Uchida, K. Photochromism of Dithienylethenes with Electron-Donating Substituents. *J. Org. Chem.* **1995**, *60*, 8305–8309.

(86) Pu, S.; Zheng, C.; Le, Z.; Liu, G.; Fan, C. Substituent Effects on the Properties of Photochromic Diarylethenes. *Tetrahedron* **2008**, *64*, 2576–2585.

(87) Irie, M.; Fukaminato, T.; Matsuda, K.; Kobatake, S. Photochromism of Diarylethene Molecules and Crystals: Memories, Switches, and Actuators. *Chem. Rev.* **2014**, *114*, 12174–12277.

(88) Nakamura, S.; Yokojima, S.; Uchida, K.; Tsujioka, T.; Goldberg, A.; Murakami, A.; Shinoda, K.; Mikami, M.; Kobayashi, T.; Kobatake, S.; et al. Theoretical Investigation on Photochromic Diarylethene: A Short Review. *J. Photochem. Photobiol. A Chem.* **2008**, *200*, 10–18.

(89) Tian, H.; Yang, S. Recent Progresses on Diarylethene Based Photochromic Switches. *Chem. Soc. Rev.* **2004**, *33*, 85–97.

(90) Tian, H.; Wang, S. Photochromic Bisthienylethene as Multi-Function Switches. *Chem. Commun.* **2007**, No. 8, 781–792.

(91) Irie, M. Diarylethenes for Memories and Switches. *Chem. Rev.* **2000**, *100*, 1685–1716.

(92) Tian, H.; Feng, Y. Next Step of Photochromic Switches? *J. Mater. Chem.* **2008**, *18*, 1617–1622.

(93) Pu, S. Z.; Sun, Q.; Fan, C. Bin; Wang, R. J.; Liu, G. Recent Advances in Diarylethene-Based Multi-Responsive Molecular Switches. *J. Mater. Chem. C* **2016**, *4*, 3075–3093.

(94) Natali, M.; Giordani, S. Molecular Switches as Photocontrollable "Smart" Receptors. *Chem. Soc. Rev.* **2012**, *41*, 4010–4029.

(95) Harvey, E. C.; Feringa, B. L.; Vos, J. G.; Browne, W. R.; Pryce, M. T. Transition Metal Functionalized Photo- and Redox-Switchable Diarylethene Based Molecular Switches. *Coord. Chem. Rev.* **2015**, *282–283*, 77–86.

(96) Zhang, J.; Tian, H. The Endeavor of Diarylethenes: New Structures, High Performance, and Bright Future. *Adv. Opt. Mater.* **2018**, *6*, 1701278.

(97) Yao, X.; Li, T.; Wang, J.; Ma, X.; Tian, H. Recent Progress in Photoswitchable Supramolecular Self-Assembling Systems. *Adv. Opt. Mater.* **2016**, *4*, 1322–1349.

(98) Stobbe, H. Ein Produkt Der Lichtwirkung Auf Diphenylfulgid Und Der Polymerisation Der Phenylpropiolsäure. *Berichte der Dtsch. Chem. Gesellschaft* **1907**, *40*, 3372–3382.

(99) Santiago, A.; Becker, R. S. Photochromic Fulgides. Spectroscopy and Mechanism of Photoreactions. *J. Am. Chem. Soc.* **1968**, *90*, 3654–3658.

(100) Yokoyama, Y. Fulgides for Memories and Switches. *Chem. Rev.* **2000**, *100*, 1717–1740.

(101) Yokoyama, Y.; Inoue, T.; Yokoyama, M.; Goto, T.; Iwai, T.; Kera, N.; Hitomi, I.; Kurita, Y. Effects of Steric Bulkiness of Substituents on Quantum Yields of Photochromic Reactions of Furylfulgides. *Bull. Chem. Soc. Jpn.* **1994**, *67*, 3297–3303.

(102) Yokoyama, Y.; Kurita, Y. Photochromism of Fulgides and Related Compounds. *Mol. Cryst. Liq. Cryst. Sci.* **1994**, *246*, 87–94.

(103) Kiji, J.; Okano, T.; Kitamura, H.; Yokoyama, Y.; Kubota, S.; Kurita, Y. Synthesis and Photochromic Properties of Fulgides with a T-Butyl Substituent on the Furyl- or Thienylmethylidene Moiety. *Bull. Chem. Soc. Jpn.* **1995**, *68*, 616–619.

(104) Yokoyama, Y.; Sagisaka, T.; Mizuno, Y.; Yokoyama, Y. Role of the Methoxy Substituents on the Photochromic Indolyfulgides. Absorption Maximum vs. Molar Absorption Coefficient of the Colored Form. *Chem. Lett.* **1996**, *25*, 587–588.

(105) Tomoda, A.; Kaneko, A.; Tsuboi, H.; Matsushima, R. Effect of 2 Electron-Donating Substituents on Photochromism of Aryl Fulgide, 2-(2,6-Dimethyl-3,5-Substituted Benzylidene)-3-Isopropylidenesuccinic Anhydride. *Bull. Chem. Soc. Jpn.* **1992**, *65*, 2352–2358.

(106) Tomoda, A.; Kaneko, A.; Tsuboi, H.; Matsushima, R. Photochromism of Heterocyclic Fulgides. IV. Relationship between Chemical Structure and Photochromic Performance. *Bull. Chem. Soc. Jpn.* **1993**, *66*, 330–333.

(107) Johnson, W. S.; Daub, G. H. The Stobbe Condensation. In *Organic Reactions*; 1951; pp 1–73.

(108) Dickinson, R.; Heilbron, I. M. CCXVIII.—Styrylpyrylium Salts. Part IX. Colour Phenomena Associated with Benzonaphtha- and Dinaphtha-Spiropyrans. *J. Chem. Soc.* **1927**, 1699–1705.

(109) Fischer, E.; Hirshberg, Y. Formation of Coloured Forms of Spirans by Low-Temperature Irradiation. *J. Chem. Soc.* **1952**, No. 4518, 4522–4524.

(110) Berkovic, G.; Krongauz, V.; Weiss, V. Spiropyrans and Spirooxazines for Memories and Switches. *Chem. Rev.* **2000**, *100*, 1741–1754.

(111) Paramonov, S. V.; Lokshin, V.; Fedorova, O. A. Spiropyran, Chromene or Spirooxazine Ligands: Insights into Mutual Relations between Complexing and Photochromic Properties. *J. Photochem. Photobiol. C Photochem. Rev.* **2011**, *12*, 209–236.

(112) Klajn, R. Spiropyran-Based Dynamic Materials. *Chem. Soc. Rev.* **2014**, *43*, 148–184.

(113) Minkin, V. I. Photo-, Thermo-, Solvato-, and Electrochromic Spiroheterocyclic Compounds. *Chem. Rev.* **2004**, *104*, 2751–2776.

(114) Davis, D. A.; Hamilton, A.; Yang, J.; Cremar, L. D.; Van Gough, D.; Potisek, S. L.; Ong, M. T.; Braun, P. V.; Martínez, T. J.; White, S. R.; et al. Force-Induced Activation of Covalent Bonds in Mechanoresponsive Polymeric Materials. *Nature* **2009**, *459*, 68–72.

(115) Sheng, Y.; Leszczynski, J.; Garcia, A. A.; Rosario, R.; Gust, D.; Springer, J. Comprehensive Theoretical Study of the Conversion Reactions of Spiropyrans: Substituent and Solvent Effects. *J. Phys. Chem. B* **2004**, *108*, 16233–16243.

(116) Wojtyk, J. T. C.; Wasey, A.; Kazmaier, P. M.; Hoz, S.; Buncel, E. Thermal Reversion Mechanism of N-Functionalized Merocyanines to Spiropyrans: A Solvatochromic, Solvatokinetic, and Semiempirical Study. *J. Phys. Chem. A* **2000**, *104*, 9046–9055.

(117) Winkler, J. D.; Bowen, C. M.; Michelet, V. Photodynamic Fluorescent Metal Ion Sensors with Parts per Billion Sensitivity. *J. Am. Chem. Soc.* **1998**, *120*, 3237–3242.

(118) Swansburg, S.; Buncel, E.; Lemieux, R. P. Thermal Racemization of Substituted Indolinobenzospiropyrans: Evidence of Competing Polar and Nonpolar Mechanisms. *J. Am. Chem. Soc.* **2000**, *122*, 6594–6600.

(119) Lukyanov, B. S.; Lukyanova, M. B. Spiropyrans: Synthesis, Properties, and Application. *Chem. Heterocycl. Compd.* **2005**, *41*, 281–311.

(120) Baillet, G.; Campredon, M.; Guglielmetti, R.; Giusti, G.; Aubert, C. Dealkylation of N-Substituted Indolinospironaphthoxazine Photochromic Compounds under UV Irradiation. *J. Photochem. Photobiol. A Chem.* **1994**, *83*, 147–151.

(121) Radu, A.; Scarmagnani, S.; Byrne, R.; Slater, C.; Tong Lau, K.; Diamond, D. Photonic Modulation of Surface Properties: A Novel Concept in Chemical Sensing. *J. Phys. D. Appl. Phys.* **2007**, *40*, 7238–7244.

(122) Shao, N.; Zhang, Y.; Cheung, S. M.; Yang, R. H.; Chan, W. H.; Mo, T.; Li, K. A.; Liu, F. Copper Ion-Selective Fluorescent Sensor Based on the Inner Filter Effect Using a Spiropyran Derivative. *Anal. Chem.* **2005**, *77*, 7294–7303.

(123) Menju, A.; Hayashi, K.; Irie, M. Photoresponsive Polymers. 3. Reversible Solution Viscosity Change of Poly(Methacrylic Acid) Having Spirobenzopyran Pendant Groups in Methanol. *Macromolecules* **1981**, *14*, 755–758.

(124) Neilson, B. M.; Bielawski, C. W. Illuminating Photoswitchable Catalysis. *ACS Catal.* **2013**, *3*, 1874–1885.

(125) Fox, R. E. Research Reports and Test Items Pertaining to Eye Protection of Air Crew Personnel, Final Rept. on Contract. AF 41(657)-215, AD 440,226, 1961.

(126) Hovey, R. J.; Chu, N. Y. C. Photochromic Compounds. U.S. Patent 4,215,010, 1980.

(127) Lokshin, V.; Samat, A.; Metelitsa, A. V. Spirooxazines: Synthesis, Structure, Spectral and

Photochromic Properties. *Russ. Chem. Rev.* **2002**, *71*, 893–916.

(128) Pottier, E.; Sergent, M.; Luu, R. P. T.; Guglielmetti, R. Synthese De Quelques Spiro[Indoline-Naphtoxazines] Et Spiro[Indoline-Pyridobenzoxazines] Photochromiques. Application De La Methodologie De La Recherche Experimentale. *Bull. des Sociétés Chim. Belges* **1992**, *101*, 719–739.

(129) Xiong, Y.; Vargas Jentzsch, A.; Osterrieth, J. W. M.; Sezgin, E.; Sazanovich, I. V.; Reglinski, K.; Galiani, S.; Parker, A. W.; Eggeling, C.; Anderson, H. L. Spironaphthoxazine Switchable Dyes for Biological Imaging. *Chem. Sci.* **2018**, *9*, 3029–3040.

(130) Vantomme, G.; Gelebart, A. H.; Broer, D. J.; Meijer, E. W. A Four-Blade Light-Driven Plastic Mill Based on Hydrazone Liquid-Crystal Networks. *Tetrahedron* **2017**, *73*, 4963–4967.

(131) Mart, R. J.; Allemann, R. K. Azobenzene Photocontrol of Peptides and Proteins. *Chem. Commun.* **2016**, *52*, 12262–12277.

(132) Hugel, T.; Holland, N. B.; Cattani, A.; Moroder, L.; Seitz, M.; Gaub, H. E. Single-Molecule Optomechanical Cycle. *Science* **2002**, *296*, 1103–1106.

(133) Gelebart, A. H.; Vantomme, G.; Meijer, E. W.; Broer, D. J. Mastering the Photothermal Effect in Liquid Crystal Networks: A General Approach for Self-Sustained Mechanical Oscillators. *Adv. Mater.* **2017**, *29*, 1606712.

(134) Baigl, D. Photo-Actuation of Liquids for Light-Driven Microfluidics: State of the Art and Perspectives. *Lab Chip* **2012**, *12*, 3637–3653.

(135) Guo, F.; Guo, Z. Inspired Smart Materials with External Stimuli Responsive Wettability: A Review. *RSC Adv.* **2016**, *6*, 36623–36641.

(136) Wagner, N.; Theato, P. Light-Induced Wettability Changes on Polymer Surfaces. *Polymer* **2014**, *55*, 3436–3453.

(137) Xin, B.; Hao, J. Reversibly Switchable Wettability. *Chem. Soc. Rev.* **2010**, *39*, 769–782.

(138) Anastasiadis, S. H.; Lygeraki, M. I.; Athanassiou, A.; Farsari, M.; Pisignano, D. Reversibly Photo-Responsive Polymer Surfaces for Controlled Wettability. *J. Adhes. Sci. Technol.* **2008**, *22*, 1853–1868.

(139) WANG, S.; SONG, Y.; JIANG, L. Photoresponsive Surfaces with Controllable Wettability. *J. Photochem. Photobiol. C Photochem. Rev.* **2007**, *8*, 18–29.

(140) Liu, Y.; Mu, L.; Liu, B.; Kong, J. Controlled Switchable Surface. *Chem. Eur. J.* **2005**, *11*, 2622–2631.

(141) Yang, D.; Piech, M.; Bell, N. S.; Gust, D.; Vail, S.; Garcia, A. A.; Schneider, J.; Park, C.-D.; Hayes, M. A.; Picraux, S. T. Photon Control of Liquid Motion on Reversibly Photoresponsive Surfaces. *Langmuir* **2007**, *23*, 10864–10872.

(142) Siewierski, L. M.; Brittain, W. J.; Petrash, S.; Foster, M. D. Photoresponsive Monolayers Containing In-Chain Azobenzene. *Langmuir* **1996**, *12*, 5838–5844.

(143) Jiang, W.; Wang, G.; He, Y.; Wang, X.; An, Y.; Song, Y.; Jiang, L. Photo-Switched Wettability on an Electrostatic Self-Assembly Azobenzene Monolayer. *Chem. Commun.* **2005**, No. 28, 3550.

(144) Samanta, S.; Locklin, J. Formation of Photochromic Spiropyran Polymer Brushes via Surface-Initiated, Ring-Opening Metathesis Polymerization: Reversible Photocontrol of Wetting Behavior and Solvent Dependent Morphology Changes. *Langmuir* **2008**, *24*, 9558–9565.

(145) Joseph, G.; Pichardo, J.; Chen, G. Reversible Photo-/Thermoresponsive Structured Polymer Surfaces Modified with a Spirobenzopyran-Containing Copolymer for Tunable Wettability. *Analyst* **2010**, *135*, 2303–2308.

(146) Uyama, A.; Yamazoe, S.; Shigematsu, S.; Morimoto, M.; Yokojima, S.; Mayama, H.; Kojima, Y.; Nakamura, S.; Uchida, K. Reversible Photocontrol of Surface Wettability between Hydrophilic and

Superhydrophobic Surfaces on an Asymmetric Diarylethene Solid Surface. *Langmuir* **2011**, *27*, 6395–6400.

(147) Athanassiou, A.; Lygeraki, M. I.; Pisignano, D.; Lakiotaki, K.; Varda, M.; Mele, E.; Fotakis, C.; Cingolani, R.; Anastasiadis, S. H. Photocontrolled Variations in the Wetting Capability of Photochromic Polymers Enhanced by Surface Nanostructuring. *Langmuir* **2006**, *22*, 2329–2333.

(148) Rosario, R.; Gust, D.; Garcia, A. A.; Hayes, M.; Taraci, J. L.; Clement, T.; Dailey, J. W.; Picraux, S. T. Lotus Effect Amplifies Light-Induced Contact Angle Switching. *J. Phys. Chem. B* **2004**, *108*, 12640–12642.

(149) Feng, C. L.; Zhang, Y. J.; Jin, J.; Song, Y. L.; Xie, L. Y.; Qu, G. R.; Jiang, L.; Zhu, D. Ben. Reversible Wettability of Photoresponsive Fluorine-Containing Azobenzene Polymer in Langmuir-Blodgett Films. *Langmuir* **2001**, *17*, 4593–4597.

(150) Subramanian, R. S. Motion of Drops on Gradient Surfaces. In *Soft Matter Gradient Surfaces*; John Wiley & Sons, Inc.: Hoboken, NJ, USA, 2012; pp 407–429.

(151) Ichimura, K.; Oh, S. K.; Nakagawa, M. Light-Driven Motion of Liquids on a Photoresponsive Surface. *Science* **2000**, *288*, 1624–1626.

(152) Oh, S.-K.; Nakagawa, M.; Ichimura, K. Photocontrol of Liquid Motion on an Azobenzene Monolayer. *J. Mater. Chem.* **2002**, *12*, 2262–2269.

(153) Rosario, R.; Gust, D.; Hayes, M.; Jahnke, F.; Springer, J.; Garcia, A. A. Photon-Modulated Wettability Changes on Spiropyran-Coated Surfaces. *Langmuir* **2002**, *18*, 8062–8069.

(154) Monobe, H.; Ohzono, T.; Akiyama, H.; Sumaru, K.; Shimizu, Y. Manipulation of Liquid Filaments on Photoresponsive Microwrinkles. *ACS Appl. Mater. Interfaces* **2012**, *4*, 2212–2217.

(155) Muto, M.; Ayako, Y.; Yamamoto, K.; Yamamoto, M.; Kondo, Y.; Motosuke, M. Photochemical Migration of Liquid Column in a Glass Tube. *Eur. Phys. J. Spec. Top.* **2017**, *226*, 1199–1205.

(156) Diguet, A.; Guillermic, R.-M.; Magome, N.; Saint-Jalmes, A.; Chen, Y.; Yoshikawa, K.; Baigl, D. Photomanipulation of a Droplet by the Chromocapillary Effect. *Angew. Chem. Int. Ed.* **2009**, *48*, 9281–9284.

(157) Okano, K.; Shinohara, M.; Yamashita, T. Light-Induced Deformation of Photoresponsive Liquid Crystals on a Water Surface. *Chem. Eur. J.* **2009**, *15*, 3657–3660.

(158) Masiero, S.; Lena, S.; Pieraccini, S.; Spada, G. P. The Direct Conversion of Light into Continuous Mechanical Energy by Photoreversible Self-Assembly: A Prototype of a Light-Powered Engine. *Angew. Chem. Int. Ed.* **2008**, *47*, 3184–3187.

(159) McHale, G.; Newton, M. I. Liquid Marbles: Topical Context within Soft Matter and Recent Progress. *Soft Matter* **2015**, *11*, 2530–2546.

(160) Kavokine, N.; Anyfantakis, M.; Morel, M.; Rudiuk, S.; Bickel, T.; Baigl, D. Light-Driven Transport of a Liquid Marble with and against Surface Flows. *Angew. Chem. Int. Ed.* **2016**, *55*, 11183–11187.

(161) Rapp, B. E. Marangoni Effect. In *Microfluidics: Modelling, Mechanics and Mathematics*; Elsevier, 2017; pp 442–443.

(162) Ma, S.; Kuwahara, Y.; Nagano, H.; Hatae, N.; Ogata, T.; Kim, S.; Kurihara, S. Photo-Controlled Manipulation of Micrometer-Scale Objects on Polyethyleneglycol Thin Films with Azobenzene Compounds. *Mol. Cryst. Liq. Cryst.* **2014**, *601*, 126–133.

(163) Yamamoto, T.; Yoshida, M. Photochemical Manipulation of Microparticles on Azobenzene-Doped Liquid-Crystal Films with Homogeneous or Homeotropic Alignment Structures. In *Proc. SPIE 8475, Liquid Crystals XVI*; Khoo, I. C., Ed.; 2012; p 847505.

(164) Yamamoto, T.; Yoshida, M. Photoinduced Directional Motions of Microparticles at Air–Liquid-Crystal Interfaces of Azobenzene-Doped Liquid-Crystal Films with Homeotropic or Homogeneous

Alignment Structures. *Appl. Phys. Express* **2012**, *5*, 101701.

(165) Kausar, A.; Nagano, H.; Ogata, T.; Nonaka, T.; Kurihara, S. Photocontrolled Translational Motion of a Microscale Solid Object on Azobenzene-Doped Liquid-Crystalline Films. *Angew. Chem. Int. Ed.* **2009**, *48*, 2144–2147.

(166) Kausar, A.; Nagano, H.; Kuwahara, Y.; Ogata, T.; Kurihara, S. Photocontrolled Manipulation of a Microscale Object: A Rotational or Translational Mechanism. *Chem. Eur. J.* **2011**, *17*, 508–515.

(167) Eelkema, R.; Pollard, M. M.; Vicario, J.; Katsonis, N.; Ramon, B. S.; Bastiaansen, C. W. M.; Broer, D. J.; Feringa, B. L. Molecular Machines: Nanomotor Rotates Microscale Objects. *Nature* **2006**, *440*, 163.

(168) Varanakkottu, S. N.; George, S. D.; Baier, T.; Hardt, S.; Ewald, M.; Biesalski, M. Particle Manipulation Based on Optically Controlled Free Surface Hydrodynamics. *Angew. Chem. Int. Ed.* **2013**, *52*, 7291–7295.

(169) Lv, C.; Varanakkottu, S. N.; Baier, T.; Hardt, S. Controlling the Trajectories of Nano/Micro Particles Using Light-Actuated Marangoni Flow. *Nano Lett.* **2018**, *18*, 6924–6930.

(170) Norikane, Y.; Tanaka, S.; Uchida, E. Azobenzene Crystals Swim on Water Surface Triggered by Light. *CrystEngComm* **2016**, *18*, 7225–7228.

(171) Suematsu, N. J.; Nakata, S. Evolution of Self-Propelled Objects: From the Viewpoint of Nonlinear Science. *Chem. Eur. J.* **2018**, *24*, 6308–6324.

(172) Xu, L.; Mou, F.; Gong, H.; Luo, M.; Guan, J. Light-Driven Micro/Nanomotors: From Fundamentals to Applications. *Chem. Soc. Rev.* **2017**, *46*, 6905–6926.

(173) Brown, P.; Eral, H. B. Smart and Stimuli-Responsive Colloids. In *Nanocolloids*; Elsevier, 2016; pp 389–426.

(174) Zhao, G.; Pumera, M. Macroscopic Self-Propelled Objects. *Chem. Asian J.* **2012**, *7*, 1994–2002.

(175) Wang, J.; Xiong, Z.; Zheng, J.; Zhan, X.; Tang, J. Light-Driven Micro/Nanomotor for Promising Biomedical Tools: Principle, Challenge, and Prospect. *Acc. Chem. Res.* **2018**, *51*, 1957–1965.

(176) Safdar, M.; Simmchen, J.; Jänis, J. Light-Driven Micro- and Nanomotors for Environmental Remediation. *Environ. Sci. Nano* **2017**, *4*, 1602–1616.

(177) Zhang, D.; Sun, Y.; Li, M.; Zhang, H.; Song, B.; Dong, B. A Phototactic Liquid Micromotor. *J. Mater. Chem. C* **2018**, *6*, 12234–12239.

(178) Florea, L.; Wagner, K.; Wagner, P.; Wallace, G. G.; Benito-Lopez, F.; Officer, D. L.; Diamond, D. Photo-Chemopropulsion - Light-Stimulated Movement of Microdroplets. *Adv. Mater.* **2014**, *26*, 7339–7345.

(179) Feldmann, D.; Maduar, S. R.; Santer, M.; Lomadze, N.; Vinogradova, O. I.; Santer, S. Manipulation of Small Particles at Solid Liquid Interface: Light Driven Diffusioosmosis. *Sci. Rep.* **2016**, *6*, 36443.

(180) Xiao, Y.; Zarghami, S.; Wagner, K.; Wagner, P.; Gordon, K. C.; Florea, L.; Diamond, D.; Officer, D. L. Moving Droplets in 3D Using Light. *Adv. Mater.* **2018**, 1801821.

(181) Kaneko, S.; Asakura, K.; Banno, T. Phototactic Behavior of Self-Propelled Micrometer-Sized Oil Droplets in a Surfactant Solution. *Chem. Commun.* **2017**, *53*, 2237–2240.

(182) Abid, J.-P.; Frigoli, M.; Pansu, R.; Szeftel, J.; Zyss, J.; Larpent, C.; Brasselet, S. Light-Driven Directed Motion of Azobenzene-Coated Polymer Nanoparticles in an Aqueous Medium. *Langmuir* **2011**, *27*, 7967–7971.

(183) Eremin, A.; Hirankittiwong, P.; Chattham, N.; Nádasi, H.; Stannarius, R.; Limtrakul, J.; Haba, O.; Yonetake, K.; Takezoe, H. Optically Driven Translational and Rotational Motions of Microrod Particles in a Nematic Liquid Crystal. *Proc. Natl. Acad. Sci.* **2015**, *112*, 1716–1720.

(184) Kuwahara, Y.; Oda, T.; Kim, S.; Ogata, T.; Kurihara, S. Photo-Responsive Traveling of Small-Particles Modified with Azobenzene Groups as Molecular Motors in a Liquid Crystal. *Mater. Lett.* **2016**, *181*, 257–260.

(185) Yamamoto, T.; Yamamoto, J.; Lev, B. I.; Yokoyama, H. Light-Induced Assembly of Tailored Droplet Arrays in Nematic Emulsions. *Appl. Phys. Lett.* **2002**, *81*, 2187–2189.

(186) Li, W.; Wu, X.; Qin, H.; Zhao, Z.; Liu, H. Light-Driven and Light-Guided Microswimmers. *Adv. Funct. Mater.* **2016**, *26*, 3164–3171.

(187) Yuan, Y.; Abuhaimed, G. N.; Liu, Q.; Smalyukh, I. I. Self-Assembled Nematic Colloidal Motors Powered by Light. *Nat. Commun.* **2018**, *9*, 5040.

(188) Seki, T. A Wide Array of Photoinduced Motions in Molecular and Macromolecular Assemblies at Interfaces. *Bull. Chem. Soc. Jpn.* **2018**, *91*, 1026–1057.

(189) Seki, T.; Sekizawa, H.; Ichimura, K. Morphological Changes in Monolayer of a Photosensitive Polymer Observed by Brewster Angle Microscopy. *Polymer* **1997**, *38*, 725–728.

(190) Seki, T.; Sekizawa, H.; Tanaka, K.; Matsuzawa, Y.; Ichimura, K. Photoresponsive Monolayers on Water and Solid Surfaces. *Supramol. Sci.* **1998**, *5*, 373–377.

(191) Seki, T.; Sekizawa, H.; Morino, S.-Y.; Ichimura, K. Inherent and Cooperative Photomechanical Motions in Monolayers of an Azobenzene Containing Polymer at the Air−Water Interface. *J. Phys. Chem. B* **1998**, *102*, 5313–5321.

(192) Grogan, C.; Florea, L.; Koprivica, S.; Scarmagnani, S.; O'Neill, L.; Lyng, F.; Pedreschi, F.; Benito-Lopez, F.; Raiteri, R. Microcantilever Arrays Functionalised with Spiropyran Photoactive Moieties as Systems to Measure Photo-Induced Surface Stress Changes. *Sensors Actuators B Chem.* **2016**, *237*, 479–486.

(193) Guo, S.; Matsukawa, K.; Miyata, T.; Okubo, T.; Kuroda, K.; Shimojima, A. Photoinduced Bending

of Self-Assembled Azobenzene–Siloxane Hybrid. *J. Am. Chem. Soc.* **2015**, *137*, 15434–15440.

(194) Ji, H.-F.; Feng, Y.; Xu, X.; Purushotham, V.; Thundat, T.; Brown, G. M. Photon-Driven Nanomechanical Cyclic Motion. *Chem. Commun.* **2004**, No. 22, 2532.

(195) Nabetani, Y.; Takamura, H.; Hayasaka, Y.; Sasamoto, S.; Tanamura, Y.; Shimada, T.; Masui, D.; Takagi, S.; Tachibana, H.; Tong, Z.; et al. An Artificial Muscle Model Unit Based on Inorganic Nanosheet Sliding by Photochemical Reaction. *Nanoscale* **2013**, *5*, 3182–3193.

(196) Nabetani, Y.; Takamura, H.; Hayasaka, Y.; Shimada, T.; Takagi, S.; Tachibana, H.; Masui, D.; Tong, Z.; Inoue, H. A Photoactivated Artificial Muscle Model Unit: Reversible, Photoinduced Sliding of Nanosheets. *J. Am. Chem. Soc.* **2011**, *133*, 17130–17133.

(197) Kauscher, U.; Holme, M. N.; Björnmalm, M.; Stevens, M. M. Physical Stimuli-Responsive Vesicles in Drug Delivery: Beyond Liposomes and Polymersomes. *Adv. Drug Deliv. Rev.* **2018**.

(198) Fredy, J. W.; Méndez-Ardoy, A.; Kwangmettatam, S.; Bochicchio, D.; Matt, B.; Stuart, M. C. A.; Huskens, J.; Katsonis, N.; Pavan, G. M.; Kudernac, T. Molecular Photoswitches Mediating the Strain-Driven Disassembly of Supramolecular Tubules. *Proc. Natl. Acad. Sci.* **2017**, *114*, 11850–11855.

(199) Kwangmettatam, S.; Kudernac, T. Light-Fuelled Reversible Expansion of Spiropyran-Based Vesicles in Water. *Chem. Commun.* **2018**, *54*, 5311–5314.

(200) Hamada, T.; Sato, Y. T.; Yoshikawa, K.; Nagasaki, T. Reversible Photoswitching in a Cell-Sized Vesicle. *Langmuir* **2005**, *21*, 7626–7628.

(201) Pernpeintner, C.; Frank, J. A.; Urban, P.; Roeske, C. R.; Pritzl, S. D.; Trauner, D.; Lohmüller, T. Light-Controlled Membrane Mechanics and Shape Transitions of Photoswitchable Lipid Vesicles. *Langmuir* **2017**, *33*, 4083–4089.

(202) Georgiev, V. N.; Grafmüller, A.; Bléger, D.; Hecht, S.; Kunstmann, S.; Barbirz, S.; Lipowsky, R.;

Dimova, R. Area Increase and Budding in Giant Vesicles Triggered by Light: Behind the Scene. *Adv. Sci.* **2018**, *5*, 1800432.

(203) Shen, G.; Xue, G.; Cai, J.; Zou, G.; Li, Y.; Zhang, Q. Photo-Induced Reversible Uniform to Janus Shape Change of Vesicles Composed of PNIPAM-b-PAzPy2. *Soft Matter* **2013**, *9*, 2512–2517.

(204) Shen, G.; Xue, G.; Cai, J.; Zou, G.; Li, Y.; Zhong, M.; Zhang, Q. In Situ Observation of Azobenzene Isomerization along with Photo-Induced Swelling of Cross-Linked Vesicles by Laser-Trapping Raman Spectroscopy. *Soft Matter* **2012**, *8*, 9127–9131.

(205) Hu, J.; Yu, H.; Gan, L. H.; Hu, X. Photo-Driven Pulsating Vesicles from Self-Assembled Lipid-like Azopolymers. *Soft Matter* **2011**, *7*, 11345–11350.

(206) Han, K.; Su, W.; Zhong, M.; Yan, Q.; Luo, Y.; Zhang, Q.; Li, Y. Reversible Photocontrolled Swelling-Shrinking Behavior of Micron Vesicles Self-Assembled from Azopyridine-Containing Diblock Copolymer. *Macromol. Rapid Commun.* **2008**, *29*, 1866–1870.

(207) Lin, L.; Feng, Z.; Yu, Q.; Yan, Z.; Yen, C.-C.; Yu, Y. Self-Assembly and Photoresponsive Behavior of Amphiphilic Diblock Copolymers Containing Azobenzene Moieties. *Mol. Cryst. Liq. Cryst.* **2009**, *508*, 214/[576]-225/[587].

(208) Han, L.-H.; Tang, T.; Chen, S. Tuning the Absorptions of Au Nanospheres on a Microshell by Photo-Deformation. *Nanotechnology* **2006**, *17*, 4600–4605.

(209) Rochon, P.; Batalla, E.; Natansohn, A. Optically Induced Surface Gratings on Azoaromatic Polymer Films. *Appl. Phys. Lett.* **1995**, *66*, 136–138.

(210) Kim, D. Y.; Tripathy, S. K.; Li, L.; Kumar, J. Laser-induced Holographic Surface Relief Gratings on Nonlinear Optical Polymer Films. *Appl. Phys. Lett.* **1995**, *66*, 1166–1168.

(211) Kim, D. Y.; Li, L.; Jiang, X. L.; Shivshankar, V.; Kumar, J.; Tripathy, S. K. Polarized Laser Induced Holographic Surface Relief Gratings on Polymer Films. *Macromolecules* **1995**, *28*, 8835–

8839.

(212) Viswanathan, N. K.; Kim, D. Y.; Bian, S.; Williams, J.; Liu, W.; Li, L.; Samuelson, L.; Kumar, J.; Tripathy, S. K. Surface Relief Structures on Azo Polymer Films. *J. Mater. Chem.* **1999**, *9*, 1941–1955.

(213) Seki, T. Light-Directed Alignment, Surface Morphing and Related Processes: Recent Trends. *J. Mater. Chem. C* **2016**, *4*, 7895–7910.

(214) Hendrikx, M.; Schenning, A. P. H. J.; Debije, M. G.; Broer, D. J. Light-Triggered Formation of Surface Topographies in Azo Polymers. *Crystals* **2017**, *7*, 231.

(215) Hvilsted, S.; Sánchez, C.; Alcalá., R. The Volume Holographic Optical Storage Potential in Azobenzene Containing Polymers. *J. Mater. Chem.* **2009**, *19*, 6641–6648.

(216) Yadavalli, N. S.; Loebner, S.; Papke, T.; Sava, E.; Hurduc, N.; Santer, S. A Comparative Study of Photoinduced Deformation in Azobenzene Containing Polymer Films. *Soft Matter* **2016**, *12*, 2593–2603.

(217) Bennani, O. R.; Al-Hujran, T. A.; Nunzi, J.-M.; Sabat, R. G.; Lebel, O. Surface Relief Grating Growth in Thin Films of Mexylaminotriazine-Functionalized Glass-Forming Azobenzene Derivatives. *New J. Chem.* **2015**, *39*, 9162–9170.

(218) Moujdi, S.; Rahmouni, A.; Mahfoud, T.; Nesterenko, D. V.; Halim, M.; Sekkat, Z. Surface Relief Gratings in Azo-Polymers Revisited. *J. Appl. Phys.* **2018**, *124*, 213103.

(219) Hurduc, N.; Donose, B. C.; Macovei, A.; Paius, C.; Ibanescu, C.; Scutaru, D.; Hamel, M.; Branza-Nichita, N.; Rocha, L. Direct Observation of Athermal Photofluidisation in Azo-Polymer Films. *Soft Matter* **2014**, *10*, 4640–4647.

(220) Yadavalli, N. S.; Korolkov, D.; Moulin, J.-F.; Krutyeva, M.; Santer, S. Probing Opto-Mechanical Stresses within Azobenzene-Containing Photosensitive Polymer Films by a Thin Metal Film

Placed Above. *ACS Appl. Mater. Interfaces* **2014**, *6*, 11333–11340.

(221) Di Florio, G.; Bründermann, E.; Yadavalli, N. S.; Santer, S.; Havenith, M. Polarized 3D Raman and Nanoscale Near-Field Optical Microscopy of Optically Inscribed Surface Relief Gratings: Chromophore Orientation in Azo-Doped Polymer Films. *Soft Matter* **2014**, *10*, 1544–1554.

(222) Di Florio, G.; Bründermann, E.; Yadavalli, N. S.; Santer, S.; Havenith, M. Graphene Multilayer as Nanosized Optical Strain Gauge for Polymer Surface Relief Gratings. *Nano Lett.* **2014**, *14*, 5754–5760.

(223) Fang, G. J.; Maclennan, J. E.; Yi, Y.; Glaser, M. A.; Farrow, M.; Korblova, E.; Walba, D. M.; Furtak, T. E.; Clark, N. A. Athermal Photofluidization of Glasses. *Nat. Commun.* **2013**, *4*, 1521.

(224) Yadavalli, N. S.; Santer, S. In-Situ Atomic Force Microscopy Study of the Mechanism of Surface Relief Grating Formation in Photosensitive Polymer Films. *J. Appl. Phys.* **2013**, *113*, 224304.

(225) Ambrosio, A.; Maddalena, P.; Marrucci, L. Molecular Model for Light-Driven Spiral Mass Transport in Azopolymer Films. *Phys. Rev. Lett.* **2013**, *110*, 146102.

(226) Accary, J.-B.; Teboul, V. How Does the Isomerization Rate Affect the Photoisomerization-Induced Transport Properties of a Doped Molecular Glass-Former? *J. Chem. Phys.* **2013**, *139*, 034501.

(227) Ilnytskyi, J. M.; Neher, D.; Saphiannikova, M. Opposite Photo-Induced Deformations in Azobenzene-Containing Polymers with Different Molecular Architecture: Molecular Dynamics Study. *J. Chem. Phys.* **2011**, *135*, 044901.

(228) Teboul, V.; Saiddine, M.; Nunzi, J.-M.; Accary, J.-B. An Isomerization-Induced Cage-Breaking Process in a Molecular Glass Former below T G. *J. Chem. Phys.* **2011**, *134*, 114517.

(229) Hurduc, N.; Donose, B. C.; Rocha, L.; Ibanescu, C.; Scutaru, D. Azo-Polymers Photofluidisation – a Transient State of Matter Emulated by Molecular Motors. *RSC Adv.* **2016**, *6*, 27087–27093.

(230) Toshchevikov, V.; Saphiannikova, M.; Heinrich, G. Microscopic Theory of Light-Induced Deformation in Amorphous Side-Chain Azobenzene Polymers. *J. Phys. Chem. B* **2009**, *113*, 5032–5045.

(231) Veer, P. U.; Pietsch, U.; Mueller, A. D. Alteration of the Mechanical Properties of Azopolymer Film in the Process of Surface Relief Grating Formation. *Appl. Phys. Lett.* **2009**, *94*, 231911.

(232) Ilnytskyi, J. M.; Neher, D.; Saphiannikova, M.; Marro, J.; Garrido, P. L.; Hurtado, P. I. Molecular Dynamics Simulations of Photo-Induced Deformations in Azobenzene-Containing Polymers. In *AIP Conference Proceedings*; AIP, 2009; pp 253–255.

(233) Juan, M. L.; Plain, J.; Bachelot, R.; Royer, P.; Gray, S. K.; Wiederrecht, G. P. Multiscale Model for Photoinduced Molecular Motion in Azo Polymers. *ACS Nano* **2009**, *3*, 1573–1579.

(234) Juan, M. L.; Plain, J.; Bachelot, R.; Royer, P.; Gray, S. K.; Wiederrecht, G. P. Stochastic Model for Photoinduced Surface Relief Grating Formation through Molecular Transport in Polymer Films. *Appl. Phys. Lett.* **2008**, *93*, 153304.

(235) Inoue, N.; Nozue, M.; Yamane, O.; Umegaki, S. Driving Force for Formation of a Surface Relief Grating on an Azobenzene-Containing Polymer. *J. Appl. Phys.* **2008**, *104*, 023106.

(236) He, L. H. Surface Deformation of Nematic Elastomers under Striped Illumination. *Phys. Rev. E* **2007**, *75*, 041702.

(237) Pawlik, G.; Kordas, W.; Mitus, A. C.; Sahraoui, B.; Czaplicki, R.; Kajzar, F. Model Kinetics of Surface Relief Gratings Formation in Organic Thin Films: Experimental and Monte Carlo Studies. In *Proc. SPIE 4087, Applications of Photonic Technology 4*; Grote, J. G., Kajzar, F., Lindgren, M., Eds.; 2007; p 674007.

(238) Yager, K. G.; Tanchak, O. M.; Godbout, C.; Fritzsche, H.; Barrett, C. J. Photomechanical Effects in Azo-Polymers Studied by Neutron Reflectometry. *Macromolecules* **2006**, *39*, 9311–9319.

(239) Ilnytskyi; Saphiannikova; Neher. Photo-Induced Deformations in Azobenzene-Containing Side-Chain Polymers: Molecular Dynamics Study. *Condens. Matter Phys.* **2006**, *9*, 87.

(240) Böckmann, M.; Doltsinis, N. L. Towards Understanding Photomigration: Insights from Atomistic Simulations of Azopolymer Films Explicitly Including Light-Induced Isomerization Dynamics. *J. Chem. Phys.* **2016**, *145*, 154701.

(241) Saphiannikova, M.; Neher, D. Thermodynamic Theory of Light-Induced Material Transport in Amorphous Azobenzene Polymer Films. *J. Phys. Chem. B* **2005**, *109*, 19428–19436.

(242) STILLER, B.; GEUE, T.; MORAWETZ, K.; SAPHIANNIKOVA, M. Optical Patterning in Azobenzene Polymer Films. *J. Microsc.* **2005**, *219*, 109–114.

(243) Yager, K. G.; Barrett, C. J. Temperature Modeling of Laser-Irradiated Azo-Polymer Thin Films. *J. Chem. Phys.* **2004**, *120*, 1089–1096.

(244) Saphiannikova, M.; Geue, T. M.; Henneberg, O.; Morawetz, K.; Pietsch, U. Linear Viscoelastic Analysis of Formation and Relaxation of Azobenzene Polymer Gratings. *J. Chem. Phys.* **2004**, *120*, 4039–4045.

(245) Henneberg, O.; Geue, T.; Pietsch, U.; Saphiannikova, M.; Winter, B. Investigation of Azobenzene Side Group Orientation in Polymer Surface Relief Gratings by Means of Photoelectron Spectroscopy. *Appl. Phys. Lett.* **2004**, *84*, 1561–1563.

(246) Sharma, L.; Matsuoka, T.; Kimura, T.; Matsuda, H. Investigation into the Surface Relief Grating Mechanism via XPS in New Azobenzene Based Optical Material. *Polym. Adv. Technol.* **2002**, *13*, 481–486.

(247) Baldus, O.; Zilker, S. J. Surface Relief Gratings in Photoaddressable Polymers Generated by Cw Holography. *Appl. Phys. B* **2001**, *72*, 425–427.

(248) Fukuda, T.; Sumaru, K.; Kimura, T.; Matsuda, H. Photofabrication of Surface Relief Structure —

Mechanism and Application. *J. Photochem. Photobiol. A Chem.* **2001**, *145*, 35–39.

(249) Labarthet, F. L.; Buffeteau, T.; Sourisseau, C. Time Dependent Analysis of the Formation of a Half-Period Surface Relief Grating on Amorphous Azopolymer Films. *J. Appl. Phys.* **2001**, *90*, 3149–3158.

(250) Labarthet, F. L.; Bruneel, J. L.; Sourisseau, C.; Huber, M. R.; Börger, V.; Menzel, H. Microspectrometric Study of Azobenzene Chromophore Orientations in a Holographic Diffraction Grating Inscribed on a p(HEMA-Co-MMA) Functionalized Copolymer Film. *J. Raman Spectrosc.* **2001**, *32*, 665–675.

(251) Ciobotarescu, S.; Hurduc, N.; Teboul, V. How Does the Motion of the Surrounding Molecules Depend on the Shape of a Folding Molecular Motor? *Phys. Chem. Chem. Phys.* **2016**, *18*, 14654–14661.

(252) Fiorini, C.; Prudhomme, N.; de Veyrac, G.; Maurin, I.; Raimond, P.; Nunzi, J.-M. Molecular Migration Mechanism for Laser Induced Surface Relief Grating Formation. *Synth. Met.* **2000**, *115*, 121–125.

(253) Lagugne´ Labarthet, F.; Bruneel, J.-L.; Buffeteau, T.; Sourisseau, C.; Huber, M. R.; Zilker, S. J.; Bieringer, T. Photoinduced Orientations of Azobenzene Chromophores in Two Distinct Holographic Diffraction Gratings as Studied by Polarized Raman Confocal Microspectrometry. *Phys. Chem. Chem. Phys.* **2000**, *2*, 5154–5167.

(254) Helgert, M.; Fleck, B.; Wenke, L.; Hvilsted, S.; Ramanujam, P. S. An Improved Method for Separating the Kinetics of Anisotropic and Topographic Gratings in Side-Chain Azobenzene Polyesters. *Appl. Phys. B* **2000**, *70*, 803–807.

(255) Fukuda, T.; Sumaru, K.; Yamanaka, T.; Matsuda, H. Photo-Induced Formation of the Surface Relief Grating on Azobenzene Polymers: Analysis Based on the Fluid Mechanics. *Mol. Cryst. Liq. Cryst. Sci.* **2000**, *345*, 263–268.

(256) Fukuda, T.; Matsuda, H.; Sumaru, K.; Yamanaka, T. Fluid Mechanics Model and Analysis for the Photofabrication of Surface Relief Grating on Azo Polymers. *MRS Proc.* **1999**, *598*, BB3.23.

(257) Kumar, J.; Li, L.; Jiang, X. L.; Kim, D.-Y.; Lee, T. S.; Tripathy, S. Gradient Force: The Mechanism for Surface Relief Grating Formation in Azobenzene Functionalized Polymers. *Appl. Phys. Lett.* **1998**, *72*, 2096–2098.

(258) Pedersen, T. G.; Johansen, P. M.; Holme, N. C. R.; Ramanujam, P. S.; Hvilsted, S. Mean-Field Theory of Photoinduced Formation of Surface Reliefs in Side-Chain Azobenzene Polymers. *Phys. Rev. Lett.* **1998**, *80*, 89–92.

(259) Barrett, C. J.; Rochon, P. L.; Natansohn, A. L. Model of Laser-Driven Mass Transport in Thin Films of Dye-Functionalized Polymers. *J. Chem. Phys.* **1998**, *109*, 1505–1516.

(260) Lefin, P.; Fiorini, C.; Nunzi, J.-M. Anisotropy of the Photo-Induced Translation Diffusion of Azobenzene Dyes in Polymer Matrices. *Pure Appl. Opt. J. Eur. Opt. Soc. Part A* **1998**, *7*, 71–82.

(261) Lefin, P.; Fiorini, C.; Nunzi, J.-M. Anisotropy of the Photoinduced Translation Diffusion of Azo-Dyes. *Opt. Mater. (Amst).* **1998**, *9*, 323–328.

(262) Vapaavuori, J.; Laventure, A.; Bazuin, C. G.; Lebel, O.; Pellerin, C. Submolecular Plasticization Induced by Photons in Azobenzene Materials. *J. Am. Chem. Soc.* **2015**, *137*, 13510–13517.

(263) Naydenova, I.; Nikolova, L.; Todorov, T.; Holme, N. C. R.; Ramanujam, P. S.; Hvilsted, S. Diffraction from Polarization Holographic Gratings with Surface Relief in Side-Chain Azobenzene Polyesters. *J. Opt. Soc. Am. B* **1998**, *15*, 1257.

(264) Lagugné Labarthet, F.; Buffeteau, T.; Sourisseau, C. Analyses of the Diffraction Efficiencies, Birefringence, and Surface Relief Gratings on Azobenzene-Containing Polymer Films. *J. Phys. Chem. B* **1998**, *102*, 2654–2662.

(265) Holme, N. C. R.; Nikolova, L.; Ramanujam, P. S.; Hvilsted, S. An Analysis of the Anisotropic and

Topographic Gratings in a Side-Chain Liquid Crystalline Azobenzene Polyester. *Appl. Phys. Lett.* **1997**, *70*, 1518–1520.

(266) Barrett, C. J.; Natansohn, A. L.; Rochon, P. L. Mechanism of Optically Inscribed High-Efficiency Diffraction Gratings in Azo Polymer Films. *J. Phys. Chem.* **1996**, *100*, 8836–8842.

(267) Garrot, D.; Lassailly, Y.; Lahlil, K.; Boilot, J. P.; Peretti, J. Real-Time near-Field Imaging of Photoinduced Matter Motion in Thin Solid Films Containing Azobenzene Derivatives. *Appl. Phys. Lett.* **2009**, *94*, 033303.

(268) Leopold, A.; Wolff, J.; Baldus, O.; Huber, M. R.; Bieringer, T.; Zilker, S. J. Thermally Induced Surface Relief Gratings in Azobenzene Polymers. *J. Chem. Phys.* **2000**, *113*, 833–837.

(269) Geue, T.; Schultz, M.; Grenzer, J.; Pietsch, U.; Natansohn, A.; Rochon, P. X-Ray Investigations of the Molecular Mobility within Polymer Surface Gratings. *J. Appl. Phys.* **2000**, *87*, 7712–7719.

(270) Sumaru, K.; Yamanaka, T.; Fukuda, T.; Matsuda, H. Photoinduced Surface Relief Gratings on Azopolymer Films: Analysis by a Fluid Mechanics Model. *Appl. Phys. Lett.* **1999**, *75*, 1878–1880.

(271) Viswanathan, N. K.; Balasubramanian, S.; Li, L.; Kumar, J.; Tripathy, S. K. Surface-Initiated Mechanism for the Formation of Relief Gratings on Azo-Polymer Films. *J. Phys. Chem. B* **1998**, *102*, 6064–6070.

(272) Lee, J.-D.; Kim, M.-J.; Nakayama, T. A Single-Dipole Model of Surface Relief Grating Formation on Azobenzene Polymer Films. *Langmuir* **2008**, *24*, 4260–4264.

(273) Harrison, J. M.; Goldbaum, D.; Corkery, T. C.; Barrett, C. J.; Chromik, R. R. Nanoindentation Studies to Separate Thermal and Optical Effects in Photo-Softening of Azo Polymers. *J. Mater. Chem. C* **2015**, *3*, 995–1003.

(274) Bin, J.; Oates, W. S. A Unified Material Description for Light Induced Deformation in Azobenzene Polymers. *Sci. Rep.* **2015**, *5*, 14654.

(275) Saphiannikova, M.; Toshchevikov, V. Optical Deformations of Azobenzene Polymers: Orientation Approach vs. Photofluidization Concept. *J. Soc. Inf. Disp.* **2015**, *23*, 146–153.

(276) Teboul, V. Stimuli Thresholds for Isomerization-Induced Molecular Motions in Azobenzene-Containing Materials. *J. Phys. Chem. B* **2015**, *119*, 3854–3859.

(277) Yadavalli, N. S.; Linde, F.; Kopyshev, A.; Santer, S. Soft Matter Beats Hard Matter: Rupturing of Thin Metallic Films Induced by Mass Transport in Photosensitive Polymer Films. *ACS Appl. Mater. Interfaces* **2013**, *5*, 7743–7747.

(278) Kim, C. Bin; Wistrom, J. C.; Ha, H.; Zhou, S. X.; Katsumata, R.; Jones, A. R.; Janes, D. W.; Miller, K. M.; Ellison, C. J. Marangoni Instability Driven Surface Relief Grating in an Azobenzene-Containing Polymer Film. *Macromolecules* **2016**, *49*, 7069–7076.

(279) Sasaki, T.; Izawa, M.; Noda, K.; Nishioka, E.; Kawatsuki, N.; Ono, H. Temporal Formation of Optical Anisotropy and Surface Relief during Polarization Holographic Recording in Polymethylmethacrylate with Azobenzene Side Groups. *Appl. Phys. B* **2014**, *114*, 373–380.

(280) Matsui, T.; Yamamoto, S.; Ozaki, M.; Yoshino, K.; Kajzar, F. Relaxation Kinetics of Photoinduced Surface Relief Grating on Azopolymer Films. *J. Appl. Phys.* **2002**, *92*, 6959–6965.

(281) Fabbri, F.; Lassailly, Y.; Monaco, S.; Lahlil, K.; Boilot, J. P.; Peretti, J. Kinetics of Photoinduced Matter Transport Driven by Intensity and Polarization in Thin Films Containing Azobenzene. *Phys. Rev. B* **2012**, *86*, 115440.

(282) Fabbri, F.; Garrot, D.; Lahlil, K.; Boilot, J. P.; Lassailly, Y.; Peretti, J. Evidence of Two Distinct Mechanisms Driving Photoinduced Matter Motion in Thin Films Containing Azobenzene Derivatives. *J. Phys. Chem. B* **2011**, *115*, 1363–1367.

(283) Kang, H. S.; Lee, S.; Park, J.-K. Monolithic, Hierarchical Surface Reliefs by Holographic Photofluidization of Azopolymer Arrays: Direct Visualization of Polymeric Flows. *Adv. Funct.*

Mater. **2011**, *21*, 4412–4422.

(284) Miniewicz, A.; Sznitko, L.; Szlapa, E. N.; Karpinski, P.; Mitus, A. C.; Pawlik, G.; Schab-Balcerzak, E. Laser Inscription of Surface Structures and Induction of Optical Anisotropy in Azo-Benzene Substituted Photochromic Polymers and Other Systems. In *Proc. SPIE 8983, Organic Photonic Materials and Devices XVI*; Tabor, C. E., Kajzar, F., Kaino, T., Koike, Y., Eds.; 2014; p 89830L.

(285) Sobolewska, A.; Zawada, J.; Bartkiewicz, S. Biphotonic Photochromic Reaction Results in an Increase in the Efficiency of the Holographic Recording Process in an Azo Polymer. *Langmuir* **2014**, *30*, 17–21.

(286) Sánchez, C.; Cases, R.; Alcalá, R.; López, A.; Quintanilla, M.; Oriol, L.; Millaruelo, M. Biphotonic Holographic Recording in a Liquid Crystalline Cyanoazobenzene Side-Chain Polymethacrylate. Polarization, Intensity, and Relief Gratings. *J. Appl. Phys.* **2001**, *89*, 5299–5306.

(287) Jäger, C.; Bieringer, T.; Zilker, S. J. Bicolor Surface Reliefs in Azobenzene Side-Chain Polymers. *Appl. Opt.* **2001**, *40*, 1776.

(288) Sánchez, C.; Alcalá, R.; Hvilsted, S.; Ramanujam, P. S. Biphotonic Holographic Gratings in Azobenzene Polyesters: Surface Relief Phenomena and Polarization Effects. *Appl. Phys. Lett.* **2000**, *77*, 1440–1442.

(289) Wu, X.; Nguyen, T. T. N.; Ledoux-Rak, I.; Nguyen, C. T.; Lai, N. D. UV Beam-Assisted Efficient Formation of Surface Relief Grating on Azobenzene Polymers. *Appl. Phys. B* **2012**, *107*, 819–822.

(290) Yang, K.; Yang, S.; Wang, X.; Kumar, J. Enhancing the Inscription Rate of Surface Relief Gratings with an Incoherent Assisting Light Beam. *Appl. Phys. Lett.* **2004**, *84*, 4517–4519.

(291) Nakata, Y.; Yoshida, M.; Miyanaga, N. Parallel Fabrication of Spiral Surface Structures by Interference Pattern of Circularly Polarized Beams. *Sci. Rep.* **2018**, *8*, 13448.

(292) Wu, X.; Nguyen, T. T. N.; Sun, D. Y.; Ledoux-Rak, I.; Nguyen, C. T.; Lai, N. D. Incoherent

UV/VIS Lasers Assisted Surface Relief Grating Formation. *Adv. Mater. Res.* **2012**, *560–561*, 456–461.

(293) Barille, R.; Ahmadi-Kandjani, S.; Ortyl, E.; Kucharski, S.; Nunzi, J.-M. Cooperative Interaction in Azopolymers upon Irradiation. *New J. Chem.* **2009**, *33*, 1207–1210.

(294) Konieczkowska, J.; Schab-Balcerzak, E.; Libera, M.; Mihaila, I.; Sava, I. Surface Relief Gratings in Azopolyimides Induced by Pulsed Laser Irradiation. *Eur. Polym. J.* **2019**, *110*, 85–89.

(295) Sava, E.; Simionescu, B.; Hurduc, N.; Sava, I. Considerations on the Surface Relief Grating Formation Mechanism in Case of Azo-Polymers, Using Pulse Laser Irradiation Method. *Opt. Mater. (Amst).* **2016**, *53*, 174–180.

(296) Damian, V.; Resmerita, E.; Stoica, I.; Ibanescu, C.; Sacarescu, L.; Rocha, L.; Hurduc, N. Surface Relief Gratings Induced by Pulsed Laser Irradiation in Low Glass-Transition Temperature Azopolysiloxanes. *J. Appl. Polym. Sci.* **2014**, *131*, 41015.

(297) Stoica, I.; Epure, L.; Sava, I.; Damian, V.; Hurduc, N. An Atomic Force Microscopy Statistical Analysis of Laser-Induced Azo-Polyimide Periodic Tridimensional Nanogrooves. *Microsc. Res. Tech.* **2013**, *76*, 914–923.

(298) Li, L.; Yan, F.; Samuelson, L. A.; Kumar, J. Simple Two-Photon Inscription of Surface Relief Gratings with Azobenzene Functionalized Polymer. *J. Macromol. Sci. Part A* **2011**, *48*, 1027–1030.

(299) Veer, P. U.; Pietsch, U.; Rochon, P. L.; Saphiannikova, M. Temperature Dependent Analysis of Grating Formation on Azobenzene Polymer Films. *Mol. Cryst. Liq. Cryst.* **2008**, *486*, 66/[1108]-78/[1120].

(300) Baldus, O.; Leopold, A.; Hagen, R.; Bieringer, T.; Zilker, S. J. Surface Relief Gratings Generated by Pulsed Holography: A Simple Way to Polymer Nanostructures without Isomerizing Side-Chains. *J. Chem. Phys.* **2001**, *114*, 1344–1349.

(301) Lee, G. J.; Oh, C. H.; Lee, Y.; Kang, I. A.; Han, Y. K. Surface Relief Grating Formation in Liquid-Crystalline Side-Chain Azopolymers by Femtosecond Pulse Holography. *J. Appl. Phys.* **2005**, *97*, 093101.

(302) Ubukata, T.; Higuchi, T.; Zettsu, N.; Seki, T.; Hara, M. Spontaneous Motion Observed in Highly Sensitive Surface Relief Formation System. *Colloids Surfaces A Physicochem. Eng. Asp.* **2005**, *257–258*, 123–126.

(303) Minabe, J.; Yasuda, S.; Kawano, K.; Maruyama, T.; Yamada, H. Photofabrication of Kinoforms as Multilevel Relief Structures on Azobenzene-Containing Polymer Films. *Jpn. J. Appl. Phys.* **2003**, *42*, L426–L428.

(304) Yasuda, S.; Minabe, J.; Kawano, K.; Maruyama, T.; Yamada, H. Single-Step Photo Fabrication of Kinoforms in Use of Azobenzene-Containing Polymer Films. *MRS Proc.* **2002**, *734*, B9.50.

(305) Holme, N. C. R.; Nikolova, L.; Hvilsted, S.; Rasmussen, P. H.; Berg, R. H.; Ramanujam, P. S. Optically Induced Surface Relief Phenomena in Azobenzene Polymers. *Appl. Phys. Lett.* **1999**, *74*, 519–521.

(306) Wen-Xuan, W.; Yan-Hua, L.; Xu-Sheng, C.; Xiu-Jie, T.; Wei-Wei, Q.; Xi-Feng, R.; Bing, Z.; Qi-Jin, Z. Effect of Zeroth-Order Beam on Azobenzene Polymer Surface Relief Gratings Fabricated by Phase-Mask Method. *Chinese Phys. Lett.* **2010**, *27*, 094202.

(307) Sobolewska, A.; Miniewicz, A. On the Inscription of Period and Half-Period Surface Relief Gratings in Azobenzene-Functionalized Polymers. *J. Phys. Chem. B* **2008**, *112*, 4526–4535.

(308) Sasaki, T.; Nishioka, E.; Noda, K.; Kondo, M.; Kawatsuki, N.; Ono, H. Analysis of Nonsinusoidal Surface Relief Structures Formed by Elliptical Polarization Holography on Azobenzene-Containing Polymeric Films. *Jpn. J. Appl. Phys.* **2014**, *53*, 02BB06.

(309) Nishioka, E.; Kawasaki, N.; Emoto, A.; Ono, H.; Kondo, M. Blazed Surface Relief Formation in

Azobenzene-Containing Polymeric Films by Asymmetric Polarization Holography. *J. Photopolym. Sci. Technol.* **2012**, *25*, 669–673.

(310) Kawatsuki, N.; Nishioka, E.; Emoto, A.; Ono, H.; Kondo, M. Blazed Surface Relief Formation in Azobenzene-Containing Polymeric Films by Asymmetric Polarization Holography. *Appl. Phys. Express* **2012**, *5*, 041601.

(311) Kim, M.-J.; Kumar, J.; Kim, D.-Y. Photofabrication of Superhelix-Like Patterns on Azobenzene Polymer Films. *Adv. Mater.* **2003**, *15*, 2005–2008.

(312) Bian, S.; Williams, J. M.; Kim, D. Y.; Li, L.; Balasubramanian, S.; Kumar, J.; Tripathy, S. Photoinduced Surface Deformations on Azobenzene Polymer Films. *J. Appl. Phys.* **1999**, *86*, 4498–4508.

(313) Wei, R.; Xu, Z.; Wang, X. Epoxy-Based Azo Polymer for Photofabricating Surface-Relief Quasi-Crystal Structures. *Opt. Mater. Express* **2015**, *5*, 1348–1355.

(314) Barille, R.; Nunzi, J.-M.; Ahmadi-Kandjani, S.; Ortyl, E.; Kucharski, S. One Step Inscription of Surface Relief Micrograting. *Opt. Commun.* **2007**, *280*, 217–220.

(315) Fabbri, F.; Lassailly, Y.; Lahlil, K.; Boilot, J. P.; Peretti, J. Alternating Photoinduced Mass Transport Triggered by Light Polarization in Azobenzene Containing Sol-Gel Films. *Appl. Phys. Lett.* **2010**, *96*, 081908.

(316) Gritsai, Y.; Goldenberg, L. M.; Kulikovska, O.; Stumpe, J. 3D Structures Using Surface Relief Gratings of Azobenzene Materials. *J. Opt. A Pure Appl. Opt.* **2008**, *10*, 125304.

(317) Kang, H. S.; Lee, S.; Lee, S.-A.; Park, J.-K. Multi-Level Micro/Nanotexturing by Three-Dimensionally Controlled Photofluidization and Its Use in Plasmonic Applications. *Adv. Mater.* **2013**, *25*, 5490–5497.

(318) Guo, M.; Xu, Z.; Wang, X. Photofabrication of Two-Dimensional Quasi-Crystal Patterns on UV-

Curable Molecular Azo Glass Films. *Langmuir* **2008**, *24*, 2740–2745.

(319) Vapaavuori, J.; Ras, R. H. A.; Kaivola, M.; Bazuin, C. G.; Priimagi, A. From Partial to Complete Optical Erasure of Azobenzene–Polymer Gratings: Effect of Molecular Weight. *J. Mater. Chem. C* **2015**, *3*, 11011–11016.

(320) Lagugné-Labarthet, F.; Buffeteau, T.; Sourisseau, C. Optical Erasures and Unusual Surface Reliefs of Holographic Gratings Inscribed on Thin Films of an Azobenzene Functionalized Polymer. *Phys. Chem. Chem. Phys.* **2002**, *4*, 4020–4029.

(321) Jiang, X. L.; Li, L.; Kumar, J.; Kim, D. Y.; Tripathy, S. K. Unusual Polarization Dependent Optical Erasure of Surface Relief Gratings on Azobenzene Polymer Films. *Appl. Phys. Lett.* **1998**, *72*, 2502–2504.

(322) Park, J. H.; Park, K. J.; Jiang, T.; Sun, Q.; Huh, J.-H.; Wang, Z. L.; Lee, S.; Cho, J. H. Light-Transformable and -Healable Triboelectric Nanogenerators. *Nano Energy* **2017**, *38*, 412–418.

(323) Sobolewska, A.; Bartkiewicz, S.; Priimagi, A. High-Modulation-Depth Surface Relief Gratings Using s – s Polarization Configuration in Supramolecular Polymer–Azobenzene Complexes. *J. Phys. Chem. C* **2014**, *118*, 23279–23284.

(324) Li, W.; Dohi, T.; Hara, M.; Nagano, S.; Haba, O.; Yonetake, K.; Seki, T. Phototriggered Mass Migration Consorted with Surface Dewetting in Thin Films of a Liquid Crystalline Azobenzene-Containing Dendrimer. *Macromolecules* **2012**, *45*, 6618–6627.

(325) Wu, S.; Huang, J. One-Step Fabrication of Hierarchically Ordered Structures on Photoresponsive Azobenzene-Containing Polymers with Phase Masks. *RSC Adv.* **2012**, *2*, 12084–12087.

(326) Lee, S.; Jeong, Y.-C.; Park, J.-K. Unusual Surface Reliefs from Photoinduced Creeping and Aggregation Behavior of Azopolymer. *Appl. Phys. Lett.* **2008**, *93*, 031912.

(327) Park, K. J.; Park, J. H.; Huh, J.-H.; Kim, C. H.; Ho, D. H.; Choi, G. H.; Yoo, P. J.; Cho, S. M.; Cho,

J. H.; Lee, S. Petal-Inspired Diffractive Grating on a Wavy Surface: Deterministic Fabrications and Applications to Colorizations and LED Devices. *ACS Appl. Mater. Interfaces* **2017**, *9*, 9935–9944.

(328) Papke, T.; Yadavalli, N. S.; Henkel, C.; Santer, S. Mapping a Plasmonic Hologram with Photosensitive Polymer Films: Standing versus Propagating Waves. *ACS Appl. Mater. Interfaces* **2014**, *6*, 14174–14180.

(329) König, T.; Goldenberg, L. M.; Kulikovska, O.; Kulikovsky, L.; Stumpe, J.; Santer, S. Reversible Structuring of Photosensitive Polymer Films by Surface Plasmon near Field Radiation. *Soft Matter* **2011**, *7*, 4174–4178.

(330) König, T.; Santer, S. Visualization of Surface Plasmon Interference by Imprinting Intensity Patterns on a Photosensitive Polymer. *Nanotechnology* **2012**, *23*, 485304.

(331) König, T.; Nataraja Sekhar, Y.; Santer, S. Surface Plasmon Nanolithography: Impact of Dynamically Varying near-Field Boundary Conditions at the Air–Polymer Interface. *J. Mater. Chem.* **2012**, *22*, 5945–5950.

(332) Derouard, M.; Hazart, J.; Lérondel, G.; Bachelot, R.; Adam, P.-M.; Royer, P. Polarization-Sensitive Printing of Surface Plasmon Interferences. *Opt. Express* **2007**, *15*, 4238–4246.

(333) Ohdaira, Y.; Noguchi, K.; Shinbo, K.; Kato, K.; Kaneko, F. Nano-Fabrication of Surface Relief Gratings on Azo Dye Films Utilizing Interference of Evanescent Waves on Prism. *Colloids Surfaces A Physicochem. Eng. Asp.* **2006**, *284–285*, 556–560.

(334) Ohdaira, Y.; Hoshiyama, S.; Kawakami, T.; Shinbo, K.; Kato, K.; Kaneko, F. Fabrication of Surface Relief Gratings on Azo Dye Thin Films Utilizing an Interference of Evanescent Waves. *Appl. Phys. Lett.* **2005**, *86*, 051102.

(335) Hendrikx, M.; ter Schiphorst, J.; van Heeswijk, E. P. A.; Koçer, G.; Knie, C.; Bléger, D.; Hecht, S.; Jonkheijm, P.; Broer, D. J.; Schenning, A. P. H. J. Re- and Preconfigurable Multistable Visible

Light Responsive Surface Topographies. *Small* **2018**, *14*, 1803274.

(336) Li, W.; Nagano, S.; Seki, T. Photo-Crosslinkable Liquid-Crystalline Azo-Polymer for Surface Relief Gratings and Persistent Fixation. *New J. Chem.* **2009**, *33*, 1343–1348.

(337) Wang, D.; He, Y.; Deng, W.; Wang, X. The Photoinduced Surface-Relief-Grating Formation Behavior of Side-Chain Azo Polymers with Narrow Mr Distribution. *Dye. Pigment.* **2009**, *82*, 286–292.

(338) Zielińska, S.; Ortyl, E.; Barille, R.; Kucharski, S. Preparation and Characteristics of New Chiral Photochromic Copolymers. *Opt. Mater. (Amst).* **2009**, *32*, 198–206.

(339) Yu*, H.; Naka, Y.; Shishido, A.; Iyoda, T.; Ikeda, T. Effect of Recording Time on Grating Formation and Enhancement in an Amphiphilic Diblock Liquid-Crystalline Copolymer. *Mol. Cryst. Liq. Cryst.* **2009**, *498*, 29–39.

(340) Emoto, A.; Fukuda, T.; Barada, D. Asymmetric Polarization Conversion in Polarization Holograms with Surface Relief. *Jpn. J. Appl. Phys.* **2008**, *47*, 3568–3571.

(341) Wang, G.; Zhu, X.; Wu, J.; Zhu, J.; Chen, X.; Cheng, Z. Synthesis and Photoinduced Surface-Relief Grating of Well-Defined Azo-Containing Polymethacrylates via Atom Transfer Radical Polymerization. *J. Appl. Polym. Sci.* **2007**, *106*, 1234–1242.

(342) Carvalho, L. L.; Borges, T. F. C.; Cardoso, M. R.; Mendonça, C. R.; Balogh, D. T. Molecular Weight Effect on the Photoinduced Birefringence and Surface Relief Gratings Formation of a Methacrylate Azopolymer. *Eur. Polym. J.* **2006**, *42*, 2589–2595.

(343) Yang, J.; Zhang, J.; Liu, J.; Wang, P.; Ma, H.; Ming, H.; Li, Z.; Zhang, Q. Holographic Grating Recording in Azobenzene Polymer Films. *Opt. Mater. (Amst).* **2004**, *27*, 527–532.

(344) Börger, V.; Kuliskovska, O.; G.-Hubmann, K.; Stumpe, J.; Huber, M.; Menzel, H. Novel Polymers to Study the Influence of the Azobenzene Content on the Photo-Induced Surface Relief Grating

Formation. *Macromol. Chem. Phys.* **2005**, *206*, 1488–1496.

(345) Börger, V.; Menzel, H.; Huber, M. R. Influence of the Molecular Weight of Azopolymers on the Photo-Induced Formation of Surface Relief Gratings. *Mol. Cryst. Liq. Cryst.* **2005**, *430*, 89–97.

(346) Golghasemi Sorkhabi, S.; Ahmadi-Kandjani, S.; Cousseau, F.; Loumaigne, M.; Zielinska, S.; Ortyl, E.; Barille, R. Surface Quasi Periodic and Random Structures Based on Nanomotor Lithography for Light Trapping. *J. Appl. Phys.* **2017**, *122*, 015303.

(347) Zettsu, N.; Seki, T. Highly Efficient Photogeneration of Surface Relief Structure and Its Immobilization in Cross-Linkable Liquid Crystalline Azobenzene Polymers. *Macromolecules* **2004**, *37*, 8692–8698.

(348) Labarthet, F. L.; Bruneel, J. L.; Buffeteau, T.; Sourisseau, C. Chromophore Orientations upon Irradiation in Gratings Inscribed on Azo-Dye Polymer Films: A Combined AFM and Confocal Raman Microscopic Study. *J. Phys. Chem. B* **2004**, *108*, 6949–6960.

(349) Lagugné-Labarthet, F.; Buffeteau, T.; Sourisseau, C. Inscription of Holographic Gratings Using Circularly Polarized Light: Influence of the Optical Set-up on the Birefringence and Surface Relief Grating Properties. *Appl. Phys. B Lasers Opt.* **2002**, *74*, 129–137.

(350) Martin, G.; Toussaere, E.; Soulier, L.; Zyss, J. Photo-Induced Non-Linear Susceptibility Patterns in Electro-Optic Polymers. *Synth. Met.* **2002**, *127*, 49–52.

(351) Choi, D. H.; Kim, J. H. Stability of the Surface Relief Grating on the Thin Film of the Polyurethane and the Polymethacrylate Containing an Aminonitroazobenzene Moiety. *Polym. Bull.* **2001**, *46*, 395–402.

(352) Nunzi, J.-M.; Fiorini, C.; Raimond, P.; Sertova, N.; Petkov, I. Optically Structured Plastic Electro-Optic Devices: About the Particular Photoinduced Migration Mechanism of Bis-Azodyes Doped into Polymers. In *Proceedings of 2001 3rd International Conference on Transparent Optical*

Networks (IEEE Cat. No.01EX488); IEEE; pp 135–138.

(353) Andruzzi, L.; Altomare, A.; Ciardelli, F.; Solaro, R.; Hvilsted, S.; Ramanujam, P. S. Holographic Gratings in Azobenzene Side-Chain Polymethacrylates. *Macromolecules* **1999**, *32*, 448–454.

(354) Mendonça, C. R.; Dhanabalan, A.; Balogh, D. T.; Misoguti, L.; dos Santos, D. S.; Pereira-da-Silva, M. A.; Giacometti, J. A.; Zilio, S. C.; Oliveira, O. N. Optically Induced Birefringence and Surface Relief Gratings in Composite Langmuir−Blodgett (LB) Films of Poly[4‘-[[2-(Methacryloyloxy)Ethyl]Ethylamino]-2-Chloro-4-Nitroazobenzene] (HPDR13) and Cadmium Stearate. *Macromolecules* **1999**, *32*, 1493–1499.

(355) Henneberg, O.; Geue, T.; Saphiannikova, M.; Pietsch, U.; Chi, L. F.; Rochon, P.; Natansohn, A. L. Atomic Force Microscopy Inspection of the Early State of Formation of Polymer Surface Relief Gratings. *Appl. Phys. Lett.* **2001**, *79*, 2357–2359.

(356) Cao, H. Z.; Zhang, W.; Zhu, J.; Chen, X. R.; Cheng, Z. P.; Wu, J. H.; Zhu, X. L. Azo Polymers with Electronical Push and Pull Structures Prepared via RAFT Polymerization and Its Photoinduced Birefringence Behavior. *Express Polym. Lett.* **2008**, *2*, 589–601.

(357) Choi, H. Microstructure of a Reflection Holographic Grating Inscribed in an Absorptive Azopolymer Film. *J. Korean Phys. Soc.* **2015**, *67*, 1630–1633.

(358) Zhang, Y.; Cheng, Z.; Chen, X.; Zhang, W.; Wu, J.; Zhu, J.; Zhu, X. Synthesis and Photoresponsive Behaviors of Well-Defined Azobenzene-Containing Polymers via RAFT Polymerization. *Macromolecules* **2007**, *40*, 4809–4817.

(359) Zettsu, N.; Ubukata, T.; Seki, T.; Ichimura, K. Soft Crosslinkable Azo Polymer for Rapid Surface Relief Formation and Persistent Fixation. *Adv. Mater.* **2001**, *13*, 1693–1697.

(360) Yu, H.; Naka, Y.; Shishido, A.; Ikeda, T. Well-Defined Liquid-Crystalline Diblock Copolymers with an Azobenzene Moiety: Synthesis, Photoinduced Alignment and Their Holographic

Properties. *Macromolecules* **2008**, *41*, 7959–7966.

(361) Wang, D.; Ye, G.; Zhu, Y.; Wang, X. Photoinduced Mass-Migration Behavior of Two Amphiphilic Side-Chain Azo Diblock Copolymers with Different Length Flexible Spacers. *Macromolecules* **2009**, *42*, 2651–2657.

(362) Huang, B.-Y.; Yu, K.-Y.; Huang, S.-Y.; Kuo, C.-T. The Investigation of the Two-Dimensional Surface Relief Grating on Dye-Doped Polymer Film. *Opt. Mater. Express* **2014**, *4*, 308–314.

(363) Kopyshev, A.; Galvin, C. J.; Genzer, J.; Lomadze, N.; Santer, S. Opto-Mechanical Scission of Polymer Chains in Photosensitive Diblock-Copolymer Brushes. *Langmuir* **2013**, *29*, 13967–13974.

(364) Zhu, Y.; Zhou, Y.; Wang, X. Photoresponsive Behavior of Two Well-Defined Azo Polymers with Different Electron-Withdrawing Groups on Push–Pull Azo Chromophores. *Dye. Pigment.* **2013**, *99*, 209–219.

(365) Kulikovska, O.; Gharagozloo-Hubmann, K.; Stumpe, J.; Huey, B. D.; Bliznyuk, V. N. Formation of Surface Relief Grating in Polymers with Pendant Azobenzene Chromophores as Studied by AFM/UFM. *Nanotechnology* **2012**, *23*, 485309.

(366) Nishioka, E.; Kondo, M.; Emoto, A.; Ono, H.; Kawatsuki, N. Surface Relief Formation in Azobenzene-Containing Polymers Using 325 Nm Holography. *Jpn. J. Appl. Phys.* **2012**, *51*, 021601.

(367) Isayama, J.; Nagano, S.; Seki, T. Phototriggered Mass Migrating Motions in Liquid Crystalline Azobenzene Polymer Films with Systematically Varied Thermal Properties. *Macromolecules* **2010**, *43*, 4105–4112.

(368) Schab-Balcerzak, E.; Sobolewska, A.; Stumpe, J.; Hamryszak, L.; Bujak, P. Surface Relief Gratings in Azobenzene Supramolecular Systems Based on Polyimides. *Opt. Mater. (Amst).* **2012**, *35*, 155–167.

(369) Sobolewska, A.; Bartkiewicz, S. Surface Relief Grating in Azo-Polymer Obtained for s-s Polarization Configuration of the Writing Beams. *Appl. Phys. Lett.* **2012**, *101*, 193301.

(370) Sava, I.; Hurduc, N.; Sacarescu, L.; Apostol, I.; Damian, V. Study of the Nanostructuration Capacity of Some Azopolymers with Rigid or Flexible Chains. *High Perform. Polym.* **2013**, *25*, 13–24.

(371) Schab-Balcerzak, E.; Siwy, M.; Kawalec, M.; Sobolewska, A.; Chamera, A.; Miniewicz, A. Synthesis, Characterization, and Study of Photoinduced Optical Anisotropy in Polyimides Containing Side Azobenzene Units. *J. Phys. Chem. A* **2009**, *113*, 8765–8780.

(372) Sava, I.; Sacarescu, L.; Stoica, I.; Apostol, I.; Damian, V.; Hurduc, N. Photochromic Properties of Polyimide and Polysiloxane Azopolymers. *Polym. Int.* **2009**, *58*, 163–170.

(373) Sava, I.; Resmerita, A.-M.; Lisa, G.; Damian, V.; Hurduc, N. Synthesis and Photochromic Behavior of New Polyimides Containing Azobenzene Side Groups. *Polymer* **2008**, *49*, 1475–1482.

(374) Schab-Balcerzak, E.; Sobolewska, A.; Miniewicz, A.; Jurusik, J. Chromophore Concentration Effect on Holographic Grating Formation Efficiency in Novel Azobenzene-Functionalized Polymers. *Polym. Eng. Sci.* **2008**, *48*, 1755–1767.

(375) Schab-Balcerzak, E.; Sobolewska, A.; Miniewicz, A.; Jurusik, J.; Jarzabek, B. Photoinduced Holographic Gratings in Azobenzene-Functionalized Poly(Amideimide)S. *Polym. J.* **2007**, *39*, 659–669.

(376) Sobolewska, A.; Miniewicz, A.; Kusto, J.; Moczko, K.; Sek, D.; Schab-Balcerzak, E.; Grabiec, E.; Kajzar, F. Optically Induced Gratings in Azo-Functionalized Polymers Studied by a Moving Grating Technique. In *Proc. SPIE 5724, Organic Photonic Materials and Devices VII*; Grote, J. G., Kaino, T., Kajzar, F., Eds.; 2005; p 21.

(377) Sek, D.; Grabiec, E.; Miniewicz, A.; Sobolewska, A. Influence of Poly(Amide-Imide)s Structures

on Holographic Grating Recording. In *Proc. SPIE 5724, Organic Photonic Materials and Devices VII*; Grote, J. G., Kaino, T., Kajzar, F., Eds.; 2005; p 311.

(378) Chen, J. P.; Lagugné-Labarthet, F.; Natansohn, A.; Rochon, P. Highly Stable Optically Induced Birefringence and Holographic Surface Gratings on a New Azocarbazole-Based Polyimide. *Macromolecules* **1999**, *32*, 8572–8579.

(379) Kozanecka-Szmigiel, A.; Antonowicz, J.; Szmigiel, D.; Makowski, M.; Siemion, A.; Konieczkowska, J.; Trzebicka, B.; Schab-Balcerzak, E. On Stress – Strain Responses and Photoinduced Properties of Some Azo Polymers. *Polymer* **2018**, *140*, 117–121.

(380) Sava, I.; Stoica, I.; Mihaila, I.; Pohoata, V.; Topala, I.; Stoian, G.; Lupu, N. Nanoscale Analysis of Laser-Induced Surface Relief Gratings on Azo-Copolyimide Films before and after Gold Coating. *Polym. Test.* **2018**, *72*, 407–415.

(381) Kozanecka-Szmigiel, A.; Konieczkowska, J.; Szmigiel, D.; Antonowicz, J.; Małecki, J.; Schab-Balcerzak, E. Blue-Light-Induced Processes in a Series of Azobenzene Poly(Ester Imide)S. *J. Photochem. Photobiol. A Chem.* **2017**, *347*, 177–185.

(382) Sava, I.; Burescu, A.; Stoica, I.; Musteata, V.; Cristea, M.; Mihaila, I.; Pohoata, V.; Topala, I. Properties of Some Azo-Copolyimide Thin Films Used in the Formation of Photoinduced Surface Relief Gratings. *RSC Adv.* **2015**, *5*, 10125–10133.

(383) Schab-Balcerzak, E.; Flakus, H.; Jarczyk-Jedryka, A.; Konieczkowska, J.; Siwy, M.; Bijak, K.; Sobolewska, A.; Stumpe, J. Photochromic Supramolecular Azopolyimides Based on Hydrogen Bonds. *Opt. Mater. (Amst).* **2015**, *47*, 501–511.

(384) Konieczkowska, J.; Wojtowicz, M.; Sobolewska, A.; Noga, J.; Jarczyk-Jedryka, A.; Kozanecka-Szmigiel, A.; Schab-Balcerzak, E. Thermal, Optical and Photoinduced Properties of a Series of Homo and Co-Polyimides with Two Kinds of Covalently Bonded Azo-Dyes and Their Supramolecular Counterparts. *Opt. Mater. (Amst).* **2015**, *48*, 139–149.

(385) Schab-Balcerzak, E.; Skorus, B.; Siwy, M.; Janeczek, H.; Sobolewska, A.; Konieczkowska, J.; Wiacek, M. Characterization of Poly(Amic Acid)s and Resulting Polyimides Bearing Azobenzene Moieties Including Investigations of Thermal Imidization Kinetics and Photoinduced Anisotropy. *Polym. Int.* **2015**, *64*, 76–87.

(386) Yadavalli, N. S.; König, T.; Santer, S. Selective Mass Transport of Azobenzene-Containing Photosensitive Films towards or Away from the Light Intensity. *J. Soc. Inf. Disp.* **2015**, *23*, 154–162.

(387) Frascella, F.; Angelini, A.; Ricciardi, S.; Pirri, F.; Descrovi, E. Surface-Relief Formation in Azo-Polyelectrolyte Layers with a Protective Polymer Coating. *Opt. Mater. Express* **2016**, *6*, 444–450.

(388) Berberova, N.; Daskalova, D.; Strijkova, V.; Kostadinova, D.; Nazarova, D.; Nedelchev, L.; Stoykova, E.; Marinova, V.; Chi, C. H.; Lin, S. H. Polarization Holographic Recording in Thin Films of Pure Azopolymer and Azopolymer Based Hybrid Materials. *Opt. Mater. (Amst).* **2017**, *64*, 212–216.

(389) Yadavalli, N. S.; Saphiannikova, M.; Santer, S. Photosensitive Response of Azobenzene Containing Films towards Pure Intensity or Polarization Interference Patterns. *Appl. Phys. Lett.* **2014**, *105*, 051601.

(390) Orofino, A. B.; Galante, M. J.; Oyanguren, P. A. Analyses of Surface Relief Gratings Inscription in Epoxy-Azo Linear and Crosslinked Polymers. *J. Polym. Sci. Part B Polym. Phys.* **2017**, *55*, 1542–1552.

(391) Zhou, Y.; Tang, B.; Wang, X. Photoinduced Deformation Behavior of a Series of Newly Synthesized Epoxy-Based Polymers Bearing Push–Pull Azo Chromophores. *Polymer* **2015**, *60*, 292–301.

(392) Viswanathan, N. K.; Balasubramanian, S.; Li, L.; Tripathy, S. K.; Kumar, J. A Detailed Investigation of the Polarization-Dependent Surface-Relief-Grating Formation Process on Azo

Polymer Films. *Jpn. J. Appl. Phys.* **1999**, *38*, 5928–5937.

(393) Orofino, A. B.; Arenas, G.; Zucchi, I.; Galante, M. J.; Oyanguren, P. A. A Simple Strategy to Generate Light-Responsive Azobenzene-Containing Epoxy Networks. *Polymer* **2013**, *54*, 6184–6190.

(394) Wang, X.; Yin, J.; Wang, X. Self-Structured Surface Patterns on Epoxy-Based Azo Polymer Films Induced by Laser Light Irradiation. *Macromolecules* **2011**, *44*, 6856–6867.

(395) Wang, X.; Yin, J.; Wang, X. Epoxy-Based Polymers Functionalized with Bisazo Chromophores: Synthesis, Characterization and Photoresponsive Behavior. *Polymer* **2011**, *52*, 3344–3356.

(396) Goldenberg, L. M.; Kulikovsky, L.; Gritsai, Y.; Kulikovska, O.; Tomczyk, J.; Stumpe, J. Very Efficient Surface Relief Holographic Materials Based on Azobenzene-Containing Epoxy Resins Cured in Films. *J. Mater. Chem.* **2010**, *20*, 9161–9171.

(397) Goldenberg, L. M.; Kulikovsky, L.; Kulikovska, O.; Stumpe, J. Extremely High Patterning Efficiency in Easily Made Azobenzene-Containing Polymer Films. *J. Mater. Chem.* **2009**, *19*, 6103–6105.

(398) He, Y.; Yin, J.; Che, P.; Wang, X. Epoxy-Based Polymers Containing Methyl-Substituted Azobenzene Chromophores and Photoinduced Surface Relief Gratings. *Eur. Polym. J.* **2006**, *42*, 292–301.

(399) Hwang, U.-J.; Kim, J.-S.; You, S.-Y.; Lee, H.-K.; Oh, C.-H.; Song, S.-H.; Kim, P.-S.; Han, Y.-K. Surface Relief Grating Formation on an Azo-Polymer. In *Proc. SPIE 5212, Linear and Nonlinear Optics of Organic Materials III*; Kuzyk, M. G., Eich, M., Norwood, R. A., Eds.; 2003; p 308.

(400) He, Y.; Wang, X.; Zhou, Q. Epoxy-Based Azo Polymers: Synthesis, Characterization and Photoinduced Surface-Relief-Gratings. *Polymer* **2002**, *43*, 7325–7333.

(401) Sukwattanasinitt, M.; Wang, X.; Li, L.; Jiang, X.; Kumar, J.; Tripathy, S. K.; Sandman, D. J.

Functionalizable Self-Assembling Polydiacetylenes and Their Optical Properties. *Chem. Mater.* **1998**, *10*, 27–29.

(402) Zhao, R.; Zhan, X.; Yao, J.; Sun, G.; Chen, Q.; Xie, Z.; Ma, Y. Reversible Photo-Controlled Mass Transfer in a Photo-Responsive Conjugated Main-Chain Polymer Film for High Contrast Surface Patterning. *Polym. Chem.* **2013**, *4*, 5382–5386.

(403) Huang, C.-W.; Ji, W.-Y.; Kuo, S.-W. Stimuli-Responsive Supramolecular Conjugated Polymer with Phototunable Surface Relief Grating. *Polym. Chem.* **2018**, *9*, 2813–2820.

(404) Zettsu, N.; Ubukata, T.; Seki, T. Two-Dimensional Manipulation of Poly(3-Dodecylthiophene) Using Light-Driven Instant Mass Migration as a Molecular Conveyer. *Jpn. J. Appl. Phys.* **2004**, *43*, L1169–L1171.

(405) Chun, C.; Seo, E.-M.; Kim, M. J.; Shin, Y.-D.; Lee, J.-S.; Kim, D. Y. Photoinduced Behaviors of Isocyanate-Based Azo Molecular Glass and Polymer. *Opt. Mater. (Amst).* **2007**, *29*, 970–974.

(406) Sáiz, L. M.; Ainchil, P.; Zucchi, I. A.; Oyanguren, P. A.; Galante, M. J. Surface Relief Gratings Inscription in Linear and Crosslinked Azo Modified Epoxy-Isocyanate Polymers. *J. Polym. Sci. Part B Polym. Phys.* **2015**, *53*, 587–594.

(407) Marański, K.; Kucharski, S.; Ortyl, E.; Nunzi, J.-M.; Ahmadi-Kandjani, S.; Dabos-Seignon, S.; Chan, S.-W.; Barille, R. Second Harmonic Generation and Photochromic Grating in Polyurethane Films Containing Diazo Isoxazole Chromophore. *Opt. Mater. (Amst).* **2008**, *30*, 1832–1839.

(408) Watanabe, O.; Narita, M.; Ikawa, T.; Tsuchimori, M. Photo-Induced Deformation Behavior Depending on the Glass Transition Temperature on the Surface of Urethane Copolymers Containing a Push–Pull Type Azobenzene Moiety. *Polymer* **2006**, *47*, 4742–4749.

(409) Wu, Y.; Natansohn, A.; Rochon, P. Photoinduced Birefringence and Surface Relief Gratings in Polyurethane Elastomers with Azobenzene Chromophore in the Hard Segment. *Macromolecules*

2004, *37*, 6090–6095.

(410) Itoh, M.; Harada, K.; Matsuda, H.; Ohnishi, S.; Parfenov, A.; Tamaoki, N.; Yatagai, T. Photomodification of Polymer Films: Azobenzene-Containing Polyurethanes. *J. Phys. D. Appl. Phys.* **1998**, *31*, 463–471.

(411) Lee, T. S.; Kim, D.-Y.; Jiang, X. L.; Li, L.; Kumar, J.; Tripathy, S. Photoinduced Surface Relief Gratings in High-Tg Main-Chain Azoaromatic Polymer Films. *J. Polym. Sci. Part A Polym. Chem.* **1998**, *36*, 283–289.

(412) Wu, Y.; Natansohn, A.; Rochon, P. Photoinduced Birefringence and Surface Relief Gratings in Novel Polyurethanes with Azobenzene Groups in the Main Chain. *Macromolecules* **2001**, *34*, 7822–7828.

(413) Che, Y.; Sugihara, O.; Egami, C.; Fujimura, H.; Kawata, Y.; Okamoto, N.; Tsuchimori, M.; Watanabe, O. Fabrication of Surface Relief Grating with Second-Order Nonlinearity Using Urethane-Urea Copolymer Films. *Jpn. J. Appl. Phys.* **1999**, *38*, 6316–6320.

(414) Zhang, J.; Zhang, H.; Zhang, Q.; Jiang, Z.; Chen, Q.; Zhang, Y. Novel Photoactive Poly(Aryl Ether)s Containing Bisazobenzene Pendants for Optical Storage. *High Perform. Polym.* **2016**, *28*, 518–524.

(415) Xu, D.; Zhang, Y.; Ren, D.; Chen, X.; Zhang, H.; Jiang, Z. Photoactive Poly(Aryl Ether)s Containing Azobenzene Moieties on Pendants for Fabrication of Thermal Stable Surface Relief Gratings. *Chem. Res. Chinese Univ.* **2013**, *29*, 384–388.

(416) Zhang, J.; Zhang, H.; Chen, X.; Pang, J.; Zhang, Y.; Wang, Y.; Chen, Q.; Pei, S.; Peng, W.; Jiang, Z. Synthesis and Photoresponsive Behaviors of Novel Poly(Arylene Ether)s with Di-Azobenzene Pendants. *React. Funct. Polym.* **2011**, *71*, 553–560.

(417) Jiang, X.; Chen, X.; Yue, X.; Zhang, J.; Guan, S.; Zhang, H.; Zhang, W.; Chen, Q. Synthesis and

Characterization of Photoactive Poly(Arylene Ether Sulfone)s Containing Azobenzene Moieties in Their Main Chains. *React. Funct. Polym.* **2010**, *70*, 616–621.

(418) Jiang, X.; Wang, H.; Chen, X.; Li, X.; Lei, L.; Mu, J.; Wang, G.; Zhang, S. A Novel Photoactive Hyperbranched Poly(Aryl Ether Ketone) with Azobenzene End Groups for Optical Storage Applications. *React. Funct. Polym.* **2010**, *70*, 699–705.

(419) Chen, X.; Zhang, Y.; Liu, B.; Zhang, J.; Wang, H.; Zhang, W.; Chen, Q.; Pei, S.; Jiang, Z. Novel Photoactive Hyperbranched Poly(Aryl Ether)s Containing Azobenzene Chromophores for Optical Storage. *J. Mater. Chem.* **2008**, *18*, 5019–5026.

(420) Chun, C.; Ghim, J.; Kim, M.-J.; Kim, D. Y. Photofabrication of Surface Relief Gratings from Azobenzene Containing Perfluorocyclobutane Aryl Ether Polymer. *J. Polym. Sci. Part A Polym. Chem.* **2005**, *43*, 3525–3532.

(421) Desbœufs, N.; Vu, A.-D.; Lahlil, K.; Lassailly, Y.; Martinelli, L.; Boilot, J.-P.; Peretti, J.; Gacoin, T. Optical Patterning of Sol-Gel Silica Coatings. *Adv. Opt. Mater.* **2016**, *4*, 313–320.

(422) Xue, X.; Zhu, J.; Zhang, Z.; Zhou, N.; Zhu, X. Synthesis and Photoresponsive Behavior of the High-Tg Azobenzene Polymers via RAFT Polymerization. *React. Funct. Polym.* **2010**, *70*, 456–462.

(423) Xu, Z.-S.; Drnoyan, V.; Natansohn, A.; Rochon, P. Novel Polyesters with Amino-Sulfone Azobenzene Chromophores in the Main Chain. *J. Polym. Sci. Part A Polym. Chem.* **2000**, *38*, 2245–2253.

(424) Wang, J.; Wu, B.; Li, S.; Sinawang, G.; Wang, X.; He, Y. Synthesis and Characterization of Photoprocessable Lignin-Based Azo Polymer. *ACS Sustain. Chem. Eng.* **2016**, *4*, 4036–4042.

(425) Bian, S.; Liu, W.; Williams, J.; Samuelson, L.; Kumar, J.; Tripathy, S. Photoinduced Surface Relief Grating on Amorphous Poly(4-Phenylazophenol) Films. *Chem. Mater.* **2000**, *12*, 1585–1590.

(426) Zhang, C.; Zhao, X.; Chao, D.; Lu, X.; Chen, C.; Wang, C.; Zhang, W. Rapid Bending of a Nonliquid Crystal Azobenzene Polymer Film and Characteristics of Surface Relief Grating. *J. Appl. Polym. Sci.* **2009**, *113*, 1330–1334.

(427) Gao, J.; He, Y.; Liu, F.; Zhang, X.; Wang, Z.; Wang, X. Azobenzene-Containing Supramolecular Side-Chain Polymer Films for Laser-Induced Surface Relief Gratings. *Chem. Mater.* **2007**, *19*, 3877–3881.

(428) Priimagi, A.; Cavallo, G.; Forni, A.; Gorynsztejn-Leben, M.; Kaivola, M.; Metrangolo, P.; Milani, R.; Shishido, A.; Pilati, T.; Resnati, G.; et al. Halogen Bonding versus Hydrogen Bonding in Driving Self-Assembly and Performance of Light-Responsive Supramolecular Polymers. *Adv. Funct. Mater.* **2012**, *22*, 2572–2579.

(429) Kulikovska, O.; Goldenberg, L. M.; Stumpe, J. Supramolecular Azobenzene-Based Materials for Optical Generation of Microstructures. *Chem. Mater.* **2007**, *19*, 3343–3348.

(430) Ahmed, R.; Priimagi, A.; Faul, C. F. J.; Manners, I. Redox-Active, Organometallic Surface-Relief Gratings from Azobenzene-Containing Polyferrocenylsilane Block Copolymers. *Adv. Mater.* **2012**, *24*, 926–931.

(431) Zhang, Y.; Zhang, J.; Cui, Z.; Chen, Q.; Zhang, H.; Jiang, Z. Fabrication of Fluorescent Holographic Micropatterns Based on the Rare Earth Complexes Using Azobenzene-Containing Poly(Aryl Ether)s as Macromolecular Ligands. *J. Polym. Sci. Part A Polym. Chem.* **2015**, *53*, 936–943.

(432) Nakano, H.; Tanino, T.; Takahashi, T.; Ando, H.; Shirota, Y. Relationship between Molecular Structure and Photoinduced Surface Relief Grating Formation Using Azobenzene-Based Photochromic Amorphous Molecular Materials. *J. Mater. Chem.* **2008**, *18*, 242–246.

(433) Nakano, H.; Tanino, T.; Shirota, Y. Surface Relief Grating Formation on a Single Crystal of 4-(Dimethylamino)Azobenzene. *Appl. Phys. Lett.* **2005**, *87*, 061910.

(434) Sahraoui, B.; Luc, J.; Meghea, A.; Czaplicki, R.; Fillaut, J.-L.; Migalska-Zalas, A. Nonlinear Optics and Surface Relief Gratings in Alkynyl–Ruthenium Complexes. *J. Opt. A Pure Appl. Opt.* **2009**, *11*, 024005.

(435) Luca, A. R.; Moleavin, I.-A.; Hurduc, N.; Hamel, M.; Rocha, L. Mass Transport in Low Tg Azo-Polymers: Effect on the Surface Relief Grating Induction and Stability of Additional Side Chain Groups Able to Generate Physical Interactions. *Appl. Surf. Sci.* **2014**, *290*, 172–179.

(436) Hurduc, N.; Macovei, A.; Paius, C.; Raicu, A.; Moleavin, I.; Branza-Nichita, N.; Hamel, M.; Rocha, L. Azo-Polysiloxanes as New Supports for Cell Cultures. *Mater. Sci. Eng. C* **2013**, *33*, 2440–2445.

(437) Kulikovska, O.; Goldenberg, L. M.; Kulikovsky, L.; Stumpe, J. Smart Ionic Sol−Gel-Based Azobenzene Materials for Optical Generation of Microstructures. *Chem. Mater.* **2008**, *20*, 3528–3534.

(438) Kang, D. J.; Kim, J.-K.; Bae, B.-S. Simple Fabrication of Diffraction Gratings by Two-Beam Interference Method in Highly Photosensitive Hybrid Sol-Gel Films. *Opt. Express* **2004**, *12*, 3947–3953.

(439) Darracq, B.; Chaput, F.; Lahlil, K.; Lévy, Y.; Boilot, J.-P. Photoinscription of Surface Relief Gratings on Azo-Hybrid Gels. *Adv. Mater.* **1998**, *10*, 1133–1136.

(440) Fukuda, T.; Matsuda, H.; Shiraga, T.; Kimura, T.; Kato, M.; Viswanathan, N. K.; Kumar, J.; Tripathy, S. K. Photofabrication of Surface Relief Grating on Films of Azobenzene Polymer with Different Dye Functionalization. *Macromolecules* **2000**, *33*, 4220–4225.

(441) Xue, X.; Zhu, J.; Zhang, Z.; Zhou, N.; Tu, Y.; Zhu, X. Soluble Main-Chain Azobenzene Polymers via Thermal 1,3-Dipolar Cycloaddition: Preparation and Photoresponsive Behavior. *Macromolecules* **2010**, *43*, 2704–2712.

(442) Ramanujam, P. S.; Holme, N. C. R.; Hvilsted, S. Atomic Force and Optical Near-field Microscopic Investigations of Polarization Holographic Gratings in a Liquid Crystalline Azobenzene Side-chain Polyester. *Appl. Phys. Lett.* **1996**, *68*, 1329–1331.

(443) Gao, J.; He, Y.; Xu, H.; Song, B.; Zhang, X.; Wang, Z.; Wang, X. Azobenzene-Containing Supramolecular Polymer Films for Laser-Induced Surface Relief Gratings. *Chem. Mater.* **2007**, *19*, 14–17.

(444) Wang, X.; Vapaavuori, J.; Wang, X.; Sabat, R. G.; Pellerin, C.; Bazuin, C. G. Influence of Supramolecular Interaction Type on Photoresponsive Azopolymer Complexes: A Surface Relief Grating Formation Study. *Macromolecules* **2016**, *49*, 4923–4934.

(445) Saccone, M.; Dichiarante, V.; Forni, A.; Goulet-Hanssens, A.; Cavallo, G.; Vapaavuori, J.; Terraneo, G.; Barrett, C. J.; Resnati, G.; Metrangolo, P.; et al. Supramolecular Hierarchy among Halogen and Hydrogen Bond Donors in Light-Induced Surface Patterning. *J. Mater. Chem. C* **2015**, *3*, 759–768.

(446) Priimagi, A.; Lindfors, K.; Kaivola, M.; Rochon, P. Efficient Surface-Relief Gratings in Hydrogen-Bonded Polymer−Azobenzene Complexes. *ACS Appl. Mater. Interfaces* **2009**, *1*, 1183–1189.

(447) Zettsu, N.; Ogasawara, T.; Mizoshita, N.; Nagano, S.; Seki, T. Photo-Triggered Surface Relief Grating Formation in Supramolecular Liquid Crystalline Polymer Systems with Detachable Azobenzene Unit. *Adv. Mater.* **2008**, *20*, 516–521.

(448) Huang, C.-W.; Wu, P.-W.; Su, W.-H.; Zhu, C.-Y.; Kuo, S.-W. Stimuli-Responsive Supramolecular Materials: Photo-Tunable Properties and Molecular Recognition Behavior. *Polym. Chem.* **2016**, *7*, 795–806.

(449) Zhang, Q.; Wang, X.; Barrett, C. J.; Bazuin, C. G. Spacer-Free Ionic Dye−Polyelectrolyte Complexes: Influence of Molecular Structure on Liquid Crystal Order and Photoinduced Motion. *Chem. Mater.* **2009**, *21*, 3216–3227.

(450) Mitsui, S.; Nagano, S.; Hara, M.; Seki, T. SRG Inscription in Supramolecular Liquid Crystalline Polymer Film: Replacement of Mesogens. *Crystals* **2017**, *7*, 52.

(451) Stumpel, J.; Saccone, M.; Dichiarante, V.; Lehtonen, O.; Virkki, M.; Metrangolo, P.; Priimagi, A. Surface-Relief Gratings in Halogen-Bonded Polymer–Azobenzene Complexes: A Concentration-Dependence Study. *Molecules* **2017**, *22*, 1844.

(452) Sobolewska, A.; Bartkiewicz, S. Single Beam Test (SBT) as a Criterion for the Resolution of Holographic Recording. *J. Mater. Chem. C* **2015**, *3*, 5616–5620.

(453) Koskela, J. E.; Vapaavuori, J.; Ras, R. H. A.; Priimagi, A. Light-Driven Surface Patterning of Supramolecular Polymers with Extremely Low Concentration of Photoactive Molecules. *ACS Macro Lett.* **2014**, *3*, 1196–1200.

(454) Koskela, J. E.; Vapaavuori, J.; Hautala, J.; Priimagi, A.; Faul, C. F. J.; Kaivola, M.; Ras, R. H. A. Surface-Relief Gratings and Stable Birefringence Inscribed Using Light of Broad Spectral Range in Supramolecular Polymer-Bisazobenzene Complexes. *J. Phys. Chem. C* **2012**, *116*, 2363–2370.

(455) Vapaavuori, J.; Valtavirta, V.; Alasaarela, T.; Mamiya, J.-I.; Priimagi, A.; Shishido, A.; Kaivola, M. Efficient Surface Structuring and Photoalignment of Supramolecular Polymer–Azobenzene Complexes through Rational Chromophore Design. *J. Mater. Chem.* **2011**, *21*, 15437–15441.

(456) Vapaavuori, J.; Priimagi, A.; Kaivola, M. Photoinduced Surface-Relief Gratings in Films of Supramolecular Polymer–Bisazobenzene Complexes. *J. Mater. Chem.* **2010**, *20*, 5260–5264.

(457) Schab-Balcerzak, E.; Konieczkowska, J.; Siwy, M.; Sobolewska, A.; Wojtowicz, M.; Wiacek, M. Comparative Studies of Polyimides with Covalently Bonded Azo-Dyes with Their Supramolecular Analoges: Thermo-Optical and Photoinduced Properties. *Opt. Mater. (Amst).* **2014**, *36*, 892–902.

(458) Vapaavuori, J.; Heikkinen, I. T. S.; Dichiarante, V.; Resnati, G.; Metrangolo, P.; Sabat, R. G.; Bazuin, C. G.; Priimagi, A.; Pellerin, C. Photomechanical Energy Transfer to Photopassive

Polymers through Hydrogen and Halogen Bonds. *Macromolecules* **2015**, *48*, 7535–7542.

(459) Kulikovska, O.; Kulikovsky, L.; Goldenberg, L. M.; Stumpe, J. Generation of Microstructures in Novel Supramolecular Ionic Materials Based on Azobenzene. In *Proc. SPIE 6999, Organic Optoelectronics and Photonics III*; Heremans, P. L., Muccini, M., Meulenkamp, E. A., Eds.; 2008; p 69990I.

(460) Wang, X.; Balasubramanian, S.; Kumar, J.; Tripathy, S. K.; Li, L. Azo Chromophore-Functionalized Polyelectrolytes. 1. Synthesis, Characterization, and Photoprocessing. *Chem. Mater.* **1998**, *10*, 1546–1553.

(461) Zucolotto, V.; He, J.-A.; Constantino, C. J. L.; Barbosa Neto, N. M.; Rodrigues, J. J.; Mendonça, C. R.; Zílio, S. C.; Li, L.; Aroca, R. F.; Oliveira, O. N.; et al. Mechanisms of Surface-Relief Gratings Formation in Layer-by-Layer Films from Azodyes. *Polymer* **2003**, *44*, 6129–6133.

(462) He, J.-A.; Bian, S.; Li, L.; Kumar, J.; Tripathy, S. K.; Samuelson, L. A. Photochemical Behavior and Formation of Surface Relief Grating on Self-Assembled Polyion/Dye Composite Film. *J. Phys. Chem. B* **2000**, *104*, 10513–10521.

(463) Zhang, Y.; Chen, S. Rare Earth Complexes Using Azobenzene-Containing Poly(Aryl Ether)s with Different Absorption Wavelengths as Macromolecular Ligands: Synthesis, Characterization, Fluorescence Properties and Fabrication of Fluorescent Holographic Micropatterns. *RSC Adv.* **2018**, *8*, 37348–37355.

(464) Kollarigowda, R. H.; Fedele, C.; Rianna, C.; Calabuig, A.; Manikas, A. C.; Pagliarulo, V.; Ferraro, P.; Cavalli, S.; Netti, P. A. Light-Responsive Polymer Brushes: Active Topographic Cues for Cell Culture Applications. *Polym. Chem.* **2017**, *8*, 3271–3278.

(465) Kopyshev, A.; Galvin, C. J.; Genzer, J.; Lomadze, N.; Santer, S. Polymer Brushes Modified by Photosensitive Azobenzene Containing Polyamines. *Polymer* **2016**, *98*, 421–428.

(466) Kopyshev, A.; Lomadze, N.; Feldmann, D.; Genzer, J.; Santer, S. Making Polymer Brush Photosensitive with Azobenzene Containing Surfactants. *Polymer* **2015**, *79*, 65–72.

(467) Lomadze, N.; Kopyshev, A.; Rühe, J.; Santer, S. Light-Induced Chain Scission in Photosensitive Polymer Brushes. *Macromolecules* **2011**, *44*, 7372–7377.

(468) Schuh, C.; Lomadze, N.; Rühe, J.; Kopyshev, A.; Santer, S. Photomechanical Degrafting of Azo-Functionalized Poly(Methacrylic Acid) (PMAA) Brushes. *J. Phys. Chem. B* **2011**, *115*, 10431–10438.

(469) Koskela, J. E.; Liljeström, V.; Lim, J.; Simanek, E. E.; Ras, R. H. A.; Priimagi, A.; Kostiainen, M. A. Light-Fuelled Transport of Large Dendrimers and Proteins. *J. Am. Chem. Soc.* **2014**, *136*, 6850–6853.

(470) Vapaavuori, J.; Priimagi, A.; Soininen, A. J.; Canilho, N.; Kasëmi, E.; Ruokolainen, J.; Kaivola, M.; Ikkala, O. Photoinduced Surface Patterning of Azobenzene-Containing Supramolecular Dendrons, Dendrimers and Dendronized Polymers. *Opt. Mater. Express* **2013**, *3*, 711–722.

(471) Galgano, J. J.; Karunatilaka, C.; Rethwisch, D. G.; Tivanski, A. V. Atomic Force Microscopy Study of Photoreversible Nanoscale Surface Relief Grating Patterns on Side Chain Dendritic Polyester Thin Films. *Colloids Surfaces A Physicochem. Eng. Asp.* **2010**, *360*, 167–174.

(472) He, Y.; Gu, X.; Guo, M.; Wang, X. Dendritic Azo Compounds as a New Type Amorphous Molecular Material with Quick Photoinduced Surface-Relief-Grating Formation Ability. *Opt. Mater. (Amst).* **2008**, *31*, 18–27.

(473) Yin, J.; Ye, G.; Wang, X. Star-Shaped Molecules Containing Both Azo Chromophores and Carbazole Units as a New Type of Photoresponsive Amorphous Material. *J. Mater. Chem. C* **2013**, *1*, 3794–3801.

(474) Yin, J.; Ye, G.; Wang, X. Self-Structured Surface Patterns on Molecular Azo Glass Films Induced

by Laser Light Irradiation. *Langmuir* **2010**, *26*, 6755–6761.

(475) Ishow, E.; Camacho-Aguilera, R.; Guérin, J.; Brosseau, A.; Nakatani, K. Spontaneous Formation of Complex Periodic Superstructures under High Interferential Illumination of Small-Molecule-Based Photochromic Materials. *Adv. Funct. Mater.* **2009**, *19*, 796–804.

(476) Alam, M. Z.; Ogata, T.; Kuwahara, Y.; Kurihara, S. Photoresponsive Behaviors of Azobenzene Functionalized 2-Arm, 3-Arm, and 4-Arm Telomers: A Comparative Study. *Int. J. Polym. Mater. Polym. Biomater.* **2014**, *63*, 620–623.

(477) Alam, M. Z.; Shibahara, A.; Ogata, T.; Kurihara, S. Synthesis of Azobenzene-Functionalized Star Polymers via RAFT and Their Photoresponsive Properties. *Polymer* **2011**, *52*, 3696–3703.

(478) Tomczyk, J.; Sobolewska, A.; Nagy, Z. T.; Guillon, D.; Donnio, B.; Stumpe, J. Photo- and Thermal-Processing of Azobenzene-Containing Star-Shaped Liquid Crystals. *J. Mater. Chem. C* **2013**, *1*, 924–932.

(479) Gharagozloo-Hubmann, K.; Kulikovska, O.; Börger, V.; Menzel, H.; Stumpe, J. Surface Relief Gratings in Azobenzene-Containing Polymers with Linear and Star-Branched Architectures: A Comparison. *Macromol. Chem. Phys.* **2009**, *210*, 1809–1817.

(480) Zarins, E.; Balodis, K.; Ruduss, A.; Kokars, V.; Ozols, A.; Augustovs, P.; Saharovs, D. Molecular Glasses of Azobenzene for Holographic Data Storage Applications. *Opt. Mater. (Amst).* **2018**, *79*, 45–52.

(481) Goldenberg, L. M.; Gritsai, Y.; Stumpe, J. Efficient Surface Relief Grating Generated in Azobenzene-Containing Material Using an He–Ne Laser. *J. Opt.* **2011**, *13*, 075601.

(482) Nakano, H. Photoinduced Surface-Relief-Grating Formation Using a Mixed Film of 4-[Bis(4-Methylphenyl)Amino]Azobenzene and 4,4′,4″-Tris[3-Methylphenyl(Phenyl)Amino]Triphenylamine. *Chem. Lett.* **2011**, *40*, 473–475.

(483) Nakano, H.; Yoshitake, M. Photoinduced Surface Relief Grating Formation Using Mixed Amorphous Films of Molecular Materials: 4-[4'-Stearoyloxybiphenyl-4-Yl(Biphenyl-4-Yl)-Amino]Azobenzene-4,4',4''-Tris[3-Methylphenyl-(Phenyl)Amino]Triphenylamine System. *J. Photopolym. Sci. Technol.* **2011**, *24*, 527–529.

(484) Goldenberg, L. M.; Kulikovsky, L.; Kulikovska, O.; Tomczyk, J.; Stumpe, J. Thin Layers of Low Molecular Azobenzene Materials with Effective Light-Induced Mass Transport. *Langmuir* **2010**, *26*, 2214–2217.

(485) Nakano, H.; Takahashi, T.; Tanino, T.; Shirota, Y. Synthesis and Photoinduced Surface Relief Grating Formation of Novel Photo-Responsive Amorphous Molecular Materials, 4-[Bis(9,9-Dimethylfluoren-2-Yl)Amino]-4′-Cyanoazobenzene and 4-[Bis(9,9-Dimethylfluoren-2-Yl)-Amino]-4′-Nitroazobenzene. *Dye. Pigment.* **2010**, *84*, 102–107.

(486) Ye, G.; Wang, D.; He, Y.; Wang, X. Nunchaku-like Molecules Containing Both an Azo Chromophore and a Biphenylene Unit as a New Type of High-Sensitivity Photo-Storage Material. *J. Mater. Chem.* **2010**, *20*, 10680–10687.

(487) Laventure, A.; Bourotte, J.; Vapaavuori, J.; Karperien, L.; Sabat, R. G.; Lebel, O.; Pellerin, C. Photoactive/Passive Molecular Glass Blends: An Efficient Strategy to Optimize Azomaterials for Surface Relief Grating Inscription. *ACS Appl. Mater. Interfaces* **2017**, *9*, 798–808.

(488) Mazaheri, L.; Bobbara, S. R.; Lebel, O.; Nunzi, J.-M. Photoinduction of Spontaneous Surface Relief Gratings on Azo DR1 Glass. *Opt. Lett.* **2016**, *41*, 2958–2961.

(489) Wei, R.; Xu, Z.; Liu, X.; He, Y.; Wang, X. Liquid-Crystalline Compounds Containing Both a Strong Push–Pull Azo Chromophore and a Cholesteryl Unit as Photoresponsive Molecular Glass Materials. *J. Mater. Chem. C* **2015**, *3*, 10925–10933.

(490) Gerbreders, A.; Bulanovs, A.; Mikelsone, J.; Traskovskis, K.; Potanina, E.; Vembris, A.; Teteris, J. Photoinduced Mass Transport in Low Molecular Organic Glasses and Its Practical Application

in Holography. *J. Non. Cryst. Solids* **2015**, *421*, 48–53.

(491) Kirby, R.; Sabat, R. G.; Nunzi, J.-M.; Lebel, O. Disperse and Disordered: A Mexylaminotriazine-Substituted Azobenzene Derivative with Superior Glass and Surface Relief Grating Formation. *J. Mater. Chem. C* **2014**, *2*, 841–847.

(492) Yadavalli, N. S.; Saphiannikova, M.; Lomadze, N.; Goldenberg, L. M.; Santer, S. Structuring of Photosensitive Material below Diffraction Limit Using Far Field Irradiation. *Appl. Phys. A* **2013**, *113*, 263–272.

(493) Jacquart, A.; Morin, E.; Yang, F.; Geffroy, B.; Ishow, E. Influence of Extrinsic and Intrinsic Parameters onto the Formation of Surface Relief Gratings in Polar Azo Molecular Glasses. *Dye. Pigment.* **2012**, *92*, 790–797.

(494) Nakano, H.; Takahashi, T.; Shirota, Y. Photoinduced Surface Relief Grating Formation Using a Photochromic Amorphous Molecular Material, N,N'-Bis(9,9-Dimethylfluoren-2-Yl)-4-(4-Pyridylazo)Aniline. *J. Photopolym. Sci. Technol.* **2009**, *22*, 253–255.

(495) Nakano, H. Photoinduced Surface Relief Grating Formation Using Azobenzene-Based Molecular Materials: A New Photochromic Amorphous Molecular Material, N-(Biphenyl-4-Yl)-N-(4'-Methoxybiphenyl-4-Yl)-4-Phenylazoaniline. *J. Photopolym. Sci. Technol.* **2008**, *21*, 545–547.

(496) Nakano, H.; Takahashi, T.; Tanino, T.; Shirota, Y. Synthesis and Photoinduced Surface Relief Grating Formation of a Novel Azobenzene-Based Photochromic Amorphous Molecular Material, 4-[Bis(9,9-Dimethylfluoren-2-Yl)Amino]-4'-Nitro-Azobenzene. *J. Photopolym. Sci. Technol.* **2007**, *20*, 87–89.

(497) Takahashi, T.; Tanino, T.; Ando, H.; Nakano, H.; Shirota, Y. Surface Relief Grating Formation Using a Novel Azobenzene-Based Photochromic Amorphous Molecular Material, Tris[4-(Phenylazo)Phenyl]Amine. *Mol. Cryst. Liq. Cryst.* **2005**, *430*, 9–14.

(498) Ueda, H.; Tanino, T.; Ando, H.; Nakano, H.; Shirota, Y. Significant Effect of Molecular Structure on Surface Relief Grating Formation for Novel Azobenzene-Based Photochromic Amorphous Molecular Materials. *Chem. Lett.* **2004**, *33*, 1152–1153.

(499) Reinke, N.; Draude, A.; Fuhrmann, T.; Franke, H.; Lessard, R. A. Electric Field Assisted Holographic Recording of Surface Relief Gratings in an Azo-Glass. *Appl. Phys. B Lasers Opt.* **2004**, *78*, 205–209.

(500) Nakano, H.; Takahashi, T.; Kadota, T.; Shirota, Y. Formation of a Surface Relief Grating Using a Novel Azobenzene-Based Photochromic Amorphous Molecular Material. *Adv. Mater.* **2002**, *14*, 1157.

(501) Ishow, E.; Lebon, B.; He, Y.; Wang, X.; Bouteiller, L.; Galmiche, L.; Nakatani, K. Structural and Photoisomerization Cross Studies of Polar Photochromic Monomeric Glasses Forming Surface Relief Gratings. *Chem. Mater.* **2006**, *18*, 1261–1267.

(502) Nakano, H. Photoinduced Surface Relief Grating Formation for a Single Crystal of 4-Aminoazobenzene. *Int. J. Mol. Sci.* **2010**, *11*, 1311–1320.

(503) Nakano, H. Photoinduced Surface Relief Grating Formation on a (100) Surface of a Single Crystal of 4-(Dimethylamino)Azobenzene. *J. Phys. Chem. C* **2008**, *112*, 16042–16045.

(504) Nakano, H. Photoinduced Surface Relief Grating Formation on a Co-Crystal of 4-[Bis(9,9-Dimethylfluoren-2-Yl)Amino]Azobenzene and Ethyl Acetate. *ChemPhysChem* **2008**, *9*, 2174–2176.

(505) Priimagi, A.; Saccone, M.; Cavallo, G.; Shishido, A.; Pilati, T.; Metrangolo, P.; Resnati, G. Photoalignment and Surface-Relief-Grating Formation Are Efficiently Combined in Low-Molecular-Weight Halogen-Bonded Complexes. *Adv. Mater.* **2012**, *24*, OP345–OP352.

(506) Kim, M.-J.; Seo, E.-M.; Vak, D.; Kim, D.-Y. Photodynamic Properties of Azobenzene Molecular

Films with Triphenylamines. *Chem. Mater.* **2003**, *15*, 4021–4027.

(507) Ando, H.; Tanino, T.; Nakano, H.; Shirota, Y. Photoinduced Surface Relief Grating Formation Using New Polymers Containing the Same Azobenzene Chromophore as a Photochoromic Amorphous Molecular Material. *Mater. Chem. Phys.* **2009**, *113*, 376–381.

(508) Ando, H.; Takahashi, T.; Nakano, H.; Shirota, Y. Comparative Studies of the Formation of Surface Relief Grating. Amorphous Molecular Material vs Vinyl Polymer. *Chem. Lett.* **2003**, *32*, 710–711.

(509) Kawatsuki, N.; Hasegawa, T.; Ono, H.; Tamoto, T. Formation of Polarization Gratings and Surface Relief Gratings in Photocrosslinkable Polymer Liquid Crystals by Polarization Holography. *Adv. Mater.* **2003**, *15*, 991–994.

(510) Zettsu, N.; Fukuda, T.; Matsuda, H.; Seki, T. Unconventional Polarization Characteristic of Rapid Photoinduced Material Motion in Liquid Crystalline Azobenzene Polymer Films. *Appl. Phys. Lett.* **2003**, *83*, 4960–4962.

(511) Yoneyama, S.; Yamamoto, T.; Tsutsumi, O.; Kanazawa, A.; Shiono, T.; Ikeda, T. High-Performance Material for Holographic Gratings by Means of a Photoresponsive Polymer Liquid Crystal Containing a Tolane Moiety with High Birefringence. *Macromolecules* **2002**, *35*, 8751–8758.

(512) Ubukata, T.; Seki, T.; Ichimura, K. Surface Relief Gratings in Host-Guest Supramolecular Materials. *Adv. Mater.* **2000**, *12*, 1675–1678.

(513) Xiang Tong Li; Natansohn, A.; Kobayashi, S.; Rochon, P. An Optically Controlled Liquid Crystal Device Using Azopolymer Films. *IEEE J. Quantum Electron.* **2000**, *36*, 824–827.

(514) Stracke, A.; Wendorff, J. H.; Goldmann, D.; Janietz, D. Optical Storage in a Smectic Mesophase: Thermal Amplification of Light-Induced Chromophore Orientations and Surface Relief Gratings. *Liq. Cryst.* **2000**, *27*, 1049–1057.

(515) Stracke, A.; Wendorff, J. H.; Goldmann, D.; Janietz, D.; Stiller, B. Gain Effects in Optical Storage: Thermal Induction of a Surface Relief Grating in a Smectic Liquid Crystal. *Adv. Mater.* **2000**, *12*, 282–285.

(516) Torres-Rocha, O. L.; Rodríguez-González, R. J.; Larios-López, L.; Martínez-Ponce, G.; Solano, C.; Navarro-Rodríguez, D. Structural and Photoresponsive Behavior of a Series of (Phenylene)Azobenzene-Containing Liquid-Crystalline Methacrylic Copolymers. *Polym. Int.* **2014**, *63*, 652–659.

(517) Zettsu, N.; Ogasawara, T.; Arakawa, R.; Nagano, S.; Ubukata, T.; Seki, T. Highly Photosensitive Surface Relief Gratings Formation in a Liquid Crystalline Azobenzene Polymer: New Implications for the Migration Process. *Macromolecules* **2007**, *40*, 4607–4613.

(518) Yu, H.; Shishido, A.; Iyoda, T.; Ikeda, T. Photoinduced Alignment and Multi-Processes of Refractive-Index Gratings in Pre-Irradiated Films of an Azobenzene-Containing Liquid-Crystalline Polymer. *Mol. Cryst. Liq. Cryst.* **2007**, *470*, 71–81.

(519) You, F.; Paik, M. Y.; Häckel, M.; Kador, L.; Kropp, D.; Schmidt, H.-W.; Ober, C. K. Control and Suppression of Surface Relief Gratings in Liquid-Crystalline Perfluoroalkyl–Azobenzene Polymers. *Adv. Funct. Mater.* **2006**, *16*, 1577–1581.

(520) Rodríguez, F. J.; Sánchez, C.; Villacampa, B.; Alcalá, R.; Cases, R.; Millaruelo, M.; Oriol, L. Surface Relief Gratings Induced by a Nanosecond Pulse in a Liquid-Crystalline Azo-Polymethacrylate. *Appl. Phys. Lett.* **2005**, *87*, 201914.

(521) Gherab, K. N.; Gatri, R.; Hank, Z.; Dick, B.; Kutta, R.-J.; Winter, R.; Luc, J.; Sahraoui, B.; Fillaut, J.-L. Design and Photoinduced Surface Relief Grating Formation of Photoresponsive Azobenzene Based Molecular Materials with Ruthenium Acetylides. *J. Mater. Chem.* **2010**, *20*, 2858–2864.

(522) Luc, J.; Bouchouit, K.; Czaplicki, R.; Fillaut, J.-L.; Sahraoui, B. Study of Surface Relief Gratings on Azo Organometallic Films in Picosecond Regime. *Opt. Express* **2008**, *16*, 15633–15639.

(523) McGee, D. J.; Ferrie, J.; Plachy, A.; Joo, Y.; Choi, J.; Kanimozhi, C.; Gopalan, P. Photo-Induced Refractive Index and Topographical Surface Gratings in Functionalized Nanocarbon Solid Film. *Appl. Phys. Lett.* **2015**, *107*, 181102.

(524) Zhao, R.; Zhan, X.; Yao, L.; Chen, Q.; Xie, Z.; Ma, Y. Electrochemical Deposition of Azobenzene-Containing Network Films with High-Contrast and Stable Photoresponse. *Macromol. Rapid Commun.* **2016**, *37*, 610–615.

(525) Han, G.; Zhang, H.; Chen, J.; Sun, Q.; Zhang, Y.; Zhang, H. Easily Crosslinkable Side-Chain Azobenzene Polymers for Fast and Persistent Fixation of Surface Relief Gratings. *New J. Chem.* **2015**, *39*, 1410–1420.

(526) Takase, H.; Natansohn, A.; Rochon, P. Photocrosslinked Surface Relief Gratings on Azobenzene-Containing Copolymer Films. *Polymer* **2003**, *44*, 7345–7351.

(527) Takase, H.; Natansohn, A.; Rochon, P. Immobilization of Surface Relief Gratings and Poled Alignment in Amorphous Azobenzene-Containing Polymers by Photopolymerization. *J. Photopolym. Sci. Technol.* **2001**, *14*, 189–192.

(528) Yamaki, S.; Nakagawa, M.; Morino, S.; Ichimura, K. Surface Relief Gratings Generated by a Photocrosslinkable Polymer with Styrylpyridine Side Chains. *Appl. Phys. Lett.* **2000**, *76*, 2520–2522.

(529) Zhou, J.; Yang, J.; Ke, Y.; Shen, J.; Zhang, Q.; Wang, K. Fabrication of Polarization Grating and Surface Relief Grating in Crosslinked and Non-Crosslinking Azopolymer by Polarization Holography Method. *Opt. Mater. (Amst).* **2008**, *30*, 1787–1795.

(530) Goldenberg, L. M.; Kulikovsky, L.; Kulikovska, O.; Stumpe, J. New Materials with Detachable Azobenzene: Effective, Colourless and Extremely Stable Surface Relief Gratings. *J. Mater. Chem.* **2009**, *19*, 8068–8071.

(531) Zhou, X.; Du, Y.; Wang, X. Azo Polymer Microspheres with Photo-Manipulated Surface and Topographic Structure. *Macromol. Chem. Phys.* **2016**, *217*, 765–772.

(532) Lambeth, R. H.; Moore, J. S. Light-Induced Shape Changes in Azobenzene Functionalized Polymers Prepared by Ring-Opening Metathesis Polymerization. *Macromolecules* **2007**, *40*, 1838–1842.

(533) Barillé, R.; Tajalli, P.; Zielinska, S.; Ortyl, E.; Kucharski, S.; Nunzi, J. M. Surface Relief Grating Formation on Nano-Objects. *Appl. Phys. Lett.* **2009**, *95*, 053102.

(534) Veer, P. U.; Pietsch, U.; Saphiannikova, M. Time and Temperature Dependence of Surface Relief Grating Formation in Polymers Containing Azobenzene Groups with Different Dipole Moment. *J. Appl. Phys.* **2009**, *106*, 014909.

(535) Kim, M.-J.; Lee, J.; Chun, C.; Kim, D.-Y.; Higuchi, S.; Nakayama, T. Control of Photodynamic Motions of Azobenzene-Derivative Polymers by Laser Excitation Wavelength. *Macromol. Chem. Phys.* **2007**, *208*, 1753–1763.

(536) Vapaavuori, J.; Goulet-Hanssens, A.; Heikkinen, I. T. S.; Barrett, C. J.; Priimagi, A. Are Two Azo Groups Better than One? Investigating the Photoresponse of Polymer-Bisazobenzene Complexes. *Chem. Mater.* **2014**, *26*, 5089–5096.

(537) Sobolewska, A.; Miniewicz, A.; Grabiec, E.; Sek, D. Holographic Grating Recording in Azobenzene Functionalized Polymers. *Open Chem.* **2006**, *4*.

(538) Kawatsuki, N.; Matsushita, H.; Washio, T.; Kozuki, J.; Kondo, M.; Sasaki, T.; Ono, H. Photoinduced Orientation of Photoresponsive Polymers with N -Benzylideneaniline Derivative Side Groups. *Macromolecules* **2014**, *47*, 324–332.

(539) Ji, R.; Fu, S.; Zhang, X.; Han, X.; Liu, S.; Wang, X.; Liu, Y. Fluorescent Holographic Fringes with a Surface Relief Structure Based on Merocyanine Aggregation Driven by Blue-Violet Laser. *Sci.*

Rep. **2018**, *8*, 3818.

(540) Park, J. W.; Nagano, S.; Yoon, S.-J.; Dohi, T.; Seo, J.; Seki, T.; Park, S. Y. High Contrast Fluorescence Patterning in Cyanostilbene-Based Crystalline Thin Films: Crystallization-Induced Mass Flow Via a Photo-Triggered Phase Transition. *Adv. Mater.* **2014**, *26*, 1354–1359.

(541) Ubukata, T.; Yamaguchi, S.; Yokoyama, Y. Photoinduced Surface Relief Structures Formed on Polymer Films Mixed with Diarylethenes. *Chem. Lett.* **2007**, *36*, 1224–1225.

(542) Ortyl, E.; Jaworowska, J.; Tajalli Seifi, P.; Barille, R.; Kucharski, S. Photochromic Polymer and Hybrid Materials Containing Azo Methylisoxazole Dye. *Soft Mater.* **2011**, *9*, 335–346.

(543) Ikoma, H.; Kondo, M.; Kawatsuki, N. Photoinduced Reorientation and Surface Relief Formation in Diblock and Random Copolymers with Benzoic Acid and Alkyloxy Side Groups. *Macromolecules* **2018**, *51*, 5392–5400.

(544) Kawatsuki, N.; Hosoda, R.; Kondo, M.; Sasaki, T.; Ono, H. Molecularly Oriented Surface Relief Formation in Polymethacrylates Comprising N -Benzylideneaniline Derivative Side Groups. *Jpn. J. Appl. Phys.* **2014**, *53*, 128002.

(545) Kawatsuki, N.; Matsushita, H.; Kondo, M.; Sasaki, T.; Ono, H. Photoinduced Reorientation and Polarization Holography in a New Photopolymer with 4-Methoxy- N -Benzylideneaniline Side Groups. *APL Mater.* **2013**, *1*, 022103.

(546) Ubukata, T.; Fujii, S.; Arimatsu, K.; Yokoyama, Y. Phototriggered Micromanufacturing Using Photoresponsive Amorphous Spirooxazine Films. *J. Mater. Chem.* **2012**, *22*, 14410–14417.

(547) Ubukata, T.; Fujii, S.; Yokoyama, Y. Reversible Phototriggered Micromanufacturing Using Amorphous Photoresponsive Spirooxazine Film. *J. Mater. Chem.* **2009**, *19*, 3373–3377.

(548) Ubukata, T.; Takahashi, K.; Yokoyama, Y. Photoinduced Surface Relief Structures Formed on Polymer Films Doped with Photochromic Spiropyrans. *J. Phys. Org. Chem.* **2007**, *20*, 981–984.

(549) Lim, T.; Kim, K.-H.; Song, S. A.; Lim, S. N.; Kim, K. Y.; Jeong, Y.-C. Effect of Hierarchical Surface Relief Grating on Light Extraction of Polymer Light-Emitting Diodes. *Macromol. Res.* **2017**, *25*, 786–791.

(550) Kim, J.; Park, H.; Na, S.-I.; Noh, Y.-Y.; Kim, D.-Y. A Facile Approach to Improve Light Extraction for Organic Light Emitting Diodes via Azobenzene Surface Relief Gratings. *Jpn. J. Appl. Phys.* **2014**, *53*, 08NF02.

(551) Paterson, J.; Natansohn, A.; Rochon, P.; Callender, C. L.; Robitaille, L. Optically Inscribed Surface Relief Diffraction Gratings on Azobenzene-containing Polymers for Coupling Light into Slab Waveguides. *Appl. Phys. Lett.* **1996**, *69*, 3318–3320.

(552) Goldenberg, L. M.; Lisinetskii, V.; Gritsai, Y.; Stumpe, J.; Schrader, S. Second Order DFB Lasing Using Reusable Grating Inscribed in Azobenzene-Containing Material. *Opt. Mater. Express* **2012**, *2*, 11–19.

(553) Goldenberg, L. M.; Lisinetskii, V.; Gritsai, Y.; Stumpe, J.; Schrader, S. Single Step Optical Fabrication of a DFB Laser Device in Fluorescent Azobenzene-Containing Materials. *Adv. Mater.* **2012**, *24*, 3339–3343.

(554) Döring, S.; Rabe, T.; Rosenhauer, R.; Kulikovska, O.; Hildebrandt, N.; Stumpe, J. Azobenzene-Based Surface Relief Gratings for Thin Film Distributed Feedback Lasers. In *Proc. SPIE 7722, Organic Photonics IV*; Heremans, P. L., Coehoorn, R., Adachi, C., Eds.; 2010; p 77221H.

(555) Ubukata, T.; Isoshima, T.; Hara, M. Wavelength Programmable Organic Distributed Feedback Laser Using a Photoinduced Surface Relief Grating. *Mol. Cryst. Liq. Cryst.* **2006**, *445*, 269/[559]-273/[563].

(556) Ubukata, T.; Isoshima, T.; Hara, M. Wavelength-Programmable Organic Distributed-Feedback Laser Based on a Photoassisted Polymer-Migration System. *Adv. Mater.* **2005**, *17*, 1630–1633.

(557) Chen, X.; Liu, B.; Zhang, H.; Guan, S.; Zhang, J.; Zhang, W.; Chen, Q.; Jiang, Z.; Guiver, M. D. Fabrication of Fluorescent Holographic Micropatterns Based on Azobenzene-Containing Host−Guest Complexes. *Langmuir* **2009**, *25*, 10444–10446.

(558) Jacquart, A.; Tauc, P.; Nakatani, K.; Ishow, E. Formation of Fluorescence Reliefs Photocontrolled by Collective Mass Migration. *J. Mater. Chem.* **2009**, *19*, 8999–9005.

(559) Ishow, E.; Brosseau, A.; Clavier, G.; Nakatani, K.; Pansu, R. B.; Vachon, J.-J.; Tauc, P.; Chauvat, D.; Mendonça, C. R.; Piovesan, E. Two-Photon Fluorescent Holographic Rewritable Micropatterning. *J. Am. Chem. Soc.* **2007**, *129*, 8970–8971.

(560) Choi, S.; Kim, K. R.; Oh, K.; Chun, C. M.; Kim, M. J.; Yoo, S. J.; Kim, D. Y. Interferometric Inscription of Surface Relief Gratings on Optical Fiber Using Azo Polymer Film. *Appl. Phys. Lett.* **2003**, *83*, 1080–1082.

(561) Jefferies, J.; Sabat, R. G. Surface-Relief Diffraction Gratings' Optimization for Plasmonic Enhancements in Thin-Film Solar Cells. *Prog. Photovoltaics Res. Appl.* **2014**, *22*, 648–655.

(562) Sabat, R. G.; Santos, M. J. L.; Rochon, P. Surface Relief Diffraction Gratings for Plasmonic Photocurrent Enhancements in P3HT-PCBM Solar Cells. In *Proc. SPIE 8007, Photonics North*; Kashyap, R., Têtu, M., Kleiman, R. N., Eds.; 2011; p 80071U.

(563) Sabat, R. G.; Santos, M. J. L.; Rochon, P. Surface Plasmon-Induced Band Gap in the Photocurrent Response of Organic Solar Cells. *Int. J. Photoenergy* **2010**, *2010*, 1–5.

(564) Na, S.-I.; Kim, S.-S.; Jo, J.; Oh, S.-H.; Kim, J.; Kim, D.-Y. Efficient Polymer Solar Cells with Surface Relief Gratings Fabricated by Simple Soft Lithography. *Adv. Funct. Mater.* **2008**, *18*, 3956–3963.

(565) Na, S.-I.; Kim, S.-S.; Kwon, S.-S.; Jo, J.; Kim, J.; Lee, T.; Kim, D.-Y. Surface Relief Gratings on Poly(3-Hexylthiophene) and Fullerene Blends for Efficient Organic Solar Cells. *Appl. Phys. Lett.*

2007, *91*, 173509.

(566) Cocoyer, C.; Rocha, L.; Sicot, L.; Geffroy, B.; de Bettignies, R.; Sentein, C.; Fiorini-Debuisschert, C.; Raimond, P. Implementation of Submicrometric Periodic Surface Structures toward Improvement of Organic-Solar-Cell Performances. *Appl. Phys. Lett.* **2006**, *88*, 133108.

(567) Cocoyer, C.; Rocha, L.; Fiorini-Debuisschert, C.; Sicot, L.; Vaufrey, D.; Sentein, C.; Geffroy, B.; Raimond, P. Implementation of a Submicrometer Patterning Technique in Azopolymer Films towards Optimization of Photovoltaic Solar Cells Efficiency. *Thin Solid Films* **2006**, *511–512*, 517–522.

(568) Wang, J.; Wang, X.; He, Y. Fabrication of Fluorescent Surface Relief Patterns Using AIE Polymer through a Soft Lithographic Approach. *J. Polym. Sci. Part B Polym. Phys.* **2016**, *54*, 1838–1845.

(569) Liu, B.; Wang, M.; He, Y.; Wang, X. Duplication of Photoinduced Azo Polymer Surface-Relief Gratings through a Soft Lithographic Approach. *Langmuir* **2006**, *22*, 7405–7410.

(570) Liu, B.; He, Y.; Wang, X. Fabrication of Photoprocessible Azo Polymer Microwires through a Soft Lithographic Approach. *Langmuir* **2006**, *22*, 10233–10237.

(571) Nishizawa, K.; Nagano, S.; Seki, T. Micropatterning of Titanium Oxide Film via Phototactic Mass Transport. *J. Mater. Chem.* **2009**, *19*, 7191–7194.

(572) Kim, M.; Kang, B.; Yang, S.; Drew, C.; Samuelson, L. A.; Kumar, J. Facile Patterning of Periodic Arrays of Metal Oxides. *Adv. Mater.* **2006**, *18*, 1622–1626.

(573) Yang, S.; Yang, K.; Niu, L.; Nagarajan, R.; Bian, S.; Jain, A. K.; Kumar, J. Patterning of Substrates Using Surface Relief Structures on an Azobenzene-Functionalized Polymer Film. *Adv. Mater.* **2004**, *16*, 693–696.

(574) Li, L.; Yan, F.; Cazeca, M.; Samuelson, L.; Kumar, J. Fabrication of Gold Nano-Structures with Azopolymer Templates. *J. Macromol. Sci. Part A* **2007**, *44*, 1299–1303.

(575) Pale, V.; Kauppinen, C.; Selin, J.; Sopanen, M.; Tittonen, I. Fluorescence-Enhancing Plasmonic Silver Nanostructures Using Azopolymer Lithography. *RSC Adv.* **2016**, *6*, 48129–48136.

(576) Kauppinen, C.; Haggren, T.; Kravchenko, A.; Jiang, H.; Huhtio, T.; Kauppinen, E.; Dhaka, V.; Suihkonen, S.; Kaivola, M.; Lipsanen, H.; et al. A Technique for Large-Area Position-Controlled Growth of GaAs Nanowire Arrays. *Nanotechnology* **2016**, *27*, 135601.

(577) Moerland, R. J.; Koskela, J. E.; Kravchenko, A.; Simberg, M.; van der Vegte, S.; Kaivola, M.; Priimagi, A.; Ras, R. H. A. Large-Area Arrays of Three-Dimensional Plasmonic Subwavelength-Sized Structures from Azopolymer Surface-Relief Gratings. *Mater. Horiz.* **2014**, *1*, 74–80.

(578) Kravchenko, A.; Shevchenko, A.; Ovchinnikov, V.; Priimagi, A.; Kaivola, M. Optical Interference Lithography Using Azobenzene-Functionalized Polymers for Micro- and Nanopatterning of Silicon. *Adv. Mater.* **2011**, *23*, 4174–4177.

(579) Kravchenko, A.; Shevchenko, A.; Grahn, P.; Ovchinnikov, V.; Kaivola, M. Photolithographic Periodic Patterning of Gold Using Azobenzene-Functionalized Polymers. *Thin Solid Films* **2013**, *540*, 162–167.

(580) Yang, S.; Yang, K.; Jain, A.; Nagarajan, R.; Kumar, J. Patterning Flexible Substrates Using Surface Relief Structures in Azobenzene Functionalized Polymer Films. *J. Macromol. Sci. Part A* **2008**, *45*, 938–941.

(581) Lomadze, N.; Kopyshev, A.; Bargheer, M.; Wollgarten, M.; Santer, S. Mass Production of Polymer Nano-Wires Filled with Metal Nano-Particles. *Sci. Rep.* **2017**, *7*, 8506.

(582) Nair, S.; Escobedo, C.; Sabat, R. G. Crossed Surface Relief Gratings as Nanoplasmonic Biosensors. *ACS Sensors* **2017**, *2*, 379–385.

(583) Nair, S.; Gomez-Cruz, J.; Manjarrez-Hernandez, Á.; Ascanio, G.; Sabat, R.; Escobedo, C. Selective Uropathogenic E. Coli Detection Using Crossed Surface-Relief Gratings. *Sensors* **2018**, *18*, 3634.

(584) Koçer, G.; ter Schiphorst, J.; Hendrikx, M.; Kassa, H. G.; Leclère, P.; Schenning, A. P. H. J.; Jonkheijm, P. Light-Responsive Hierarchically Structured Liquid Crystal Polymer Networks for Harnessing Cell Adhesion and Migration. *Adv. Mater.* **2017**, *29*, 1606407.

(585) Rianna, C.; Ventre, M.; Cavalli, S.; Radmacher, M.; Netti, P. A. Micropatterned Azopolymer Surfaces Modulate Cell Mechanics and Cytoskeleton Structure. *ACS Appl. Mater. Interfaces* **2015**, *7*, 21503–21510.

(586) Rianna, C.; Calabuig, A.; Ventre, M.; Cavalli, S.; Pagliarulo, V.; Grilli, S.; Ferraro, P.; Netti, P. A. Reversible Holographic Patterns on Azopolymers for Guiding Cell Adhesion and Orientation. *ACS Appl. Mater. Interfaces* **2015**, *7*, 16984–16991.

(587) Barillé, R.; Janik, R.; Kucharski, S.; Eyer, J.; Letournel, F. Photo-Responsive Polymer with Erasable and Reconfigurable Micro- and Nano-Patterns: An in Vitro Study for Neuron Guidance. *Colloids Surfaces B Biointerfaces* **2011**, *88*, 63–71.

(588) Loebner, S.; Jelken, J.; Yadavalli, N.; Sava, E.; Hurduc, N.; Santer, S. Motion of Adsorbed Nano-Particles on Azobenzene Containing Polymer Films. *Molecules* **2016**, *21*, 1663.

(589) Snell, K. E.; Stéphant, N.; Pansu, R. B.; Audibert, J.-F.; Lagugné-Labarthet, F.; Ishow, E. Nanoparticle Organization through Photoinduced Bulk Mass Transfer. *Langmuir* **2014**, *30*, 2926–2935.

(590) Capeluto, M. G.; Fernández Salvador, R.; Eceiza, A.; Goyanes, S.; Ledesma, S. A. Azopolymer Film as an Actuator for Organizing Multiwall Carbon Nanotubes. *Opt. Mater. (Amst).* **2017**, *66*, 247–252.

(591) Wang, D.; Ye, G.; Wang, X.; Wang, X. Graphene Functionalized with Azo Polymer Brushes: Surface-Initiated Polymerization and Photoresponsive Properties. *Adv. Mater.* **2011**, *23*, 1122–1125.

(592) Ubukata, T.; Hara, M.; Ichimura, K.; Seki, T. Phototactic Mass Transport in Polymer Films for Micropatterning and Alignment of Functional Materials. *Adv. Mater.* **2004**, *16*, 220–223.

(593) Kim, M.-H.; Kim, J.-D.; Fukuda, T.; Matsuda, H. Alignment Control of Liquid Crystals on Surface Relief Gratings. *Liq. Cryst.* **2000**, *27*, 1633–1640.

(594) Parfenov, A.; Tamaoki, N.; Ohnishi, S. Photoinduced Alignment of Nematic Liquid Crystal on the Polymer Surface Microrelief. *J. Appl. Phys.* **2000**, *87*, 2043–2045.

(595) Li, X. T.; Natansohn, A.; Rochon, P. Photoinduced Liquid Crystal Alignment Based on a Surface Relief Grating in an Assembled Cell. *Appl. Phys. Lett.* **1999**, *74*, 3791–3793.

(596) Madani, A.; Khoshsima, H.; Tajalli, H.; Ahmadi, S. Experimental Study of Liquid-Crystal Alignment on a Surface Relief Grating. *Laser Phys.* **2006**, *16*, 1197–1201.

(597) Morikawa, Y.; Nagano, S.; Watanabe, K.; Kamata, K.; Iyoda, T.; Seki, T. Optical Alignment and Patterning of Nanoscale Microdomains in a Block Copolymer Thin Film. *Adv. Mater.* **2006**, *18*, 883–886.

(598) Cardoso, M. R.; Tribuzi, V.; Balogh, D. T.; Misoguti, L.; Mendonca, C. R. Laser Microstructuring of Azopolymers via Surface Relief Gratings: Controlling Hydrophobicity. *J. Optoelectron. Adv. Mater.* **2010**, *12*, 745–748.

(599) Mazaheri, L.; Ahmadi-Kandjani, S.; Nunzi, J.-M. Influence of Temperature on the Relaxation Kinetics of Spontaneous Pattern Formation in an Azo–Polymer Film. *Opt. Commun.* **2013**, *298–299*, 150–153.

(600) Wang, X.; Yin, J.; Wang, X. Photoinduced Self-Structured Surface Pattern on a Molecular Azo Glass Film: Structure–Property Relationship and Wavelength Correlation. *Langmuir* **2011**, *27*, 12666–12676.

(601) Hubert, C.; Fiorini-Debuisschert, C.; Rocha, L.; Raimond, P.; Nunzi, J.-M. Spontaneous

Photoinduced Patterning of Azo-Dye Polymer Films: The Facts. *J. Opt. Soc. Am. B* **2007**, *24*, 1839.

(602) Ciuchi, F.; Mazzulla, A.; Carbone, G.; Cipparrone, G. Complex Structures of Surface Relief Induced by Holographic Recording in Azo-Dye-Doped Elastomer Thin Films. *Macromolecules* **2003**, *36*, 5689–5693.

(603) Morikawa, Y.; Kondo, T.; Nagano, S.; Seki, T. Photoinduced 3D Ordering and Patterning of Microphase-Separated Nanostructure in Polystyrene-Based Block Copolymer. *Chem. Mater.* **2007**, *19*, 1540–1542.

(604) Korbut, A.; Zielińska, S.; Barille, R.; Pigłowski, J.; Ortyl, E. The Novel Photoresponsive Oligomers Containing Azo Derivatives of Sulfamerazine for Spontaneous Surface Relief Grating Inscription. *Eur. Polym. J.* **2017**, *90*, 392–406.

(605) Ambrosio, A.; Girardo, S.; Camposeo, A.; Pisignano, D.; Maddalena, P. Controlling Spontaneous Surface Structuring of Azobenzene-Containing Polymers for Large-Scale Nano-Lithography of Functional Substrates. *Appl. Phys. Lett.* **2013**, *102*, 093102.

(606) Noga, J.; Sobolewska, A.; Bartkiewicz, S.; Virkki, M.; Priimagi, A. Periodic Surface Structures Induced by a Single Laser Beam Irradiation. *Macromol. Mater. Eng.* **2017**, *302*, 1600329.

(607) Hubert, C.; Fiorini-Debuisschert, C.; Maurin, I.; Nunzi, J.-M.; Raimond, P. Spontaneous Patterning of Hexagonal Structures in an Azo-Polymer Using Light-Controlled Mass Transport. *Adv. Mater.* **2002**, *14*, 729.

(608) Mazaheri, L.; Sabat, R. G.; Lebel, O.; Nunzi, J.-M. Unraveling the Nucleation and Growth of Spontaneous Surface Relief Gratings. *Opt. Mater. (Amst).* **2016**, *62*, 378–391.

(609) Teboul, V.; Barillé, R.; Tajalli, P.; Ahmadi-Kandjani, S.; Tajalli, H.; Zielinska, S.; Ortyl, E. Light Mediated Emergence of Surface Patterns in Azopolymers at Low Temperatures. *Soft Matter* **2015**, *11*, 6444–6449.

(610) Hubert, C.; Malcor, E.; Maurin, I.; Nunzi, J.-M.; Raimond, P.; Fiorini, C. Microstructuring of Polymers Using a Light-Controlled Molecular Migration Processes. *Appl. Surf. Sci.* **2002**, *186*, 29–33.

(611) Lee, S.; Shin, J.; Kang, H. S.; Lee, Y.-H.; Park, J.-K. Deterministic Nanotexturing by Directional Photofluidization Lithography. *Adv. Mater.* **2011**, *23*, 3244–3250.

(612) Ishitobi, H.; Nakamura, I.; Kobayashi, T.; Hayazawa, N.; Sekkat, Z.; Kawata, S.; Inouye, Y. Nanomovement of Azo Polymers Induced by Longitudinal Fields. *ACS Photonics* **2014**, *1*, 190–197.

(613) Bobrovsky, A.; Mochalov, K.; Chistyakov, A.; Oleinikov, V.; Shibaev, V. AFM Study of Laser-Induced Crater Formation in Films of Azobenzene-Containing Photochromic Nematic Polymer and Cholesteric Mixture. *J. Photochem. Photobiol. A Chem.* **2014**, *275*, 30–36.

(614) Ambrosio, A.; Borbone, F.; Carella, A.; Centore, R.; Fusco, S.; Kuball, H.-G.; Maddalena, P.; Romano, C.; Roviello, A.; Stolte, M. Cis–Trans Isomerization and Optical Laser Writing in New Heterocycle Based Azo-Polyurethanes. *Opt. Mater. (Amst).* **2012**, *34*, 724–728.

(615) Savoini, M.; Biagioni, P.; Finazzi, M.; Duò, L. Macroscopic Movement of Azo Polymer Chains by Near-Field Probes: Dependence on the Illumination Conditions. *Phys. Status Solidi B* **2010**, *247*, 2067–2070.

(616) Ishitobi, H.; Shoji, S.; Hiramatsu, T.; Sun, H.-B.; Sekkat, Z.; Kawata, S. Two-Photon Induced Polymer Nanomovement. *Opt. Express* **2008**, *16*, 14106–14114.

(617) Fukuda, T.; Barada, D. Photoinduced Mass Transport by One-Dimensional Gaussian Beam Irradiation: Width and Polarization Dependence. *Jpn. J. Appl. Phys.* **2006**, *45*, 470–474.

(618) Zhang, D.; Wang, P.; Lu, Y.; Bai, M.; Yang, J.; Tang, L.; Zhang, J.; Ming, H.; Zhang, Q.; Liu, J.; et al. Near-Field Lithography on the Azobenzene Polymer Liquid Crystal Films. *Chinese Opt. Lett.*

2005, *03*, 107-107-.

(619) Sumaru, K.; Fukuda, T.; Kimura, T.; Matsuda, H.; Yamanaka, T. Photoinduced Surface Relief Formation on Azopolymer Films: A Driving Force and Formed Relief Profile. *J. Appl. Phys.* **2002**, *91*, 3421–3430.

(620) Bian, S.; Li, L.; Kumar, J.; Kim, D. Y.; Williams, J.; Tripathy, S. K. Single Laser Beam-Induced Surface Deformation on Azobenzene Polymer Films. *Appl. Phys. Lett.* **1998**, *73*, 1817–1819.

(621) Ishitobi, H.; Tanabe, M.; Sekkat, Z.; Kawata, S. Nanomovement of Azo Polymers Induced by Metal Tip Enhanced Near-Field Irradiation. *Appl. Phys. Lett.* **2007**, *91*, 091911.

(622) Barada, D.; Fukuda, T.; Itoh, M.; Yatagai, T. Numerical Analysis of Photoinduced Surface Relief Formed on Azobenzene Polymer Film by Optical Near-Field Exposure. *Jpn. J. Appl. Phys.* **2006**, *45*, 6730–6737.

(623) Zhang, Y.; Demesy, G.; Haggui, M.; Gérard, D.; Béal, J.; Dodson, S.; Xiong, Q.; Plain, J.; Bonod, N.; Bachelot, R. Nanoscale Switching of Near-Infrared Hot Spots in Plasmonic Oligomers Probed by Two-Photon Absorption in Photopolymers. *ACS Photonics* **2018**, *5*, 918–928.

(624) Ishitobi, H.; Kobayashi, T.; Ono, A.; Inouye, Y. Near-Field Optical Mapping of Single Gold Nano Particles Using Photo-Induced Polymer Movement of Azo-Polymers. *Opt. Commun.* **2017**, *387*, 24–29.

(625) Teulle, A.; Sanchot, A.; Ishow, E.; Sharma, J.; Dujardin, E. Photochemical Mapping of the Multimodal Plasmonic Response of 2D Gold Crystals. *J. Phys. Chem. C* **2017**, *121*, 15908–15914.

(626) Kim, M.; Huh, J.-H.; Lee, J.; Woo, H. J.; Kim, K.; Jung, D.-W.; Yi, G.-R.; Jeong, M. S.; Lee, S.; Song, Y. J. Photofluidic Near-Field Mapping of Electric-Field Resonance in Plasmonic Metasurface Assembled with Gold Nanoparticles. *J. Phys. Chem. Lett.* **2017**, *8*, 3745–3751.

(627) Galarreta, B. C.; Rupar, I.; Young, A.; Lagugné-Labarthet, F. Mapping Hot-Spots in Hexagonal

Arrays of Metallic Nanotriangles with Azobenzene Polymer Thin Films. *J. Phys. Chem. C* **2011**, *115*, 15318–15323.

(628) Hubert, C.; Rumyantseva, A.; Lerondel, G.; Grand, J.; Kostcheev, S.; Billot, L.; Vial, A.; Bachelot, R.; Royer, P.; Chang, S.; et al. Near-Field Photochemical Imaging of Noble Metal Nanostructures. *Nano Lett.* **2005**, *5*, 615–619.

(629) König, T.; Yadavalli, N. S.; Santer, S. Near-Field Induced Reversible Structuring of Photosensitive Polymer Films: Gold Versus Silver Nano-Antennas. *Plasmonics* **2012**, *7*, 535–542.

(630) Masuda, K.; Nakano, S.; Barada, D.; Kumakura, M.; Miyamoto, K.; Omatsu, T. Azo-Polymer Film Twisted to Form a Helical Surface Relief by Illumination with a Circularly Polarized Gaussian Beam. *Opt. Express* **2017**, *25*, 12499–12507.

(631) Ambrosio, A.; Marrucci, L.; Borbone, F.; Roviello, A.; Maddalena, P. Light-Induced Spiral Mass Transport in Azo-Polymer Films under Vortex-Beam Illumination. *Nat. Commun.* **2012**, *3*, 989.

(632) Watabe, M.; Juman, G.; Miyamoto, K.; Omatsu, T. Light Induced Conch-Shaped Relief in an Azo-Polymer Film. *Sci. Rep.* **2015**, *4*, 4281.

(633) Sorkhabi, S. G.; Barille, R.; Ahmadi-Kandjani, S.; Zielinska, S.; Ortyl, E. A New Method for Patterning Azopolymer Thin Film Surfaces. *Opt. Mater. (Amst).* **2017**, *66*, 573–579.

(634) Fedele, C.; De Gregorio, M.; Netti, P. A.; Cavalli, S.; Attanasio, C. Azopolymer Photopatterning for Directional Control of Angiogenesis. *Acta Biomater.* **2017**, *63*, 317–325.

(635) Rianna, C.; Rossano, L.; Kollarigowda, R. H.; Formiggini, F.; Cavalli, S.; Ventre, M.; Netti, P. A. Spatio-Temporal Control of Dynamic Topographic Patterns on Azopolymers for Cell Culture Applications. *Adv. Funct. Mater.* **2016**, *26*, 7572–7580.

(636) Rossano, L.; Cimmino, C.; Cavalli, S.; Ventre, M.; Netti, P. A. Regulating Fibroblast Shape and Mechanics through Photoresponsive Surfaces with Concentric Circular Topographic Patterns. *Adv.*

Mater. Interfaces **2018**, *5*, 1800890.

(637) Stumpel, J. E.; Ziółkowski, B.; Florea, L.; Diamond, D.; Broer, D. J.; Schenning, A. P. H. J. Photoswitchable Ratchet Surface Topographies Based on Self-Protonating Spiropyran–NIPAAM Hydrogels. *ACS Appl. Mater. Interfaces* **2014**, *6*, 7268–7274.

(638) Stumpel, J. E.; Liu, D.; Broer, D. J.; Schenning, A. P. H. J. Photoswitchable Hydrogel Surface Topographies by Polymerisation-Induced Diffusion. *Chem. Eur. J.* **2013**, *19*, 10922–10927.

(639) Szilágyi, A.; Sumaru, K.; Sugiura, S.; Takagi, T.; Shinbo, T.; Zrínyi, M.; Kanamori, T. Rewritable Microrelief Formation on Photoresponsive Hydrogel Layers. *Chem. Mater.* **2007**, *19*, 2730–2732.

(640) Liu, D.; Broer, D. J. Liquid Crystal Polymer Networks: Switchable Surface Topographies. *Liq. Cryst. Rev.* **2013**, *1*, 20–28.

(641) Seki, T. Meso- and Microscopic Motions in Photoresponsive Liquid Crystalline Polymer Films. *Macromol. Rapid Commun.* **2014**, *35*, 271–290.

(642) Liu, D. Volume Generation towards Dynamic Surface Morphing in Liquid Crystal Polymer Networks. *Liq. Cryst.* **2016**, *43*, 2136–2143.

(643) Liu, Y.; Genzer, J.; Dickey, M. D. "2D or Not 2D": Shape-Programming Polymer Sheets. *Prog. Polym. Sci.* **2016**, *52*, 79–106.

(644) Feng, W.; Broer, D. J.; Liu, D. Combined Light and Electric Response of Topographic Liquid Crystal Network Surfaces. *Adv. Funct. Mater.* **2019**, 1901681.

(645) Lancia, F.; Ryabchun, A.; Katsonis, N. Life-like Motion Driven by Artificial Molecular Machines. *Nat. Rev. Chem.* **2019**, *3*, 536–551.

(646) Liu, D.; Bastiaansen, C. W. M.; den Toonder, J. M. J.; Broer, D. J. Photo-Switchable Surface Topologies in Chiral Nematic Coatings. *Angew. Chem. Int. Ed.* **2012**, *51*, 892–896.

(647) Liu, D.; Bastiaansen, C. W. M.; den Toonder, J. M. J.; Broer, D. J. Light-Induced Formation of Dynamic and Permanent Surface Topologies in Chiral–Nematic Polymer Networks. *Macromolecules* **2012**, *45*, 8005–8012.

(648) McConney, M. E.; Martinez, A.; Tondiglia, V. P.; Lee, K. M.; Langley, D.; Smalyukh, I. I.; White, T. J. Topography from Topology: Photoinduced Surface Features Generated in Liquid Crystal Polymer Networks. *Adv. Mater.* **2013**, *25*, 5880–5885.

(649) Liu, D.; Broer, D. J. New Insights into Photoactivated Volume Generation Boost Surface Morphing in Liquid Crystal Coatings. *Nat. Commun.* **2015**, *6*, 8334.

(650) He, L.-H. Deformation of Amorphous Azobenzene-Containing Polymer Films Induced by Polarized Light. *Acta Mech. Sin.* **2012**, *28*, 1203–1208.

(651) Loebner, S.; Lomadze, N.; Kopyshev, A.; Koch, M.; Guskova, O.; Saphiannikova, M.; Santer, S. Light-Induced Deformation of Azobenzene-Containing Colloidal Spheres: Calculation and Measurement of Opto-Mechanical Stresses. *J. Phys. Chem. B* **2018**, *122*, 2001–2009.

(652) Ortyl, E.; Zielinska, S.; Barillé, R.; Almohamed, Y.; Nunzi, J.-M. Instantaneous Photoinduced Patterning of an Azopolymer Colloidal Nanosphere Assembly. *Opt. Mater. Express* **2016**, *6*, 2925–2932.

(653) Fan, W.; Tong, X.; Li, G.; Zhao, Y. Photoresponsive Liquid Crystalline Polymer Single-Chain Nanoparticles. *Polym. Chem.* **2017**, *8*, 3523–3529.

(654) Snell, K. E.; Mevellec, J.-Y.; Humbert, B.; Lagugné-Labarthet, F.; Ishow, E. Photochromic Organic Nanoparticles as Innovative Platforms for Plasmonic Nanoassemblies. *ACS Appl. Mater. Interfaces* **2015**, *7*, 1932–1942.

(655) Lin, S.; Wang, Y.; Cai, C.; Xing, Y.; Lin, J.; Chen, T.; He, X. Tuning Self-Assembly and Photo-Responsive Behavior of Azobenzene-Containing Triblock Copolymers by Combining

Homopolymers. *Nanotechnology* **2013**, *24*, 085602.

(656) Wu, S.; Wang, L.; Kroeger, A.; Wu, Y.; Zhang, Q.; Bubeck, C. Block Copolymers of PS-b-PEO Co-Assembled with Azobenzene-Containing Homopolymers and Their Photoresponsive Properties. *Soft Matter* **2011**, *7*, 11535–11545.

(657) Barillé, R.; Tajalli, P.; Kucharski, S.; Ortyl, E.; Nunzi, J.-M. Photoinduced Deformation of Azopolymer Nanometric Spheres. *Appl. Phys. Lett.* **2010**, *96*, 163104.

(658) Wang, D.; Liu, J.; Ye, G.; Wang, X. Amphiphilic Block Copolymers Bearing Strong Push–Pull Azo Chromophores: Synthesis, Micelle Formation and Photoinduced Shape Deformation. *Polymer* **2009**, *50*, 418–427.

(659) Liu, J.; He, Y.; Wang, X. Azo Polymer Colloidal Spheres Containing Different Amounts of Functional Groups and Their Photoinduced Deformation Behavior. *Langmuir* **2008**, *24*, 678–682.

(660) Wang, D.; Ye, G.; Wang, X. Synthesis of Aminoazobenzene-Containing Diblock Copolymer and Photoinduced Deformation Behavior of Its Micelle-Like Aggregates. *Macromol. Rapid Commun.* **2007**, *28*, 2237–2243.

(661) Li, Y.; He, Y.; Tong, X.; Wang, X. Photoinduced Deformation of Amphiphilic Azo Polymer Colloidal Spheres. *J. Am. Chem. Soc.* **2005**, *127*, 2402–2403.

(662) Hsu, C.; Xu, Z.; Wang, X. Symmetry-Breaking Response of Azo Molecular Glass Microspheres to Interfering Circularly Polarized Light: From Shape Manipulation to 3D Patterning. *Adv. Funct. Mater.* **2019**, *29*, 1806703.

(663) Huang, J.; Beckemper, S.; Wu, S.; Shen, J.; Zhang, Q.; Wang, K.; Gillner, A. Light Driving Force for Surface Patterning on Azobenzene-Containing Polymers. *Phys. Chem. Chem. Phys.* **2011**, *13*, 16150–16158.

(664) Liu, B.; He, Y.; Fan, P.; Wang, X. Azo Polymer Microspherical Cap Array: Soft-Lithographic

Fabrication and Photoinduced Shape Deformation Behavior. *Langmuir* **2007**, *23*, 11266–11272.

(665) Bublitz, D.; Helgert, M.; Fleck, B.; Wenke, L.; Hvilsted, S.; Ramanujam, P. S. Photoinduced Deformation of Azobenzene Polyester Films. *Appl. Phys. B* **2000**, *70*, 863–865.

(666) Yin, X.; Dong, H.; Wang, S.; Liang, Y.; Zhang, W.; Gao, N.; Liu, X.; Wang, X.; Li, G. Coupling of Photoinduced Mass Immigration with Polymer Networks to Produce Nanostructured Materials Capable of Reversibly Creating Arbitrary Deformations. *Macromol. Chem. Phys.* **2018**, *219*, 1800113.

(667) Pirani, F.; Angelini, A.; Frascella, F.; Rizzo, R.; Ricciardi, S.; Descrovi, E. Light-Driven Reversible Shaping of Individual Azopolymeric Micro-Pillars. *Sci. Rep.* **2016**, *6*, 31702.

(668) Liu, B.; Zhou, Y.; Zhou, X.; Wang, X. Photodeformable Microspheres from Methacrylate-Based Azo Homopolymers. *Macromol. Chem. Phys.* **2017**, *218*, 1700020.

(669) Huang, J.; Wu, S.; Beckemper, S.; Gillner, A.; Zhang, Q.; Wang, K. All-Optical Fabrication of Ellipsoidal Caps on Azobenzene Functional Polymers. *Opt. Lett.* **2010**, *35*, 2711–2713.

(670) Zhou, Y.; Liu, B.; Wang, X. Microspheres of Polyurethanes Functionalized with Push - Pull Type Azo Chromophores and Their Photoinduced Deformation Behavior. *Polymer* **2017**, *111*, 229–238.

(671) Zhou, Y.; Wang, X. G. Photodeformable Microspheres from Amphiphilic Azo Polyurethane. *Macromol. Chem. Phys.* **2015**, *216*, 2040–2047.

(672) Liu, J.; He, Y.; Wang, X. Influence of Chromophoric Electron-Withdrawing Groups on Photoinduced Deformation of Azo Polymer Colloids. *Polymer* **2010**, *51*, 2879–2886.

(673) Li, Y.; He, Y.; Tong, X.; Wang, X. Stretching Effect of Linearly Polarized Ar + Laser Single-Beam on Azo Polymer Colloidal Spheres. *Langmuir* **2006**, *22*, 2288–2291.

(674) Li, N.; Ye, G.; He, Y.; Wang, X. Hollow Microspheres of Amphiphilic Azo Homopolymers: Self-

Assembly and Photoinduced Deformation Behavior. *Chem. Commun.* **2011**, *47*, 4757.

(675) Wei, R.; Ma, J.; Zhang, H.; He, Y. Synthesis, Characterization, and Photo-Responsive Properties of Y-Shaped Amphiphilic Azo Triblock Copolymer. *J. Appl. Polym. Sci.* **2016**, *133*, DOI: 10.1002/app.43695.

(676) Wei, R.-B.; Wang, X.-G.; He, Y.-N. Synthesis, Self-Assembly and Photo-Responsive Behavior of AB2 Shaped Amphiphilic Azo Block Copolymer. *Chinese Chem. Lett.* **2015**, *26*, 857–861.

(677) Xing, Y.; Lin, S.; Lin, J.; He, X. Synthesis, Self-Assembly and Responsive Properties of PEG-b-PDMAEMA-b-PMMAzo Triblock Copolymers. *Chinese J. Polym. Sci.* **2013**, *31*, 833–840.

(678) Wang, Y.; Lin, S.; Zang, M.; Xing, Y.; He, X.; Lin, J.; Chen, T. Self-Assembly and Photo-Responsive Behavior of Novel ABC2-Type Block Copolymers Containing Azobenzene Moieties. *Soft Matter* **2012**, *8*, 3131–3138.

(679) Jin, C.; Zhang, T.; Wang, L.; He, M.; Yuan, T.; Jiang, B.; Xiao, D.; Yin, Q. Photoinduced Deformation of Hollow Nanospheres Formed by the Self-Assembly of Amphiphilic Random Copolymers and Small Azo Molecules. *RSC Adv.* **2014**, *4*, 45890–45894.

(680) Liu, J.; He, Y.; Wang, X. Size-Dependent Light-Driven Effect Observed for Azo Polymer Colloidal Spheres with Different Average Diameters. *Langmuir* **2009**, *25*, 5974–5979.

(681) Huang, H.; Su, Y.; Zhou, X.; Liao, C.; Hsu, C.; Du, Y.; Xu, J.; Wang, X. Shaping Monodispersed Azo Molecular Glass Microspheres Using Polarized Light. *Soft Matter* **2018**, *14*, 5847–5855.

(682) Tang, B.; Zhou, Y.; Xiong, Z.; Wang, X. Photodeformable Microspheres from an Azo Molecule Containing a 1,4,3,6-Dianhydrosorbitol Core and Cinnamate Peripheral Groups. *RSC Adv.* **2016**, *6*, 64203–64207.

(683) Wang, J.; Wang, S.; Zhou, Y.; Wang, X.; He, Y. Fast Photoinduced Large Deformation of Colloidal Spheres from a Novel 4-Arm Azobenzene Compound. *ACS Appl. Mater. Interfaces* **2015**, *7*,

16889–16895.

(684) Kang, H. S.; Lee, S.; Choi, J.; Lee, H.; Park, J.-K.; Kim, H.-T. Light-Induced Surface Patterning of Silica. *ACS Nano* **2015**, *9*, 9837–9848.

(685) Choi, J.; Jo, W.; Lee, S. Y.; Jung, Y. S.; Kim, S.-H.; Kim, H.-T. Flexible and Robust Superomniphobic Surfaces Created by Localized Photofluidization of Azopolymer Pillars. *ACS Nano* **2017**, *11*, 7821–7828.

(686) Pirani, F.; Angelini, A.; Ricciardi, S.; Frascella, F.; Descrovi, E. Laser-Induced Anisotropic Wettability on Azopolymeric Micro-Structures. *Appl. Phys. Lett.* **2017**, *110*, 101603.

(687) Oscurato, S. L.; Borbone, F.; Maddalena, P.; Ambrosio, A. Light-Driven Wettability Tailoring of Azopolymer Surfaces with Reconfigured Three-Dimensional Posts. *ACS Appl. Mater. Interfaces* **2017**, *9*, 30133–30142.

(688) Lee, S.; Kang, H. S.; Ambrosio, A.; Park, J.-K.; Marrucci, L. Directional Superficial Photofluidization for Deterministic Shaping of Complex 3D Architectures. *ACS Appl. Mater. Interfaces* **2015**, *7*, 8209–8217.

(689) Gritsai, Y.; Goldenberg, L. M.; Stumpe, J. Efficient Single-Beam Light Manipulation of 3D Microstructures in Azobenzene-Containing Materials. *Opt. Express* **2011**, *19*, 18687–18695.

(690) Kong, X.; Wang, X.; Luo, T.; Yao, Y.; Li, L.; Lin, S. Photomanipulated Architecture and Patterning of Azopolymer Array. *ACS Appl. Mater. Interfaces* **2017**, *9*, 19345–19353.

(691) Lee, S.; Kang, H. S.; Park, J.-K. High-Resolution Patterning of Various Large-Area, Highly Ordered Structural Motifs by Directional Photofluidization Lithography: Sub-30-Nm Line, Ellipsoid, Rectangle, and Circle Arrays. *Adv. Funct. Mater.* **2011**, *21*, 1770–1778.

(692) Wang, W.; Shen, D.; Li, X.; Yao, Y.; Lin, J.; Wang, A.; Yu, J.; Wang, Z. L.; Hong, S. W.; Lin, Z.; et al. Light-Driven Shape-Memory Porous Films with Precisely Controlled Dimensions. *Angew.*

Chem. Int. Ed. **2018**, *57*, 2139–2143.

(693) Choi, J.; Kang, H. S.; Jo, W.; Kim, S.-H.; Jung, Y. S.; Kim, H.-T. Photo-Reconfigurable Azopolymer Etch Mask: Photofluidization-Driven Reconfiguration and Edge Rectangularization. *Small* **2018**, *14*, 1703250.

(694) Wang, W.; Yao, Y.; Luo, T.; Chen, L.; Lin, J.; Li, L.; Lin, S. Deterministic Reshaping of Breath Figure Arrays by Directional Photomanipulation. *ACS Appl. Mater. Interfaces* **2017**, *9*, 4223–4230.

(695) Wang, W.; Du, C.; Wang, X.; He, X.; Lin, J.; Li, L.; Lin, S. Directional Photomanipulation of Breath Figure Arrays. *Angew. Chem. Int. Ed.* **2014**, *53*, 12116–12119.

(696) Lee, S.-A.; Kang, H. S.; Park, J.-K.; Lee, S. Vertically Oriented, Three-Dimensionally Tapered Deep-Subwavelength Metallic Nanohole Arrays Developed by Photofluidization Lithography. *Adv. Mater.* **2014**, *26*, 7521–7528.

(697) Li, C.; Wang, W.; Wang, X.; Jiang, H.; Zhu, J.; Lin, S. Fabrication of Porous Polymer Microspheres by Tuning Amphiphilicity of the Polymer and Emulsion–Solvent Evaporation Processing. *Eur. Polym. J.* **2015**, *68*, 409–418.

(698) Li, Y.; Tong, X.; He, Y.; Wang, X. Formation of Ordered Mesoporous Films from In Situ Structure Inversion of Azo Polymer Colloidal Arrays. *J. Am. Chem. Soc.* **2006**, *128*, 2220–2221.

(699) Gao, F.; Xing, Y.; Yao, Y.; Sun, L.; Sun, Y.; He, X.; Lin, S. Self-Assembly and Multi-Stimuli Responsive Behavior of PAA- b -PAzoMA- b -PNIPAM Triblock Copolymers. *Polym. Chem.* **2017**, *8*, 7529–7536.

(700) Ichikawa, R.; Nakano, H. Photoinduced Change in Phase-Separated Structure of a Binary Film Composed of 4-[Bis(9,9-Dimethylfluoren-2-Yl)Amino]-4'-Nitroazobenzene and Poly(Vinyl Acetate). *J. Photopolym. Sci. Technol.* **2017**, *30*, 661–665.

(701) Hsu, C.; Du, Y.; Wang, X. Janus and Strawberry-like Particles from Azo Molecular Glass and

Polydimethylsiloxane Oligomer. *Langmuir* **2017**, *33*, 10645–10654.

(702) Zhou, X.; Chen, S.; Liu, B.; Wang, X. Azo-Polymer Janus Particles Assembled by Solvent-Induced Microphase Separation and Their Photoresponsive Behavior. *Chem. Asian J.* **2016**, *11*, 3443–3448.

(703) Zhou, X.; Du, Y.; Wang, X. Azo Polymer Janus Particles Possessing Photodeformable and Magnetic-Field-Responsive Dual Functions. *Chem. Asian J.* **2016**, *11*, 2130–2134.

(704) Zhou, X.; Du, Y.; Wang, X. Azo Polymer Janus Particles and Their Photoinduced, Symmetry-Breaking Deformation. *ACS Macro Lett.* **2016**, *5*, 234–237.

(705) Nakano, H.; Ichikawa, R.; Ukai, H.; Kitano, A. Photoinduced Shape Changes of Mixed Molecular Glass Particles Containing Azobenzene-Based Photochromic Amorphous Molecular Materials Fixed in Agar Gel. *J. Phys. Chem. B* **2018**, *122*, 7775–7781.

(706) Kitano, A.; Ichikawa, R.; Nakano, H. Photomechanical Response Observed for Azobenzene-Based Photochromic Amorphous Molecular Films Fabricated on the Surface of Agar Gel. *Opt. Mater. (Amst).* **2018**, *86*, 51–55.

(707) Ichikawa, R.; Nakano, H. Photoinduced Change in the Shape of Azobenzene-Based Molecular Glass Particles Fixed in Agar Gel. *RSC Adv.* **2016**, *6*, 36761–36765.

(708) Choi, J.; Cho, W.; Jung, Y. S.; Kang, H. S.; Kim, H.-T. Direct Fabrication of Micro/Nano-Patterned Surfaces by Vertical-Directional Photofluidization of Azobenzene Materials. *ACS Nano* **2017**, *11*, 1320–1327.

(709) Gao, F.; Yao, Y.; Wang, W.; Wang, X.; Li, L.; Zhuang, Q.; Lin, S. Light-Driven Transformation of Bio-Inspired Superhydrophobic Structure via Reconfigurable PAzoMA Microarrays: From Lotus Leaf to Rice Leaf. *Macromolecules* **2018**, *51*, 2742–2749.

(710) Jeong, Y. J.; Park, K. J.; Kim, K.; Lee, S.; Yoo, P. J. Uniaxial Alignment of ZnO Nanowires via Light-Induced Directional Migration of Azopolymeric Microspheres. *Polymer* **2018**, *138*, 180–

187.

(711) Li, J.; Chen, L.; Xu, J.; Wang, K.; Wang, X.; He, X.; Dong, H.; Lin, S.; Zhu, J. Photoguided Shape Deformation of Azobenzene-Containing Polymer Microparticles. *Langmuir* **2015**, *31*, 13094–13100.

(712) Kang, H. S.; Kim, H.-T.; Park, J.-K.; Lee, S. Light-Powered Healing of a Wearable Electrical Conductor. *Adv. Funct. Mater.* **2014**, *24*, 7273–7283.

(713) Lee, S.; Shin, J.; Lee, Y.-H.; Fan, S.; Park, J.-K. Directional Photofluidization Lithography for Nanoarchitectures with Controlled Shapes and Sizes. *Nano Lett.* **2010**, *10*, 296–304.

(714) Lee, S.; Shin, J.; Lee, Y.-H.; Park, J.-K. Fabrication of the Funnel-Shaped Three-Dimensional Plasmonic Tip Arrays by Directional Photofluidization Lithography. *ACS Nano* **2010**, *4*, 7175–7184.

(715) Wie, J. J.; Wang, D. H.; Lee, K. M.; White, T. J.; Tan, L.-S. The Contribution of Hydrogen Bonding to the Photomechanical Response of Azobenzene-Functionalized Polyamides. *J. Mater. Chem. C* **2018**, *6*, 5964–5974.

(716) Baczkowski, M. L.; Wang, D. H.; Lee, D. H.; Lee, K. M.; Smith, M. L.; White, T. J.; Tan, L.-S. Photomechanical Deformation of Azobenzene-Functionalized Polyimides Synthesized with Bulky Substituents. *ACS Macro Lett.* **2017**, *6*, 1432–1437.

(717) Wang, D. H.; Wie, J. J.; Lee, K. M.; White, T. J.; Tan, L.-S. Impact of Backbone Rigidity on the Photomechanical Response of Glassy, Azobenzene-Functionalized Polyimides. *Macromolecules* **2014**, *47*, 659–667.

(718) Lee, K. M.; Wang, D. H.; Koerner, H.; Vaia, R. A.; Tan, L.-S.; White, T. J. Enhancement of Photogenerated Mechanical Force in Azobenzene-Functionalized Polyimides. *Angew. Chem. Int. Ed.* **2012**, *51*, 4117–4121.

(719) Wie, J. J.; Chatterjee, S.; Wang, D. H.; Tan, L.-S.; Ravi Shankar, M.; White, T. J. Azobenzene-Functionalized Polyimides as Wireless Actuators. *Polymer* **2014**, *55*, 5915–5923.

(720) Lee, K. M.; Wang, D. H.; Koerner, H.; Vaia, R. A.; Tan, L.-S.; White, T. J. Photomechanical Response of Pre-Strained Azobenzene-Functionalized Polyimide Materials. *Macromol. Chem. Phys.* **2013**, *214*, 1189–1194.

(721) Wang, D. H.; Lee, K. M.; Yu, Z.; Koerner, H.; Vaia, R. A.; White, T. J.; Tan, L.-S. Photomechanical Response of Glassy Azobenzene Polyimide Networks. *Macromolecules* **2011**, *44*, 3840–3846.

(722) Wie, J. J.; Wang, D. H.; Lee, K. M.; Tan, L.-S.; White, T. J. Molecular Engineering of Azobenzene-Functionalized Polyimides To Enhance Both Photomechanical Work and Motion. *Chem. Mater.* **2014**, *26*, 5223–5230.

(723) Skandani, A. A.; Chatterjee, S.; Wang, D. H.; Tan, L.-S.; White, T. J.; Shankar, M. R.; Smith, M. L. Relaxation Dynamics and Strain Persistency of Azobenzene-Functionalized Polymers and Actuators. *Macromol. Mater. Eng.* **2017**, *302*, 1700256.

(724) Lee, B. K. M.; Koerner, H.; Wang, D. H.; Tan, L.-S.; White, T. J.; Vaia, R. A. Tailoring the Photomechanical Response of Glassy, Azobenzene-Functionalized Polyimides by Physical Aging. *Macromolecules* **2012**, *45*, 7527–7534.

(725) Wie, J. J.; Wang, D. H.; Tondiglia, V. P.; Tabiryan, N. V.; Vergara-Toloza, R. O.; Tan, L.-S.; White, T. J. Photopiezoelectric Composites of Azobenzene-Functionalized Polyimides and Polyvinylidene Fluoride. *Macromol. Rapid Commun.* **2014**, *35*, 2050–2056.

(726) Nakano, H. Direction Control of Photomechanical Bending of a Photochromic Molecular Fiber. *J. Mater. Chem.* **2010**, *20*, 2071–2074.

(727) Nakano, H.; Suzuki, M. Photoinduced Mass Flow of Photochromic Molecular Materials. *J. Mater.*

Chem. **2012**, *22*, 3702–3704.

(728) Suzuki, M.; Nakano, H. Moving Fragments of Photochromic Molecular Glass of 4-[Bis(9,9-Dimethylfluoren-2-Yl)Amino]-4^|^rsquo;-Cyanoazobenzene. *J. Photopolym. Sci. Technol.* **2012**, *25*, 159–160.

(729) Merian, E. Steric Factors Influencing the Dyeing of Hydrophobic. Fibers. *Text. Res. J.* **1966**, *36*, 612–618.

(730) Husy, H.; Merian, E.; Schetty, G. Steric Factors Influencing the Dyeing of Hydrophobic Fibers. *Text. Res. J.* **1969**, *39*, 94–94.

(731) Blair, H. S.; Law, T.-K. Photocontractile Effects in Nylon-6,6 Films Containing β-Carotene, and 4-Nitro-4′-Hydroxy-α-Cyanostilbene. *Polymer* **1980**, *21*, 1475–1476.

(732) Wen, H.; Zhang, W.; Weng, Y.; Hu, Z. Photomechanical Bending of Linear Azobenzene Polymer. *RSC Adv.* **2014**, *4*, 11776–11781.

(733) Li, S.; Han, G.; Zhang, W. Concise Synthesis of Photoresponsive Polyureas Containing Bridged Azobenzenes as Visible-Light-Driven Actuators and Reversible Photopatterning. *Macromolecules* **2018**, *51*, 4290–4297.

(734) Athanassiou, A.; Kalyva, M.; Lakiotaki, K.; Georgiou, S.; Fotakis, C. All-Optical Reversible Actuation of Photochromic-Polymer Microsystems. *Adv. Mater.* **2005**, *17*, 988–992.

(735) Athanassiou, A.; Lakiotaki, K.; Kalyva, M.; Georgiou, S.; Fotakis, C. Photoswitches Operating upon Ns Pulsed Laser Irradiation. *Appl. Surf. Sci.* **2005**, *248*, 56–61.

(736) Athanassiou, A.; Kalyva, M.; Lakiotaki, K.; Fotakis, C. Laser Controlled Mechanical Actuation of Photochromic-Polymer Microsystems. *Rev. Adv. Mater. Sci.* **2003**, *5*, 245–251.

(737) Mahimwalla, Z. S.; Ngai, Y.; Barrett, C. J. Photomechanical Effect of Azobenzene Thin Polymer

Films Measured with an AFM Cantilever Based Sensor. In *Proc. SPIE 7712, Nanophotonics III*; Andrews, D. L., Nunzi, J.-M., Ostendorf, A., Eds.; 2010; p 771217.

(738) Kim, H.-K.; Wang, X.-S.; Fujita, Y.; Sudo, A.; Nishida, H.; Fujii, M.; Endo, T. A Rapid Photomechanical Switching Polymer Blend System Composed of Azobenzene-Carrying Poly(Vinylether) and Poly(Carbonate). *Polymer* **2005**, *46*, 5879–5883.

(739) Tanaka, S.; Kim, H.-K.; Sudo, A.; Nishida, H.; Endo, T. Anisotropic Photomechanical Response of Stretched Blend Film Made of Polycaprolactone-Polyvinyl Ether with Azobenzene Group as Side Chain. *Macromol. Chem. Phys.* **2008**, *209*, 2071–2077.

(740) Li, S.; Tu, Y.; Bai, H.; Hibi, Y.; Wiesner, L. W.; Pan, W.; Wang, K.; Giannelis, E. P.; Shepherd, R. F. Simple Synthesis of Elastomeric Photomechanical Switches That Self-Heal. *Macromol. Rapid Commun.* **2019**, *40*, 1800815.

(741) Xiong, Y.; Zhang, L.; Weis, P.; Naumov, P.; Wu, S. A Solar Actuator Based on Hydrogen-Bonded Azopolymers for Electricity Generation. *J. Mater. Chem. A* **2018**, *6*, 3361–3366.

(742) Zhang, L.; Naumov, P. Light- and Humidity-Induced Motion of an Acidochromic Film. *Angew. Chem. Int. Ed.* **2015**, *54*, 8642–8647.

(743) Zhang, L.; Liang, H.; Jacob, J.; Naumov, P. Photogated Humidity-Driven Motility. *Nat. Commun.* **2015**, *6*, 7429.

(744) Shang, J.; Lin, S.; Theato, P. UV-Triggered Shape-Controllable PP Fabric. *Polym. Chem.* **2018**, *9*, 3232–3237.

(745) Zhou, L.; Liu, Q.; Lv, X.; Gao, L.; Fang, S.; Yu, H. Photoinduced Triple Shape Memory Polyurethane Enabled by Doping with Azobenzene and GO. *J. Mater. Chem. C* **2016**, *4*, 9993–9997.

(746) Bian, S.; Robinson, D.; Kuzyk, M. G. Optically Activated Cantilever Using Photomechanical

Effects in Dye-Doped Polymer Fibers. *J. Opt. Soc. Am. B* **2006**, *23*, 697.

(747) Kuzyk, M. G.; Bian, S.; Robinson, D. An All-Optical Polymer Fiber Cantilever. In *Proc. SPIE 6331, Linear and Nonlinear Optics of Organic Materials VI*; Norwood, R. A., Ed.; 2006; p 63310T.

(748) Han, G.; Nie, J.; Zhang, H. Facile Preparation of Recyclable Photodeformable Azobenzene Polymer Fibers with Chemically Crosslinked Networks. *Polym. Chem.* **2016**, *7*, 5088–5092.

(749) Kim, H.-K.; Wang, X.-S.; Fujita, Y.; Sudo, A.; Nishida, H.; Fujii, M.; Endo, T. Photomechanical Switching Behavior of Semi-Interpenetrating Polymer Network Consisting of Azobenzene-Carrying Crosslinked Poly(Vinyl Ether) and Polycarbonate. *Macromol. Rapid Commun.* **2005**, *26*, 1032–1036.

(750) Kim, H.-K.; Wang, X.-S.; Fujita, Y.; Sudo, A.; Nishida, H.; Fujii, M.; Endo, T. Reversible Photo-Mechanical Switching Behavior of Azobenzene-Containing Semi-Interpenetrating Network under UV and Visible Light Irradiation. *Macromol. Chem. Phys.* **2005**, *206*, 2106–2111.

(751) Phua, D. I.; Herman, K.; Balaceanu, A.; Zakrevski, J.; Pich, A. Reversible Size Modulation of Aqueous Microgels via Orthogonal or Combined Application of Thermo- and Phototriggers. *Langmuir* **2016**, *32*, 3867–3879.

(752) Liu, J.; Nie, J.; Zhao, Y.; He, Y. Preparation and Properties of Different Photoresponsive Hydrogels Modulated with UV and Visible Light Irradiation. *J. Photochem. Photobiol. A Chem.* **2010**, *211*, 20–25.

(753) Karmalkar, R. N.; Premnath, V.; Kulkarni, M. G.; Mashelkar, R. A. Switching Biomimetic Hydrogels. *Proc. R. Soc. A Math. Phys. Eng. Sci.* **2000**, *456*, 1305–1320.

(754) Ishihara, K.; Hamada, N.; Kato, S.; Shinohara, I. Photoinduced Swelling Control of Amphiphilic Azoaromatic Polymer Membrane. *J. Polym. Sci. Polym. Chem. Ed.* **1984**, *22*, 121–128.

(755) Zhang, Q. M.; Li, X.; Islam, M. R.; Wei, M.; Serpe, M. J. Light Switchable Optical Materials from

Azobenzene Crosslinked Poly(N -Isopropylacrylamide)-Based Microgels. *J. Mater. Chem. C* **2014**, *2*, 6961–6965.

(756) Zakrevskyy, Y.; Richter, M.; Zakrevska, S.; Lomadze, N.; von Klitzing, R.; Santer, S. Light-Controlled Reversible Manipulation of Microgel Particle Size Using Azobenzene-Containing Surfactant. *Adv. Funct. Mater.* **2012**, *22*, 5000–5009.

(757) Abraham, G.; Purushothaman, E. Synthesis and Photostimulated Dilation Changes of Polymers with Azobenzene Cross-Links. *Indian J. Chem. Technol.* **1998**, *5*, 213–216.

(758) Montagna, M.; Guskova, O. Photosensitive Cationic Azobenzene Surfactants: Thermodynamics of Hydration and the Complex Formation with Poly(Methacrylic Acid). *Langmuir* **2018**, *34*, 311–321.

(759) Schimka, S.; Lomadze, N.; Rabe, M.; Kopyshev, A.; Lehmann, M.; von Klitzing, R.; Rumyantsev, A. M.; Kramarenko, E. Y.; Santer, S. Photosensitive Microgels Containing Azobenzene Surfactants of Different Charges. *Phys. Chem. Chem. Phys.* **2017**, *19*, 108–117.

(760) Schimka, S.; Gordievskaya, Y. D.; Lomadze, N.; Lehmann, M.; von Klitzing, R.; Rumyantsev, A. M.; Kramarenko, E. Y.; Santer, S. Communication: Light Driven Remote Control of Microgels' Size in the Presence of Photosensitive Surfactant: Complete Phase Diagram. *J. Chem. Phys.* **2017**, *147*, 031101.

(761) Hosono, N.; Yoshikawa, M.; Furukawa, H.; Totani, K.; Yamada, K.; Watanabe, T.; Horie, K. Photoinduced Deformation of Rigid Azobenzene-Containing Polymer Networks. *Macromolecules* **2013**, *46*, 1017–1026.

(762) Kulawardana, E. U.; Kuruwita-Mudiyanselage, T.; Neckers, D. C. Dual Responsive Poly(N -Isopropylacrylamide) Hydrogels Having Spironaphthoxazines as Pendant Groups. *J. Polym. Sci. Part A Polym. Chem.* **2009**, *47*, 3318–3325.

(763) Mudiyanselage, T. K.; Neckers, D. C. Photochromic Superabsorbent Polymers. *Soft Matter* **2008**, *4*, 768–774.

(764) Sun, Z.; Liu, S.; Li, K.; Tan, L.; Cen, L.; Fu, G. Well-Defined and Biocompatible Hydrogels with Toughening and Reversible Photoresponsive Properties. *Soft Matter* **2016**, *12*, 2192–2199.

(765) Satoh, T.; Sumaru, K.; Takagi, T.; Kanamori, T. Fast-Reversible Light-Driven Hydrogels Consisting of Spirobenzopyran-Functionalized Poly(N-Isopropylacrylamide). *Soft Matter* **2011**, *7*, 8030–8034.

(766) Edahiro, J.; Sumaru, K.; Takagi, T.; Shinbo, T.; Kanamori, T.; Sudoh, M. Analysis of Photo-Induced Hydration of a Photochromic Poly(N-Isopropylacrylamide) – Spiropyran Copolymer Thin Layer by Quartz Crystal Microbalance. *Eur. Polym. J.* **2008**, *44*, 300–307.

(767) Sumaru, K.; Ohi, K.; Takagi, T.; Kanamori, T.; Shinbo, T. Photoresponsive Properties of Poly(N-Isopropylacrylamide) Hydrogel Partly Modified with Spirobenzopyran. *Langmuir* **2006**, *22*, 4353–4356.

(768) Filipcsei, G.; Sumaru, K.; Takagi, T.; Kanamori, T.; Zrinyi, M. Swelling Degree and Shape Change of Photo- and Thermo-Response of Spirobenzopyran-Functionalized Porous PNIPAAm Hydrogels. *J. Mol. Liq.* **2014**, *189*, 63–67.

(769) Ziółkowski, B.; Florea, L.; Theobald, J.; Benito-Lopez, F.; Diamond, D. Porous Self-Protonating Spiropyran-Based NIPAAm Gels with Improved Reswelling Kinetics. *J. Mater. Sci.* **2016**, *51*, 1392–1399.

(770) Dunne, A.; Delaney, C.; Florea, L.; Diamond, D. Solvato-Morphologically Controlled, Reversible NIPAAm Hydrogel Photoactuators. *RSC Adv.* **2016**, *6*, 83296–83302.

(771) Francis, W.; Dunne, A.; Delaney, C.; Florea, L.; Diamond, D. Spiropyran Based Hydrogels Actuators—Walking in the Light. *Sensors Actuators B Chem.* **2017**, *250*, 608–616.

(772) ter Schiphorst, J.; Coleman, S.; Stumpel, J. E.; Ben Azouz, A.; Diamond, D.; Schenning, A. P. H. J. Molecular Design of Light-Responsive Hydrogels, For in Situ Generation of Fast and Reversible Valves for Microfluidic Applications. *Chem. Mater.* **2015**, *27*, 5925–5931.

(773) Ziółkowski, B.; Florea, L.; Theobald, J.; Benito-Lopez, F.; Diamond, D. Self-Protonating Spiropyran-Co-NIPAM-Co-Acrylic Acid Hydrogel Photoactuators. *Soft Matter* **2013**, *9*, 8754–8760.

(774) Saez, J.; Glennon, T.; Czugala, M.; Tudor, A.; Ducreé, J.; Diamond, D.; Florea, L.; Benito-Lopez, F. Reusable Ionogel-Based Photo-Actuators in a Lab-on-a-Disc. *Sensors Actuators B Chem.* **2018**, *257*, 963–970.

(775) Czugala, M.; O'Connell, C.; Blin, C.; Fischer, P.; Fraser, K. J.; Benito-Lopez, F.; Diamond, D. Swelling and Shrinking Behaviour of Photoresponsive Phosphonium-Based Ionogel Microstructures. *Sensors Actuators B Chem.* **2014**, *194*, 105–113.

(776) Byrne, R.; Ventura, C.; Benito Lopez, F.; Walther, A.; Heise, A.; Diamond, D. Characterisation and Analytical Potential of a Photo-Responsive Polymeric Material Based on Spiropyran. *Biosens. Bioelectron.* **2010**, *26*, 1392–1398.

(777) Benito-Lopez, F.; Byrne, R.; Răduţă, A. M.; Vrana, N. E.; McGuinness, G.; Diamond, D. Ionogel-Based Light-Actuated Valves for Controlling Liquid Flow in Micro-Fluidic Manifolds. *Lab Chip* **2010**, *10*, 195–201.

(778) Lei, Z.; Chen, B.; Koo, Y.-M.; MacFarlane, D. R. Introduction: Ionic Liquids. *Chem. Rev.* **2017**, *117*, 6633–6635.

(779) ter Schiphorst, J.; Melpignano, G. G.; Amirabadi, H. E.; Houben, M. H. J. M.; Bakker, S.; den Toonder, J. M. J.; Schenning, A. P. H. J. Photoresponsive Passive Micromixers Based on Spiropyran Size-Tunable Hydrogels. *Macromol. Rapid Commun.* **2018**, *39*, 1700086.

(780) Delaney, C.; McCluskey, P.; Coleman, S.; Whyte, J.; Kent, N.; Diamond, D. Precision Control of Flow Rate in Microfluidic Channels Using Photoresponsive Soft Polymer Actuators. *Lab Chip* **2017**, *17*, 2013–2021.

(781) Coleman, S.; ter Schiphorst, J.; Ben Azouz, A.; Bakker, S.; Schenning, A. P. H. J.; Diamond, D. Tuning Microfluidic Flow by Pulsed Light Oscillating Spiropyran-Based Polymer Hydrogel Valves. *Sensors Actuators B Chem.* **2017**, *245*, 81–86.

(782) Czugala, M.; Fay, C.; O'Connor, N. E.; Corcoran, B.; Benito-Lopez, F.; Diamond, D. Portable Integrated Microfluidic Analytical Platform for the Monitoring and Detection of Nitrite. *Talanta* **2013**, *116*, 997–1004.

(783) Sugiura, S.; Szilágyi, A.; Sumaru, K.; Hattori, K.; Takagi, T.; Filipcsei, G.; Zrínyi, M.; Kanamori, T. On-Demand Microfluidic Control by Micropatterned Light Irradiation of a Photoresponsive Hydrogel Sheet. *Lab Chip* **2009**, *9*, 196–198.

(784) Sugiura, S.; Sumaru, K.; Ohi, K.; Hiroki, K.; Takagi, T.; Kanamori, T. Photoresponsive Polymer Gel Microvalves Controlled by Local Light Irradiation. *Sensors Actuators A Phys.* **2007**, *140*, 176–184.

(785) ter Schiphorst, J.; van den Broek, M.; de Koning, T.; Murphy, J. N.; Schenning, A. P. H. J.; Esteves, A. C. C. Dual Light and Temperature Responsive Cotton Fabric Functionalized with a Surface-Grafted Spiropyran–NIPAAm-Hydrogel. *J. Mater. Chem. A* **2016**, *4*, 8676–8681.

(786) Xuan, C.; Jin, L. Concurrent Reaction and Diffusion in Photo-Responsive Hydrogels. *J. Mech. Phys. Solids* **2019**, *124*, 599–611.

(787) Dehghany, M.; Zhang, H.; Naghdabadi, R.; Hu, Y. A Thermodynamically-Consistent Large Deformation Theory Coupling Photochemical Reaction and Electrochemistry for Light-Responsive Gels. *J. Mech. Phys. Solids* **2018**, *116*, 239–266.

(788) Kuksenok, O.; Balazs, A. C. Modeling the Photoinduced Reconfiguration and Directed Motion of Polymer Gels. *Adv. Funct. Mater.* **2013**, *23*, 4601–4610.

(789) Singh, A.; Kuksenok, O.; Balazs, A. C. Embedding Flexible Fibers into Responsive Gels to Create Composites with Controllable Dexterity. *Soft Matter* **2016**, *12*, 9170–9184.

(790) Kuksenok, O.; Balazs, A. C. Designing Dual-Functionalized Gels for Self-Reconfiguration and Autonomous Motion. *Sci. Rep.* **2015**, *5*, 9569.

(791) Masoud, H.; Bingham, B. I.; Alexeev, A. Designing Maneuverable Micro-Swimmers Actuated by Responsive Gel. *Soft Matter* **2012**, *8*, 8944–8951.

(792) Li, S.; Feng, Y.; Wang, W.; Ji, T.; Han, J.; Long, P.; Cao, C.; Feng, W. Polarization-Induced Alignment of Azobenzene/Fluorinated Polyimide for Three-Dimensional Shape-Persistent and Photo-Responsive Elastic Helixes. *Compos. Sci. Technol.* **2019**, *169*, 158–166.

(793) Qin, C.; Feng, Y.; An, H.; Han, J.; Cao, C.; Feng, W. Tetracarboxylated Azobenzene/Polymer Supramolecular Assemblies as High-Performance Multiresponsive Actuators. *ACS Appl. Mater. Interfaces* **2017**, *9*, 4066–4073.

(794) Qin, C.; Feng, Y.; Luo, W.; Cao, C.; Hu, W.; Feng, W. A Supramolecular Assembly of Cross-Linked Azobenzene/Polymers for a High-Performance Light-Driven Actuator. *J. Mater. Chem. A* **2015**, *3*, 16453–16460.

(795) Si, Q.; Feng, Y.; Yang, W.; Fu, L.; Yan, Q.; Dong, L.; Long, P.; Feng, W. Controllable and Stable Deformation of a Self-Healing Photo-Responsive Supramolecular Assembly for an Optically Actuated Manipulator Arm. *ACS Appl. Mater. Interfaces* **2018**, *10*, 29909–29917.

(796) Pan, M.; Yuan, Q.-J.; Gong, X.-L.; Zhang, S.; Li, B.-J. A Tri-Stimuli-Responsive Shape-Memory Material Using Host-Guest Interactions as Molecular Switches. *Macromol. Rapid Commun.* **2016**, *37*, 433–438.

(797) Zhang, Y.; Ma, Y.; Sun, J. Reversible Actuation of Polyelectrolyte Films: Expansion-Induced Mechanical Force Enables Cis–Trans Isomerization of Azobenzenes. *Langmuir* **2013**, *29*, 14919–14925.

(798) Finkelmann, H.; Nishikawa, E.; Pereira, G. G.; Warner, M. A New Opto-Mechanical Effect in Solids. *Phys. Rev. Lett.* **2001**, *87*, 1–4.

(799) Wei, J.; Yu, Y. Photodeformable Polymer Gels and Crosslinked Liquid-Crystalline Polymers. *Soft Matter* **2012**, *8*, 8050–8059.

(800) Mamiya, J. Photomechanical Energy Conversion Based on Cross-Linked Liquid-Crystalline Polymers. *Polym. J.* **2013**, *45*, 239–246.

(801) Ube, T.; Ikeda, T. Photomobile Polymer Materials with Crosslinked Liquid-Crystalline Structures: Molecular Design, Fabrication, and Functions. *Angew. Chem. Int. Ed.* **2014**, *53*, 10290–10299.

(802) Priimagi, A.; Barrett, C. J.; Shishido, A. Recent Twists in Photoactuation and Photoalignment Control. *J. Mater. Chem. C* **2014**, *2*, 7155–7162.

(803) Hogan, P. M.; Tajbakhsh, A. R.; Terentjev, E. M. Uv Manipulation of Order and Macroscopic Shape in Nematic Elastomers. *Phys. Rev. E* **2002**, *65*, 10.

(804) Qing, X.; Qin, L.; Gu, W.; Yu, Y. Deformation of Cross-Linked Liquid Crystal Polymers by Light – from Ultraviolet to Visible and Infrared. *Liq. Cryst.* **2016**, *43*, 2114–2135.

(805) Bushuyev, O. S.; Aizawa, M.; Shishido, A.; Barrett, C. J. Shape-Shifting Azo Dye Polymers: Towards Sunlight-Driven Molecular Devices. *Macromol. Rapid Commun.* **2018**, *39*, 1700253.

(806) Bisoyi, H. K.; Li, Q. Light-Driven Liquid Crystalline Materials: From Photo-Induced Phase Transitions and Property Modulations to Applications. *Chem. Rev.* **2016**, *116*, 15089–15166.

(807) Jiang, H.; Kelch, S.; Lendlein, A. Polymers Move in Response to Light. *Adv. Mater.* **2006**, *18*,

1471–1475.

(808) Barrett, C. J.; Mamiya, J.; Yager, K. G.; Ikeda, T. Photo-Mechanical Effects in Azobenzene-Containing Soft Materials. *Soft Matter* **2007**, *3*, 1249–1261.

(809) Ikeda, T.; Mamiya, J.; Yu, Y. Photomechanics of Liquid-Crystalline Elastomers and Other Polymers. *Angew. Chem. Int. Ed.* **2007**, *46*, 506–528.

(810) Yu, H.; Ikeda, T. Photocontrollable Liquid-Crystalline Actuators. *Adv. Mater.* **2011**, *23*, 2149–2180.

(811) Fang, L.; Han, G.; Zhang, J.; Zhang, H.; Zhang, H. Synthesis of Well-Defined Easily Crosslinkable Azobenzene Side-Chain Liquid Crystalline Polymers via Reversible Addition–Fragmentation Chain Transfer Polymerization and Photomechanical Properties of Their Post-Crosslinked Fibers. *Eur. Polym. J.* **2015**, *69*, 592–604.

(812) Fang, L.; Zhang, H.; Li, Z.; Zhang, Y.; Zhang, Y.; Zhang, H. Synthesis of Reactive Azobenzene Main-Chain Liquid Crystalline Polymers via Michael Addition Polymerization and Photomechanical Effects of Their Supramolecular Hydrogen-Bonded Fibers. *Macromolecules* **2013**, *46*, 7650–7660.

(813) Kondo, M.; Yu, Y.; Ikeda, T. How Does the Initial Alignment of Mesogens Affect the Photoinduced Bending Behavior of Liquid-Crystalline Elastomers? *Angew. Chem. Int. Ed.* **2006**, *45*, 1378–1382.

(814) Lv, J.; Wang, W.; Xu, J.; Ikeda, T.; Yu, Y. Photoinduced Bending Behavior of Cross-Linked Azobenzene Liquid-Crystalline Polymer Films with a Poly(Oxyethylene) Backbone. *Macromol. Rapid Commun.* **2014**, *35*, 1266–1272.

(815) White, T. J.; Broer, D. J. Programmable and Adaptive Mechanics with Liquid Crystal Polymer Networks and Elastomers. *Nat. Mater.* **2015**, *14*, 1087–1098.

(816) Kondo, M.; Mamiya, J.; Kinoshita, M.; Ikeda, T.; Yu, Y. Photoinduced Deformation Behavior of Crosslinked Azobenzene Liquid-Crystalline Polymer Films with Unimorph and Bimorph Structure. *Mol. Cryst. Liq. Cryst.* **2007**, *478*, 245/[1001]-257/[1013].

(817) Gelebart, A. H.; Jan Mulder, D.; Varga, M.; Konya, A.; Vantomme, G.; Meijer, E. W.; Selinger, R. L. B.; Broer, D. J. Making Waves in a Photoactive Polymer Film. *Nature* **2017**, *546*, 632–636.

(818) Kumar, K.; Knie, C.; Bléger, D.; Peletier, M. A.; Friedrich, H.; Hecht, S.; Broer, D. J.; Debije, M. G.; Schenning, A. P. H. J. A Chaotic Self-Oscillating Sunlight-Driven Polymer Actuator. *Nat. Commun.* **2016**, *7*, 11975.

(819) Wani, O. M.; Zeng, H.; Wasylczyk, P.; Priimagi, A. Programming Photoresponse in Liquid Crystal Polymer Actuators with Laser Projector. *Adv. Opt. Mater.* **2018**, *6*, 1700949.

(820) Iamsaard, S.; Anger, E.; Aßhoff, S. J.; Depauw, A.; Fletcher, S. P.; Katsonis, N. Fluorinated Azobenzenes for Shape-Persistent Liquid Crystal Polymer Networks. *Angew. Chem. Int. Ed.* **2016**, *55*, 9908–9912.

(821) Yu, Y.; Nakano, M.; Ikeda, T. Directed Bending of a Polymer Film by Light. *Nature* **2003**, *425*, 145–145.

(822) Yu, Y.; Nakano, M.; Ikeda, T. Photoinduced Bending and Unbending Behavior of Liquid-Crystalline Gels and Elastomers. *Pure Appl. Chem.* **2004**, *76*, 1467–1477.

(823) Yu, Y.; Nakano, M.; Shishido, A.; Shiono, T.; Ikeda, T. Effect of Cross-Linking Density on Photoinduced Bending Behavior of Oriented Liquid-Crystalline Network Films Containing Azobenzene. *Chem. Mater.* **2004**, *16*, 1637–1643.

(824) Yu, Y.; Nakano, M.; Maeda, T.; Kondo, M.; Ikeda, T. Precisely Direction-Controllable Bending of Cross-Linked Liquid-Crystalline Polymer Films by Light. *Mol. Cryst. Liq. Cryst.* **2005**, *436*, 281/[1235]-290/[1244].

(825) Ikeda, T.; Nakano, M.; Yu, Y.; Tsutsumi, O.; Kanazawa, A. Anisotropic Bending and Unbending Behavior of Azobenzene Liquid-Crystalline Gels by Light Exposure. *Adv. Mater.* **2003**, *15*, 201–205.

(826) Yu, H.; Dong, C.; Zhou, W.; Kobayashi, T.; Yang, H. Wrinkled Liquid-Crystalline Microparticle-Enhanced Photoresponse of PDLC-like Films by Coupling with Mechanical Stretching. *Small* **2011**, *7*, 3039–3045.

(827) Braun, L. B.; Hessberger, T.; Pütz, E.; Müller, C.; Giesselmann, F.; Serra, C. A.; Zentel, R. Actuating Thermo- and Photo-Responsive Tubes from Liquid Crystalline Elastomers. *J. Mater. Chem. C* **2018**, *6*, 9093–9101.

(828) Yu, Y.; Ikeda, T. Photodeformable Polymers: A New Kind of Promising Smart Material for Micro- and Nano-Applications. *Macromol. Chem. Phys.* **2005**, *206*, 1705–1708.

(829) White, T. J.; Serak, S. V.; Tabiryan, N. V.; Vaia, R. A.; Bunning, T. J. Polarization-Controlled, Photodriven Bending in Monodomain Liquid Crystal Elastomer Cantilevers. *J. Mater. Chem.* **2009**, *19*, 1080–1085.

(830) Tabiryan, N.; Serak, S.; Dai, X.-M.; Bunning, T. Polymer Film with Optically Controlled Form and Actuation. *Opt. Express* **2005**, *13*, 7442–7448.

(831) Lee, K. M.; Tabiryan, N. V.; Bunning, T. J.; White, T. J. Photomechanical Mechanism and Structure-Property Considerations in the Generation of Photomechanical Work in Glassy, Azobenzene Liquid Crystal Polymer Networks. *J. Mater. Chem.* **2012**, *22*, 691–698.

(832) Lee, K. M.; White, T. J. Photochemical Mechanism and Photothermal Considerations in the Mechanical Response of Monodomain, Azobenzene-Functionalized Liquid Crystal Polymer Networks. *Macromolecules* **2012**, *45*, 7163–7170.

(833) Lv, J.; Wang, W.; Wu, W.; Yu, Y. A Reactive Azobenzene Liquid-Crystalline Block Copolymer

as a Promising Material for Practical Application of Light-Driven Soft Actuators. *J. Mater. Chem. C* **2015**, *3*, 6621–6626.

(834) Iamsaard, S.; Aßhoff, S. J.; Matt, B.; Kudernac, T.; Cornelissen, J. J. L. M.; Fletcher, S. P.; Katsonis, N. Conversion of Light into Macroscopic Helical Motion. *Nat. Chem.* **2014**, *6*, 229–235.

(835) Iamsaard, S.; Villemin, E.; Lancia, F.; Aβhoff, S.-J.; Fletcher, S. P.; Katsonis, N. Preparation of Biomimetic Photoresponsive Polymer Springs. *Nat. Protoc.* **2016**, *11*, 1788–1797.

(836) Kondo, M.; Sugimoto, M.; Yamada, M.; Naka, Y.; Mamiya, J. I.; Kinoshita, M.; Shishido, A.; Yu, Y.; Ikeda, T. Effect of Concentration of Photoactive Chromophores on Photomechanical Properties of Crosslinked Azobenzene Liquid-Crystalline Polymers. *J. Mater. Chem.* **2010**, *20*, 117–122.

(837) Lee, K. M.; Koerner, H.; Vaia, R. A.; Bunning, T. J.; White, T. J. Relationship between the Photomechanical Response and the Thermomechanical Properties of Azobenzene Liquid Crystalline Polymer Networks. *Macromolecules* **2010**, *43*, 8185–8190.

(838) Fang, L.; Zhang, H. H.; Li, Z.; Zhang, Y. Y.; Zhang, Y. Y.; Zhang, H. H. Synthesis of Reactive Azobenzene Main-Chain Liquid Crystalline Polymers via Michael Addition Polymerization and Photomechanical Effects of Their Supramolecular Hydrogen-Bonded Fibers. *Macromolecules* **2013**, *46*, 7650–7660.

(839) Mamiya, J.; Yoshitake, A.; Kondo, M.; Yu, Y.; Ikeda, T. Is Chemical Crosslinking Necessary for the Photoinduced Bending of Polymer Films? *J. Mater. Chem.* **2008**, *18*, 63–65.

(840) Liao, J.; Yang, M.; Liu, Z.; Zhang, H. Fast Photoinduced Deformation of Hydrogen-Bonded Supramolecular Polymers Containing α-Cyanostilbene Derivative. *J. Mater. Chem. A* **2019**, *7*, 2002–2008.

(841) Deng, W.; Li, M.-H.; Wang, X.; Keller, P. Light-Responsive Wires from Side-on Liquid Crystalline Azo Polymers. *Liq. Cryst.* **2009**, *36*, 1023–1029.

(842) Hosono, N.; Kajitani, T.; Fukushima, T.; Ito, K.; Sasaki, S.; Takata, M.; Aida, T. Large-Area Three-Dimensional Molecular Ordering of a Polymer Brush by One-Step Processing. *Science* **2010**, *330*, 808–811.

(843) Priimagi, A.; Shimamura, A.; Kondo, M.; Hiraoka, T.; Kubo, S.; Mamiya, J.-I.; Kinoshita, M.; Ikeda, T.; Shishido, A. Location of the Azobenzene Moieties within the Cross-Linked Liquid-Crystalline Polymers Can Dictate the Direction of Photoinduced Bending. *ACS Macro Lett.* **2012**, *1*, 96–99.

(844) Cheng, Z.; Ma, S.; Zhang, Y.; Huang, S.; Chen, Y.; Yu, H. Photomechanical Motion of Liquid-Crystalline Fibers Bending Away from a Light Source. *Macromolecules* **2017**, *50*, 8317–8324.

(845) Zhang, Y.; Xu, J.; Cheng, F.; Yin, R.; Yen, C.-C.; Yu, Y. Photoinduced Bending Behavior of Crosslinked Liquid-Crystalline Polymer Films with a Long Spacer. *J. Mater. Chem.* **2010**, *20*, 7123–7130.

(846) van Oosten, C. L.; Harris, K. D.; Bastiaansen, C. W. M.; Broer, D. J. Glassy Photomechanical Liquid-Crystal Network Actuators for Microscale Devices. *Eur. Phys. J. E* **2007**, *23*, 329–336.

(847) Chung, H.; Choi, J.; Yun, J.-H.; Cho, M. Light and Thermal Responses of Liquid-Crystal-Network Films: A Finite Element Study. *Phys. Rev. E* **2015**, *91*, 042503.

(848) Dunn, M. L. Photomechanics of Mono- and Polydomain Liquid Crystal Elastomer Films. *J. Appl. Phys.* **2007**, *102*, 013506.

(849) Wang, H.; Lee, K. M.; White, T. J.; Oates, W. S. Trans-Cis and Trans-Cis-Trans Microstructure Evolution of Azobenzene Liquid-Crystal Polymer Networks. *Macromol. Theory Simulations* **2012**, *21*, 285–301.

(850) Oates, W. S.; Bin, J. Thermodynamics and Nonlinear Mechanics of Materials with Photoresponsive Microstructure. In *Proc. SPIE 9058, Behavior and Mechanics of Multifunctional Materials and*

Composites; Goulbourne, N. C., Naguib, H. E., Eds.; 2014; p 90580Y.

(851) Li, C.; Moon, J.; Yun, J.-H.; Kim, H.; Cho, M. Influence of External Loads on Structure and Photoactuation in Densely Crosslinked Azo-Incorporated Liquid Crystalline Polymers. *Polymer* **2017**, *129*, 252–260.

(852) Yun, J.-H.; Li, C.; Chung, H.; Choi, J.; Cho, M. Photo Deformation in Azobenzene Liquid-Crystal Network: Multiscale Model Prediction and Its Validation. *Polymer* **2015**, *75*, 51–56.

(853) Toshchevikov, V. P.; Saphiannikova Grenzer, M.; Heinrich, G. Effects of the Liquid-Crystalline Order on the Light-Induced Deformation of Azobenzene Elastomers. In *Proc. SPIE 8545, Optical Materials and Biomaterials in Security and Defence Systems Technology IX*; Zamboni, R., Kajzar, F., Szep, A. A., Eds.; 2012; p 854507.

(854) Toshchevikov, V.; Saphiannikova, M. Theory of Light-Induced Deformation of Azobenzene Elastomers: Effects of the Liquid-Crystalline Interactions and Biaxiality. *J. Phys. Chem. B* **2014**, *118*, 12297–12309.

(855) Petrova, T.; Toshchevikov, V.; Saphiannikova, M. Light-Induced Deformation of Polymer Networks Containing Azobenzene Chromophores and Liquid Crystalline Mesogens. *Soft Matter* **2015**, *11*, 3412–3423.

(856) Corbett, D.; Warner, M. Nonlinear Photoresponse of Disordered Elastomers. *Phys. Rev. Lett.* **2006**, *96*, 237802.

(857) Van Oosten, C. L.; Corbett, D.; Davies, D.; Warner, M.; Bastiaansen, C. W. M.; Broer, D. J. Bending Dynamics and Directionality Reversal in Liquid Crystal Network Photoactuators. *Macromolecules* **2008**, *41*, 8592–8596.

(858) Yun, J.-H.; Li, C.; Chung, H.; Choi, J.; Cho, M. Multiscale Modeling and Its Validation of the Trans-Cis-Trans Reorientation-Based Photodeformation in Azobenzene-Doped Liquid Crystal

Polymer. *Int. J. Solids Struct.* **2017**, *128*, 36–49.

(859) Hrozhyk, U.; Serak, S.; Tabiryan, N.; White, T. J.; Bunning, T. J. Bidirectional Photoresponse of Surface Pretreated Azobenzene Liquid Crystal Polymer Networks. *Opt. Express* **2009**, *17*, 716–722.

(860) Wen, Z.-B.; Liu, D.; Li, X.-Y.; Zhu, C.-H.; Shao, R.-F.; Visvanathan, R.; Clark, N. A.; Yang, K.-K.; Wang, Y.-Z. Fabrication of Liquid Crystalline Polyurethane Networks with a Pendant Azobenzene Group to Access Thermal/Photoresponsive Shape-Memory Effects. *ACS Appl. Mater. Interfaces* **2017**, *9*, 24947–24954.

(861) Yin, R.; Xu, W.; Kondo, M.; Yen, C.-C.; Mamiya, J.; Ikeda, T.; Yu, Y. Can Sunlight Drive the Photoinduced Bending of Polymer Films? *J. Mater. Chem.* **2009**, *19*, 3141–3143.

(862) Cheng, F.; Zhang, Y.; Yin, R.; Yu, Y. Visible Light Induced Bending and Unbending Behavior of Crosslinked Liquid-Crystalline Polymer Films Containing Azotolane Moieties. *J. Mater. Chem.* **2010**, *20*, 4888–4896.

(863) Liu, Y.; Wu, W.; Wei, J.; Yu, Y. Visible Light Responsive Liquid Crystal Polymers Containing Reactive Moieties with Good Processability. *ACS Appl. Mater. Interfaces* **2017**, *9*, 782–789.

(864) Cheng, F.; Yin, R.; Zhang, Y.; Yen, C.-C.; Yu, Y. Fully Plastic Microrobots Which Manipulate Objects Using Only Visible Light. *Soft Matter* **2010**, *6*, 3447.

(865) Wu, W.; Yao, L.; Yang, T.; Yin, R.; Li, F.; Yu, Y. NIR-Light-Induced Deformation of Cross-Linked Liquid-Crystal Polymers Using Upconversion Nanophosphors. *J. Am. Chem. Soc.* **2011**, *133*, 15810–15813.

(866) Jiang, Z.; Xu, M.; Li, F.; Yu, Y. Red-Light-Controllable Liquid-Crystal Soft Actuators via Low-Power Excited Upconversion Based on Triplet–Triplet Annihilation. *J. Am. Chem. Soc.* **2013**, *135*, 16446–16453.

(867) Sasaki, S.; Ube, T.; Katayama, K.; Muramatsu, M.; Miyasaka, H.; Ikeda, T. Two-Photon Actuation of Crosslinked Liquid-Crystalline Polymers Utilizing Energy Transfer System. *Mol. Cryst. Liq. Cryst.* **2018**, *662*, 53–60.

(868) Cheng, Z.; Wang, T.; Li, X.; Zhang, Y.; Yu, H. NIR–Vis–UV Light-Responsive Actuator Films of Polymer-Dispersed Liquid Crystal/Graphene Oxide Nanocomposites. *ACS Appl. Mater. Interfaces* **2015**, *7*, 27494–27501.

(869) Lu, X.; Zhang, H.; Fei, G.; Yu, B.; Tong, X.; Xia, H.; Zhao, Y. Liquid-Crystalline Dynamic Networks Doped with Gold Nanorods Showing Enhanced Photocontrol of Actuation. *Adv. Mater.* **2018**, *30*, 1706597.

(870) Ryabchun, A.; Li, Q.; Lancia, F.; Aprahamian, I.; Katsonis, N. Shape-Persistent Actuators from Hydrazone Photoswitches. *J. Am. Chem. Soc.* **2019**, *141*, 1196–1200.

(871) Lee, K. M.; Koerner, H.; Vaia, R. A.; Bunning, T. J.; White, T. J. Light-Activated Shape Memory of Glassy, Azobenzene Liquid Crystalline Polymer Networks. *Soft Matter* **2011**, *7*, 4318–4324.

(872) Min Lee, K.; Lynch, B. M.; Luchette, P.; White, T. J. Photomechanical Effects in Liquid Crystal Polymer Networks Prepared with M-Fluoroazobenzene. *J. Polym. Sci. Part A Polym. Chem.* **2014**, *52*, 876–882.

(873) Akamatsu, N.; Tashiro, W.; Saito, K.; Mamiya, J.; Kinoshita, M.; Ikeda, T.; Takeya, J.; Fujikawa, S.; Priimagi, A.; Shishido, A. Facile Strain Analysis of Largely Bending Films by a Surface-Labelled Grating Method. *Sci. Rep.* **2015**, *4*, 5377.

(874) Pang, X.; Xu, B.; Qing, X.; Wei, J.; Yu, Y. Photo-Induced Bending Behavior of Post-Crosslinked Liquid Crystalline Polymer/Polyurethane Blend Films. *Macromol. Rapid Commun.* **2018**, *39*, 1–7.

(875) Wie, J. J.; Lee, K. M.; Smith, M. L.; Vaia, R. A.; White, T. J. Torsional Mechanical Responses in Azobenzene Functionalized Liquid Crystalline Polymer Networks. *Soft Matter* **2013**, *9*, 9303–

9310.

(876) Harris, K. D.; Cuypers, R.; Scheibe, P.; Van Oosten, C. L.; Bastiaansen, C. W. M.; Lub, J.; Broer, D. J. Large Amplitude Light-Induced Motion in High Elastic Modulus Polymer Actuators. *J. Mater. Chem.* **2005**, *15*, 5043–5048.

(877) Yu, Y.; Ikeda, T. Soft Actuators Based on Liquid-Crystalline Elastomers. *Angew. Chem. Int. Ed.* **2006**, *45*, 5416–5418.

(878) Yu, Y.; Maeda, T.; Mamiya, J.; Ikeda, T. Photomechanical Effects of Ferroelectric Liquid-Crystalline Elastomers Containing Azobenzene Chromophores. *Angew. Chem. Int. Ed.* **2007**, *46*, 881–883.

(879) Kondo, M.; Miyasato, R.; Naka, Y.; Mamiya, J.; Kinoshita, M.; Yu, Y.; Barrett, C. J.; Ikeda, T. Photomechanical Properties of Azobenzene Liquid-Crystalline Elastomers. *Liq. Cryst.* **2009**, *36*, 1289–1293.

(880) Yoshino, T.; Kondo, M.; Mamiya, J.; Kinoshita, M.; Yu, Y.; Ikeda, T. Three-Dimensional Photomobility of Crosslinked Azobenzene Liquid-Crystalline Polymer Fibers. *Adv. Mater.* **2010**, *22*, 1361–1363.

(881) Li, M.-H.; Keller, P.; Li, B.; Wang, X.; Brunet, M. Light-Driven Side-On Nematic Elastomer Actuators. *Adv. Mater.* **2003**, *15*, 569–572.

(882) Tanchak, O. M.; Barrett, C. J. Light-Induced Reversible Volume Changes in Thin Films of Azo Polymers: The Photomechanical Effect. *Macromolecules* **2005**, *38*, 10566–10570.

(883) Fleischmann, E.-K.; Zentel, R. Liquid-Crystalline Ordering as a Concept in Materials Science: From Semiconductors to Stimuli-Responsive Devices. *Angew. Chem. Int. Ed.* **2013**, *52*, 8810–8827.

(884) Ionov, L. Polymeric Actuators. *Langmuir* **2015**, *31*, 5015–5024.

(885) Li, C.-C.; Chen, C.-W.; Yu, C.-K.; Jau, H.-C.; Lv, J.-A.; Qing, X.; Lin, C.-F.; Cheng, C.-Y.; Wang, C.-Y.; Wei, J.; et al. Arbitrary Beam Steering Enabled by Photomechanically Bendable Cholesteric Liquid Crystal Polymers. *Adv. Opt. Mater.* **2017**, *5*, 1600824.

(886) Ohm, C.; Brehmer, M.; Zentel, R. Liquid Crystalline Elastomers as Actuators and Sensors. *Adv. Mater.* **2010**, *22*, 3366–3387.

(887) Ikeda, T.; Ube, T. Photomobile Polymer Materials: From Nano to Macro. *Mater. Today* **2011**, *14*, 480–487.

(888) Mahimwalla, Z.; Yager, K. G.; Mamiya, J. I.; Shishido, A.; Priimagi, A.; Barrett, C. J. *Azobenzene Photomechanics: Prospects and Potential Applications*; 2012; Vol. 69.

(889) Jiang, H.; Li, C.; Huang, X. Actuators Based on Liquid Crystalline Elastomer Materials. *Nanoscale* **2013**, *5*, 5225–5240.

(890) Aßhoff, S. J.; Lancia, F.; Iamsaard, S.; Matt, B.; Kudernac, T.; Fletcher, S. P.; Katsonis, N. High-Power Actuation from Molecular Photoswitches in Enantiomerically Paired Soft Springs. *Angew. Chem. Int. Ed.* **2017**, *56*, 3261–3265.

(891) White, T. J.; Tabiryan, N. V.; Serak, S. V.; Hrozhyk, U. A.; Tondiglia, V. P.; Koerner, H.; Vaia, R. A.; Bunning, T. J. A High Frequency Photodriven Polymer Oscillator. *Soft Matter* **2008**, *4*, 1796–1798.

(892) Serak, S.; Tabiryan, N.; Vergara, R.; White, T. J.; Vaia, R. A.; Bunning, T. J. Liquid Crystalline Polymer Cantilever Oscillators Fueled by Light. *Soft Matter* **2010**, *6*, 779–783.

(893) Lee, K. M.; White, T. J. Photomechanical Response of Composite Structures Built from Azobenzene Liquid Crystal Polymer Networks. *Polymers* **2011**, *3*, 1447–1457.

(894) Lee, K. M.; Smith, M. L.; Koerner, H.; Tabiryan, N.; Vaia, R. A.; Bunning, T. J.; White, T. J. Photodriven, Flexural-Torsional Oscillation of Glassy Azobenzene Liquid Crystal Polymer

Networks. *Adv. Funct. Mater.* **2011**, *21*, 2913–2918.

(895) Tang, R.; Liu, Z.; Xu, D.; Liu, J.; Yu, L.; Yu, H. Optical Pendulum Generator Based on Photomechanical Liquid-Crystalline Actuators. *ACS Appl. Mater. Interfaces* **2015**, *7*, 8393–8397.

(896) Zhu, Y.; Zheng, L.; Liu, Z.; Liu, H.; Yu, Y. Photodeformable Polymer Materials: Towards Light-Driven Spoke-Type Micromotor Application. *Appl. Phys. A* **2014**, *115*, 1167–1172.

(897) Yamada, M.; Kondo, M.; Mamiya, J.; Yu, Y.; Kinoshita, M.; Barrett, C. J.; Ikeda, T. Photomobile Polymer Materials: Towards Light-Driven Plastic Motors. *Angew. Chem. Int. Ed.* **2008**, *47*, 4986–4988.

(898) Camacho-Lopez, M.; Finkelmann, H.; Palffy-Muhoray, P.; Shelley, M. Fast Liquid-Crystal Elastomer Swims into the Dark. *Nat. Mater.* **2004**, *3*, 307–310.

(899) Yamada, M.; Kondo, M.; Miyasato, R.; Naka, Y.; Mamiya, J.; Kinoshita, M.; Shishido, A.; Yu, Y.; Barrett, C. J.; Ikeda, T. Photomobile Polymer Materials—Various Three-Dimensional Movements. *J. Mater. Chem.* **2009**, *19*, 60–62.

(900) Huang, C.; Lv, J.; Tian, X.; Wang, Y.; Yu, Y.; Liu, J. Miniaturized Swimming Soft Robot with Complex Movement Actuated and Controlled by Remote Light Signals. *Sci. Rep.* **2015**, *5*, 17414.

(901) Zeng, H.; Wasylczyk, P.; Parmeggiani, C.; Martella, D.; Burresi, M.; Wiersma, D. S. Light-Fueled Microscopic Walkers. *Adv. Mater.* **2015**, *27*, 3883–3887.

(902) Rogóż, M.; Zeng, H.; Xuan, C.; Wiersma, D. S.; Wasylczyk, P. Light-Driven Soft Robot Mimics Caterpillar Locomotion in Natural Scale. *Adv. Opt. Mater.* **2016**, *4*, 1689–1694.

(903) Palagi, S.; Mark, A. G.; Reigh, S. Y.; Melde, K.; Qiu, T.; Zeng, H.; Parmeggiani, C.; Martella, D.; Sanchez-Castillo, A.; Kapernaum, N.; et al. Structured Light Enables Biomimetic Swimming and Versatile Locomotion of Photoresponsive Soft Microrobots. *Nat. Mater.* **2016**, *15*, 647–653.

(904) Zeng, H.; Wani, O. M.; Wasylczyk, P.; Priimagi, A. Light-Driven, Caterpillar-Inspired Miniature Inching Robot. *Macromol. Rapid Commun.* **2018**, *39*, 1700224.

(905) Wang, M.; Lin, B.-P.; Yang, H. A Plant Tendril Mimic Soft Actuator with Phototunable Bending and Chiral Twisting Motion Modes. *Nat. Commun.* **2016**, *7*, 13981.

(906) Wie, J. J.; Shankar, M. R.; White, T. J. Photomotility of Polymers. *Nat. Commun.* **2016**, *7*, 13260.

(907) Lu, X.; Guo, S.; Tong, X.; Xia, H.; Zhao, Y. Tunable Photocontrolled Motions Using Stored Strain Energy in Malleable Azobenzene Liquid Crystalline Polymer Actuators. *Adv. Mater.* **2017**, *29*, 1–7.

(908) Hines, L.; Petersen, K.; Lum, G. Z.; Sitti, M. Soft Actuators for Small-Scale Robotics. *Adv. Mater.* **2017**, *29*, 1603483.

(909) Zeng, H.; Wasylczyk, P.; Wiersma, D. S.; Priimagi, A. Light Robots: Bridging the Gap between Microrobotics and Photomechanics in Soft Materials. *Adv. Mater.* **2018**, *30*, 1703554.

(910) Lahikainen, M.; Zeng, H.; Priimagi, A. Reconfigurable Photoactuator through Synergistic Use of Photochemical and Photothermal Effects. *Nat. Commun.* **2018**, *9*, 4148.

(911) Zeng, H.; Wani, O. M.; Wasylczyk, P.; Kaczmarek, R.; Priimagi, A. Self-Regulating Iris Based on Light-Actuated Liquid Crystal Elastomer. *Adv. Mater.* **2017**, *29*, 1701814.

(912) Palagi, S.; Fischer, P. Bioinspired Microrobots. *Nat. Rev. Mater.* **2018**, *3*, 113–124.

(913) Wani, O. M.; Zeng, H.; Priimagi, A. A Light-Driven Artificial Flytrap. *Nat. Commun.* **2017**, *8*, 15546.

(914) van Oosten, C. L.; Bastiaansen, C. W. M.; Broer, D. J. Printed Artificial Cilia from Liquid-Crystal Network Actuators Modularly Driven by Light. *Nat. Mater.* **2009**, *8*, 677–682.

(915) Yan, Z.; Ji, X.; Wu, W.; Wei, J.; Yu, Y. Light-Switchable Behavior of a Microarray of Azobenzene

Liquid Crystal Polymer Induced by Photodeformation. *Macromol. Rapid Commun.* **2012**, *33*, 1362–1367.

(916) Gelebart, A. H.; Mc Bride, M.; Schenning, A. P. H. J.; Bowman, C. N.; Broer, D. J. Photoresponsive Fiber Array: Toward Mimicking the Collective Motion of Cilia for Transport Applications. *Adv. Funct. Mater.* **2016**, *26*, 5322–5327.

(917) Lv, J.; Liu, Y.; Wei, J.; Chen, E.; Qin, L.; Yu, Y. Photocontrol of Fluid Slugs in Liquid Crystal Polymer Microactuators. *Nature* **2016**, *537*, 179–184.

(918) Kobatake, S.; Takami, S.; Muto, H.; Ishikawa, T.; Irie, M. Rapid and Reversible Shape Changes of Molecular Crystals on Photoirradiation. *Nature* **2007**, *446*, 778–781.

(919) Kuroki, L.; Takami, S.; Yoza, K.; Morimoto, M.; Irie, M. Photoinduced Shape Changes of Diarylethene Single Crystals: Correlation between Shape Changes and Molecular Packing. *Photochem. Photobiol. Sci.* **2010**, *9*, 221–225.

(920) Kitagawa, D.; Iwaihara, C.; Nishi, H.; Kobatake, S. Quantitative Evaluation of Photoinduced Bending Speed of Diarylethene Crystals. *Crystals* **2015**, *5*, 551–561.

(921) Kitagawa, D.; Tanaka, R.; Kobatake, S. Dependence of Photoinduced Bending Behavior of Diarylethene Crystals on Irradiation Wavelength of Ultraviolet Light. *Phys. Chem. Chem. Phys.* **2015**, *17*, 27300–27305.

(922) Kitagawa, D.; Kobatake, S. Crystal Thickness Dependence of the Photoinduced Crystal Bending of 1-(5-Methyl-2-(4-(p-Vinylbenzoyloxymethyl)Phenyl)-4-Thiazolyl)-2-(5-Methyl-2-Phenyl-4-Thiazolyl)Perfluorocyclopentene. *Photochem. Photobiol. Sci.* **2014**, *13*, 764–769.

(923) Terao, F.; Morimoto, M.; Irie, M. Light-Driven Molecular-Crystal Actuators: Rapid and Reversible Bending of Rodlike Mixed Crystals of Diarylethene Derivatives. *Angew. Chem. Int. Ed.* **2012**, *51*, 901–904.

(924) Colombier, I.; Spagnoli, S.; Corval, A.; Baldeck, P. L.; Giraud, M.; Leaustic, A.; Yu, P.; Irie, M. Diarylethene Microcrystals Make Directional Jumps upon Ultraviolet Irradiation. *J. Chem. Phys.* **2007**, *126*, 011101.

(925) Tong, F.; Kitagawa, D.; Dong, X.; Kobatake, S.; Bardeen, C. J. Photomechanical Motion of Diarylethene Molecular Crystal Nanowires. *Nanoscale* **2018**, *10*, 3393–3398.

(926) Kitagawa, D.; Kawasaki, K.; Tanaka, R.; Kobatake, S. Mechanical Behavior of Molecular Crystals Induced by Combination of Photochromic Reaction and Reversible Single-Crystal-to-Single-Crystal Phase Transition. *Chem. Mater.* **2017**, *29*, 7524–7532.

(927) Kitagawa, D.; Tanaka, R.; Kobatake, S. Photoinduced Stepwise Bending Behavior of Photochromic Diarylethene Crystals. *CrystEngComm* **2016**, *18*, 7236–7240.

(928) Kitagawa, D.; Kobatake, S. Crystal Thickness Dependence of Photoinduced Crystal Bending of 1,2-Bis(2-Methyl-5-(4-(1-Naphthoyloxymethyl)Phenyl)-3-Thienyl)Perfluorocyclopentene. *J. Phys. Chem. C* **2013**, *117*, 20887–20892.

(929) Kitagawa, D.; Nishi, H.; Kobatake, S. Photoinduced Twisting of a Photochromic Diarylethene Crystal. *Angew. Chem. Int. Ed.* **2013**, *52*, 9320–9322.

(930) Kobatake, S.; Hasegawa, H.; Miyamura, K. High-Convertible Photochromism of a Diarylethene Single Crystal Accompanying the Crystal Shape Deformation. *Cryst. Growth Des.* **2011**, *11*, 1223–1229.

(931) Uchida, K.; Sukata, S.; Matsuzawa, Y.; Akazawa, M.; de Jong, J. J. D.; Katsonis, N.; Kojima, Y.; Nakamura, S.; Areephong, J.; Meetsma, A.; et al. Photoresponsive Rolling and Bending of Thin Crystals of Chiral Diarylethenes. *Chem. Commun.* **2008**, No. 3, 326–328.

(932) Peng, J.; Zhao, J.; Ye, K.; Gao, H.; Sun, J.; Lu, R. Light-Induced Bending of Needle-Like Crystals of Naphthylvinylbenzoxazole Triggered by Trans – Cis Isomerization. *Chem. – An Asian J.* **2018**,

13, 1719–1724.

(933) Morimoto, M.; Irie, M. A Diarylethene Cocrystal That Converts Light into Mechanical Work. *J. Am. Chem. Soc.* **2010**, *132*, 14172–14178.

(934) Hatano, E.; Morimoto, M.; Hyodo, K.; Yasuda, N.; Yokojima, S.; Nakamura, S.; Uchida, K. Photosalient Effect of a Diarylethene with a Perfluorocyclohexene Ring. *Chem. Eur. J.* **2016**, *22*, 12680–12683.

(935) Kitagawa, D.; Tsujioka, H.; Tong, F.; Dong, X.; Bardeen, C. J.; Kobatake, S. Control of Photomechanical Crystal Twisting by Illumination Direction. *J. Am. Chem. Soc.* **2018**, *140*, 4208–4212.

(936) Hirano, A.; Hashimoto, T.; Kitagawa, D.; Kono, K.; Kobatake, S. Dependence of Photoinduced Bending Behavior of Diarylethene Crystals on Ultraviolet Irradiation Power. *Cryst. Growth Des.* **2017**, *17*, 4819–4825.

(937) Chizhik, S.; Sidelnikov, A.; Zakharov, B.; Naumov, P.; Boldyreva, E. Quantification of Photoinduced Bending of Dynamic Molecular Crystals: From Macroscopic Strain to Kinetic Constants and Activation Energies. *Chem. Sci.* **2018**, *9*, 2319–2335.

(938) Nath, N. K.; Pejov, L.; Nichols, S. M.; Hu, C.; Saleh, N.; Kahr, B.; Naumov, P. Model for Photoinduced Bending of Slender Molecular Crystals. *J. Am. Chem. Soc.* **2014**, *136*, 2757–2766.

(939) Dong, X.; Tong, F.; Hanson, K. M.; Al-Kaysi, R. O.; Kitagawa, D.; Kobatake, S.; Bardeen, C. J. Hybrid Organic–Inorganic Photon-Powered Actuators Based on Aligned Diarylethene Nanocrystals. *Chem. Mater.* **2019**, acs.chemmater.8b04568.

(940) Kitagawa, D.; Kobatake, S. Photoreversible Current ON/OFF Switching by the Photoinduced Bending of Gold-Coated Diarylethene Crystals. *Chem. Commun.* **2015**, *51*, 4421–4424.

(941) Tong, F.; Liu, M.; Al-Kaysi, R. O.; Bardeen, C. J. Surfactant-Enhanced Photoisomerization and

Photomechanical Response in Molecular Crystal Nanowires. *Langmuir* **2018**, *34*, 1627–1634.

(942) Zhu, L.; Tong, F.; Zaghloul, N.; Baz, O.; Bardeen, C. J.; Al-Kaysi, R. O. Characterization of a P-Type Photomechanical Molecular Crystal Based on the E → Z Photoisomerization of 9-Divinylanthracene Malonitrile. *J. Mater. Chem. C* **2016**, *4*, 8245–8252.

(943) Takanabe, A.; Tanaka, M.; Johmoto, K.; Uekusa, H.; Mori, T.; Koshima, H.; Asahi, T. Optical Activity and Optical Anisotropy in Photomechanical Crystals of Chiral Salicylidenephenylethylamines. *J. Am. Chem. Soc.* **2016**, *138*, 15066–15077.

(944) Koshima, H.; Nakaya, H.; Uchimoto, H.; Ojima, N. Photomechanical Motion of Furylfulgide Crystals. *Chem. Lett.* **2012**, *41*, 107–109.

(945) Koshima, H.; Matsuo, R.; Matsudomi, M.; Uemura, Y.; Shiro, M. Light-Driven Bending Crystals of Salicylidenephenylethylamines in Enantiomeric and Racemate Forms. *Cryst. Growth Des.* **2013**, *13*, 4330–4337.

(946) Koshima, H.; Takechi, K.; Uchimoto, H.; Shiro, M.; Hashizume, D. Photomechanical Bending of Salicylideneaniline Crystals. *Chem. Commun.* **2011**, *47*, 11423.

(947) Koshima, H.; Matsudomi, M.; Uemura, Y.; Kimura, F.; Kimura, T. Light-Driven Bending of Polymer Films in Which Salicylidenephenylethylamine Crystals Are Aligned Magnetically. *Chem. Lett.* **2013**, *42*, 1517–1519.

(948) Hao, Y.; Huang, S.; Guo, Y.; Zhou, L.; Hao, H.; Barrett, C. J.; Yu, H. Photoinduced Multi-Directional Deformation of Azobenzene Molecular Crystals. *J. Mater. Chem. C* **2019**, *7*, 503–508.

(949) Bushuyev, O. S.; Tomberg, A.; Friščić, T.; Barrett, C. J. Shaping Crystals with Light: Crystal-to-Crystal Isomerization and Photomechanical Effect in Fluorinated Azobenzenes. *J. Am. Chem. Soc.* **2013**, *135*, 12556–12559.

(950) Koshima, H.; Ojima, N. Photomechanical Bending of 4-Aminoazobenzene Crystals. *Dye. Pigment.*

2012, *92*, 798–801.

(951) Koshima, H.; Ojima, N.; Uchimoto, H. Mechanical Motion of Azobenzene Crystals upon Photoirradiation. *J. Am. Chem. Soc.* **2009**, *131*, 6890–6891.

(952) Bushuyev, O. S.; Singleton, T. A.; Barrett, C. J. Fast, Reversible, and General Photomechanical Motion in Single Crystals of Various Azo Compounds Using Visible Light. *Adv. Mater.* **2013**, *25*, 1796–1800.

(953) Bushuyev, O. S.; Corkery, T. C.; Barrett, C. J.; Friščić, T. Photo-Mechanical Azobenzene Cocrystals and in Situ X-Ray Diffraction Monitoring of Their Optically-Induced Crystal-to-Crystal Isomerisation. *Chem. Sci.* **2014**, *5*, 3158–3164.

(954) Taniguchi, T.; Fujisawa, J.; Shiro, M.; Koshima, H.; Asahi, T. Mechanical Motion of Chiral Azobenzene Crystals with Twisting upon Photoirradiation. *Chem. Eur. J.* **2016**, *22*, 7950–7958.

(955) Hu, J.; Li, X.; Ni, Y.; Ma, S.; Yu, H. A Programmable and Biomimetic Photo-Actuator: A Composite of a Photo-Liquefiable Azobenzene Derivative and Commercial Plastic Film. *J. Mater. Chem. C* **2018**, *6*, 10815–10821.

(956) Liu, Z.; Tang, R.; Xu, D.; Liu, J.; Yu, H. Precise Actuation of Bilayer Photomechanical Films Coated with Molecular Azobenzene Chromophores. *Macromol. Rapid Commun.* **2015**, *36*, 1171–1176.

(957) Lee, J.; Oh, S.; Pyo, J.; Kim, J.-M.; Je, J. H. A Light-Driven Supramolecular Nanowire Actuator. *Nanoscale* **2015**, *7*, 6457–6461.

(958) Uchida, E.; Azumi, R.; Norikane, Y. Light-Induced Crawling of Crystals on a Glass Surface. *Nat. Commun.* **2015**, *6*, 7310.

(959) Stoddart, J. F. The Chemistry of the Mechanical Bond. *Chem. Soc. Rev.* **2009**, *38*, 1802–1820.

(960) Kay, E. R.; Leigh, D. A. Rise of the Molecular Machines. *Angew. Chem. Int. Ed.* **2015**, *54*, 10080–10088.

(961) Wasserman, E. The Preparation of Interlocking Rings: A Catenane. *J. Am. Chem. Soc.* **1960**, *82*, 4433–4434.

(962) Sauvage, Jean-pierre; Dietrich-Buchecker, C. UNE NOUVELLE FAMILLE DE MOLECULES : LES METALLO-CATENANES. *Tetrahedron Lett.* **1983**, No. 46, 5095–5098.

(963) Livoreil, A.; Dietrich-Buchecker, C. O.; Sauvage, J.-P. Electrochemically Triggered Swinging of a [2]-Catenate. *J. Am. Chem. Soc.* **1994**, *116*, 9399–9400.

(964) Cárdenas, D. J.; Livoreil, A.; Sauvage, J.-P. Redox Control of the Ring-Gliding Motion in a Cu-Complexed Catenane: A Process Involving Three Distinct Geometries. *J. Am. Chem. Soc.* **1996**, *118*, 11980–11981.

(965) Ashton, P. R.; Pérez-García, L.; Stoddart, J. F.; Ballardini, R.; Balzani, V.; Credi, A.; Gandolfi, M. T.; Prodi, L.; Venturi, M.; Menzer, S.; et al. Molecular Meccano. 4. The Self-Assembly of [2]Catenanes Incorporating Photoactive and Electroactive π-Extended Systems. *J. Am. Chem. Soc.* **1995**, *117*, 11171–11197.

(966) Gil-Ramírez, G.; Leigh, D. A.; Stephens, A. J. Catenanes: Fifty Years of Molecular Links. *Angew. Chem. Int. Ed.* **2015**, *54*, 6110–6150.

(967) Leigh, D. A.; Wong, J. K. Y.; Dehez, F.; Zerbetto, F. Unidirectional Rotation in a Mechanically Interlocked Molecular Rotor. *Nature* **2003**, *424*, 174–179.

(968) Wilson, M. R.; Solà, J.; Carlone, A.; Goldup, S. M.; Lebrasseur, N.; Leigh, D. A. An Autonomous Chemically Fuelled Small-Molecule Motor. *Nature* **2016**, *534*, 235–240.

(969) Hernandez, J. V. A Reversible Synthetic Rotary Molecular Motor. *Science* **2004**, *306*, 1532–1537.

(970) Anelli, P. L.; Spencer, N.; Fraser Stoddart, J. A Molecular Shuttle. *J. Am. Chem. Soc.* **1991**, *113*, 5131–5133.

(971) Bissell, R. A.; Cordova, E.; Kaifer, A. E.; Stoddart, J. F. A Chemically and Electrochemically Switchable Molecular Shuttle. *Nature* **1994**, *369*, 133–137.

(972) Badjic, J. D.; Balzani, V.; Credi, A.; Silvi, S.; Stoddart, J. F. A Molecular Elevator. *Science* **2004**, *303*, 1845–1849.

(973) Ragazzon, G.; Baroncini, M.; Silvi, S.; Venturi, M.; Credi, A. Light-Powered Autonomous and Directional Molecular Motion of a Dissipative Self-Assembling System. *Nat. Nanotechnol.* **2015**, *10*, 70–75.

(974) Pezzato, C.; Nguyen, M. T.; Cheng, C.; Kim, D. J.; Otley, M. T.; Stoddart, J. F. An Efficient Artificial Molecular Pump. *Nat. Nanotechnol.* **2017**, *73*, 4849–4857.

(975) Ashton, P. R.; Ballardini, R.; Balzani, V.; Baxter, I.; Credi, A.; Fyfe, M. C. T.; Gandolfi, M. T.; Gómez-López, M.; Martínez-Díaz, M. V.; Piersanti, A.; et al. Acid-Base Controllable Molecular Shuttles. *J. Am. Chem. Soc.* **1998**, *120*, 11932–11942.

(976) Balzani, V.; Clemente-Leon, M.; Credi, A.; Ferrer, B.; Venturi, M.; Flood, A. H.; Stoddart, J. F. Autonomous Artificial Nanomotor Powered by Sunlight. *Proc. Natl. Acad. Sci.* **2006**, *103*, 1178–1183.

(977) Serreli, V.; Lee, C. F.; Kay, E. R.; Leigh, D. A. A Molecular Information Ratchet. *Nature* **2007**, *445*, 523–527.

(978) Lewandowski, B.; De Bo, G.; Ward, J. W.; Papmeyer, M.; Kuschel, S.; Aldegunde, M. J.; Gramlich, P. M. E.; Heckmann, D.; Goldup, S. M.; D'Souza, D. M.; et al. Sequence-Specific Peptide Synthesis by an Artificial Small-Molecule Machine. *Science* **2013**, *339*, 189–193.

(979) Li, H.; Cheng, C.; McGonigal, P. R.; Fahrenbach, A. C.; Frasconi, M.; Liu, W. G.; Zhu, Z.; Zhao,

Y.; Ke, C.; Lei, J.; et al. Relative Unidirectional Translation in an Artificial Molecular Assembly Fueled by Light. *J. Am. Chem. Soc.* **2013**, *135*, 18609–18620.

(980) Consuelo Jimenez, M.; Dietrich-buchecker, C.; Sauvage, J.-P. Towards Synthetic Molecular Muscles : *Angew. Chem. Int. Ed. Engl.* **2000**, *1*, 3284–3287.

(981) Chang, J.-C.; Tseng, S.-H.; Lai, C.-C.; Liu, Y.-H.; Peng, S.-M.; Chiu, S.-H. Mechanically Interlocked Daisy-Chain-like Structures as Multidimensional Molecular Muscles. *Nat. Chem.* **2017**, *9*, 128–134.

(982) Aoki, D.; Aibara, G.; Uchida, S.; Takata, T. A Rational Entry to Cyclic Polymers via Selective Cyclization by Self-Assembly and Topology Transformation of Linear Polymers. *J. Am. Chem. Soc.* **2017**, *139*, 6791–6794.

(983) Wu, J.; Leung, K. C. F.; Benítez, D.; Han, J. Y.; Cantrill, S. J.; Fang, L.; Stoddart, J. F. An Acid-Base-Controllable [C2]Daisy Chain. *Angew. Chem. Int. Ed.* **2008**, *47*, 7470–7474.

(984) Romuald, C.; Busseron, E.; Coutrot, F. A New PH-Switchable Dimannosyl [C2] Daisy Chain Molecular. *Org. Lett.* **2008**, *10*, 3741–3744.

(985) Coutrot, F. A Focus on Triazolium as a Multipurpose Molecular Station for PH-Sensitive Interlocked Crown-Ether-Based Molecular Machines. *ChemistryOpen* **2015**, *4*, 556–576.

(986) Wolf, A. A.; Cid, J.; Moulin, E.; Niess, F.; Du, G.; Goujon, A.; Busseron, E.; Ruff, A.; Ludwigs, S.; Giuseppone, N. Unsymmetric Bistable [C2]Daisy Chain Rotaxanes Which Combine Two Types of Electroactive Stoppers. *Eur. J. Org. Chem.* **2019**.

(987) Dawson, R. E.; Lincoln, S. F.; Easton, C. J. The Foundation of a Light Driven Molecular Muscle Based on Stilbene and α-Cyclodextrin. *Chem. Commun.* **2008**, No. 34, 3980–3982.

(988) Tsukagoshi, S.; Miyawaki, A.; Takashima, Y.; Yamaguchi, H.; Harada, A. Contraction of Supramolecular Double-Threaded Dimer Formed by r -Cyclodextrin with a Long Alkyl Chain.

Org. Lett. **2007**, *9*, 1053–1055.

(989) Bruns, C. J.; Frasconi, M.; Iehl, J.; Hartlieb, K. J.; Schneebeli, S. T.; Cheng, C.; Stupp, S. I.; Stoddart, J. F. Redox Switchable Daisy Chain Rotaxanes Driven by Radical-Radical Interactions. *J. Am. Chem. Soc.* **2014**, *136*, 4714–4723.

(990) Silvi, S.; Venturi, M.; Credi, A. Artificial Molecular Shuttles: From Concepts to Devices. *J. Mater. Chem.* **2009**, *19*, 2279–2294.

(991) Erbas-Cakmak, S.; Leigh, D. A.; McTernan, C. T.; Nussbaumer, A. L. Artificial Molecular Machines. *Chem. Rev.* **2015**, *115*, 10081–10206.

(992) Collier, C. P.; Mattersteig, G.; Wong, E. W.; Luo, Y.; Beverly, K.; Sampaio, J.; Raymo, F. M.; Stoddart, J. F.; Heath, J. R. A [2]Catenane-Based Solid State Electronically Reconfigurable Switch. *Science* **2000**, *289*, 1172–1175.

(993) Mendes, P. M.; Flood, A. H.; Stoddart, J. F. Nanoelectronic Devices from Self-Organized Molecular Switches. *Appl. Phys. A* **2005**, *80*, 1197–1209.

(994) Balzani, V.; Credi, A.; Mattersteig, G.; Matthews, O. A.; Raymo, F. M.; Stoddart, J. F.; Venturi, M.; White, A. J. P.; Williams, D. J. Switching of Pseudorotaxanes and Catenanes Incorporating a Tetrathiafulvalene Unit by Redox and Chemical Inputs †. *J. Org. Chem.* **2000**, *65*, 1924–1936.

(995) Diehl, M. R.; Steuerman, D. W.; Tseng, H.-R.; Vignon, S. A.; Star, A.; Celestre, P. C.; Stoddart, J. F.; Heath, J. R. Single-Walled Carbon Nanotube Based Molecular Switch Tunnel Junctions. *ChemPhysChem* **2003**, *4*, 1335–1339.

(996) Klajn, R.; Fang, L.; Coskun, A.; Olson, M. A.; Wesson, P. J.; Stoddart, J. F.; Grzybowski, B. A. Metal Nanoparticles Functionalized with Molecular and Supramolecular Switches. *J. Am. Chem. Soc.* **2009**, *131*, 4233–4235.

(997) Wu, Q.; Rauscher, P. M.; Lang, X.; Wojtecki, R. J.; de Pablo, J. J.; Hore, M. J. A.; Rowan, S. J.

Poly[n]Catenanes: Synthesis of Molecular Interlocked Chains. *Science* **2017**, *358*, 1434–1439.

(998) Xing, H.; Li, Z.; Wu, Z. L.; Huang, F. Catenane Crosslinked Mechanically Adaptive Polymer Gel. *Macromol. Rapid Commun.* **2018**, *39*, 1700361.

(999) Fahrenbach, A. C.; Warren, S. C.; Incorvati, J. T.; Avestro, A.-J.; Barnes, J. C.; Stoddart, J. F.; Grzybowski, B. A. Organic Switches for Surfaces and Devices. *Adv. Mater.* **2013**, *25*, 331–348.

(1000) Collier, C. P.; Jeppesen, J. O.; Luo, Y.; Perkins, J.; Wong, E. W.; Heath, J. R.; Stoddart, J. F. Molecular-Based Electronically Switchable Tunnel Junction Devices. *J. Am. Chem. Soc.* **2001**, *123*, 12632–12641.

(1001) Luo, Y.; Collier, C. P.; Jeppesen, J. O.; Nielsen, K. A.; DeIonno, E.; Ho, G.; Perkins, J.; Tseng, H.-R.; Yamamoto, T.; Stoddart, J. F.; et al. Two-Dimensional Molecular Electronics Circuits. *ChemPhysChem* **2002**, *3*, 519–525.

(1002) Nørgaard, K.; Laursen, B. W.; Nygaard, S.; Kjaer, K.; Tseng, H.-R.; Flood, A. H.; Stoddart, J. F.; Bjørnholm, T. Structural Evidence of Mechanical Shuttling in Condensed Monolayers of Bistable Rotaxane Molecules. *Angew. Chem. Int. Ed.* **2005**, *44*, 7035–7039.

(1003) Green, J. E.; Wook Choi, J.; Boukai, A.; Bunimovich, Y.; Johnston-Halperin, E.; Deionno, E.; Luo, Y.; Sheriff, B. A.; Xu, K.; Shik Shin, Y.; et al. A 160-Kilobit Molecular Electronic Memory Patterned at 1011bits per Square Centimetre. *Nature* **2007**, *445*, 414–417.

(1004) Ball, P. A Switch in Time. *Nature* **2007**, *445*, 362–363.

(1005) Coskun, A.; Spruell, J. M.; Barin, G.; Dichtel, W. R.; Flood, A. H.; Botros, Y. Y.; Stoddart, J. F. High Hopes: Can Molecular Electronics Realise Its Potential? *Chem. Soc. Rev.* **2012**, *41*, 4827–4859.

(1006) Huang, T. J.; Tseng, H.-R.; Sha, L.; Lu, W.; Brough, B.; Flood, A. H.; Yu, B.-D.; Celestre, P. C.; Chang, J. P.; Stoddart, J. F.; et al. Mechanical Shuttling of Linear Motor-Molecules in Condensed

Phases on Solid Substrates. *Nano Lett.* **2004**, *4*, 2065–2071.

(1007) Huang, T. J.; Brough, B.; Ho, C.-M.; Liu, Y.; Flood, A. H.; Bonvallet, P. A.; Tseng, H.-R.; Stoddart, J. F.; Baller, M.; Magonov, S. A Nanomechanical Device Based on Linear Molecular Motors. *Appl. Phys. Lett.* **2004**, *85*, 5391–5393.

(1008) Liu, Y.; Flood, A. H.; Bonvallet, P. A.; Vignon, S. A.; Northrop, B. H.; Tseng, H.-R.; Jeppesen, J. O.; Huang, T. J.; Brough, B.; Baller, M.; et al. Linear Artificial Molecular Muscles. *J. Am. Chem. Soc.* **2005**, *127*, 9745–9759.

(1009) Juluri, B. K.; Kumar, A. S.; Liu, Y.; Ye, T.; Yang, Y.-W.; Flood, A. H.; Fang, L.; Stoddart, J. F.; Weiss, P. S.; Huang, T. J. A Mechanical Actuator Driven Electrochemically by Artificial Molecular Muscles. *ACS Nano* **2009**, *3*, 291–300.

(1010) Zheng, Y. B.; Yang, Y.-W.; Jensen, L.; Fang, L.; Juluri, B. K.; Flood, A. H.; Weiss, P. S.; Stoddart, J. F.; Huang, T. J. Active Molecular Plasmonics: Controlling Plasmon Resonances with Molecular Switches. *Nano Lett.* **2009**, *9*, 819–825.

(1011) Jia, C.; Li, H.; Jiang, J.; Wang, J.; Chen, H.; Cao, D.; Stoddart, J. F.; Guo, X. Interface-Engineered Bistable [2]Rotaxane-Graphene Hybrids with Logic Capabilities. *Adv. Mater.* **2013**, *25*, 6752–6759.

(1012) Katz, E.; Lioubashevsky, O.; Willner, I. Electromechanics of a Redox-Active Rotaxane in a Monolayer Assembly on an Electrode. *J. Am. Chem. Soc.* **2004**, *126*, 15520–15532.

(1013) Berná, J.; Leigh, D. A.; Lubomska, M.; Mendoza, S. M.; Pérez, E. M.; Rudolf, P.; Teobaldi, G.; Zerbetto, F. Macroscopic Transport by Synthetic Molecular Machines. *Nat. Mater.* **2005**, *4*, 704–710.

(1014) Heinrich, T.; Traulsen, C. H.-H.; Holzweber, M.; Richter, S.; Kunz, V.; Kastner, S. K.; Krabbenborg, S. O.; Huskens, J.; Unger, W. E. S.; Schalley, C. A. Coupled Molecular Switching

Processes in Ordered Mono- and Multilayers of Stimulus-Responsive Rotaxanes on Gold Surfaces. *J. Am. Chem. Soc.* **2015**, *137*, 4382–4390.

(1015) Schwarz, F. B.; Heinrich, T.; Lippitz, A.; Unger, W. E. S.; Schalley, C. A. A Photoswitchable Rotaxane Operating in Monolayers on Solid Support. *Chem. Commun.* **2016**, *52*, 14458–14461.

(1016) Nguyen, T. D.; Tseng, H.-R.; Celestre, P. C.; Flood, A. H.; Liu, Y.; Stoddart, J. F.; Zink, J. I. A Reversible Molecular Valve. *Proc. Natl. Acad. Sci. U. S. A.* **2005**, *102*, 10029–10034.

(1017) Nguyen, T. D.; Liu, Y.; Saha, S.; Leung, K. C.-F.; Stoddart, J. F.; Zink, J. I. Design and Optimization of Molecular Nanovalves Based on Redox-Switchable Bistable Rotaxanes. *J. Am. Chem. Soc.* **2007**, *129*, 626–634.

(1018) Coskun, A.; Wesson, P. J.; Klajn, R.; Trabolsi, A.; Fang, L.; Olson, M. A.; Dey, S. K.; Grzybowski, B. A.; Stoddart, J. F. Molecular-Mechanical Switching at the Nanoparticle−Solvent Interface: Practice and Theory. *J. Am. Chem. Soc.* **2010**, *132*, 4310–4320.

(1019) Cao, Z.-Q.; Miao, Q.; Zhang, Q.; Li, H.; Qu, D.-H.; Tian, H. A Fluorescent Bistable [2]Rotaxane Molecular Switch on SiO 2 Nanoparticles. *Chem. Commun.* **2015**, *51*, 4973–4976.

(1020) Takata, T.; Aoki, D. Topology-Transformable Polymers: Linear–Branched Polymer Structural Transformation via the Mechanical Linking of Polymer Chains. *Polym. J.* **2018**, *50*, 127–147.

(1021) Zhang, W.; DeIonno, E.; Dichtel, W. R.; Fang, L.; Trabolsi, A.; Olsen, J.-C.; Benítez, D.; Heath, J. R.; Stoddart, J. F. A Solid-State Switch Containing an Electrochemically Switchable Bistable Poly[n]Rotaxane. *J. Mater. Chem.* **2011**, *21*, 1487–1495.

(1022) Lin, Q.; Hou, X.; Ke, C. Ring Shuttling Controls Macroscopic Motion in a Three-Dimensional Printed Polyrotaxane Monolith. *Angew. Chem. Int. Ed.* **2017**, *56*, 4452–4457.

(1023) Takashima, Y.; Hayashi, Y.; Osaki, M.; Kaneko, F.; Yamaguchi, H.; Harada, A. A Photoresponsive Polymeric Actuator Topologically Cross-Linked by Movable Units Based on a

[2]Rotaxane. *Macromolecules* **2018**, *51*, 4688–4693.

(1024) Sakuda, J.; Yasuda, T.; Kato, T. Liquid-Crystalline Catenanes and Rotaxanes. *Isr. J. Chem.* **2012**, *52*, 854–862.

(1025) Aprahamian, I.; Yasuda, T.; Ikeda, T.; Saha, S.; Dichtel, W. R.; Isoda, K.; Kato, T.; Stoddart, J. F. A Liquid-Crystalline Bistable [2]Rotaxane. *Angew. Chem. Int. Ed.* **2007**, *46*, 4675–4679.

(1026) Yasuda, T.; Tanabe, K.; Tsuji, T.; Coti, K. K.; Aprahamian, I.; Stoddart, J. F.; Kato, T. A Redox-Switchable [2]Rotaxane in a Liquid-Crystalline State. *Chem. Commun.* **2010**, *46*, 1224–1226.

(1027) Vukotic, V. N.; Harris, K. J.; Zhu, K.; Schurko, R. W.; Loeb, S. J. Metal–Organic Frameworks with Dynamic Interlocked Components. *Nat. Chem.* **2012**, *4*, 456–460.

(1028) Zhu, K.; Vukotic, V. N.; O'Keefe, C. A.; Schurko, R. W.; Loeb, S. J. Metal–Organic Frameworks with Mechanically Interlocked Pillars: Controlling Ring Dynamics in the Solid-State via a Reversible Phase Change. *J. Am. Chem. Soc.* **2014**, *136*, 7403–7409.

(1029) Zhu, K.; O'Keefe, C. A.; Vukotic, V. N.; Schurko, R. W.; Loeb, S. J. A Molecular Shuttle That Operates inside a Metal-Organic Framework. *Nat. Chem.* **2015**, *7*, 514–519.

(1030) Chen, K.-J.; Tsai, Y.-C.; Suzaki, Y.; Osakada, K.; Miura, A.; Horie, M. Rapid and Reversible Photoinduced Switching of a Rotaxane Crystal. *Nat. Commun.* **2016**, *7*, 13321.

(1031) Chen, K.-J.; Chen, P.-L.; Horie, M. Dynamic Pseudorotaxane Crystals Containing Metallocene Complexes. *Sci. Rep.* **2017**, *7*, 14195.

(1032) Cheng, S.-C.; Chen, K.-J.; Suzaki, Y.; Tsuchido, Y.; Kuo, T.-S.; Osakada, K.; Horie, M. Reversible Laser-Induced Bending of Pseudorotaxane Crystals. *J. Am. Chem. Soc.* **2018**, *140*, 90–93.

(1033) Chen, K.-J.; Tan, A. C.; Wang, C.-H.; Kuo, T.-S.; Chen, P.-L.; Horie, M. Photoinduced

Mechanical Motions of Biferrocene-Containing Pseudorotaxane Crystals. *Cryst. Growth Des.* **2019**, *19*, 17–22.

(1034) Shukla, T.; Arumugaperumal, R.; Raghunath, P.; Lin, M.-C.; Lin, C.-M.; Lin, H.-C. Novel Supramolecular Conjugated Polyrotaxane as an Acid-Base Controllable Optical Molecular Switch. *Sensors Actuators B Chem.* **2017**, *243*, 84–95.

(1035) Cao, Z.-Q.; Luan, Z.-L.; Zhang, Q.; Gu, R.-R.; Ren, J.; Qu, D.-H. An Acid/Base Responsive Side-Chain Polyrotaxane System with a Fluorescent Signal. *Polym. Chem.* **2016**, *7*, 1866–1870.

(1036) Leigh, D. A.; Morales, M. Á. F.; Pérez, E. M.; Wong, J. K. Y.; Saiz, C. G.; Slawin, A. M. Z.; Carmichael, A. J.; Haddleton, D. M.; Brouwer, A. M.; Buma, W. J.; et al. Patterning through Controlled Submolecular Motion: Rotaxane-Based Switches and Logic Gates That Function in Solution and Polymer Films. *Angew. Chem. Int. Ed.* **2005**, *44*, 3062–3067.

(1037) Klajn, R.; Olson, M. A.; Wesson, P. J.; Fang, L.; Coskun, A.; Trabolsi, A.; Soh, S.; Stoddart, J. F.; Grzybowski, B. A. Dynamic Hook-and-Eye Nanoparticle Sponges. *Nat. Chem.* **2009**, *1*, 733–738.

(1038) Zhou, H.; Wang, Y.; Zheng, Z.; Ding, X.; Peng, Y. Periodic Auto-Active Gels with Topologically "Polyrotaxane-Interlocked" Structures. *Chem. Commun.* **2014**, *50*, 6372–6374.

(1039) Krans, J. L. The Sliding Filament Theory of Muscle Contraction. *Nat. Educ.* **2010**, *3*, 66–69.

(1040) Jiménez, M. C.; Dietrich-Buchecker, C.; Sauvage, J.-P. Towards Synthetic Molecular Muscles: Contraction and Stretching of a Linear Rotaxane Dimer. *Angew. Chem. Int. Ed.* **2000**, *39*, 3284–3287.

(1041) Goujon, A.; Moulin, E.; Fuks, G.; Giuseppone, N. [C2]Daisy Chain Rotaxanes as Molecular Muscles. *CCS Chem.* **2019**, *1*, 83–96.

(1042) Tsuda, S.; Aso, Y.; Kaneda, T. Linear Oligomers Composed of a Photochromically Contractible

and Extendable Janus [2]Rotaxane. *Chem. Commun.* **2006**, No. 29, 3072–3075.

(1043) Fang, L.; Hmadeh, M.; Wu, J.; Olson, M. A.; Spruell, J. M.; Trabolsi, A.; Yang, Y.-W.; Elhabiri, M.; Albrecht-Gary, A.-M.; Stoddart, J. F. Acid−Base Actuation of [c 2]Daisy Chains. *J. Am. Chem. Soc.* **2009**, *131*, 7126–7134.

(1044) Clark, P. G.; Day, M. W.; Grubbs, R. H. Switching and Extension of a [C2]Daisy-Chain Dimer Polymer. *J. Am. Chem. Soc.* **2009**, *131*, 13631–13633.

(1045) Hmadeh, M.; Fang, L.; Trabolsi, A.; Elhabiri, M.; Albrecht-Gary, A.-M.; Stoddart, J. F. On the Thermodynamic and Kinetic Investigations of a [C2]Daisy Chain Polymer. *J. Mater. Chem.* **2010**, *20*, 3422–3430.

(1046) Clark, P. G.; Day, M. W.; Grubbs, R. H. Switching and Extension of a [C2]Daisy-Chain Dimer Polymer. *J. Am. Chem. Soc.* **2009**, *131*, 13631–13633.

(1047) Du, G.; Moulin, E.; Jouault, N.; Buhler, E.; Giuseppone, N. Muscle-like Supramolecular Polymers: Integrated Motion from Thousands of Molecular Machines. *Angew. Chem. Int. Ed.* **2012**, *51*, 12504–12508.

(1048) Zhao, Y.-L.; Zhang, R.-Q.; Minot, C.; Hermann, K.; Van Hove, M. A. Revealing Highly Unbalanced Energy Barriers in the Extension and Contraction of the Muscle-like Motion of a [C2]Daisy Chain. *Phys. Chem. Chem. Phys.* **2015**, *17*, 18318–18326.

(1049) Zhao, Y.-L.; Zhang, R.-Q.; Minot, C.; Hermann, K.; Van Hove, M. A. Computational Prediction of Optimal Metal Ions to Induce Coordinated Polymerization of Muscle-like [C2]Daisy Chains. *Phys. Chem. Chem. Phys.* **2016**, *18*, 7419–7426.

(1050) Gao, L.; Zhang, Z.; Zheng, B.; Huang, F. Construction of Muscle-like Metallo-Supramolecular Polymers from a Pillar[5]Arene-Based [C2]Daisy Chain. *Polym. Chem.* **2014**, *5*, 5734–5739.

(1051) Goujon, A.; Du, G.; Moulin, E.; Fuks, G.; Maaloum, M.; Buhler, E.; Giuseppone, N. Hierarchical

Self-Assembly of Supramolecular Muscle-Like Fibers. *Angew. Chem. Int. Ed.* **2016**, *55*, 703–707.

(1052) Marangoni, T.; Bonifazi, D. Nano- and Microstructuration of Supramolecular Materials Driven by H-Bonded Uracil·2,6-Diamidopyridine Complexes. *Nanoscale* **2013**, *5*, 8837–8851.

(1053) Wolf, A.; Moulin, E.; Cid Martín, J. J.; Goujon, A.; Du, G.; Busseron, E.; Fuks, G.; Giuseppone, N. PH and Light-Controlled Self-Assembly of Bistable [C2] Daisy Chain Rotaxanes. *Chem. Commun.* **2015**, *51*, 4212–4215.

(1054) Goujon, A.; Mariani, G.; Lang, T.; Moulin, E.; Rawiso, M.; Buhler, E.; Giuseppone, N. Controlled Sol-Gel Transitions by Actuating Molecular Machine Based Supramolecular Polymers. *J. Am. Chem. Soc.* **2017**, *139*, 4923–4928.

(1055) Van Beek, D. J. M.; Spiering, A. J. H.; Peters, G. W. M.; Te Nijenhuis, K.; Sijbesma, R. P. Unidirectional Dimerization and Stacking of Ureidopyrimidinone End Groups in Polycaprolactone Supramolecular Polymers. *Macromolecules* **2007**, *40*, 8464–8475.

(1056) Mariani, G.; Goujon, A.; Moulin, E.; Rawiso, M.; Giuseppone, N.; Buhler, E. Integration of Molecular Machines into Supramolecular Materials: Actuation between Equilibrium Polymers and Crystal-like Gels. *Nanoscale* **2017**, *9*, 18456–18466.

(1057) Tao, R.; Zhang, Q.; Rao, S.; Zheng, X.; Li, M.; Qu, D. Supramolecular Gelator Based on a [C2]Daisy Chain Rotaxane: Efficient Gel-Solution Transition by Ring-Sliding Motion. *Sci. China Chem.* **2019**, *62*, 245–250.

(1058) Iwaso, K.; Takashima, Y.; Harada, A. Fast Response Dry-Type Artificial Molecular Muscles with [C2]Daisy Chains. *Nat. Chem.* **2016**, *8*, 625–632.

(1059) Ikejiri, S.; Takashima, Y.; Osaki, M.; Yamaguchi, H.; Harada, A. Solvent-Free Photoresponsive Artificial Muscles Rapidly Driven by Molecular Machines. *J. Am. Chem. Soc.* **2018**, *140*, 17308–17315.

(1060) Goujon, A.; Lang, T.; Mariani, G.; Moulin, E.; Fuks, G.; Raya, J.; Buhler, E.; Giuseppone, N. Bistable [c 2] Daisy Chain Rotaxanes as Reversible Muscle-like Actuators in Mechanically Active Gels. *J. Am. Chem. Soc.* **2017**, *139*, 14825–14828.

(1061) Zhang, Q.; Rao, S.-J.; Xie, T.; Li, X.; Xu, T.-Y.; Li, D.-W.; Qu, D.-H.; Long, Y.-T.; Tian, H. Muscle-like Artificial Molecular Actuators for Nanoparticles. *Chem* **2018**, *4*, 2670–2684.

(1062) Kottas, G. S.; Clarke, L. I.; Horinek, D.; Michl, J. Artificial Molecular Rotors. *Chem. Rev.* **2005**, *105*, 1281–1376.

(1063) Kemp, J. D.; Pitzer, K. S. Hindered Rotation of the Methyl Groups in Ethane. *J. Chem. Phys.* **1936**, *4*, 749–749.

(1064) Khuong, T. A. V.; Nunez, J. E.; Godinez, C. E.; Garcia-Garibay, M. A. Crystalline Molecular Machines: A Quest toward Solid-State Dynamics and Function. *Acc. Chem. Res.* **2006**, *39*, 413–422.

(1065) Vicsek, T.; Zafeiris, A. Collective Motion. *Phys. Rep.* **2012**, *517*, 71–140.

(1066) Garcia-Garibay, M. A. Crystalline Molecular Machines: Encoding Supramolecular Dynamics into Molecular Structure. *Proc. Natl. Acad. Sci.* **2005**, *102*, 10771–10776.

(1067) Vogelsberg, C. S.; Garcia-Garibay, M. A. Crystalline Molecular Machines: Function, Phase Order, Dimensionality, and Composition. *Chem. Soc. Rev.* **2012**, *41*, 1892–1910.

(1068) Turiv, T.; Lazo, I.; Brodin, A.; Lev, B. I.; Reiffenrath, V.; Nazarenko, V. G.; Lavrentovich, O. D. Effect of Collective Molecular Reorientations on Brownian Motion of Colloids in Nematic Liquid Crystal. *Science* **2013**, *342*, 1351–1354.

(1069) Gavezzotti, A. Theoretical Studies of Molecular Motions and Reactivity in Organic Crystals. *Mol. Cryst. Liq. Cryst.* **1988**, *156*, 25–33.

(1070) Gong, C.; Li, L.; Li, Z.; Ji, H.; Stern, A.; Xia, Y.; Cao, T.; Bao, W.; Wang, C.; Wang, Y.; et al. Discovery of Intrinsic Ferromagnetism in Two-Dimensional van Der Waals Crystals. *Nature* **2017**, *546*, 265–269.

(1071) Liu, Y.; Weiss, N. O.; Duan, X.; Cheng, H.-C.; Huang, Y.; Duan, X. Van Der Waals Heterostructures and Devices. *Nat. Rev. Mater.* **2016**, *1*, 16042.

(1072) Cooper, A. I. Porous Molecular Solids and Liquids. *ACS Cent. Sci.* **2017**, *3*, 544–553.

(1073) Lemouchi, C.; Mézière, C.; Zorina, L.; Simonov, S.; Rodríguez-Fortea, A.; Canadell, E.; Wzietek, P.; Auban-Senzier, P.; Pasquier, C.; Giamarchi, T.; et al. Design and Evaluation of a Crystalline Hybrid of Molecular Conductors and Molecular Rotors. *J. Am. Chem. Soc.* **2012**, *134*, 7880–7891.

(1074) Hoatson, G. L.; Vold, R. L. 2H-NMR Spectroscopy of Solids and Liquid Crystals. In *Solid-State NMR III Organic Matter*; Springer Berlin Heidelberg: Berlin, Heidelberg, 1994; pp 1–67.

(1075) Simpson, J. H.; Rice, D. M.; Karasz, F. E. 2H NMR Characterization of Phenylene Ring Flip Motion in Poly(p-Phenylene Vinylene) Films. *J. Polym. Sci. Part B Polym. Phys.* **1992**, *30*, 11–18.

(1076) Kubo, R.; Tomita, K. A General Theory of Magnetic Resonance Absorption. *J. Phys. Soc. Japan* **1954**, *9*, 888–919.

(1077) Ōki, M. Unusually High Barriers to Rotation Involving the Tetrahedral Carbon Atom. *Angew. Chem. Int. Ed. Engl.* **1976**, *15*, 87–93.

(1078) Hounshell, W. D.; Iroff, L. D.; Iverson, D. J.; Wroczynski, R. J.; Mislow, K. Is the Effective Size of an Alkyl Group a Gauge of Dynamic Gearing? *Isr. J. Chem.* **1980**, *20*, 65–71.

(1079) Hounshell, W. D.; Johnson, C. A.; Guenzi, A.; Cozzi, F.; Mislow, K. Stereochemical Consequences of Dynamic Gearing in Substituted Bis(9-Triptycyl) Methanes and Related Molecules. *Proc. Natl. Acad. Sci.* **1980**, *77*, 6961–6964.

(1080) Gust, D. Restricted Rotation in Hexaarylbenzenes. *J. Am. Chem. Soc.* **1977**, *99*, 6980–6982.

(1081) Gust, D.; Mislow, K. Analysis of Isomerization in Compounds Displaying Restricted Rotation of Aryl Groups. *J. Am. Chem. Soc.* **1973**, *95*, 1535–1547.

(1082) Iwamura, H. Stable Isomers of 1,6-Bis-(1-Cyano-1-Methylethyl)Triptycenes. *J. Chem. Soc. Chem. Commun.* **1973**, 232.

(1083) Thanasekaran, P.; Huang, C.-Y.; Lu, K.-L. Synthesis, Structure, and Dynamic Behavior of Discrete Metallacyclic Rotors. *Chem. Lett.* **2013**, *42*, 776–784.

(1084) Rappoport, Z.; Biali, S. E. Threshold Rotational Mechanisms and Enantiomerization Barriers of Polyarylvinyl Propellers. *Acc. Chem. Res.* **1997**, *30*, 307–314.

(1085) Mislow, K. Stereochemical Consequences of Correlated Rotation in Molecular Propellers. *Acc. Chem. Res.* **1976**, *9*, 26–33.

(1086) Kawada, Y.; Iwamura, H. Unconventional Synthesis and Conformational Flexibility of Bis(1-Triptycyl) Ether. *J. Org. Chem.* **1980**, *45*, 2547–2548.

(1087) Kawada, Y.; Iwamura, H. Bis(4-Chloro-1-Triptycyl) Ether. Separation of a Pair of Phase Isomers of Labeled Bevel Gears. *J. Am. Chem. Soc.* **1981**, *103*, 958–960.

(1088) Iwamura, H.; Ito, T.; Ito, H.; Toriumi, K.; Kawada, Y.; Osawa, E.; Fujiyoshi, T.; Jaime, C. Crystal and Molecular Structure of Bis(9-Triptycyl) Ether. *J. Am. Chem. Soc.* **1984**, *106*, 4712–4717.

(1089) Iwamura, H. Molecular Design of Correlated Internal Rotation. *J. Mol. Struct.* **1985**, *126*, 401–412.

(1090) Koga, N.; Iwamura, H. Barrier to Coupled Internal Rotation in Bis(9-Triptycyl) Ether. Kinetics of Intramolecular Exciplex Formation in Racemic 2,3-Benzo-9-Triptycyl 2-(N,N-Dimethylaminomethyl)-9-Triptycyl Ether. *J. Am. Chem. Soc.* **1985**, *107*, 1426–1427.

(1091) Koga, N.; Iwamura, H. A Kinetic Study of Coupled Internal Rotation in Racemic 2,3-Benzo-9-Triptycyl 2-(Dimethylaminomethyl)-9-Triptycyl Ether by Means of Exciplex Fluorescence Dynamics. *Chem. Lett.* **1986**, *15*, 247–250.

(1092) Kawada, Y.; Yamazaki, H.; Koga, G.; Murata, S.; Iwamura, H. Bis(9-Triptycyl)Amines, a Missing Link between the Corresponding Methanes and Ethers. An Unconventional Synthesis and Influence of Nitrogen Configurational Inversion on the Coupled Disrotatory Trajectory. *J. Org. Chem.* **1986**, *51*, 1472–1477.

(1093) Kawada, Y.; Ishikawa, J.; Yamazaki, H.; Koga, G.; Murata, S.; Iwamura, H. Correlation of the Two Torsional Degrees of Freedom about the Bonds Connecting the Bridgehead Carbons to the Sulfur Atom in Bis (9-Triptycyl) Sulfide. *Tetrahedron Lett.* **1987**, *28*, 445–448.

(1094) Iwamura, H.; Mislow, K. Stereochemical Consequences of Dynamic Gearing. *Acc. Chem. Res.* **1988**, *21*, 175–182.

(1095) Chance, J. M.; Geiger, J. H.; Mislow, K. A Parity Restriction on Dynamic Gearing Immobilizes the Rotors in Tris(9-Triptycyl)Germanium Chloride and Tris(9-Triptycyl)Cyclopropenium Perchlorate. *J. Am. Chem. Soc.* **1989**, *111*, 2326–2327.

(1096) Chance, J. M.; Geiger, J. H.; Okamoto, Y.; Aburatani, R.; Mislow, K. Stereochemical Consequences of a Parity Restriction on Dynamic Gearing in Tris(9-Triptycyl)Germanium Chloride and Tris(9-Triptycyl)Cyclopropenium Perchlorate. *J. Am. Chem. Soc.* **1990**, *112*, 3540–3547.

(1097) Kawada, Y.; Iwamura, H. Phase Isomerism in Gear-Shaped Molecules. *Tetrahedron Lett.* **1981**, *22*, 1533–1536.

(1098) Cozzi, F.; Guenzi, A.; Johnson, C. A.; Mislow, K.; Hounshell, W. D.; Blount, J. F. Stereoisomerism and Correlated Rotation in Molecular Gear Systems. Residual Diastereomers of Bis(2,3-Dimethyl-9-Triptycyl)Methane. *J. Am. Chem. Soc.* **1981**, *103*, 957–958.

(1099) Johnson, C. A.; Guenzi, A.; Mislow, K. Restricted Gearing and Residual Stereoisomerism in Bis(1,4-Dimethyl-9-Triptycyl)Methane. *J. Am. Chem. Soc.* **1981**, *103*, 6240–6242.

(1100) Johnson, C. A.; Guenzi, A.; Nachbar, R. B.; Blount, J. F.; Wennerstroem, O.; Mislow, K. Crystal and Molecular Structure of Bis(9-Triptycyl) Ketone and Bis(9-Triptycyl)Methane. *J. Am. Chem. Soc.* **1982**, *104*, 5163–5168.

(1101) Kawada, Y.; Iwamura, H. Correlated Rotation in Bis(9-Triptycyl)Methanes and Bis(9-Triptycyl) Ethers. Separation and Interconversion of the Phase Isomers of Labeled Bevel Gears. *J. Am. Chem. Soc.* **1983**, *105*, 1449–1459.

(1102) Kawada, Y.; Okamoto, Y.; Iwamura, H. Correlated Internal Rotation in Bis(2,6-Dichloro-9-Triptycyl)Methane. To What Extent Can Phase Isomers Be Separated and Identified? *Tetrahedron Lett.* **1983**, *24*, 5359–5362.

(1103) Buergi, H. B.; Hounshell, W. D.; Nachbar, R. B.; Mislow, K. Conformational Dynamics of Propane, Di-Tert-Butylmethane, and Bis(9-Triptycyl)Methane. An Analysis of the Symmetry of Two Threefold Rotors on a Rigid Frame in Terms of Nonrigid Molecular Structure and Energy Hypersurfaces. *J. Am. Chem. Soc.* **1983**, *105*, 1427–1438.

(1104) Guenzi, A.; Johnson, C. A.; Cozzi, F.; Mislow, K. Dynamic Gearing and Residual Stereoisomerism in Labeled Bis(9-Triptycyl)Methane and Related Molecules. Synthesis and Stereochemistry of Bis(2,3-Dimethyl-9-Triptycyl)Methane, Bis(2,3-Dimethyl-9-Triptycyl)Carbinol, and Bis(1,4-Dimethyl-9-Triptycyl)Methane. *J. Am. Chem. Soc.* **1983**, *105*, 1438–1448.

(1105) Chen, C.-F.; Ma, Y.-X. *Iptycenes Chemistry*; Springer Berlin Heidelberg: Berlin, Heidelberg, 2013.

(1106) Yamamoto, G.; Ohta, S.; Kaneko, M.; Mouri, K.; Ohkuma, M.; Mikami, R.; Uchiyama, Y.; Minoura, M. Static and Dynamic Stereochemistry of Tris(9-Triptycyl)Stannane Derivatives. *Bull.*

Chem. Soc. Jpn. **2005**, *78*, 487–497.

(1107) Yamamoto, G.; Kaneko, M.; Ohkuma, M.; Minoura, M. Dynamic Stereochemistry of Alkyltris(9-Triptycyl)Stannanes. *Chem. Lett.* **2003**, *32*, 964–965.

(1108) Stevens, A. M.; Richards, C. J. A Metallocene Molecular Gear. *Tetrahedron Lett.* **1997**, *38*, 7805–7808.

(1109) Kawada, Y.; Sakai, H.; Oguri, M.; Koga, G. Preparation of and Dynamic Gearing in Cis-1,2-Bis(9-Triptycyl)Ethylene. *Tetrahedron Lett.* **1994**, *35*, 139–142.

(1110) Kawada, Y.; Kimura, Y.; Yamazaki, H.; Ishikawa, J.; Sakai, H.; Oguri, M.; Koga, G. Further Studies on the Dependence of the Barriers for Gear Slippage on the Joint Group in Bis(9-Triptycyl)X Type Molecules. Bis(9-Triptycyl)Phosphine, the Missing Link in the Series along the Third Row of the Periodic Table. *Chem. Lett.* **1994**, *23*, 1311–1314.

(1111) Nikitin, K.; Müller-Bunz, H.; Ortin, Y.; Risse, W.; McGlinchey, M. J. Twin Triptycyl Spinning Tops: A Simple Case of Molecular Gearing with DynamicC2 Symmetry. *Eur. J. Org. Chem.* **2008**, *2008*, 3079–3084.

(1112) Wang, G.; Ma, L.; Xiang, J.; Wang, Y.; Chen, X.; Che, Y.; Jiang, H. 2,6-Pyridodicarboxamide-Bridged Triptycene Molecular Transmission Devices: Converting Rotation to Rocking Vibration. *J. Org. Chem.* **2015**, *80*, 11302–11312.

(1113) Kao, C.-Y.; Hsu, Y.-T.; Lu, H.-F.; Chao, I.; Huang, S.-L.; Lin, Y.-C.; Sun, W.-T.; Yang, J.-S. Toward a Four-Toothed Molecular Bevel Gear with C 2 -Symmetrical Rotors. *J. Org. Chem.* **2011**, *76*, 5782–5792.

(1114) Koga, N.; Kawada, Y.; Iwamura, H. Recognition of the Phase Relationship between Remote Substituents in 9,10-Bis(3-Chloro-9-Triptycyloxy)Triptycene Molecules Undergoing Rapid Internal Rotation Cooperatively. *J. Am. Chem. Soc.* **1983**, *105*, 5498–5499.

(1115) Toyota, S.; Kawahata, K.; Sugahara, K.; Wakamatsu, K.; Iwanaga, T. Triple and Quadruple Triptycene Gears in Rigid Macrocyclic Frameworks. *Eur. J. Org. Chem.* **2017**, *2017*, 5696–5707.

(1116) Sanada, K.; Ube, H.; Shionoya, M. Rotational Control of a Dirhodium-Centered Supramolecular Four-Gear System by Ligand Exchange. *J. Am. Chem. Soc.* **2016**, *138*, 2945–2948.

(1117) Ube, H.; Yamada, R.; Ishida, J.; Sato, H.; Shiro, M.; Shionoya, M. A Circularly Arranged Sextuple Triptycene Gear Molecule. *J. Am. Chem. Soc.* **2017**, *139*, 16470–16473.

(1118) Harrington, L. E.; Cahill, L. S.; McGlinchey, M. J. Toward an Organometallic Molecular Brake with a Metal Foot Pedal: Synthesis, Dynamic Behavior, and X-Ray Crystal Structure of [(9-Indenyl)Triptycene]Chromium Tricarbonyl. *Organometallics* **2004**, *23*, 2884–2891.

(1119) Setaka, W.; Nirengi, T.; Kabuto, C.; Kira, M. Introduction of Clutch Function into a Molecular Gear System by Silane-Silicate Interconversion. *J. Am. Chem. Soc.* **2008**, *130*, 15762–15763.

(1120) Ube, H.; Yasuda, Y.; Sato, H.; Shionoya, M. Metal-Centred Azaphosphatriptycene Gear with a Photo- and Thermally Driven Mechanical Switching Function Based on Coordination Isomerism. *Nat. Commun.* **2017**, *8*, 14296.

(1121) Tashiro, K.; Konishi, K.; Aida, T. Metal Bisporphyrinate Double-Decker Complexes as Redox-Responsive Rotating Modules. Studies on Ligand Rotation Activities of the Reduced and Oxidized Forms Using Chirality as a Probe. *J. Am. Chem. Soc.* **2000**, *122*, 7921–7926.

(1122) Ikeda, M.; Takeuchi, M.; Shinkai, S.; Tani, F.; Naruta, Y. Synthesis of New Diaryl-Substituted Triple-Decker and Tetraaryl-Substituted Double-Decker Lanthanum(III) Porphyrins and Their Porphyrin Ring Rotational Speed as Compared with That of Double-Decker Cerium(IV) Porphyrins. *Bull. Chem. Soc. Jpn.* **2001**, *74*, 739–746.

(1123) Alessio, E.; Geremia, S.; Mestroni, S.; Iengo, E.; Srnova, I.; Slouf, M. Solution and Solid State Structure of a Canted, Side-to-Face, Bis(Porphyrin) Adduct. *Inorg. Chem.* **1999**, *38*, 869–875.

(1124) Funatsu, K.; Imamura, T.; Ichimura, A.; Sasaki, Y. Synthesis and Properties of Cyclic Ruthenium(II) Porphyrin Tetramers. *Inorg. Chem.* **1998**, *37*, 1798–1804.

(1125) Funatsu, K.; Kimura, A.; Imamura, T.; Ichimura, A.; Sasaki, Y. Perpendicularly Arranged Ruthenium Porphyrin Dimers and Trimers. *Inorg. Chem.* **1997**, *36*, 1625–1635.

(1126) Kariya, N.; Imamura, T.; Sasaki, Y. Synthesis, Characterization, and Spectral Properties of New Perpendicularly Linked Osmium(II) Porphyrin Oligomers 1. *Inorg. Chem.* **1997**, *36*, 833–839.

(1127) Kimura, A.; Funatsu, K.; Imamura, T.; Kido, H.; Sasaki, Y. Vertically Linked Ruthenium(II) Porphyrin Oligomers. *Chem. Lett.* **1995**, *24*, 207–208.

(1128) Alessio, E.; Macchi, M.; Heath, S.; Marzilli, L. G. A Novel Open-Box Shaped Pentamer of Vertically Linked Porphyrins That Selectively Recognizes S-Bonded Me2SO Complexes. *Chem. Commun.* **1996**, 1411–1412.

(1129) Ogi, S.; Ikeda, T.; Wakabayashi, R.; Shinkai, S.; Takeuchi, M. A Bevel-Gear-Shaped Rotor Bearing a Double-Decker Porphyrin Complex. *Chem. Eur. J.* **2010**, *16*, 8285–8290.

(1130) Ogi, S.; Ikeda, T.; Wakabayashi, R.; Shinkai, S.; Takeuchi, M. Mechanically Interlocked Porphyrin Gears Propagating Two Different Rotational Frequencies. *Eur. J. Org. Chem.* **2011**, *2011*, 1831–1836.

(1131) Ogi, S.; Ikeda, T.; Takeuchi, M. Synthetic Molecular Gear Based on Double-Decker Porphyrin Complexes. *J. Inorg. Organomet. Polym. Mater.* **2013**, *23*, 193–199.

(1132) Bulo, R. E.; Allaart, F.; Ehlers, A. W.; de Kanter, F. J. J.; Schakel, M.; Lutz, M.; Spek, A. L.; Lammertsma, K. Circumambulatory Rearrangement with Characteristics of a 2:1 Covalent Molecular Bevel Gear. *J. Am. Chem. Soc.* **2006**, *128*, 12169–12173.

(1133) Romeo, R.; Carnabuci, S.; Fenech, L.; Plutino, M. R.; Albinati, A. Overcrowded Organometallic Platinum(II) Complexes That Behave as Molecular Gears. *Angew. Chem. Int. Ed.* **2006**, *45*, 4494–

4498.

(1134) Khan, N. S.; Perez-Aguilar, J. M.; Kaufmann, T.; Hill, P. A.; Taratula, O.; Lee, O.-S.; Carroll, P. J.; Saven, J. G.; Dmochowski, I. J. Multiple Hindered Rotators in a Gyroscope-Inspired Tribenzylamine Hemicryptophane. *J. Org. Chem.* **2011**, *76*, 1418–1424.

(1135) Toyota, S.; Shimizu, T.; Iwanaga, T.; Wakamatsu, K. Structures and Conformational Analysis of 1,8-Bis(9-Triptycylethynyl)Anthracene and Its Derivatives as Prototypes of Molecular Spur Gears. *Chem. Lett.* **2011**, *40*, 312–314.

(1136) Frantz, D. K.; Linden, A.; Baldridge, K. K.; Siegel, J. S. Molecular Spur Gears Comprising Triptycene Rotators and Bibenzimidazole-Based Stators. *J. Am. Chem. Soc.* **2012**, *134*, 1528–1535.

(1137) Huang, F.; Wang, G.; Ma, L.; Wang, Y.; Chen, X.; Che, Y.; Jiang, H. Molecular Spur Gears Based on a Switchable Quinquepyridine Foldamer Acting as a Stator. *J. Org. Chem.* **2017**, *82*, 12106–12111.

(1138) Liu, S.; Kondratuk, D. V.; Rousseaux, S. A. L.; Gil-Ramírez, G.; O'Sullivan, M. C.; Cremers, J.; Claridge, T. D. W.; Anderson, H. L. Caterpillar Track Complexes in Template-Directed Synthesis and Correlated Molecular Motion. *Angew. Chem. Int. Ed.* **2015**, *54*, 5355–5359.

(1139) Hiraoka, S.; Harano, K.; Tanaka, T.; Shiro, M.; Shionoya, M. Quantitative Formation of Sandwich-Shaped Trinuclear Silver(I) Complexes and Dynamic Nature of TheirP?M Flip Motion in Solution. *Angew. Chem. Int. Ed.* **2003**, *42*, 5182–5185.

(1140) Hiraoka, S.; Shiro, M.; Shionoya, M. Heterotopic Assemblage of Two Different Disk-Shaped Ligands through Trinuclear Silver(I) Complexation: Ligand Exchange-Driven Molecular Motion. *J. Am. Chem. Soc.* **2004**, *126*, 1214–1218.

(1141) Hiraoka, S.; Hirata, K.; Shionoya, M. A Molecular Ball Bearing Mediated by Multiligand Exchange in Concert. *Angew. Chem. Int. Ed.* **2004**, *43*, 3814–3818.

(1142) Hiraoka, S.; Hisanaga, Y.; Shiro, M.; Shionoya, M. A Molecular Double Ball Bearing: An AgI-PtII Dodecanuclear Quadruple-Decker Complex with Three Rotors. *Angew. Chem. Int. Ed.* **2010**, *49*, 1669–1673.

(1143) Hiraoka, S.; Okuno, E.; Tanaka, T.; Shiro, M.; Shionoya, M. Ranging Correlated Motion (1.5 Nm) of Two Coaxially Arranged Rotors Mediated by Helix Inversion of a Supramolecular Transmitter. *J. Am. Chem. Soc.* **2008**, *130*, 9089–9098.

(1144) Tabe, Y.; Yokoyama, H. Coherent Collective Precession of Molecular Rotors with Chiral Propellers. *Nat. Mater.* **2003**, *2*, 806–809.

(1145) Zhao, R.; Zhao, Y.-L.; Qi, F.; Hermann, K. E.; Zhang, R.-Q.; Van Hove, M. A. Interlocking Mechanism between Molecular Gears Attached to Surfaces. *ACS Nano* **2018**, *12*, 3020–3029.

(1146) Zhao, R.; Qi, F.; Zhang, R.-Q.; Van Hove, M. A. How Does the Flexibility of Molecules Affect the Performance of Molecular Rotors? *J. Phys. Chem. C* **2018**, *122*, 25067–25074.

(1147) Zhao, R.; Qi, F.; Zhao, Y.-L.; Hermann, K. E.; Zhang, R.-Q.; Van Hove, M. A. Interlocking Molecular Gear Chains Built on Surfaces. *J. Phys. Chem. Lett.* **2018**, *9*, 2611–2619.

(1148) Chiaravalloti, F.; Gross, L.; Rieder, K.-H.; Stojkovic, S. M.; Gourdon, A.; Joachim, C.; Moresco, F. A Rack-and-Pinion Device at the Molecular Scale. *Nat. Mater.* **2007**, *6*, 30–33.

(1149) Mishra, P.; Hill, J. P.; Vijayaraghavan, S.; Rossom, W. Van; Yoshizawa, S.; Grisolia, M.; Echeverria, J.; Ono, T.; Ariga, K.; Nakayama, T.; et al. Current-Driven Supramolecular Motor with In Situ Surface Chiral Directionality Switching. *Nano Lett.* **2015**, *15*, 4793–4798.

(1150) Wasio, N. A.; Slough, D. P.; Smith, Z. C.; Ivimey, C. J.; Thomas III, S. W.; Lin, Y.-S.; Sykes, E. C. H. Correlated Rotational Switching in Two-Dimensional Self-Assembled Molecular Rotor Arrays. *Nat. Commun.* **2017**, *8*, 16057.

(1151) Écija, D.; Auwärter, W.; Vijayaraghavan, S.; Seufert, K.; Bischoff, F.; Tashiro, K.; Barth, J. V.

Assembly and Manipulation of Rotatable Cerium Porphyrinato Sandwich Complexes on a Surface. *Angew. Chem. Int. Ed.* **2011**, *50*, 3872–3877.

(1152) Tanaka, H.; Ikeda, T.; Takeuchi, M.; Sada, K.; Shinkai, S.; Kawai, T. Molecular Rotation in Self-Assembled Multidecker Porphyrin Complexes. *ACS Nano* **2011**, *5*, 9575–9582.

(1153) Lei, S.-B.; Deng, K.; Yang, Y.-L.; Zeng, Q.-D.; Wang, C.; Jiang, J.-Z. Electric Driven Molecular Switching of Asymmetric Tris(Phthalocyaninato) Lutetium Triple-Decker Complex at the Liquid/Solid Interface. *Nano Lett.* **2008**, *8*, 1836–1843.

(1154) Zhang, Y.; Kersell, H.; Stefak, R.; Echeverria, J.; Iancu, V.; Perera, U. G. E.; Li, Y.; Deshpande, A.; Braun, K.-F.; Joachim, C.; et al. Simultaneous and Coordinated Rotational Switching of All Molecular Rotors in a Network. *Nat. Nanotechnol.* **2016**, *11*, 706–712.

(1155) Rodríguez-Molina, B.; Farfán, N.; Romero, M.; Méndez-Stivalet, J. M.; Santillan, R.; Garcia-Garibay, M. A. Anisochronous Dynamics in a Crystalline Array of Steroidal Molecular Rotors: Evidence of Correlated Motion within 1D Helical Domains. *J. Am. Chem. Soc.* **2011**, *133*, 7280–7283.

(1156) Kaleta, J.; Bastien, G.; Císařová, I.; Batail, P.; Michl, J. Molecular Rods: Facile Desymmetrization of 1,4-Diethynylbicyclo[2.2.2]Octane. *Eur. J. Org. Chem.* **2018**, *2018*, 5137–5142.

(1157) Schwab, P. F. H.; Smith, J. R.; Michl, J. Synthesis and Properties of Molecular Rods. 2. Zig-Zag Rods. *Chem. Rev.* **2005**, *105*, 1197–1280.

(1158) Schwab, P. F. H.; Noll, B. C.; Michl, J. Synthesis and Structure of Trigonal and Tetragonal Connectors for a “Tinkertoy” Construction Set. *J. Org. Chem.* **2002**, *67*, 5476–5485.

(1159) Bastien, G.; Lemouchi, C.; Allain, M.; Wzietek, P.; Rodríguez-Fortea, A.; Canadell, E.; Iliopoulos, K.; Gindre, D.; Chrysos, M.; Batail, P. Changing Gears to Neutral in a Polymorph of One-Dimensional Arrays of Cogwheel-like Pairs of Molecular Rotors. *CrystEngComm* **2014**, *16*, 1241–

1244.

(1160) Kaleta, J.; Michl, J.; Mézière, C.; Simonov, S.; Zorina, L.; Wzietek, P.; Rodríguez-Fortea, A.; Canadell, E.; Batail, P. Gearing Motion in Cogwheel Pairs of Molecular Rotors: Weak-Coupling Limit. *CrystEngComm* **2015**, *17*, 7829–7834.

(1161) Lemouchi, C.; Iliopoulos, K.; Zorina, L.; Simonov, S.; Wzietek, P.; Cauchy, T.; Rodríguez-Fortea, A.; Canadell, E.; Kaleta, J.; Michl, J.; et al. Crystalline Arrays of Pairs of Molecular Rotors: Correlated Motion, Rotational Barriers, and Space-Inversion Symmetry Breaking Due to Conformational Mutations. *J. Am. Chem. Soc.* **2013**, *135*, 9366–9376.

(1162) Simonov, S.; Zorina, L.; Wzietek, P.; Rodríguez-Fortea, A.; Canadell, E.; Mézière, C.; Bastien, G.; Lemouchi, C.; Garcia-Garibay, M. A.; Batail, P. Static Modulation Wave of Arrays of Halogen Interactions Transduced to a Hierarchy of Nanoscale Change Stimuli of Crystalline Rotors Dynamics. *Nano Lett.* **2018**, *18*, 3780–3784.

(1163) Kassem, S.; van Leeuwen, T.; Lubbe, A. S.; Wilson, M. R.; Feringa, B. L.; Leigh, D. A. Artificial Molecular Motors. *Chem. Soc. Rev.* **2017**, *46*, 2592–2621.

(1164) Boyer, P. D. The ATP Synthase—A Splendid Molecular Machine. *Annu. Rev. Biochem.* **1997**, *66*, 717–749.

(1165) Koumura, N.; Zijlstra, R. W. J.; van Delden, R. A.; Harada, N.; Feringa, B. L. Light-Driven Monodirectional Molecular Rotor. *Nature* **1999**, *401*, 152–155.

(1166) Roke, D.; Wezenberg, S. J.; Feringa, B. L. Molecular Rotary Motors: Unidirectional Motion around Double Bonds. *Proc. Natl. Acad. Sci.* **2018**, *115*, 9423–9431.

(1167) Lehn, J.-M. Conjecture: Imines as Unidirectional Photodriven Molecular Motors—Motional and Constitutional Dynamic Devices. *Chem. Eur. J.* **2006**, *12*, 5910–5915.

(1168) Greb, L.; Lehn, J.-M. Light-Driven Molecular Motors: Imines as Four-Step or Two-Step

Unidirectional Rotors. *J. Am. Chem. Soc.* **2014**, *136*, 13114–13117.

(1169) Guentner, M.; Schildhauer, M.; Thumser, S.; Mayer, P.; Stephenson, D.; Mayer, P. J.; Dube, H. Sunlight-Powered KHz Rotation of a Hemithioindigo-Based Molecular Motor. *Nat. Commun.* **2015**, *6*, 8406.

(1170) Wang, J.; Feringa, B. L. Dynamic Control of Chiral Space in a Catalytic Asymmetric Reaction Using a Molecular Motor. *Science* **2011**, *331*, 1429–1432.

(1171) Zhao, D.; van Leeuwen, T.; Cheng, J.; Feringa, B. L. Dynamic Control of Chirality and Self-Assembly of Double-Stranded Helicates with Light. *Nat. Chem.* **2017**, *9*, 250–256.

(1172) Lubbe, A. S.; Liu, Q.; Smith, S. J.; de Vries, J. W.; Kistemaker, J. C. M.; de Vries, A. H.; Faustino, I.; Meng, Z.; Szymanski, W.; Herrmann, A.; et al. Photoswitching of DNA Hybridization Using a Molecular Motor. *J. Am. Chem. Soc.* **2018**, *140*, 5069–5076.

(1173) García-López, V.; Chen, F.; Nilewski, L. G.; Duret, G.; Aliyan, A.; Kolomeisky, A. B.; Robinson, J. T.; Wang, G.; Pal, R.; Tour, J. M. Molecular Machines Open Cell Membranes. *Nature* **2017**, *548*, 567–572.

(1174) van Leeuwen, T.; Lubbe, A. S.; Štacko, P.; Wezenberg, S. J.; Feringa, B. L. Dynamic Control of Function by Light-Driven Molecular Motors. *Nat. Rev. Chem.* **2017**, *1*, 0096.

(1175) Browne, W. R.; Feringa, B. L. Making Molecular Machines Work. *Nat. Nanotechnol.* **2006**, *1*, 25–35.

(1176) Cnossen, A.; Pijper, D.; Kudernac, T.; Pollard, M. M.; Katsonis, N.; Feringa, B. L. A Trimer of Ultrafast Nanomotors: Synthesis, Photochemistry and Self-Assembly on Graphite. *Chem. Eur. J.* **2009**, *15*, 2768–2772.

(1177) Chen, K.-Y.; Ivashenko, O.; Carroll, G. T.; Robertus, J.; Kistemaker, J. C. M.; London, G.; Browne, W. R.; Rudolf, P.; Feringa, B. L. Control of Surface Wettability Using Tripodal Light-

Activated Molecular Motors. *J. Am. Chem. Soc.* **2014**, *136*, 3219–3224.

(1178) Vives, G.; Tour, J. M. Synthesis of Single-Molecule Nanocars. *Acc. Chem. Res.* **2009**, *42*, 473–487.

(1179) Kudernac, T.; Ruangsupapichat, N.; Parschau, M.; Maciá, B.; Katsonis, N.; Harutyunyan, S. R.; Ernst, K.-H.; Feringa, B. L. Electrically Driven Directional Motion of a Four-Wheeled Molecule on a Metal Surface. *Nature* **2011**, *479*, 208–211.

(1180) Wang, Y.; Li, Q. Light-Driven Chiral Molecular Switches or Motors in Liquid Crystals. *Adv. Mater.* **2012**, *24*, 1926–1945.

(1181) van Delden, R. A.; Koumura, N.; Harada, N.; Feringa, B. L. Unidirectional Rotary Motion in a Liquid Crystalline Environment: Color Tuning by a Molecular Motor. *Proc. Natl. Acad. Sci.* **2002**, *99*, 4945–4949.

(1182) Eelkema, R.; Feringa, B. L. Reversible Full-Range Color Control of a Cholesteric Liquid-Crystalline Film by Using a Molecular Motor. *Chem. – An Asian J.* **2006**, *1*, 367–369.

(1183) Eelkema, R.; Pollard, M. M.; Vicario, J.; Katsonis, N.; Ramon, B. S.; Bastiaansen, C. W. M.; Broer, D. J.; Feringa, B. L. Nanomotor Rotates Microscale Objects. *Nature* **2006**, *440*, 163–163.

(1184) Eelkema, R.; Pollard, M. M.; Katsonis, N.; Vicario, J.; Broer, D. J.; Feringa, B. L. Rotational Reorganization of Doped Cholesteric Liquid Crystalline Films. *J. Am. Chem. Soc.* **2006**, *128*, 14397–14407.

(1185) Pijper, D.; Jongejan, M. G. M.; Meetsma, A.; Feringa, B. L. Light-Controlled Supramolecular Helicity of a Liquid Crystalline Phase Using a Helical Polymer Functionalized with a Single Chiroptical Molecular Switch. *J. Am. Chem. Soc.* **2008**, *130*, 4541–4552.

(1186) Bosco, A.; Jongejan, M. G. M.; Eelkema, R.; Katsonis, N.; Lacaze, E.; Ferrarini, A.; Feringa, B. L. Photoinduced Reorganization of Motor-Doped Chiral Liquid Crystals: Bridging Molecular

Isomerization and Texture Rotation. *J. Am. Chem. Soc.* **2008**, *130*, 14615–14624.

(1187) Pijper, D.; Feringa, B. L. Molecular Transmission: Controlling the Twist Sense of a Helical Polymer with a Single Light-Driven Molecular Motor. *Angew. Chem. Int. Ed.* **2007**, *46*, 3693–3696.

(1188) Loussert, C.; Iamsaard, S.; Katsonis, N.; Brasselet, E. Subnanowatt Opto-Molecular Generation of Localized Defects in Chiral Liquid Crystals. *Adv. Mater.* **2014**, *26*, 4242–4246.

(1189) Orlova, T.; Lancia, F.; Loussert, C.; Iamsaard, S.; Katsonis, N.; Brasselet, E. Revolving Supramolecular Chiral Structures Powered by Light in Nanomotor-Doped Liquid Crystals. *Nat. Nanotechnol.* **2018**, *13*, 304–308.

(1190) Bléger, D. Continuously Revolving Patterns. *Nat. Nanotechnol.* **2018**, *13*, 274–275.

(1191) Sun, J.; Lan, R.; Gao, Y.; Wang, M.; Zhang, W.; Wang, L.; Zhang, L.; Yang, Z.; Yang, H. Stimuli-Directed Dynamic Reconfiguration in Self-Organized Helical Superstructures Enabled by Chemical Kinetics of Chiral Molecular Motors. *Adv. Sci.* **2018**, *5*, 1700613.

(1192) Poloni, C.; Stuart, M. C. A.; Van Der Meulen, P.; Szymanski, W.; Feringa, B. L. Light and Heat Control over Secondary Structure and Amyloid-like Fiber Formation in an Overcrowded-Alkene-Modified Trp Zipper. *Chem. Sci.* **2015**, *6*, 7311–7318.

(1193) van Dijken, D. J.; Chen, J.; Stuart, M. C. A. A.; Hou, L.; Feringa, B. L. Amphiphilic Molecular Motors for Responsive Aggregation in Water. *J. Am. Chem. Soc.* **2016**, *138*, 660–669.

(1194) Chen, J.; Leung, F. K.-C.; Stuart, M. C. A.; Kajitani, T.; Fukushima, T.; van der Giessen, E.; Feringa, B. L. Artificial Muscle-like Function from Hierarchical Supramolecular Assembly of Photoresponsive Molecular Motors. *Nat. Chem.* **2018**, *10*, 132–138.

(1195) Yu, J. J.; Cao, Z. Q.; Zhang, Q.; Yang, S.; Qu, D. H.; Tian, H. Photo-Powered Stretchable Nano-Containers Based on Well-Defined Vesicles Formed by an Overcrowded Alkene Switch. *Chem.*

Commun. **2016**, *52*, 12056–12059.

(1196) van Leeuwen, T.; Heideman, G. H.; Zhao, D.; Wezenberg, S. J.; Feringa, B. L. In Situ Control of Polymer Helicity with a Non-Covalently Bound Photoresponsive Molecular Motor Dopant. *Chem. Commun.* **2017**, *53*, 6393–6396.

(1197) Wezenberg, S. J.; Croisetu, C. M.; Stuart, M. C. A.; Feringa, B. L. Reversible Gel–Sol Photoswitching with an Overcrowded Alkene-Based Bis-Urea Supergelator. *Chem. Sci.* **2016**, *7*, 4341–4346.

(1198) Li, Q.; Fuks, G.; Moulin, E.; Maaloum, M.; Rawiso, M.; Kulic, I.; Foy, J. T.; Giuseppone, N. Macroscopic Contraction of a Gel Induced by the Integrated Motion of Light-Driven Molecular Motors. *Nat. Nanotechnol.* **2015**, *10*, 161–165.

(1199) Li, Q.; Foy, J. T.; Colard-Itté, J.-R.; Goujon, A.; Dattler, D.; Fuks, G.; Moulin, E.; Giuseppone, N. Gram Scale Synthesis of Functionalized and Optically Pure Feringa's Motors. *Tetrahedron* **2017**, *73*, 4874–4882.

(1200) Colard-Itté, J.-R.; Li, Q.; Collin, D.; Mariani, G.; Fuks, G.; Moulin, E.; Buhler, E.; Giuseppone, N. Mechanical Behaviour of Contractile Gels Based on Light-Driven Molecular Motors. *Nanoscale* **2019**, *11*, 5197–5202.

(1201) Foy, J. T.; Li, Q.; Goujon, A.; Colard-Itté, J.-R.; Fuks, G.; Moulin, E.; Schiffmann, O.; Dattler, D.; Funeriu, D. P.; Giuseppone, N. Dual-Light Control of Nanomachines That Integrate Motor and Modulator Subunits. *Nat. Nanotechnol.* **2017**, *12*, 540–545.

BIOGRAPHIES

Damien Dattler received his master degree in Molecular and Supramolecular chemistry from the University of Strasbourg in 2016. After a master internship, he continued his research in Giuseppone's group as Ph.D. student under the supervision of Prof. Nicolas Giuseppone and is currently in the 3rd year. His Ph.D. studies are mainly focus on the synthesis and the integration of photoactive molecular motor in supramolecular systems.

Gad Fuks studied chemistry at the University of Strasbourg and then completed a PhD (2004–2007) working under the supervision of Dr Didier Bourissou and Prof. Guy Bertrand both at the University of Toulouse and at the University of California (Riverside) working on singlet diradicals. He then started a postdoctoral work at the IMRCP laboratory in Toulouse with Dr Fabienne Gauffre working on biohybrid block copolymers. Then, he worked one year at the LPCNO (Toulouse) working on metallic nanoparticles under the supervision of Dr Céline Nayral and Dr Fabien Delpech. He moved to Strasbourg in 2010 where he is now assistant professor working with Prof. Nicolas Giuseppone in the SAMS research group on the amplification of molecular motions.

Joakim Heiser studied chemistry at the University of Strasbourg where he obtained a Master degree in Molecular and Supramolecular Chemistry. In 2017, he obtained a PhD grant from the Fond National de la Recherche Luxembourg and began working under the supervision of Nicolas Giuseppone. His project is titled "Integration of light-fuelled molecular motors combined with releasing units into a contractile gel" and will be focused on the elaboration of mechanical oscillator materials as well as the synthesis of functionalized photoswitches.

Emilie Moulin completed her PhD in organic synthesis in 2006 in Strasbourg under the supervision of Prof. Nicolas Winssinger working on the total synthesis of resorcylic macrolides. She then joined the group of Prof. Aloïs Fürstner at the Max-Planck-Institute für Kohlenforschung in Mülheim an der Ruhr (Germany) as a Alexander von Humboldt post-doctoral fellow working on the total synthesis of polyene macroclides (2007-2008). Since 2008, she holds a "Chargé de Recherche" CNRS position at the Institut Charles Sadron in Strasbourg working in the group of Prof. Nicolas Giuseppone, where she has actively developed the supramolecular chemistry of triarylamine molecules. In 2014, she completed her habilitation (HDR) and her current research interests focus on merging the fields of polymer, supramolecular and organic chemistry to produce functional materials, in particular using molecular machines.

Alexis Perrot obtained his master's degree "International Master of Polymer Sciences" at the University of Strasbourg (France) and the Albert-Ludwigs-Universität Freiburg (Germany) in 2017. He then started his PhD under the supervision of Prof. Nicolas Giuseppone and Dr. Emilie Moulin, where he studies the influence of the polymeric backbone on the photomechanical behavior of materials incorporating photoactive rotary molecular motors. His current research interests are material sciences, particularly advanced functional materials.

Xuyang Yao obtained his PhD in applied chemistry in 2016 under the supervision of Prof. He Tian from East China University of Science and Technology (ECUST). During his PhD, he also worked in a collaborative project that combined supramolecular self-assembling systems with nanopore technology with Professor Yitao Long's group. After obtaining his PhD, he worked for one year in the same institute with Prof. Xiang Ma to study room-temperature-phosphorescence materials before moving to the University of Freiburg as post-doc for the joint FRIAS-USIAS project between Profs. Andreas Walther

and Nicolas Giuseppone. His research interest focuses on controllable and functional supramolecular self-assemblies, polymers, and supramolecular light-responsive systems and optical materials.

Nicolas Giuseppone received his PhD in asymmetric catalysis (laboratory of Prof. H.B. Kagan), performed a post-doctoral research in total synthesis (laboratory of Prof. K.C. Nicolaou), and entered the field of supramolecular chemistry as a CNRS researcher (laboratory of Prof. J.-M. Lehn). In 2008 he started his independent research group and was awarded the ERC Starting Grant from the European Research Council in 2010. In 2013 he was promoted Full Professor of Chemistry at the University of Strasbourg (Unistra) and nominated as a junior member of the Institut Universitaire the France (IUF). In 2016, he was promoted Distinguished Professor at the Unistra. He is currently deputy director of the Institut Charles Sadron (CNRS) and director of the Research Federation on Materials and Nanoscience for the Grand Est Region. His research interests are focused on supramolecular chemistry, molecular machines, and functional materials.

Graphical TOC